

Technical Report Documentation Page

1. Report No. FHWA/TX-13/0-6564-1		2. Government Accession No.		3. Recipient's Catalog No.	
4. Title and Subtitle Improved Cross Frame Details for Steel Bridges			5. Report Date October 2013; Published May 2014		
			6. Performing Organization Code		
7. Author(s) Anthony Battistini, Weihua Wang, Sean Donahue, Todd Helwig, Michael Engelhardt, Karl Frank			8. Performing Organization Report No. 0-6564-1		
9. Performing Organization Name and Address Center for Transportation Research The University of Texas at Austin 1616 Guadalupe St., Suite 4.202 Austin, TX 78701			10. Work Unit No. (TRAIS)		
			11. Contract or Grant No. 0-6564		
12. Sponsoring Agency Name and Address Texas Department of Transportation Research and Technology Implementation Office P.O. Box 5080 Austin, TX 78763-5080			13. Type of Report and Period Covered Technical Report September 2009–August 2012		
			14. Sponsoring Agency Code		
15. Supplementary Notes Project performed in cooperation with the Texas Department of Transportation and the Federal Highway Administration.					
16. Abstract <p>Cross frames are critical members for the stability of straight and curved steel bridges. Conventional cross frames are often fabricated from steel angles; however these members have relatively poor structural behavior. Because of the low buckling strength, cross frames with angle diagonals are often designed as tension-only systems, therefore increasing the necessary steel. The angles are also connected through one leg resulting in eccentric connections causing bending of the members and potentially reducing the fatigue performance.</p> <p>Improved behavior may result if concentric members are utilized for the cross frames. The increased buckling strength of tubes and double angles results in effective members in both tension and compression, and a single diagonal cross frame can provide effective bracing. Although there are structural advantages of utilizing concentric members, a suitable connection must be developed. Tubes are often connected by slitting the tube in the center and welding to a connection plate, which requires precise fabrication and relatively poor fatigue behavior. One proposed solution is to use a steel casting designed to connect easily to the beams and to seal the end of the tube (preventing exposure to atmospheric conditions).</p> <p>In addition, the report covers in detail the categorization of the single angle detail for both X and K frame configurations. To date, the determination of the single angle fatigue detail has been largely based on component tests only. The project incorporated both component and full-scale cross frame fatigues tests to fully examine the interaction of the cross frame members with the overall structure. Finally, the project also examined the stiffness behavior of cross frames, using a combination of full-scale laboratory tests and computational finite element model analysis.</p>					
17. Key Words steel bridges, cross frames, tubular members, steel castings, stability, fatigue, stiffness, single angle behavior			18. Distribution Statement No restrictions. This document is available to the public through the National Technical Information Service, Springfield, Virginia 22161; www.ntis.gov .		
19. Security Classif. (of report) Unclassified		20. Security Classif. (of this page) Unclassified		21. No. of pages 412	
22. Price					



**THE UNIVERSITY OF TEXAS AT AUSTIN
CENTER FOR TRANSPORTATION RESEARCH**

Improved Cross Frame Details for Steel Bridges

Anthony Battistini
Weihua Wang
Sean Donahue
Todd Helwig
Michael Engelhardt
Karl Frank

CTR Technical Report:	0-6564-1
Report Date:	October 2013
Project:	0-6564
Project Title:	Improved Cross Frame Details
Sponsoring Agency:	Texas Department of Transportation
Performing Agency:	Center for Transportation Research at The University of Texas at Austin

Project performed in cooperation with the Texas Department of Transportation and the Federal Highway Administration.

Center for Transportation Research
The University of Texas at Austin
1616 Guadalupe St, Suite 4.202
Austin, TX 78701

www.utexas.edu/research/ctr

Disclaimers

Author's Disclaimer: The contents of this report reflect the views of the authors, who are responsible for the facts and the accuracy of the data presented herein. The contents do not necessarily reflect the official view or policies of the Federal Highway Administration or the Texas Department of Transportation (TxDOT). This report does not constitute a standard, specification, or regulation.

Patent Disclaimer: There was no invention or discovery conceived or first actually reduced to practice in the course of or under this contract, including any art, method, process, machine manufacture, design or composition of matter, or any new useful improvement thereof, or any variety of plant, which is or may be patentable under the patent laws of the United States of America or any foreign country.

Notice: The United States Government and the State of Texas do not endorse products or manufacturers. If trade or manufacturers' names appear herein, it is solely because they are considered essential to the object of this report.

Engineering Disclaimer

NOT INTENDED FOR CONSTRUCTION, BIDDING, OR PERMIT PURPOSES.

Project Engineer: Todd Helwig
Professional Engineer License State and Number: Texas No. 94280
P. E. Designation: Research Supervisor

Acknowledgments

The authors would like to acknowledge the Texas Department of Transportation for funding this research project. In particular, the authors would like to thank TxDOT bridge engineer Michelle Romage, the former project director, for her continued participation in the research. In addition, Wade Odell, from TxDOT RTI has provided the researchers a great deal of assistance in the administration of the contract and his guidance is greatly appreciated. The authors also recognize the staff of Quality Electric Steel Castings for the information they provided in regards to the steel castings. Finally, the authors are grateful to the engineers and welding crew at Hirschfeld Industries for their input on the fabrication of steel bridge cross frames and for construction of some test specimens.

Table of Contents

Chapter 1. Introduction.....	1
1.1 Problem Statement.....	1
1.2 Objectives of TxDOT Project 0-6564.....	3
1.3 Report Outline.....	4
Chapter 2. Background	5
2.1 Introduction.....	5
2.2 Stability of Bridges	5
2.2.1 Lateral Torsional Buckling	6
2.2.2 Bracing Requirements.....	7
2.2.3 Fundamentals of Beam Bracing.....	9
2.2.4 Beam Bracing Stiffness.....	11
2.2.5 Equivalent Stiffness of Cross Frames	14
2.3 Beam Bracing Strength.....	16
2.3.1 Compressive Strength of Single Angles	16
2.3.2 Compressive Strength of Gusset plates.....	17
2.4 Fatigue Design of Steel Bridges	17
2.4.1 Introduction to Fatigue.....	18
2.4.2 Geometrical Discontinuities.....	18
2.4.3 Material Defects.....	19
2.5 AASHTO Bridge Fatigue Design Methodology	22
2.5.1 Fatigue Design	22
2.5.2 Live Load Stress Range	22
2.5.3 AASHTO Fatigue Design Categories	23
2.5.4 Nominal Fatigue Resistance	24
2.5.5 AASHTO S-N Chart	25
2.5.6 Fatigue Testing Methods and Failure Criteria	26
2.6 Fatigue Behavior of Single Angle Members	27
2.6.1 Effect of Angle Eccentricity	27
2.6.2 Fatigue Classification of Single Angle Detail.....	28
2.6.3 Previous Fatigue Tests of Single Angle Detail	29
2.6.4 Discussion of Previous Fatigue Tests of Single Angle Detail	30
2.6.5 Previous Finite Element Analysis (FEA) of Single Angle Detail.....	31
2.7 Fatigue Behavior of Transverse Fillet Welds	31
2.8 Fatigue Behavior of Knife Plate Detail.....	34
2.9 Tubular Braces in Literature	35
2.9.1 Offshore Industry	35
2.9.2 Concentrically Braced Frames.....	36
2.9.3 European Bridges.....	36

2.9.4 Wichita Falls, TX Bridge Retrofit	36
2.10 Advantages of Tubular Members	37
2.10.1 Compression Capacity	37
2.10.2 Fatigue Behavior	38
2.11 Steel Castings in Literature.....	38
2.11.1 Greenbank Telescope.....	38
2.11.2 Earthquake Connections	39
2.11.3 Crane Connections	40
2.12 Advantages of Steel Castings	40
2.12.1 Fatigue Behavior	41
2.12.2 Efficient Use of Material.....	41
2.12.3 Seals Tube	41
2.12.4 Standardization	41
2.13 TxDOT Design Practice.....	42
Chapter 3. Background on Steel Castings	45
3.1 Steel Casting Types	45
3.1.1 Investment Casting.....	45
3.1.2 Sand Casting	46
3.2 Steel Casting Process: Pattern Construction.....	46
3.2.1 Working with the Foundry.....	46
3.2.2 Constructing the Pattern.....	47
3.3 Steel Casting Process: Sand Mold Formation.....	50
3.3.1 Sand Slurry Composition.....	51
3.3.2 Forming the Raw Sand Mold.....	51
3.3.3 Coating the Sand Mold	52
3.3.4 Creating the Sand Cores.....	53
3.3.5 Completing the Sand Mold	54
3.4 Steel Casting Process: Pouring the Steel	55
3.4.1 Melting the Steel	55
3.4.2 Checking the Chemistry of the Steel.....	56
3.4.3 Checking the Temperature of the Steel.....	56
3.4.4 Pouring the Steel	58
3.4.5 Casting Steel Material Test Blocks.....	59
3.5 Steel Casting Process: Finishing the Part	60
3.5.1 Casting Shake-Out	60
3.5.2 Shot Blast	60
3.5.3 Torching and Air Carbon Arc Gouging.....	61
3.5.4 Weld Repair and Grinding	61
3.5.5 Heat Treatment.....	61
3.6 Casting Defects	61
3.6.1 Shrinkage	61
3.6.2 Gas Porosity	62

3.6.3 Surface Flaws.....	62
3.6.4 Inclusions	62
3.6.5 Segregation	63
3.7 Quality Assurance.....	63
3.7.1 Chemical Analysis	63
3.7.2 Mechanical Testing.....	65
3.7.3 Visual Inspection	66
3.7.4 Magnetic Particle Inspection.....	66
3.7.5 Liquid Dye Penetrant	66
3.7.6 Radiography	66
3.7.7 Ultrasonic Inspection	67
3.8 Cost Analysis	67
3.9 Summary	67
Chapter 4. Cross Frame Connections	69
4.1 Introduction.....	69
4.2 Cross Frame Connection Laboratory Experiments.....	69
4.2.1 Testing Machine.....	69
4.2.2 Stiffness Tests	71
4.2.3 Ultimate Strength Tests.....	73
4.2.4 Fatigue Tests	74
<i>Part I: Cast Connection</i>	<i>75</i>
4.3 Cast Connection Design.....	75
4.3.1 Features	75
4.3.2 Dimensions	77
4.3.3 Analysis.....	79
4.4 Cast Connection Laboratory Experiments.....	81
4.4.1 Stiffness Tests	81
4.4.2 Ultimate Strength Test	83
4.4.3 Fatigue Tests	85
4.5 Cast Connection Observations.....	87
<i>Part II: T-Stem Connection.....</i>	<i>87</i>
4.6 T-Stem Connection Design.....	87
4.6.1 Features	88
4.6.2 Dimensions	88
4.6.3 Analysis.....	89
4.7 T-Stem Connection Laboratory Experiments	95
4.7.1 Stiffness Tests	95
4.7.2 Ultimate Strength Tests.....	96
4.7.3 Fatigue Tests	99
4.8 T-Stem Connection Test Observations	103

<i>Part III: Knife-Plate Connection</i>	103
4.9 Knife-Plate Connection Design	103
4.9.1 Stress Relief Hole	103
4.9.2 Slot Fabrication	104
4.10 Knife-Plate Connection Lab Experiments	105
4.10.1 Stiffness Tests	105
4.10.2 Ultimate Strength Tests.....	105
4.10.3 Fatigue Tests	105
4.11 Knife-Plate Connection Observations	107
<i>Part IV: Double Angle Connection</i>	107
4.12 Double Angle Connection Design	107
4.13 Double Angle Connection Laboratory Experiments	108
4.13.1 Stiffness Tests	108
4.13.2 Ultimate Strength Test	109
4.13.3 Fatigue Tests	110
4.14 Double Angle Connection Observations	112
<i>Part V: Single Angle Connection</i>	112
4.15 Single Angle Connection Design.....	112
4.16 Single Angle Connection Lab Experiments.....	113
4.16.1 Stiffness Tests	113
4.16.2 Ultimate Strength Test	114
4.16.3 Fatigue Tests	115
4.17 Single Angle Connection Observations	115
<i>Part VI: Connection Comparison</i>	116
4.18 Connection Stiffness Comparison	116
4.18.1 Calculation Procedure	116
4.18.2 Test Specimen Summary	117
4.18.3 Test Results	120
4.18.4 Relative Behavior of the Connections	121
4.18.5 Connection Stiffness	121
4.18.6 Effect on Cross Frame Stiffness	122
4.18.7 Connection Stiffness Observations	124
4.19 Connection Fatigue Comparison	125
4.20 Cross Frame Connection Conclusions.....	128
Chapter 5. Laboratory Tests for Cross Frame Strength and Stiffness.....	129
5.1 Introduction.....	129
5.2 Test Setup	129
5.2.1 Test Frame	129
5.2.2 Loading and Moments Measurement.....	131

5.2.3 Measurement of Rotations	134
5.2.4 Measurement of Member Axial Forces	136
5.3 Cross Frame Test Program	137
5.4 Single Angle X-frame.....	139
5.4.1 Stiffness Test – Single Angle X-frame	141
5.4.2 Ultimate Strength Test – Single Angle X-frame.....	142
5.5 Single Angle K-frame.....	145
5.5.1 Stiffness Test – Single Angle K-frame	147
5.5.2 Ultimate Strength Test – Single Angle K-frame.....	148
5.6 Square Tube Z-frame	151
5.6.1 Stiffness Test – Square Tube Z-frame	152
5.6.2 Ultimate Strength Test – Square Tube Z-frame.....	153
5.7 Double Angle Z-frame.....	154
5.7.1 Stiffness Test – Double Angle Z-frame	156
5.7.2 Ultimate Strength Test – Double Angle Z-frame.....	157
5.8 Double Angle Z-frame 2 (with Double Angle Struts)	158
5.8.1 Stiffness Test – Double Angle Z-frame 2	160
5.8.2 Ultimate Strength Test – Double Angle Z-frame.....	160
5.9 Single Angle Z-frame	161
5.9.1 Stiffness Test – Single Angle Z-frame.....	162
5.9.2 Ultimate Strength Test – Single Angle Z-frame	163
5.10 Single Angle Unequal Leg X-frame	167
5.10.1 Stiffness Test – Single Angle Unequal Leg X-frame	167
5.10.2 Ultimate Strength Test – Single Angle Unequal Leg X-frame.....	168
5.11 Coupon Tension Tests	169
5.12 Summary of Cross Frame Test Results.....	169
Chapter 6: Models for Cross Frame Stiffness.....	173
6.1 Introduction.....	173
6.2 Analytical Stiffness Reduction for a Single Angle	173
6.2.1 Bending Due to the Eccentric Connection.....	174
6.2.2 Stiffness Reduction Due to Bending.....	177
6.2.3 Typical Values of ρ , γ and R_{member}	180
6.3 Analytical Stiffness Reduction for Cross Frames.....	182
6.3.1 Bending Stiffness of Gusset Plate.....	183
6.3.2 Single Angle X-Frame	184
6.3.3 Single Angle K-Frame	188
6.3.4 Single Angle Z-Frame.....	190
6.3.5 Double Angle Z-Frame	194
6.3.6 Summary of the Analytical Solutions for Stiffness Reduction in Cross Frames	195
6.4 Parametric Studies for the Stiffness Reduction Factor Using Analytical Solutions.....	196

6.5 Conclusions of the Analytical Solution	198
6.6 Parametric Studies for Stiffness of Single Angle X-Frame	199
6.6.1 Introduction	199
6.6.2 Parametric Study with Linear Analysis	200
6.6.3 Parametric Study with Out-of-Plane Bending Constrained	200
6.6.4 Parametric Study with Out-of-Plane Bending Allowed.....	201
6.6.5 Stiffness Estimate Using Analytical Stiffness Reduction Factor.....	203
6.6.6 Stiffness Comparison Using Tension-Only Diagonal Model	208
6.6.7 Stiffness Reduction from Regression Method	209
6.6.8 Parametric Study with Nonlinear Buckling Analysis	213
6.6.9 Parametric Study for Cross Frame with Unequal Legs Angles	216
6.6.10 Summary of Parametric Studies for Single Angle X-Frame	219
6.7 FEA Parametric Studies for Stiffness of Single Angle K-Frame	220
6.7.1 Introduction.....	220
6.7.2 Parametric Study with Linear Analysis	220
6.7.3 Parametric Study with Out-of-Plane Bending Constrained	220
6.7.4 Parametric Study with Out-of-Plane Bending Allowed.....	221
6.7.5 Estimate Stiffness by Using Analytical Stiffness Reduction Factor.....	223
6.7.6 Estimate Stiffness with Regression Method	225
6.7.7 Parametric Study with Nonlinear Buckling Analysis	228
6.7.8 Parametric Study with Unequal Legs	229
6.7.9 Summary of Parametric Studies for Single Angle K-Frames	231
Chapter 7. Cross Frame Fatigue Tests	233
7.1 Introduction.....	233
7.2 Cross Frame Fatigue Test Setup	235
7.2.1 Built-Up Test Girders	237
7.2.2 Deck Beams	238
7.2.3 Wall Beam Supports	238
7.2.4 Double Angle Stiffening Elements	238
7.2.5 Lateral Bracing.....	238
7.2.6 Stiffeners	239
7.2.7 Loading System	239
7.2.8 Fabrication Methods	239
7.3 Cross Frame Specimen Details	241
7.3.1 Cross Frame Fabrication and Specimen Designation	241
7.3.2 Cross Frame Welds	242
7.3.3 Testing Procedures.....	243
7.3.4 Testing Equipment.....	244
<i>Part I: X Frames—Equal Leg Angles</i>	<i>245</i>
7.4 X Frame—Equal Leg Angle Design.....	245
7.4.1 X Frame Test Variables	247
7.4.2 X Frame Tests of Current TxDOT Detail (XF_1,3,4)	248

7.4.3 X Frame Tests of TxDOT Detail with Tension Diagonal away from Gusset-Stiffener Weld (XF_2,5,8)	251
7.4.4 X Frame Tests of TxDOT Detail with Increased Spacing between Angle-gusset Weld and Gusset-Stiffener Weld (XF_6,7)	253
7.4.5 X Frame Conclusions.....	256
<i>Part II: X Frames—Unequal Leg Angles</i>	256
7.5 X Frame—Unequal Leg Angle Design	256
<i>Part III: K Frames—Equal Leg Angles</i>	259
7.6 K Frame—Equal Leg Angle Design.....	259
7.6.1 K Frame Test Variables	261
7.6.2 K Frame Tests of Current TxDOT Detail (KF_2,3,4)	261
7.6.3 K Frame Tests of TxDOT Detail Rotated 180 Degrees (KF_1,5).....	266
7.6.4 K Frame Tests with L4x4x3/4 Strut (KF_6,7).....	268
7.6.5 K Frame Conclusions.....	269
<i>Part IV: Z Frames—HSS Tubes</i>	271
7.7 Z Frame—HSS Tube Design.....	271
7.7.1 Z Frame HSS Test Variables	272
7.7.2 Z Frame Tests using HSS5x5x3/8 Members (ZF_HSS_1,2,3).....	273
7.7.3 Z Frame Tests using HSS6x3x5/16 Members (ZF_HSS_4).....	275
7.7.4 Z Frame HSS Conclusions.....	277
<i>Part V: Z Frames—Equal Leg Double Angles</i>	277
7.8 Z Frame—Equal Leg Double Angle Design	277
7.8.1 Z Frame Double Angle Test Variables	278
7.8.2 Z Frame Tests using 2L4x4x3/8 Members (ZF_DA_1,2,3)	278
7.8.3 Z Frame Double Angle Conclusions.....	281
7.9 Summary of Conclusions.....	281
Chapter 8. Finite Element Studies of Cross Frame Forces.....	283
8.1 Introduction.....	283
8.2 Comparison to Commercial Software.....	283
8.2.1 Case Study Details	283
8.2.2 Software for Steel Bridge Analysis.....	288
8.2.3 ANSYS Model	291
8.2.4 Initial Design Comparison	294
8.2.5 Final Design Comparison	296
8.2.6 Use of R Factor for Calculation of Force Range	298
8.2.7 Application of R to General Computer Software.....	300
8.2.8 Case Study Conclusions.....	300
Chapter 9. Conclusions and Recommendations.....	301
9.1 Introduction.....	301
9.2 Applicability of Cast Steel Connections.....	301

9.3 Cross Frame Member Strength, Stiffness, and Fatigue Tests.....	302
9.4 Full Scale Cross Frame Stiffness and Ultimate Strength Tests	304
9.5 Cross Frame Stiffness and Ultimate Strength Parametric Studies.....	306
9.6 Full Scale Cross Frame Fatigue Tests.....	308
9.7 Comparison of Cross Frame Fatigue Forces to Commercial Software	309
9.8 Recommendations to Improve Current TxDOT Cross Frame Details	309
References.....	311
Appendix A. Cross Frame Fatigue Test Details.....	317
Appendix B. TxDOT Bridge Details for FEA Comparison	377

List of Figures

Figure 1.1: Typical X-type Cross Frame with Steel Angles	1
Figure 1.2: Single Diagonal Tubular Cross Frame	2
Figure 2.1: Effect of Brace Stiffness for Column Buckling	7
Figure 2.2: Normalized Axial Load vs. Normalized Displacement for Braced Winter Column with Initial Out-of-straightness	8
Figure 2.3: P vs. F for Braced Winter Column with Initial Out-of-straightness	8
Figure 2.4: Stiffness of a Cross Frame.....	12
Figure 2.5: Stiffness Formulas for Twin Girder Cross Frames (Yura 1992).....	13
Figure 2.6 Brace Stiffness for Twin Girders Buckle in Opposite Directions	13
Figure 2.7: Equivalent Stiffness (AASHTO/NSBA Steel Bridge Collaboration 2011),	14
Figure 2.8: Whitmore Width.....	17
Figure 2.9: Stress Concentration due to Geometrical Discontinuities at the Cross Frame Connection	18
Figure 2.10: Undercut at Toe of Fillet Weld Connection (Schematic).....	19
Figure 2.11: Undercut at Toe of Fillet Weld Connection (Example)	20
Figure 2.12: Slag Inclusion in Fillet Weld (Schematic)	20
Figure 2.13: Slag Inclusion in Fillet Weld (Example).....	21
Figure 2.14: Porosity in Fillet Weld (Schematic)	21
Figure 2.15: Porosity in Cross Section of Fillet Weld (Example)	22
Figure 2.16: AASHTO Fatigue Design Truck [AASHTO 2012].....	23
Figure 2.17: AASHTO Fatigue Design Tandem	23
Figure 2.18: S-N Plot indicating AASHTO Fatigue Categories.....	26
Figure 2.19: Fatigue Testing Procedure.....	27
Figure 2.20: (a) Eccentric Connection of Angle and (b) Bending of Angle due to Eccentricity	28
Figure 2.21: Single Angle Fatigue Crack Failure Locations	30
Figure 2.22: Typical Cruciform Joint with Fatigue Crack.....	32
Figure 2.23: Comparison of Cruciform Joint to Uniformly Loaded Plate with Crack.....	33
Figure 2.24: Lack of Weld Root Fusion Inherent to T-stem and Cast Steel Connections.....	33
Figure 2.25: Knife Plate Connection with Stress Concentration Locations	34
Figure 2.26: Large Cast Steel Bearing in Tubular Arch Bridge [FHA 2001].....	36
Figure 2.27: Tubular Bracing Retrofit of Curved Steel Bridge in Wichita Falls, TX with Close-up of Connections [Turco 2009].....	37

Figure 2.28: (a) Green Bank Radio Telescope and (b) Steel Casting.....	39
Figure 2.29: Cast ConneX Cast Steel Connections [de Oliveira and Stine 2008].....	40
Figure 2.30: Cast Steel Connection used in Tower Crane Construction [Soderberg 2010]	40
Figure 3.1: Investment Casting Process [Ningbo Yinzhou KST 2010].....	45
Figure 3.2: Rapid Prototyping Machine.....	47
Figure 3.3: (a) Roller and (b) Laser	48
Figure 3.4: (a) Removal of Powder Block and (b) Cleaning of Prototype	48
Figure 3.5: Prototype of Cross Frame Connection	49
Figure 3.6: Wooden Pattern for Use in Sand Casting.....	50
Figure 3.7: Polyurethane Core Box	50
Figure 3.8: (a) Pouring Sand Slurry into Pattern Box and (b) Compacting Sand Mold.....	52
Figure 3.9: (a) Removing Pattern from Sand Mold and (b) Adding Vents along Parting Line	52
Figure 3.10: (a) Flow Coating the Sand Mold and (b) Burning the Sand Mold.....	53
Figure 3.11: (a) Cores used for Cross Frame Connection and (b) Large Sand Core.....	54
Figure 3.12: (a) Setting the Cores and (b) Closing the Sand Mold.....	54
Figure 3.13: (a) Electric Arc Furnace and (b) Small Induction Furnace	55
Figure 3.14: (a) Sample Taken from Furnace and (b) Cooled Sample for Chemical Analysis.....	56
Figure 3.15: Example of Steel Casting with Incomplete Run-Out.....	57
Figure 3.16: (a) Ladle and (b) Pouring Steel into Ladle.....	57
Figure 3.17: Gating System	58
Figure 3.18: Approximate Position of Riser for Cast Connection.....	59
Figure 3.19: Pouring the Steel into the Sand Molds	59
Figure 3.20: Casting Steel Material Test Blocks	60
Figure 3.21: Cross Frame Connections Following Shot-Blast	61
Figure 3.22: (a) Spectrometer with (b) Sample for Analysis.....	63
Figure 3.23: Sample Data from Chemical Analysis	64
Figure 3.24: Graville Diagram for First Round of Cast Steel Connections [Kaufmann, Viscomi, Lu 1995]	65
Figure 4.1: 220 kip MTS Testing Machine with Specimen.....	70
Figure 4.2: Test Setup (a) Front View and (b) Side View	71
Figure 4.3: Displacement Dial Gage with (a) 0.001" Accuracy and (b) 0.0001" Accuracy	72

Figure 4.4: Test Setup Front View with Dial Gages.....	72
Figure 4.5: Close Up View of Dial Gages and Angle Clamps	73
Figure 4.6: Close-Up View of Strain Gage.....	73
Figure 4.7: Basic Fatigue Setup	74
Figure 4.8: Cast Steel Connection Design Process.....	75
Figure 4.9: Prototype Cross Frame Connection.....	76
Figure 4.10: Prototype Cross Frame Connection (Side View)	76
Figure 4.11: Cast Steel Cross Frame Connection	77
Figure 4.12: Cast Steel Cross Frame Connection (Side View).....	77
Figure 4.13: Two Dimensional Drawing of Cast Steel Connection	78
Figure 4.14: Three Dimensional Drawing of Cast Steel Connection	79
Figure 4.15: Load and Boundary Conditions for Steel Casting Analysis.....	80
Figure 4.16: Elastic Analysis on Steel Casting Connected to Gusset Plate.....	80
Figure 4.17: Inelastic Analysis on Steel Casting Connected to Gusset Plate	81
Figure 4.18: Cast Steel Connection Stiffness Tests with Dial Gages	82
Figure 4.19: Cast Steel Connection Stiffness	83
Figure 4.20: Cast Steel Connection Test in 550 kip MTS Testing Machine	84
Figure 4.21: Cast Steel Connection Ultimate Strength Test Results	85
Figure 4.22: Cast Steel Connection Fatigue Results.....	86
Figure 4.23: Eccentric Nature of Fillet Weld.....	86
Figure 4.24: Cast Steel Connection Fatigue Crack.....	87
Figure 4.25: T-Stem Connection Detail Concept	88
Figure 4.26: Square HSS Specimen with T-Stem Connection Detail	90
Figure 4.27: Typical Boundary Conditions Used for Preliminary T-Stem Analysis.....	91
Figure 4.28: Axial Stress in HSS Tube Wall (a) Perpendicular to Stem and (b) Parallel to Stem	91
Figure 4.29: Round HSS Specimen with T-Stem Connection Detail.....	92
Figure 4.30: Axial Stress in Round HSS Tube Wall	93
Figure 4.31: Diamond HSS Specimen with T-Stem Connection Detail.....	94
Figure 4.32: Axial Stress in Diamond HSS Tube Wall	94
Figure 4.33: Strain Gages Applied to Tube Wall	95
Figure 4.34: T-Stem Connection Stiffness Data	96
Figure 4.35: Ultimate Strength Test of Square HSS 5 x 5 x 3/8 and WT 9 x 35.5.....	97

Figure 4.36: Fracture in Fillet Weld Connection	97
Figure 4.37: HSS 5 x 5 x 3/16 and WT 12 x 31 Stiffness Data	98
Figure 4.38: Fractured Connection	98
Figure 4.39: T-stem Connection Weld Eccentricity (with Weld Penetration Enhanced).....	99
Figure 4.40: Complete Joint Penetration Groove Weld Detail	100
Figure 4.41: Fatigue Test Results	101
Figure 4.42: Example of Fatigue Crack Forming at Fillet Weld Root in Square HSS Connection	101
Figure 4.43: Example of Fatigue Crack Forming at CJP Weld Toe in Square HSS Connection	102
Figure 4.44: Example of Fatigue Crack Forming at Fillet Weld Root in Round HSS Connection	102
Figure 4.45: Example of Fatigue Crack Forming at Fillet Weld Root in Diamond HSS Connection	102
Figure 4.46: Knife-Plate Connection	103
Figure 4.47: Knife-Plate Connection with Drilled Stress Relief Hole.....	104
Figure 4.48: Fabrication of Knife-Plate Connection Using (a) Band Saw and (b) Plasma Torch.....	104
Figure 4.49: Knife-Plate Connection Stiffness Test Results	105
Figure 4.50: Fatigue Tests of Knife-Plate Connections.....	106
Figure 4.51: Knife-Plate Connection Fatigue Crack (Stress Relief Hole).....	106
Figure 4.52: Knife-Plate Connection Fatigue Crack (Torch-Cut Slots)	107
Figure 4.53: Double Angle Detail.....	108
Figure 4.54: Double Angle Connection Stiffness Test Results	109
Figure 4.55: Double Angle Connection Ultimate Strength Test Results.....	110
Figure 4.56: Double Angle Fatigue Test Results.....	111
Figure 4.57: Double Angle Connection Fatigue Crack (Angle Member)	111
Figure 4.58: Double Angle Connection Fatigue Crack (Gusset Plate).....	112
Figure 4.59: Single Angle Connection.....	112
Figure 4.60: Single Angle Connection Stiffness Test Results.....	113
Figure 4.61: Single Angle Connection Eccentricity	114
Figure 4.62: Single Angle Connection Ultimate Strength Test Results	114
Figure 4.63: Deformed Single Angle Connection	115
Figure 4.64: (a) Tension-Only System and (b) Compression System	116

Figure 4.65: Test Specimens- (a) T-Stem and Square HSS, (b) T-Stem and Diamond HSS, (c) T-Stem and Round HSS, (d) Cast Connection, (e) Knife-Plate Connection, (f) Double Angle Connection, and (g) Single Angle Connection	119
Figure 4.66: Summary of Stiffness Test Results- Knife-Plate, Double Angle, and Single Angle.....	120
Figure 4.67: Relative Performance of Different Connections	121
Figure 4.68: Fatigue Performance of Various Details	126
Figure 5.1: Overall View of Cross Frame Test.....	130
Figure 5.2: Cross Frame Test Plan Drawing.....	130
Figure 5.3: Details of Test Setup	131
Figure 5.4: Load Cell for Actuator	132
Figure 5.5: Strain Gage on Reaction Strut.....	132
Figure 5.6: Calibration of Force Measurement.....	132
Figure 5.7: Free-body of Test Setup	133
Figure 5.8: Equilibrium of a Load Beam	134
Figure 5.9: Cross Frame Rotation in Test Setup.....	135
Figure 5.10: Displacement Measurements.....	136
Figure 5.11: Linear Potentiometers Locations.....	136
Figure 5.12: Force Measurement of Cross Frame Member	137
Figure 5.13: Single Angle X-frame Drawing	140
Figure 5.14: Single Angle X-frame Specimen.....	140
Figure 5.15: Locations of Strain Gages – Single Angle X-frame.....	141
Figure 5.16: Load and Deflection Relationship of Single Angle X-frame	141
Figure 5.17: Axial Forces in Single Angle Members – Single Angle X-frame.....	142
Figure 5.18: Step one - Buckling of the compression diagonal.....	143
Figure 5.19: Step two - Buckling of the top strut	143
Figure 5.20: F_{equiv} . vs. Rotation θ	144
Figure 5.21: Axial Member Force vs. Rotation θ	144
Figure 5.22: Mid-section Out-of-plane Deflection	145
Figure 5.23: Single Angle K-frame Drawing	146
Figure 5.24: Single Angle K-frame Specimen.....	146
Figure 5.25: Locations of Strain Gages – Single Angle K-frame.....	147
Figure 5.26: Load and Deflection Relationship of Single Angle K-frame	147

Figure 5.27: Axial Forces in Single Angle Members – Single Angle K-frame.....	148
Figure 5.28: Buckling of the Single Angle K-frame.....	149
Figure 5.29: Axial Member Force vs. Rotation θ – K-frame.....	149
Figure 5.30: $F_{equiv.}$ vs. Rotation θ	150
Figure 5.31 Out-of-plane Deflection.....	150
Figure 5.32: Slotted Tube Connection Fabrication.....	151
Figure 5.33: Square Tube Z-frame Drawing.....	152
Figure 5.34: Square Tube Z-frame Specimen.....	152
Figure 5.35: Load and Deflection Relationship of Square Tube Z-frame	153
Figure 5.36: Failure of Square Tube Z-frame	153
Figure 5.37: $F_{equiv.}$ vs. Rotation θ	154
Figure 5.38: Axial Member Force vs. Rotation θ	154
Figure 5.39: Double Angle Z-frame Drawing	155
Figure 5.40: Double Angle Z-frame Specimen.....	156
Figure 5.41: Load and Deflection Relationship of Double Angle Z-frame	156
Figure 5.42: Failure of Double Angle Z-frame.....	157
Figure 5.43: $F_{equiv.}$ vs. Rotation θ	158
Figure 5.44: Axial Member Force vs. Rotation θ	158
Figure 5.45: Double Angle Z-frame with Single Angle Struts Drawing (Repeated)	159
Figure 5.46: Double Angle Z-frame 2 Specimen.....	159
Figure 5.47: Load and Deflection Relationship of Double Angle Z-frame 2.....	160
Figure 5.48: Failure of Double Angle Z-frame.....	161
Figure 5.49: Single Angle Z-frame Drawing.....	161
Figure 5.50: Single Angle Z-frame Specimen	162
Figure 5.51: Load and Deflection Relationship of Single Angle Z-frame	163
Figure 5.52: Failure at Top Strut.....	164
Figure 5.53: Failure at Diagonal	164
Figure 5.54: $F_{equiv.}$ vs. Rotation θ – Failure at Top Strut.....	165
Figure 5.55: Axial Member Force vs. Rotation θ – Failure in Top Strut	165
Figure 5.56: $F_{equiv.}$ vs. Rotation θ – Failure at Diagonal	166
Figure 5.57: Axial Member Force vs. Rotation θ – Failure at Diagonal	166
Figure 5.58: Single Angle Unequal Leg X-frame Specimen.....	167
Figure 5.59: Load and Deflection Relationship of Single Angle Unequal Leg X-frame	168

Figure 5.60: Failure of Single Angle Unequal Leg X-frame	168
Figure 6.1: Single Angle with Eccentric Connection in Tension	174
Figure 6.2: Free Body Diagram for Angle.....	175
Figure 6.3: Free Body Diagram for a Gusset plate	175
Figure 6.4: Deformation of angle and gusset plate	176
Figure 6.5: Deflection Due to Eccentric Loading	178
Figure 6.6: FEA Analysis of Single Angle Specimen	180
Figure 6.7: Shape Factors for Equal Leg Angles.....	181
Figure 6.8: Rmember vs. kP	182
Figure 6.9: Rmember vs. L	182
Figure 6.10: Rmember vs. L	183
Figure 6.11: Out-of-plane Deflection for X-Frame	185
Figure 6.12: Typical TxDOT Cross Frame (Texas Department of Transportation, 2006).....	186
Figure 6.13: Revised Geometry of the Compression-Tension Model	187
Figure 6.14: Out-of-plane Deflection for K-Frame	190
Figure 6.15: Revised Geometry for Tension-only Model.....	192
Figure 6.16: Analytical Stiffness Reduction Factor of Single Angle X-Frame	197
Figure 6.17: Analytical Stiffness Reduction Factor of Single Angle K-Frame	198
Figure 6.18: $\beta_{comp-ten}$ VS $\beta_{FEA-SX-no-bending}$	201
Figure 6.19: $\beta_{comp-ten}$ VS β_{FEA-SX}	202
Figure 6.20: Errors of $\beta_{comp-ten}$	203
Figure 6.21: $\beta_{ana-SX'}$ VS β_{FEA-SX}	204
Figure 6.22: Errors of $\beta_{ana-SX'}$	204
Figure 6.23: Errors of $\beta_{ana-SX'}$ VS. Thickness of Angle (t).....	205
Figure 6.24: $0.85\beta_{ana-SX'}$ VS β_{FEA-SX}	206
Figure 6.25: $0.5\beta_{comp-ten}$ VS β_{FEA-SX}	207
Figure 6.26: Errors of $0.5\beta_{comp-ten}$	207
Figure 6.27: $\beta_{tension}$ VS β_{FEA-SX}	208
Figure 6.28: Errors of $\beta_{tension}$	209
Figure 6.29: RFEA-SX VS \bar{y}	210
Figure 6.30: RFEA-SX VS S/hb.....	211
Figure 6.31: RFEA-SX' VS S/hb.....	212
Figure 6.32: β_{reg-SX} VS β_{FEA-SX}	213

Figure 6.33: Errors of β_{reg-SX}	213
Figure 6.34: Example of Load-Deflection Curve	214
Figure 6.35: Statistics on P	216
Figure 6.36: RFEA-SX VS \bar{y} for Cross Frame with Unequal Legs Angles	217
Figure 6.37: β_{reg-SX} VS β_{FEA-SX} for Cross Frame with Unequal Legs Angles	218
Figure 6.38: Rest-SX-adj VS RFEA-SX for Cross Frame with Unequal Legs Angles.....	218
Figure 6.39: β_K VS $\beta_{FEA-SK-no-bending}$	221
Figure 6.40: β_K VS β_{FEA-SK}	222
Figure 6.41: Errors of β_K	222
Figure 6.42: β_{ana-SK} VS β_{FEA-SK}	223
Figure 6.43: Errors of β_{ana-SK}	224
Figure 6.44: $0.5\beta_K$ VS β_{FEA-SX}	224
Figure 6.45: Errors of $0.5\beta_K$	225
Figure 6.46: RFEA-SK VS \bar{y}	226
Figure 6.47: RFEA-SK VS S/hb.....	227
Figure 6.48: β_{reg-SK} VS β_{FEA-SK}	228
Figure 6.49: Statistics on N.....	229
Figure 6.50: RFEA-SK VS \bar{y} for Cross Frame with Unequal Legs Angles	230
Figure 6.51: β_{reg-SK} VS β_{FEA-SK} for Cross Frame with Unequal Legs Angles	231
Figure 7.1: Eccentric Single Angle Connection	233
Figure 7.2: Single Angle Strength Test Bending	234
Figure 7.3: CAD Drawing of Cross Frame Fatigue Setup.....	235
Figure 7.4: Completed Cross Frame Fatigue Test Setup	235
Figure 7.5: Front View of Cross Frame Fatigue Setup.....	236
Figure 7.6: Front View of Cross Frame Fatigue Setup (Details).....	236
Figure 7.7: Side View of Cross Frame Fatigue Setup	237
Figure 7.8: Side View of Cross Frame Fatigue Setup (Details)	237
Figure 7.9: (a) Hydraulic Actuator, (b) Load Cell, and (c) Spherical Head	239
Figure 7.10: Drilling Holes for Wall Beams.....	240
Figure 7.11: Flame Cutting Web	240
Figure 7.12: Completed Wall Support.....	241
Figure 7.13: Surface Condition (a) After Flame Cut and (b) After Subsequent Grinding	241
Figure 7.14: Cross Frame Layout during Fabrication.....	242

Figure 7.15: Test Setup and Load Application	243
Figure 7.16: Schematic of Force Controlled System	245
Figure 7.17: Typical TxDOT X Frame Detail [TxDOT 2010]	246
Figure 7.18: Typical X Frame Specimen in Test Setup	246
Figure 7.19: Typical X Frame Internal Forces from Load Applied	247
Figure 7.20: X Frame with Tension Diagonal on Stiffener Side of Cross Frame (i.e. XF_1,3,4)	248
Figure 7.21: X Frame with Tension Diagonal away from Stiffener Side of Cross Frame (i.e. XF_2,5,8)	248
Figure 7.22: Overlap of Angle-Gusset Weld and Gusset-Stiffener Weld (XF_1)	249
Figure 7.23: Overlap of Angle-Gusset Weld and Gusset-Stiffener Weld (XF_4)	249
Figure 7.24: Typical TxDOT Spacing between End of Angle and Edge of Stiffener [TxDOT 2010]	250
Figure 7.25: Cross Frame Fatigue Results of Specimens XF_1,3,4 with Weld Intersection	250
Figure 7.26: Fatigue Crack at Forward Edge of Fillet Weld into Angle Member (XF_2)	251
Figure 7.27: Additional Transverse Fillet Weld on Reverse Side of Angle-Gusset Connection (XF_2)	252
Figure 7.28: Cross Frame Fatigue Results of Specimens XF_2,5,8 with Tension Diagonal away from Gusset-Stiffener Weld; XF_5,8 has No Additional Transverse Weld	253
Figure 7.29: Hot Spot Stress in Gusset Plate due to Angle-Gusset Connection	254
Figure 7.30: Cross Frame Fatigue Results of Specimens XF_6,7 with Increased Weld Spacing (Relative to Typical TxDOT Details in XF_1,3,4)	255
Figure 7.31: Typical Failure Crack in X Frame with Increased Weld Spacing (XF_6)	255
Figure 7.32: Cross Frame Fatigue Results of X Frames with Equal Leg Angles	256
Figure 7.33: Typical Unequal Leg X Frame Specimen with Internal Forces due to Load	257
Figure 7.34: Typical Unequal Leg X Frame in Test Setup	257
Figure 7.35: Typical Unequal Leg X Frame Fatigue Crack (XF_UL_1,2)	258
Figure 7.36: Typical Unequal Leg X Frame Fatigue Crack (XF_UL_3)	258
Figure 7.37: Cross Frame Fatigue Results of Unequal Leg Angles	259
Figure 7.38: TxDOT Standard K Frame Detail [2010]	260
Figure 7.39: Typical K Frame Specimen in Test Setup	260
Figure 7.40: Typical K Frame Internal Forces from Load Applied	261
Figure 7.41: K Frame Orientation in Test Setup as given by TxDOT Detail (KF_2,3,4)	262
Figure 7.42: K Frame with Fatigue Crack in Strut (KF_2)	263

Figure 7.43: K Frame Fatigue Crack Repair in Strut (KF_2).....	263
Figure 7.44: K Frame Fatigue Crack in Tension Diagonal (KF_2).....	264
Figure 7.45: Cross Frame Fatigue Results of Specimens KF_2,3,4.....	264
Figure 7.46: Absence of Additional Transverse Weld on Reverse Side of Angle.....	265
Figure 7.47: TxDOT Standard K Frame Detail with Strut Orientation Indicated [2010].....	265
Figure 7.48: Cross Frame Orientation of KF_1,5.....	266
Figure 7.49: Cross Frame Fatigue Results of Specimens KF_1,5.....	267
Figure 7.50: Crack in Tension Strut (KF_1).....	267
Figure 7.51: K Frame Specimen Details (KF_6,7).....	268
Figure 7.52: Cross Frame Fatigue Results of K Frame Specimens.....	269
Figure 7.53: Fatigue Crack in Tension Diagonal (KF_7).....	269
Figure 7.54: Suggested Improvements to TxDOT Standard K Frame Detail.....	270
Figure 7.55: X Frame to K Frame Comparison for Different Geometries and Cross Sections.....	271
Figure 7.56: Z Frame HSS Specimen in Fatigue Test Setup.....	272
Figure 7.57: Z Frame HSS Internal Forces due to Fatigue Test Loading.....	272
Figure 7.58: Typical Z Frame HSS Fatigue Crack (ZF_HSS_2).....	273
Figure 7.59: Typical Z Frame HSS Fatigue Crack (ZF_HSS_3).....	273
Figure 7.60: Cross Frame Fatigue Results of Specimens ZF_HSS_1,2,3.....	274
Figure 7.61: Large Bending Stress Causes Loss of Fatigue Life in Z Frames.....	275
Figure 7.62: Rectangular HSS Z Frame in Test Setup.....	275
Figure 7.63: Example of Fatigue Crack (ZF_HSS_4).....	276
Figure 7.64: Cross Frame Fatigue Results of Z Frame HSS Specimens.....	276
Figure 7.65: Z Frame Double Angle Specimen in Fatigue Test Setup.....	277
Figure 7.66: Z Frame Double Angle Internal Forces due to Fatigue Test Loading.....	278
Figure 7.67: Cross Frame Fatigue Results of Z Frame DA Specimens.....	279
Figure 7.68: Typical Z Frame Double Angle Fatigue Crack (ZF_DA_1).....	279
Figure 7.69: Typical Z Frame Double Angle Fatigue Crack (ZF_DA_2).....	280
Figure 7.70: Typical Z Frame Double Angle Fatigue Failure Mode (ZF_DA_3).....	280
Figure 8.1: Boundary and Loading Conditions for Cross Frame Rotation Calculation in Typical Grillage Model.....	289
Figure 8.2: Displaced Shape Cross Frame Stiffness Calculation in Typical Grillage Model.....	289

Figure 8.3: Displaced Shape of Equivalent Beam in Grillage Model.....	290
Figure 8.4: Top View of ANSYS Model.....	292
Figure 8.5: Isometric View of ANSYS Model	292
Figure 8.6: Application of Design Lane Live Load in ANSYS.....	293
Figure 8.7: Application of Design Truck Loads in ANSYS.....	294
Figure 8.8: Location of Maximum/Minimum Forces in ANSYS and Grillage Model (Initial Design).....	295
Figure 8.9: Location of Maximum/Minimum Forces in ANSYS and Grillage Model (Final Design)	297
Figure 9.1: Z Frame Cross Frame Layout.....	301
Figure 9.2: Cast Steel Connection	302
Figure 9.3: Test Specimens- (a) T-Stem and Square HSS, (b) T-Stem and Diamond HSS,(c) T-Stem and Round HSS, (d) Cast Connection, (e) Knife-Plate Connection, (f) Double Angle Connection, and (g) Single Angle Connection	303
Figure 9.4: Eccentricity of Load Relative to Angle Center of Gravity.....	304
Figure 9.5: TxDOT Standard X Frame Detail [2010].....	305
Figure 9.6: TxDOT Standard K Frame Detail [2010].....	305
Figure 9.7: Suggested Improvements to TxDOT Standard X Frame Detail.....	309
Figure 9.8: Increased Spacing between End of Angle and Edge of Stiffener.....	310
Figure 9.9: Suggested Improvements to TxDOT Standard K Frame Detail.....	310

List of Tables

Table 2.1 Equivalent Stiffness Example.....	15
Table 2.2: Detail Category Constant, A [AASHTO Table 6.6.1.2.5-1 2012]	25
Table 2.3: Constant-Amplitude Fatigue Thresholds [AASHTO Table 6.6.1.2.5-3 2012].....	25
Table 2.4: Standard Angle Sizes and Properties.....	42
Table 2.5: Angle Tensile Strength vs. Tube Buckling Strength	43
Table 3.1: Comparison of Cast Steel Composition with ASTM A588 Specification	64
Table 3.2: Comparison of Cast Steel Mechanical Properties with ASTM A588 Specification	66
Table 4.1: Angle Tensile Strength vs. Tube Buckling Strength	78
Table 4.2: Proposed Experimental Test Program for the T-Stem Connection	89
Table 4.3: Test Specimen Geometry.....	119
Table 4.4: Calculation of Connection Stiffness based upon Laboratory Tests.....	122
Table 4.5: Calculation of Cross Frame Stiffness Including the Effect of Member Connections.....	124
Table 4.6: Fatigue Test Summary of Various Details.....	127
Table 5.1 Key Parameters in Test Setup.....	134
Table 5.2 Cross Frame Test Program	138
Table 5.3 Average Results from the Tension Coupon Tests	169
Table 5.4 Cross Frame Test Results Summary	170
Table 6.1 Summary of Brace Stiffness by Analytical Solution.....	196
Table 6.2 Summary of Variables in the Parametric Study.....	196
Table 6.3 Summary of Variables in the Parametric Study.....	200
Table 6.4. Summary of Variables in the Parametric Study.....	216
Table 6.5 Summary of Cross Section Parameters of Unequal Legs Angle Members	219
Table 6.6 Summary of Variables in the Parametric Study.....	222
Table 6.7 Summary of Variables in the Parametric Study.....	230
Table 6.8 Summary of Cross Section Parameters of Unequal Legs Angle Members	232
Table 7.1: Cross Frame Types and Specimen Designation	242
Table 8.1: Initial Design Bridge Details	285
Table 8.2: Final Design Bridge Details.....	287
Table 8.3: Calculation of Beam Equivalent Moment of Inertia.....	291

Table 8.4: Results for Cross Frame Member Forces in Center Bay of Initial Design	296
Table 8.5: Results for Cross Frame Member Forces in Center Bays of Final Design.....	298
Table 8.6: Results for Cross Frame Member Forces in Center Bay of Initial Design Including the R Factor	299
Table 8.7: Ratio of Cross Frame Member Forces in Center Bay of Initial Design Including the R Factor to the Original Calculation.....	299

Chapter 1. Introduction

1.1 Problem Statement

Cross frames are critical bracing elements for the stability of straight and curved steel bridges. The cross frames provide lateral stability to the bridge system and increase the capacity and stiffness of the girder system. Effective stability bracing must satisfy both strength and stiffness requirements [Winter 1958]. Steel bridge cross frames are usually designed as torsional braces, which increase the overall strength and stiffness of the individual girders by creating a girder system that translates and rotates as a unit along the bracing lines.

Conventional cross frames are often fabricated using steel angles, consisting of two diagonal members and two horizontal struts to create an X-type brace, as shown in Figure 1.1. As discussed later in the report, other cross frame configurations such as K-type cross frames are also often used.

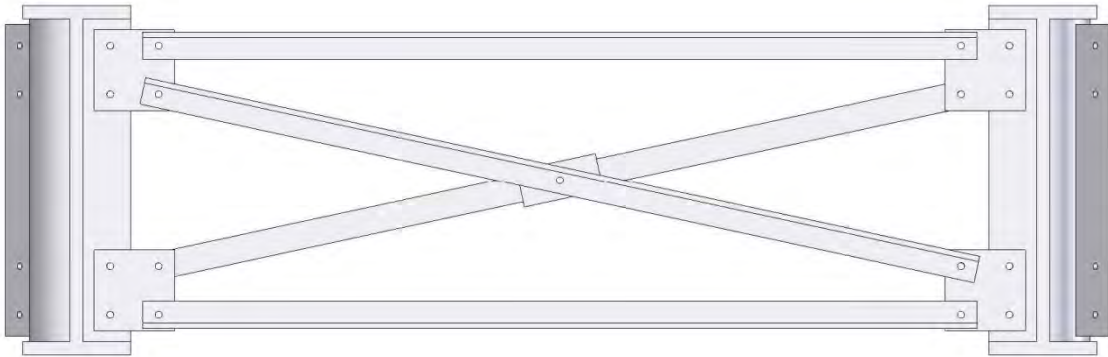


Figure 1.1: Typical X-type Cross Frame with Steel Angles

Although the X-type cross frame is very widely used in Texas bridges, there are a number of potential concerns with these cross frames. Due to the relatively poor buckling resistance of angle members, X-type cross frames are often designed as a “tension-only-diagonal” system. In a tension-only-diagonal system, the compression diagonal is conservatively neglected in strength and stiffness calculations. However, neglecting the contribution of the compression diagonal to cross frame stiffness and strength can lead to heavier diagonals and potentially higher cost for the cross frame. In addition, the angles are connected to the end plates along only one leg of the member, resulting in an eccentric connection. Results from laboratory tests and three-dimensional finite element studies on this project demonstrated that the eccentricity causes out-of-plane bending of the members and decreases its stiffness and fatigue performance. Further, because of the many members and connections that make up an X-type cross frame, the cost of fabrication can be substantial.

The fabrication difficulties as well as connection eccentricities create uncertainties in the behavior of cross frames that require deeper study including the following:

- the impact of the connection eccentricity for angle members on the strength and stiffness of the cross frames;

- the potential for improvements in cross frame behavior with the use of additional shapes besides angles;
- a measure of the fatigue performance of the different cross frames both at the member and system behavior.

Improved structural behavior may result by using concentric members to construct the cross frame. HSS tubular members and double angle members have significant buckling strength, allowing the diagonal to be utilized in both tension and compression. Further, these members allow for concentric connections, thereby reducing potential problems with eccentric connections. Thus, a single diagonal cross frame with concentric members can provide an effective brace for the steel bridge girders.

Additionally, the use of four steel angles in the X configuration shown in Figure 1.1 necessitates multiple rotations of the cross frame during fabrication to accommodate weld placement. By reducing the number of cross frame members, handling requirements in the fabrication shop should be reduced. Figure 1.2 shows an example of a single diagonal tubular cross frame.

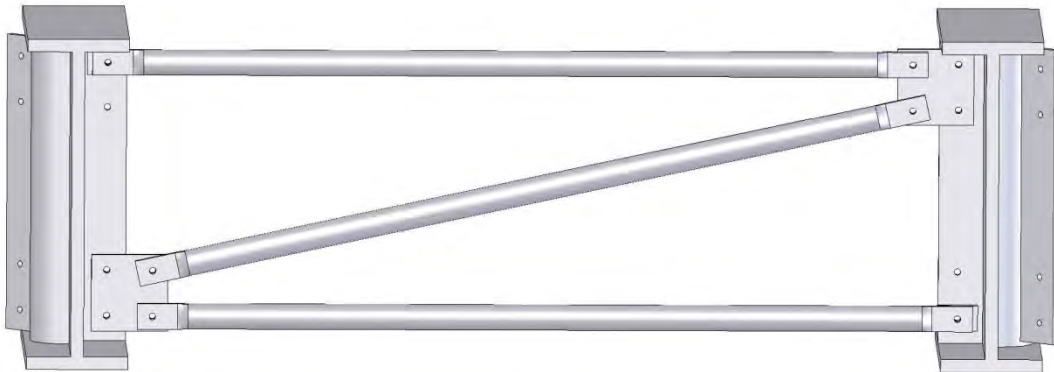


Figure 1.2: Single Diagonal Tubular Cross Frame

Although there are several structural advantages of utilizing tubular members, one drawback is designing a simple means of connecting the circular cross section to a flat plate. Frequently, tubes are slotted to allow the reception of the connection plate, and then welded. This slotted-tube detail however, has been reported to have relatively poor fatigue behavior [Liu et al. 2006] and is difficult to fabricate. Moreover, the detail leaves the tube open to the atmosphere, attracting dirt, debris, water, birds, and insects that may compromise the corrosion resistance of the member.

A potential connection for tubular members in cross frames that was proposed at the outset of TxDOT Research Project 0-6564 was a steel casting that provided streamlined behavior from a stress perspective, but also would seal off the end of the tube. The steel casting can be engineered to account for the complex geometry of the connection, and once produced, would be relatively easy to use in cross frame fabrication.

Additionally, the slotted tube detail was investigated to provide information on tubular members of the dimensions necessary to accommodate the required brace forces. The potential use of the double angle detail was also examined. As noted earlier, in addition to the questions

regarding the use of tubular members, there are a number of uncertainties in the stiffness and strength behavior of traditional cross frames comprised of simple angle members.

1.2 Objectives of TxDOT Project 0-6564

The objectives TxDOT Project 0-6564 are to investigate the behavior of cross frames from both a stiffness and strength perspective. The strength of the cross frames include both the static strength and the fatigue strength. The prevailing design methodology for cross frame design was assessed to understand the current performance of both the X-type and K-type cross frame configurations.

Furthermore, the use of tubular members in steel bridge cross frames were explored to verify the structural adequacy of utilizing a single diagonal cross frame configuration and to quantify the fatigue performance of the connection. The behavior of cross frames comprised of angles was also a major focus of the study. The research included experimental tests on individual components of the cross frame as well as full scale cross frames. Parametrical finite element analyses were carried out on the cross frames as well as straight and horizontally curved steel girder systems. The research was carried out at Ferguson Structural Engineering Laboratory at the University of Texas at Austin.

Project 0-6564 included the following major tasks:

- Review the existing available technical literature concerning previous studies on full cross frame systems, as well as the use of steel castings in structural applications.
- Meet with steel casting manufacturers and steel fabricators to understand the requirements, procedures, and limiting factors for using tubular members in cross frame design.
- Survey existing TxDOT bridge designs to understand the impact of using single diagonal cross frames and to determine typical ranges of cross frame dimensions.
- Alter existing validated finite element analysis (FEA) models for steel girder systems to be applicable to cross frames using a single diagonal member. Conduct parametric analyses to determine the design requirements for the cross frame system.
- Develop FEA models of tubular members and the connection region for use in developing optimized prototype connections for laboratory testing.
- Develop FEA models of a cast connection to analyze its strength and work with steel foundry engineers to optimize the design for production.
- Conduct buckling tests on two or three girder systems with bracing at midspan to validate the behavior of single diagonal cross frame systems.
- Conduct axial tension and compression tests on tubular members to validate connection behavior.
- Conduct fatigue tests on the proposed cross frame members to develop a fatigue rating for the connection and the member.

- Conduct load tests to failure on full cross frames to fully understand the failure mechanism and capacity for design applications.
- Conduct fatigue tests on full scale cross frame systems.
- Conduct a case study to compare cross frame design software used at TxDOT with three dimensional FEA models.
- Make design recommendations based upon laboratory and computational results and provide recommended connection details.
- Develop design methodologies for specifying single diagonal cross frames in straight and curved steel bridges.

1.3 Report Outline

This report serves as the final report for TxDOT Project 0-6564 and marks the completion of the project.

The report consists of nine chapters. Chapter 2 provides background information on the stability of steel bridges, as well as the previous use of tubular members in bracing applications and the use of steel castings in structures. A summary of TxDOT bridge practice and current details is also included in Chapter 2 and information on the fatigue design of cross frames is given.

An introduction to steel castings is provided in Chapter 3, including important terminology and a detailed discussion of the process required to create steel castings. Attention is also given to potential defects in the cast steel material and the variety of measures that can be conducted to detect these flaws.

A summary of the connection design process is provided in Chapter 4. This chapter contains the proposed connections under investigation, including laboratory test results involving a number of different members and corresponding connections. For tubular members, three connections were evaluated: 1) cast steel connections, 2) T-stem connections, and 3) knife-plate connection. In addition to tubular members, double angle members and single angle members and the resulting gusset plate connections were also studied. In addition to experiments, finite element analyses on the different members and connections were also carried out, which is discussed in Chapter 4.

Results from the large-scale cross frame stiffness and ultimate strength tests are highlighted in Chapter 5. Information on the test setup for the stiffness tests is provided, followed by the results for several cross frame layouts both currently in use and proposed.

The associated computational models for the cross frame stiffness and preliminary recommendations are described in Chapter 6.

The test setup and results involving the full scale fatigue testing of cross frames are outlined in Chapter 7. Recommendations based on test results and observations are made.

Additional computational modeling efforts are detailed in Chapter 8. A discussion of the FEA models is provided as well as a summary of the parametric studies for the project.

Chapter 9 provides a summary of the study, including key conclusions and recommendations.

Chapter 2. Background

2.1 Introduction

Steel plate-girders are commonly used in highway bridge construction. The ability to fabricate, transport, and splice the girders are attractive for applications with spans larger than approximately 150 feet. The 150 feet span limit is based upon shipping limitations that often preclude the use of precast concrete beams. Steel members can be shipped in smaller lengths and spliced together in the field to create longer spans than possible with precast concrete bridges. Plate-girder bridges are usually composed of multiple I-beams with a composite concrete slab and other bracing components. In straight bridges, the girders primarily support vertical loads that cause bending in the members. In horizontally curved bridges, the geometry also results in significant torsion.

I-shaped sections are efficient sections for cases where bending is primarily in one plane. The use of two flanges connected by the web makes efficient use of the material by maximizing the major axis moment inertia I_x , which gives a large flexural stiffness. However, due to the relatively low lateral stiffness (I_y) the I-shape sections are susceptible to lateral torsional buckling unless adequate bracing is provided. In the finished bridge, a composite concrete slab provides continuous lateral and torsional restraint to the girders and lateral torsional buckling is generally not a major problem. However, the wet concrete does not provide any restraint to the girder during construction. Therefore, the critical stage for lateral torsional buckling typically occurs during construction and adequate stability bracing must be provided.

While cross frames are important structural members for providing girder stability and improving the torsional stiffness of the bridge, the braces in the completed bridge are susceptible to fatigue crack formation from repeated stress cycles from traffic loads such as heavy truck traffic. The cross frame forces leading to fatigue issues primarily result from differential deflection of adjacent girder lines. Therefore, the fatigue design of these braces also plays a key role in the overall design of the bracing system.

This chapter outlines the background information for both stability and fatigue design aspects of cross frames for I-girder bridges. Following those sections is relevant information regarding the current use of the single angle member in cross frame design and then for some of the proposed design solutions. The background information provides a basis for the following chapters that include laboratory test results, parametric finite element studies, and design recommendations.

2.2 Stability of Bridges

Stability is often a crucial design consideration for steel girder bridges. To prevent lateral torsional buckling of the beams, cross frames are used to help restrain girder twist. The critical stage for cross frames is often during construction, when the full weight of the wet concrete slab acts on the non-composite steel girder section. The cutting, fitting, and welding required to construct cross frames is a very labor-intensive process. Consequently, cross frames are generally the most expensive component per unit weight of a steel bridge.

2.2.1 Lateral Torsional Buckling

Timoshenko (Timoshenko and Gere 1961) derived the buckling solution for doubly-symmetric sections subjected to uniform moment. The solution was based upon the assumption that the sections were restrained from twist at the ends; however the end sections are free to warp as outlined below. The expression for the critical lateral torsional buckling moment for a beam subjected to uniform moment is given in the following equation:

$$M_{cr} = \frac{\pi}{L_b} \sqrt{EI_y GJ + \frac{\pi^2 E^2 C_w I_y}{L_b^2}} \quad (2.1)$$

where:

M_{cr} = buckling moment

L_b = unbraced length

I_y = weak-axis moment of inertia

E = elastic modulus

G = shear modulus of elasticity

J = torsional constant

C_w = torsional warping constant

The torsional stiffness of a member can generally be divided into two components: the uniform torsional stiffness and the non-uniform torsional stiffness. The first term under the radical in Equation 2.1 is often referred to as the St. Venant term, and is related to the uniform torsional stiffness. The second term under the radical is related to the non-uniform torsional stiffness and is often referred to as the warping term. The warping term is the torsional stiffness that is related to lateral bending of the flanges that occurs during twisting of the girder. The warping stiffness is significantly affected by the unbraced length of the flanges as well as the support conditions. Equation ((2.1) was derived with the assumption that the ends of the unbraced length are free to warp. Although design specifications do not typically include an effective length factor on the unbraced length to account for warping restraints, the methods of accounting for warping restraint are outlined in sources such as the SSRC Guide (SSRC 2010).

In Timoshenko's original derivation of the beam buckling solution, the stated assumptions for the support conditions included restraints of torsional and lateral deformations at the ends of the unbraced length; however only the assumption about twist restraint was utilized. Provided that a point is restrained from twisting, whether the section can translate laterally has no impact on the lateral torsional buckling capacity. Twist of the section can be effectively controlled by either providing bracing that specifically prevents twist of the cross section (torsional bracing) or by providing braces that stop lateral movement of the compression flange (lateral bracing). The focus of the research outlined in this dissertation are cross frames which fit into the category of torsional bracing since the braces control twist by connecting adjacent beams. Although a plate diaphragm is sometimes utilized, the most common form of bracing in steel bridges is the cross frames that form a truss structure for controlling the girder twist. Some of the factors that impact the behavior of torsional braces are discussed later in this chapter; however the next section focuses on the fundamental properties that are necessary for effective stability bracing.

2.2.2 Bracing Requirements

As outlined in Chapter 1, an adequate bracing system must possess both adequate stiffness and strength. This section describes how these requirements are determined for column and beam systems. Although the primary focus of the study is on beam systems, column bracing requirements are first discussed since the derivation of the column bracing requirements are relatively simple to convey. In addition, many of the basic stability requirements for column bracing are applicable to beam bracing.

The concept of bracing requirements was first developed for column bracing by Winter (Winter 1958). The relationship between the brace stiffness, β_L , and the buckling capacity, P_{cr} , is graphed in Figure 2.1 for a perfectly straight column with discrete brace located at mid-height. As shown in the figure, the column will buckle between the brace points if the stiffness of brace, β_L , is greater than $2P_e/L_b$. In this case, the column will achieve the full buckling capacity predicted, $P_e = \pi^2 EI/L_b^2$, which is often referred to as the Euler buckling load as a tribute to Leonhard Euler who was the first individual to recognize column buckling and developed much of the mathematical theory necessary in the derivation. This minimum stiffness of the brace for the column to achieve full buckling capacity is referred to as the ideal stiffness (β_i) of the brace. Therefore, the ideal stiffness is the minimum brace stiffness necessary so that a perfectly straight member will buckle between the brace points.

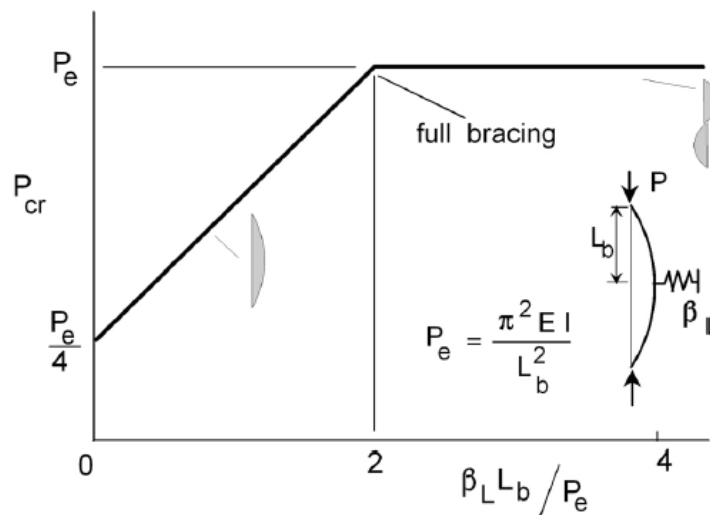


Figure 2.1: Effect of Brace Stiffness for Column Buckling

However, a real column that possesses out-of-straightness, will be unable to reach the load corresponding to buckling between the brace points if the ideal stiffness is provided (Winter 1958), as shown by the large deformation that occur if the ideal stiffness, β_i , is provided in Figure 2.2. If instead a value of twice the ideal stiffness is provided, the amount of deformation that occurs at the brace will be equal to the magnitude of the initial imperfection, Δ_0 . Providing stiffness magnitudes larger than the ideal value results in even smaller deformations at the brace location.

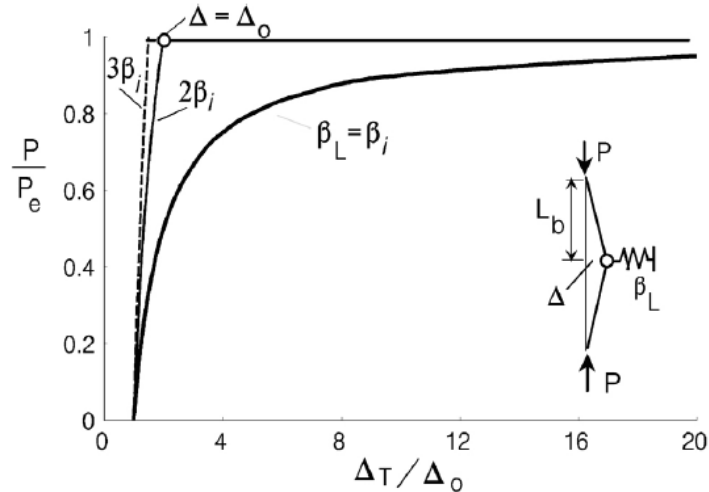


Figure 2.2: Normalized Axial Load vs. Normalized Displacement for Braced Winter Column with Initial Out-of-straightness

Since the brace forces are a function of the brace stiffness and the amount of deformation that occurs at the brace, providing the ideal stiffness will also result in very large brace forces as the load corresponding to buckling between the brace points is approached. This is demonstrated in Figure 2.3 which shows the bracing force for an imperfect column (imperfection is in the magnitude of 1/500 of total column length) and three cases of different brace stiffness that are referenced relative to the ideal stiffness, β_i . If only the ideal stiffness is provided, the brace force will theoretically tend towards infinity when the buckling load is approached. Therefore, a stiffness larger than the ideal stiffness needs to be provided to control brace forces. Winter developed a simple rigid link model that could be used for determining the ideal stiffness requirements (Winter 1958). Winter's model can also be used to determine the brace forces as a function of the magnitude of the initial imperfection and the stiffness of the brace that is provided.

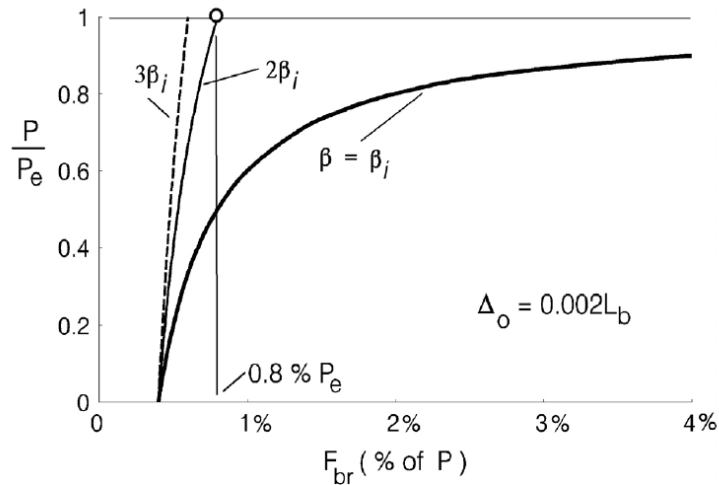


Figure 2.3: P vs. F for Braced Winter Column with Initial Out-of-straightness

Many bracing provisions recommend a brace stiffness of twice the ideal stiffness to control brace forces and member deformations. Figure 2.3 shows the brace forces that are predicted using Winter's model and for a stiffness of twice the ideal value, the force requirement is 0.8% of P_e of the column. The brace strength requirement that is published for column discrete (often referred to as nodal) bracing is actual 1.0% of the column load. The higher requirement comes from finite element solutions of imperfect columns which result in a brace force of 1.05% of the column load for the case of a single brace at mid-height and an imperfection of $L_b/500$ (Helwig 1994). The larger force compared to Winter's model comes from internal forces that develop in the column member. The case of a single intermediate brace is actually the worst case and for columns with several intermediate braces, the brace force tends towards 0.8% of the column load as predicted by Winter's model.

Although beam bracing systems are generally more complex than axially loaded columns, the fundamental concepts related to the stiffness and strength requirements are essentially the same. Like columns, effective beam bracing must possess sufficient stiffness and strength. The following section provides a discussion of beam torsional bracing with an overview of the many factors that have an impact on the effectiveness of the bracing.

2.2.3 Fundamentals of Beam Bracing

The purpose of beam bracing is to improve the lateral torsional buckling capacity of a member. Lateral torsional buckling is a mode of failure that involves both lateral movement and twist of the cross section. Effective beam bracing can be achieved by either preventing lateral movement of the compression flange (lateral bracing) or twist of the cross-section (torsional bracing). Furthermore the torsional bracing system can be divided into discrete bracing and continuous bracing. The cross frames or diaphragms between bridge girders provide torsional restraint to girders at the bracing points, and therefore are categorized as discrete torsional braces.

Equation ((2.2) can be used to quantify the buckling capacity of a beam with continuous torsional bracing. The expression was developed for doubly symmetric beams subjected to uniform moment loading (Taylor and Ojalvo 1966).

$$M_{cr} = \sqrt{M_0^2 + \bar{\beta}_b EI_y} \quad (2.2)$$

where:

M_0 = buckling capacity of the unbraced beam, kip-in

$\bar{\beta}_b$ = torsional brace stiffness (in-k/rad per in. length)

This expression was updated to consider the impact of discrete torsional braces and general loading conditions as shown in the following expression: (Yura 1992).

$$M_{cr} = \sqrt{C_{bu}^2 M_0^2 + \frac{C_{bb}^2 \bar{\beta}_T EI_{eff}}{C_T}} \leq M_y \text{ or } M_{bp} \quad (2.3)$$

where:

C_{bu} = C_b factor corresponding to an beam with no intermediate braces

C_{bb} = C_b factor corresponding to beam fully brace at location of intermediate cross frames

C_T = top flange loading modification factor; $C_T=1.2$ for top flange loading and $C_T=1.0$ for centroidal loading

$\bar{\beta}_T$ = equivalent effective continuous torsional brace stiffness, determined by:
 $\beta_T n/L$

β_T = torsional stiffness provided by single cross frame.

n = number of intermediate braces

L = length of span

The torsional stiffness (β_T) provided by a single intermediate cross frame is a major topic of this research and is discussed more in later sections.

The ideal stiffness of the torsional bracing can be obtained by rearranging Equation ((2.3). Similar to columns the stiffness required to control brace forces and deformations are obtained by using at least twice the ideal stiffness. The expression in the brackets of the following expression comes from solving Equation 2.3 for the stiffness while the 2 outside the brackets doubles this stiffness:

$$\bar{\beta}_T^* = 2 \left[(M_{cr}^2 - C_{bu}^2 M_0^2) \frac{C_T}{C_{bb}^2 EI_{eff}} \right] \quad (2.4)$$

The stiffness in the above equations is expressed for a continuous bracing system and can be modified as follows for n discretely spaced braces along the girder of length L :

$$\beta_T^* = \bar{\beta}_T^* L/n \quad (2.5)$$

In the Appendix 6 bracing provisions in the AISC specification (AISC 2010), the initial capacity of the girder with no bracing is conservatively neglected. If M_{cr} is then set to the design moment and top flange loading is assumed ($C_T = 1.2$), the required stiffness is given by the following expression:

$$\beta_T = \frac{2.4LM_r^2}{nEI_y C_b^2} \quad (2.6)$$

where:

M_r = the required flexural strength of the beam.

The strength requirements for the torsional braces, are a function of the initial imperfection. Imperfections that are critical for beams typically involved an initial twist (θ_0) so that the required brace moment can be determined. Similar to columns, if twice the ideal stiffness is provided the amount of deformation is approximately equal to the initial imperfection and the resulting brace moment is given by the following expression:

$$M_{br} = \beta_T^* \theta_0 \quad (2.7)$$

With regards to the critical shape of the imperfection, Wang and Helwig (2008) studied the shape of the imperfection and found that a shape in which the top flange was displaced lateral while the bottom flange remained straight tended to give the worst case for stability induced forces. Following the AISC Code of Standard Practice (2012) for erection tolerances the amount of sweep of the top flange is taken as $L_b/500$. Therefore the magnitude of the twist imperfection is given as $0.002L_b/h$. The resulting bracing moment is given by the following expression:

$$M_{br} = \beta_T \theta_o = \left(\frac{2.4LM_r^2}{nEI_y C_b^2} \right) \frac{L_b}{500h} = \frac{0.005LM_r^2 L_b}{nEI_y C_b^2} \quad (2.8)$$

The above expression differs from the expression given in the AISC Appendix 6 provisions due to some simplifications as outlined in the Commentary of the AISC Specification.

2.2.4 Beam Bracing Stiffness

The stiffness predicted by Equation 2.6 is the required stiffness to result in twice the ideal value. The actual stiffness of the cross frame on the bridge is a function of several components. In general, the stiffness of a beam torsional brace can be divided into three major parts (Yura 1992) as expressed in Equation ((2.9)).

$$\frac{1}{\beta_T} = \frac{1}{\beta_b} + \frac{1}{\beta_{sec}} + \frac{1}{\beta_g} \quad (2.9)$$

where:

β_b = brace stiffness

β_{sec} = web distortional stiffness

β_g = girder system stiffness

Previous studies have addressed the impact of the cross sectional distortion and the in-plane stiffness of the girders. The research outlined in this dissertation has focused on the brace stiffness denoted by β_b in the expression. More detailed information of how the β_{sec} , β_g are quantified can be found in (Yura 1992).

The stiffness of a torsional brace is sensitive to the buckling mode of the girders. Because cross frames have a depth that is a significant percentage of the overall depth of the girder, the buckling mode of the girders usually involve twisting and displacing laterally in the same direction as depicted in Figure 2.4. The loading on the cross frame from a stiffness and strength demand can be viewed as moments with equal magnitude and opposite sign (reverse curvature bending) as shown in Figure 2.4. The restraining moment provided by the cross frame is essentially a torque on the girder, which is why the braces are referred to as a torsional braces. The effect of the brace moments on the cross frame can be represented by the force couples (Fh_b) as denoted in the figure. The cross frame will deform under the force couple leading to a girder rotation θ . The brace stiffness is defined as the ratio M/θ .

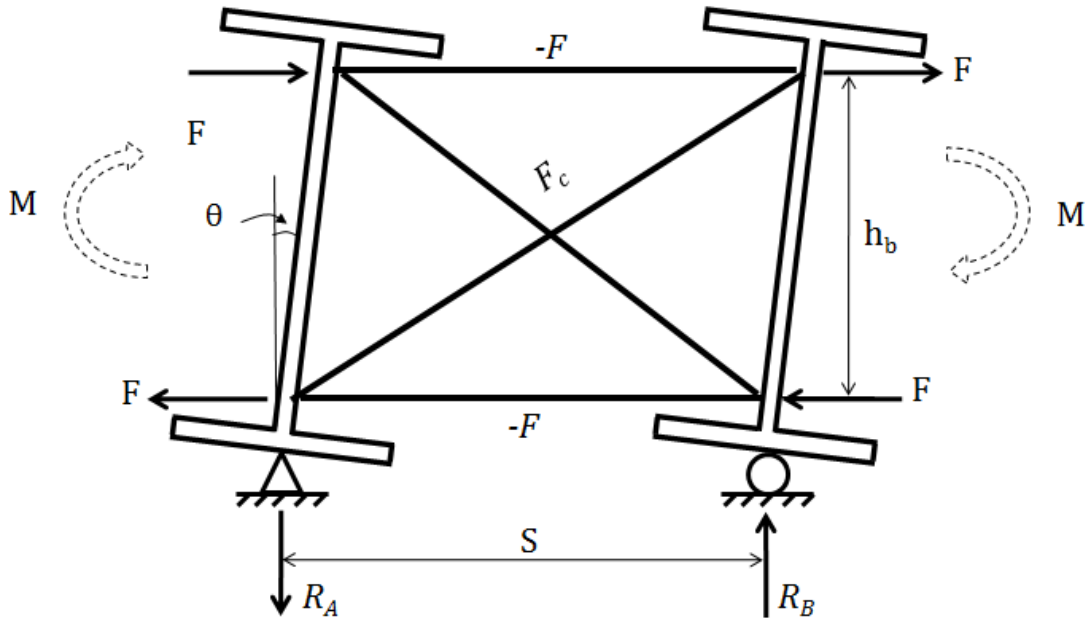
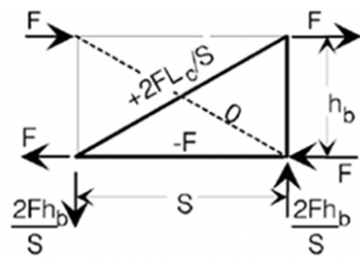


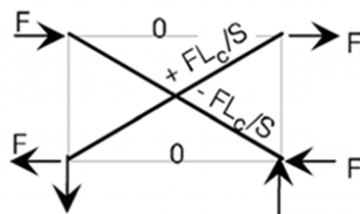
Figure 2.4: Stiffness of a Cross Frame

A simplified truss model representation for the cross frame leads to stiffness and axial force representations as depicted in Figure 2.5.



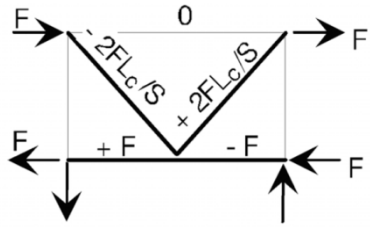
$$\beta_b = \frac{ES^2 h_b^2}{\frac{2L_c^3}{A_c} + \frac{S^3}{A_h}} \quad (2.10)$$

(a) Tension-only Diagonal System



$$\beta_b = \frac{A_c ES^2 h_b^2}{L_c^3} \quad (2.11)$$

(b) Compression-tension Diagonal System



$$\beta_b = \frac{2ES^2h_b^2}{\frac{8L_c^3}{A_c} + \frac{S^3}{A_h}} \quad (2.12)$$

(c) K-brace System

A_h = area of horizontal members

L_c = length of diagonal members

A_c = area of diagonal members

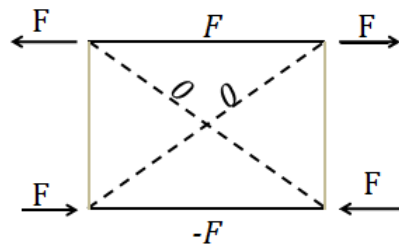
S = spacing of girders

E = modulus of elasticity

h_b = height of the cross frame

Figure 2.5: Stiffness Formulas for Twin Girder Cross Frames (Yura 1992)

According to Figure 2.5, the top and bottom struts of the compression-tension diagonal system are zero force members. And the top strut of a K-brace system is also a zero force member. However, it does not imply that these members are dispensable for an effective cross frame system. The reason is that these members are only zero force members when the twin girder buckling mode is as depicted in Figure 2.4. If the twin girders buckle in a mode in which the top flanges separate instead of the same direction, the top and bottom struts of these cross frames are actually not zero force members. A sketch of this condition is shown in Figure 2.6. The corresponding brace stiffness is shown in Equation (2.13). This equation was derived by conservatively assuming that the two diagonals are not connected at the intersection. The condition depicted by Figure 2.6 will be the controlling case for top and bottom strut if their sizes are chosen to be different from the diagonal members. However, for majority of cross frames that all members are in the same size, the critical condition is the one depicted by Figure 2.4.



$$\beta_b = \frac{EAh_b^2}{S} \quad (2.13)$$

Figure 2.6 Brace Stiffness for Twin Girders Buckle in Opposite Directions

The X-frame comprised by single angles that were introduced in Chapter 1 is conventionally designed by representing the system as a tension-only diagonal system. Considering the low compression strength of a single angle member, designers may conservatively ignore the contribution of the diagonal in compression. On the other hand, the compression-tension model assumes the compression diagonal contributes as much as the tension member. The K-frame must have diagonals that have sufficient compression resistance to be viable.

2.2.5 Equivalent Stiffness of Cross Frames

The method in evaluating bracing stiffness introduced in Section 2.2.4 is specifically designed for checking girder stability. However, the stiffness of the cross frame is also needed in many other occasions. Engineers often rely on computer software in analyzing bridges for the strength and deflections. One of the widely used bridge analysis models is the two-dimensional (2D) grillage method, in which the girder lines and the cross frames are all simplified as beam elements in the same 2-D plane. Engineering practice has shown that this method can predict bridge behaviors with relatively low modeling and computation cost if compared with three-dimensional (3-D) models. One of the challenges of this method is to simulate cross frame truss with beam element, which should possess stiffness equivalent to the cross frame in order to accurately predict the structural behavior of the whole bridge. According to *G13.1 Guidelines for Steel Girder Bridge Analysis* (AASHTO/NSBA Steel Bridge Collaboration 2011), two methods of obtaining equivalent stiffness for X-frames were traditionally used by bridge designers. As shown in Figure 2.7, one method is to determine the equivalent stiffness by calculating the flexural stiffness on a propped cantilever model and another one is by calculating the shear stiffness on a pure shear model. An equivalent moment of inertia I_{equiv} will be then obtained from either method and will be used in the bridge grid analysis.

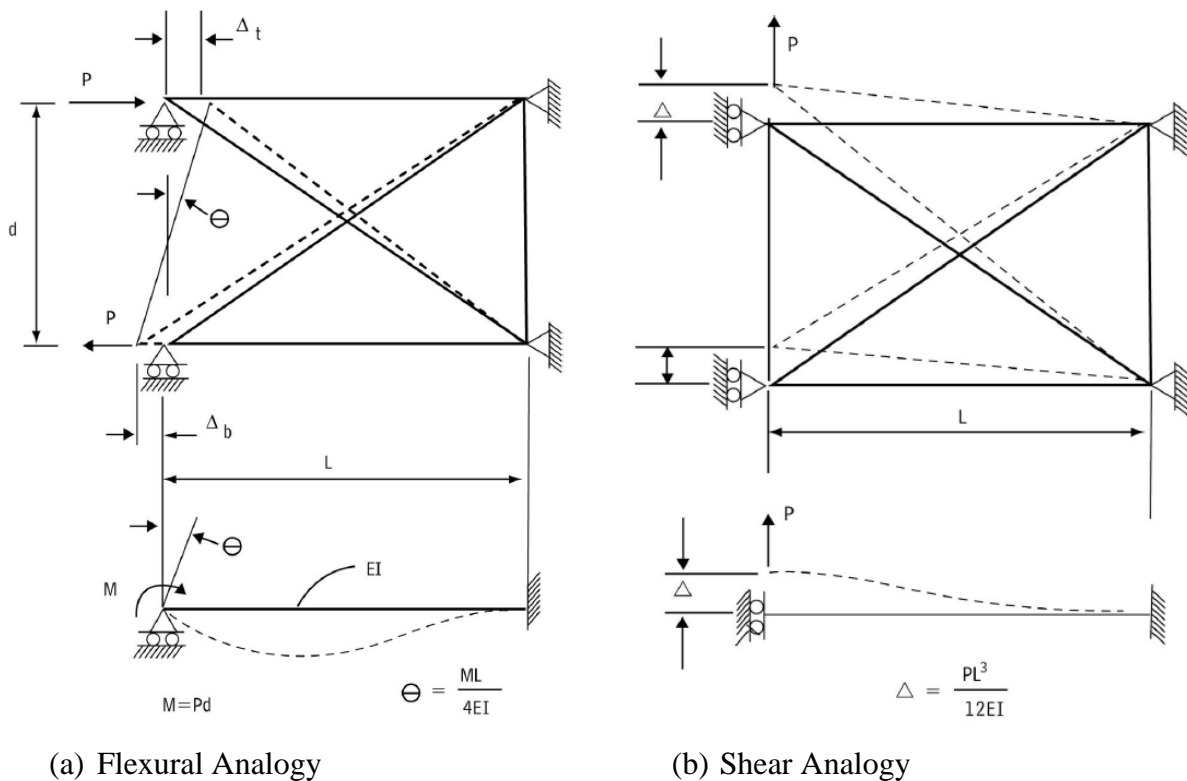


Figure 2.7: Equivalent Stiffness (AASHTO/NSBA Steel Bridge Collaboration 2011),

As the figure indicates, both approaches consider the contribution from both tension and compression diagonals of the cross frame, so the resulting stiffness from the expressions should be comparable to the compression and tension diagonal model under double curvature type of loading computed by Equation (2.11). For the model under double curvature type of loading, an

equivalent moment of inertia can be obtained by using a similar approach. The resulting I_{equiv} from these three approaches for an example cross frame are listed in Table 2.1. The geometry in the example is chosen to be consistent with the laboratory tests introduced later in this report.

Table 2.1 Equivalent Stiffness Example

Cross Frame: 114.5" (S) x 53.74" (h_b), Member:L4x4x3/8	
Approach	Equivalent Moment of Inertia I_{equiv}, in⁴
Flexural Analogy	1,829
Shear Analogy	1,039
Double Curvature Analogy (Compression and Tension Diagonal Model (Eq. 2.11))	1,039

As the example shows, the double curvature analogy gives the same equivalent stiffness as the shear analogy. The finding suggests that the double curvature model is only a variant of the pure shear model. This can be also proved by comparing the deformed shapes. Both the double curvature analogy and shear analogy cause shear deformation in the cross frame. The deformed shape of the cross frame remains a parallelogram and the girder webs remain parallel.

The flexural analogy and shear analogy (or double curvature analogy) give different results and research has been conducted to identify their impact in predicting bridge behaviors (Chang 2005)(Ozgun 2007). However, there has not been conclusive determination of whether either approach is sufficient. As commented in the *G13.1 Guidelines for Steel Girder Bridge Analysis* (AASHTO/NSBA Steel Bridge Collaboration 2011):

“None of these approaches is wrong in and of itself but each approach focuses only on one of several stiffness parameters, while others are neglected. In an actual bridge, there is the potential that both stiffness parameters may have noticeable influence on the overall structural response of the bridge. Differential deflection of adjacent girders might primarily engage the shear stiffness of the cross frames, while differential rotation (twisting) of adjacent girders might be more likely to engage the flexural stiffness of the cross frames.”

“Regardless of the type of modeling being performed (2D, 3D, others) most designers will omit refined consideration of the flexibility of connection details such as bolted gusset plate connections. Instead, for truss-type cross frames, most designers assume that the chord and diagonals act as pin-ended truss members for analysis modeling as well as for detailed design checks.”

No matter what type of truss analogy is employed, the current practices always neglect the flexibility of connection details and the details of connections.

2.3 Beam Bracing Strength

In addition to the stiffness, the cross frames depicted in Figure 2.5 also show the axial forces resulting from using a truss analogy in the different members of the cross frame. The strength of a given cross frame will be controlled by the weakest member in the system compared to the resulting member force. The respective member strengths need to reflect tensile strengths or buckling strengths for members subjected to either tension or compression. In the following subsections, a few methods necessary for evaluating the compressive strength of single angle members and gusset plates are summarized.

2.3.1 Compressive Strength of Single Angles

To accurately determine the strength of a single angle cross frame, the compression capacity of a single angle member needs to be determined. Due to the difficulty in accounting for the end restraints and eccentricity of end connections, the evaluation of the compressive capacity single angle members have varied in design specifications over the years. Historically the AISC Specification adopted two methods: a Beam Column Method and Effective Length Method.

When a single angle member is connected with gusset plates at both ends, the eccentricity of the connection can result in significant bending in the member. Therefore, a beam column method was traditionally recommended by ASIC. The expression used to limit the effects of combined bending and axial force is shown in Equation (2.14). The strength of the member is a function of the factored axial force, P and the factored moments about two principle axes, M_{uw} and M_{uz} . The nominal strength of the member as a column is denoted as P_n and nominal strength of the member as a beam about the respective w and z axes are denoted by M_{nw} and M_{nz} . The resistance factors for column behavior and bending behavior are identified as ϕ_c and ϕ_b . The upper limit of 1.0 on the expression limits the impact of the combined load effects.

$$\left| \frac{P_u}{\phi P_n} + \frac{8}{9} \left(\frac{M_{uw}}{\phi_b M_{nw}} + \frac{M_{uz}}{\phi_b M_{nz}} \right) \right| \leq 1.0 \quad (2.14)$$

The evaluation of using the beam column method in the single angle member was a tedious procedure that often resulted in relatively conservative solutions, which led AISC 360-05 to adopt a simpler method based upon an effective length method. The effective length method was developed from a method introduced by Design of Latticed Steel Transmission Structure (ASCE 1997). It was based on a review of many years of tower industry experience and the results of laboratory and full-scale tower tests. Equations (2.15) and (2.16) can be used to correct the slenderness of the eccentrically connected single angle in a planar truss. The resulting slenderness could be directly applied to equations of the compressive strength of column.

When $0 \leq \frac{L}{r_x} \leq 80$:

$$\frac{KL}{r} = 72 + 0.75 \frac{L}{r_x} \quad (2.15)$$

When $\frac{L}{r_x} > 80$

$$\frac{KL}{r} = 32 + 1.25 \frac{L}{r_x} \quad (2.16)$$

The effective length method provides reasonable predictions for the buckling resistance of single angle members and is generally much simpler to use than the beam-column approach.

2.3.2 Compressive Strength of Gusset plates

The thickness of gusset plates for cross frames are usually specified by state transportation authorities. For example, TxDOT specifies a typical thickness of 0.5 inch. However, the design of gusset plates based on its strength is difficult due to lack of the understanding impact of the connection on the buckling resistance due to potentially complex geometry. The most well-known method in evaluating strength of gusset plate was proposed by Whitmore (Whitmore 1952) and this method was adopted by FHWA in its latest rating guidance of gusset plates (FHWA 2009). The proposed method recommends that the gusset plates be checked for strength using the width based on the connection length as shown in Figure 2.8. It is assumed that the load spreads at an angle of 30 degrees from the start of the connection and therefore the gusset plate needs to resist the design load at the end of the connection based on the Whitmore width. This geometry does not take into the account any gusset plate material that is outside of the Whitmore width. Common practice has adopted this method and uses it for welded and bolted connections even though it was originally intended for bolted connections only.

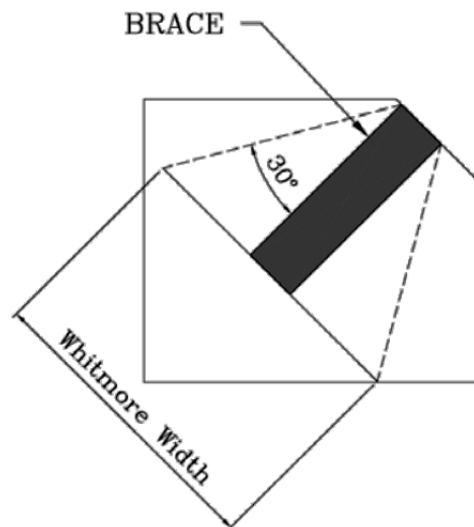


Figure 2.8: Whitmore Width

2.4 Fatigue Design of Steel Bridges

A major aspect of the research conducted within this project was the assessment and development of cross frame connections for use in steel bridge applications. The following

information provides a brief overview of the classification of bridge details for fatigue design, including information on the current use of single angle members.

2.4.1 Introduction to Fatigue

Fatigue is the phenomenon by which localized structural damage occurs to the material due to cyclic loading. It is often grouped into two classifications: low-cycle fatigue, typically less than 10,000 cycles, and high-cycle fatigue, more than 10,000 cycles. In the determination of fatigue life, the stress range, S_R , applied to the member is related to the number of cycles, N , to failure. Low-cycle fatigue is characterized by stress ranges near the yield stress of the material (F_y), namely $S_R \approx F_y$. High-cycle fatigue involves stress ranges much lower than the yield strength of the material, or $S_R \ll F_y$.

In steel bridges, the designer is concerned with high-cycle fatigue. The members of the bridge are subjected to periodic loads due to the passing of traffic on the superstructure. These stresses are usually much lower than the yield strength of the material, especially in cross frame members.

2.4.2 Geometrical Discontinuities

Fatigue cracks will often form at geometrical discontinuities, such as that caused by the cross frame member connection to the gusset plates as well as at the attachment of the cross frame gusset plates to the connection plates. The local geometry causes an increase in stress to build up at a specific point, thereby exceeding the yield stress and causing permanent damage. The damage initiates on a microscopic level and often over the course of thousands of cycles, the crack will grow. Figure 2.9 shows the eccentric single angle detail studied in the research. Note how the stress transfer from the angle member to the gusset plate leads to a build-up of stress at the forward edge of the fillet weld connection. In addition, a secondary stress concentration occurs at the back end of the member in the gusset plate at the weld.

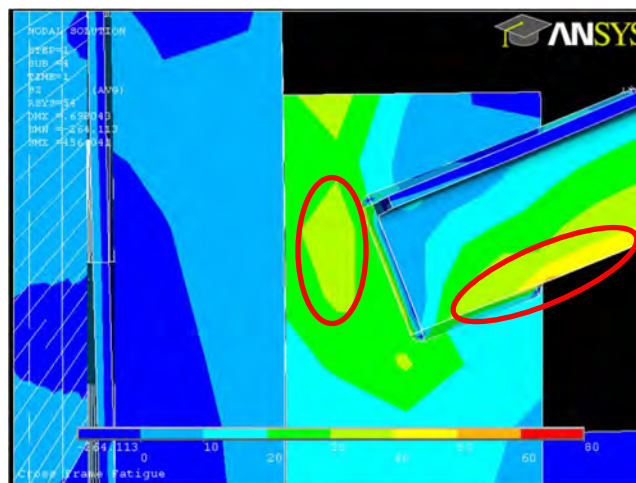


Figure 2.9: Stress Concentration due to Geometrical Discontinuities at the Cross Frame Connection

A major focus of the research is to identify the effect geometrical discontinuities can have on the formation and growth of fatigue cracks. Due to the nature of the welded connections,

stress concentrations arising from rapid changes in geometry are inevitable. The research aims to identify the probable locations of fatigue cracks, track the relative growth rate of the crack compared to the overall fatigue life, and provide guidance on the magnitude of stress concentration in the connection.

2.4.3 Material Defects

At the most basic level, fatigue cracks will form at defects in the material. There are many possible sources of the defects, which range from the atomic level to the macroscopic level. For instance, in an ordinary plate of steel, atomic vacancies in the lattice structure of the material cause microscopic stress risers, similar to the stress concentration formed in the classic example of a uniaxially loaded plate with a hole. Although the cracks start small, they continue to grow under repeated cycling of stress.

Likewise, defects in the weld material frequently lead to the development of fatigue cracks. Since the quality of the welded connections in the cross frames is unique to the each weld, it is important to maintain strict quality control on the welding process to ensure the fatigue cracks do not emanate from weld defects.

Undercut

Undercut is a notch-type defect occurring in the base metal at the welded connection and is related to the temperature and placement of the weld metal. If the input heat is too high, or the weld is directed into one plate more than the other, the base metal at the edge of the weld will melt, creating a divot at the weld toe (as seen in Figure 2.10 and Figure 2.11). The divot can cause localized stress concentrations, amplifying the concentration already existing at the weld toe, resulting in lower fatigue life. The permissible depth of undercut is $\frac{3}{64}$ in. or less [AWS 2012].

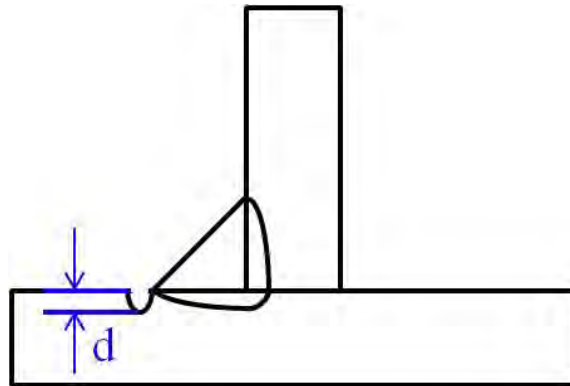


Figure 2.10: Undercut at Toe of Fillet Weld Connection (Schematic)

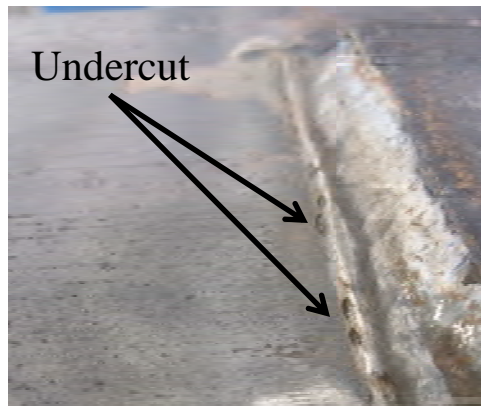


Figure 2.11: Undercut at Toe of Fillet Weld Connection (Example)

Incomplete Fusion

Incomplete fusion is the failure of the weld to fully penetrate the base metal, particularly at the root of the weld, thus reducing the strength of the weld. Insufficient welding current, lack of access to the weld, and poor preweld cleaning are the leading causes of incomplete fusion [Connor 1987]. In terms of fatigue, incomplete fusion can lead to an increase of stress at the toe of the weld reducing the fatigue life.

Slag Inclusions

Slag inclusions are nonmetallic solid materials that get trapped in the weld metal as a result of poor technique and inaccessibility of the connection [Connor 1987]. The slag is only present in the methods that use a solid material to shield the weld from the air, which includes the basic Shielded Metal Arc Welding (SMAW) and the Flux-Cored Arc Welding (FCAW) processes. In a properly welded connection, the slag will float to the top of the molten weld and act as a buffer to the air, preventing other defects like porosity (covered in next subsection) from occurring. If the slag gets trapped in the weld, there can be a large vacancy which cannot distribute load. The vacancy can lead to fatigue crack initiation and eventually failure. A schematic of a slag inclusion is shown in Figure 2.12 and an example in Figure 2.13.

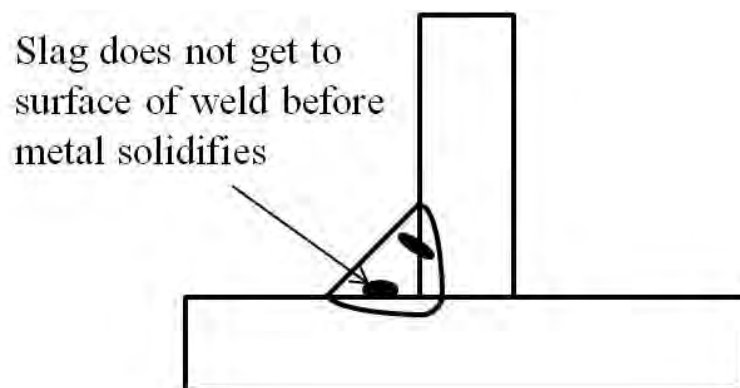


Figure 2.12: Slag Inclusion in Fillet Weld (Schematic)

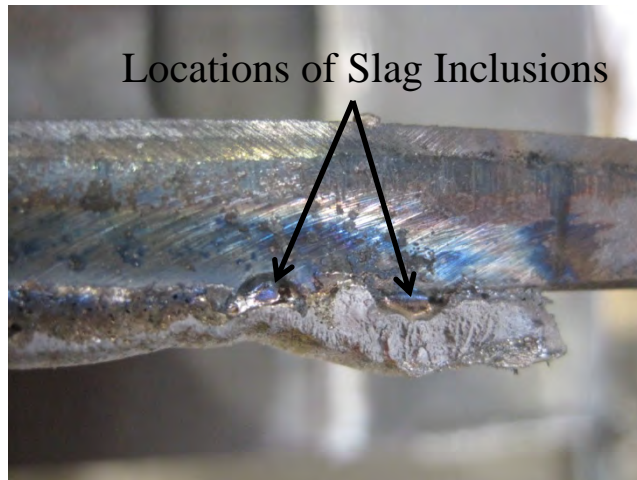


Figure 2.13: Slag Inclusion in Fillet Weld (Example)

Porosity

The last and perhaps most common defect is porosity, which involves gas becoming entrapped in the solidifying weld metal [Connor 1987]. In a weld metal, the molten weld pool could contain the following gases: hydrogen, oxygen, nitrogen, carbon monoxide, carbon dioxide, water vapor, hydrogen sulphide, argon, and helium. Of these, hydrogen, oxygen, and nitrogen are the only ones that diffuse in high concentration into the liquid metal. Hydrogen, the major cause of porosity, can be from several sources, including, but not limited to, the hydrogen in the atmosphere immediately surrounding the weld, the hydrogen that can form from constituents like cellulose in the flux or electrode covering, and the hydrogen from dissociation of water. Water can be from excessive humidity or rainwater in the vicinity of the weld. Oxygen can enter the molten pool through oxides on filler wire or base metal, flux and electrode covering, and from the atmosphere [Connor 1987]. Porosity leads to small vacancies that can become the initiation points for fatigue cracks in the connection. A schematic of porosity is shown in Figure 2.14 and porosity in a fillet weld is shown in Figure 2.15.

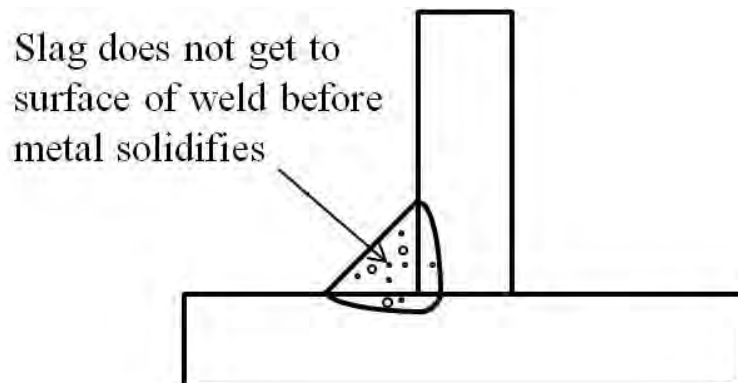


Figure 2.14: Porosity in Fillet Weld (Schematic)



Figure 2.15: Porosity in Cross Section of Fillet Weld (Example)

2.5 AASHTO Bridge Fatigue Design Methodology

With the numerous potential defects present at welded connections, fatigue loading on the connection needs to be considered. The American Association of State Highway and Transportation Officials (AASHTO) LRFD Bridge Design Specification [2012] designs for fatigue using different categories based on the type of connections on the bridge. In conjunction with the detail category, the average daily truck traffic on the bridge is the other prevailing factor in the fatigue design of the steel bridge. The following subsections outline the methodology AASHTO uses when designing for fatigue.

2.5.1 Fatigue Design

In LRFD design, the factored resistance to fatigue cracking of the detail must exceed the factored load demand on the detail. AASHTO specifies in Article 6.6.1.2.2 that any load-induced fatigue detail needs to satisfy the following condition:

$$\gamma(\Delta f) \leq (\Delta F)_n \quad (2.17)$$

where,

γ = Load Factor specified in Table 3.4.1-1

(Δf) = Force Effect, or the Live Load Stress Range (specified in Article 3.6.1.4)

$(\Delta F)_n$ = Nominal Fatigue Resistance (specified in Article 6.6.1.2.5)

2.5.2 Live Load Stress Range

The fatigue loading magnitude and configuration is covered in AASHTO Article 3.6.1.4.1 and is used to determine the factored live load stress range acting on the detail, or (Δf) [2012]. The specification uses one design truck (as specified in Article 3.6.1.2.2) but with a constant spacing of 30 ft between the 32 kip axles for the truck. Furthermore, you must also consider the design tandem, which consists of two 25 kip axles spaced at 4 ft apart. Unless short spans are used, the design truck, with the much higher load, will govern the strength behavior of the bridge and often the fatigue stresses [Frank 2008]. The geometry and loading associated with the fatigue design truck and the tandem are given in Figure 2.16 and Figure 2.17.

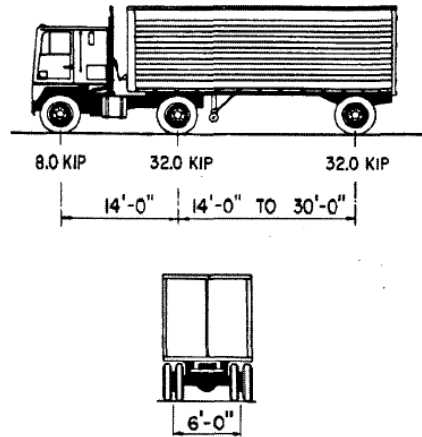


Figure 2.16: AASHTO Fatigue Design Truck [AASHTO 2012]

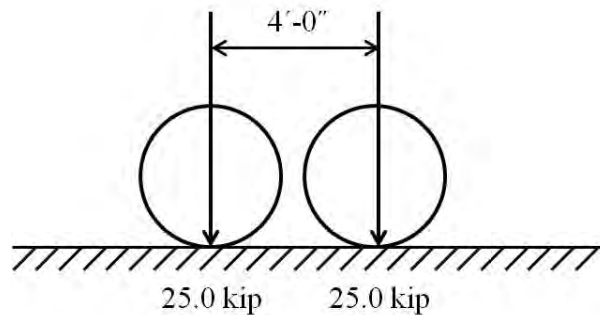


Figure 2.17: AASHTO Fatigue Design Tandem

Article 3.6.1.4.3 specifies the fatigue load distribution to determine the fatigue forces in the various bridge components. Simply stated, the fatigue truck or tandem shall be placed transversely and longitudinally to maximize the stress range at the detail under consideration, regardless of the traffic position or lane designations [AASHTO 2012]. Any additional live load will also be applied to the structure in the computation of the stress range [AASHTO 6.6.1.2.1 2012]. Chapter 10 highlights the results from a fatigue design comparison between ANSYS and MDX in which the placement of the fatigue load will be discussed in more detail.

2.5.3 AASHTO Fatigue Design Categories

In an attempt to simplify fatigue design, AASHTO designates categories to different connection types that account for the stress concentration resulting from geometrical discontinuities and local notch stresses. There are currently eight categories in the AASHTO specification: A, B, B', C, C', D, E, and E' (pronounced 'E prime') [AASHTO 6.6.1.2.3 2012]. In order to be used in steel bridge design, the detail must meet one of these fatigue categories. AASHTO Table 6.6.1.2.3-1 gives an extensive list of the categories for different connection and other details typically found in steel bridges [2012].

The basic premise is that Category A pertains to the base metal of steel, that simply accounts for material defects in the base metal away from any connection details or geometric anomalies. Each category below A, B through E', applies to increasing severity of stress

concentrations or lower fatigue resistance, with E' being the lowest category. The category method helps determine the resistance of the detail to the development of fatigue cracks, which must be larger than the applied loads in LRFD design.

2.5.4 Nominal Fatigue Resistance

The nominal fatigue resistance is covered in Article 6.6.1.2.5 and is separated into two load combinations [AASHTO 2012]. Using the Fatigue I load combination and considering infinite life for the detail:

$$(\Delta F)_n \leq (\Delta F)_{TH} \quad (2.18)$$

where,

$(\Delta F)_n$ = Nominal Fatigue Resistance (specified in Article 6.6.1.2.5)

$(\Delta F)_{TH}$ = Constant Amplitude Fatigue Threshold (specified in Table 6.6.1.2.5-3)

Alternatively, the Fatigue II load combination is used and the designer considers a finite life for the detail as follows:

$$(\Delta F)_n \leq \left(\frac{A}{N}\right)^{\frac{1}{3}} \quad (2.19)$$

where,

$(\Delta F)_n$ = Nominal Fatigue Resistance (specified in Article 6.6.1.2.5)

A = Constant, taken from Table 6.6.1.2.5-1 related to fatigue category

N = Number of stress cycles over the life of the bridge

$$N = (365)(75)n(ADTT)_{SL} \quad (2.20)$$

where,

365 = Days per year

75 = 75 year design life, typical in AASHTO

n = Number of stress range cycles per truck passage (Table 6.6.1.2.5-2)

$(ADTT)_{SL}$ = Single lane average daily truck traffic (Article 3.6.1.4)

AASHTO specifies the frequency of the fatigue loading to be taken as the single-lane average daily truck traffic $(ADTT)_{SL}$ which, without better information, is taken as a percentage of the average daily truck traffic (ADTT) of the bridge [2012]. For simple spans longer than 40 ft, n is taken as 1.0; for continuous spans longer than 40 ft, n is taken as 1.5 [AASHTO 2012].

The values for A and $(\Delta F)_{TH}$ in Equations (2.18) and (2.19) are given in Table 2.2 and Table 2.3 respectively.

Table 2.2: Detail Category Constant, A [AASHTO Table 6.6.1.2.5-1 2012]

Detail Category	Constant, A times 10^8 (ksi ³)
A	250.0
B	120.0
B'	61.0
C	44.0
C'	44.0
D	22.0
E	11.0
E'	3.9
M 164 (A325) Bolts in Axial Tension	17.1
M 253 (A490) Bolts in Axial Tension	31.5

Table 2.3: Constant-Amplitude Fatigue Thresholds [AASHTO Table 6.6.1.2.5-3 2012]

Detail Category	Threshold (ksi)
A	24.0
B	16.0
B'	12.0
C	10.0
C'	12.0
D	7.0
E	4.5
E'	2.6
M 164 (A 325) Bolts in Axial Tension	31.0
M 253 (A 490) Bolts in Axial Tension	38.0

2.5.5 AASHTO S-N Chart

When determining the associated fatigue performance of a typical detail using the AASHTO design code, it is useful to graph the results of Equations (2.18) and (2.19) on an S-N plot. The S-N plot is a log-log plot of the constant-amplitude stress range (S) versus the number of cycles to failure (N). An S-N plot with the fatigue categories of AASHTO is given in Figure 2.18.

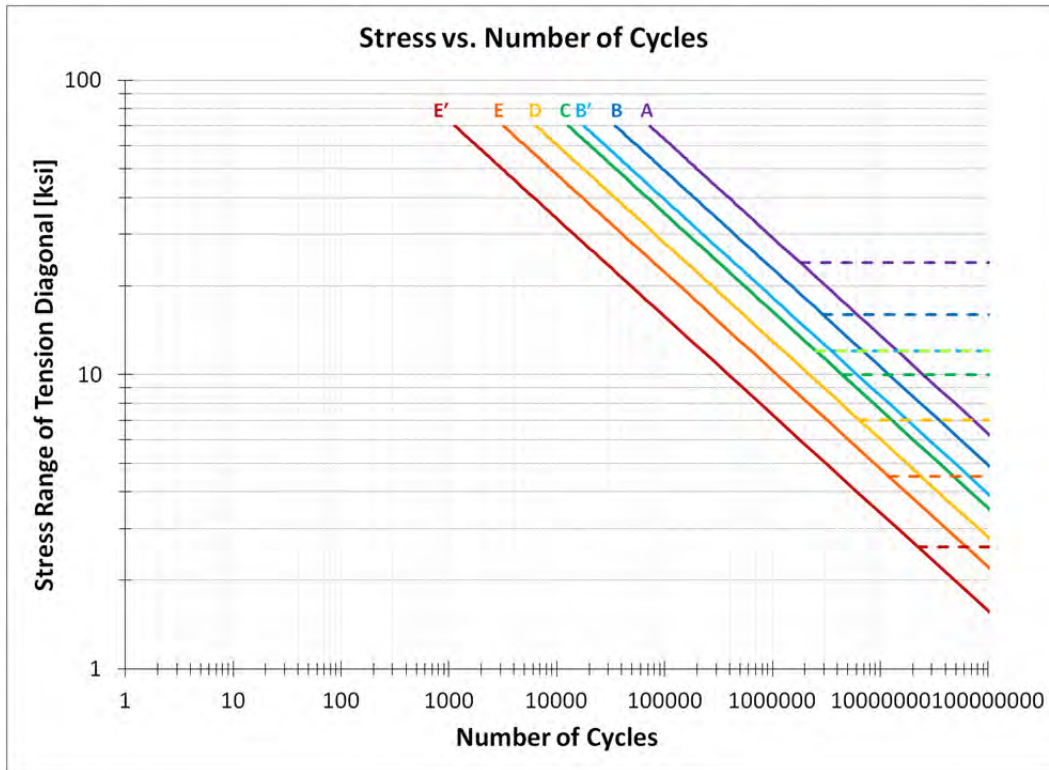


Figure 2.18: S-N Plot indicating AASHTO Fatigue Categories

Data points that lie above and to the right of the finite life portions of the curve are considered adequate. The finite life portion is the sloped line on the graph, which on the log-log scale has a slope of 3, the generally accepted value resulting from fatigue tests performed on numerous steel details in previous research.

If it is determined the stress range acting on a detail is lower than the infinite life portion of the design curves (the dashed lines in Figure 2.18), then the detail is considered to have infinite life according to the code.

For ease of design, AASHTO only considers the constant-amplitude stress range, and applies different load factors to the Fatigue I and Fatigue II loadings to adjust for load variation according to a perceived stress range distribution function [AASHTO 2012]. For a more detailed analysis, advanced techniques utilizing rain flow counting methods or the Palmgren-Miner rule can account for variation in stress range, but is not carried out in the current research.

2.5.6 Fatigue Testing Methods and Failure Criteria

In order to assess the fatigue life of a given detail, numerous connections are tested to rate the connection according to the categories outlined in AASHTO. The connections tested can be either small scale (uniaxial tension tests) or large scale (full scale cross frame tests) in nature. The testing method employed usually consists of specimens that are tested at a constant stress range, verified and updated by external measurements of force/stress and strain. The connections are typically tested at the maximum frequency at which the test setup remains stable.

During most laboratory tests, once a stress range is selected for the test, the detail is cycled until failure. The number of cycles-to-failure are recorded and compared to the AASHTO fatigue categories to classify the behavior of the detail. Failure is usually taken as the point at

which the specified force for the stress range can no longer be sustained. The process is outlined in Figure 2.19.

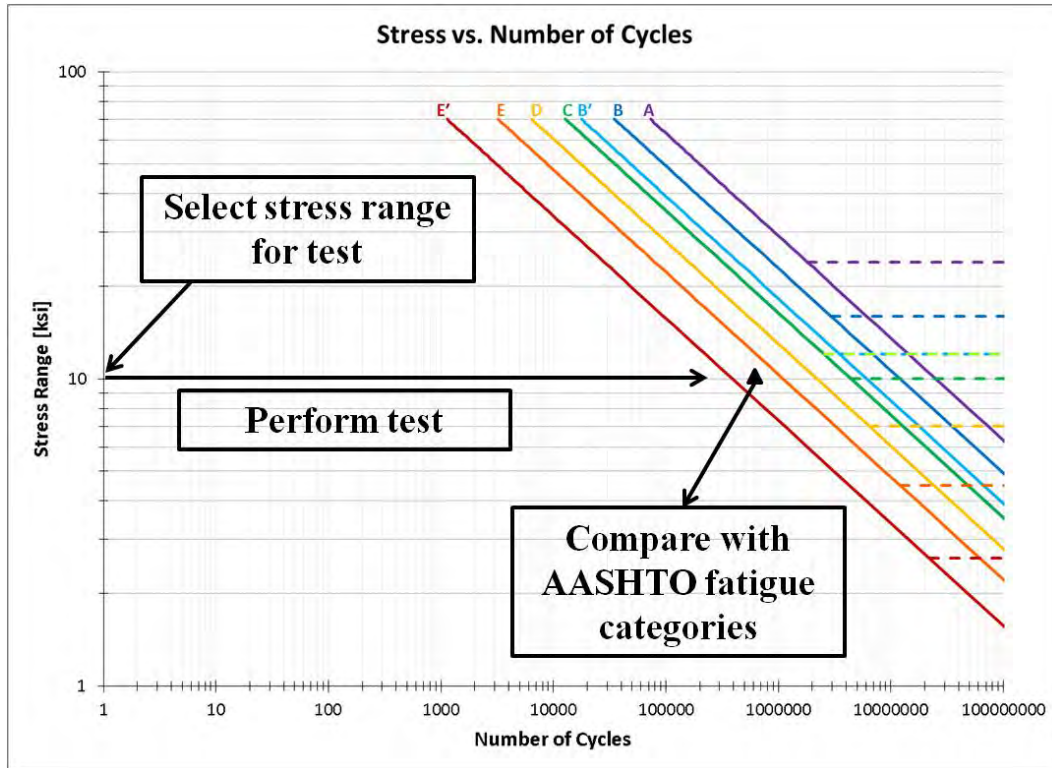


Figure 2.19: Fatigue Testing Procedure

2.6 Fatigue Behavior of Single Angle Members

The majority of steel bridge cross frames constructed utilize single angle members. The angles are typically welded to the gusset plates along only one leg of the angle, resulting in an eccentric connection. While the single angle detail has been used for numerous years, there is relatively little information on the corresponding fatigue performance. Fortunately, the eccentric single angle detail has not caused widespread fatigue problems within the cross frame bridges. However, as analysis tools become more advanced and the prevailing bridge codes allow more direct analysis, designers may begin to place higher force demands on the cross frames by using smaller cross frames with a larger spacing. It is important to therefore understand the behavior of this connection and the potential failure modes.

2.6.1 Effect of Angle Eccentricity

In a cross frame, forces are transmitted to the cross frame members from the girder via the gusset plate. Due to the eccentricity of the angle centroid from the gusset plate centroid, a moment is applied to the member in addition to the axial force. Figure 2.20 shows a typical angle to gusset plate connection alongside the associated bending that occurs when a uniaxial tension is applied to the gusset plates.



Figure 2.20: (a) Eccentric Connection of Angle and (b) Bending of Angle due to Eccentricity

The test shown in Figure 2.20(b) was performed as part of research conducted by McDonald and Frank [2009] for the American Institute for Iron and Steel. During the tests, lateral deformation of the angle was reported to be approximately 1 in at mid-length of a short 4 ft specimen.

2.6.2 Fatigue Classification of Single Angle Detail

Prior to 2012, there was little guidance given in the AASHTO LRFD Bridge Design Specification regarding the fatigue classification of the single angle detail. A Category E detail was recommended by the LRFD Design Manual for Highway Bridge Superstructures [Grubb et al. 2007], which takes into account the fatigue performance for shear on the throat of the fillet weld, but does not consider the geometric differences provided by the angle.

The current specification recommends the detail to be Category E, as referenced in AASHTO Table 6.6.1.2.3-1 [2012]. The table goes on to specify that fatigue stress range be based on the effective net area of the member, A_e , which includes a shear lag factor, U , as given in the following equations.

$$A_e = UA_g \quad (2.21)$$

where,

A_e = Effective area of the angle

U = Shear lag factor

A_g = Gross area of the member

$$U = 1 - \frac{\bar{x}}{L} \quad (2.22)$$

where,

- \bar{x} = Distance from the centroid of the member to the surface of the gusset or connection plate
- L = Maximum length of the longitudinal welds

The AASHTO code cites the research by McDonald and Frank [2009] regarding the behavior of the single angle connection, and specifies that the moment due to the eccentricities in the connections shall be ignored when calculating the fatigue stress range [AASHTO 2012].

2.6.3 Previous Fatigue Tests of Single Angle Detail

The research conducted by McDonald and Frank [2009] was motivated by the lack of laboratory testing performed on the single angle detail in fatigue. The research program consisted of three angle cross section arrangements, the L4x4x3/8 angle, the L5x3x3/8 angle with the short leg connected to the gusset plate, and the L5x3x3/8 angle with the long leg connected to the gusset plate. The angles were connected to the gusset plates with 5/16 in fillet welds, and the specimen longitudinal weld lengths were either “equal” or “balanced”. Equal means the weld lengths were the same along the outstanding leg and the horizontal leg. Balanced means the weld length along the horizontal leg was reduced so that the center of gravity of the weld resistance was in line with the center of gravity of the member [McDonald and Frank 2009].

The specimens were tested in a 550 kip MTS universal testing machine. Due to the large amount of bending resulting from the angle eccentricity (shown in Figure 2.20), there was concern the moment on the grips could cause damage to the test machine from cyclic loading during a fatigue test. Therefore, the tests were primarily performed with two specimens back-to-back. A spacer plate was positioned between the gusset plate ends to allow the angles to deform out-of-plane and to prevent the contact pressure between the plates from changing the force distribution on the angles. The gusset plate ends were also thicker than plates typically used in practice to ensure cracking occurred in the angle member [McDonald and Frank 2009]. The symmetric nature of two specimens tested back to back eliminated the impact of the bending from the eccentricity, which may have impacted the fatigue performance.

Results from the fatigue tests showed three types of failures: (i) cracking at the forward weld toe of the angle-gusset weld propagating into the toe of the horizontal leg of the angle; (ii) cracking at the forward weld toe of the angle-gusset weld propagating into the heel of the angle; and (iii) cracking at the end weld toe propagating into the gusset plate [McDonald and Frank 2009]. A summary of the crack locations is given in Figure 2.21.

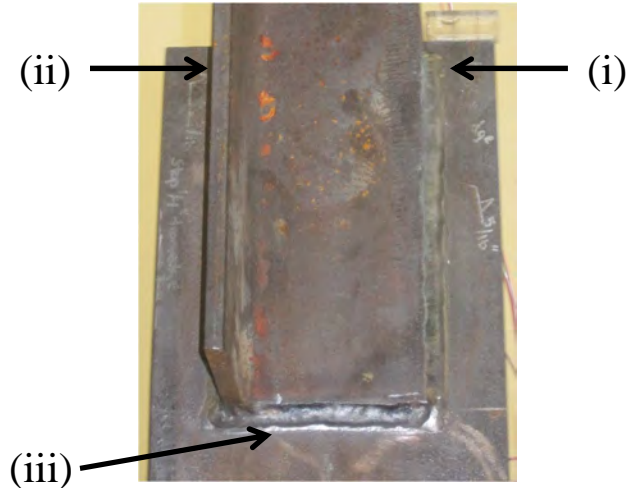


Figure 2.21: Single Angle Fatigue Crack Failure Locations

Analysis of the test data showed that calculating the fatigue stress range using the effective net area of the member, which accounts for shear lag in the connection, reduced the scatter of the results. The connections tested ranged from Category E' to Category D, with the majority of the connections classified as Category E' and Category E [McDonald and Frank 2009]. In particular, it is noted the specimens with “equal” weld length were primarily on the lower end of performance.

Tests on angle connections were also performed by Wilbur Wilson, and reported in Munse's *Fatigue of Welded Structures* [1964]. The geometry was much different than seen in typical cross frame construction, with the horizontal leg of the angle tapering from the width of the angle to the thickness of the angle over the connection length. Although being significantly different, fatigue performance of the connection was similar to the aforementioned results (Category E' to Category E) as discussed by McDonald and Frank [2009].

2.6.4 Discussion of Previous Fatigue Tests of Single Angle Detail

Although the tests conducted by McDonald and Frank [2009] seem to indicate that Category E' would represent an appropriate lower bound prediction of fatigue failure, the AASHTO specification still considers the detail as Category E [AASHTO 2012]. Perhaps considering the mean of the test data would justify this classification.

In addition, the previous tests had thicker gusset plates than typically used in cross frame construction and were tested back-to-back in the test machine to minimize the eccentric moment applied to the grips. It is theorized the stress concentration at the angle-gusset weld connection due to the increased bending that would occur as a result of thinner plates and allowing out-of-plane bending would further reduce the fatigue life of the single angle detail. In fact, the one test data point completed which allowed bending had the worst performance of all specimens tested [McDonald and Frank 2009].

Axial tests performed in the research of this project (Chapter 4) showed similar testing problems with the bending moment induced at the grips. The solution was to test the entire cross frame assembly in fatigue, using weld details and member sizes indicative of common plate girder design. The results of this test series are documented in Chapter 7.

2.6.5 Previous Finite Element Analysis (FEA) of Single Angle Detail

As part of the research conducted by McDonald and Frank [2009], an extensive parametric study was undertaken to determine the effect certain variables on the behavior of the connection. Following the DNV method for hot spot stress extrapolation, the stress concentration factor (SCF) at the forward edge of the fillet weld on both the horizontal and vertical angle legs (Locations (i) and (ii) in Figure 2.21) was determined, and the maximum value recorded. More information on finite element modeling for fatigue hot spot stress extrapolation is provided later in the chapter.

The results of the FEA study showed that the SCF increased as the thickness of the gusset plate decreased, following approximately linear behavior. According to the equation provided in Eq. (2.23), the SCF using a thickness of 1.5 in, corresponding to the tests performed, is 3.72 [McDonald and Frank 2009]. Using the typical 0.5 in gusset plates seen in construction, the SCF would be 4.21, an increase of 13%. The increase may contribute to reduced fatigue life.

$$SCF = -0.49x + 4.4542 \quad (2.23)$$

where,

SCF = Stress Concentration Factor

x = Gusset Plate Thickness

Further FEA showed the SCF to increase with increasing length of the outstanding leg of the angle. The outstanding leg increases the eccentricity, and although the stiffness of the angle is also increased, the eccentricity seems to significantly affect the behavior of the angle and heightens the effect of the stress concentration. This variable showed the greatest effect on the SCF [McDonald and Frank 2009].

Other variables had small effects on the SCF: increasing the gusset plate length slightly increased the SCF; increasing the angle length reduced the SCF; and increasing the angle thickness reduced the SCF. The gusset plate width, weld lengths, and horizontal angle leg width did not significantly change the SCF and no discernible trend was shown [McDonald and Frank 2009].

2.7 Fatigue Behavior of Transverse Fillet Welds

One aim of the research documented in this report is to provide alternative details that offer similar or improved fatigue performance compared to existing details. The T-stem and cast connections outlined in Chapter 2 require transversely loaded fillet welds to transfer the forces from the tubular members to the gusset plates. In addition to the advantages of the tube in compression, the concentric connection the tube provides may improve the fatigue strength of the diagonal members relative to angles. In order to make sure the fatigue behavior of the tubular members is superior, various methods of connecting the members were investigated, including the T-stem and cast steel connections.

One shortcoming of current design rules is the fatigue strength of fillet weld connections failing through the throat of the weld are based on data obtained from simple cruciform joints tested in tension under normal stresses [Maddox 2008]. Figure 2.22 shows a typical fatigue test on a cruciform joint, with the loading direction and failure crack indicated.

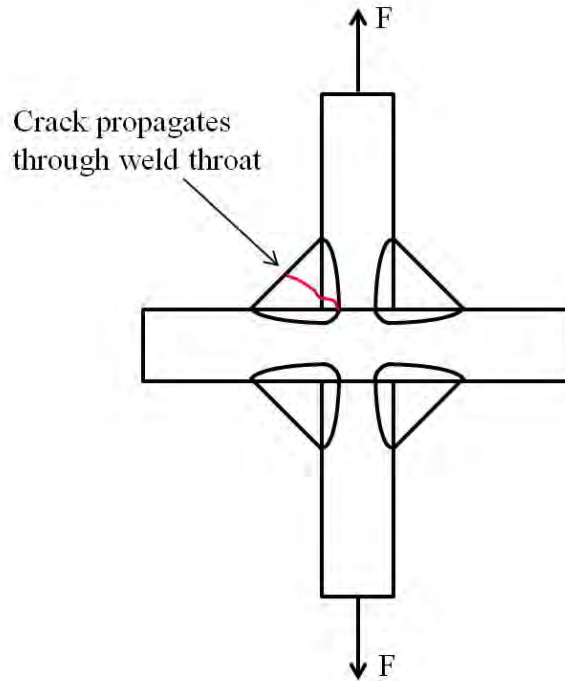


Figure 2.22: Typical Cruciform Joint with Fatigue Crack

Although useful, the cruciform joint test fails to include other factors that could affect the fatigue life of the joint, such as non-uniform stress along the length of the weld, bending/shear stresses on the weld throat, and the size of the unfused zone at the weld root [Maddox 2008]. In particular, due to the geometry of the T-stem connections, there is a stress concentration located along the weld near the stem of the WT.

Another factor is the effect of the unfused zone at the root for both the T-stem and cast steel connection. The cruciform joint can be compared to the classic fracture mechanics analysis of a uniformly loaded plate with a crack in it, with the thickness of the loaded plate being the width of the initial crack. Since the fillet welds to the tubular members will only be welded to the outside wall, the lack of connection at the weld root through the member thickness could lead to potential problems. Figure 2.23 and Figure 2.24 summarize these considerations.

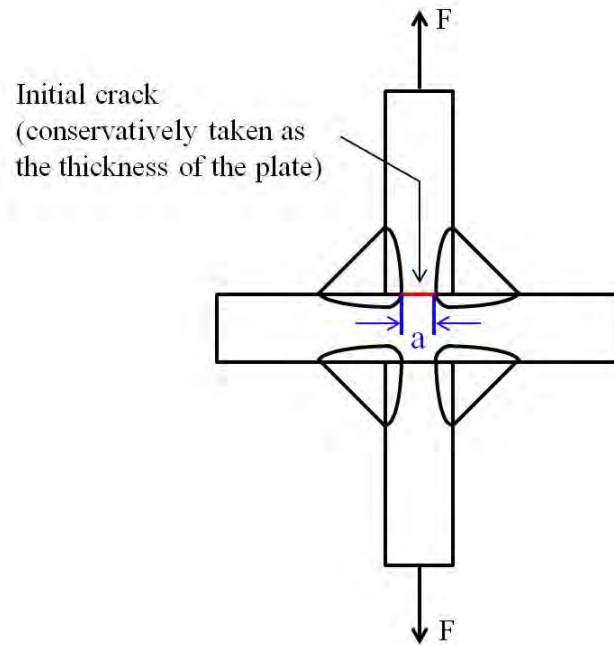


Figure 2.23: Comparison of Cruciform Joint to Uniformly Loaded Plate with Crack

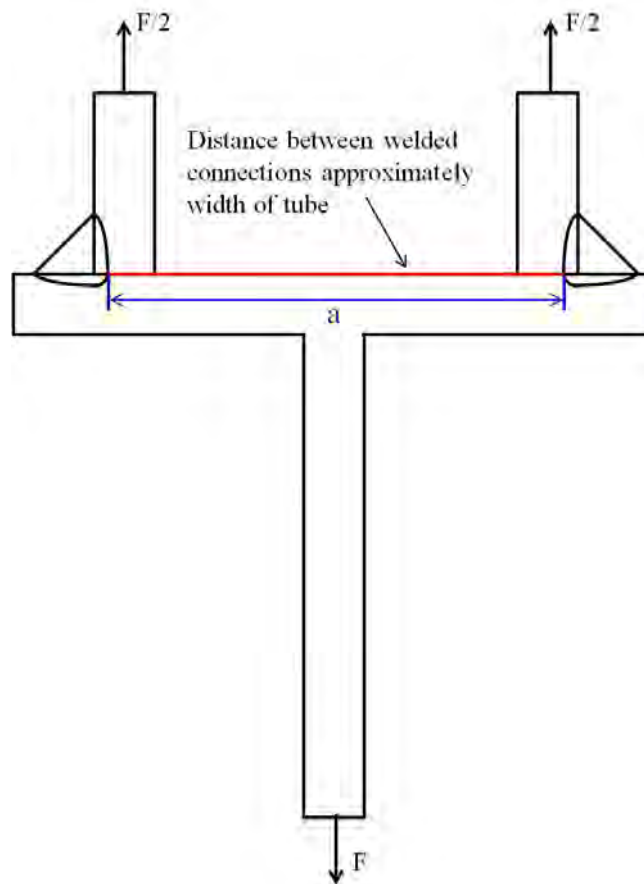


Figure 2.24: Lack of Weld Root Fusion Inherent to T-stem and Cast Steel Connections

Results from cruciform joint tests show that the fatigue strength is a function of the weld size, weld penetration, and plate thickness [Frank 1979]. Using the results of previous research in combination with fracture mechanics solutions, Frank [1979] proposes an equation to predict the stress range required to achieve a desired life in the welded joint. As the plate thickness becomes large, i.e. the distance between weld roots increases, the required stress range is reduced. The concern in a tubular connection is the distance between weld roots will not be the thickness of the tube; rather it will be the width of the tube.

Using the T-stem detail in the research, the fit-up of the connection was closely monitored. The ends of the tube were saw-cut and ground to create a flush interface between the tube and the WT flange. Previous research by Mori et al. [2000] reported that gaps up to 3 mm (0.118 in) in cruciform joints did not affect the fatigue performance of the connection [Maddox 2008].

While there may be potential problems for the fatigue resistance of transversely loaded fillet welds, the ease and availability of this detail made it worthwhile to investigate. Details from the tests are given in Chapter 4.

2.8 Fatigue Behavior of Knife Plate Detail

One way used to avoid eccentric connections in tubular members is to cut a slot in the tube, allowing the insertion of a gusset plate, which can then be welded in place and act as the connecting element. This procedure was selected for ease in the Wichita Falls, TX bridge retrofit (as discussed later in this chapter). However, there is evidence that this configuration may not have good fatigue performance due to stress concentrations at the end of the slot. An example of this type of connection is shown in Figure 2.25.

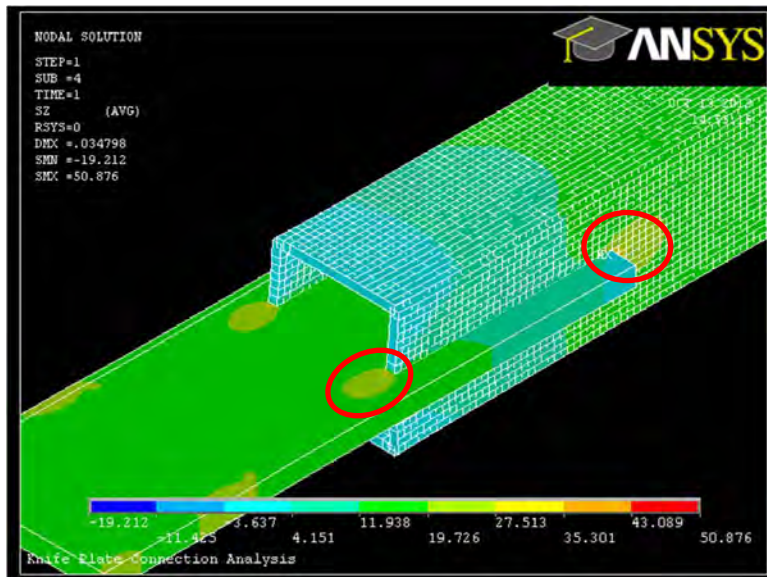


Figure 2.25: Knife Plate Connection with Stress Concentration Locations

The typical mode of tension failure in slotted end HSS connections is either circumferential tensile fracture of the HSS member or tear-out along the weld [Martinez-Saucedo and Packer 2009]. Tests have indicated that a significant shear lag exists in the detail connection

type, which makes the weld to the gusset plate become the critical section [Martinez-Saucedo and Packer 2009, Willibald et al. 2006].

Furthermore, tests presented by Liu et al. [2006] showed specimens with this type of connection failed in fatigue at a relatively low number of cycles. The fatigue stress concentration cracks typically formed in the HSS walls at the forward edge of the fillet weld connecting the HSS member to the knife plate [Liu et al. 2006]. The locations of these stress concentrations are given in Figure 2.25.

Due to imperfect fabrication and construction tolerances, it is difficult to obtain good fit-up between the end of the slot and the gusset plate. If the gap is large, it is often left unfilled and the knife plate is only connected by two longitudinal welds [Liu et al. 2006]. In general, it is impractical to try and fill this gap with weld material due to the aforementioned tolerances [Dowswell and Barber 2005]. In some cases, the area at the gap is drilled to reduce the stress concentration and possibly increase the fatigue life [Liu et al. 2006, Soderberg 2010].

The tests performed by Liu et al. [2006] involved both static and fatigue tests performed on HSS4x4x1/4 and HSS4x4x3/16 sections. The typical failure cracks originated at the forward ends of the fillet welds connecting the knife plate to the HSS member, with the cracks propagating into the HSS tube wall. The tests were performed at various stress ranges, and the effect of different knife plate thickness and slot lengths was investigated [Liu et al. 2006]. The number of cycles at first crack initiation was also recorded.

The knife plate connection tends to show evidence of failure at a very early stage in the cyclic loading history. The average time of first detection was 9% of the number of cycles at ultimate failure [Liu et al. 2006], showing that the connection, although cracking early, is fairly resilient and offers significant time for identification of fatigue cracks prior to failure.

The tests also showed thicker knife plates have a longer fatigue life at lower stress ranges and a shorter fatigue life at higher stress ranges when compared to a specimen that is 2/3 the thickness [Liu et al. 2006]. The previous finding indicates the stress concentration at the forward edge of the fillet weld causes the specimen data to not follow a slope of 3 on the standard S-N curve.

Another important finding from the research shows the slot gap between the HSS member and knife plate does not have a significant effect on the overall fatigue life of the specimens [Liu et al. 2006]. Therefore, while every effort will be made to ensure good fabrication techniques, small deviations will not affect the research results on these connections.

To improve the performance of the tubes cast steel nodes were considered in this study and are discussed in Chapter 4.

2.9 Tubular Braces in Literature

While tubular braces may not be commonly used in steel bridge design, there are a variety of structural applications where tubular members and braces have been used. The following sections highlight the documented use of tubular members.

2.9.1 Offshore Industry

Tubular members have long been the primary cross-section used in the construction of offshore platforms for the oil industry. Their increased strength in compression helps to resist the large overturning moments caused by waves acting on the structure. Also, because the tube is axisymmetrical, it helps to simplify the analysis as the tidal forces may act on the members from

any direction. Lastly, using tubular members helps to resist any torsional loads acting on the platform.

2.9.2 Concentrically Braced Frames

In addition to the offshore industry, tubular members have seen increased use in structures designed to resist earthquakes. Again, the superior strength of tubes in compression, as compared to other available structural shapes, is the motivating reason for their use.

2.9.3 European Bridges

Overseas, use of tubular members in structures has been steadily growing. One emerging type of bridge involves a three-dimensional steel space truss structure made composite with a concrete deck. The truss consists of hollow tubular members and is usually connected with cast steel nodes [Haldimann-Sturm and Nussbaumer 2007]. Tubular members have also been used as the primary support structures of arch bridges, such as the Humboldtshafen Rail Bridge in Germany shown in Figure 2.26 [FHA 2001]. Coincidentally, the steel bearing connections shown were cast specifically for this bridge.



Figure 2.26: Large Cast Steel Bearing in Tubular Arch Bridge [FHA 2001]

2.9.4 Wichita Falls, TX Bridge Retrofit

Tubular braces were also utilized in a recent retrofit to a curved steel I-girder bridge located in Wichita Falls, TX. Two three-span steel bridge units were constructed as part of a direct connector ramp to take traffic from northbound US-82 to westbound US-277. Each unit consisted of 235 ft end spans and a 250 ft center span, resulting in an unfavorable span ratio approaching 1.0. Due to site restrictions, these span ratios were necessary to accommodate support placement. In addition, the bridge had an 819 ft radius of horizontal curvature further complicating design [Turco 2009].

After placement of the concrete deck, excessive rotations were observed in the superstructure. To accommodate the design ramp speed, a cross slope of 6 percent was desired in the finished deck. However, survey measurements indicated the slope was significantly less than required, approaching a minimum of 1 percent near mid-length of the end spans [Turco 2009].

The existing cross frame system consisted of the X-type braces using L4x4x3/8 members and set at approximately 17 ft spacing. When the problems were discovered, further analysis using a finite element model was conducted, revealing torsional flexibility in the system as a result of the disadvantageous span arrangement as well as high length-to-width ratio [Turco 2009].

To solve the problem, a retrofit was necessary requiring removal of the concrete deck over the end spans. Shore towers were then installed and the bridge was jacked into proper position, followed by the addition of a lateral truss connected to the bottom flange as shown in Figure 2.27. Once the concrete deck was placed and hardened, the bottom flange braces formed a quasi-closed box with significant torsional stiffness compared to the open I-girder system. Because some members of the braces may experience significant torsion, HSS 6x6x5/8 tubular braces were selected. The connection detail consisted of a split tube connection also shown in Figure 2.27. The torsional stiffness of the retrofitted bridge proved to be significantly higher than the open I-girder system [Turco 2009].



Figure 2.27: Tubular Bracing Retrofit of Curved Steel Bridge in Wichita Falls, TX with Close-up of Connections [Turco 2009]

2.10 Advantages of Tubular Members

Tubular members offer several advantages over the use of other readily available structural shapes. The behavior of tubes is well understood, allowing a more accurate prediction of structural forces and deflections as compared to angles, which are subject to biaxial bending. Tubular members are available in a wide array of sizes, allowing the designer to select the appropriate cross-section for a given application.

2.10.1 Compression Capacity

The main reason for selecting tubular members for use in steel bridge braces is to allow the use of a single diagonal cross frame layout. In order to provide an effective torsional brace, the single diagonal needs to handle both tension and compression, depending upon the buckling direction. For unbraced lengths on the order of 12-15 ft, tubular cross-sections are the most efficient way to resist these forces and provide an adequate design.

2.10.2 Fatigue Behavior

In addition to the advantages of the tube in compression, the fatigue strength of the diagonal members should also be improved relative to angles. In order to make sure the fatigue behavior of the tubular members is superior, various methods of connecting the members will be investigated. By using the tubular members, this eccentricity is avoided as a connection passing through the centroid is possible.

Slotted-Tube Detail

One way used to avoid eccentric connections in tubular members is to cut a slot in the tube, allowing the insertion of a gusset plate, which can then be welded in place and act as the connecting element. This procedure was selected for ease in the Wichita Falls, TX bridge retrofit (Figure 2.27). However, there is evidence that this configuration may not have good fatigue performance due to stress concentrations at the end of the slot.

The typical mode of tension failure in slotted end HSS connections is either circumferential tensile fracture of the HSS member or tear out along the weld [Martinez-Saucedo and Packer 2009]. Tests have indicated that a significant shear lag exists in this connection type, which makes the weld to the gusset plate become the critical section [Martinez-Saucedo and Packer 2009, Willibald et al. 2006]. Furthermore, tests presented by Liu et al. [2006] showed specimens with this type of connection failed in fatigue at a relatively low number of cycles.

To improve the fatigue and fracture performance of the tubes with the slotted end connection, properly designed cast steel nodes are a viable alternative.

2.11 Steel Castings in Literature

Historically, steel castings were once relatively common in structural engineering applications when complex connections were required. However, with modern welding technology, fabricated connections using wrought steel materials became more economical, significantly reducing the use of castings in structural engineering [de Oliveira 2006]. A lack of knowledge in the behavior of steel castings has caused most engineers today to be hesitant of using castings in design. The following case studies document some current uses of steel castings and the advantages cast steel can offer.

2.11.1 Greenbank Telescope

One modern application of steel castings is concerned the construction of the Green Bank Radio Telescope shown in Figure 2.28. Due to the complex geometry and large number of connections, steel castings provided an economical solution to simplify construction of the telescope.



Figure 2.28: (a) Green Bank Radio Telescope and (b) Steel Casting

2.11.2 Earthquake Connections

Perhaps the most predominant use of steel cast connections occurs in seismic applications. These castings are designed to help column bracing resist earthquake forces as well as aid in retrofitting steel members after an earthquake event. Two examples are provided in this section.

Kaiser Bolted Bracket

The Kaiser bolted bracket, developed by Steel Cast Connections, Lehigh University, and IFC Kaiser Engineers, is a high-strength, haunched steel bracket designed to connect the flanges of a beam to a column [Adan and Gibb 2008]. The brackets, which are bolted to the column and either bolted or welded to the beam, were engineered so that yielding and plastic hinge formation occurs primarily in the beams at the tip of the bracket. The brackets come in various sizes and are proportioned to handle the probable moment required to fully yield the beam cross-section [Adan and Gibb 2008].

Cast ConneX

Similarly, Cast ConneX has developed high-strength cast steel connections for use with concentrically braced frames comprised of HSS members (Figure 2.29) [de Oliveira et al. 2008]. These connectors are designed to handle the expected forces developed in the HSS brace during a seismic event. This protocol ensures the brace member will yield or buckle prior to connection failure allowing the connections to be prequalified by AISC for use in seismic applications. This behavior is important because yielding and buckling are the primary methods concentrically braced frames dissipate energy from the earthquake [de Oliveira et al. 2008].

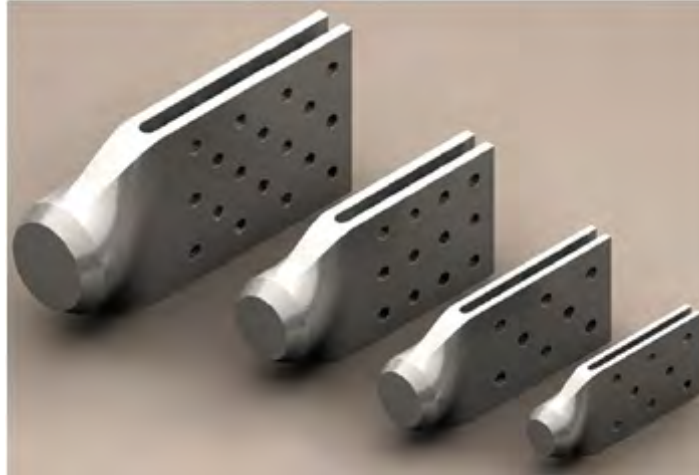


Figure 2.29: Cast ConneX Cast Steel Connections [de Oliveira and Stine 2008]

2.11.3 Crane Connections

Lastly, cast connections have been used in the construction industry to aid in the assembly of large tower cranes. By using a pin-type end connector welded to the ends of steel tubular members, construction workers can quickly piece together the support structure for large tower crane. In addition, the simplified connection helps avoid confusion on the job site [Soderberg 2010]. A sample of the connection is shown in Figure 2.30.

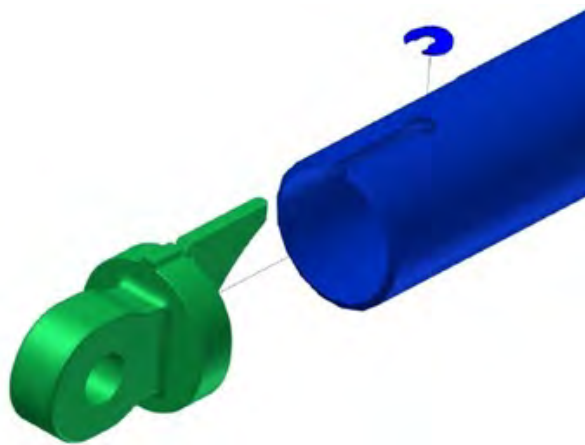


Figure 2.30: Cast Steel Connection used in Tower Crane Construction [Soderberg 2010]

2.12 Advantages of Steel Castings

Since cast steel connections are formed from liquid metal, complex geometries can be fabricated. Moreover, steel castings can be designed to specific applications, potentially allowing the inclusion of items like holes for erection bolts or increased thicknesses to facilitate welding. This ability has the potential to greatly reduce fabrication and construction time.

The economy of steel castings will also improve as the necessary quantity increases. Typical current practice involves creating a prototype of the connection from a plastic polymer

or metal. The prototype part is then placed in a mold box, where chemically treated sand is inserted and compacted. Once the sand is hardened, the pattern is removed to form a negative space, where ultimately the molten steel will be poured to create the final product [Steel Founders' Society of America 2009]. It is evident from the creation process that once an initial prototype is engineered and created that the part can be easily mass produced.

2.12.1 Fatigue Behavior

Due to the geometric flexibility of casting liquid steel, castings can be tapered to create smooth transitions, minimizing stress concentrations and improving fatigue performance. Experimental tests conducted by Haldimann-Sturm and Nussbaumer [2008] showed the fatigue behavior of tubular members with cast nodes were governed by the fracture resistance of the butt welds used to connect the two components.

2.12.2 Efficient Use of Material

Because steel castings are designed for specific applications, the required steel material can be optimized, resulting in the most efficient use of the material. Accordingly, material can be added to lower the stress in the part, which can also aid in improving fatigue behavior.

2.12.3 Seals Tube

One of the most important tasks accomplished by the cast steel connection is the sealing of the tube. If the tube is open to the atmosphere, rain, dirt, debris, animals, and insects are capable of getting inside the tube, potentially decreasing the corrosion resistance of the metal. Moreover, because the corrosion would work from the inside of the tube, a visual inspection of the member would not reveal any structural deficiency. Thus, it is important to develop a cast connection which will isolate the inside of the tube from the elements.

2.12.4 Standardization

Lastly, the use of steel castings is only economically feasible when large amounts of castings are required. As a case study, the direct connector linking Texas SH 71 East with Texas SH 130 North was examined. The connector consists of 10 steel spans of varying length and 4 I-girders across. The following calculations summarize the quantity of steel castings that would be required for this project.

107 cross frame lines

x 3 cross frames

321 cross frames

321 cross frames

x 6 connections

1926 Cast Connections

With such a large number of cross frame connections, steel castings could greatly reduce the time necessary to construct these braces. Furthermore, the casting can be designed to handle

more than one tubular cross-section, allowing its use in potentially all cross frames in steel bridges. As TxDOT Project 0-6564 continues, standardization of the cast connection will remain an important task to accomplish. Computational modeling will be the main tool used, allowing the researchers to determine an expected range of forces in the cross frame members, and then to design the casting to accommodate tubular sections that can withstand those forces.

2.13 TxDOT Design Practice

In conversations with various TxDOT bridge engineers, it seems the current TxDOT selection of cross frames utilizes conservative “rules of thumb” to initially size the cross frame members. Based upon a known girder spacing and depth, the engineer selects an appropriate size member for the chosen cross frame layout. While, the X-type brace configuration is the most common for newly constructed steel I-girder bridges, other brace orientations may be selected and members sized accordingly. Similar practices are used to layout the locations of the cross frames. Once the geometry has been finalized, computer models are used to verify the cross frame layout and the cross frame members are adequate.

When looking at the TxDOT standard plans, three typical angle sizes are utilized for cross frames [TxDOT 2006]. The angle properties are given in Table 2.4, assuming A36 Grade steel which is common in angles.

Table 2.4: Standard Angle Sizes and Properties

Angle Size	Area	Tension Capacity
L4 x 4 x 3/8	2.86 in ²	92.7 k
L5 x 5 x 1/2	4.75 in ²	154 k
L6 x 6 x 9/16	6.45 in ²	209 k

The angle sizes listed are to be used in cross frames for depths of 52 in to 96 in with varying spacing [TxDOT 2006]. For a baseline comparison between the strengths of tubes and angles, a typical brace diagonal length of 13 ft will be assumed. This would approximately correspond to the extreme case of a 96 in depth, along with a 120 in girder spacing. From various plans of recent steel bridge construction provided by TxDOT, this diagonal length seems to be a reasonable benchmark. The comparison given in Table 2.5 indicates the approximate size of the tubes that are necessary to deliver the same performance as the angles. Recall, the angle systems are designed as tension-only braces. Therefore, if a one tube diagonal is to replace two angle diagonals, the tension and compression strength of the tube needs to meet or exceed the tension strength of the angle. The buckling strength of the HSS sections of Table 2.5 were determined from the AISC manual [2005] assuming a buckling length coefficient $k = 1.0$ and using LRFD values. This condition corresponds to a member with pinned ends.

Table 2.5: Angle Tensile Strength vs. Tube Buckling Strength

Angle Size	Angle Capacity (36 ksi)	Tube Size	Tube Capacity^{1,2}
L4 x 4 x 3/8	92.7 k	HSS 5 x 5 x 3/16	88.6 k
		HSS 5.563 x 0.258	99.6 k
L5 x 5 x 1/2	154 k	HSS 5 x 5 x 3/8	160 k
		HSS 5.563 x 0.375	139 k
L6 x 6 x 9/16	209 k	HSS 5 x 5 x 1/2	199 k
		HSS 6.000 x 0.500	207 k

1. Tube capacity was calculated using a length of 13 ft

2. Yield stress (F_y) is assumed to be 46 ksi for square tubes and 42 ksi for round tubes [AISC 2005]

Chapter 3. Background on Steel Castings

3.1 Steel Casting Types

One of the objectives of this research project was to investigate the feasibility of using steel castings as connections for tubular members in cross frames. This chapter provides background information on steel castings and discusses the development of prototype castings for possible use in bridge cross frames.

Steel castings can offer several advantages over conventional fabricated steel connections. The primary advantage, since cast steel is poured into a mold, is that it can easily accommodate complex geometries. The final shape of the casting can be engineered for its particular application, therefore allowing more efficient use of the steel material and reducing stress concentrations, which can lead to better fatigue behavior. In addition, the mechanical properties of cast steel are isotropic, which is beneficial in cases where three-dimensional states of stress could present a problem for design [de Oliveira 2006]. Finally, in situations where the casting design can be standardized, such as for the proposed cross frame connection, the casting can potentially become a cost competitive alternative to the normal fabricated connection.

3.1.1 Investment Casting

While there are a variety of methods available for casting steel, the two main types identified for possible use with creating a connection for tubular cross frame braces were investment casting and sand casting.

Investment casting, also referred to as the “lost-wax” method (Figure 3.1), begins with a pattern matching the final shape of the cast part that is created from an expendable material such as wax or plastic. The patterns are invested in a ceramic slurry, which hardens to create a shell encasing the parts. Next, the wax or plastic is melted to leave the ceramic shell hollow. The cast steel is then poured into the shell to solidify into the final product.

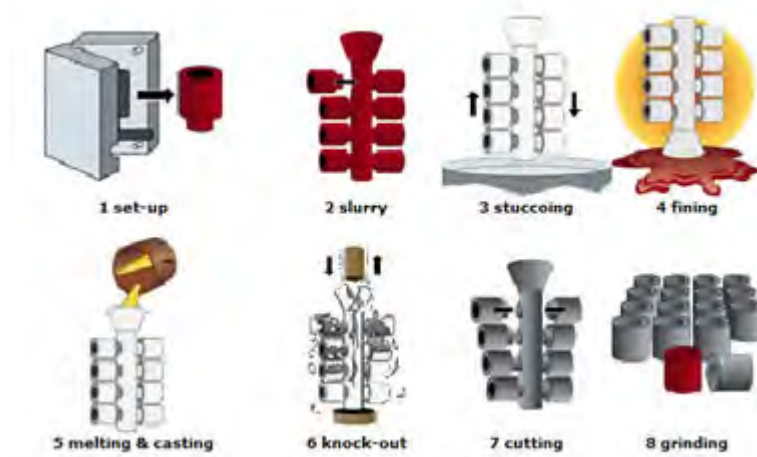


Figure 3.1: Investment Casting Process [Ningbo Yinzhou KST 2010]

One advantage to using investment castings is the ceramic shell better controls the geometry of the final part, resulting in lower geometric tolerances and better quality surface

finish as compared to sand castings. However, investment castings tend to be more expensive per unit weight and are limited to overall size. Investment castings are often cast along a “tree” with the final parts branching off from the main portion. The arrangement of the parts limits the weight of each casting. While de Oliveira [2006] reports investment castings can weigh up to 154 lb (70 kg), the facilities investigated in Texas had weight limits near or below the approximate weight of the prototype connection, about 45 lbs. Furthermore, the process is more time-consuming than sand casting, which translates into increased cost. Therefore, sand casting was the process selected for the cast connection for TxDOT Project 0-6564.

3.1.2 Sand Casting

Sand casting receives its name from the green sand often used to create the molds. Sand casting begins with a pattern, typically constructed from wood, which is used to form a negative shape of the finished casting in the sand mold. The flexibility in creating the sand molds allows the castings to weigh from only a few pounds up to several tons and to be virtually any shape. The following section further explores the steel casting process and provides detailed information on the manufacture of the cast steel connection proposed for use with tubular cross frames.

3.2 Steel Casting Process: Pattern Construction

The steel casting process begins with identifying a foundry capable of producing the desired part, in this case, the cast steel connection for use with tubular cross frame members. While many foundries specialize in bronze and aluminum castings, fewer foundries specialize in steel castings, particularly structural grades of steel. The project team identified Quality Electric Steel Castings, a foundry in Houston, TX, as suitable for the needs of the project. Their previous work on suspension bridge hanger attachments and drawbridge bearings showed they had experience with the transportation industry and were capable of producing steel grades for structural applications.

In order to better understand the creation of steel castings, multiple site visits to Quality Electric Steel Castings were conducted. During the visits, foundry engineers and sales representatives met with the project team to discuss the feasibility of using cast steel connections for cross frames and to provide more detailed information on the steel casting process. The following outline of the steel casting process represents information that was gained through tours of the foundry, including the pour of the cast connections.

3.2.1 Working with the Foundry

The first stage of creating a steel casting is to develop a good relationship with the foundry. As with any project, good communication will decrease the time required to finish the job. The engineers at the foundry know the limitations of the equipment and can provide useful knowledge towards developing an optimized design for the casting.

In addition, it is important to coordinate the design of the casting. The foundry will need to design the gating system for each particular casting. The gating system simply refers to the delivery path of the molten metal to the cavity in the mold eventually becoming the completed part. The foundry has software which models the solidification of the casting to assist in the gating system layout. Using the software, the foundry can analyze the casting geometry and provide feedback on how to streamline the casting process to make the part more easily created.

3.2.2 Constructing the Pattern

The next stage of creating a casting is to make the pattern representing the finished part. The pattern is a three-dimensional model which contains all the features desired in the completed part. In terms of geometry, the pattern is usually slightly over-sized to offset the effects of shrinkage, which will cause the part to reduce in size as the liquid metal solidifies. Also, the patterns typically represent only half of the completed part. The halves will be used individually to create sand molds, so that when the two molds are matched together, the vacant space remaining will become the completed part. More information on the structural design and analysis of the steel casting can be found in Chapter 4.

Plastic Prototypes

Rapid prototyping is one method that can be employed to create patterns. There are various kinds of prototyping machines, but the majority will create three-dimensional plastic parts from a solid model computer file. Aside from pattern production, the plastic models can be a useful tool when discussing ideas with the foundry engineers, as it clearly indicates the design and function of the final product.

Prototypes of the cross frame connection for TxDOT Project 0-6564 were created in conjunction with the Mechanical Engineering Department at the University of Texas at Austin. First, the solid model of the connection was created using the computer drawing software SolidWorks 2010. From the program, the solid model was exported as an .stl file type, which takes the original solid model and creates a three-dimensional representation using small triangular elements. The file was uploaded into a software associated with the prototyping machine that divided the cast connection volume into thousands of 0.003 inch cross-sectional layers. These layers would be created sequentially by the prototyping machine to create a solid volume. The machine used was a 3D-Systems Sinterstation using selective laser sintering (SLS) technology and is shown in Figure 3.2.



Figure 3.2: Rapid Prototyping Machine

Once the computer files were input into the prototyping machine, the machine built-up the part in layers. The roller shown in Figure 3.3(a) delivers a 0.003 in thick layer of plastic

powder to the center bay. Next, the laser of Figure 3.3(b) lowers, and will move around the powder layer, melting the specific portions to become the hardened prototype. The laser retracts, the center bay lowers, and another layer of powder is placed. This process repeats until the prototype is complete.



Figure 3.3: (a) Roller and (b) Laser

Upon completion, the part remains in the machine to allow it to cool to a reasonable handling temperature. When it is ready, the plastic powder block is removed from the machine and the completed prototypes can be cleaned using brushes and compressed air as seen in Figure 3.4. An example of a finished cross frame prototype is shown in Figure 3.5.



Figure 3.4: (a) Removal of Powder Block and (b) Cleaning of Prototype



Figure 3.5: Prototype of Cross Frame Connection

While the plastic prototypes are easy to construct, the foundry did not recommend them for use in the sand casting process. Primarily, the plastic prototypes do not make a very good impression in the sand molds, which results in a relatively poor surface condition. Additionally, the means by which the sand is packed into the pattern box to create the mold would most likely damage the pattern, making it unusable for future castings.

Wooden Patterns

The most common patterns used are created from hard woods, such as pine, oak, and mahogany. Pine is the least expensive option of the woods, however, as the pattern is continually used, it is most likely to lose its original shape. On the other hand, mahogany will not degrade as quickly as pine, but it is more costly to create. At Quality Electric Steel Castings, the patterns are created by a separate vendor who works in conjunction with the foundry. Completed patterns are usually coated with a special primer to protect the surface quality. For the preliminary cast steel connection design, a wooden pattern constructed from pine was selected as most economic since the connection will be tested, and the design perhaps changed, prior to final recommendations. The wooden pattern is mounted in a pattern box for the sand mold making process, as shown in Figure 3.6.



Figure 3.6: Wooden Pattern for Use in Sand Casting

Polyurethane Patterns

The most durable type of pattern is made from polyurethane. While it is expensive to initially produce, foundry engineers indicated these patterns show almost no signs of degradation and ultimately produce the best quality castings. These patterns are most beneficial for high volume castings as the pattern would not need to be replaced frequently, if at all. An example of a polyurethane core box is shown in Figure 3.7.



Figure 3.7: Polyurethane Core Box

3.3 Steel Casting Process: Sand Mold Formation

The next major stage in the steel casting process is to create the sand mold which will be used to form the steel casting. The sand mold contains the negative image of the pattern, so that when the molten steel is poured, it will fill the cavity and harden into the desired part geometry. The procedure begins with transporting the pattern box to the sand mold assembly line, where it will be filled with sand slurry.

3.3.1 Sand Slurry Composition

The slurry used at Quality Electric Steel Castings is a combination of sand from a source in Arkansas and iron oxide, which is mixed with a binding agent, causing the sand to harden to a brick-like consistency. The foundry takes great care in selecting the sand for use in the molds as the grain size plays an important role in the surface condition of the casting.

The raw sand must be passed through a series of sieves to separate the grains according to diameter. Very fine grains are undesirable because collectively, they have a very large surface area. As the sand is mixed with the binding agent, sections with very fine grains will tend to be moister, and the binding agent may not completely burn away when preparing the casting surface. On the other hand, grains with larger diameters are likely to create an irregular geometrical profile on the surface of the sand mold, thus directly affecting the surface quality of the casting. Additionally, sections with large grains will be more porous, potentially allowing the molten liquid steel to seep into the sand. The foundry did not specifically report which grain sizes are used, as that information is considered proprietary. For good compaction and strength, it is recommended the washed and dried sand have at least 85% of the sand on four adjacent screens and an American Foundry Society grain fineness number of approximately 55 [Totten et al. 2004].

Iron oxide is mixed into the sand to provide strength. The sand molds are lifted, rotated, and transported many times prior to casting. Additionally, the sand needs to support the weight of the casting during the pour. The iron oxide helps to distribute these forces without cracking the hardened sand.

Once the iron oxide and green sand are mixed, the binding agent, a phenolic urethane resin, is added. Phenolic urethane resins are advantageous to use because they have a low viscosity, allowing them to more efficiently coat the sand [Totten et al. 2004]. Typically, the phenolic urethane resins are a three part system: Part I is a resin comprised of approximately 45% solvents and 55% solids by weight; Part II is a polymeric isocyanate; and Part III is a catalyst [Totten et al. 2004]. Phenolic urethane resins are common in “no-bake” systems, meaning the sand molds will cure without additional heat.

3.3.2 Forming the Raw Sand Mold

After the sand slurry is mixed, it is immediately poured into the pattern boxes to make the sand molds. Various methods of consolidating the sand are employed, including the use of vibratory compactors, as well as manual force. Figure 3.8 (a) shows an example of a pattern box which is then filled with sand using the depicted machine. Figure 3.8 (b) shows the pattern box on vibratory rollers, while the worker finishes the top.



Figure 3.8: (a) Pouring Sand Slurry into Pattern Box and (b) Compacting Sand Mold

Once the sand has cured, about 3-5 minutes for the prototype cross frame connection, the pattern box is flipped onto a piece of plywood to remove the sand mold, revealing the hollow cavity which will eventually become the finished steel casting. The sand molds are brushed to remove any loose sand, and air-blown to remove all loose grains. A file is used to create extra vents along the parting line to allow hot gases to escape during casting. Figure 3.9 shows the pattern removal and sand mold preparation for the cross frame connection.



Figure 3.9: (a) Removing Pattern from Sand Mold and (b) Adding Vents along Parting Line

3.3.3 Coating the Sand Mold

The next stage is to coat the sand mold to seal the surface, preventing the liquid metal from seeping into the sand. Smaller molds are suspended over a basin while workers use a low-pressured hose to flow coat the mold. Flow coatings consist of two main parts, a refractory material and a carrier. In the cast steel industry, the refractory material is usually zircon (zirconium silicate) and the carrier is either water or alcohol based [Brannon et al. 2001]. Flow coating allows both a surface and sub-surface coating to form. The surface coating helps to improve the surface finish of the casting, while the sub-surface coating fills in the voids in the

sand to prevent seepage of the molten metal [Brannon et al. 2001]. Figure 3.10 (a) shows the application of the flow coat to the sand mold.

Once coated, the sand molds continue down the assembly line to dry. If the foundry uses an alcohol-based carrier in the flow coat (such as isopropyl alcohol), the mold can be burned to eliminate the alcohol and to harden the coating. Figure 3.10 (b) shows the burning of the sand mold.



Figure 3.10: (a) Flow Coating the Sand Mold and (b) Burning the Sand Mold

3.3.4 Creating the Sand Cores

In addition to the sand molds, cores are required for castings containing hollow sections. The cores are made from sand in a similar manner to the sand molds, and are set in the completed sand mold. Large cores often contain steel rebar for reinforcement as the sand cores must be strong enough to resist the loading effect of self-weight when it is lifted and moved into place.

Smaller cores, like the ones necessary for the proposed cast steel connection, do not require reinforcement and are simply made by filling the core box with the sand slurry, and allowing the core to cure. Once completed, the cores are positioned in the main sand mold, attaching to nonessential portions of the mold. Examples of cores are shown in Figure 3.11.



Figure 3.11: (a) Cores used for Cross Frame Connection and (b) Large Sand Core

3.3.5 Completing the Sand Mold

The final stage in the preparation of the sand mold is to join the two halves of the mold. First, any cores required for the mold are placed in the drag, and glued into place, as illustrated in Figure 3.12 (a). Note the taper on the core which helps to lock it into place in the sand mold, preventing it from shifting during the pour.

Glue is also spread along the top of the drag to bond to the cope, which is flipped over and lowered on top to complete the mold, as shown in Figure 3.12 (b). Finally, clamps are inserted into the sand on either side of the parting line and tightened to create a good seal. The sand molds are then moved to the pouring line.



Figure 3.12: (a) Setting the Cores and (b) Closing the Sand Mold

For very large castings, the sand molds are coated by hand using paint brushes and rollers, rather than hosed down with the flow coat, primarily because they cannot be suspended to allow the flow coat to drain properly. Similarly, these molds are burned to remove the carrier agent, cores are set into place, and the cope and drag are united. Some large sand molds are surrounded by formwork and bound with metal straps to resist the hydrostatic force of the molten steel.

3.4 Steel Casting Process: Pouring the Steel

The third major stage in the steel casting process is the actual pouring of the molten steel into the sand molds to create the desired part. Due to the large amount of electricity required for this operation, Quality Electric Steel Castings pours steel overnight when the electricity demand is lower.

3.4.1 Melting the Steel

Depending upon the size of the job, steel is either melted in a large electric arc furnace or a smaller induction furnace according to the desired chemistry of the completed product. The foundry adds scrap steel of known chemical content to the furnace in order to produce a steel close to the material grade specified by the customer.

The electric arc furnace operates by running a large current through three carbon electrodes. The electrodes, which can move up and down vertically, are positioned to allow a small gap between the electrode tip and the steel, very similar to the procedure used in welding. When the current is turned on, an electric arc will connect the electrode tip and the steel. The arc is extremely hot (over 5400°F (3000°C)) and will quickly melt the steel [Lye 1989]. The electrodes are shifted up and down to melt all the steel in the furnace. As the arcs continuously jump around inside, the steel is also mixed, ideally leading to a homogenous mixture.

On the contrary, induction furnaces do not use electric arcs to melt the steel. Instead, the scrap steel is set into a crucible, which has an induction coil surrounding the perimeter. Alternating currents are passed through the coil creating alternate magnetic fields in the crucible. The result is an extreme amount of heat being developed in the scrap steel, enough to melt it. The alternating magnetic fields also help to mix the steel into a uniform composition [Lye 1989].

An example of an electric arc furnace and an induction furnace is shown in Figure 3.13. For the first round of castings, the small induction furnace was used since its capacity better met the needs of the project.



Figure 3.13: (a) Electric Arc Furnace and (b) Small Induction Furnace

3.4.2 Checking the Chemistry of the Steel

As the steel melts, workers monitor its chemical composition until the specified alloy of steel is achieved. Samples are taken with a small ladle, then poured into small cups made from sand, similar to the sand molds. These samples are typically submerged in water to cool and are taken to a spectrometer to perform a chemical analysis. Figure 3.14 shows a worker taking a sample from the molten steel, and what the sample looks like after it cools and is ready for analysis.

More information regarding the chemical analysis is provided later in this chapter in Section 3.7.1.

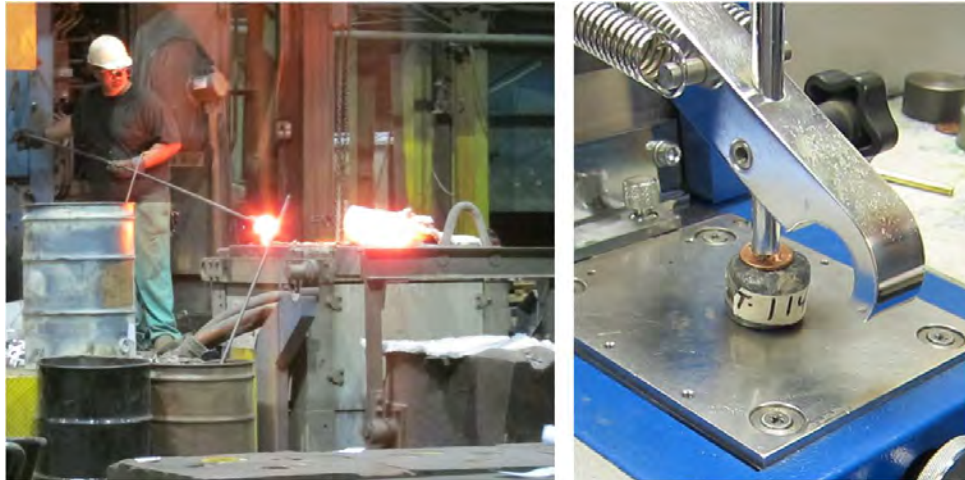


Figure 3.14: (a) Sample Taken from Furnace and (b) Cooled Sample for Chemical Analysis

3.4.3 Checking the Temperature of the Steel

The temperature of the steel plays an important role in the quality of the casting as well as in the design of the gating system. The gating system simply refers to the path the steel will take from when it is poured into the sand mold until it fills in the part cavity (more information on the gating system is given in Section 3.4.4). Using software designed for temperature and flow analysis, the foundry will design the gating system to deliver steel into the cavity at a specific velocity as well as temperature. If the flow rate is too fast, it is possible that turbulent flow will result, damaging the surface of the sand mold and decreasing the smoothness of the finished part. Turbulence can also cause sand inclusions in the cast metal. If the steel is not at the proper temperature, it will not flow properly, possibly cooling before the entire mold is filled as shown in Figure 3.15.



Figure 3.15: Example of Steel Casting with Incomplete Run-Out

Workers will check the temperature of the steel using a large thermometer specially designed and calibrated for the high temperature of the molten steel. Typically, the steel will be between 2700°F and 3000°F when it is considered ready for pouring. The steel is poured from the furnace into large ladles, which are lined with a special refractory material that protects them from the molten steel and will allow various gases to escape. Figure 3.16 (a) shows a typical ladle used at Quality Electric Steel Casting. Figure 3.16 (b) shows the molten steel from the small induction furnace being poured into a ladle.



Figure 3.16: (a) Ladle and (b) Pouring Steel into Ladle

3.4.4 Pouring the Steel

The ladle containing the molten steel is transported by crane to the pouring line. Some ladles have an opening in the bottom through which the steel will flow, while other ladles are tilted, allowing the steel to flow over the top rim. Either way, the steel enters the gating system of the sand mold, which is set up to control the flow of the steel to the casting. The gating system is designed by the foundry for each particular casting and consists of the pouring cone, pour box, runners (sluices), gates, and risers. Using temperature and flow analysis software, the foundry determines the optimum sizes to use for the gating system to feed the casting. A schematic of the gating system is shown in Figure 3.17.

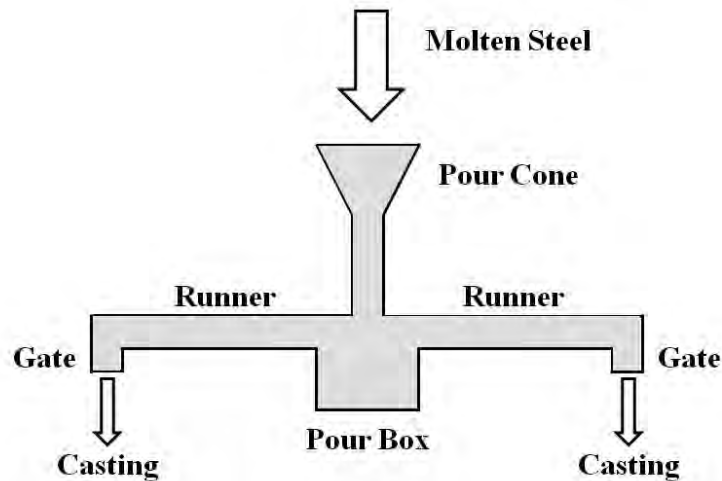


Figure 3.17: Gating System

First, the steel enters the pour cone, which helps to funnel the liquid steel into a smaller channel. The pour box helps to control the flow by reducing turbulence, and gradually fills up until the steel heads down the runners to the gates, eventually entering the casting.

Good casting designs utilize directional solidification which causes the part to cool incrementally from one side to another. Thicker sections of the casting can sometimes cause problems because they will be the last to become solid. Risers can be placed above these sections to provide a constant hydrostatic head of molten steel to the region of the casting that will cool last. The placement of the risers prevents large voids from forming in the casting due to shrinkage. Since the risers are designed to be the last section to harden, the shrinkage void will therefore lie in this region and not in the casting, and can subsequently be removed. For the first cross frame prototypes, the foundry used one riser placed as shown in Figure 3.18.

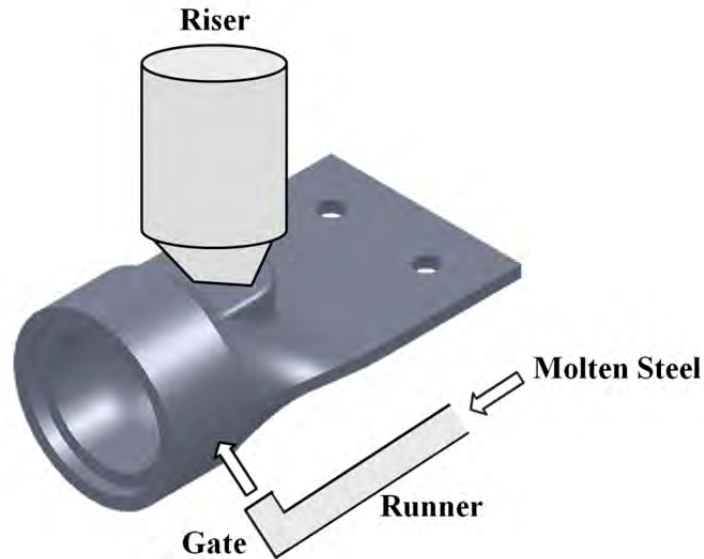


Figure 3.18: Approximate Position of Riser for Cast Connection

Figure 3.19 shows the molten steel being poured into the sand molds for the cross frame connection. Note the fire present on the surface of the previously poured molds. As the casting cools, hot gases that were diffused in the molten steel will bubble to the surface and escape through vents placed in the cope portion of the mold, as well as along the parting line. It is important for these gases to escape and not become trapped in the final product causing a defect. These gases also escape from the surface of the risers and the pour cone.



Figure 3.19: Pouring the Steel into the Sand Molds

3.4.5 Casting Steel Material Test Blocks

During the casting of the parts, the foundry will cast material test blocks for the current heat of steel. These blocks are poured at the approximate halfway point in order to provide a

representative sample of the steel. The blocks are cast into standard size molds and will be used to verify the chemistry of the final product and to produce mechanical test specimens, such as tension test coupons and Charpy V-notch specimens. Figure 3.20 shows the casting of the material test blocks.



Figure 3.20: Casting Steel Material Test Blocks

3.5 Steel Casting Process: Finishing the Part

3.5.1 Casting Shake-Out

Finally, the casting, along with the gating system, is removed from the sand mold once it has cooled to a handling temperature. The molds are transported to a shake table where the hardened sand is separated from the steel casting. The sand is reclaimed for future molds, and the part is removed for further finishing.

3.5.2 Shot Blast

The next step is to get the surface of the casting to a rough finish by using a shot blaster to polish the surface. Basically, steel pellets are shot at the casting to remove excess sand and clean the surface. Figure 3.21 shows the castings following blasting.



Figure 3.21: Cross Frame Connections Following Shot-Blast

3.5.3 Torching and Air Carbon Arc Gouging

The cast steel part is cut from the gating system using a high-powered oxy-acetylene torch. Due to the intensity of the torch, these cuts tend to be rougher and are not performed close to the casting profile. Subsequently, air carbon arc gouging is employed to remove the metal on the surface of the casting, creating a smooth geometrical profile.

3.5.4 Weld Repair and Grinding

Next, the casting is inspected for any surface flaws. If allowed by the customer, weld metal will be used to fill in any voids or cracks on the surface. The weld repairs, along with any remaining irregularities from cutting away the gating system, are ground flush to the part using regular metal disc grinders.

3.5.5 Heat Treatment

Lastly, the castings are subjected to a heat treatment procedure. This helps to relieve any internal stresses that were created during the pour as well as surface stresses caused by weld repairing. The heat treatment results in a steel part with isotropic material properties. Additionally, the typical heat treatment involves a tempering phase, which helps to increase the strength of the casting. It is anticipated the practice of weld repairing will be acceptable for the cross frame connections, so long as the heat treatment is performed to remove residual stresses.

3.6 Casting Defects

Controlling the steel casting process helps to ensure a good quality casting, free from any potential defects in the material. In order to prevent defects from compromising the behavior of the casting, a better understanding of what types of defects are possible is necessary. The following sections note the more common defects for steel castings.

3.6.1 Shrinkage

As previously discussed, shrinkage serves a major role in the design of the casting and the layout of the gating system. There are two types of shrinkage that can occur: microshrinkage

and macroshrinkage. Microshrinkage, sometimes referred to as shrinkage porosity, affects the material on the molecular level. As the steel begins to solidify, dendrites, molecules of steel creating a branched like structure, may form. Dendrite growth is related to the degree of undercooling that may occur in the casting as part of the cooling process [de Oliveira 2006]. While dendritic growth is not desirable, most castings exhibit some degree of this defect. The major problem occurs when adjacent dendrites are allowed to grow large, potentially becoming entangled and preventing liquid metal from accessing the spaces in between. As the liquid cools, thermal contraction in these spaces occurs, leaving small voids in the material. Due to the scale of this defect, it is only detectable and problematic when it affects large sections of the casting [de Oliveira 2006].

Macrosrinkage is a large-scale defect that is present in all castings that are created. The term is generally applied to the thermal contraction of the steel material as it cools from the liquid to solid phase. As the liquid begins to solidify, it begins to contract, exerting an inward pressure to those sections of the casting remaining in the liquid phase, typically regions with larger thicknesses. The pressure will expel the molten steel unless it is balanced by another pressure, typically the hydrostatic head provided by the risers. If the risers are not present nor properly designed, large voids could form in the casting [de Oliveira 2006]. In addition, macrosrinkage also incorporates solid shrinkage, which is the volumetric shrinkage taking place once the entire casting has solidified and begins to cool. This type of macrosrinkage is accounted for by creating a pattern that is slightly larger than the desired size of the casting. Typically low carbon steels exhibit about a 2.5 to 3 percent decrease in volume [de Oliveira 2006].

3.6.2 Gas Porosity

As the temperature of the steel is increased beyond its melting point, the diffusivity of gases into the metal is also increased. However, as the casting cools, the diffusivity decreases again, causing excess gases to form bubbles in the steel, ultimately leading to the formation of voids. These voids occur on the microscopic scale of the material, and similar to microshrinkage, gas porosity is only detectable when large sections of the casting exhibit this defect [de Oliveira 2006].

3.6.3 Surface Flaws

The most obvious of casting defects are those visible on the finished surface of the casting. Surface flaws can be voids, pits, or cracks along the casting profile and significantly reduce the fatigue life of the casting by providing points for crack initiation and propagation [de Oliveira 2006]. Surface flaws are usually a result of poor mold quality, poor gating system design, or inadequate cooling conditions. Often, surface voids and cracks are repaired by welding the completed casting using an arc-air gauging process. The weld is subsequently ground flush to the casting profile, and the entire casting is heat treated to relieve any residual stresses induced. While this can only be done at the discretion of the customer, it has been shown that weld repairs can improve the high-cycle fatigue life of the casting [de Oliveira 2006].

3.6.4 Inclusions

Inclusions refer to any sort of foreign particles that may accidentally be introduced to the steel casting. Examples of inclusions consist of dirt and dust particles, refractory, slag, or sand that may be picked up by the liquid during the casting process. The major concern of having

inclusions is they may create unwanted stress concentrations in the steel matrix and can therefore become an initiation site for cracking [de Oliveira 2006].

3.6.5 Segregation

The final casting defect covered in this section is segregation, which is characterized by an unequal distribution of alloying metals in the steel material. This defect can occur on the macro and micro scales, and can lead to a variation in mechanical properties at different locations throughout the casting. Adjusting the cooling rate of the casting, as well as subjecting it to a heat treatment can help mitigate the effects of segregation [de Oliveira 2006].

3.7 Quality Assurance

In order to make sure a casting does not contain any significant defects, there are a variety of methods, both invasive and non-destructive, to assure a quality product. The following methods can be prescribed as necessary based on the final application of steel casting.

3.7.1 Chemical Analysis

Throughout the entire casting process, the foundry monitors the chemistry of the molten steel to make sure it meets the requested specification. As more scrap is added to the molten steel mix, samples of the liquid are removed and analyzed. The machine used to determine the chemical breakdown is a spectrometer, shown in Figure 3.22.



Figure 3.22: (a) Spectrometer with (b) Sample for Analysis

Basically, the steel surface is melted in a small region which emits a specific color of light. The light is passed through a series of filters to determine the specific wavelengths radiated. Based upon the wavelength, each element present in the steel can be identified, and depending upon the strength of the specific wavelength, a relative percentage can be obtained. The machine outputs the results in a tabular format shown in Figure 3.23.

No	C	Mn	Si	P	S	Cr	Ni
	%	%	%	%	%	%	%
1	0.315	0.74	0.66	0.023	0.018	0.52	0.496
2	0.309	0.76	0.65	0.024	0.020	0.54	0.51
No	Mo	V	Al	Ti	Cu	Nb	Co
	%	%	%	%	%	%	%
1	0.159	0.0082	0.128	0.0029	0.112	0.0022	0.0074
2	0.167	0.0083	0.032	0.0025	0.115	0.0023	0.0087

Figure 3.23: Sample Data from Chemical Analysis

Once the steel matches the specification, the part can be cast. Along with every heat of steel for each casting order, a sample block of metal is cast to be used both for final chemical analysis as well as for supplementary mechanical tests. The block undergoes the same cooling conditions and heat treatment as the casting to maintain uniformity. Once cooled, the sample block is again tested to verify the chemical content meets the specification. The results from this final analysis are reported to the customer, often constituting an average of 2-4 separate tests. In order to maintain precision and accuracy, the foundry calibrates their spectrometer daily using several standardized test samples with a known chemical content.

A key advantage of using the cast steel connection is the customer can specify the grade of material to be made. One concern for the cast connection was its compatibility with weathering steel construction, a relatively common practice in the Texas bridges. For the first round of castings, the steel was specified to meet ASTM A588 Standard Specification for High-Strength Low-Alloy Structural Steel, up to 50 ksi Minimum Yield Point, with Atmospheric Corrosion Resistance [2005].

The material composition breakdown for the first round of cast steel connections is given in Table 3.1. Comparing the cast steel composition with the ASTM A588 specification, it is seen the appropriate requirements are met for all specified elements. ASTM A588 Grade C was the specified grade of material.

Table 3.1: Comparison of Cast Steel Composition with ASTM A588 Specification

Element	ASTM A588 Gr. C (%)	Cast Steel Sample Average (%)
Carbon	0.15 (max)	0.105
Manganese	0.80-1.35	0.97
Phosphorous	0.04 (max)	0.015
Sulfur	0.05 (max)	0.0058
Silicon	0.15-0.40	0.331
Nickel	0.25-0.50	0.298
Chromium	0.30-0.50	0.390
Copper	0.20-0.50	0.275
Vanadium	0.01-0.10	0.054

Weldability

One of the major concerns of using cast steel in structural applications is its ability to be used in welding details. The major concern for cast steel is the increased carbon content which gives the casting its strength but could compromise its ability to be welded. To help determine how easily a steel can be welded, a Graville diagram can be utilized. The diagram uses the percentage of carbon equivalent versus the percentage of carbon to determine whether or not difficulties will be encountered when welding [de Oliveira 2006]. Figure 3.24 shows a Graville diagram with the steel from the first set of castings plotted.

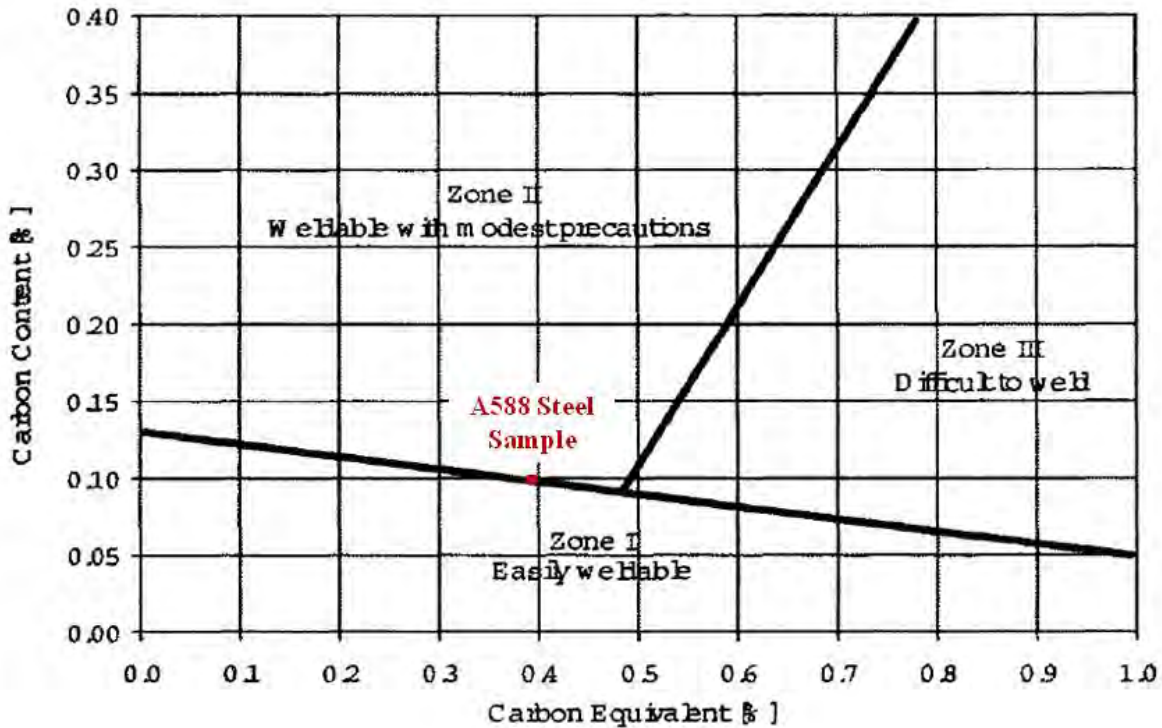


Figure 3.24: Graville Diagram for First Round of Cast Steel Connections [Kaufmann, Viscomi, Lu 1995]

3.7.2 Mechanical Testing

Mechanical testing is conducted to determine the approximate strength and toughness of the steel used to create the casting. Mechanical tests are performed on specimens, machined from the test blocks that cast with each heat of steel for every casting order.

Tensile Tests

The tensile tests conducted are the standard direct tension test on a machined bar. The results are compared to the required specification to make sure the appropriate strength is achieved. It is important to note that while the tension specimen is machined from a sample of the same heat of steel, its properties could be somewhat different than the casting due to differences in thickness and in the relative rate of cooling.

Table 3.2 summarizes the results for the tension tests from the first set of castings and how the values satisfy the ASTM A588 specification.

Table 3.2: Comparison of Cast Steel Mechanical Properties with ASTM A588 Specification

	ASTM A588	Cast Steel
Tensile Strength	70 ksi (min)	85.09 ksi
Yield Point	50 ksi (min)	68.16 ksi
Elongation (2 in)	0.21 (min)	0.29

Charpy V-Notch Tests

In order to determine the toughness of the steel used to create the castings, standard Charpy V-Notch tests can be conducted. The toughness of the steel is a representation of how susceptible the steel is to brittle fracture and hence, gives insight on the fatigue life of the casting. Many of the ASTM standards for structural steels do not include Charpy impact requirements, so it is recommended the customer specify these values for the given application. One suggested Charpy V-Notch impact test value for use in steel castings in structural applications is 27 Joules at -20°C [de Oliveira 2006].

3.7.3 Visual Inspection

In terms of inspection, the easiest to perform is a visual inspection, which examines the surface of the casting to identify the presence of any major flaws or defects. This inspection would be recommended for most any casting, and can be done in accordance with the standard ASTM A802.

3.7.4 Magnetic Particle Inspection

Magnetic particle inspection uses magnetism to reveal any voids or cracks at or near the surface. The steel casting is magnetized and subjected to magnetic particles. Cracks, pits, or voids in the steel disturb the magnetic field, attracting the particles. A visual inspection is then conducted to determine the approximate location and magnitude of the defect [de Oliveira 2006]. The governing standard specification for this test is ASTM A903.

3.7.5 Liquid Dye Penetrant

Liquid dye penetrant requires the steel casting to be covered in a colored dye. Once the casting is wiped clean of excess dye, it is covered with a powder. The powder will soak up any remaining dye, revealing the location and magnitude of the surface flaws. While this method is convenient to detect surface irregularities, it will not uncover subsurface defects [de Oliveira 2006]. The ASTM A903 standard covers liquid dye penetrant examination.

3.7.6 Radiography

One way to detect flaws internal to steel castings is to pass X-rays or gamma rays through the casting and capture the image on film. The resulting pictures can provide an indication of where surface flaws might exist, usually shown as lighter shades of gray on the film [de Oliveira 2006]. ASTM E1030 covers the use of radiography for steel castings.

3.7.7 Ultrasonic Inspection

Another way to detect internal defects in steel castings is to use ultrasonic inspection. Ultrasonic inspection applies high-frequency sound waves to the surface of the casting. Using a calibrated measuring device, the reflection of the waves through the material are measured, indicating the approximate size, location, and depth of the flaw [de Oliveira 2006]. While ultrasonic inspection is useful, it is sometimes difficult to pick up small flaws in the material. Additionally, interpreting the results requires skilled training, and depending on how the device is oriented, it can miss some defects. The standard used for this inspection is ASTM A609.

3.8 Cost Analysis

There are two main factors constituting the cost of the completed part: the amount of steel required for the casting and the amount of time to create the casting. The first factor indicates the gross steel quantity necessary to cast the part. The quantity would include the final steel weight of the casting as well as the excess metal consumed during the pour (see section 3.4). The second factor refers to the processing time required to create the sand mold and the time required after the pour to finish the part. Complex molds using multiple cores and needing an intricate gating system will increase the cost of the final product. Therefore, it is important to make sure the design is well suited for both the final application and the casting operation.

For the cross frame connections produced for this research project, Quality Electric Steel Castings in Houston, TX charged a cost of \$4.82 per pound of the finished casting weight. The prototypes weighed 44 lb, resulting in a cost \$212.08 per connection.

In addition, the foundry offered the following approximations for the cost of the patterns. To generate a wooden pattern made from pine, the cost would be roughly \$2,000-3,000. For the polyurethane pattern, the cost would be about \$8,000-10,000. To mount either pattern, it would cost about \$500. These would be only initial start-up costs to create the pattern, and subsequently, the customer would own the pattern for use in all future castings.

Initially, pine wood was used to make the prototype connection. The resulting cost was \$4235, which included the cope and drag portion for two connections, as well as a core box to make the hollow portion of the casting to reduce overall weight.

3.9 Summary

This chapter has provided a brief description of the process of producing cast steel connections. Castings provide the advantage of being able to accommodate a wide range of complex geometries and allow the development of an optimized design. In addition, castings can be made to a variety of different steel specifications, including weathering steels. This chapter has also described some of the specific steps involved in producing the castings for the tubular cross-frame connections being investigated in this research. The next chapter provides further details on the design of this cast connection, along with results of static and fatigue tests on the cast connection as well as other cross frame connections investigated in this research.

Chapter 4. Cross Frame Connections

4.1 Introduction

TxDOT Project 0-6564 focused on improving cross frame details by investigating a variety of different cross frame geometries, member types, and connection details. Much of the research investigated the feasibility of using tubular cross frame members rather than the conventional single angle members. As previously discussed, tubular members may permit the use of single diagonal cross frames, leading to potentially simpler and more cost effective cross frame. Tubular members also allow the use of concentric connections, thereby eliminating the eccentric single angle connections. Concentric connections may lead to increased cross frame stiffness and improved fatigue performance. This research project also investigated the use of double angle diagonals, which would also allow for a concentric connection.

In reviewing the background information provided in Chapter 2, it is seen there are a variety of ways to make the connection between the cross frame members and the gusset plates or cross frame connection plates. This chapter describes analysis and tests on four types of connections studied for potential use in cross frame construction. Three connections were investigated for use with the tubular cross frame members: the cast steel connection, the T-stem connection, and the knife-plate connection. The fourth connection investigated in this chapter is the welded double angle connection. For each connection type, this chapter will describe the design of the connection, the experimental tests, and the associated finite element model analyses. The single angle connection currently used in TxDOT cross frames will also be studied to investigate the expected performance of these connections and to compare with the alternative connection details considered in this research.

4.2 Cross Frame Connection Laboratory Experiments

The cross frame connection tests conducted in this research were divided into three main series of tests: stiffness tests, ultimate strength tests, and fatigue tests. The purpose of the stiffness tests was to determine the effect the connection had on the overall stiffness of the member and connection system. As previously discussed in Chapter 2, the system stiffness can be reduced by flexible connections. The stiffness tests provided data to quantify this effect.

The ultimate strength tests were used to determine the failure modes of the connections and their ultimate strength under static loading.

In addition, fatigue tests on the various connection types were performed to determine the adequacy of using these connections in cross frames from a fatigue perspective. The AASHTO LRFD Bridge Design Specification [2012] has requirements for the fatigue behavior of these connections and will be discussed shortly.

4.2.1 Testing Machine

The cross frame connection tests were performed in the 220 kip MTS Universal Testing Machine at the Ferguson Structural Engineering Laboratory at The University of Texas at Austin. The basic test setup is shown in Figure 4.1 and Figure 4.2.



Figure 4.1: 220 kip MTS Testing Machine with Specimen

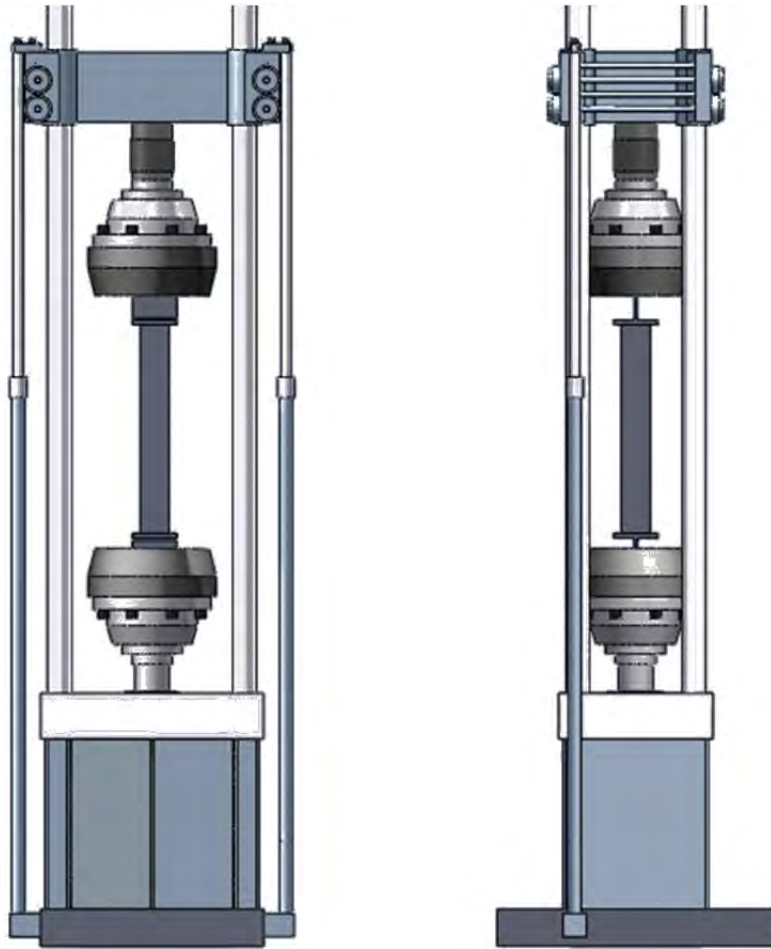


Figure 4.2: Test Setup (a) Front View and (b) Side View

4.2.2 Stiffness Tests

As previously mentioned, tests were conducted to quantify the effect of connection details on the axial stiffness of a cross frame member. Quantifying axial stiffness required measuring the axial force imposed on the member and also measuring the axial displacement of the member. Axial force was measured by the load cell in the MTS test frame. In order to measure axial displacement of the cross frame member, two dial gages were used. One gage has an accuracy of 0.001" and the other 0.0001". The gages are shown in Figure 4.3. Dial gages were chosen for the measurements due to their high accuracy.



Figure 4.3: Displacement Dial Gage with (a) 0.001" Accuracy and (b) 0.0001" Accuracy

The axial displacement of the cross frame member was measured between points at the member ends that were attached to the connection plates that were gripped by the test machine. The measurement points were located 2 in from the end of the actual cross frame member. The overall measurement arrangement can be seen in Figure 4.4 and Figure 4.5. The gage locations were slightly modified for the cast connection.



Figure 4.4: Test Setup Front View with Dial Gages

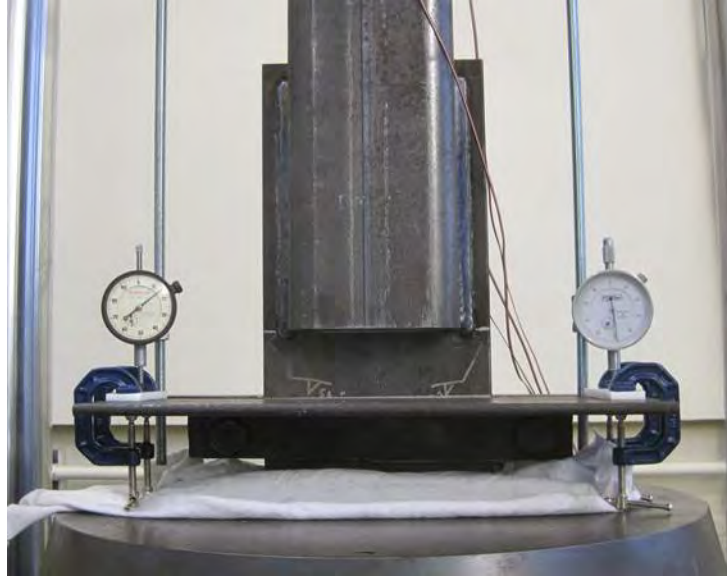


Figure 4.5: Close Up View of Dial Gages and Angle Clamps

In addition to the displacement measurements, strain data was taken to validate the results of the finite element models. The strain gages were 350-ohm general purpose strain gages produced by Micro-Measurements of the Vishay Precision Group. The gage designation was CEA-06-250UN-350/P-2 and the gages were thermally compensated for use with mild carbon steel. The placement of these gages for each specimen will be discussed in the corresponding parts of this chapter. A close-up of the strain gages are shown in Figure 4.6.

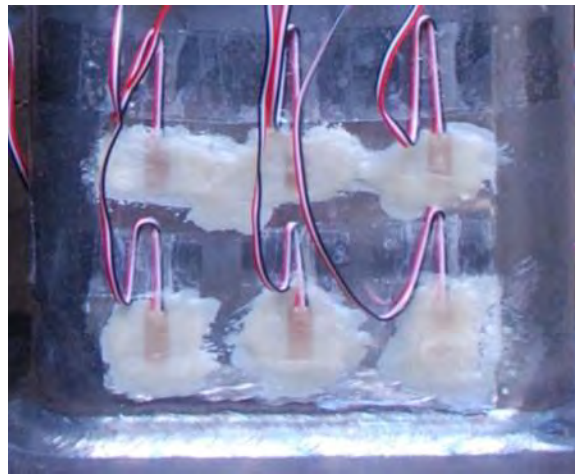


Figure 4.6: Close-Up View of Strain Gage

4.2.3 Ultimate Strength Tests

The ultimate strength tests were performed in the same setup as the stiffness tests, using the same specimens. Tests were first conducted in the elastic tension and compression range to determine the stiffness behavior. The sample was then loaded in tension to failure, or until the limits of the testing machine were reached.

4.2.4 Fatigue Tests

The fatigue tests were also performed in the 220 kip MTS Universal Testing Machine using the same basic setup as the stiffness tests, but subjecting the specimens to cyclic loads rather than tension and compression loads. The tests were conducted using close-looped force control, with the specimens exposed to sinusoidal cyclic loads and loading compensated for force errors. The specimens were initially placed under tensile stress, and then further loaded in tension to produce the desired stress range. An example setup is shown in Figure 4.7.



Figure 4.7: Basic Fatigue Setup

The results of the fatigue test were be used to obtain the applied stress range versus number of cycles to failure relationship. The values were then plotted against performance requirements from the AASHTO Bridge Design Specification to establish the fatigue category of the connection.

Part I: Cast Connection

4.3 Cast Connection Design

In order to design the cast steel connection, computer software was used to both generate a solid model and analyze it for a given load condition. SolidWorks 2010 was the CAD program selected to make the three-dimensional solid model of the connection. From the program, the model geometry was exported as an .iges solid geometry file. This format basically reduces the model into small triangular elements for use in exporting to other software. The geometry was then uploaded into ANSYS[®] Academic Research, Release 11.0, a three-dimensional finite element analysis (FEA) program. Once uploaded, the appropriate loading and boundary conditions were applied and the connection was analyzed. Figure 4.8 summarizes the design process for an early version of the cast steel cross frame connection.

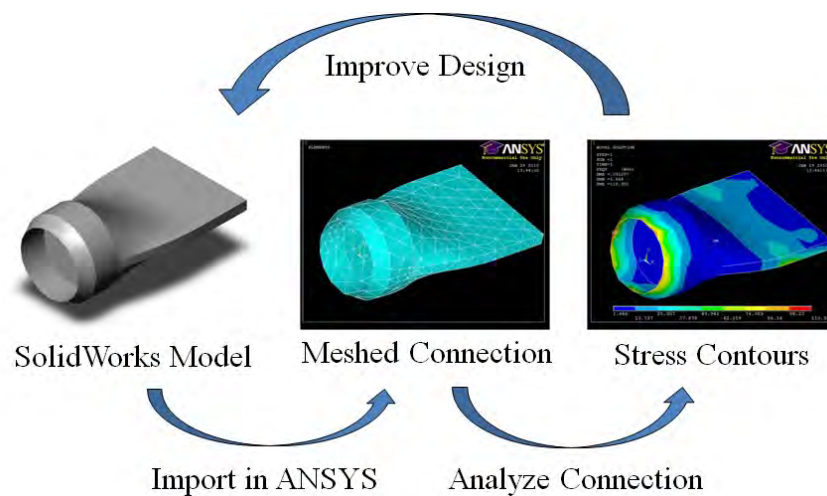


Figure 4.8: Cast Steel Connection Design Process

After iterating through the design process of Figure 4.8, a final geometry for the connection was selected.

4.3.1 Features

Initially, the prototype was designed to fit to the inside diameter of the tube to reduce the amount of steel required for casting and improve handling of the parts. However, pipes, as well as round HSS members, are specified by the outside diameter. In order to standardize the casting geometry, which improves the economy of using the connection, a prototype that fits to the outside diameter is more beneficial. Namely, fitting to the outside diameter allows one cast connection geometry to be used with pipe sizes of the same outside diameter but varying thicknesses. Therefore, the designer can use a thicker tube when a higher strength cross frame member is needed, and vice versa.

The prototype connection is given below in Figure 4.9. The design incorporates a ledge on the inside of the hollowed portion to facilitate fit-up with the circular tube. The hollow is provided to remove unnecessary material from the casting making it lighter and reducing the cost. Additionally, two erection bolt holes were added in the flat portion to aid in the

construction of the braces. Since these steel parts were cast from molten metal, features like erection bolts could be easily added with little effect on the cost of the part.

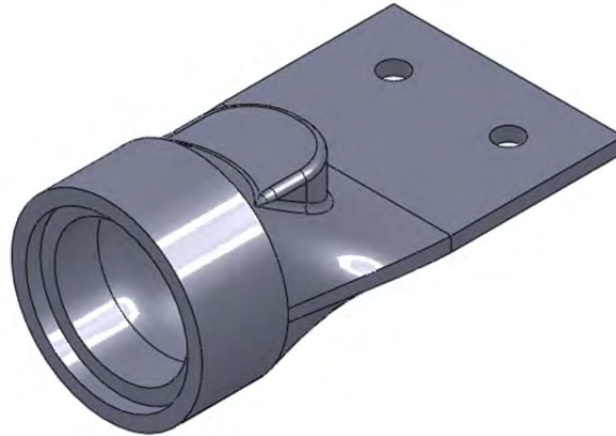


Figure 4.9: Prototype Cross Frame Connection

The prototype also features a taper from the circular cross section to a flat plate, making it easy to weld to gusset plates or cross frame connection plates, and preventing large stress concentrations from forming. After corresponding with the foundry, a steel pad was placed along the taper of the casting to ease the finishing process of the castings. As discussed in Chapter 3, risers are used in the design of the gating system to ensure the portion of the casting that cools last has liquid steel feeding it, preventing macro shrinkage. Through temperature and flow analysis software, the foundry identified the section along the taper to be critical and placed the riser pad accordingly. The pad helps reduce labor costs when the riser is cut from the casting. Finite element analyses showed the riser pad to have little effect on the flow of forces through the part. Figure 4.10 shows the taper of the casting and the final geometry of the casting.

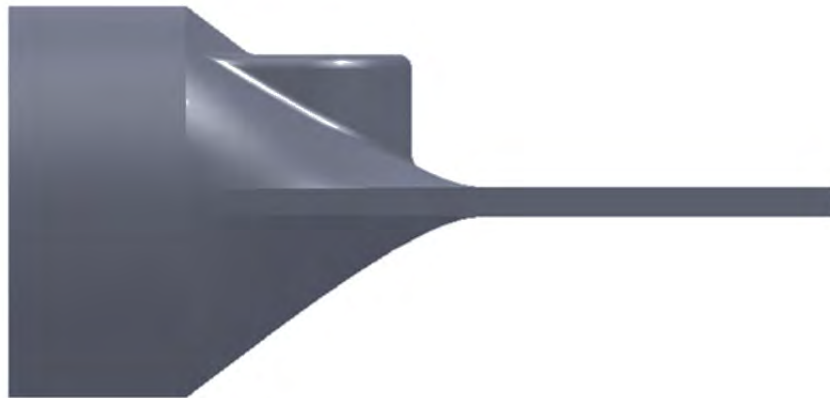


Figure 4.10: Prototype Cross Frame Connection (Side View)

It was anticipated that the connection between the tubular member and the casting would be a fillet weld. Using a fillet weld was intended to simplify fabrication as well as reduce inspection requirements. Since the weld will be situated along the circumference of the tubular

member, a setup involving some roller supports could be arranged in the fabrication shop so the welder could rotate the tube while fillet welding the connection.

The completed cast connections, after heat treatment and the finishing processes, are shown in Figure 4.11 and Figure 4.12.



Figure 4.11: Cast Steel Cross Frame Connection



Figure 4.12: Cast Steel Cross Frame Connection (Side View)

4.3.2 Dimensions

When determining the required size of the cross frame connections, the project team identified the tube sizes necessary for the single diagonal cross frame layout. The tube sizes were approximated from current TxDOT details using angle members, with the round and square tube sizes having similar capacity in compression at a length of 13 ft as the angles have in tension. The length of 13 ft was used as it approximately represents the diagonal length of a cross frame with an 8 ft (96 in) girder depth and 10 ft girder spacing. In actuality, the length would be less due to the addition of gusset plates and positioning of the members. Table 4.1 shows how the tubular member compression capacities compare to the yielding capacity of the angle.

The laboratory testing focused on the tube sizes corresponding to the L4 x 4 x 3/8 and the L5 x 5 x 1/2 angle members. Thus, the first prototype for the steel casting was designed to fit to the outside diameter of an HSS 5.563 tubular member. The other main dimensions calculated were the width and thickness of the flat portion of the casting, as it needs to also reach the appropriate strength for the connection to be successful. Using analytical strength equations, and the results from the FEA, a connection width of 8 in and thickness of 0.5 in was deemed adequate. The other dimensions for the casting were determined by performing multiple finite

element analyses, optimizing the use of material to make an efficient connection. Figure 4.13 and Figure 4.14 show the plans submitted to the foundry for use in creating the cast steel connection patterns and cores.

Table 4.1: Angle Tensile Strength vs. Tube Buckling Strength

Angle Size	Angle Capacity (36 ksi)	Tube Size	Tube Capacity ^{1,2}
L4 x 4 x 3/8	92.7 k	HSS 5 x 5 x 3/16	88.6 k
		HSS 5.563 x 0.258	99.6 k
L5 x 5 x 1/2	154 k	HSS 5 x 5 x 3/8	160 k
		HSS 5.563 x 0.375	139 k
L6 x 6 x 9/16	209 k	HSS 5 x 5 x 1/2	199 k
		HSS 6.000 x 0.500	207 k

1. Tube capacity was calculated using a length of 13 ft

2. Yield stress (F_y) is assumed to be 46 ksi for square tubes and 42 ksi for round tubes [AISC 2005]

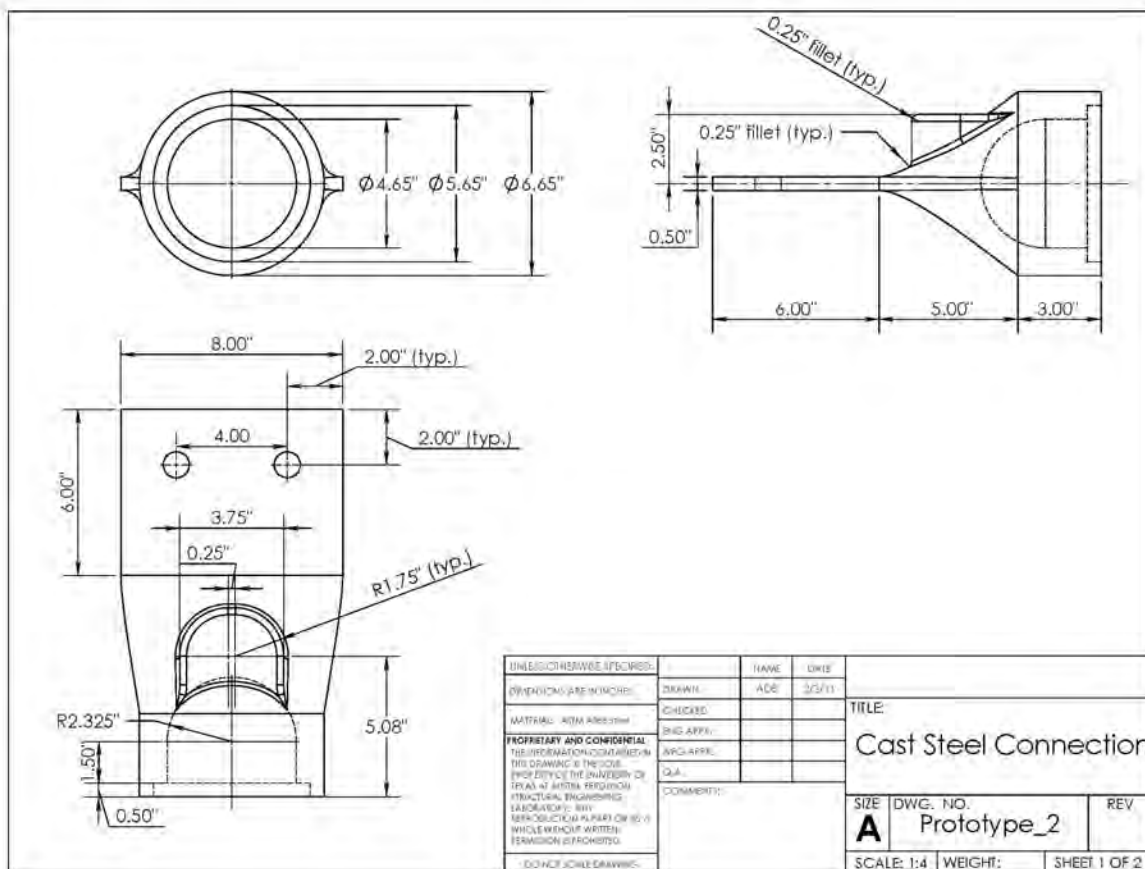


Figure 4.13: Two Dimensional Drawing of Cast Steel Connection

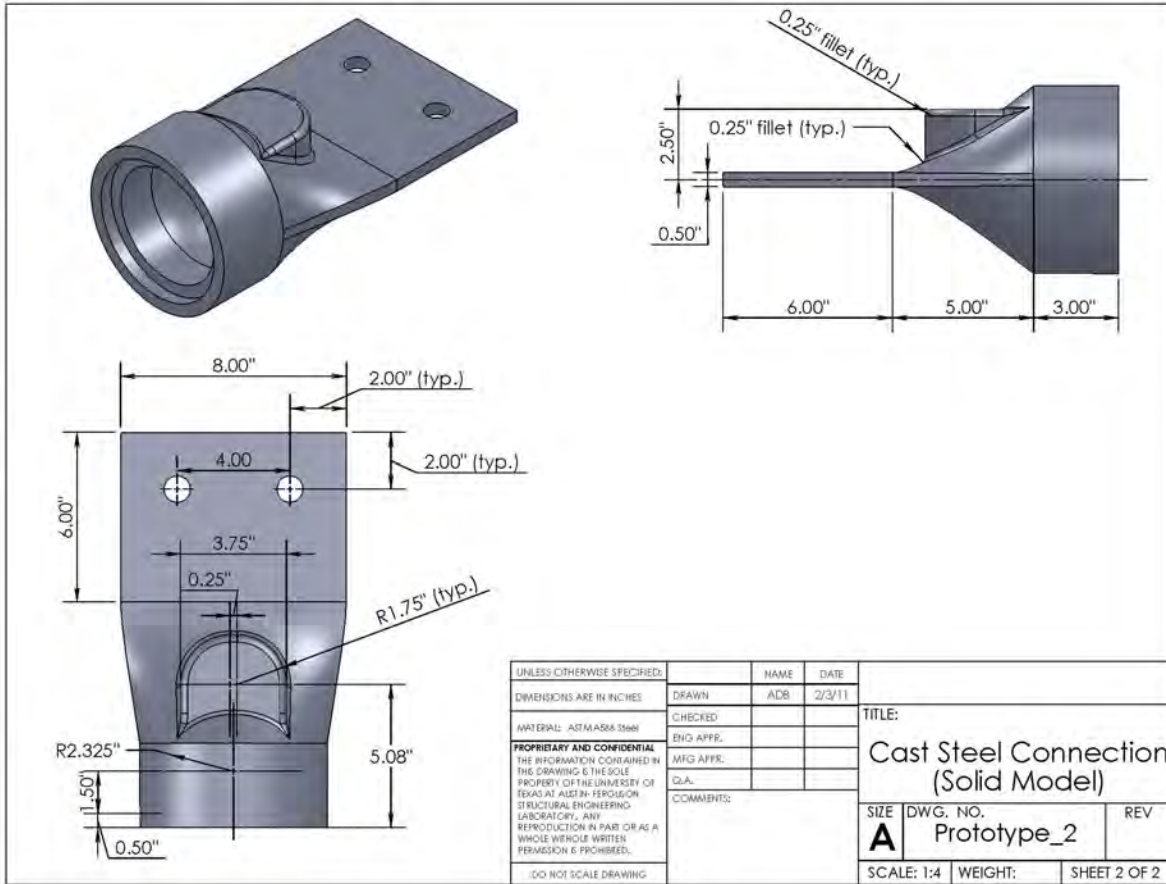


Figure 4.14: Three Dimensional Drawing of Cast Steel Connection

4.3.3 Analysis

As previously mentioned, multiple finite element analyses were performed on the cast connection geometry to determine appropriate dimensions. The primary focus of these analyses was to determine if the cast connection showed signs of stress concentration.

Using the FEA program ANSYS, the solid model file was uploaded and meshed using SOLID187 elements, which are 10-noded tetrahedral solid elements. Each node has three degrees of freedom, translation in the nodal x, y, and z directions. The element can support quadratic displacements and is well-suited to model irregular meshes [ANSYS 2011].

Figure 4.15 shows the loading and boundary conditions used for the analysis of the cast steel connection. Using the program, a 100 kip load was discretized into smaller point loads and applied uniformly to the casting at the location of the tube-to-casting fillet weld. One result of fixing nodes in an FEA model is that large stress concentrations will develop at the fixed location. To reduce this effect in the model, a gusset plate was included in the model to analyze the casting. The gusset plate was constructed of SHELL93 elements, an 8-noded plate element with six degrees of freedom at each node: three translations and three rotations. The casting was connected to the plate using MPC184 elements, multipoint constraint elements that rigidly join two nodes and are often used to model welded connections [ANSYS 2011].

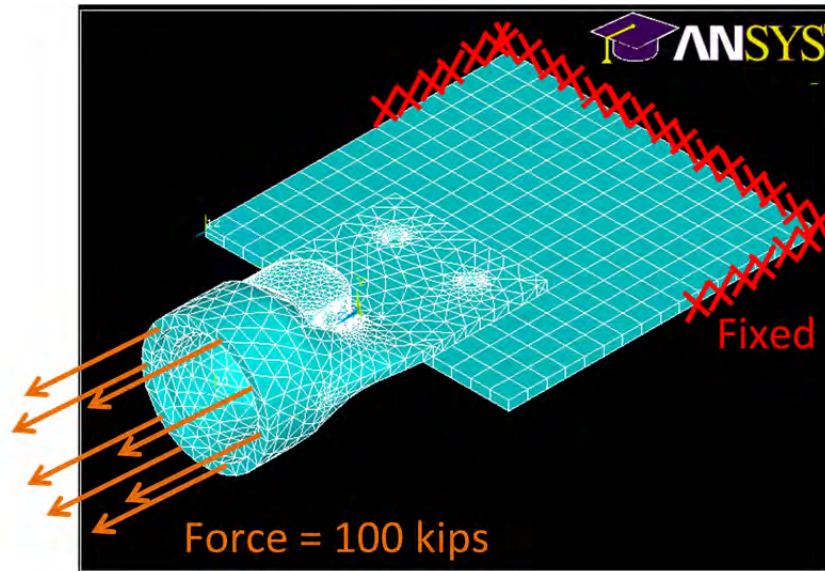


Figure 4.15: Load and Boundary Conditions for Steel Casting Analysis

Using the prescribed boundary conditions, an analysis of the cast steel connection was performed to determine if large stress concentrations were developing in the connection and if the connection was strong enough to resist the applied loads. Figure 4.16 shows the results of an elastic, static analysis of the connection.

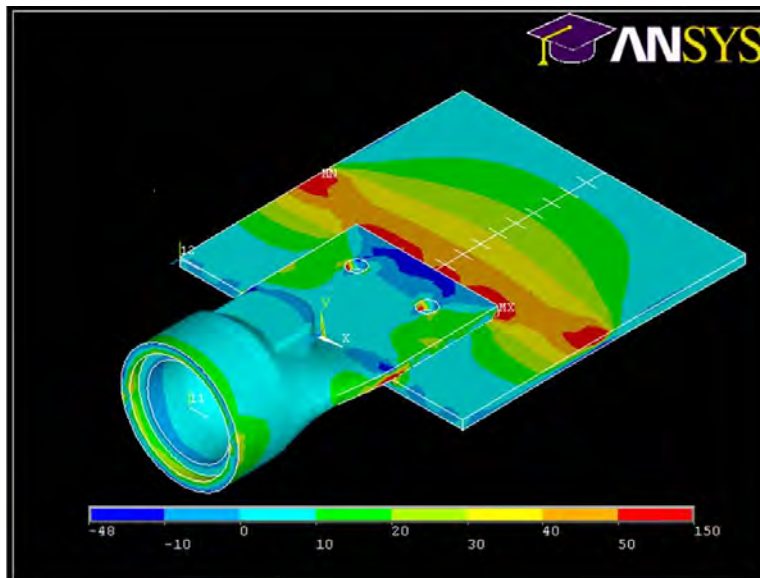


Figure 4.16: Elastic Analysis on Steel Casting Connected to Gusset Plate

While every effort was taken to minimize the effect of stress concentrations in the FEA model, some of the high localized stresses predicted by this elastic model will be reduced due to localized yielding. A subsequent analysis was carried out using an inelastic material model. A bilinear hardening material model was used with an initial modulus of elasticity of 29000 ksi to a yield stress of 50 ksi, followed by a 580 ksi modulus. Figure 4.17 shows the results of the

inelastic analysis. Note the stress pattern in the casting is similar to Figure 4.16, indicating the use of the gusset plate helps to minimize the effects of stress concentration.

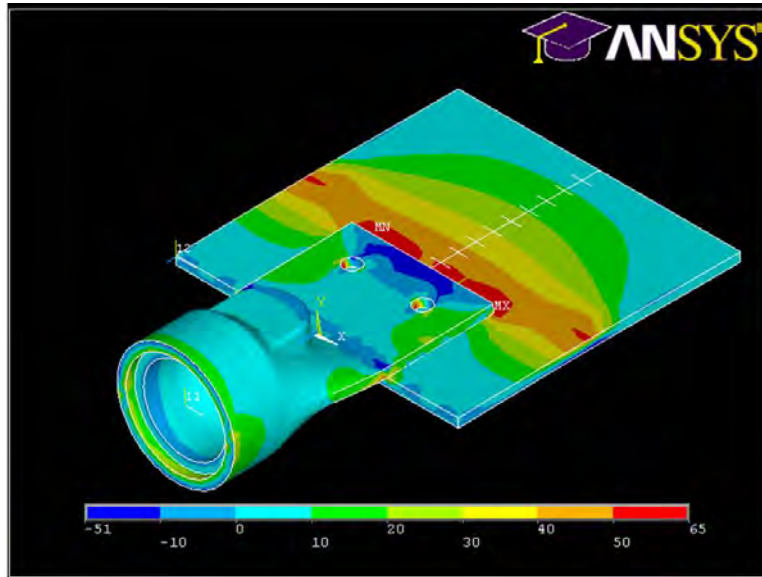


Figure 4.17: Inelastic Analysis on Steel Casting Connected to Gusset Plate

4.4 Cast Connection Laboratory Experiments

Once the design of the cast steel connection for tubular cross frame members was complete, the project team worked with a foundry to create a pattern for the design, and to cast the connections. Quality Electric Steel Castings in Houston, TX was selected for the task, and the connections were made following a procedure typical to the sand casting method. In-depth discussion of the procedure employed to form the castings and to assure a quality casting are provided in Chapter 3.

Upon delivery of the castings, the project team fabricated test specimens to determine the strength and stiffness of the connection to make sure it is adequate for the application of constructing cross frames.

4.4.1 Stiffness Tests

In order to determine if the castings are capable of resisting the designed tension and compression loads, specimens were created with the intent of determining the strength of the casting. Furthermore, these tests quantified the effect the connection has on the overall stiffness of the tubular member.

The stiffness tests were conducted in the 220 kip MTS Universal Testing Machine as outlined in Section 4.2.2 and depicted in Figure 4.18. Due to geometrical constraints, the angle clamps could not be used to support the gages, so the dial gages were attached to the casting along the sides, using smaller angle sections that were epoxied to the casting.



Figure 4.18: Cast Steel Connection Stiffness Tests with Dial Gages

Using the obtained deflection measurements, the load versus displacement relationship was plotted. The slope of the elastic portion of the curve is then equal to the stiffness. The stiffness measured is that of the combined system, meaning the stiffness of the cross frame member and the two connections at either end. Figure 4.19 depicts a plot of the displacement data. The stiffness listed was found by using a linear best fit line through the data.

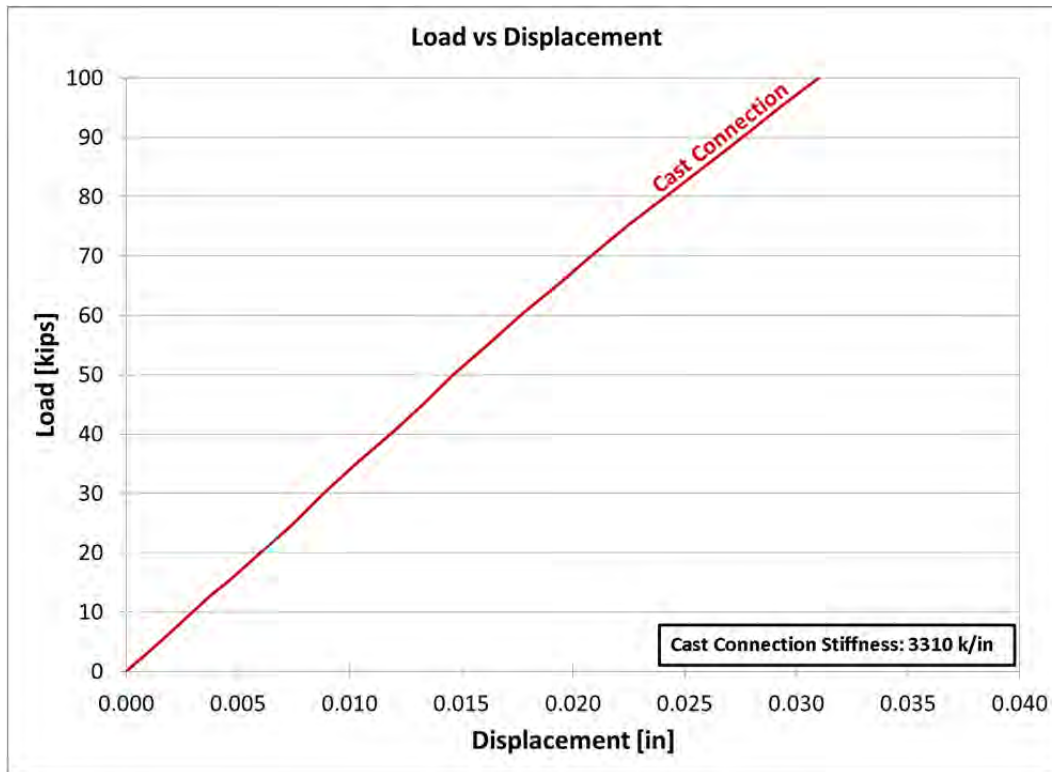


Figure 4.19: Cast Steel Connection Stiffness

4.4.2 Ultimate Strength Test

Additional tests were performed in the 550 kip MTS Universal Testing Machine to determine the ultimate strength and failure mechanism of the cast connection, and to obtain supplemental stiffness data. The specimen in the 550 kip machine is shown in Figure 4.20.



Figure 4.20: Cast Steel Connection Test in 550 kip MTS Testing Machine

Using standard steel design checks, the calculated strength of the cast steel connection was approximately 240 kips. When loaded in tension, the steel casting and welded connection exceeded these strength calculations, showing that typical checks performed on the cast steel connection and tube combination can provide a safe design. The results of the ultimate strength test are shown in Figure 4.21.

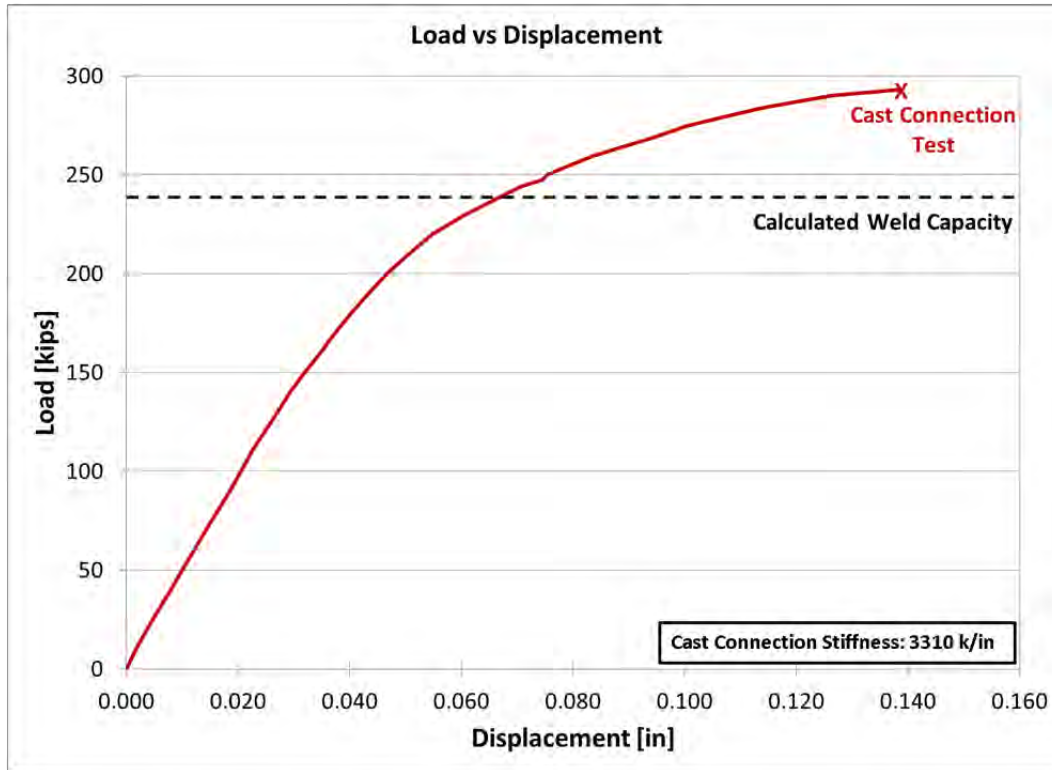


Figure 4.21: Cast Steel Connection Ultimate Strength Test Results

4.4.3 Fatigue Tests

Test specimens similar to those tested in the tension test were carried out under cyclic loading until fracture occurs. One of the key aspects of these tests was to make sure the fatigue crack initiates at the welded connection and does not originate in the casting. The tests were also used to classify the cast connection according to the fatigue categories given in the AASHTO Bridge Design Specifications.

Figure 4.22 shows the results of two fatigue tests on the cast connection and tube specimen. Unfortunately, the fatigue behavior of the welded connection was poor.

The connection was designed to be a transversely loaded fillet weld which would transfer the force from the rim of the casting into the tube wall. It was designed as a fillet weld to facilitate the fabrication process and prevent the need for costly inspection procedures. However, while the connection is concentric on the whole, at the local level it is eccentric. Figure 4.23 depicts how the load is transferred locally through the weld.

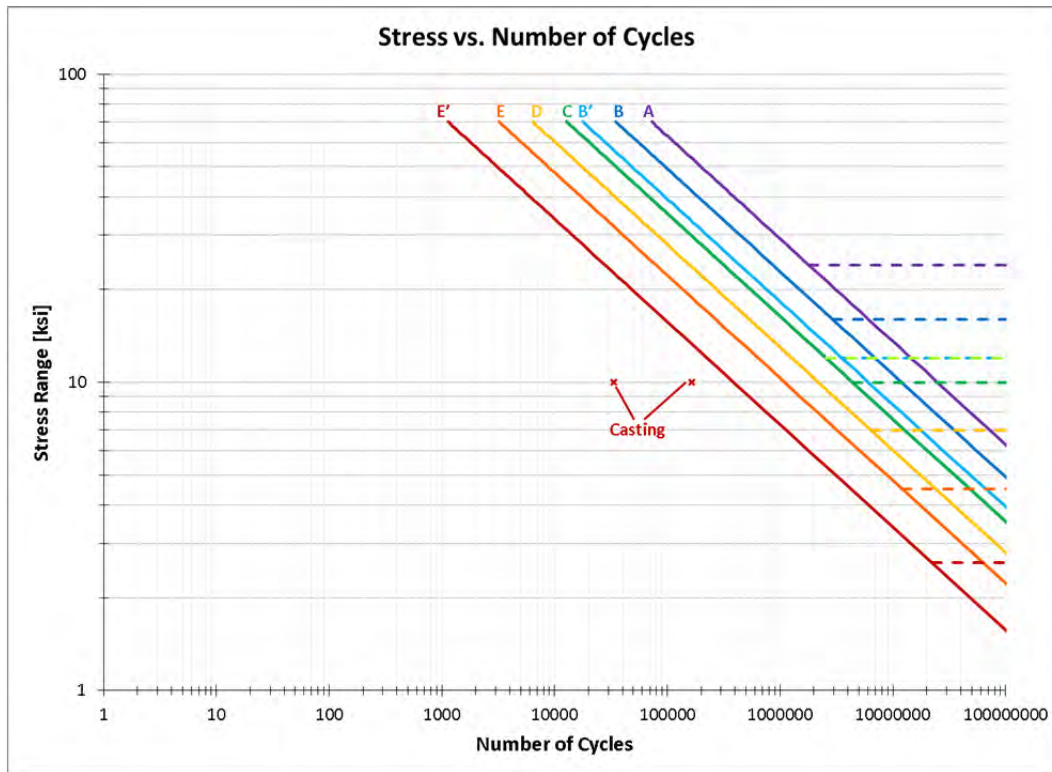


Figure 4.22: Cast Steel Connection Fatigue Results

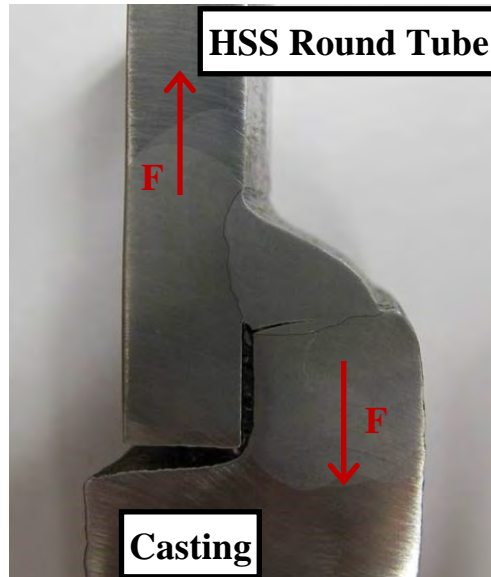


Figure 4.23: Eccentric Nature of Fillet Weld

The result of the eccentric loading pattern is a low fatigue life. The fatigue crack begins at the notch located at the root of the weld, and then propagates through the weld throat until it reaches the surface. Unfortunately, since the notch is built into the connection as a result of the geometry of the fillet weld, it cannot be improved. As seen in Figure 4.23, there was little weld

penetration into the tube wall. Therefore, a second specimen was prepared to improve the connection. The subsequent castings were sand blasted to improve surface conditions and preheated to improve weld penetration, while the weld electrode diameter was reduced and a multi-pass weld was employed to further the level of penetration. The result was a significant improvement in fatigue life, as shown in Figure 4.22, however, the number of cycles achieved was only half of what is required to meet the minimum E' category as specified by AASHTO for use in bridge components.

Additionally, when the crack becomes visible on the surface of the weld, the majority of the fatigue life of the detail has been used, meaning that there is little warning before imminent failure. An example of a fatigue crack in the cast steel connection weld is shown in Figure 4.24.



Figure 4.24: Cast Steel Connection Fatigue Crack

4.5 Cast Connection Observations

The results on the cast steel connection indicate that it is not a suitable connection for typical cross frame braces. The strength tests showed the cast connection provided a safe detail when using standard connection checks to predict strength. The connection uniformly engaged the tube and provided one of the stiffer connections as will be discussed later in the chapter. However, the poor fatigue life of the designed weld leads to its exclusion from potential cross frame details.

Part II: T-Stem Connection

4.6 T-Stem Connection Design

As an alternative to casting a steel connection piece to connect the tubular members of the cross frames, fabricated connections were also considered as part of TxDOT Project 0-6564. One of the connections details considered in the research was the T-stem detail, which is discussed below.

4.6.1 Features

The T-stem detail involves the use of a WT section to connect to the ends of the tube to a flat plate. The tubular member meets the flange of the WT shape at 90° and is fillet welded to create the connection. The stem of the WT can then easily attach to the flat cross frame connection plate or to a cross frame gusset plate. Figure 4.25 shows the basic geometry of a T-stem connection.

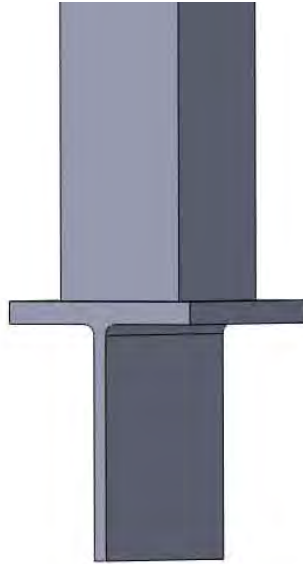


Figure 4.25: T-Stem Connection Detail Concept

One of the major advantages of the T-stem connection is it consists of standard steel rolled shapes. In comparison to the cast connection which requires special manufacture, the T-stem is readily available for fabrication. In addition, the material properties of the steel are better understood by most designers. The T-stem connection would also offer a variety of tube sizes to be used, allowing the bridge designer to customize the size of tube and connection for each particular scenario. Lastly, because of the increased availability, the T-stem connection may offer improved economy over the cast connection. In addition, like the cast connection, the T-stem connection seals the end of the tube.

4.6.2 Dimensions

Determining the optimum size of WT section to use for a connection requires several considerations. The two main criteria to evaluate are the yielding/fracture strength of the WT stem and the bending capacity of the WT flange. At the same time, the width of the flange should be selected so it does not grossly exceed the width of the HSS tube, resulting in poor efficiency of material.

For the experimental test program, it was the goal of the research team to select the WT sizes such that the full yielding capacity of the tubular members could be attained. While this is possible for thinner walled tubes, it was apparent that it was unlikely to be the case for thicker walled tubes. Furthermore, the capacity of the proposed fillet welded connection tended to control the design for some cases. Therefore, the research team decided to select two different

WT sections for the experimental program, and to use them in different combinations to study the variety of failure modes possible for this design.

Using Table 4.1 as a guide, the WT 9 x 35.5 and the WT 12 x 31 shapes were selected. With flange widths of 7.64 in and 7.04 in respectively, the use of 5 in square HSS members seemed reasonable, allowing about an inch or so along the sides in which to make the fillet weld. While the WT connection can be cut to any length and attached to the tubular member, it is proposed the WT be cut to a square flange area so the tube and flange are concentric, primarily for aesthetic purposes. The following table shows the planned experimental test program. However, not all tests were completed due to poor performance of this connection in the early tests.

Table 4.2: Proposed Experimental Test Program for the T-Stem Connection

HSS Member			WT Connection				Weld Size			
Thin	Thick	Member Size	Thin Flange	Thick Flange	Thin Web	Thick Web	Member Size	3/16	1/4	5/16
X		HSS 5 x 5 x 3/16		X		X	WT 9 x 35.5			X
X		HSS 5 x 5 x 3/16				X	WT 12 x 31		X	
	X	HSS 5 x 5 x 3/8		X		X	WT 9 x 35.5	X		
	X	HSS 5 x 5 x 3/8				X	WT 12 x 31		X	
X		HSS 5.563 x 0.258		X		X	WT 9 x 35.5			X
X		HSS 5.563 x 0.258				X	WT 12 x 31		X	
	X	HSS 5.563 x 0.500		X		X	WT 9 x 35.5		X	
	X	HSS 5.563 x 0.500				X	WT 12 x 31			X
X		HSS 5 x 5 x 3/16	X			X	PL 7 x 0.25 / PL 7 x 0.75			X
X		HSS 5 x 5 x 3/16		X	X		PL 7 x 0.75 / PL 7 x 0.25	X		
	X	HSS 5 x 5 x 3/8		X		X	PL 7 x 0.75 / PL 7 x 0.75			X
	X	HSS 5.563 x 0.500	X			X	PL 7 x 0.25 / PL 7 x 0.75			X

4.6.3 Analysis

As shown in Table 4.2, round HSS members were also being considered for use with the T-stem connection. The decision to consider round HSS members arose when preliminary analyses were performed on the connection geometries, indicating the square HSS members had a very large stress concentration. The following subsections discuss more detail on the analyses.

Square HSS Connection

In an effort to understand the flow of forces through the T-stem connection, a finite element model was constructed in ANSYS. The model uses 8-noded shell elements (SHELL93) to construct the plate regions of the WT section and the square HSS tube. The preliminary model does not account for the fillet region between the stem and flange of the WT, nor does it consider the curved corners of the square HSS members.

A major goal of the connection tests is to better understand the axial behavior of the tubular members in conjunction with the connections. Once the project team gains knowledge of these components on an elemental level, the system effect of multiple tubular members forming a cross frame can be evaluated. The preliminary boundary conditions were simplistic: the applied load is discretized into several point loads applied along the WT stem edge. To connect the

tubular member to the WT flange, multipoint constraint elements (MPC184) were used to join the nodes.

Figure 4.26 shows a typical plan for a square HSS specimen with WT connections. Figure 4.27 shows typical boundary conditions for these analyses using a square HSS member.

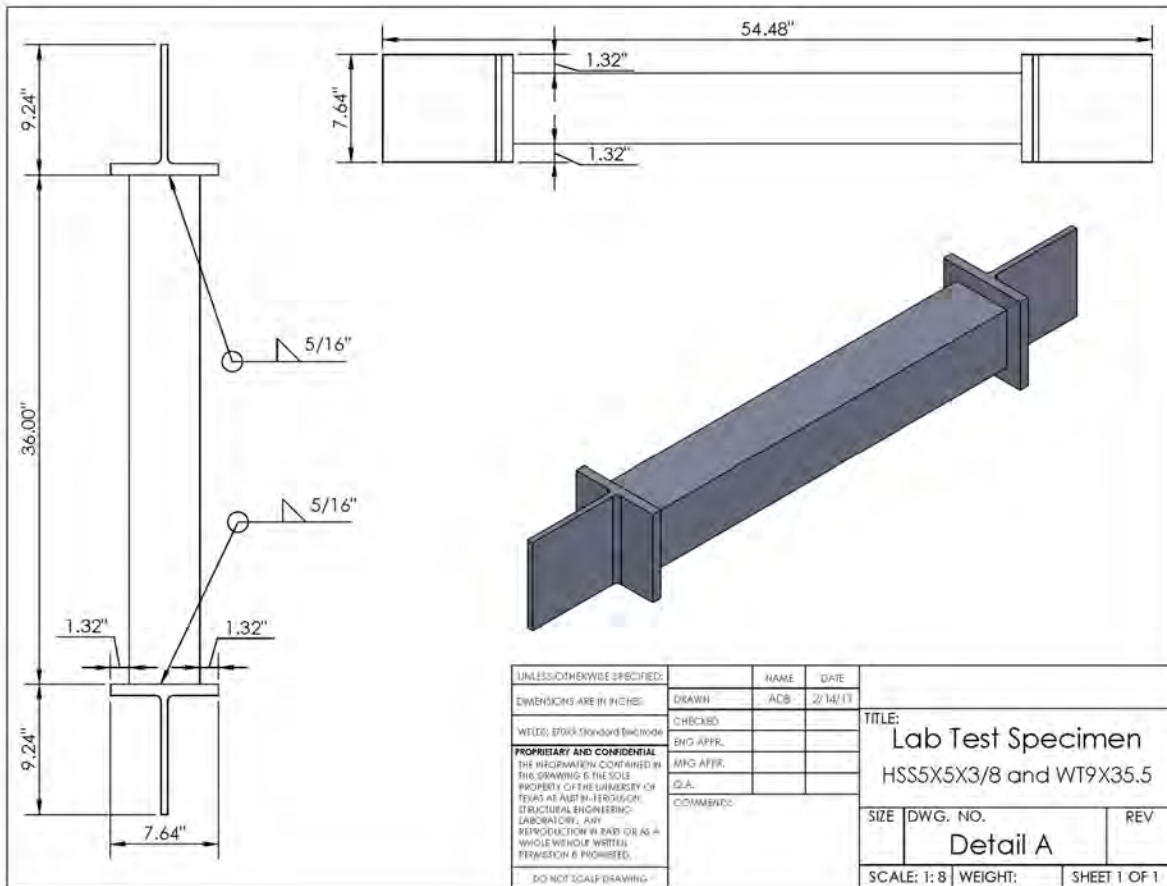


Figure 4.26: Square HSS Specimen with T-Stem Connection Detail

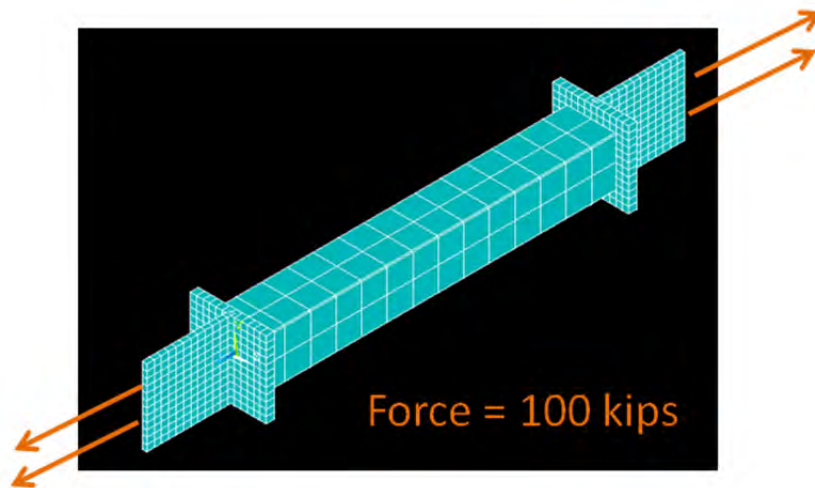


Figure 4.27: Typical Boundary Conditions Used for Preliminary T-Stem Analysis

Results from these analyses showed that an intense stress concentration developed in the wall of the HSS tube perpendicular to the WT stem (see Figure 4.28(a)). Conversely, the stress in the wall parallel to the stem is less than the average stress expected in the tube section (Figure 4.28(b)). The presence of a stress concentration in the detail is problematic because it has the potential to lead to early, unexpected failures, especially in fatigue loading.

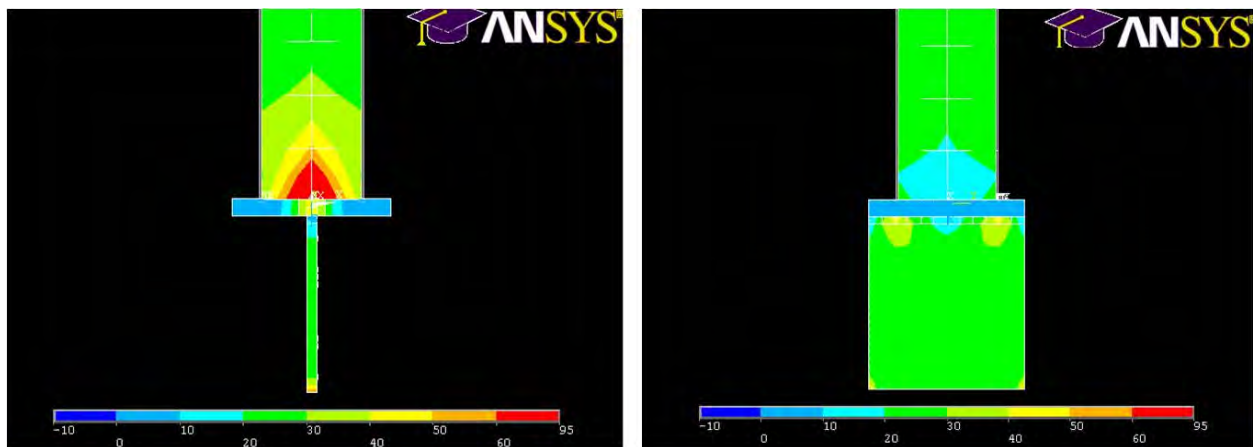


Figure 4.28: Axial Stress in HSS Tube Wall (a) Perpendicular to Stem and (b) Parallel to Stem

Round HSS Connection

Due to the stress concentration issue arising in the square HSS detail, the research team explored alternative arrangements of tubular members to determine if there was a reduction in the longitudinal stress. The first alternative used round HSS members instead of square members. The proposed detail geometry remains the same as the circular tube is centered in the square WT flange and connected with fillet welds. Figure 4.29 shows typical plans for a round HSS specimen with WT connections.

Figure 4.30 shows the preliminary analysis conducted for the round HSS members. In comparison to the square HSS detail, the round HSS seemed to significantly reduce the magnitude of the stress concentration.

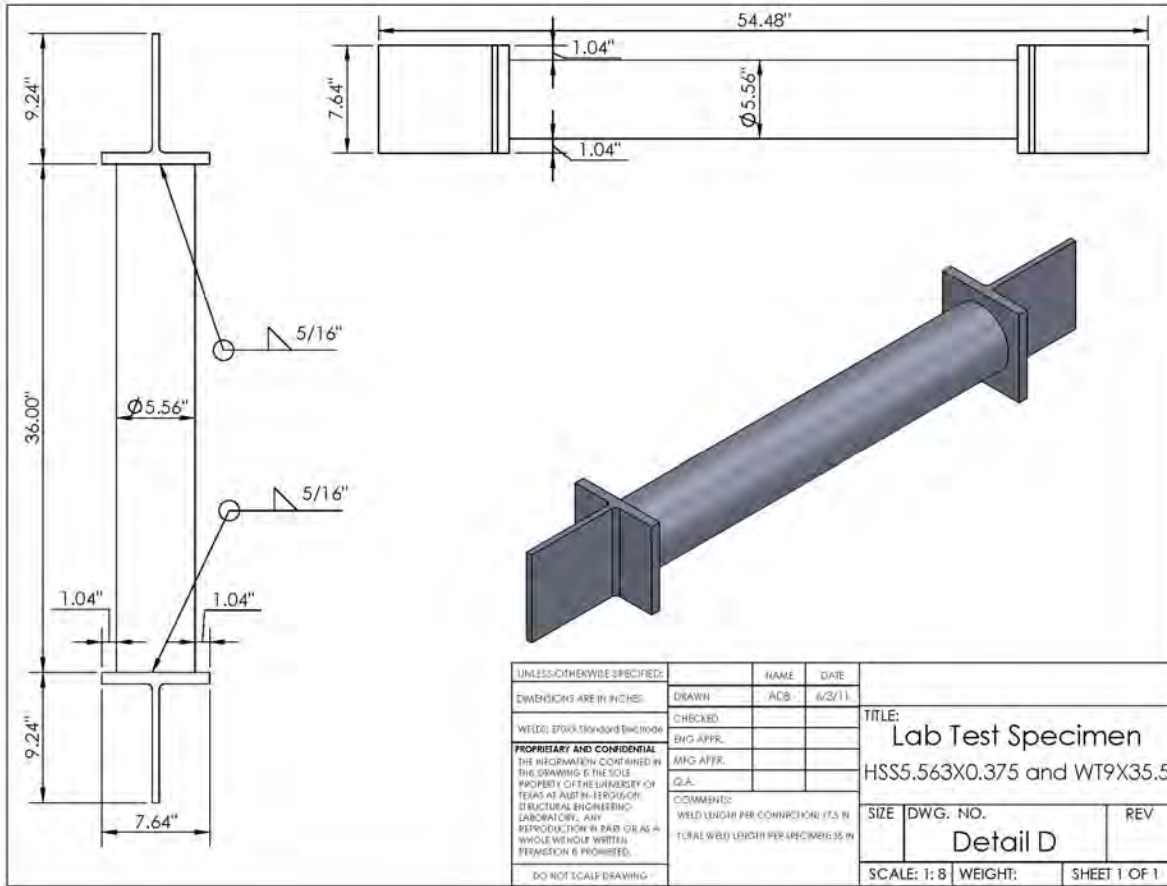


Figure 4.29: Round HSS Specimen with T-Stem Connection Detail

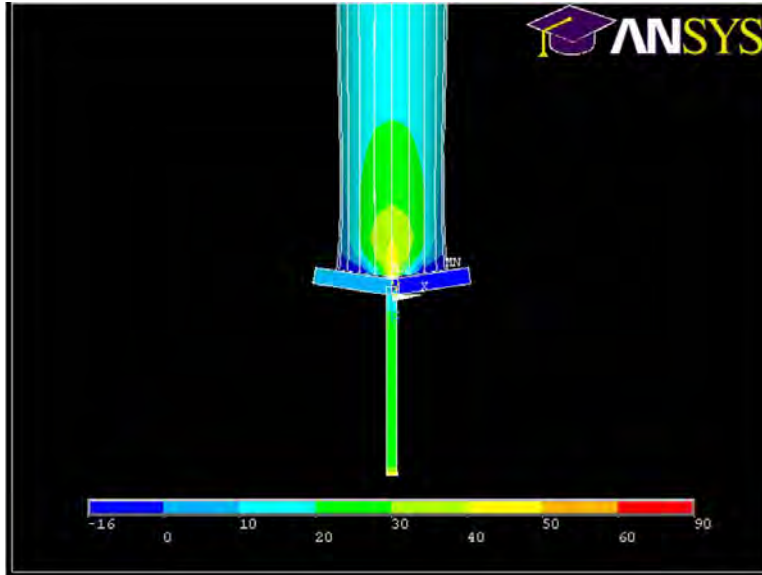


Figure 4.30: Axial Stress in Round HSS Tube Wall

Diamond HSS Connection

The second alternative to the square HSS detail is the diamond HSS connection. Utilizing the same square HSS sections, the tube is rotated 45 degrees about its longitudinal axis and attached to the flange of the WT section, as shown in Figure 4.31.

Performing an analysis on the rotated square specimen showed a further reduction in stress concentration as compared to the round HSS member, suggesting this detail may have the best fatigue performance of the three proposed options. Results of the analysis are given in Figure 4.32.

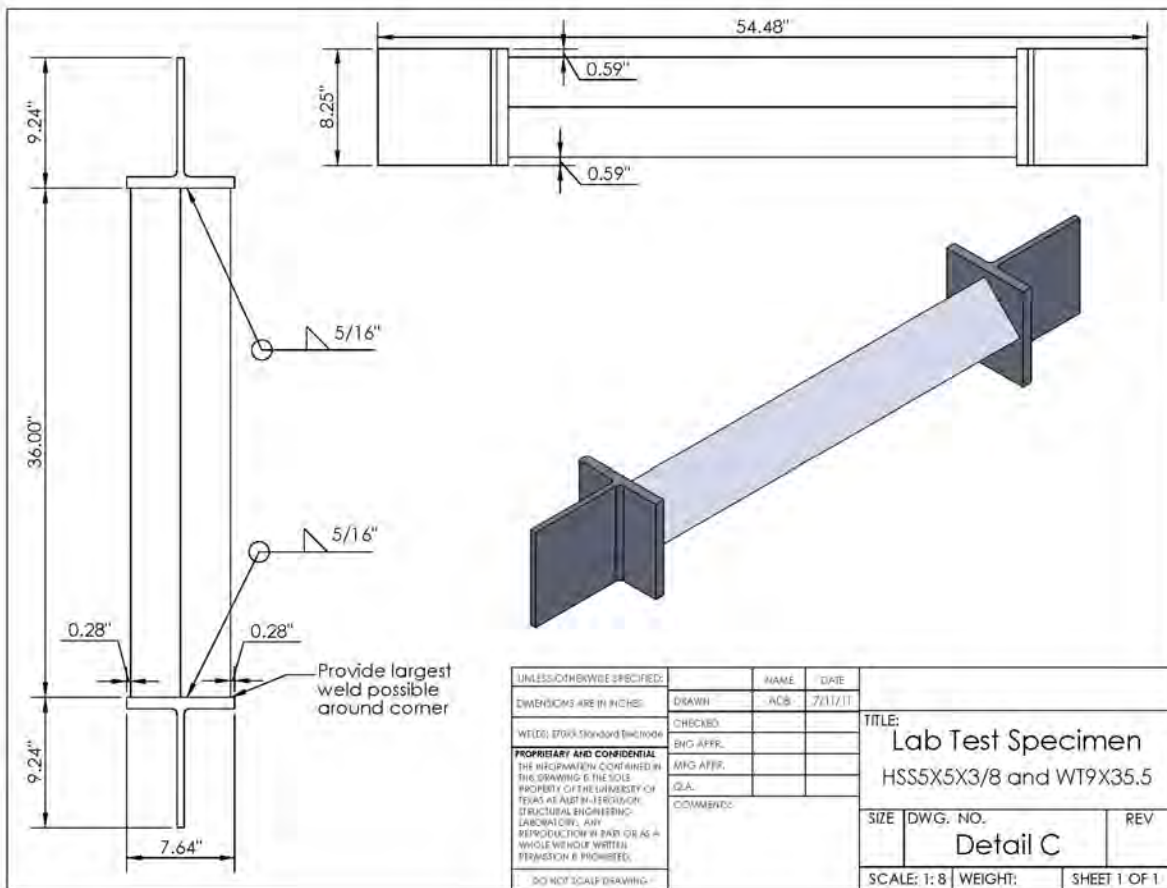


Figure 4.31: Diamond HSS Specimen with T-Stem Connection Detail

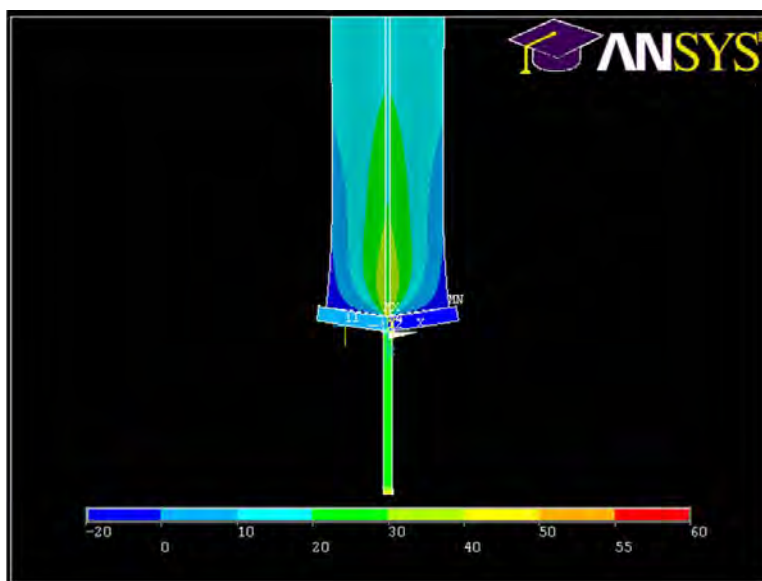


Figure 4.32: Axial Stress in Diamond HSS Tube Wall

In order to improve the finite element model associated with the experimental tests, numerous strain gages were attached to the HSS tube walls to measure the strain at various load levels. The general purpose strain gages were manufactured by Vishay Micro-Measurements and SR-4 with a 350 Ω resistance. In order to further examine the stress concentration effect, many gages were used in that particular region, as shown in Figure 4.33. Gages were also applied in the same pattern on the opposite wall to eliminate any effects from bending occurring due to an out-of-straightness of the specimen in the testing machine.

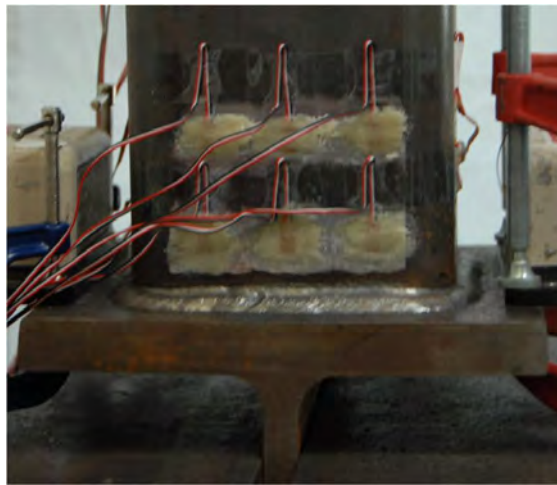


Figure 4.33: Strain Gages Applied to Tube Wall

4.7 T-Stem Connection Laboratory Experiments

4.7.1 Stiffness Tests

A series of stiffness tests were performed on the T-stem connection using an HSS 5 x 5 x 3/8 member fillet welded to the flange of WT 9 x 35.5 connections. The tests included the square, round, and diamond HSS detail as outlined in the previous section. An additional test utilizing a complete joint penetration weld with the square HSS connection was also performed and showed similar agreement to the fillet weld specimen. Figure 4.34 shows the stiffness data obtained from the tests.

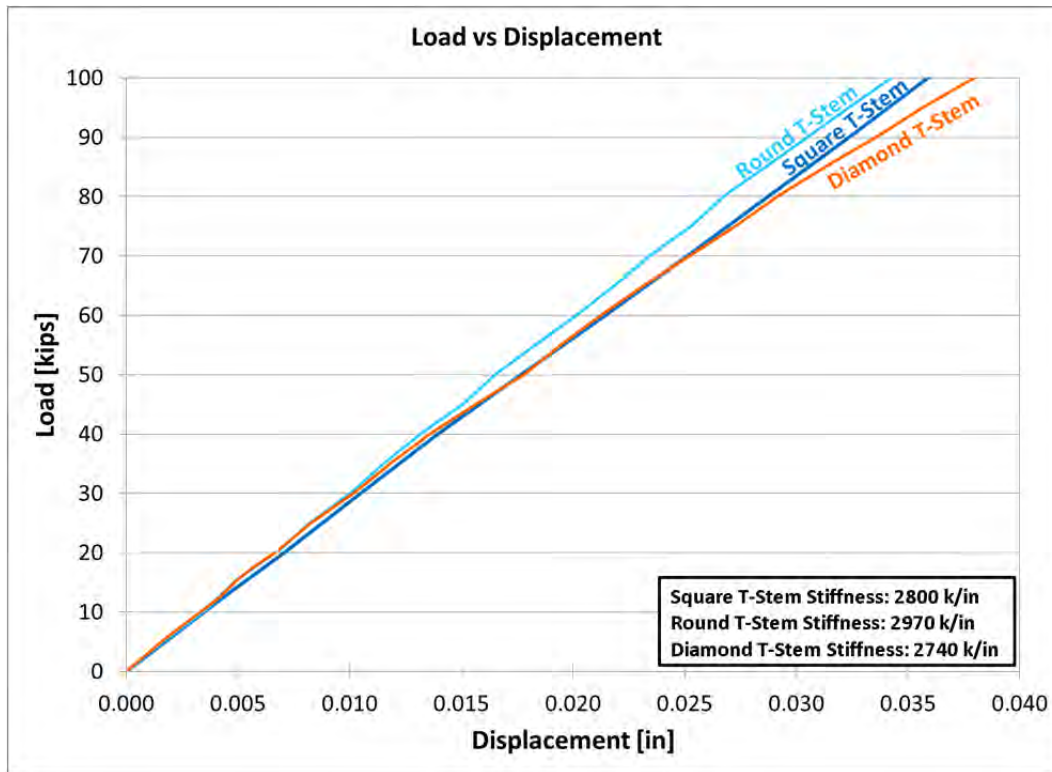


Figure 4.34: T-Stem Connection Stiffness Data

In order to compare the various connections performance, it is necessary to account for the area of the tubular member used. This will be discussed later in this chapter. However, since the square and diamond HSS connections use the same connections and tubes, their performance can be directly compared. Looking at the graph, we see the Square HSS connection is slightly stiffer than the Diamond HSS connection; however, they are practically the same, which is expected since the two specimens utilize the same connections and member.

4.7.2 Ultimate Strength Tests

After obtaining the stiffness of the T-stem connections, the tests were continued into the inelastic range to determine the ultimate strength and failure mechanism of the detail.

Square HSS 5 x 5 x 3/8 and WT 9 x 35.5 Connections

Using standard connection strength calculations, it was determined the limiting strength without resistance factors was approximately 204 kips corresponding to yielding of the WT stem. However, the weld fractured much before this at an applied load of 152 kips. The premature failure of the connection indicates the danger the aforementioned stress concentration poses on the behavior of the tubular member. The failure also highlights the necessity for a more accurate prediction method of the ultimate strength of the connection. Figure 4.35 shows the force versus displacement behavior of this connection type and Figure 4.36 shows the fractured condition of the specimen.



Figure 4.35: Ultimate Strength Test of Square HSS 5 x 5 x 3/8 and WT 9 x 35.5



Figure 4.36: Fracture in Fillet Weld Connection

Square HSS 5 x 5 x 3/16 and WT 12 x 31 Connections

A second square HSS specimen tested in tension consisted of an HSS 5 x 5 x 3/16 fillet welded to WT 12 x 31 connections. Similar to the previous test, the failure occurred in the weld prior to reaching its calculated strength. According to the strength calculations, yielding in the tube should have been the limiting state at a load of 187 kips. However, the welded connection

fractured at a load of 114 kips. Stiffness data for the test is given in Figure 4.37 and a photo of the fractured member is shown in Figure 4.38. As opposed to the thicker walled specimen, this specimen exhibited a substantial amount of ductility as the fracture in the weld spread along the tube face perpendicular to the T-stem. Figure 4.38 also exemplifies the bending in the WT flange that occurs as the weld begins to fracture.

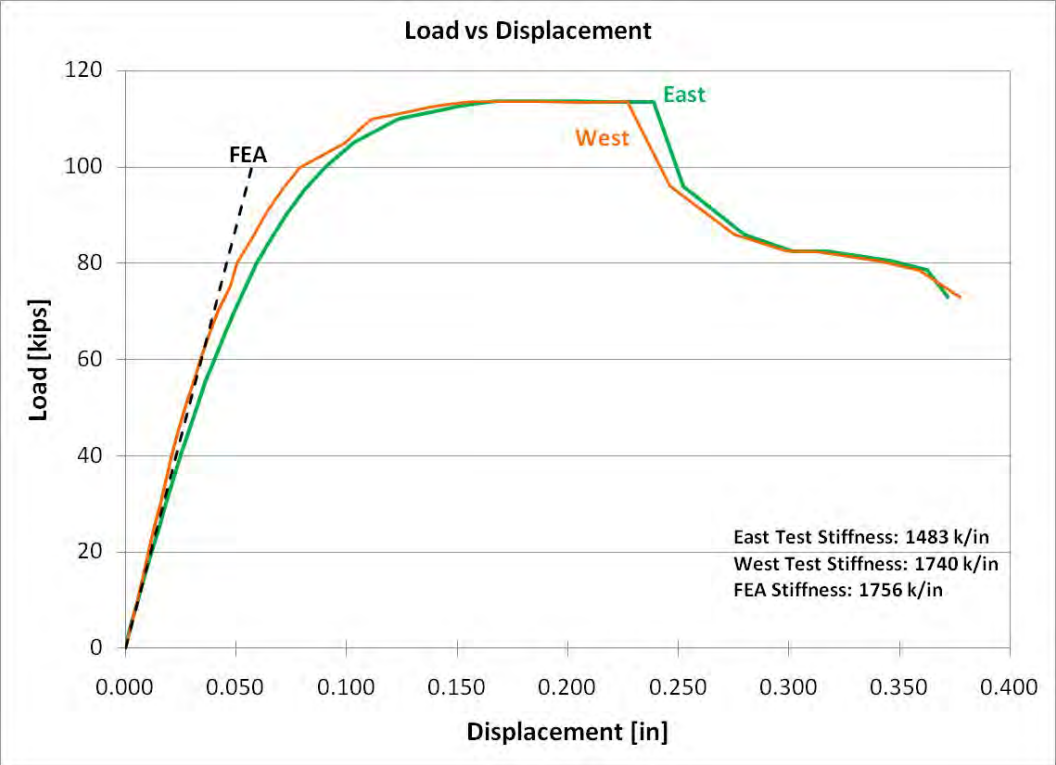


Figure 4.37: HSS 5 x 5 x 3/16 and WT 12 x 31 Stiffness Data



Figure 4.38: Fractured Connection

4.7.3 Fatigue Tests

In addition to the stiffness and strength behavior of the connections, it is necessary to determine the appropriate fatigue category for the connections according to the AASHTO Bridge design Specification. In order to assess the fatigue life, the test specimens were subjected to cyclic axial load to determine where the details rated.

Similar to the cast steel connection, the T-stem connection (square, round, or diamond) was designed to be concentric, however, at the local level, an eccentricity exists where the force is transferred from the flange of the T-stem into the wall of the tube. A cross section of the weld profile is shown in Figure 4.39.

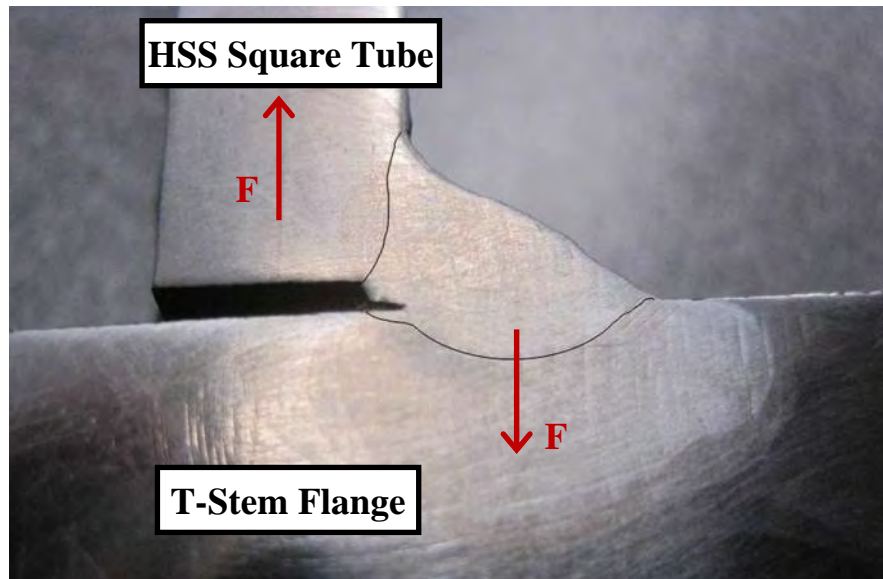


Figure 4.39: T-stem Connection Weld Eccentricity (with Weld Penetration Enhanced)

Unfortunately, this eccentricity drastically reduced the fatigue life of the connection. Due to the early failures of these HSS fillet welded specimens, a specimen utilizing a complete joint penetration groove weld was fabricated. The detail included a backup bar on the inside of the tube and was extremely difficult to fabricate. Plans of the detail are given in Figure 4.40.

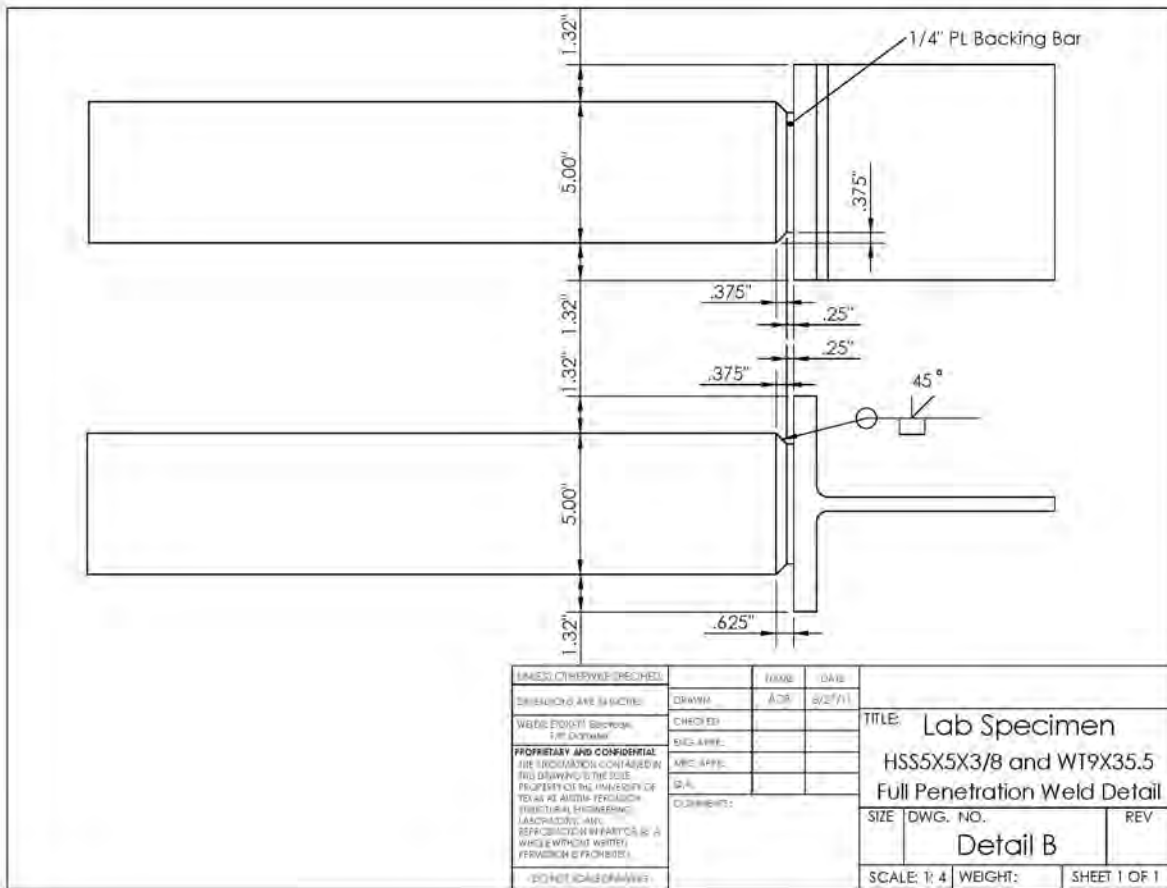


Figure 4.40: Complete Joint Penetration Groove Weld Detail

While this may not be a practical design option due to the high cost of complete joint penetration groove weld, it represented the maximum fatigue strength expected from this detail. Ultimately, this detail was tested in fatigue; however, stiffness data to a load of 100 kips (within the elastic range) was measured before fatigue testing occurred.

The tests presented in this section were conducted at stress cycles of 5 and 10 ksi applied at a 1.4 Hz frequency. The HSS tubes were connected to the WT 9 x 35.5 connections with 5/16" fillet welds. The following S-N plot was created with the results. Examples of fatigue cracks in the different details are presented in Figure 4.42 to Figure 4.45.

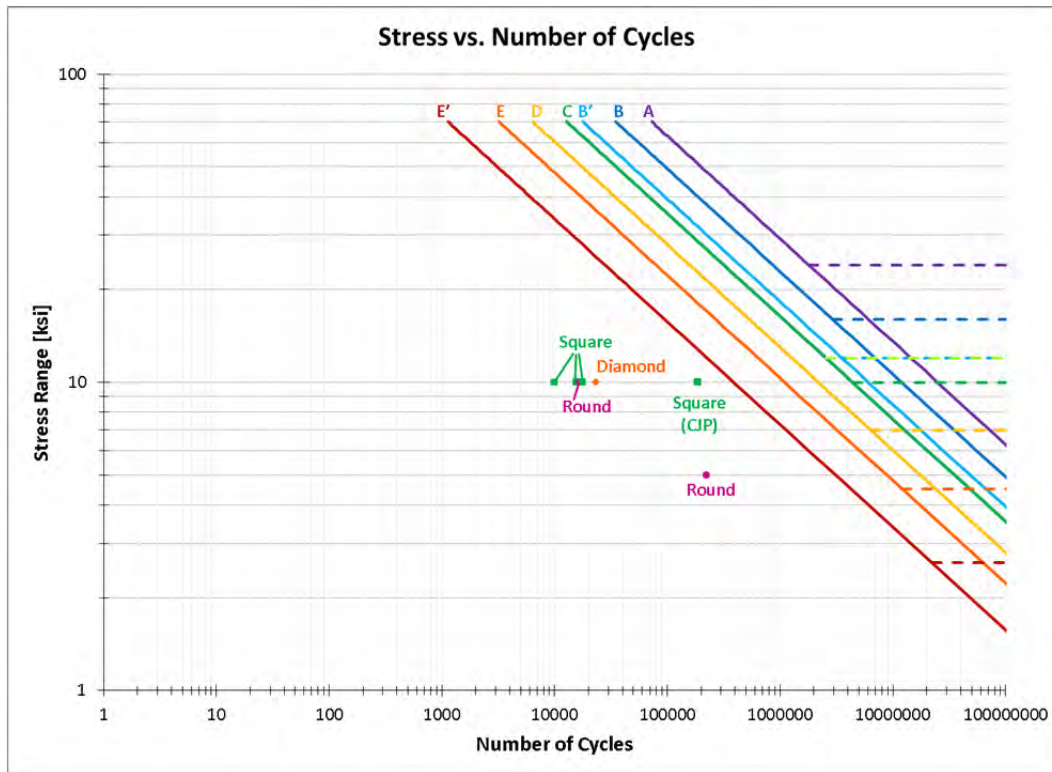


Figure 4.41: Fatigue Test Results



Figure 4.42: Example of Fatigue Crack Forming at Fillet Weld Root in Square HSS Connection



Figure 4.43: Example of Fatigue Crack Forming at CJP Weld Toe in Square HSS Connection



Figure 4.44: Example of Fatigue Crack Forming at Fillet Weld Root in Round HSS Connection



Figure 4.45: Example of Fatigue Crack Forming at Fillet Weld Root in Diamond HSS Connection

Unfortunately, none of the specimens reached the required number of cycles for fatigue categories allowed by AASHTO for use in steel bridge construction. Even the CJP specimen only reached half the life required by the E' detail, the lowest of the AASTHO allowed categories.

4.8 T-Stem Connection Test Observations

Multiple tests were performed on HSS members with T-stem connections. Due to the large stress concentration in the wall of the tube perpendicular to the stem, failure occurred in the welded connection prior to calculated failure loads using standard connection limit states. In terms of fatigue, the T-stem detail and square, round, and diamond HSS combination performs very poorly and is not recommended for use in bridge applications where fatigue problems are critical.

Part III: Knife-Plate Connection

4.9 Knife-Plate Connection Design

A third option for a connection to a tubular member is to use a knife-plate connection. The connection involves creating a slot in the tube in which the gusset plate can be inserted, then fillet welding the tube to the plate. Figure 4.46 shows a picture of the completed knife-plate connection.



Figure 4.46: Knife-Plate Connection

4.9.1 Stress Relief Hole

One way to improve the stress concentration at the forward edge of the fillet weld is to drill a stress relief hole. The hole creates a small region of compression in the vicinity of the start of the fillet weld, improving the fatigue life of the detail. The hole forces the tension stress to be “diverted” away from the forward edge, engaging the weld more uniformly along the length and minimizing the stress concentration. Figure 4.47 shows the knife-plate connection with the stress relief hole drilled.



Figure 4.47: Knife-Plate Connection with Drilled Stress Relief Hole

4.9.2 Slot Fabrication

To make the slot in the tube to receive the gusset plate, two methods were employed to determine if the fabrication had any effect on the fatigue performance of the detail. The first method involved drilling the stress relief hole and then saw-cutting the slot from the tube edge into the hole. The second method used a plasma torch to create the rectangular slot without the stress relief hole. The finish obtained with both methods are shown in Figure 4.48.



Figure 4.48: Fabrication of Knife-Plate Connection Using (a) Band Saw and (b) Plasma Torch

In all cases, the slot was centered on the wall of the square HSS 5 x 5 x 3/8 tube and the fillet weld connection length was 8 inches. The specimens with stress relief holes had diameters

of 1-5/16 inches, 1-5/16 inches, and 1-1/2 inches respectively. The gusset plates were cut from PL7 x 0.75 flat bar and were 20 inches long to allow for the connection length and suitable grip length for the MTS Universal Testing Machine. The weld was specified to be 5/16 inches.

4.10 Knife-Plate Connection Lab Experiments

Laboratory experiments were performed on the knife-plate connection to determine the stiffness of the tube and connection system as well as to determine the appropriate AASHTO fatigue category.

4.10.1 Stiffness Tests

The stiffness tests for the knife-plate specimen followed the parameters outlined at the beginning of the chapter. Figure 4.49 shows the stiffness test results.

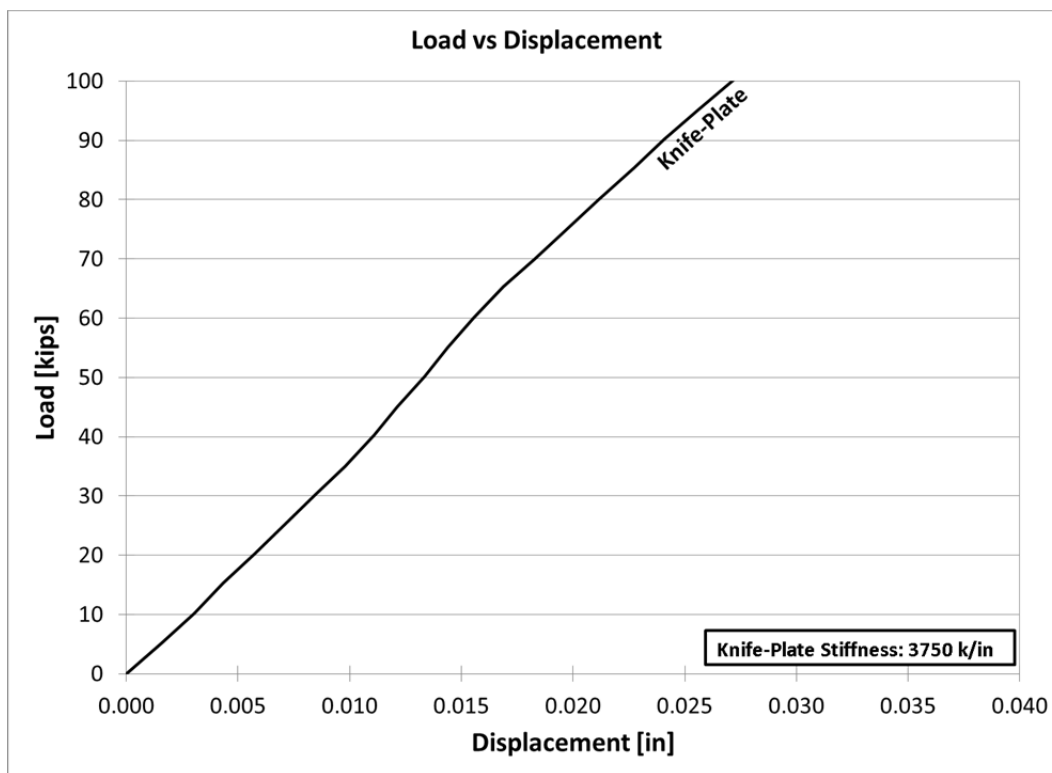


Figure 4.49: Knife-Plate Connection Stiffness Test Results

4.10.2 Ultimate Strength Tests

No ultimate strength tests were undertaken for the knife-plate connections. Numerous tests are described in the literature, and were summarized in Chapter 2.

4.10.3 Fatigue Tests

In total, six knife-plate specimens were tested in fatigue, three with the stress relief hole and three with only plasma torch-cut slots. The specimens with the stress relief hole achieved the AASHTO Category E detail, with one specimen achieving Category D. The specimens without

the stress relief hole achieved Category E', and almost made it to Category E. The one specimen failing prematurely had very large gaps in the fabrication of the torch cut slot. The results are plotted in Figure 4.50.

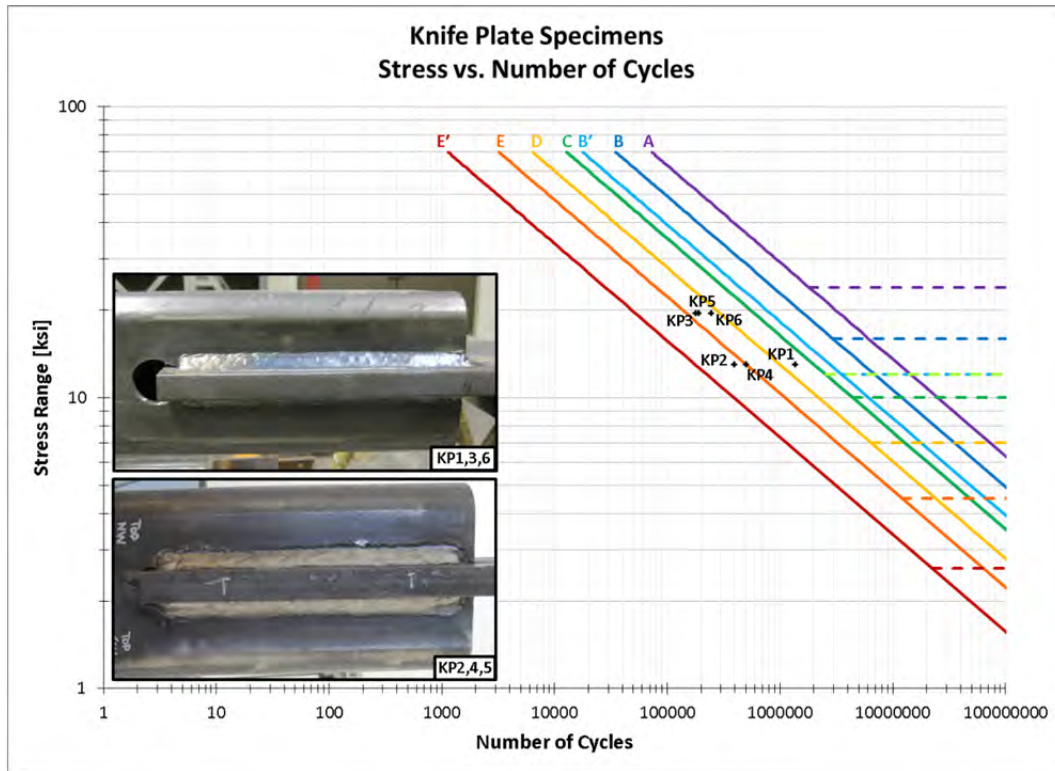


Figure 4.50: Fatigue Tests of Knife-Plate Connections

The fatigue tests indicated the knife-plate connection as a possible solution for tubular cross frame connections. Examples of fatigue cracks in the stress relief hole specimens and the torch-cut slot specimens are shown in Figure 4.51 and Figure 4.52 respectively.



Figure 4.51: Knife-Plate Connection Fatigue Crack (Stress Relief Hole)



Figure 4.52: Knife-Plate Connection Fatigue Crack (Torch-Cut Slots)

4.11 Knife-Plate Connection Observations

The test data suggests that the knife-plate connection is feasible for use with tubular members in cross-frames. In terms of fabrication, careful plasma-torching of the slot seems to be adequate to reach the AASHTO Category E detail requirements.

Part IV: Double Angle Connection

4.12 Double Angle Connection Design

A fourth option for single diagonal cross frame layouts is to use a double angle member. The connection detail would be identical to the current TxDOT X-type braces except the two diagonal angles would be aligned rather than crisscrossed. One major advantage of using a double angle along the diagonal is the elimination of connection eccentricity. The connections should have similar fatigue ratings as the current details, and may improve as the concentric connection may reduce out-of-plane bending. It is perceived the angle diagonals may still be connected at the midpoint by welding the angles to a spacer plate as this helps the double angle to work as a single member. But the resulting fabrication requirements and material usage would be identical to the current system, and may reduce as smaller angles may be possible for use on the diagonal. A picture of the double angle detail is shown in Figure 4.53.



Figure 4.53: Double Angle Detail

4.13 Double Angle Connection Laboratory Experiments

Laboratory experiments for the double angle connection included stiffness, strength, and fatigue tests. The tests involved using a double angle member sized at L4 x 4 x 3/8, a typical size utilized in current TxDOT designed braces. The connection length to both gusset plates was 8 inches.

Three different gusset plate sizes were used, each with a length of 20 inches to allow for connection and grip length. The PL7 x 0.75 connections were sized to guarantee failure in the double angle member in tension in the stiffness and strength tests, and were used in the first three fatigue tests. Since the majority of gusset plates used in real cross frames are only 0.5 in, three additional tests were conducted using PL7 x 0.5 connections. Lastly, a PL10.5 x 0.5 connection was tested, which offers the half inch thick plate while having the same area as the PL7 x 0.75 connections.

4.13.1 Stiffness Tests

The double angle detail was tested in tension according to the plan outlined at the beginning of the chapter. The results from the test are shown in Figure 4.54.

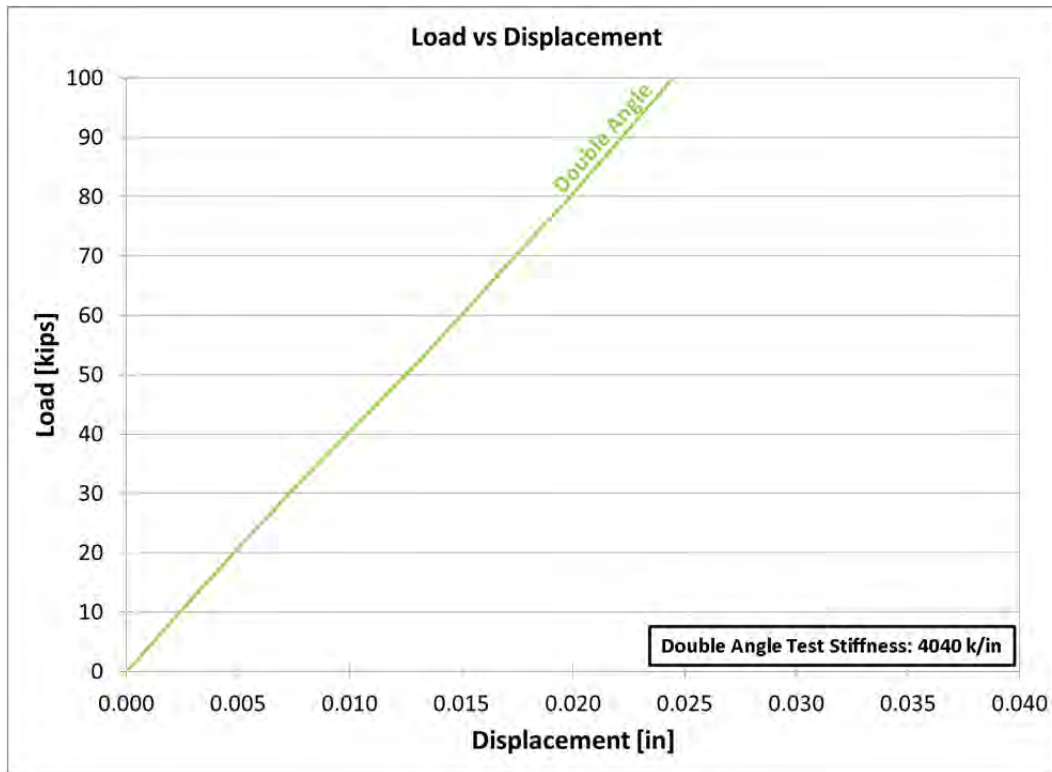


Figure 4.54: Double Angle Connection Stiffness Test Results

4.13.2 Ultimate Strength Test

To determine the strength and ductility offered by the double angle connection, tension was applied to the specimen to reach failure. However, the 220 kip MTS Universal Testing Machine did not have enough strength to fail the connection. The double angle reached the yield criteria and began to enter strain hardening region. Before its ultimate strength was achieved, the machine reached its capacity. The indication was significant ductility near yielding, and results from the single angle connection ultimate strength test confirm this speculation. Figure 4.55 shows the data obtained from the test.

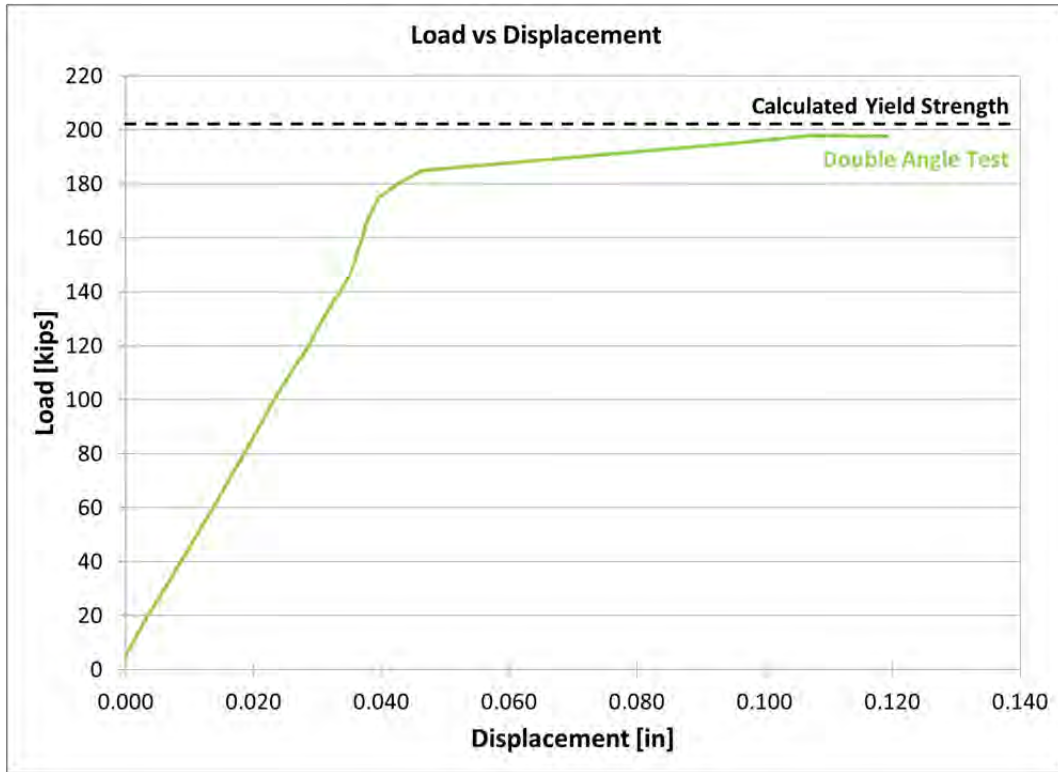


Figure 4.55: Double Angle Connection Ultimate Strength Test Results

4.13.3 Fatigue Tests

As discussed in the introduction to Section 4.13, three different gusset plate sizes were tested in fatigue. The results from the experiments are given in Figure 4.56.

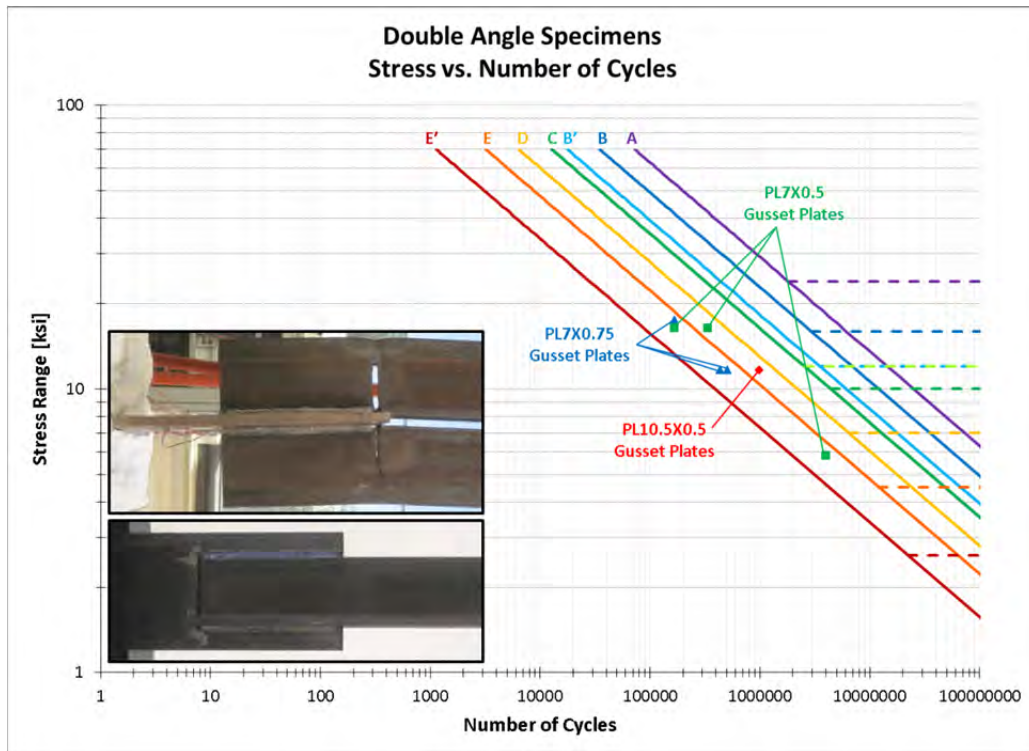


Figure 4.56: Double Angle Fatigue Test Results

From the fatigue tests, it is evident the double angle connection ranges from AASHTO Category E' to E. Examples of fatigue cracks observed in the tests are shown in Figure 4.57 and Figure 4.58. When reducing from the 0.75 in gusset plate to the 0.5 in gusset plate, two specimens experienced fatigue cracks in the gusset plate. A review of the FEA model indicates there is a second area of stress concentration at the back edge of the angles, with the effect magnified as the stress in the gusset plate increases. Since the stress in the PL7 x 0.5 plates was substantially larger than in the 2L4 x 4 x 3/8 members, the fatigue crack initiated in the plate. The PL10.5 x 0.5 specimen shows that it is only a function of the stress range in the plate and not the thickness of material as the cracks in this test occurred in the angles.



Figure 4.57: Double Angle Connection Fatigue Crack (Angle Member)



Figure 4.58: Double Angle Connection Fatigue Crack (Gusset Plate)

4.14 Double Angle Connection Observations

The double angle offers a suitable alternative to the existing single angle connection as it has the same AASHTO fatigue category (E'). However, the tests performed in fatigue seem to have the same boundary conditions as previous work for the single angles [McDonald and Frank 2009], potentially indicating the single angles may have worse fatigue behavior. Using the double angle along the diagonal only results in the same material usage as the X-type cross frame and offers the possibility of reducing the angle size to meet the same compression demands.

Part V: Single Angle Connection

4.15 Single Angle Connection Design

The single angle connection tested was the L4 x 4 x 3/8 member fillet welded to a PL7 x 0.75 gusset plate, with an overlap of 8 inches. This detail is currently used in practice and its performance was of interest to the researchers. Figure 4.59 shows the basic connection.



Figure 4.59: Single Angle Connection

4.16 Single Angle Connection Lab Experiments

Laboratory experiments for stiffness, strength, and fatigue were desired for study in TxDOT Project 0-6564. However, due to the eccentric loading of the angle, fatigue tests were not possible. Therefore, another test setup involving fatigue testing of complete cross frames was developed, and is described in Chapter 7.

4.16.1 Stiffness Tests

The single angle member was subjected to tension and the associated stiffness measured. Results from the stiffness test are plotted in Figure 4.60.

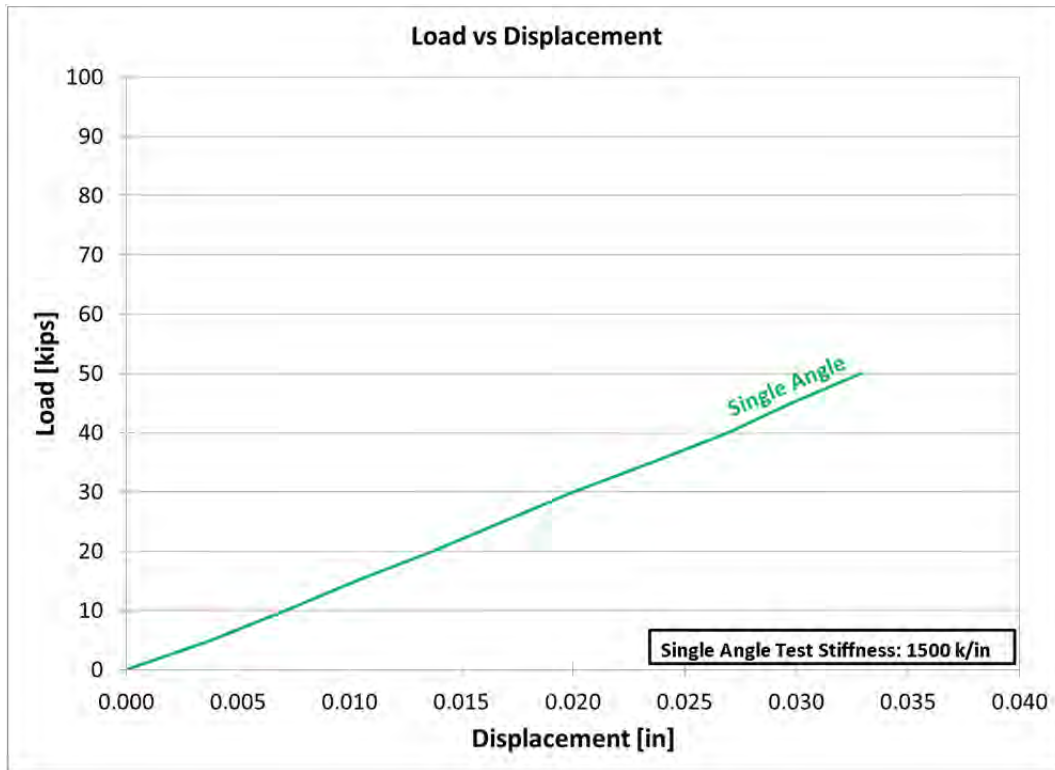


Figure 4.60: Single Angle Connection Stiffness Test Results

The eccentric loading of the angle significantly impacted the measured stiffness. Figure 4.61 shows the eccentricity of the member relative to the load through the gusset plate. The result is a substantial amount of bending, which reduces the stiffness.

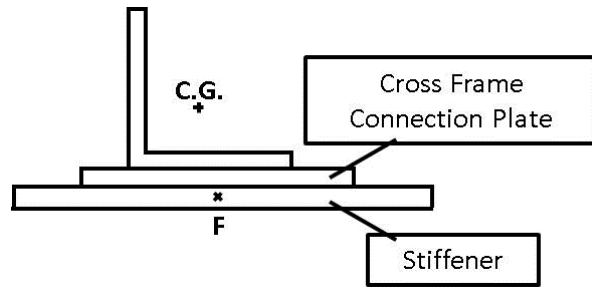


Figure 4.61: Single Angle Connection Eccentricity

4.16.2 Ultimate Strength Test

The single angle was tested to failure in the 220 kip MTS Universal Tension Machine. A significant amount of bending at the connection was observed. As the angle was loaded into the inelastic region, the angle yielded along the entire length, leading to a substantial amount of displacement. Unfortunately, the testing machine ran out of stroke length prior to fracture of the member. The data obtained is shown in Figure 4.62 and a picture of the deformed member is shown in Figure 4.63.

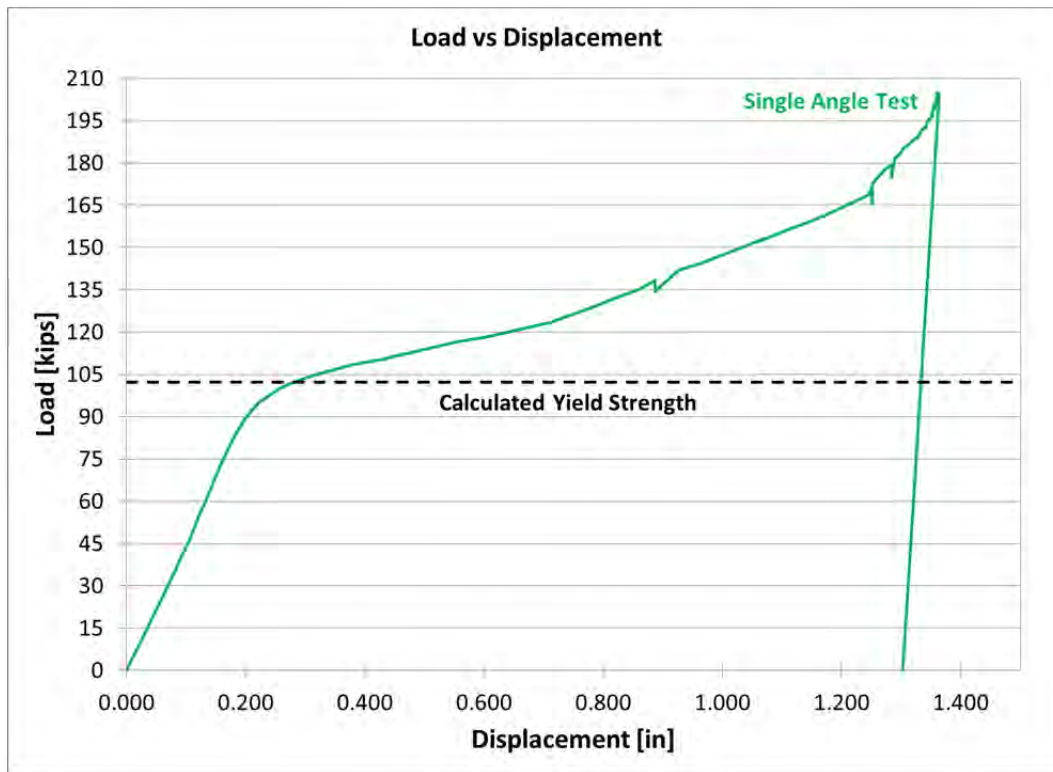


Figure 4.62: Single Angle Connection Ultimate Strength Test Results



Figure 4.63: Deformed Single Angle Connection

4.16.3 Fatigue Tests

As previously mentioned, concern for the testing machine due to the amount of bending of the single angle connection precluded the performance of any fatigue tests. Chapter 7 details an alternate test setup that was used to determine this detail's elusive fatigue behavior.

4.17 Single Angle Connection Observations

The single angle does not provide a very stiff connection due to the effect of the member bending under the eccentric loading. From a strength perspective, the detail meets typical strength checks and provides a significant amount of ductility. The fatigue behavior will be further examined in Chapter 7.

Part VI: Connection Comparison

4.18 Connection Stiffness Comparison

4.18.1 Calculation Procedure

When calculating the torsional stiffness of the cross frame, an elastic truss analysis is often employed [Yura 2001]. As previously stated in Chapter 2, for a tension-only system, the contribution of the compression diagonal is ignored, and the single diagonal model shown in Figure 4.64 (a) is analyzed.

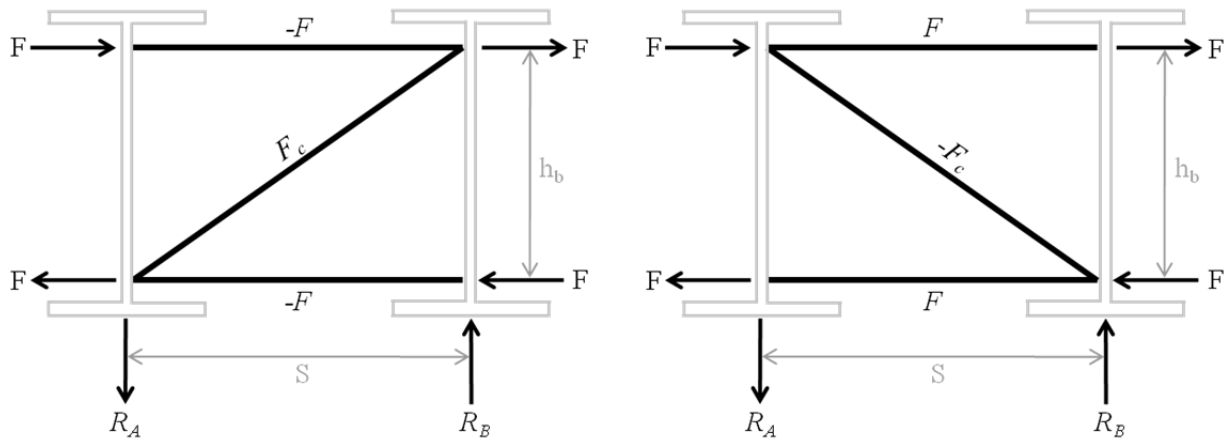


Figure 4.64: (a) Tension-Only System and (b) Compression System

Following the derivation provided by Quadrato [2010], a deflection analysis on the tension-only system is performed to determine the rotation of the cross frame, and ultimately the brace stiffness is (in accordance with the formula given by Yura [2001]):

$$\beta_{braxial} = \frac{Eh_b^2 S^2}{\frac{2L_c^3}{A_c} + \frac{S^3}{A_h}} \quad (4.1)$$

where $\beta_{braxial}$ is the torsional stiffness of the cross frame considering only the axial stiffness of the cross frame members, E is the modulus of elasticity (29000 ksi), h_b is the height of the brace (centroid of top strut to centroid of bottom strut), S is the girder spacing, L_c is the length of the diagonal member, A_c is the area of the diagonal member, and A_h is the area of each strut. Eq. 4.1 assumes that the ends of the cross frame members are pinned.

Conversely, if the diagonal has significant buckling strength, the truss analysis could be performed on the geometry of Figure 4.64 (b), resulting in the same torsional stiffness as Eq. 4.1, with the diagonal member in compression instead of tension.

Eq. 4.1 offers a useful design calculation to determine the torsional stiffness of the cross frame, but it simplifies the typical cross frame geometry and it neglects the possible impact of the member connections. To better isolate the effects of the connection, it is useful to put Eq. 4.1

in terms of the stiffness of the strut and diagonal. Eq. 4.1 assumes the strut member stiffness to be defined as:

$$k_h = \frac{A_h E}{S} \quad (4.2)$$

and the diagonal member stiffness as:

$$k_c = \frac{A_c E}{L_c} \quad (4.3)$$

Revisiting the derivation of Eq. 4.2, but substituting Eqs. 4.2 and 4.3 where appropriate, the following formula for $\beta_{braxial}$ is obtained:

$$\beta_{braxial} = \frac{h_b^2}{\frac{2L_c^2}{k_c S^2} + \frac{1}{k_h}} \quad (4.4)$$

In order to determine the stiffness of the members, the equation for springs in series will be used:

$$\frac{1}{k_T} = \frac{1}{k_{member}} + \frac{2}{k_{connection}} \quad (4.5)$$

where k_T is the total stiffness, k_{member} is the analytic stiffness of the member (Eqs. 4.2 and 4.3), and $k_{connection}$ is the stiffness of each connection.

Using the MTS universal tension machine, test data for the total stiffness of the members and connections was obtained. From the experiments, $k_{connection}$ can be determined using Eq. 4.5. Once known, Eq. 4.5 can then be used in conjunction with the cross frame geometry to determine k_c and k_h (including the contribution of the member and connection). Substituting k_c and k_h in Eq. 4.4 will give the torsional stiffness of the cross frame including member connection flexibility.

While Eqs. 4.4 and 4.5 may better represent the actual condition, it is recognized the process may not be suited for design calculations. The goal is to use the equations to estimate the magnitude of the effect of the connections and determine if it is necessary to include in design.

4.18.2 Test Specimen Summary

The T-stem connection specimens consisted of two sections of a WT member connected to square and round HSS tubes. The WT was sized to meet expected strength requirements based on the HSS tube strength, while also meeting the geometric constraint that the flange width had to exceed the tube width allowing enough space for the weld. The tube was centered on the flange of the WTs and welded to create the connection. Three types of T-stem connection specimens were created: (1) square HSS welded with the tube walls parallel to the edges of the WT flange, (2) square HSS welded with the tube walls at a 45 degree angle to the edges of the

WT flange (diamond), and (3) round HSS. Examples of the HSS specimens and WT connections are shown in Figure 4.65 (a-c).

The cast steel connection specimen comprised a round HSS member connected to two steel castings. The castings were designed to seal the tube, to minimize stress concentrations at the connection, and to allow for easy assembly. To achieve these effects, the casting fits to the outside diameter of the tube and tapers to a flat plate which can then connect to cross frame gusset plates or directly to girder stiffeners (Figure 4.65 (d)).

The knife-plate connection was fabricated by first drilling a 1-5/16 in stress relief hole (1.75 times the thickness of the knife-plate), centered approximately 8.8 in from the either end of the HSS 5 x 5 x 3/8 member. A 3/4 in slot was then saw cut to allow insertion of the gusset plate. The tube was then welded longitudinally to the knife-plates to create the connection (Figure 4.65 (e)).

The double angle connection was fabricated using 2 L 4 x 4 x 3/8 members, which is a typical size used in steel bridges [TxDOT 2006]. The members overlapped the gusset plate by 8 in, and were welded around all sides of the angles. Although designers will sometimes detail the welds for a balanced condition, i.e., the center of gravity of the weldment will align with the center of gravity of the angle, it was found the fully welded condition usually results in decreased fatigue behavior [McDonald and Frank 2009]. Since both stiffness and fatigue criteria are important in these connection tests, the fully welded condition was selected.

Similar to the double angle specimen, the single angle specimen was constructed from an L 4 x 4 x 3/8 member, overlapping the gusset plate by 8 in, and utilizing the fully welded condition. Additionally, a second transverse weld was situated on the back side of the angle, consistent with standard practice for TxDOT bridges [TxDOT 2006]. The double and single angles specimens can be seen in Figure 4.65 (f) and (g) respectively. Table 4.3 also summarizes the connection lengths for each of these variations.

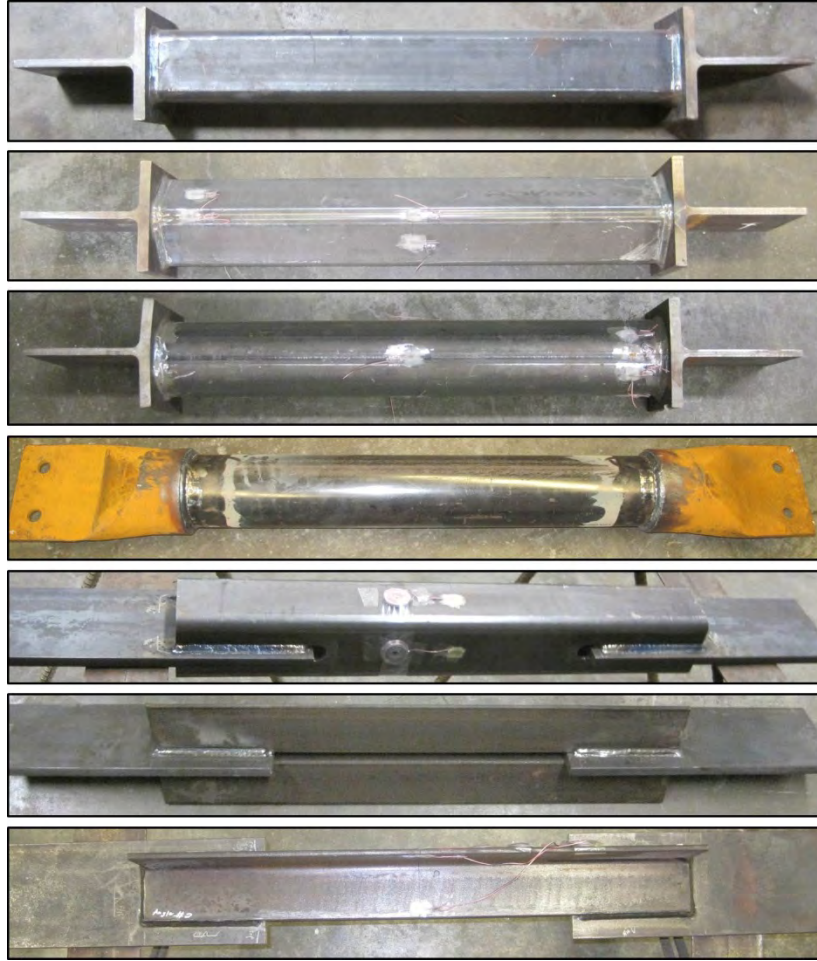


Figure 4.65: Test Specimens- (a) T-Stem and Square HSS, (b) T-Stem and Diamond HSS, (c) T-Stem and Round HSS, (d) Cast Connection, (e) Knife-Plate Connection, (f) Double Angle Connection, and (g) Single Angle Connection

Table 4.3: Test Specimen Geometry

Specimen	Member	Connection	Weld Length [in]	Weld Size [in]
T-Stem Square	HSS 5 x 5 x 3/8	WT 9 x 35.5	20	5/16
T-Stem Diamond	HSS 5 x 5 x 3/8	WT 9 x 35.5	20	5/16
T-Stem Round	HSS 5.563 x 0.375	WT 9 x 35.5	17.5	5/16
Cast Connection	HSS 5.563 x 0.375	Steel Casting	17.5	5/16
Knife-Plate	HSS 5 x 5 x 3/8	PL 7 x 0.75	32	5/16
Double Angle	2L 4 x 4 x 3/8	PL 7 x 0.75	20	5/16
Single Angle	L 4 x 4 x 3/8	PL 7 x 0.75	24	5/16

4.18.3 Test Results

Each of the specimens was placed in a uniaxial tension test machine and loaded to determine the stiffness of the assembly, as described earlier in this chapter. The stiffness of each specimen was determined by plotting the load versus deflection curve based on the measured force from the load cell in the MTS machine and the deflection read from the dial gages. Using a best-fit line through the data, the slope represents the stiffness of the specimen. Since the displacement readings include some region of the connection, which varied in width and thickness amongst the tests, the stiffness results from all the connection types are not directly comparable.

The knife-plate connection, double angle connection, and single angle connection utilized the same plate material to make the connections (PL 7 x 0.75), thereby allowing comparisons to be made between the tests. The total stiffness of the knife-plate specimen was measured to be 3750 kip/in, about 7% less than the stiffness of the double angle specimen despite having a 5% larger area. The lower stiffness may indicate the connection has a greater shear lag than the double angle specimen. Results for the knife-plate specimen, as well as the angle specimens are plotted in Figure 4.66.

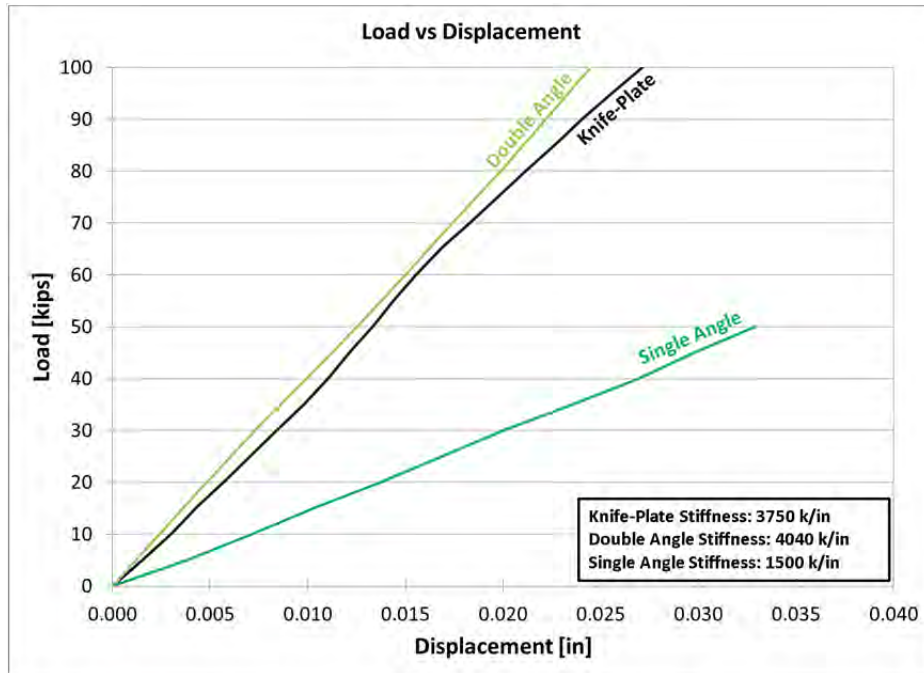


Figure 4.66: Summary of Stiffness Test Results- Knife-Plate, Double Angle, and Single Angle

The double angle specimen performed the best of these three connections, with a total stiffness of 4040 kip/in. On the contrary, the single angle specimen, representing the vast majority of cross frame members currently used, had a low stiffness of 1500 kip/in. While it would be expected the stiffness would reduce by half due to the cross-sectional area, the single angle stiffness is only 37% of the stiffness of the double angle. The most likely explanation is the eccentricity of load relative to the member. All of the other connections are concentric, reducing the amount of bending that occurs under direct tensile load. However, the single angle member is

loaded through one leg only, causing substantial bending of the member and therefore decreasing the stiffness available.

4.18.4 Relative Behavior of the Connections

In order to better understand the behavior of the connections relative to one another, an average stress versus average strain plot was created as shown in Figure 4.67. The stress was calculated using the measured force from the MTS machine and the measured area, which was calculated based upon the length of the member and the member weight. The strain utilizes the measured displacement divided by the sum of the length of the member and the distance from the end of the connections to the gage location/attachment point. The displacement was calculated by taking the average of the dial gages. By normalizing the force by the area of each member, and the strain by the length, Figure 4.67 shows the approximate performance offered by each connection.

It is observed the cast connection and the double angle connection perform the best, while the T-stem connections connected to the HSS 5 x 5 x 3/8 tubes are the most flexible. The current standard using single angle connections is not as effective as the casting, double angle, or knife-plate connections.

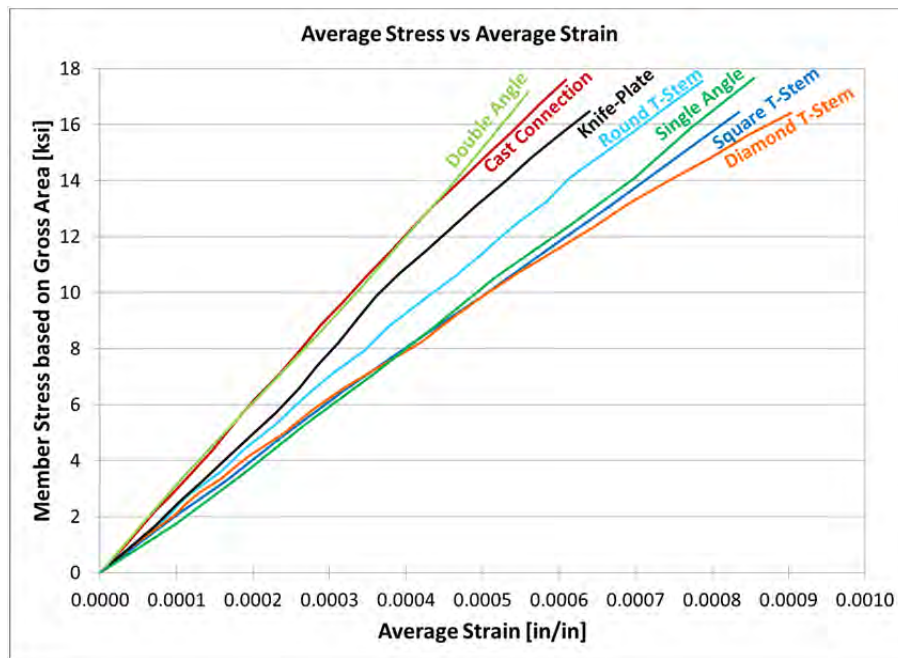


Figure 4.67: Relative Performance of Different Connections

4.18.5 Connection Stiffness

As outlined in Section 4.18.1, the connection stiffness can be calculated from the test data using Eq. 4.5. The results of these calculations are displayed in Table 4.4 and are grouped into the connections that could be compared to one another.

Table 4.4: Calculation of Connection Stiffness based upon Laboratory Tests

Specimen	Member Area [in ²]	Member Length [in]	Total Stiffness k_T [kip/in]	Member Stiffness k_{member} [kip/in]	Approximate Connection Stiffness $k_{connection}$ [kip/in]
T-Stem Square	6.09	36	2800	4910	13000
T-Stem Diamond	6.09	36	2740	4910	12400
T-Stem Round	5.69	36	2970	4580	16900
Cast Connection	5.69	36	3310	4580	23900
Knife-Plate	6.10	36	3750	4910	31700
Double Angle	5.81	36	4040	4680	59100
Single Angle	2.83	36	1500	2280	8800

Note: The connection stiffness includes the stiffness of the connecting plate, which varied between tests. Therefore, the connection stiffnesses shown are not comparable to one another.

The T-stem connection combined with square tubular members produced similar values of stiffness for the connection, about 13,000 kip/in. However, use of the round tube with the T-stem offered better performance at 16,900 kip/in.

The cast connection stiffness was determined to be 23,900 kip/in. The stiffness value of the cast connection is very useful in understanding the behavior since the casting was designed to fit a specific diameter of tubes, but multiple tube thicknesses. Therefore, the stiffness will not fluctuate due to connection plate thickness changes, weld length variations, or tube thickness changes.

The knife-plate connection had a test stiffness of 31,700 kip/in. The double angle connection was more rigid with a stiffness of 59,100 kip/in and performed better than the knife-plate while having a smaller overall area. Finally, the single angle connection was the most flexible, supplying only 8800 kip/in. It is interesting to see the detrimental effect of the eccentric loading on the single angle connection, by comparing it to the double angle comprised of the same cross-section.

4.18.6 Effect on Cross Frame Stiffness

Now that once the stiffness of each connection has been determined, the values can be combined with the cross frame member lengths to determine the effect of including connection behavior in the calculation of the torsional brace stiffness. Two extreme cases for plate girder depth, 54 in and 96 in, will be considered to identify the effect of connection stiffness on different cross frame sizes.

Using Eq. 4.5, total member stiffnesses for the struts and diagonal were found including the effect of the connection. These calculations utilized the dimensions shown in Figure 4.64, along with the standard areas given in the AISC Steel Construction Manual [2010]. Once solved for, the stiffnesses from Table 4.4 were substituted into Eq. 4.4 to determine the total torsional brace stiffness. The value was compared to Eq. 4.1 which does not include connection behavior. The results are summarized in Table 4.5.

From Table 4.5 it is observed the inclusion of connection behavior can reduce the cross frame stiffness by up to 19%. The square and diamond T-stem connections cause the biggest error, ranging from 16-17% at the larger 96 in girder depth, and from 18-19% at the shallower 54 in depth. The castings performed fairly well only reducing the stiffness by 9-10% at both girder depths considered. In reference to the double angle cross frame, it is anticipated that single angles would be used for the top and bottom struts, with a double angle along the diagonal. The inclusion of the single angles contributed to brace stiffness errors around 7-9%. Meanwhile, using all single angle sections in the tension-only calculation caused errors of 12-13%. The knife-plate cross frame was comparable to the double angle with errors of 7-9%.

Referencing Table 4.5, it is also concluded the reduction in axial brace stiffness due to connection effects is not highly sensitive to the girder depth. Comparing each connection at the two extreme depths considered, the percent decrease does not vary significantly between the two cases.

Table 4.5: Calculation of Cross Frame Stiffness Including the Effect of Member Connections

Girder Web Depth = 96 in, Girder Spacing = 10 ft							
Cross Frame Member Type	Member	Connection	k_h [kip/in]	k_c [kip/in]	$\beta_{braxial}$ (Eq. 1) [10 ⁶ kip-in/rad]	$\beta_{braxial}$ (Eq. 4) [10 ⁶ kip-in/rad]	Percent Decrease
T-Stem Square	HSS 5 x 5 x 3/8	WT 9 x 35.5	1210	1040	2.172	1.810	16.7%
T-Stem Diamond	HSS 5 x 5 x 3/8	WT 9 x 35.5	1200	1030	2.172	1.793	17.4%
T-Stem Round	HSS 5.563 x 0.375	WT 9 x 35.5	1190	1010	1.992	1.744	12.4%
Cast Connection	HSS 5.563 x 0.375	Steel Casting	1240	1050	1.992	1.814	8.9%
Knife-Plate	HSS 5 x 5 x 3/8	PL 7 x 0.75	1360	1150	2.172	2.008	7.6%
Double Angle	2L 4 x 4 x 3/8	PL 7 x 0.75	600	1090	1.721	1.596	7.3%
Single Angle	L 4 x 4 x 3/8	PL 7 x 0.75	600	500	1.048	0.921	12.1%

Girder Web Depth = 54 in, Girder Spacing = 10 ft							
Cross Frame Member Type	Member	Connection	k_h [kip/in]	k_c [kip/in]	$\beta_{braxial}$ (Eq. 1) [10 ⁶ kip-in/rad]	$\beta_{braxial}$ (Eq. 4) [10 ⁶ kip-in/rad]	Percent Decrease
T-Stem Square	HSS 5 x 5 x 3/8	WT 9 x 35.5	1210	1170	0.683	0.560	18.0%
T-Stem Diamond	HSS 5 x 5 x 3/8	WT 9 x 35.5	1200	1160	0.683	0.555	18.7%
T-Stem Round	HSS 5.563 x 0.375	WT 9 x 35.5	1190	1140	0.616	0.532	13.6%
Cast Connection	HSS 5.563 x 0.375	Steel Casting	1240	1190	0.616	0.556	9.7%
Knife-Plate	HSS 5 x 5 x 3/8	PL 7 x 0.75	1360	1300	0.683	0.624	8.6%
Double Angle	2L 4 x 4 x 3/8	PL 7 x 0.75	600	1250	0.550	0.503	8.5%
Single Angle	L 4 x 4 x 3/8	PL 7 x 0.75	600	570	0.357	0.311	12.9%

Note: The calculations for the double angle cross frame assume single angle struts and a double angle diagonal

4.18.7 Connection Stiffness Observations

Often in design, simplified formulas are used to determine the axial brace stiffness of the cross frame. These formulas typically do not consider the effect the connection may have on the stiffness of the brace. As part of using a single diagonal cross frame, experimental tests were conducted to characterize the stiffness of five different connections: (1) the T-stem connection, (2) the cast steel connection, (3) the knife-plate connection, (4) the double angle connection, and (5) the single diagonal connection. The tests showed that the round HSS tube with T-stem

connections offers higher stiffness than using square HSS members, despite having a lower cross-sectional area. Subsequent analysis showed the WT 9 x 35.5 T-stems to have a major impact on the torsional stiffness of the cross frame, reducing the value calculated by the current analytical formula by 12-20%. The cast connection performed fairly well, only resulting in a 9-10% decrease of stiffness relative to the current analytical formula.

The knife-plate connection reduced the brace stiffness by 7-9%, assuming the connection plates are similarly sized to the specimen. The eccentric loading of the single angle connection caused the reduction in brace stiffness to be larger (12-13%), but when combined with a double angle along the diagonal, the loss was limited to 7-9%. Again, these expected reductions are based on similarly sized connection plates and weld lengths.

Lastly, comparing brace stiffness reductions at a larger and smaller girder depth, the effect of including the connections led to roughly the same percent decrease between the two cases.

These stiffness calculations were determined based on specific connection sizes and details. Future parametric studies will be used to isolate the effect of the connection to apply to a broader range of connection geometries. While including the connection behavior in determining the torsional stiffness of the brace may be more accurate, it is not practical for design. For now, it seems the expected loss in stiffness is less than 10% for the connections commonly used, which can be accounted for by using appropriate safety factors.

4.19 Connection Fatigue Comparison

The fatigue behavior of the various connections is more easily compared than the stiffness properties. Using the S-N plot, the fatigue performance of all the different connections are shown in Figure 4.68 with the stress ranges, number of cycles to failure, and fatigue crack location shown in Table 4.6.

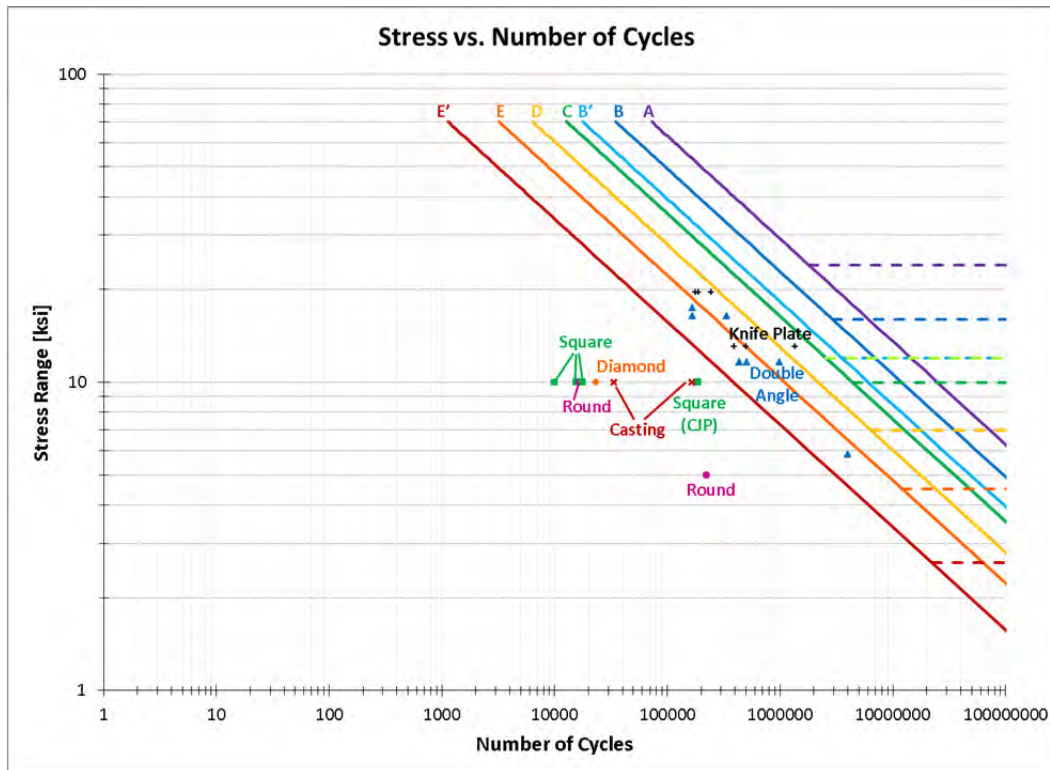


Figure 4.68: Fatigue Performance of Various Details

The following is a summary of the results of the fatigue tests:

- The Square, Round, and Diamond T-stem connections performed poorly in fatigue, most likely due to the transversely loaded fillet weld that has a slight load eccentricity when examined on the local level.
- The cast steel connection performed poorly in fatigue, similar to the T-stem connections.
- The knife-plate connections offered adequate performance, with 5 of 6 specimens achieving AASHTO Category E. The stress relief hole further increases the fatigue life, while using the saw or torch to cut the slots seems to have no effect.
- The double angle members meet the requirements of AASHTO Category E'. The cracks should form in the angles as long as the stress range in the gusset plate is not larger than in the member.
- The single angle member could not be tested due to the amount of bending that occurs due to the eccentric load pattern. An alternative test setup described in Chapter 7 will determine the fatigue behavior of these members.

Table 4.6: Fatigue Test Summary of Various Details

Fatigue Test	Member				Connection		Weld		Controlling S_R (ksi)	N	Crack Location
	Size	Nominal S_R (ksi)	Shear Lag Factor U	S_R (ksi)	Size	S_R (ksi)	Type	Size			
F-ST1	HSS 5 x 5 x 3/8	10	-	10	WT 9 x 35.5	16.61	Fillet	5/16	10	9884	Weld
F-ST2	HSS 5 x 5 x 3/8	10	-	10	WT 9 x 35.5	16.61	Fillet	5/16	10	17603	Weld
F-ST3	HSS 5 x 5 x 3/8	10	-	10	WT 9 x 35.5	16.61	Fillet	5/15	10	15669	Weld
F-ST4	HSS 5 x 5 x 3/8	10	-	10	WT 9 x 35.5	16.61	CJP	5/16	10	186692	Weld
F-RT1	HSS 5.563 x 0.375	10	-	10	WT 9 x 35.5	15.04	Fillet	5/16	10	16394	Weld
F-RT2	HSS 5.563 x 0.375	5	-	5	WT 9 x 35.5	7.53	Fillet	5/16	5	222184	Weld
F-DT1	HSS 5 x 5 x 3/8	10	-	10	WT 9 x 35.5	16.61	Fillet	5/16	10	23228	Weld
F-CC1	HSS 5.563 x 0.375	10	-	10	Casting	14.20	Fillet	5/16	10	33557	Weld
F-CC2	HSS 5.563 x 0.375	10	-	10	Casting	14.20	Fillet	5/16	10	165756	Weld
F-KP1	HSS 5 x 5 x 3/8	10	0.766	13.05	PL 7 x 0.75	11.62	Fillet	5/16	13.05	1360317	Tube
F-KP2	HSS 5 x 5 x 3/8	10	0.766	13.05	PL 7 x 0.75	11.62	Fillet	5/16	13.05	392727	Tube
F-KP3	HSS 5 x 5 x 3/8	15	0.766	19.58	PL 7 x 0.75	17.77	Fillet	5/16	19.58	190226	Tube
F-KP4	HSS 5 x 5 x 3/8	10	0.766	13.05	PL 7 x 0.75	11.62	Fillet	5/16	11.62	497842	Gusset
F-KP5	HSS 5 x 5 x 3/8	15	0.766	19.58	PL 7 x 0.75	17.77	Fillet	5/16	19.58	176546	Tube
F-KP6	HSS 5 x 5 x 3/8	15	0.766	19.58	PL 7 x 0.75	17.77	Fillet	5/16	19.58	246176	Weld
F-DA1	2L4 x 4 x 3/8	10	0.859	11.64	PL 7 x 0.75	11.12	Fillet	5/16	11.64	436278	Angle
F-DA2	2L4 x 4 x 3/8	15	0.859	17.46	PL 7 x 0.75	16.13	Fillet	5/16	17.46	166983	Angle
F-DA3	2L4 x 4 x 3/8	10	0.859	11.64	PL 7 x 0.75	10.73	Fillet	5/16	11.64	507435	Angle
F-DA4	2L4 x 4 x 3/8	10	0.859	11.64	PL 7 x 0.5	16.39	Fillet	5/16	16.39	166809	Gusset
F-DA5	2L4 x 4 x 3/8	10	0.859	11.64	PL 7 x 0.5	16.39	Fillet	5/16	16.39	335986	Gusset
F-DA6	2L4 x 4 x 3/8	5	0.859	5.82	PL 7 x 0.5	8.2	Fillet	5/16	5.82	3971604	Angle
F-DA7	2L4 x 4 x 3/8	10	0.859	11.64	PL 10.5 x 0.5	10.65	Fillet	5/16	11.64	986449	Angle

4.20 Cross Frame Connection Conclusions

There are a variety of connections that can be used to connect the cross frame members to the gusset plates. The T-stem connections, while convenient from a fabrication perspective, do not provide a very stiff connection, typically fail below calculated loads, and have poor fatigue performance. Therefore, the research team did not consider this detail further.

The cast steel connection provides a stiff connection and meets standard strength checks. However, its poor performance in fatigue prevents it from being a suitable option for steel bridge cross frames.

The knife-plate connection offers the best fatigue performance of those details investigated, but fabrication and material costs will be higher. From a fatigue standpoint, plasma torching could be used to streamline the fabrication of the slot with minimal effect on fatigue life. The knife-plate connection provides one of the stiffest connections.

The double angle connection provides a reasonably stiff connection and meets typical strength calculations. The fatigue performance meets the minimum AASHTO requirements.

The single angle connection is relatively flexible due to the eccentric loading on the angle, which leads to substantial bending of the angle at the connection. This bending prevents fatigue tests from being performed in the MTS Universal Testing Machines due to damage concerns. Chapter 7 highlights an alternative test setup to categorize the fatigue performance of the single angle.

Chapter 5. Laboratory Tests for Cross Frame Strength and Stiffness

5.1 Introduction

The experimental program that is documented in this report consisted of cross frame tests and tension coupon tests on the cross frame materials. The purpose of the cross frame tests was to measure the stiffness and the ultimate strength of cross frames from a stability bracing perspective. The results of these tests provide valuable insight into the behavior of various cross frame systems, provide data on the performance of different connections, and also provide validation data for analytical and computational models. The cross frames that were tested include conventional cross frame system as well as newly proposed cross frame systems. To achieve the desired functions, the test setup was designed and fabricated with the following capabilities:

1. Deformations were applied to the cross frames that were consistent with buckling deformations of adjacent girders. The deformations were achieved by applying loads through actuators as shown in Figure 5.1 to achieve the loading condition given in Figure 2.4. Loads and displacements values were monitored throughout the tests.
2. The focus of the tests was the stiffness of cross frame systems including the flexibilities of the cross frame members and the connections. Flexibilities discussed in Equation 2.9, such as the web distortion and the in-plane stiffness of the girders were not to be included in the tests. Efforts were made to restrain out-of-plane twists of the cross frames.
3. The test setup was designed so that cyclic loading could be applied to obtain a measure of the stiffness by racking the cross frame in both directions within the plane of the frame. The tests setup was also designed so that a measure of the ultimate strength of cross frame specimens could be obtained.
4. The test setup was designed and fabricated so that specimens could be easily removed and additional specimens installed.

In addition to the cross frame tests, material tests were also conducted on tension coupons that were removed from the cross frame members to obtain the stress versus strain characteristics of the material. Discussions of the test setup, the test program, and corresponding results are provided in the remainder of this chapter.

5.2 Test Setup

5.2.1 Test Frame

The loading condition depicted in Figure 2.4 consists of equal but opposite moments on each side of the cross frame. In order to achieve this loading condition, four equal forces must be applied to the four corners of the cross frame in the specified directions such as those depicted in Figure 5.1. The setup was fabricated at the Ferguson Structural Engineering Laboratory at The University of Texas at Austin. The setup dimensions are indicated in the plan view drawing in Figure 5.2.



Figure 5.1: Overall View of Cross Frame Test

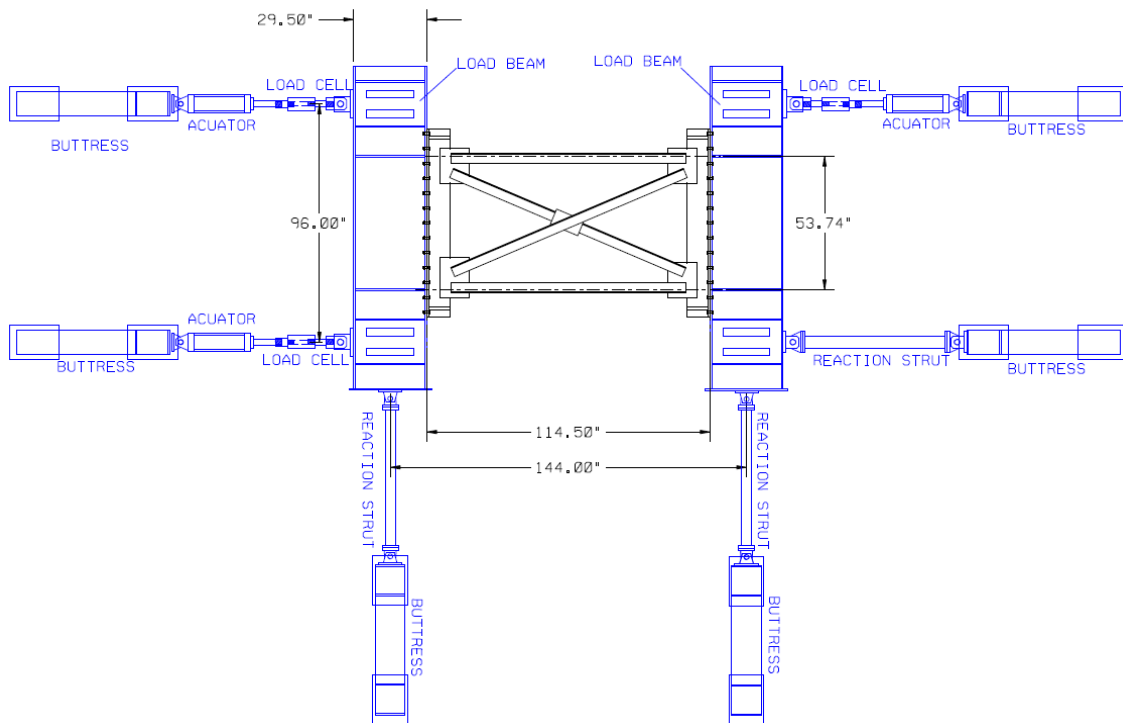
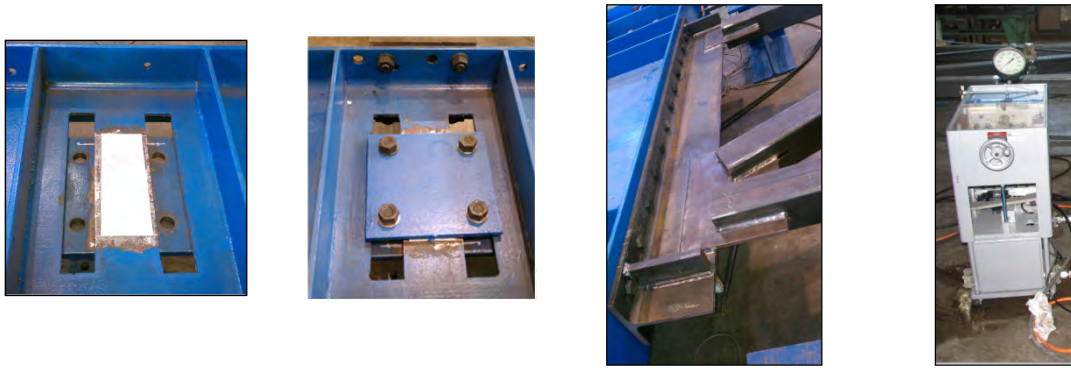


Figure 5.2: Cross Frame Test Plan Drawing

The members designated “load beams” in the figure represent the cross sections of two adjacent girders that are connected by the cross frame test specimen. The deformations that were applied through the actuators were consistent with the lateral torsional buckling deformations of two adjacent girders. W30x90 sections were used for the load beams due to the high in-plane stiffness. Bearing stiffeners were used at the locations of the struts to create a relatively rigid cross section that would not distort so that the primary stiffness being measured in the tests was

the cross frame members. The cross frame specimen was mounted into the test setup with WT members (WT9x35.5) that were bolted to the two load beams. The load beams were elevated off the floor using W21x111 supports and were also anchored by top plates (Figure 5.3 (a) and (b)). Teflon was placed between the contact surfaces of the anchoring plate and the beams to create a low-friction sliding surface as the load beams were displaced by the actuators during testing. The WT section at both ends of the cross frame specimen (Figure 5.3 (c)) provides a reasonable simulation of a connection stiffener that is welded to top and bottom flanges of the girder which is consistent with bridge detailing practices. The WT section is stiffened at both ends to prevent distortions out of the plane of the cross frame. As noted above, bolted connections were used between the WT sections and the load beams to allow multiple use of the test setup.

Loads were exerted by tension-compression actuators connected to the load beams. Actuators were installed at three corners of the test frame and the force at the fourth corner is provided by a reaction strut. Provided equal magnitude forces, F , are applied by the three actuators, with minimal friction from the sliding surfaces and fixtures, equilibrium dictates that the force in the reaction strut will be also F . Reaction struts at the bottom of the two load beams were installed to simulate roller supports. To achieve equal loads in the three actuators, a load maintainer (Figure 5.3 (d)) was used so as to control the hydraulic pressure to the three different actuators. The actuators have different compression and tensile areas, and the EDISON hydraulic load maintainer can be used to adjust the pressures to achieve and maintain equal load magnitudes in the actuators throughout the test.



(a) Teflon Bearing (b) Anchoring Plate (c) WT Connection (d) Load Maintainer

Figure 5.3: Details of Test Setup

5.2.2 Loading and Moments Measurement

The tests were conducted in a load controlled process. The applied load from the actuator was monitored by LEBOW 150 kips load cells as shown in Figure 5.4. To offer some redundancy in force measurements, the strains in the three reaction struts were monitored by strain gages installed at the mid-length on the opposite sides of the round tubes to account for bending effects (Figure 5.5). In order to obtain accurate force measurement, the load cells and the reaction struts were calibrated in a test machine before assembly into the setup. Figure 5.6 shows the calibration tests. Load levels in the calibration tests were kept in the elastic region with load levels consistent with the maximum values expected in the tests.



Figure 5.4: Load Cell for Actuator

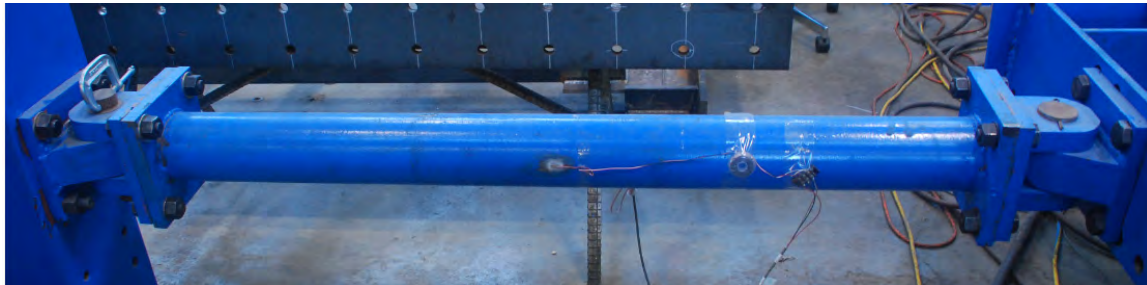


Figure 5.5: Strain Gage on Reaction Strut



Figure 5.6: Calibration of Force Measurement

The effective moment applied to the cross frame specimens can be determined based on the measured forces. A representative free body diagram of the whole test setup is depicted in Figure 5.7. The force, F , shown in the horizontal direction represents the value measured from the load cells. The force, R , shown in the vertical direction represents the force in the strut that was determined from the strain gage measurements. The applied moment at one side of the test frame could be represented as:

$$M_{applied} = FD = \frac{1}{2}RS \quad (5.1)$$

Since there is redundancy in measuring the applied moment, the average of the results from two calculations was used in later evaluation.

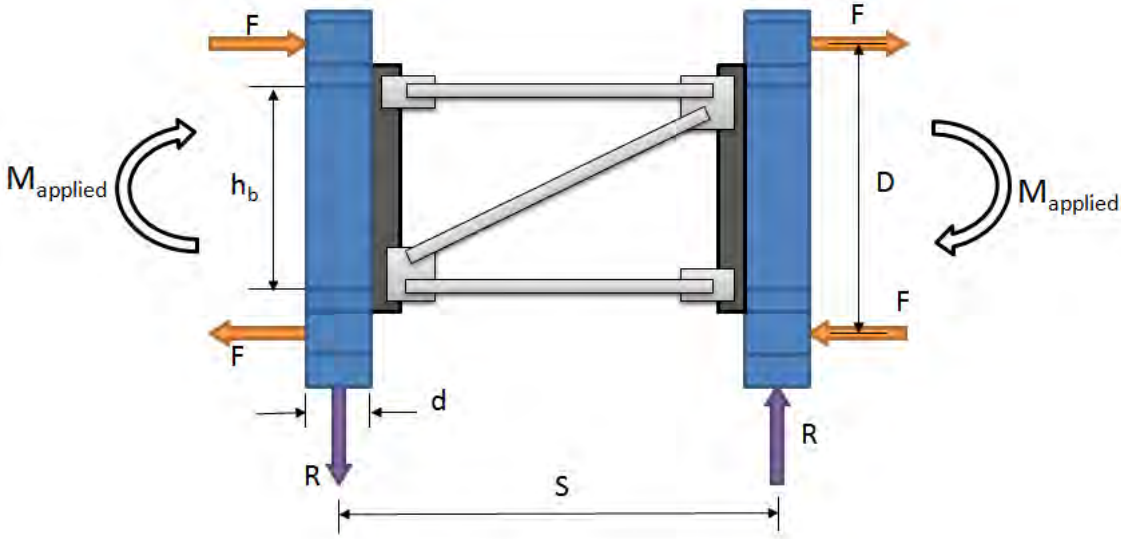


Figure 5.7: Free-body of Test Setup

The equilibrium representation of a single load beam is depicted in Figure 5.8, and the resulting moment applied at the load beam-cross frame interface could be evaluated as:

$$M_{frame} = M_{applied} - \frac{1}{2}Rd \quad (5.2)$$

M_{frame} represents the moment applied to the cross frame for use in evaluating the cross frame stiffness. M_{frame} can be also represented as a force couple of F_{equiv} , which is equivalent to the applied forces shown in the truss analogy sketch from Figure 2.4. The key geometric and mechanical parameters related to the test setup are summarized in Table 5.1

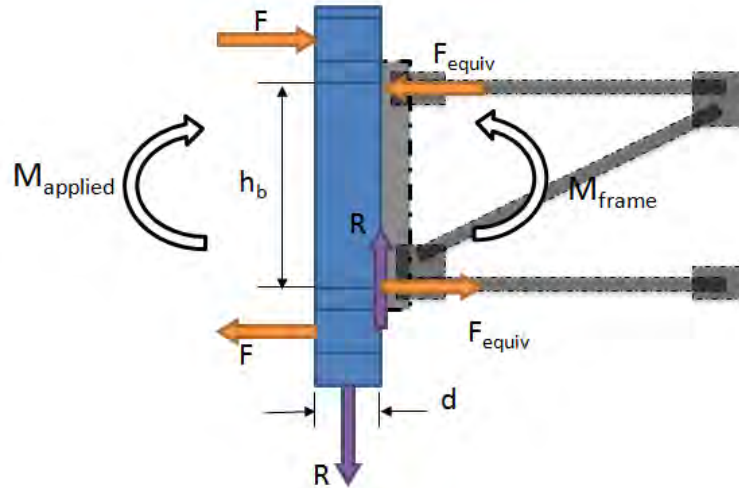


Figure 5.8: Equilibrium of a Load Beam

Table 5.1 Key Parameters in Test Setup

Parameter Name	Symbol	Value
Load Beam Spacing	S	144 in
Cross Frame Length (or Girder Spacing)	S'	114.5 in
Loading Spacing	D	98 in
Brace Height	h_b	53.74 in
Depth of Load Beam	d	29.5 in
Moment Applied on the Test Frame	$M_{applied}$	$98F$
Reaction	R	$1.36F$
Moment Applied on the Cross Frame	M_{frame}	$78F$
Equivalent Force Applied on the Cross Frame	F_{equiv}	$1.45F$

Note: F is the load reading from the actuators.

5.2.3 Measurement of Rotations

As defined in Figure 2.4, the angle, θ , represents the deformational rotation at one end of the cross frame. The deformations in the test setup are slightly different from those depicted in Figure 2.4, because the additional rotation in the vertical direction must be considered in the evaluation of total rotation, as illustrated in Figure 5.9.

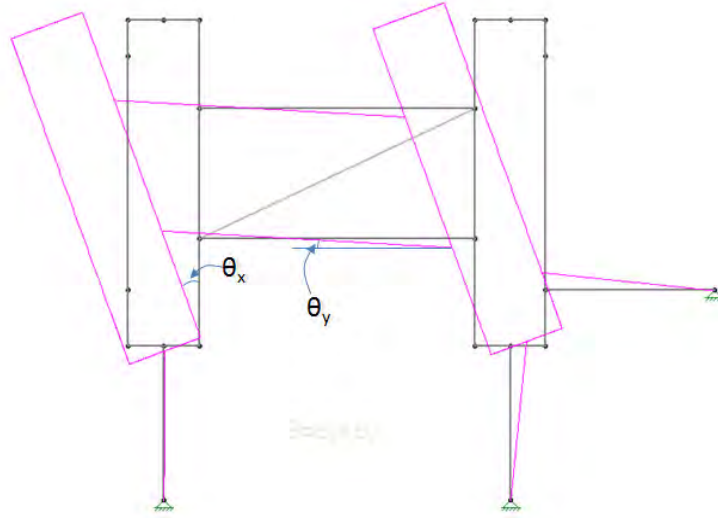


Figure 5.9: Cross Frame Rotation in Test Setup

The total rotation of one load beam is the summation of two rotational components:

$$\theta = \theta_x + \theta_y \quad (5.3)$$

Where:

$$\theta_x = \frac{(\delta_1 - \delta_2) + (\delta_3 - \delta_4)}{2h_b} \quad (5.4)$$

$$\theta_y = \frac{\delta_5 - \delta_6}{S'} \quad (5.5)$$

and $\delta_1, \delta_2, \dots, \delta_6$ are measured displacement as indicated in Figure 3.10.

It should be noted that at each location from δ_1 through δ_4 , two linear potentiometers (Precision of 0.001") were placed at the top and bottom side of the WT connection member, shown in Figure 5.10 and Figure 5.11, so the average of the two reading accounts for measurement error that may occur due to potential twist of the WT section.

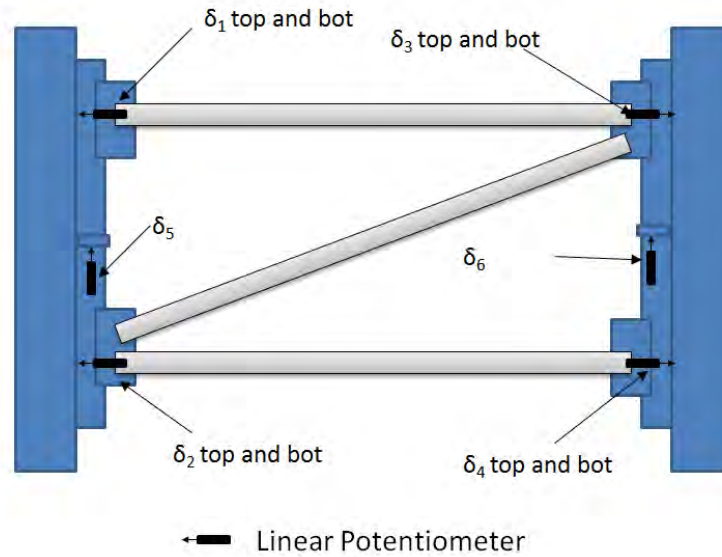


Figure 5.10: Displacement Measurements

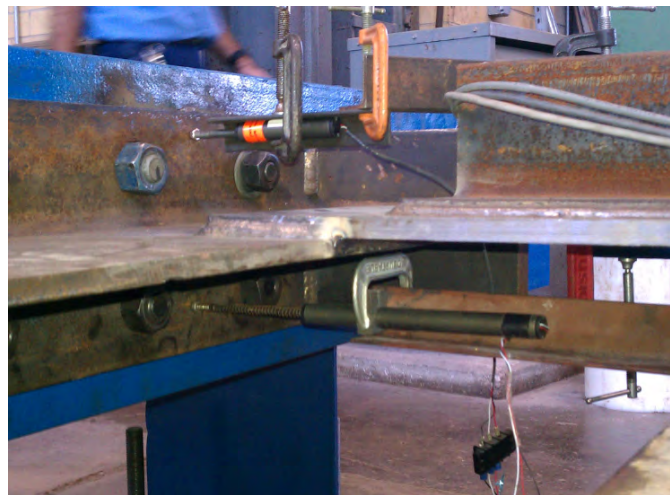


Figure 5.11: Linear Potentiometers Locations

The expression in Equation 5.6 was used to calculate the stiffness of the cross frame. The rotation θ was the average of the rotations measured from the two load beams.

$$\beta = \frac{M_{frame}}{\theta} \quad (5.6)$$

5.2.4 Measurement of Member Axial Forces

Axial forces in the cross frame members were determined from strain gage measurements from gages placed midway between connection points in the individual members. Conversion from strain to force for symmetric sections such as square tube members was obtained by averaging the two strain readings placed symmetrically on either side of the center of gravity (CG) of the section.

Estimating the axial force component in members with eccentric connections, such as single angles, can be more challenging. Previous research has shown a regression method provides a successful method for obtaining the forces in angle members (Helwig and Fan 2000), which was the method employed in this research. Four strain gages placed as depicted in Figure 5.12(b) were used to determine the forces in the angles.

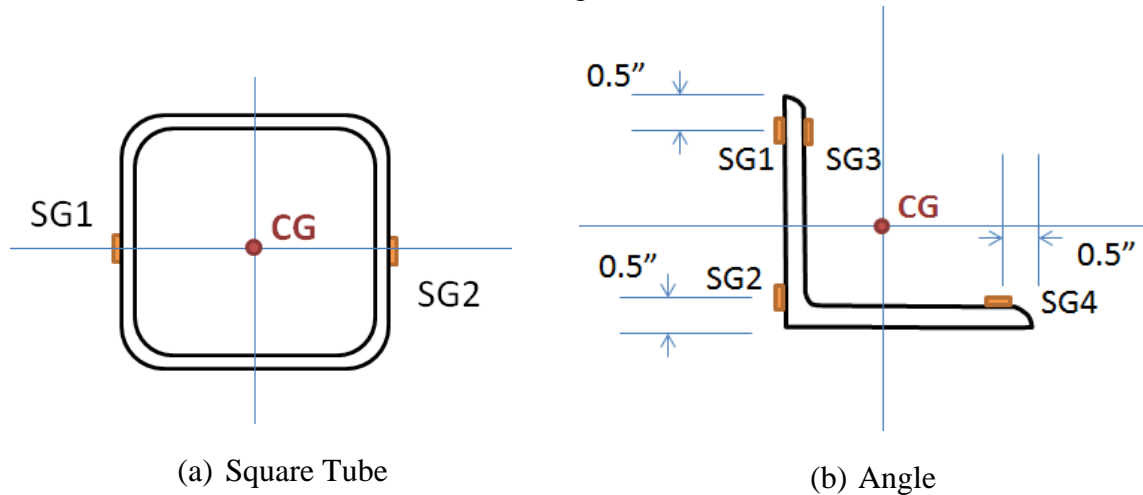


Figure 5.12: Force Measurement of Cross Frame Member

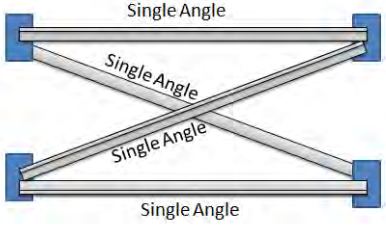
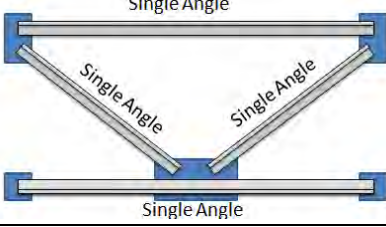
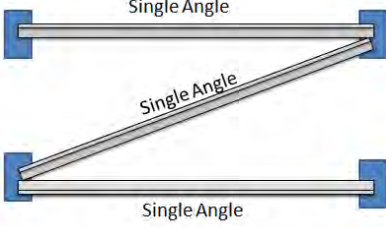
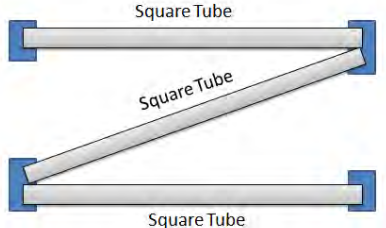
5.3 Cross Frame Test Program

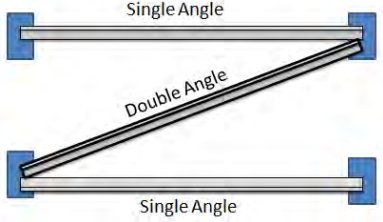
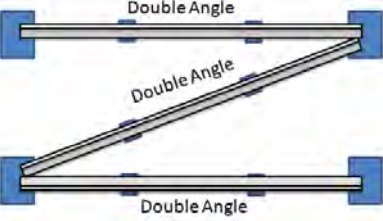
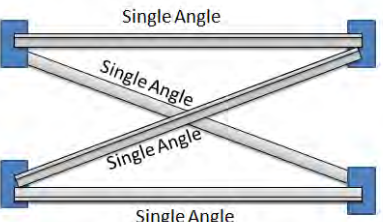
As noted earlier, the purpose of the laboratory experiments on full-size cross frames was to obtain a measure the stiffness and ultimate strength. Five different cross frames configurations were tested with a total of six specimens. The matrix of test specimens is shown in Table 5.2. Cross frames consisting of both conventional and proposed details were considered. The conventional details consist of the single angle X-frame and the single angle K-frame. The other single angle cross frame that was tested had only a single diagonal and is referred to as a single angle Z-frame. This latter specimen would not be considered for application in practice and was instead tested to represent the analytical model that is often used for the X-frame in which the compression diagonal is conservatively neglected. Two of the single-angle Z-frames were tested so that the member could be taken to failure with the diagonal in compression and in tension. The two proposed details that were tested were both Z frames (single diagonal) with either tubular members or double angle members. Both the double angles and the tubular members have substantial compression strength and therefore using the single diagonal to make the Z-shape may have applications in practice. During all tests, the two load beams were displaced in the same direction to achieve deformations that are consistent with either lateral torsional buckling of the girders or torsional deformations in curved girder applications. Two loading stages were applied: 1) Elastic stiffness tests, and 2) Ultimate load tests. In the stiffness tests, the actuator loads were incremented in 4-kip load steps to a maximum value of approximately 20 kips which was within the elastic region of the cross frames. At each 4-kip load step, data from the linear pots, load cells, and strain gages were recorded by the data acquisition system. The cross frame was then unloaded by releasing the actuator pressure in approximately 4-kip steps and data was recorded at each step. Once the pressure was released, the direction of loading was reversed and the cross frames were then loaded in the opposite direction in 4-kip steps to a

maximum actuator load of approximately 20 kips. The specimen was then unloaded to obtain one complete load cycle. Each cross frame was generally subjected to three complete load cycles to ensure repeatability in the data.

Following the elastic stiffness tests, ultimate strength tests were conducted on each cross frame. The conventional cross frames (X-frame and K-frame) are symmetrical systems and these cross frames have identical nominal failure properties in either direction. However, for single diagonal cross frames, the ultimate strengths of the cross frames are different depending on whether the diagonal is in compression or tension. Loading so that the diagonal is in compression will generally result in lower cross frame strengths.

Table 5.2 Cross Frame Test Program

Specimen Name	Specimen Sketch	No. of Specimens	Type of Test
Single Angle X-frame (SA_X)		1	Stiffness Test
			Ultimate Strength Test
Single Angle K-frame (SA_K)		1	Stiffness Test
			Ultimate Strength Test
Single Angle Z-frame (SA_Z)		2	Stiffness Test
			Ultimate Strength Test
Square Tube Z-frame (ST_Z)		1	Stiffness Test
			Ultimate Strength Test

Specimen Name	Specimen Sketch	No. of Specimens	Type of Test
Double Angle Z-frame (DA_Z)		1	Stiffness Test
			Ultimate Strength Test
Double Angle Z-frame with Double Angle Struts (DA_Z2)		1	Stiffness Test
			Ultimate Strength Test
Single Angle X-frame with Unequal Legs (SA_UL_X)		1	Stiffness Test
			Ultimate Strength Test

5.4 Single Angle X-frame

The nominal geometry of the test specimen is shown in Figure 5.13. The cross frame was designed for a girder spacing (S) of 114.5 in and a brace height (h_b) of 53.74 in. All single angles used were L4x4x3/8 sections. The basic geometry of the cross frame and size of the gusset plate were determined according to the TxDOT Standard Drawing – Steel Girder Miscellaneous Details (SGMD) (Texas Department of Transportation 2006). The two diagonals were connected at mid-span by a spacer plate. All connections between the cross frame members were made with 5/16 in. fillet welds. Figure 5.14 shows the final specimen installed in test frame.

The effective axial forces in the cross frame members were determined from the measured data using previously introduced techniques. The locations of the strain gages are shown in Figure 5.15. Since the diagonals are connected the middle, each diagonal is divided into two parts on either side of the spacer plate. Therefore, with two diagonals there are a total of four diagonal segments. The researchers were not sure how the interconnected diagonals would behave and therefore, three of the diagonal segments were monitored with strain gages to obtain effective member forces. The remaining diagonal force was determined from equilibrium of the diagonals about the splice plate.

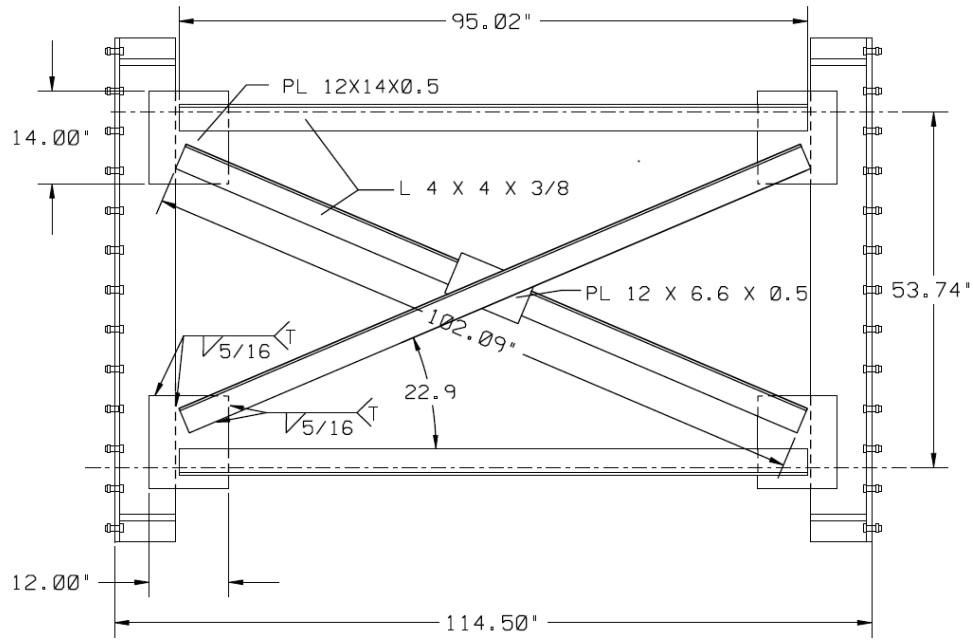


Figure 5.13: Single Angle X-frame Drawing



Figure 5.14: Single Angle X-frame Specimen

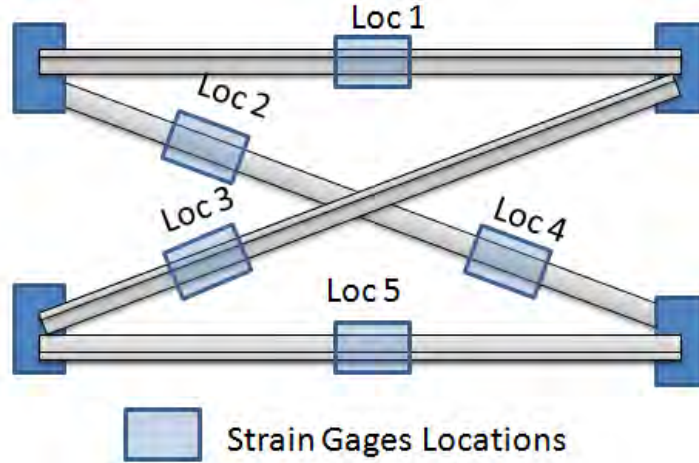


Figure 5.15: Locations of Strain Gages – Single Angle X-frame

5.4.1 Stiffness Test – Single Angle X-frame

The stiffness test was performed on this specimen with the aforementioned procedure. A graph of the measured M_{frame} and θ is plotted in Figure 5.16. The three markers at each load increment represent the test results during the three cycles of loading. The close proximity of the data markers at a given load level demonstrates the repeatability in the data. A linear trend line is graphed through the data. The measured stiffness of the cross frame, was $\beta_{brace} = 872,000$ kip-in/rad as determined from the slope of the linear trend line.

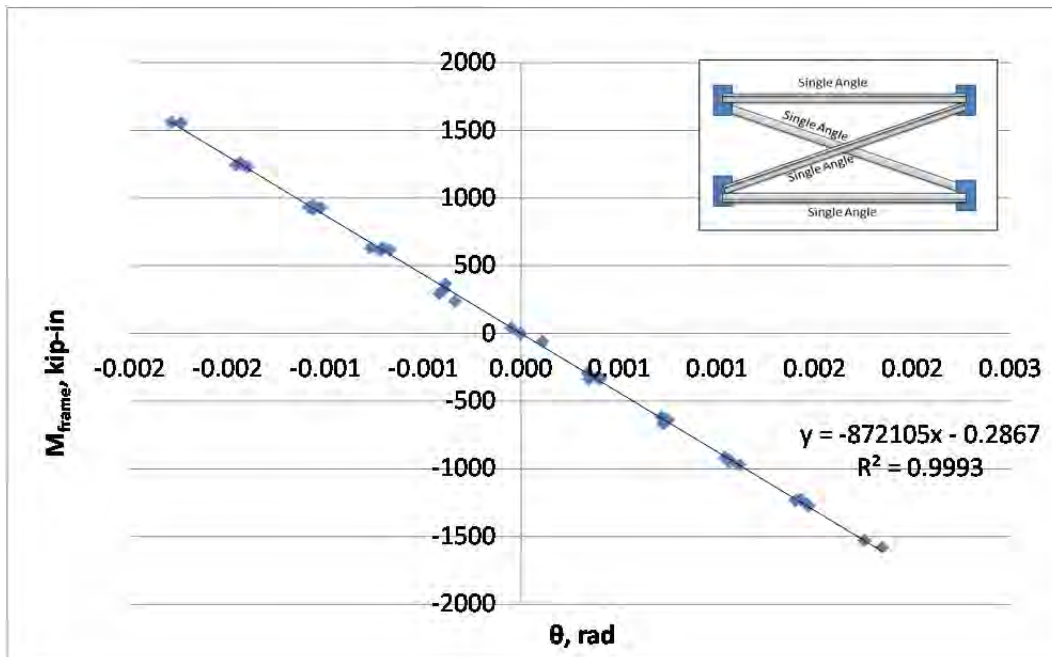


Figure 5.16: Load and Deflection Relationship of Single Angle X-frame

Based upon the strain gage readings, the effective axial force of the four cross frame members are graphed in Figure 5.17. It can be observed from the plot that the magnitude of axial

forces in the two diagonals are approximately the same with one in tension and one in compression. The axial forces in the top and bottom struts are very close to zero. Within the load range that was used for the stiffness tests, the contributions of the tension and compression diagonals are essentially the same.

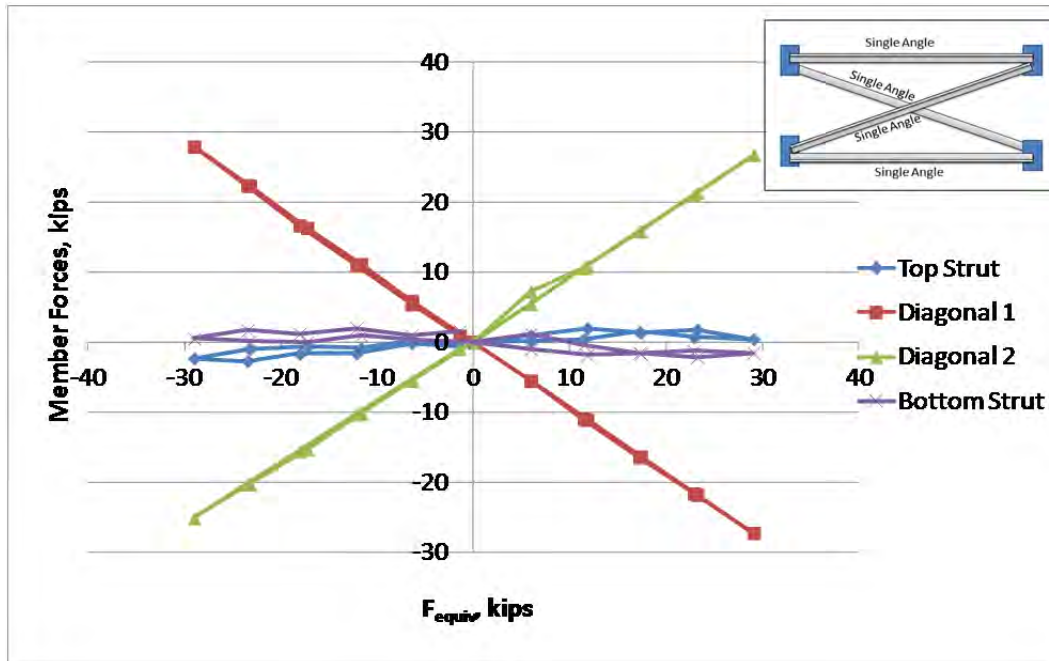


Figure 5.17: Axial Forces in Single Angle Members – Single Angle X-frame

5.4.2 Ultimate Strength Test – Single Angle X-frame

The specimen was loaded to failure after the stiffness test was completed. The failure of the specimen can be divided into two separate stages as shown in Figure 5.18 and Figure 5.19. The first failure observed was the buckling of the compression diagonal at the actuator load of 77.5 kips. The largest out-of-plane buckling deformations occurred near the midpoint of the section between the gusset plate and spacer plate (quarter point of the total diagonal length). The diagonal buckling was followed by the buckling of the top strut with no additional load increment. The maximum buckling deformations of the top strut were not at mid-span as expected but instead somewhat transversely (between the load beams) lined up with the location of the maximum buckling deformations in the compression diagonal. The likely explanation for this is that the buckling of the diagonal resulted in a rotation of the end gusset plate which resulted in bending in the upper strut as well as a reduction in the end restraint provided to the top strut at the right gusset plate. Another important observation from the tests is that the effective length of the compression diagonal was approximately half the length of the diagonal, which indicates that the connection point to the tension diagonal serves as a braced point for the compression diagonal.



Figure 5.18: Step 1: Buckling of the compression diagonal



Figure 5.19: Step 2: Buckling of the top strut

A graph of F_{equiv} and θ is shown in Figure 5.20 while Figure 5.21 shows the corresponding member forces. F_{equiv} is the effective component of the force couple as depicted earlier in Figure 5.8. As measured, the ultimate strength of the cross frame F_{equiv} is 77.5 kips or

in term of moment, M_{frame} is 4,165 kip-in. From the plotted curve, it can be found that the stiffness remained relatively constant up to a value of F_{equiv} of 60 kips, which is about 77% of the ultimate strength. The force in the compression diagonal when it buckled was 72 kips. The dashed lines in the figures represent the unloading region of the test.

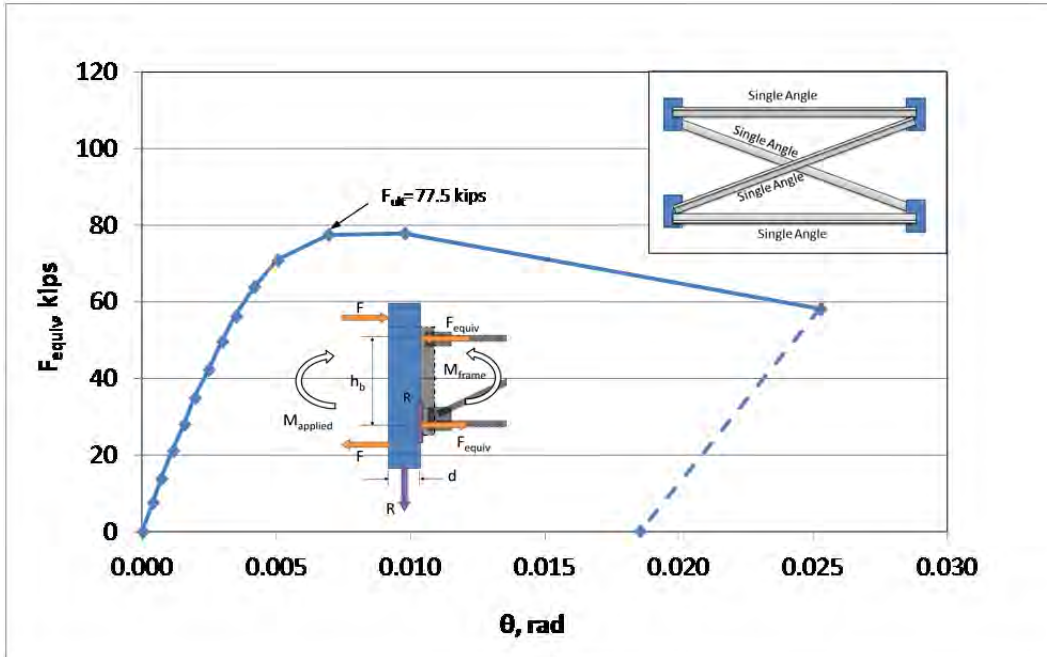


Figure 5.20: F_{equiv} vs. Rotation θ

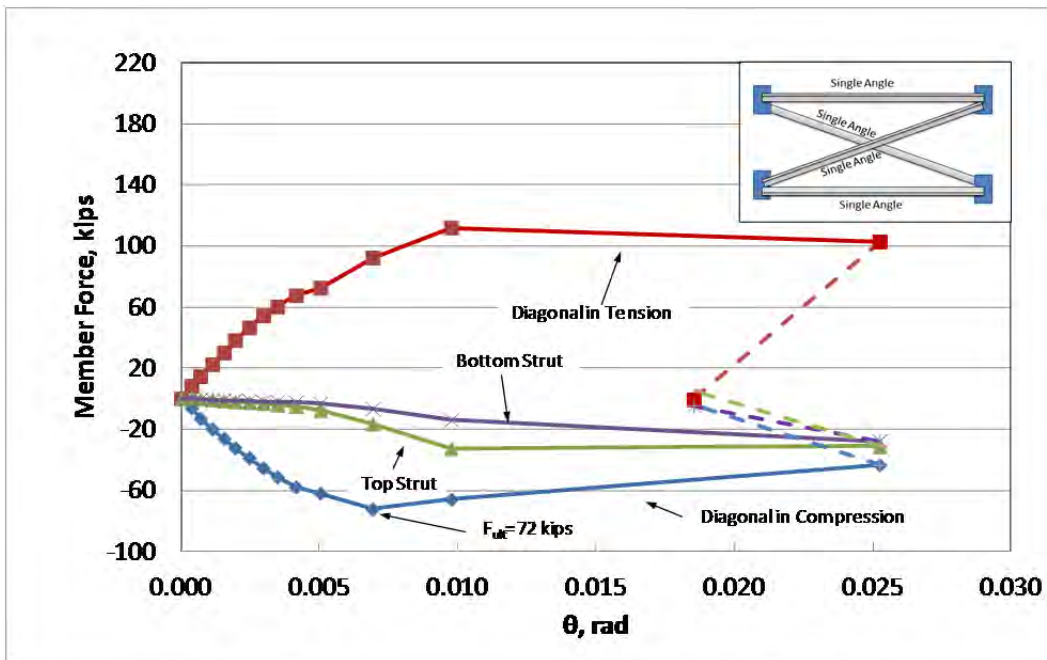


Figure 5.21: Axial Member Force vs. Rotation θ

During the test, significant out-of-plane deflection was also observed. Both diagonals had substantial deformation out-of-the-plane of the cross frame. The deflection at the intersection of the two diagonals (located at the spacer plate) was monitored with a linear potentiometer and the result is graphed against the F_{equiv} in Figure 5.22. The out-of-plane deflection is linear to the applied load before failure and it can be presumed that this bending is related to the eccentric loading for single angles. Later chapters further investigate the impact of the bending.

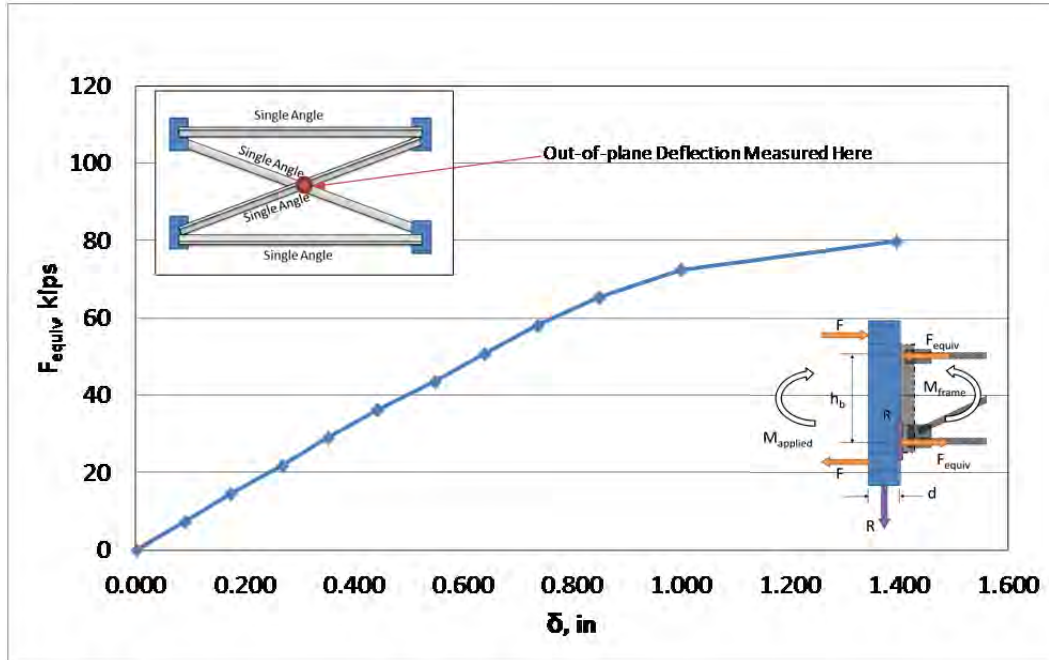


Figure 5.22: Mid-section Out-of-plane Deflection

5.5 Single Angle K-frame

The geometry of the test specimen is shown in Figure 5.23. The cross frame was fabricated with a length to simulate a girder spacing (S) of 114.5 in and a brace height (h_b) of 53.74 in. The K-frame diagonals and struts consisted of L4x4x3/8 sections. The basic geometry of the cross frame and size of the gusset plate were determined according to the TxDOT Standard Drawing SGMD (Texas Department of Transportation 2006). Figure 5.24 shows the final specimen in test frame.

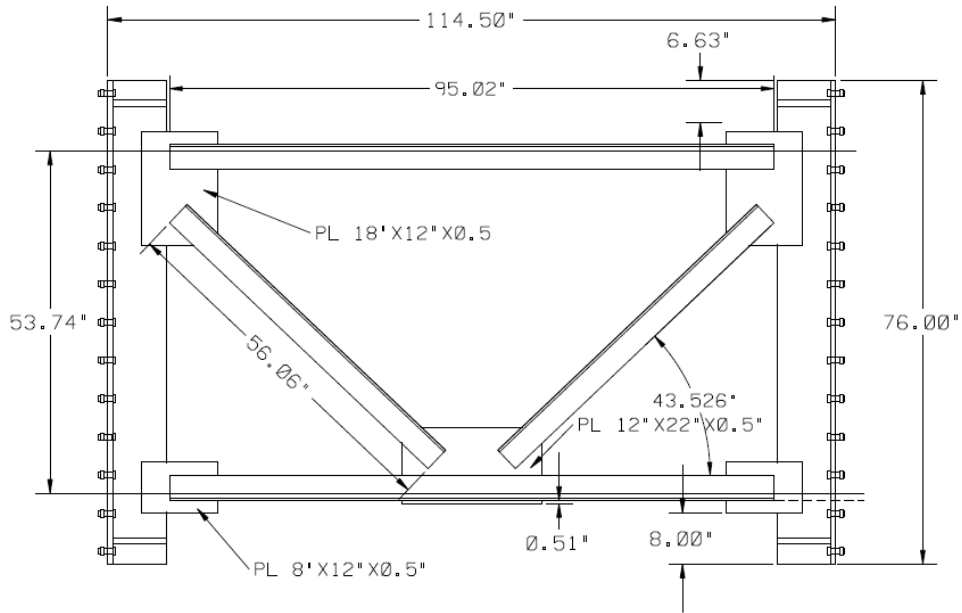


Figure 5.23: Single Angle K-frame Drawing

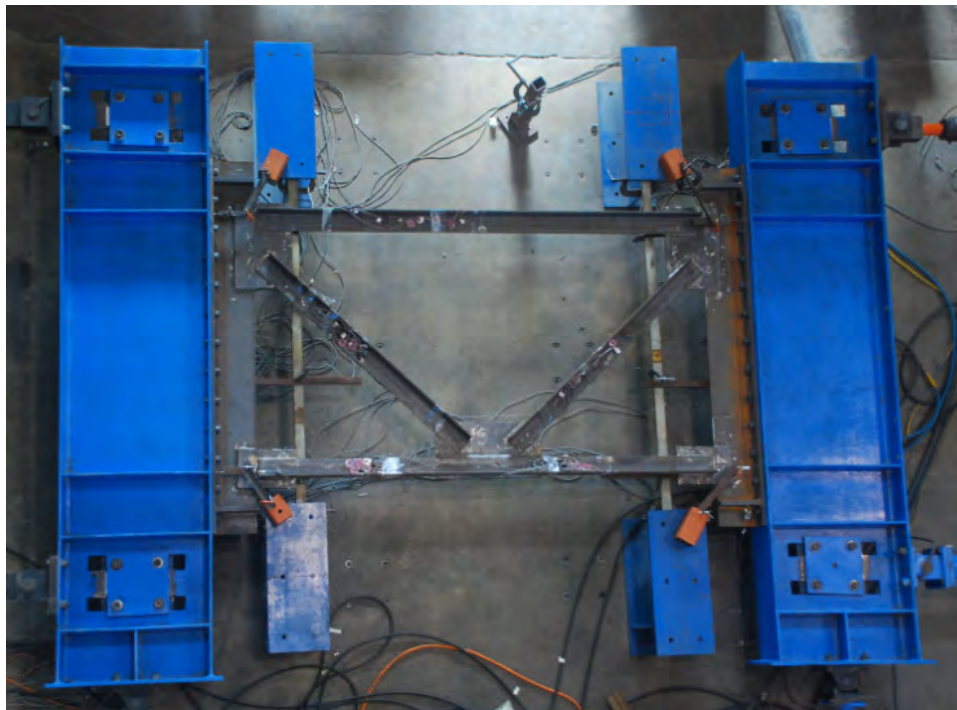


Figure 5.24: Single Angle K-frame Specimen

The member axial forces were monitored during all tests by the techniques outlined earlier in the chapter. The location of the strain gages are depicted in Figure 5.25.

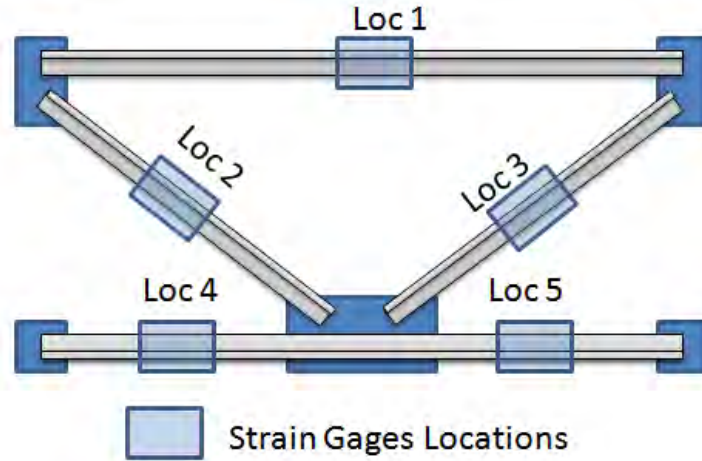


Figure 5.25: Locations of Strain Gages – Single Angle K-frame

5.5.1 Stiffness Test – Single Angle K-frame

The stiffness test followed the procedures outlined earlier in the chapter. The measured M_{frame} and θ relationship is plotted in Figure 5.26. The cross frame stiffness was obtained from the linear trend line, with a stiffness, β_{brace} , of 760,000 kip-in/rad.

The member axial forces are plotted in Figure 5.27. The top strut essentially showed zero forces as predicted by the K-frame model shown in Figure 2.5(c). Similar to the behavior exhibited by the Single Angle X-frame, the compression member contributed nearly as much as the tension member in this case.

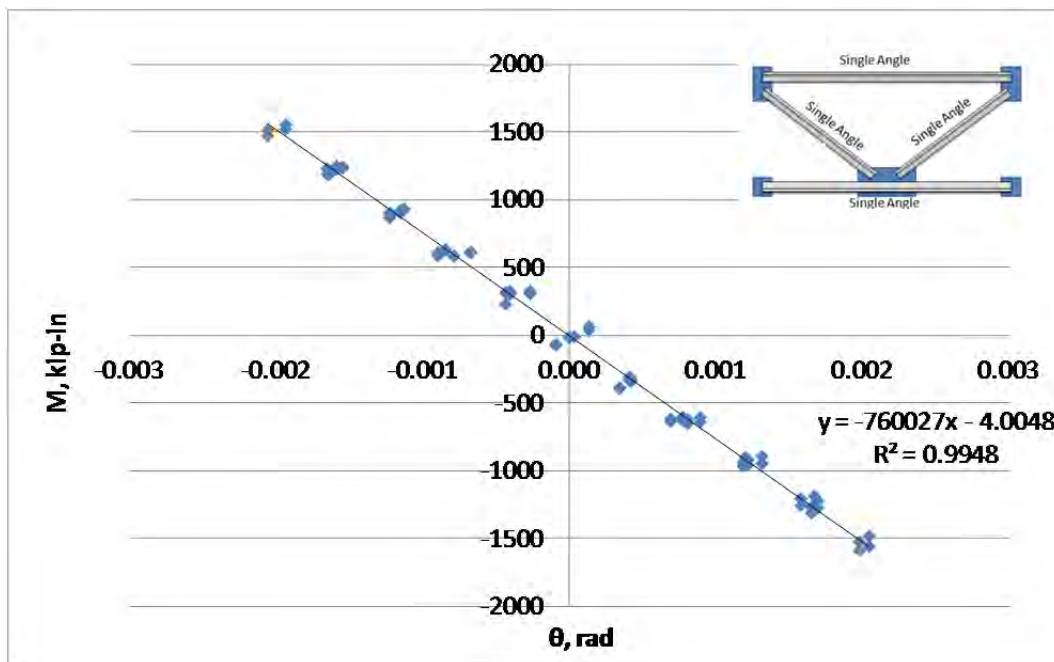


Figure 5.26: Load and Deflection Relationship of Single Angle K-frame

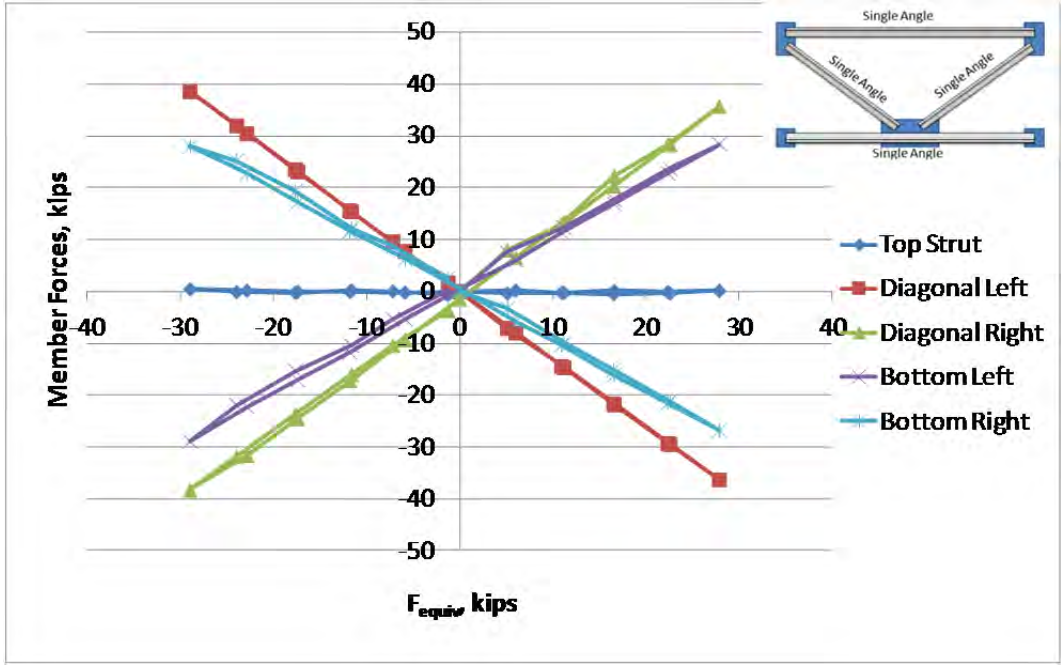


Figure 5.27: Axial Forces in Single Angle Members – Single Angle K-frame

5.5.2 Ultimate Strength Test – Single Angle K-frame

The specimen was taken to failure after the stiffness test was completed. Figure 5.28 shows the image of the failed specimen. The compression diagonal (right diagonal) failed at the mid-span when the cross frame reached its maximum capacity.

Figure 5.29 shows the relationship between F_{equiv} and rotation θ and Figure 5.30 shows the member forces (only the compression members). As measured, the ultimate strength of the cross frame F_{equiv} was 62.7 kips or in term of moment, M_{frame} was 3,369 kip-in. When the compression diagonal buckles, the ultimate axial force was 83 kips. Dashed lines in the figures represent the unloading region of the test.



Figure 5.28: Buckling of the Single Angle K-frame

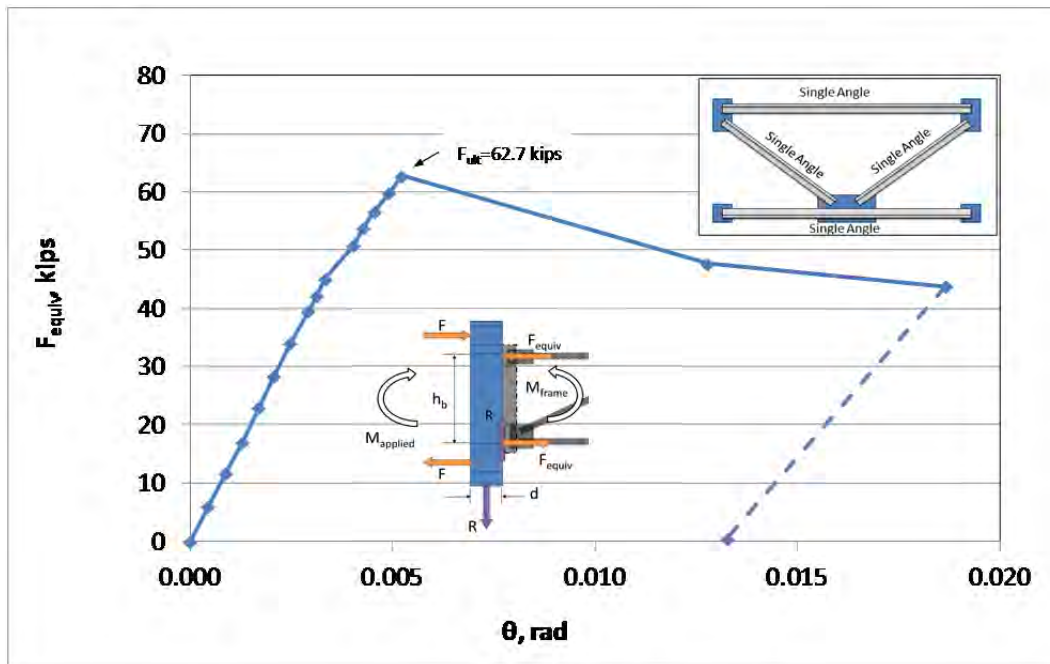


Figure 5.29: Axial Member Force vs. Rotation θ – K-frame

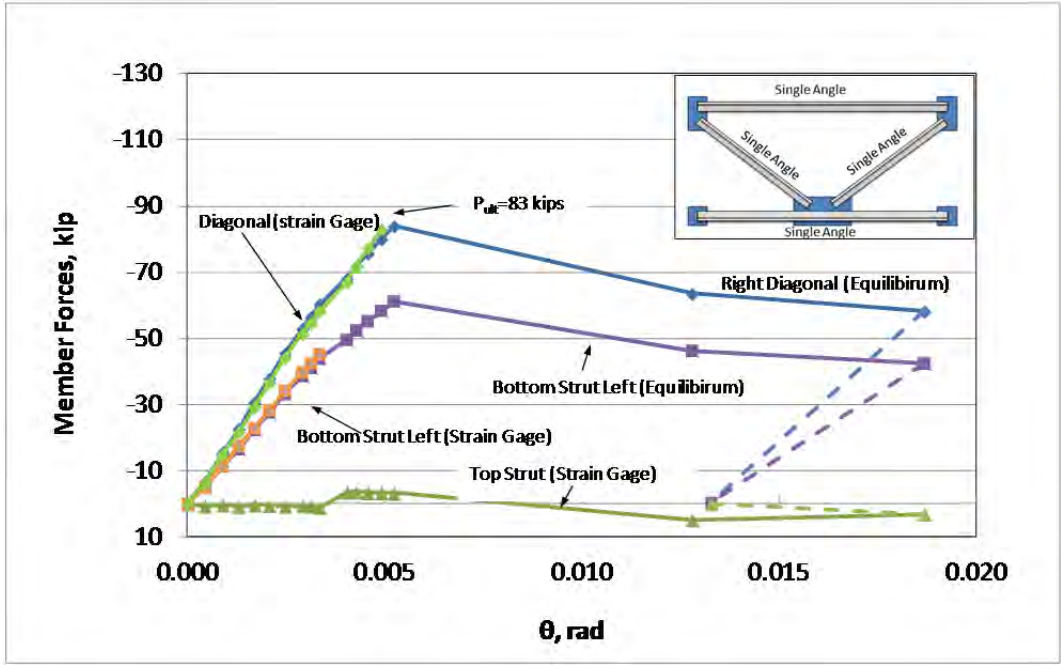


Figure 5.30: F_{equiv} vs. Rotation θ

The K-frame exhibited significant out-of-plane bending in all members similar to that observed for the Single Angle X-frame. The mid-span deflection of the compression diagonal was monitored and the results are shown in Figure 5.31.

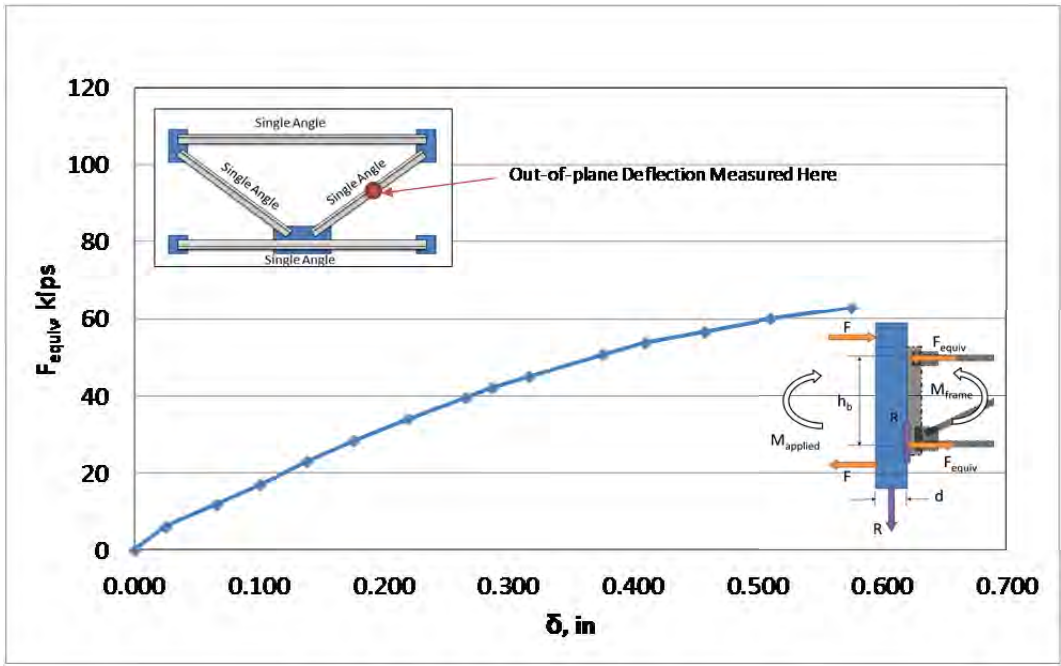


Figure 5.31 Out-of-plane Deflection

5.6 Square Tube Z-frame

The square tube Z-frame is one of the newly-proposed cross frame types that were evaluated in this research investigation. The cross frame members make a “Z-shape” with a single diagonal and all members composed of square tubes. The connection detail that was used at the end of the tubular members consisted of a slotted tube, which is a relatively common connection for these members in bracing applications. Pictures of connection fabrication are shown in Figure 5.32. Although some of the tubular members in the fatigue specimens that are reported in a later dissertation have slots cut using a plasma torch, the connection slots for the stiffness tests were cut by a metal saw to achieve a clean cut. The gusset plates were inserted into the slot and welded around. The overlap between the tube and the gusset plate was 7.5 in.

This specimen was proportioned to have similar geometry as the conventional cross frame specimens to simplify the comparisons between test specimens. The cross frame was fabricated for a simulated girder spacing (S) of 114.5 in and a brace height (h_b) of 53.74 in. The dimensional values are provided in Figure 5.33. HSS5x5x3/16 tubes were used for all members. Figure 5.34 shows the specimen as installed in the test frame. The force measurement was performed by monitoring strains at mid-span of all three members as outlined for the other cross frame specimens.



Figure 5.32: Slotted Tube Connection Fabrication

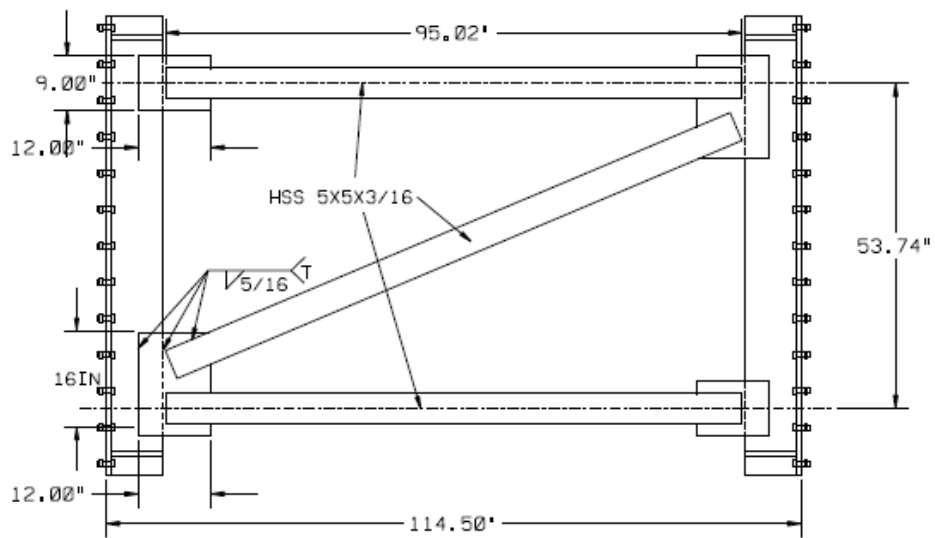


Figure 5.33: Square Tube Z-frame Drawing



Figure 5.34: Square Tube Z-frame Specimen

5.6.1 Stiffness Test – Square Tube Z-frame

The stiffness test was performed following the procedures outlined previously. The measured M_{frame} and θ relationship is plotted in Figure 5.35. As the linear trend line shows, the stiffness β_{brace} of this frame was 658,000 kip-in/rad.

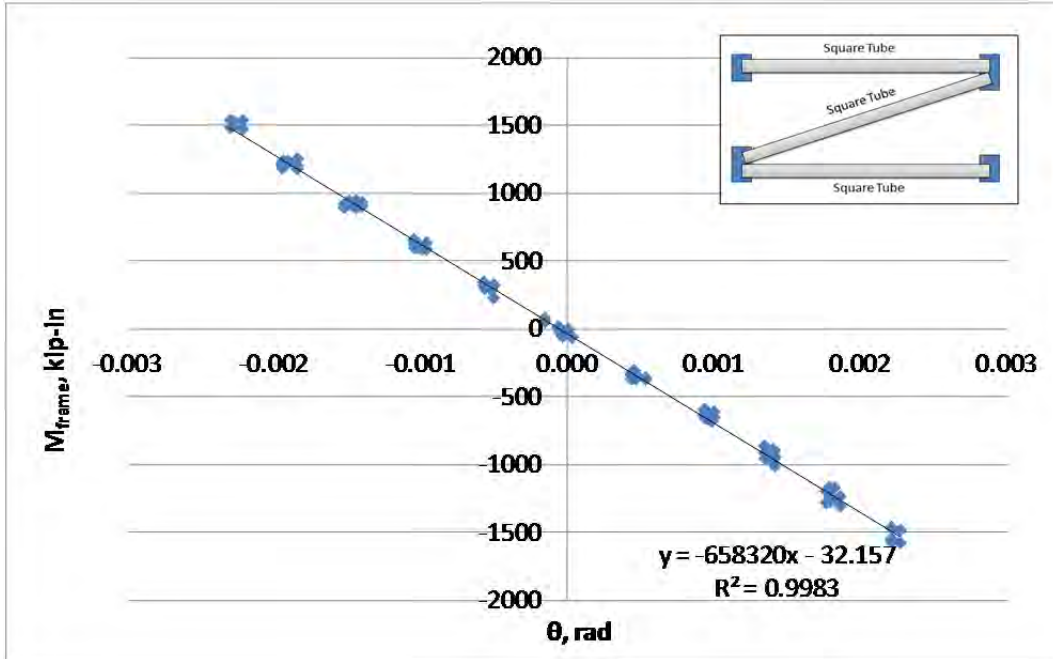


Figure 5.35: Load and Deflection Relationship of Square Tube Z-frame

5.6.2 Ultimate Strength Test – Square Tube Z-frame

The specimen was taken to failure after the stiffness test was completed. Figure 5.36 shows the final image of the failed specimen. The diagonal buckled out-of-plane at mid-span when this cross frame reached its maximum capacity.

Figure 5.37 shows the relationship between F_{equiv} and rotation θ and Figure 5.38 shows the corresponding member forces. As measured, the ultimate strength of the cross frame F_{equiv} was 74.3 kips or in term of moment, M_{frame} is 3,993 kip-in. The maximum compressive axial force in the diagonal was 156 kips and the failure mode consisted of local buckling in the wall of the tube.

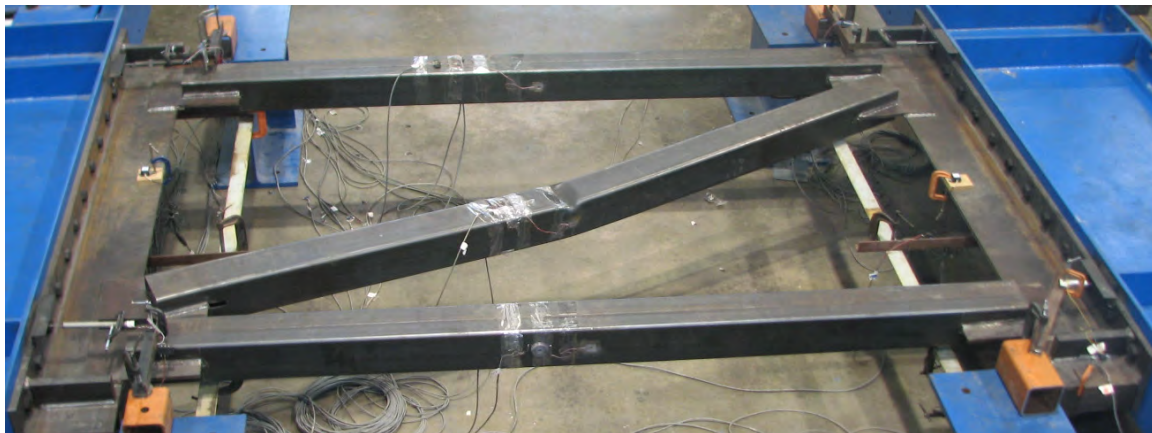


Figure 5.36: Failure of Square Tube Z-frame

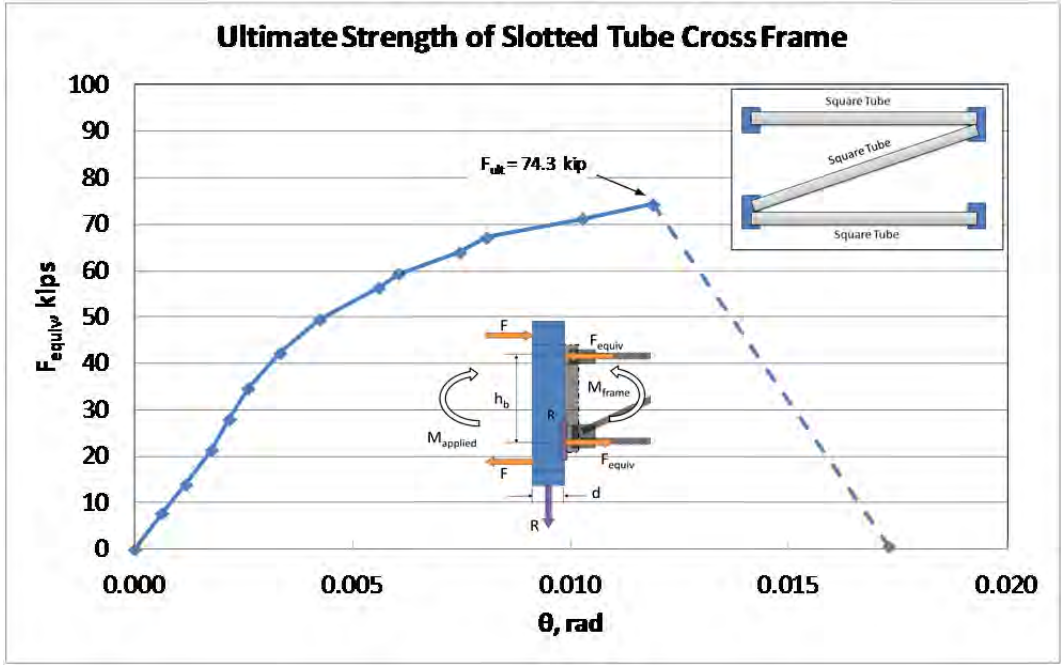


Figure 5.37: F_{equiv} vs. Rotation θ

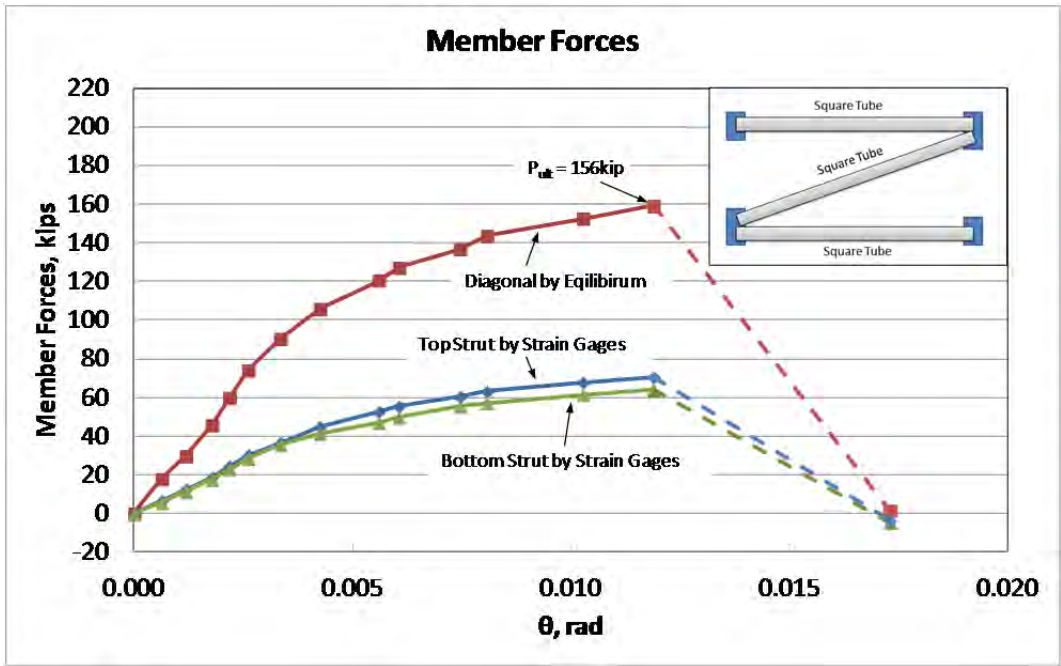


Figure 5.38: Axial Member Force vs. Rotation θ

5.7 Double Angle Z-frame

The Double Angle Z-frame is another newly-proposed cross frame geometry that is being considered in this research investigation. The Z-frame geometry has a single diagonal similar to that outlined for the tubular cross frame. The geometry of the cross frame is depicted in Figure

5.39 and is the same as the Single Angle X-frame except both diagonal angles were lined back-to-back to form a double angle section. The top and bottom struts were kept as single angles in order to simplify the design. Three intermediate connectors were used for the double angle to ensure the two angles functioned as a single unit. Figure 5.40 shows the specimen installed in the test frame. Strain gages were installed in mid-span of each angle member as previously described for the other cross frame systems with angle members.

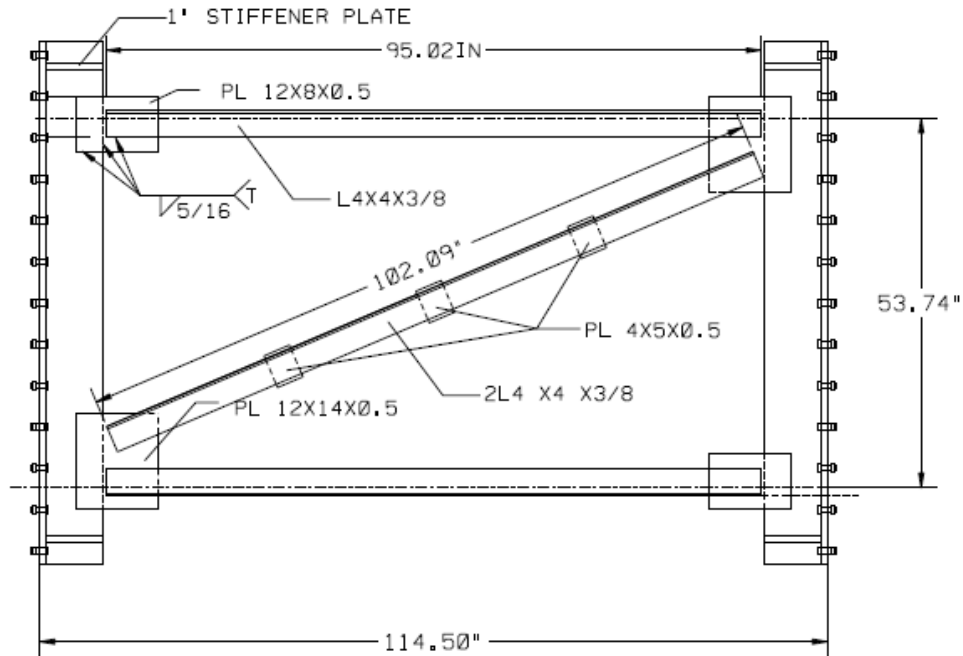


Figure 5.39: Double Angle Z-frame Drawing

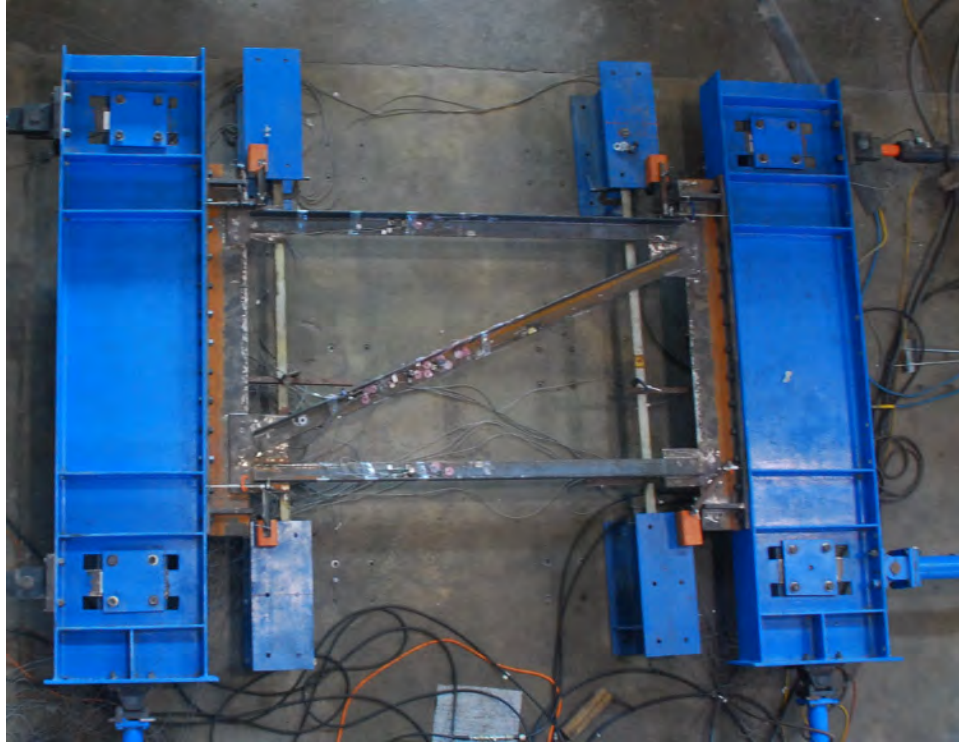


Figure 5.40: Double Angle Z-frame Specimen

5.7.1 Stiffness Test – Double Angle Z-frame

The measured M_{frame} and θ relationship is plotted in Figure 5.41. As the linear trend line shows, the stiffness β_{brace} of this frame was 593,000 kip-in/rad.

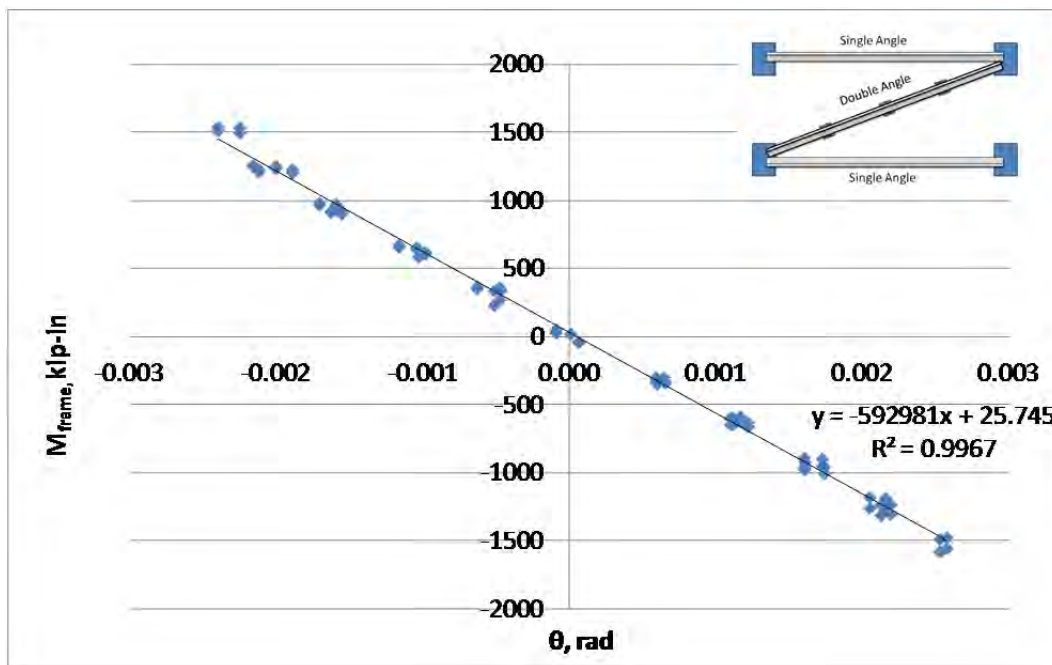


Figure 5.41: Load and Deflection Relationship of Double Angle Z-frame

5.7.2 Ultimate Strength Test – Double Angle Z-frame

The specimen was loaded to failure after the stiffness test was completed. Figure 5.42 shows the final image of the failed specimen. It was observed that significant deformation occurred in the left gusset plate and double angle diagonal.

Figure 5.43 shows the relationship between F_{equiv} and rotation θ and shows the member forces. As measured, the ultimate strength of the cross frame F_{equiv} is 94.6 kips or in term of moment, M_{frame} is 5,084 kip-in. Even though the failure happened at the gusset plate, the capacity is much higher than the previously tested specimens. Figure 5.44 shows the relationship between member forces and the rotation. It can be seen that when the cross frame reaches its maximum capacity, the axial force in the double angle was 215 kips.



Figure 5.42: Failure of Double Angle Z-frame

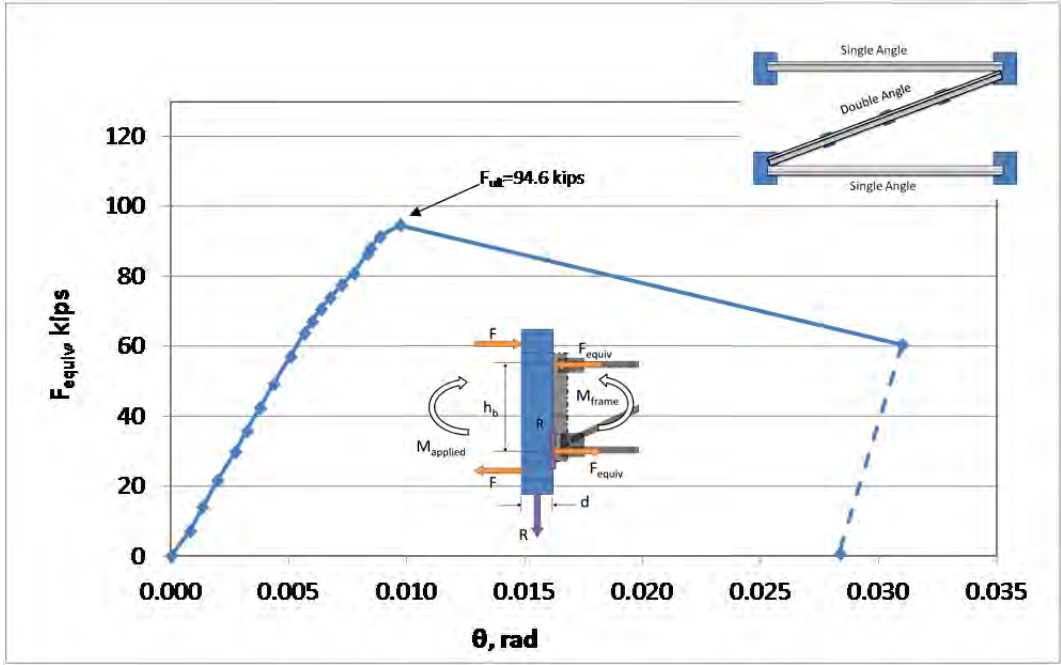


Figure 5.43: F_{equiv} vs. Rotation θ

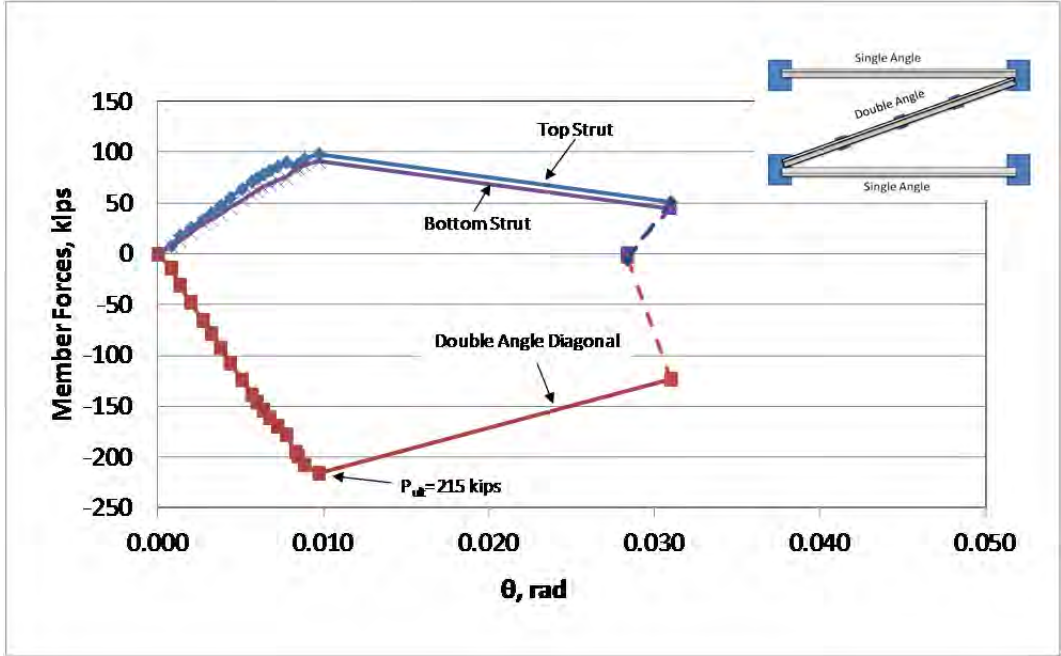


Figure 5.44: Axial Member Force vs. Rotation θ

5.8 Double Angle Z-frame 2 (with Double Angle Struts)

Similar to the previous Double Angle Z-frame, this test examined the behavior when double angle members were used for both the struts and the diagonal. For identification, this test is referred to as DA-Z2. The Z-frame geometry was identical to the Double Angle Z-frame specimen (shown in Figure 5.39 and repeated for convenience in Figure 5.45), except that double

angles were used for both the top and bottom struts. Three spacer plates of the same size were utilized on the struts, equally spaced along the length.

Figure 5.40 shows the specimen in the test frame. Strain gages were installed at around the 3/8 point of each angle member to obtain the axial force. The gage locations were offset from the middle of the length so as not to be affected by the spacer plates.

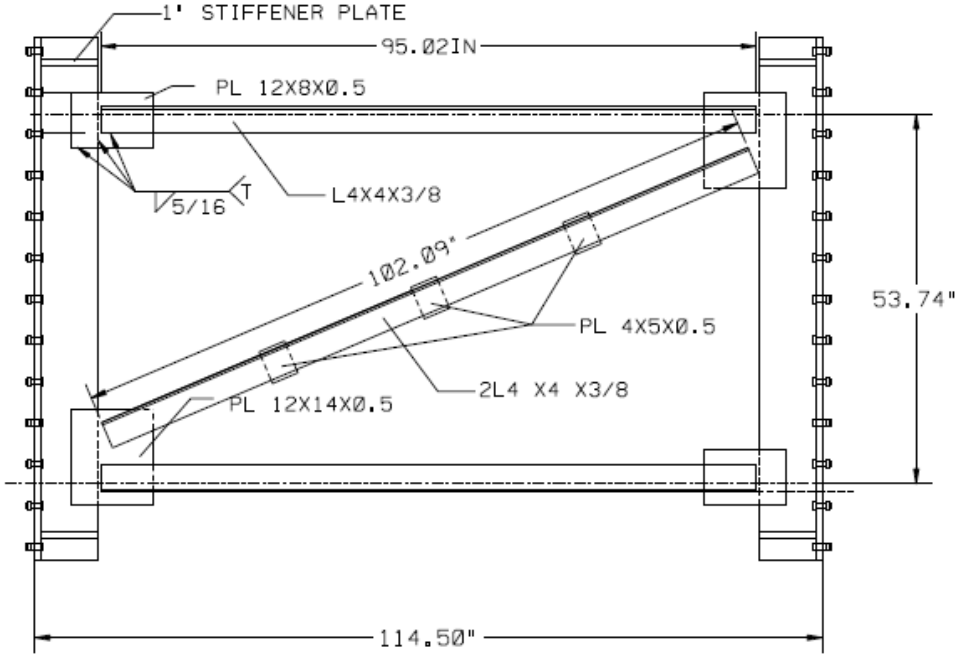


Figure 5.45: Double Angle Z-frame with Single Angle Struts Drawing (Repeated)



Figure 5.46: Double Angle Z-frame 2 Specimen

5.8.1 Stiffness Test – Double Angle Z-frame 2

The measured M_{frame} and θ relationship is plotted in Figure 5.41. As the linear trend line shows, the stiffness β_{brace} of this frame was 1,182,000 kip-in/rad.

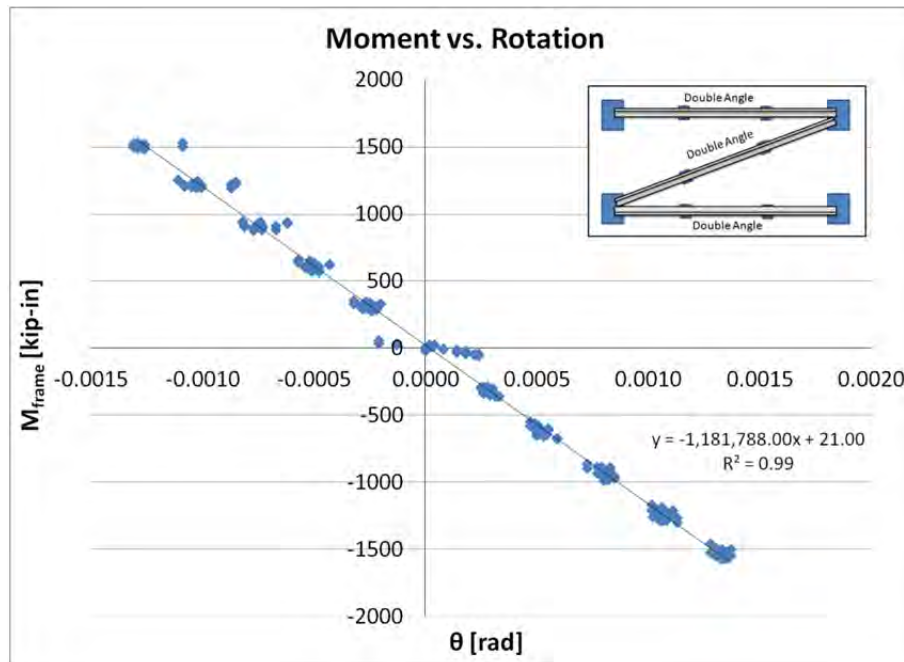


Figure 5.47: Load and Deflection Relationship of Double Angle Z-frame 2

5.8.2 Ultimate Strength Test – Double Angle Z-frame

The specimen was loaded to failure after the stiffness test was completed. Figure 5.48 shows the final image of the failed specimen. In an effort to optimize fabrication, two of the intermediate spacer plates were removed along the diagonal to examine the necessity of the plates. Based on the unbraced length of the diagonal (from the gusset plate to the center spacer plate) and the stiffness of the corresponding connections, it seems the additional spacer plates were not necessary. The AISC Specification [2010] has information on the requirements for built-up members.

It was observed that significant deformation occurred in double angle diagonal between the brace points. The double angle buckled as a unit, further confirming the spacer plates were not necessary, however, local buckling of the member did seem to precede flexural buckling. The failure also led to large deformations in the gusset plate.



Figure 5.48: Failure of Double Angle Z-frame

5.9 Single Angle Z-frame

The geometry of the Single Angle Z-frame was the same as the conventional X-frame except only a single diagonal was used as shown in Figure 5.49. Figure 5.50 shows the specimen installed in the test frame. Strain gages were installed at mid-span of each angle member similar to the previously described applications with single angle members.

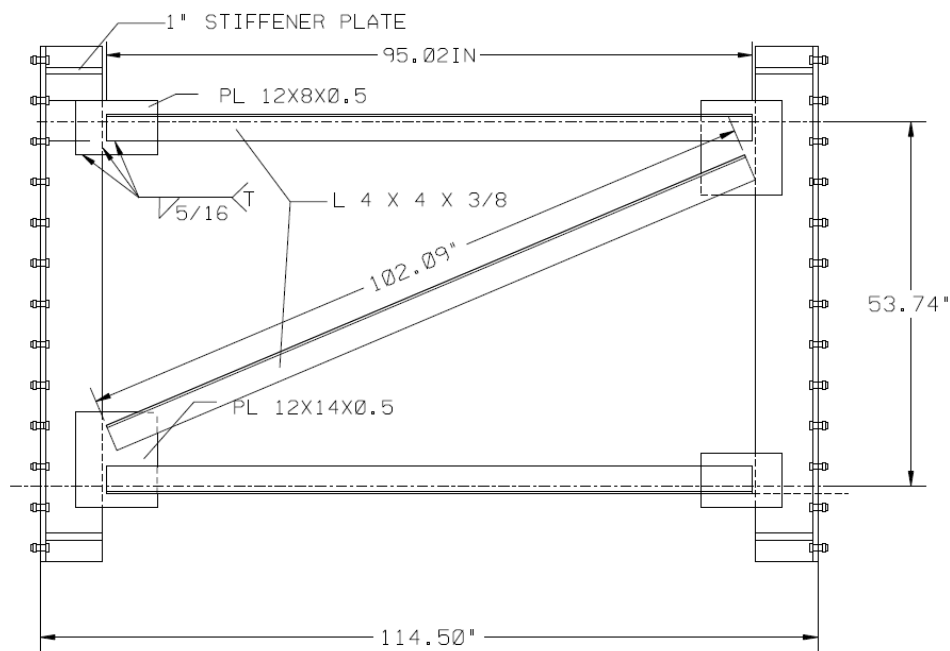


Figure 5.49: Single Angle Z-frame Drawing

Two specimens were fabricated and tested with this type of cross frame. One specimen was loaded so that the top strut failed in compression. Another one was loaded so that the diagonal failed in compression. Since the second specimen had relatively low strength, the stiffness test was only performed on the first specimen. The primary reason to test this type of cross frame was to simulate the geometry that is modeled with a “tension-only” diagonal model where the compression diagonal is conservatively neglected.

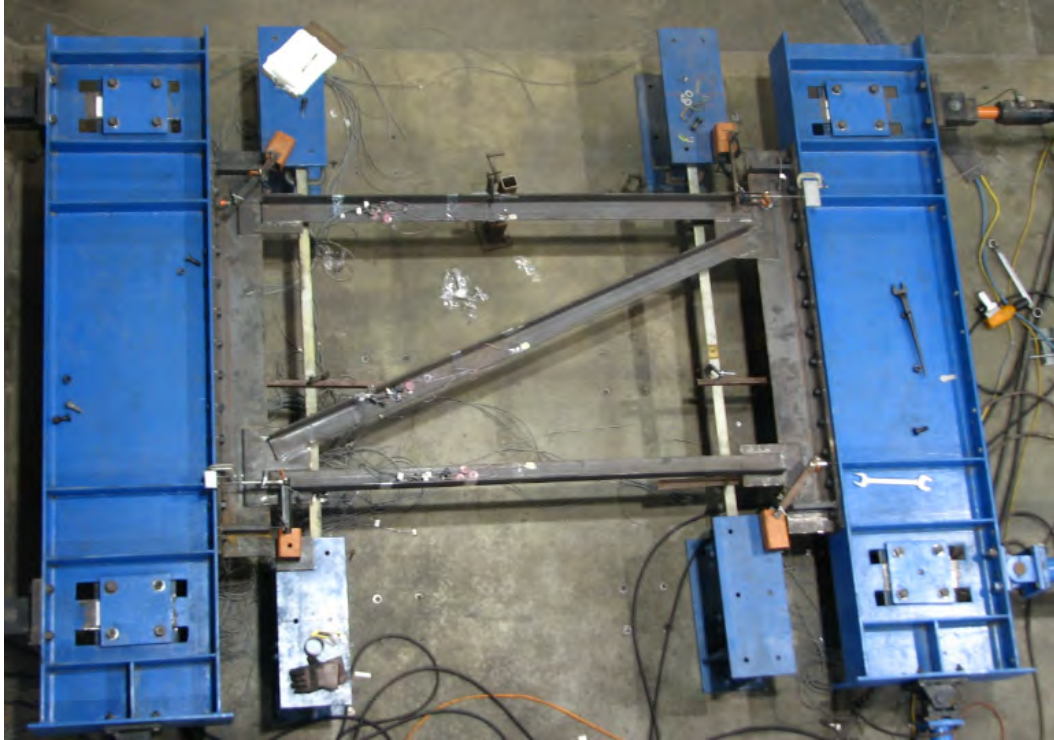


Figure 5.50: Single Angle Z-frame Specimen

5.9.1 Stiffness Test – Single Angle Z-frame

The stiffness test was done by only loading in the direction that loads diagonal in tension, because loading diagonal in compression may possibly lead to early failure. The measured M_{frame} and θ relationship is plotted in Figure 5.51. As the linear trend line shows, the stiffness β_{brace} of this frame was 352,000 kip-in/rad.

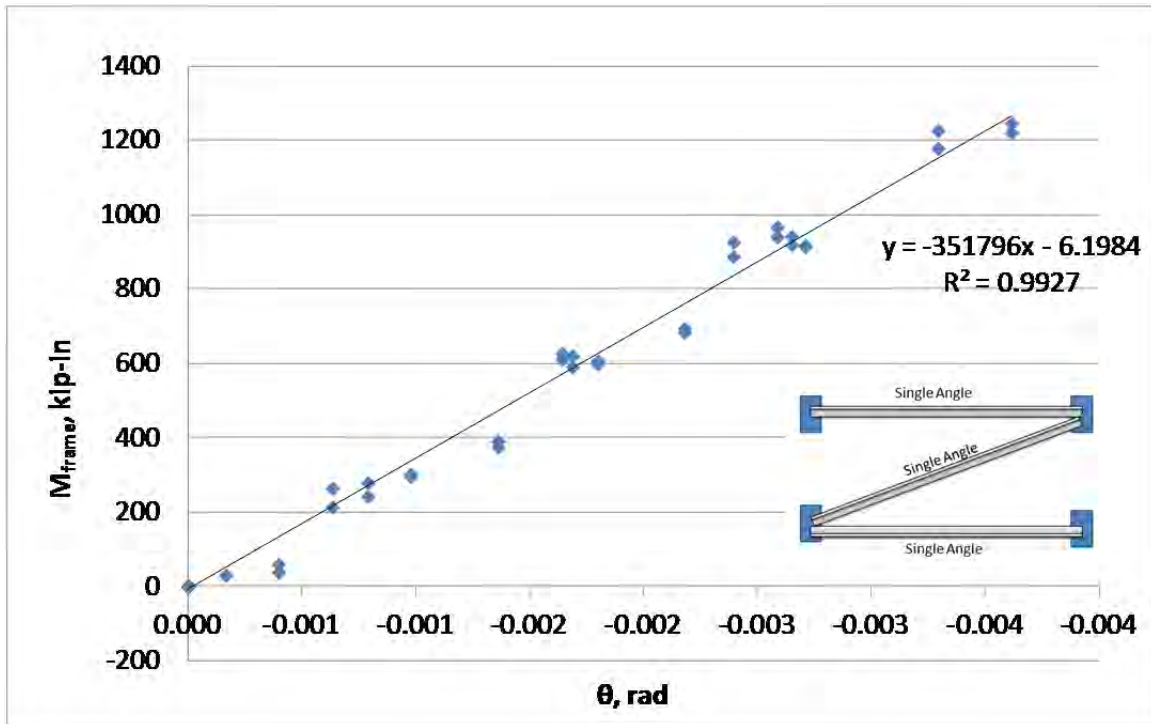


Figure 5.51: Load and Deflection Relationship of Single Angle Z-frame

5.9.2 Ultimate Strength Test – Single Angle Z-frame

Since the single angle struts and diagonal members have relatively low buckling strengths, two specimens were tested. The first test included the ultimate strength test with the diagonal in compression and the struts in tension, while the ultimate load test for the second specimen had the diagonal in tension and the struts in compression. The ultimate strength tests were performed using the aforementioned procedure. Figure 5.52 shows the image of the specimen with failed top struts and Figure 5.53 for the specimen with the failed diagonal.



Figure 5.52: Failure at Top Strut



Figure 5.53: Failure at Diagonal

For the test with the failure at top strut, Figure 5.54 shows the relationship between F_{equiv} and rotation θ . The ultimate strength of the cross frame F_{equiv} was measured to be 55 kips or in terms of moment, M_{frame} was 2,956 kip-in. The corresponding relationship between member forces and the rotation is shown in Figure 5.55. When the cross frame reached its maximum

capacity, the axial force in the top strut was 56 kips and the bottom strut force was slightly lower. The corresponding diagonal force was a little over 120 k in tension.

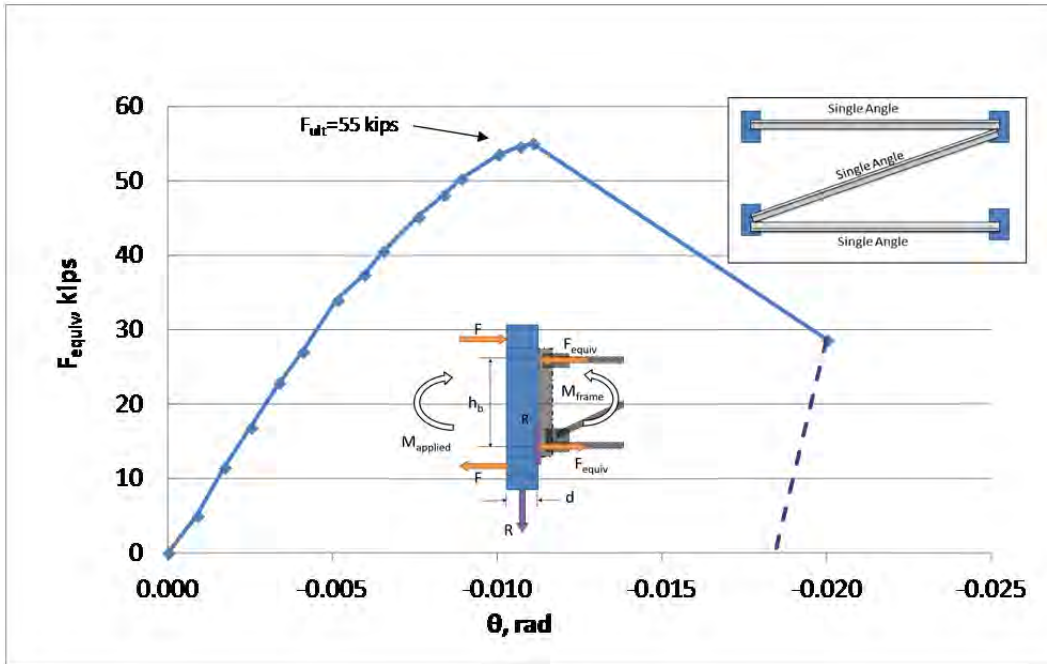


Figure 5.54: F_{equiv} vs. Rotation θ – Failure at Top Strut

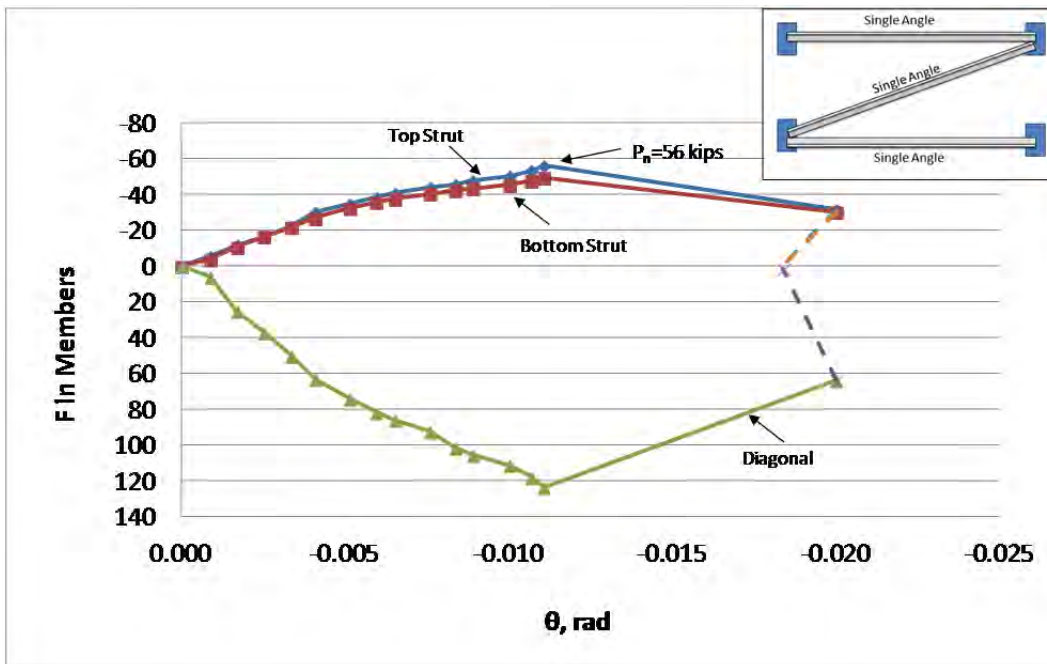


Figure 5.55: Axial Member Force vs. Rotation θ – Failure in Top Strut

Figure 5.56 shows the relationship between F_{equiv} and rotation θ when the single angle diagonal was in compression. The ultimate strength of the cross frame F_{equiv} was measured to be 21 kips or in terms of moment, M_{frame} , the strength was 1,129 kip-in. The corresponding relationship between member forces and the rotation is shown in Figure 5.57. It can be seen that when the cross frame reached its maximum capacity, the axial force in the single angle diagonal was 48 kips. Obviously the second specimen is considerably weaker than the first one due to the longer compression member in the diagonal compared to the strut in the other specimen. In addition, the stiffness during the elastic range was 357,000 kip-in/rad.

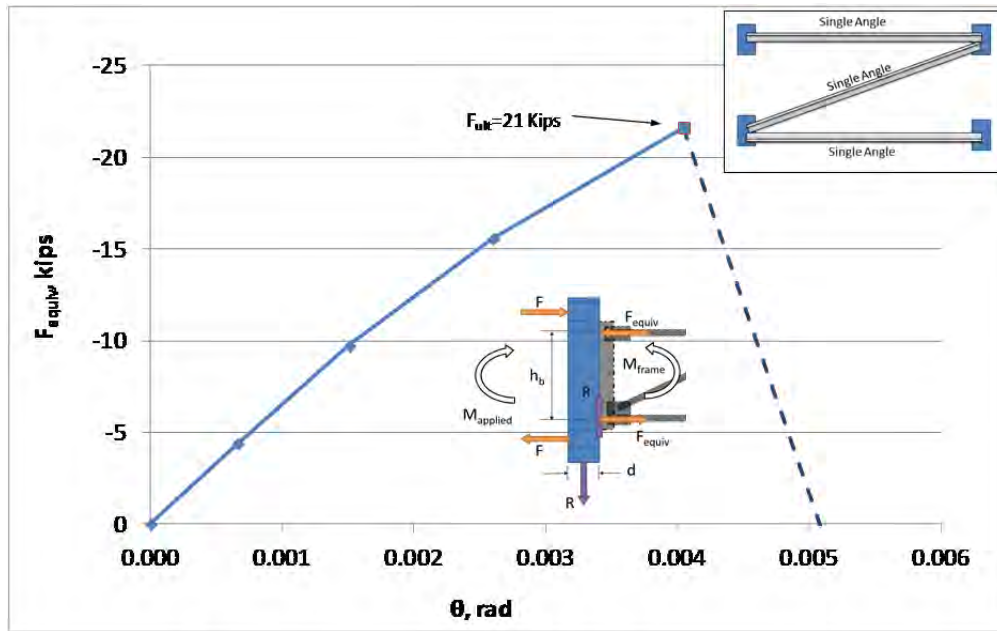


Figure 5.56: F_{equiv} vs. Rotation θ – Failure at Diagonal

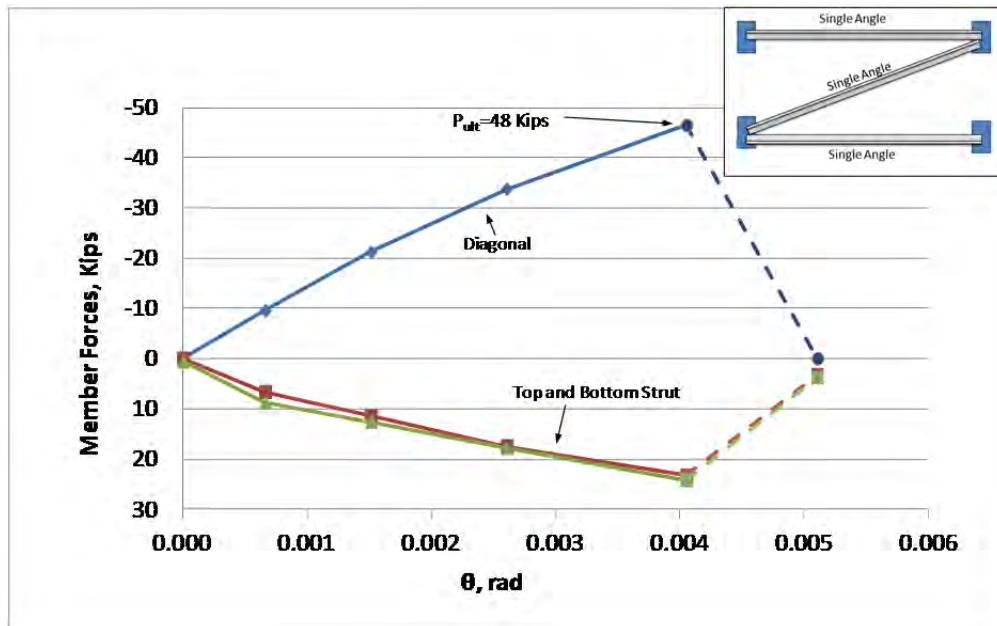


Figure 5.57: Axial Member Force vs. Rotation θ – Failure at Diagonal

5.10 Single Angle Unequal Leg X-frame

Lastly, stiffness and ultimate strength tests were conducted on a specimen utilizing unequal leg angles in an X-type configuration. The angle member selected was the L6x3.5x3/16 member which has nearly an identical area to the previously used L4x4x3/8 members. This test was done in conjunction with the ongoing fatigue tests that considered the impact of using unequal leg angles to reduce the eccentricity.

The geometry of the specimen was calculated using the TxDOT standards, with a brace height of 53.74 in to be directly comparable to the Single Angle X-frame specimen, whose geometry is given by Figure 5.13. This required the gusset plates to be slightly deeper for the specimen.

Figure 5.58 shows the specimen in the test frame. Strain gages were installed at around the quarter points of each diagonal angle member and the mid-length for each strut to obtain the axial force. The gages on the diagonal were offset to avoid effects around the connection to the other diagonal.



Figure 5.58: Single Angle Unequal Leg X-frame Specimen

5.10.1 Stiffness Test – Single Angle Unequal Leg X-frame

The measured M_{frame} and θ relationship is plotted in Figure 5.59. As the linear trend line shows, the stiffness β_{brace} of this frame was 1,156,000 kip-in/rad.

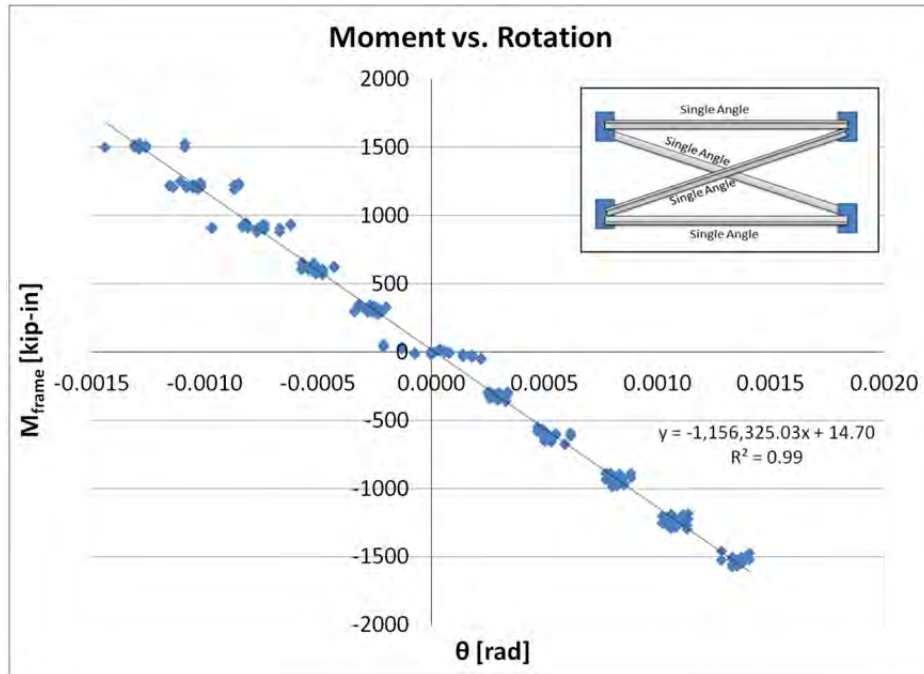


Figure 5.59: Load and Deflection Relationship of Single Angle Unequal Leg X-frame

5.10.2 Ultimate Strength Test – Single Angle Unequal Leg X-frame

The specimen was loaded to failure after the stiffness test was completed. Figure 5.60 shows the final image of the failed specimen. Similar to the Single Angle X-frame, failure was initiated by buckling of the compression diagonal between the gusset plate and center plate, followed by buckling of the adjacent strut.

It was observed that significant deformation occurred in the specimen as the researchers continued to load the specimen much beyond failure. As the specimen continued to rotate, local buckling of the lower right portion of the diagonal also occurred near the center connection. The local buckling can be observed in the figure just to the right of the connection between the diagonals.



Figure 5.60: Failure of Single Angle Unequal Leg X-frame

5.11 Coupon Tension Tests

The yield stress of the steel material was determined for consideration of the inelastic behavior of cross frame members. Tension coupons obtained from the raw steel were tested to find the yield stresses. A displacement controlled loading process was used to perform the tests. The data of the tension tests is included in Appendix. The average properties of the steel for all specimens are presented in Table 5.3.

Table 5.3 Average Results from the Tension Coupon Tests

Specimen	Average Yield Stress (ksi)	Average Tensile Stress (ksi)	Elongation	Coupon Numbers
Single Angle X-frame	46	65	37%	SA-1 SA-2 SA-3
Single Angle K-frame	57	75	34%	SAK-1 SAK-2 SAK-3
Square Tube Z-frame	51	57	26%	HSS-1 HSS-2 HSS-3
Double Angle Z-frame	46	65	37%	SA-1 SA-2 SA-3
Single Angle Z-frame - Diagonal in Compression	46	65	37%	SA-1 SA-2 SA-3
Single Angle Z-frame - Diagonal in Tension	54	74	35%	SA-4 SA-5 SA-6
Gusset Plates	56	72	38%	GP-1 GP-2 GP-3

5.12 Summary of Cross Frame Test Results

A total of five different cross frame types were tested in this series of experiments. The elastic stiffness of the cross frames and their ultimate strength in the critical direction were obtained from each cross frame. A summary of the test results is listed in Table 5.4.

Table 5.4 Cross Frame Test Results Summary

Specimen Name	Stiffness ¹ (kip-in/rad)	Ultimate Strength in M_{frame} (kip-in)	Ultimate Strength in F_{equiv} (kip)
Single Angle X-frame	872,000	4,165	77.5
Single Angle K-frame	760,000	3,369	62.7
Square Tube Z-frame	658,000	3,993	74.3
Double Angle Z-frame	593,000	5,084	94.6
Single Angle Z-frame -Diagonal in Tension	352,000	2,956	55
Single Angle Z-frame - Diagonal in Compression	Initial 357,000	1,129	21
Double Angle Z-frame 2	1,181,788	-	-
Single Angle Unequal Leg X-frame	1,156,325	-	-

Note: 1. Stiffness values are rounded to 1000 kip-in/rad

It should be noted that this table is a summary of test results. Superiority of different cross frames types can be only judged with further consideration of the size of the cross frames, the overall cost and other structural performance, such as fatigue life also need to be considered.

The test frame that was designed and fabricated provided a good means of evaluating the stiffness and strength of full scale cross frame systems. Based upon the results of the tests, the following conclusions can be made:

1. The stiffness tests showed that the measured values of the stiffness of cross frames are the same for loading in both directions within the elastic region of the component members.
2. Failure of the cross frames usually occurs following a degradation in the stiffness of one or more of the critical compressive components due to instability. The two instabilities that were observed consisted of buckling of a primary cross frame member or buckling of a gusset plate. Although most of the buckling modes in the cross frames consisted of member buckling, one of the HSS section diagonals failed due to local buckling.
3. For the Single Angle X-frame, the connection to the tension diagonal at the mid length location can be considered as a bracing point for the compression diagonal.

The next chapter provides a comparison of the test results with the analytical and computational models. After the models and tools are validated, more geometry options can be explored to make further observations of the stiffness behavior of the cross frames.

Chapter 6: Models for Cross Frame Stiffness

6.1 Introduction

The studies presented in Chapter 4 and Chapter 5 demonstrated that the single angle members that frequently comprise cross frame braces can lead to substantial reductions in the torsional brace stiffness due to the large eccentricity of the connections.

The stiffness reduction factor for a cross frame is defined as the ratio between the actual stiffness and the theoretical stiffness of the cross frame as indicated in the following expression:

$$R_{frame} = \frac{\beta_a}{\beta_b} \quad (6.1)$$

Where:

β_a = Actual stiffness of the cross frame

β_b = Theoretical stiffness of a cross frame as defined in Chapter 2.

In the first part of this chapter, the stiffness reduction problem is examined analytically in an attempt to develop a solution for the reduced stiffness of the angle. The R factors for the X and K cross frames are then derived from the individual member reduction.

Subsequently, finite element analyses of the X and K frames, validated by the experimental test results, were performed on typical cross frame geometries to develop the R factor parametrically.

6.2 Analytical Stiffness Reduction for a Single Angle

The results presented in Chapter 4 demonstrated that the reduction in the stiffness of cross frames is due to the eccentric connections from the single angle members. Therefore, it is reasonable to approach the cross frame system problem by first considering the problem on the member level. A simplified model of the problem is illustrated in Figure 6.1, which depicts a single angle with gusset plates that are idealized with fixed ends. The fixed end boundary condition was chosen to simulate the support condition of the gusset plates attached to a rigid stiffener that frames into the web of the girder. The assumed support conditions represent one of the extreme limits; however the assumption greatly simplifies the derivation. A horizontal tensile force of magnitude F is applied to the system. The length of the angle is designated as L_L , and length of the gusset plate is L_P . In the derivation, the overlap region between the angle and gusset plates, which would have a combined moment of inertia, is neglected for simplification.

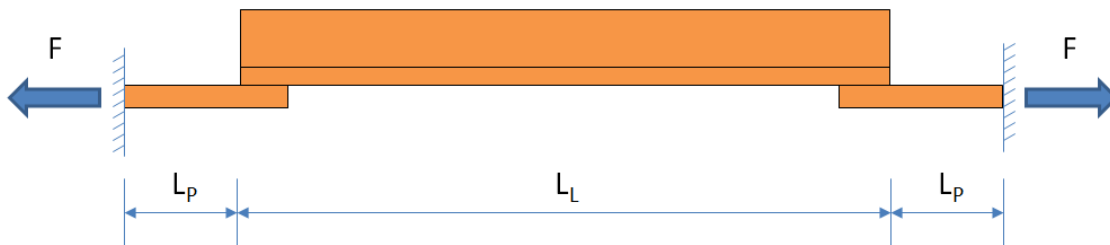


Figure 6.1: Single Angle with Eccentric Connection in Tension

For a concentrically loaded member, the theoretical axial stiffness k_t is defined as:

$$k_t = \frac{F}{\delta_a} = \frac{FEA}{FL} = \frac{EA}{L} \quad (6.2)$$

Where:

E = Elastic modulus of the material

A = Area of the member

L = Length of the member

However, the eccentric connection relative to the geometric centroid of the angle results in a bending moment that causes additional deflection along the bottom side of the angle. Based on the increased deflection, the modified axial stiffness is calculated as:

$$k_a = \frac{F}{\delta_a + \delta_b} \quad (6.3)$$

Where:

δ_a = Deflection due to axial load

δ_b = Deflection due to bending moment

The stiffness reduction factor for a member is defined as follows:

$$R_{member} = \frac{k_a}{k_t} \quad (6.4)$$

The next section focuses on the formulation of k_a so that R_{member} can be evaluated.

6.2.1 Bending Due to the Eccentric Connection

In order to solve the stiffness reduction factor of Equation (6.4), the extra deflection due to the bending is needed. The free body diagrams for the angle and the gusset plates are shown in Figure 6.2(a) and Figure 6.3, respectively. The axial force and the bending moment at the angle-

plate interface are labeled as F and M_{plate} , where M_{plate} is the restraining moment that the plate applies to the end of the angle. Based on force equilibrium, the axial force F is equal to the applied tension. In addition, for the angle, the eccentrically loaded tension, F , and moment, M_{plate} , (Figure 6.2(a)) can be replaced by an equivalent force and moment acting at the centroid of the angle, as shown in Figure 6.2(b). Then the total resultant moment at end of the angle is labeled as M_L :

$$M_L = F\bar{y} - M_{plate} \quad (6.5)$$

Where

\bar{y} = Distance between center gravity and the outer face of one leg

F = Tension force

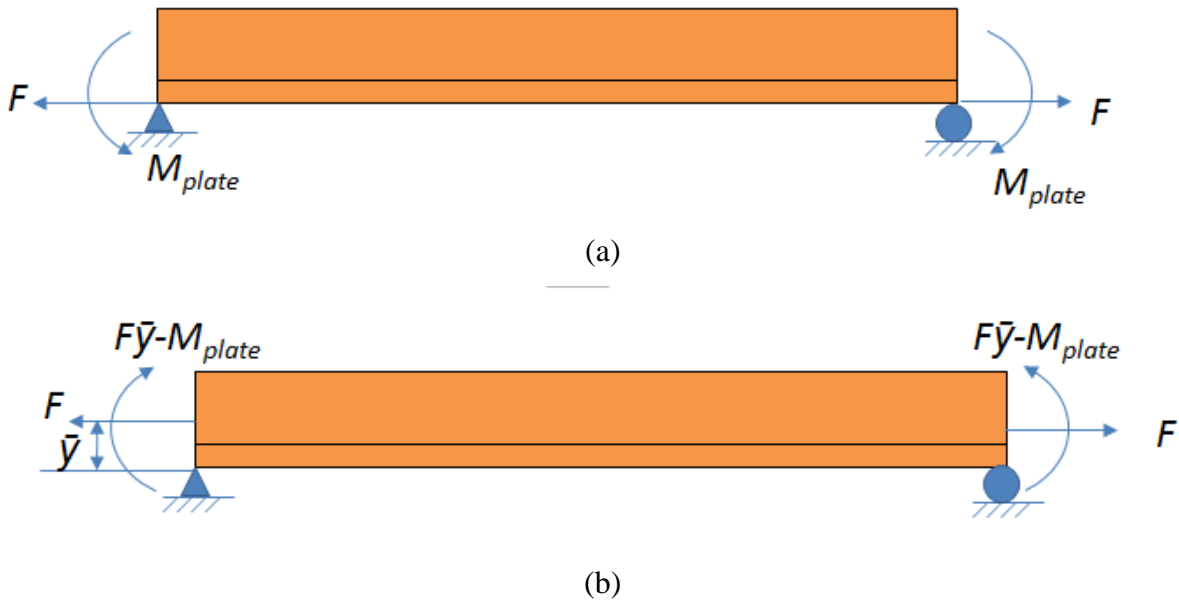


Figure 6.2: Free Body Diagram for Angle

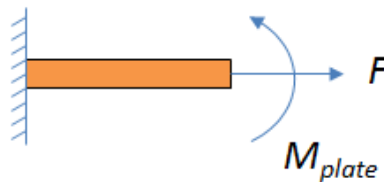


Figure 6.3: Free Body Diagram for a Gusset plate

To solve the moment, M_{plate} , between the angle and gusset plates, compatibility between the deflections of the two parts can be used. Under the applied moment, the angle and the gusset plates deform as shown in Figure 6.4.

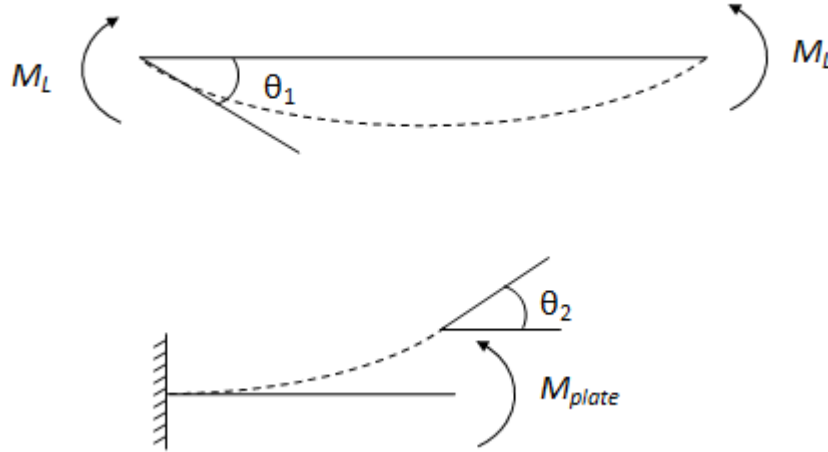


Figure 6.4: Deformation of angle and gusset plate

By compatibility (continuity of rotation at the interface of angle and gusset plate):

$$\theta_1 = \theta_2 = \theta \quad (6.6)$$

According to beam bending theory, Equation (6.6) can be rewritten as:

$$\frac{(F\bar{y} - M_{plate})}{2k_L} = \frac{M_{plate}}{k_P} = \theta \quad (6.7)$$

Where:

$$k_L = \text{Bending stiffness of the angle} = \frac{EI_L}{L_L} \quad (6.8)$$

$$k_P = \text{Bending stiffness of the gusset plate} = \frac{EI_P}{L_P} \quad (6.9)$$

Equation (6.7) can be rearranged to solve for M_{plate} :

$$M_{plate} = \frac{\frac{F\bar{y}}{2k_L}}{\frac{1}{2k_L} + \frac{1}{k_P}} \quad (6.10)$$

The total resultant moment at the angle centroid can be obtained by substituting Equation (6.10) to Equation (6.5):

$$M_L = F\bar{y} - M_{plate} = \frac{\frac{F\bar{y}}{k_P}}{\frac{1}{2k_L} + \frac{1}{k_P}} \quad (6.11)$$

The rotation at the angle-plate interface can be calculated by substituting Equation (6.10) into Equation (6.7):

$$\theta = \frac{\frac{F\bar{y}}{2k_L k_P}}{\frac{1}{2k_L} + \frac{1}{k_P}} \quad (6.12)$$

By using a parameter γ , Equation (6.11) and Equation (6.12) can be rewritten as:

$$M_L = F\bar{y} - M_{plate} = \gamma F\bar{y} \quad (6.13)$$

$$\theta = \gamma \frac{F\bar{y}}{k_L} \quad (6.14)$$

Where:

$$\gamma = \frac{1}{\frac{k_P}{2k_L} + 1} \quad (6.15)$$

At this point, the derivation of the moment and the rotation at the ends of the angle is complete. The next step is finding the effect of the rotation on the axial stiffness of the angle.

6.2.2 Stiffness Reduction Due to Bending

The actual axial stiffness of the angle in a cross frame structure is measured at the leg welded to the gusset plate. The reduction in stiffness is caused by the extra deflection due to member bending from the eccentric connection. The concept of the deflection components are depicted in Figure 6.5. The deflection due to axial load F can be calculated as:

$$\delta_a = \frac{FL}{EA} \quad (6.16)$$

In getting the extra bending deflection, it is assumed at the end of the angle that plane sections remain plane under bending and the rotation due to the bending is about the neutral axis of the section. The deformation due to the bending at the bottom should be proportional to the end rotation:

$$\delta_b = 2\theta\bar{y} = 2\gamma \frac{F\bar{y}^2}{2k_L} = \gamma \frac{FL_L\bar{y}^2}{EI} \approx \gamma \frac{FL\bar{y}^2}{EI} \quad (6.17)$$

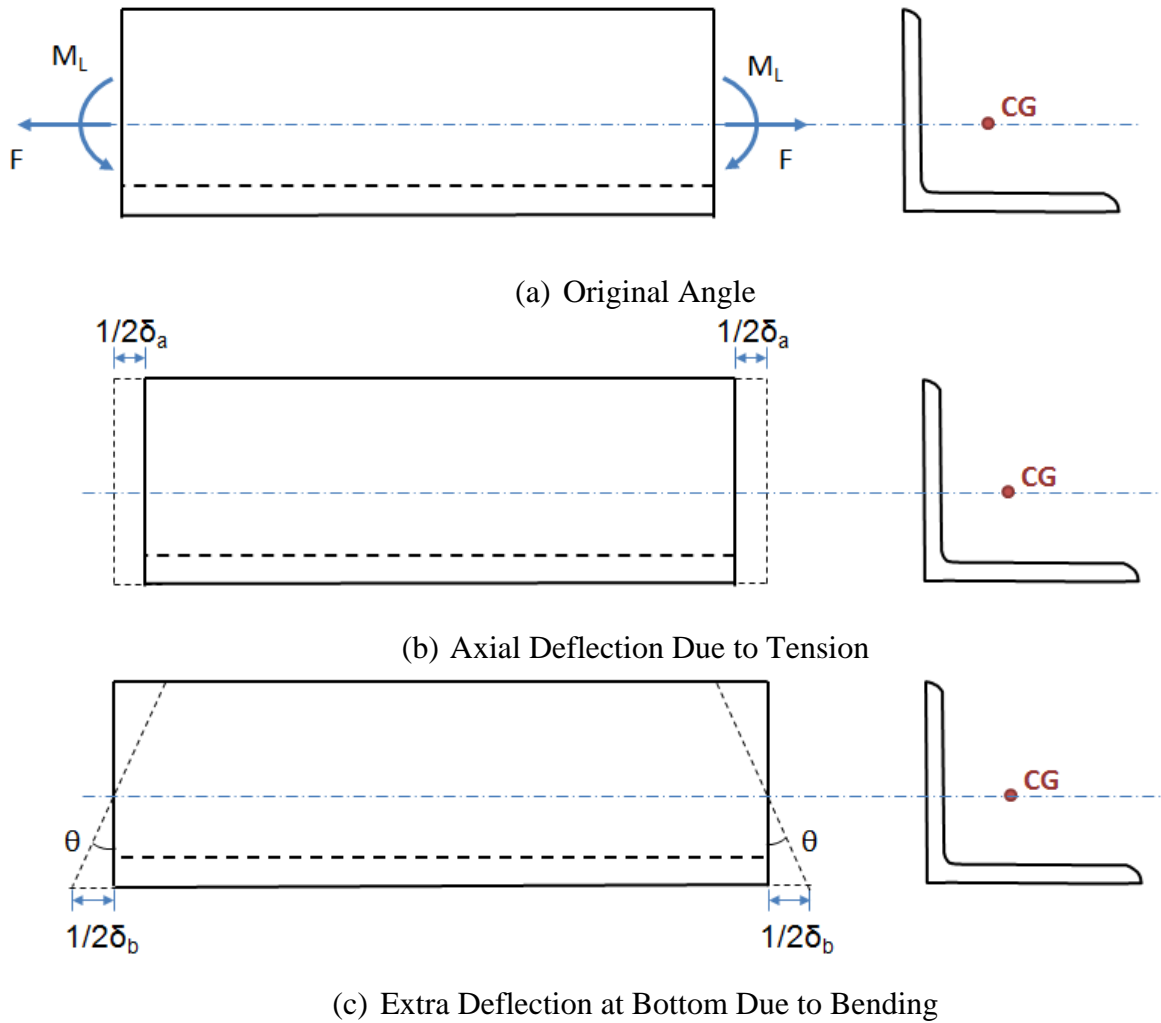


Figure 6.5: Deflection Due to Eccentric Loading

Finally, the derived δ_a and δ_b can be substituted into Equation (6.3) to get the reduced stiffness:

$$k_a = \frac{F}{\delta_a + \delta_b} = \frac{E}{L} \left(\frac{1}{\frac{1}{A} + \gamma \frac{\bar{y}}{I}} \right) = \frac{EA}{L} \left(\frac{1}{1 + \gamma \frac{A\bar{y}^2}{I}} \right) \quad (6.18)$$

This equation can be simplified by using Equation (6.2):

$$k_a = k_t \left(\frac{I}{I + \gamma A\bar{y}^2} \right) \quad (6.19)$$

Based on Equation (6.4), the stiffness reduction factor for the angle member is:

$$R_{member} = \frac{k_a}{k_t} = \frac{1}{1 + \gamma \left(\frac{A\bar{y}^2}{I} \right)} \quad (6.20)$$

Or:

$$R_{member} = \frac{1}{1 + \gamma\rho} \quad (6.21)$$

Where

$$\rho = \text{Shape factor for angle member defined as } \frac{A\bar{y}^2}{I} \quad (6.22)$$

To this point, the analytical equation for the axial stiffness of an eccentrically loaded single angle is presented by Equation (6.19), and its stiffness reduction factor is presented by Equation (6.21). The following example demonstrates the use of these expressions to predict the stiffness of the angle member test specimen described in Chapter 4.

EXAMPLE 6.1

Given:

Angle L4x4x3/8 with 7"x0.75" gusset plate.

$$L_L = 36 \text{ in}$$

$$L_p = 6.5 \text{ in}$$

Solution:

$$A_L = 2.86 \text{ in}^2, I_L = 4.32 \text{ in}^4, \bar{y} = 1.13 \text{ in}$$

$$I_{plate} = 0.246 \text{ in}^4$$

$$\rho = \frac{2.86 \times 1.13^2}{4.32} = 0.84 \quad \text{from Eq.(6.22)}$$

$$k_L = \frac{29000 \times 4.32}{36} = 3480 \text{ kip} - \text{in/rad} \quad \text{from Eq.(6.8)}$$

$$k_p = \frac{29000 \times 0.246}{6.5} = 1098 \text{ kip} - \text{in/rad} \quad \text{from Eq.(6.9)}$$

$$\gamma = \frac{1}{\frac{1098}{2 \times 3480} + 1} = 0.86 \quad \text{from Eq.(6.15)}$$

$$R_{member} = \frac{1}{1 + 0.84 \times 0.86} = 0.58 \quad \text{from Eq.(6.21)}$$

The predicted axial stiffness of the specimen is:

$$k_a = \frac{EA}{L} R_{member} = \frac{29000 \times 2.86}{36} \times 0.58 = 1336 \text{ k/in} \quad \text{from Eq. (6.19)}$$

The predicted value is 10% lower than the measured value 1500k/in. Additional verification can be done by using FEA model. Figure 6.6 shows an FEA analysis performed using ANSYS. Results of this analysis indicated that the axial stiffness of the angle member is 1288 k/in, which is only 3% lower than the predicted result of the analytical method.

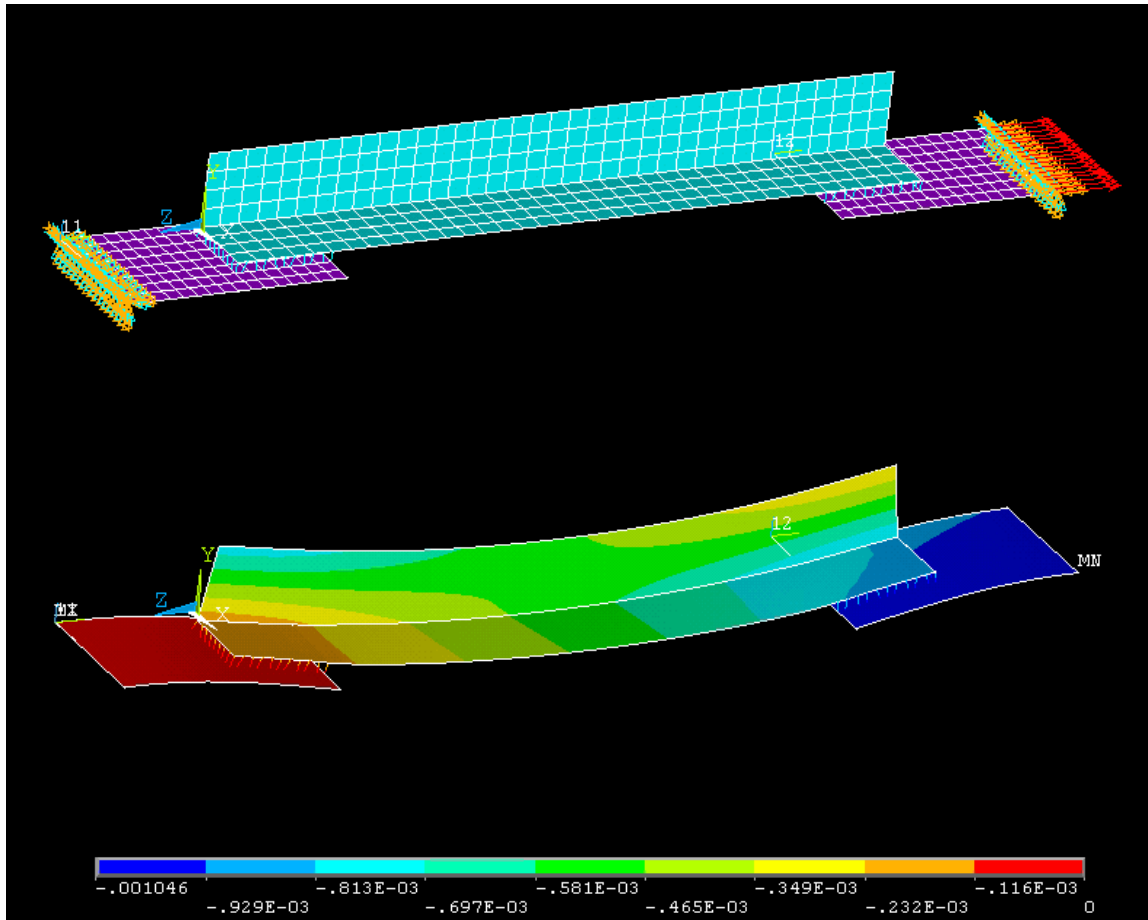


Figure 6.6: FEA Analysis of Single Angle Specimen

6.2.3 Typical Values of ρ , γ and R_{member}

The shape factor ρ is only related to three section parameters: A , \bar{y} and I . If only equal leg angles are considered, these three parameters may be interrelated. A statistic parametric analysis was performed to find the relationship of these parameters for equal leg angles.

The parametric study included angle members with leg sizes of 3", 4", 5" and 6" and thicknesses of 1/4", 3/8", 1/2" and 5/8". A , \bar{y} and I of all 16 sections were calculated and the relation of $A\bar{y}^2$ and I is graphed in Figure 6.7.

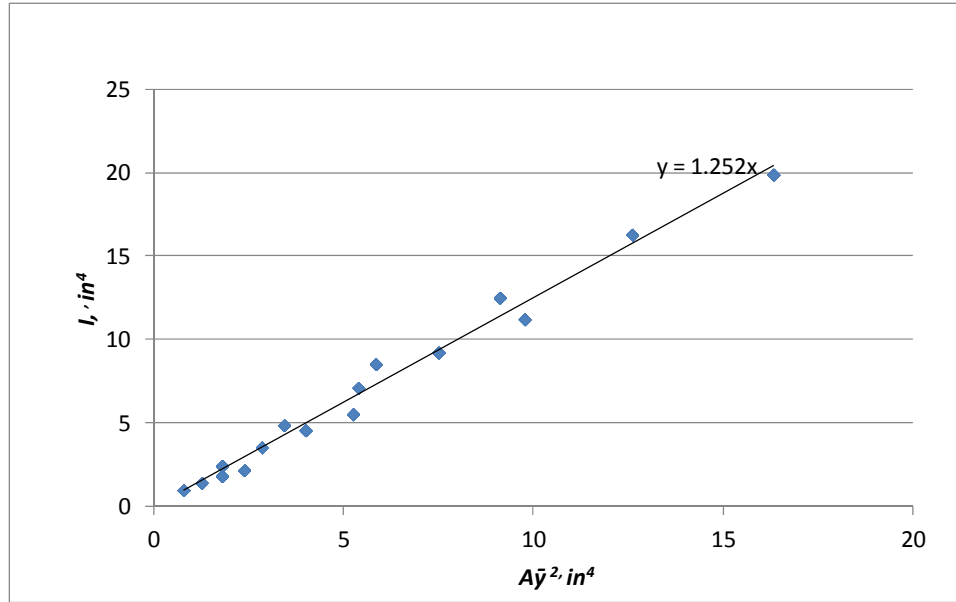


Figure 6.7: Shape Factors for Equal Leg Angles

It is obvious from this plot that the relationship between these two terms is rather linear. The generalized equation can be found:

$$I \approx 1.25A\bar{y}^2 \quad (6.23)$$

According to the relationship, ρ for the equal leg member is 0.8. Equation (6.21) can therefore be further simplified as:

$$R_{member} \approx \frac{1}{1 + 0.8\gamma} \quad (6.24)$$

The ρ value for unequal leg angles is not studied here. But the general trend of the value ρ is not difficult to recognize. When a shorter outstanding leg is used, the eccentricity \bar{y} is reduced, which leads to a lower value of ρ .

The value of γ reflects the comparison of stiffness between the angle member and the gusset plates. A stiffer gusset plate will result in a lower γ and in turn increase the axial stiffness of the member. On the other hand, if the plate is kept constant and the bending stiffness of the angle is increased, the stiffness reduction factor decreases.

Example values of R_{member} relative to k_p are presented in Figure 6.8 for a length of 120 in. It can be observed from the examples that the lower limit of R_{member} is 0.55. The upper limit of the R_{member} ranges from 0.8 and 0.9 when the gusset plate is relatively stiff.

By assuming constant gusset plate stiffness, the relation between R_{member} and the length of the angle L can be also established. As shown in Figure 6.9, increasing the length results in a slight increase in the R_{member} value; however the increase is relatively small.

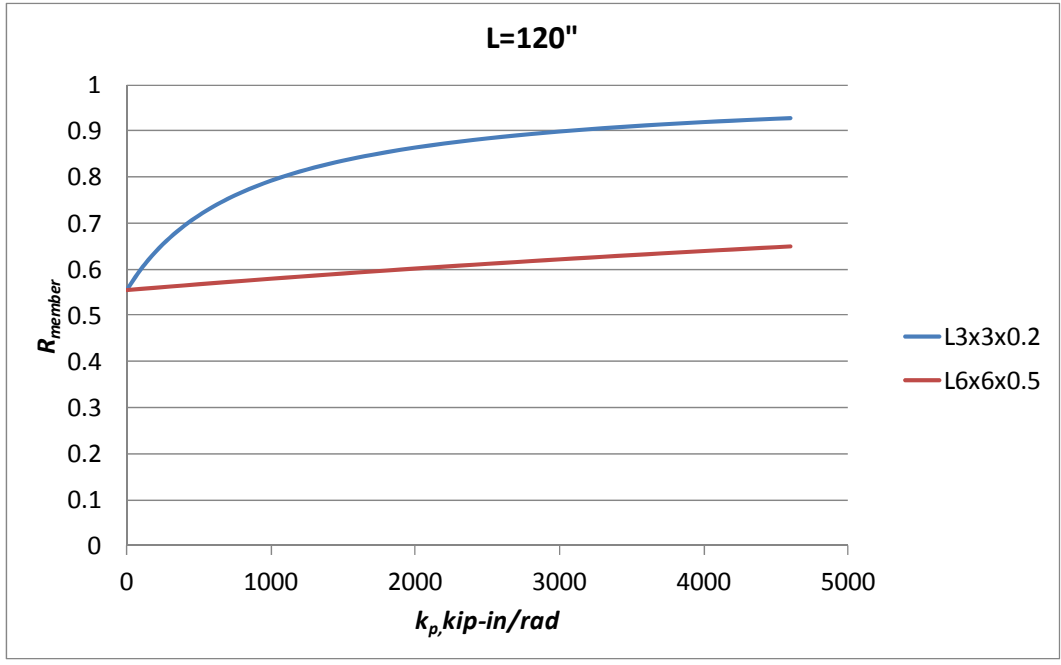


Figure 6.8: R_{member} vs. k_p

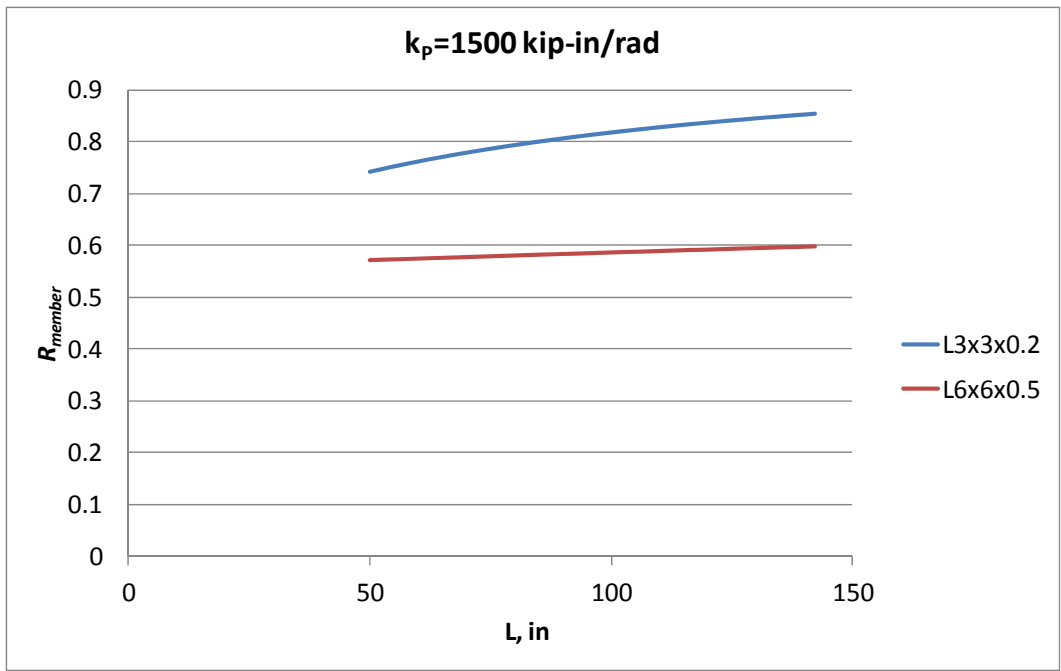


Figure 6.9: R_{member} vs. L

6.3 Analytical Stiffness Reduction for Cross Frames

Any cross frame composed of eccentrically connected single angle members will be subjected to the stiffness reduction. The stiffness reduction factor for a single angle member was

derived in the previous section, and can now be further used to develop the stiffness reduction factor for the entire cross frame.

6.3.1 Bending Stiffness of Gusset Plate

One challenge of calculating the stiffness reduction factor of a cross frame is determining the bending stiffness of the gusset plate (k_p). The complicated geometries and unclear boundary condition of the plates make an accurate estimation very difficult. But a simplified method will provide a useful approximation. As introduced in the background information presented in Chapter 2, the Whitmore effective width method is usually adopted in evaluating the strength of the gusset plate. This method could also be used to provide an approximate prediction of the bending stiffness of the gusset plate.

A sketch of a gusset plate is presented in Figure 6.10. The width of the gusset plate can be approximated as the effective width (Whitmore width), which is approximately three times the size of the angle leg. The thickness can be taken as the thickness of the stiffener, which is typically 0.5 inches in Texas. This value conservatively ignores the overlap of the stiffener and gusset plate. According to FHWA-IF-09-014(2009), the length of the plate can be taken as the average length between the fixed end and end of the member, which leads to the following expression:

$$L_p = \frac{L_1 + L_2 + L_3}{3} \quad (6.25)$$

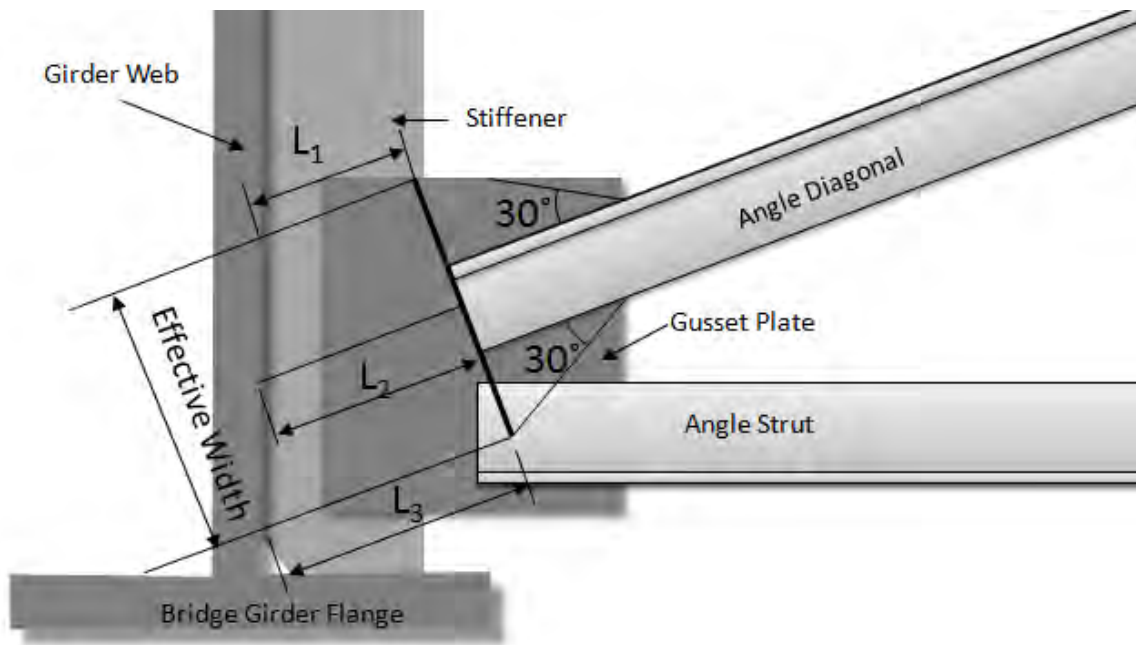


Figure 6.10: R_{member} vs. L

Based on the TxDOT Standard drawings (Texas Department of Transportation, 2006), if the minimal 8 in wide stiffener is used for all cases, L_1 is approximately 8.5 in and L_2 is approximately 9.5 in. For most cases, the lower end of the Whitmore width enters into the

bottom strut, so L_3 is set to zero, according to FHWA-IF-09-014 (2009). Then, L_p can be evaluated as follows:

$$L_p = \frac{L_1 + L_2 + L_3}{3} = \frac{8.5 + 9.5 + 0}{3} = 6in \quad \text{from Eq. (6.25)}$$

Based on these assumptions, the plate stiffness for the cross frame is as follows:

$$k_p = \frac{EI_p}{L_p} = \frac{E}{L_p} \left(\frac{3bt_p^3}{12} \right) = \frac{29000}{6} \left(\frac{3b(0.5)^3}{12} \right) = 151b$$

Where:

b = Width of the gusset plate

t_p = Thickness of the gusset plate

Finally based on the assumed geometry, the bending stiffness of the gusset plate can be approximated and the stiffness reduction for a cross frame can be determined. Examples are given to test the accuracy of these assumptions in the following subsections.

6.3.2 Single Angle X-Frame

The stiffness reduction factor for a Single Angle X-Frame (R_{ana-sx}) can be easily derived by using the compression and tension model described by Equation (2.11) along with Equation (6.24). Since the top and bottom struts are zero force members in this model and only the compression and tension diagonals contribute to the stiffness of the cross frame, the stiffness reduction factor for the cross frame should be the same as for the individual diagonals.

$$R_{ana-sx} = R_{diagonal} \quad (6.26)$$

The Single Angle X-Frame test specimen from Chapter 5 is used to demonstrate the effectiveness of using the derived analytical method.

EXAMPLE 6.2

Given:

Angle L4x4x3/8, $I=4.32 \text{ in}^4$, $\bar{y}=1.13 \text{ in}$, $E=29000 \text{ ksi}$, $A_c=2.91 \text{ in}^2$

Cross Frame: Single Angle X-Frame: $114.5'' (S) \times 53.76'' (h_b)$

$L_c= 126.48 \text{ in}$, $S_c/L_c=0.91$

Solution:

Calculate the stiffness reduction factor for the diagonal:

$$k_L = \frac{EI}{L_c} = \frac{29000 \times 4.32}{126.48} = 990.5 \text{ kip} - \text{in/rad} \quad \text{from Eq. (6.8)}$$

$$k_p = 151b = 151 \times 4 = 604 \text{ kip} - \text{in/rad} \quad \text{from Eq. (6.9)}$$

$$\gamma = \frac{1}{\frac{k_p}{2k_L} + 1} = \frac{1}{\frac{604}{2 \times 990.5} + 1} = 0.77 \quad \text{from Eq. (6.15)}$$

$$R_{diagonal} = \frac{1}{1 + 0.8\gamma} = \frac{1}{1 + 0.8 \times 0.766} = 0.62 \quad \text{from Eq. (6.21)}$$

The value of γ represents the comparison of bending stiffness between the angle and gusset plates and it can be used to estimate the bending deflection of the angle member. According to Equation 5.8, the resultant moment from eccentric loading is:

$$M_L = \gamma F_c \bar{y} = \gamma F \frac{L_c}{S_c} \bar{y} = 0.77 \times \frac{1}{0.91} \times \bar{y} F = 0.85 \bar{y} F \quad \text{from Eq. (6.13)}$$

The out-of-plane deflection at the mid-span of the diagonals:

$$\delta = \frac{M_L L_c^2}{8EI} = \frac{0.85 \times 1.13F \times 126.48^2}{8 \times 29000 \times 4.32} = 0.0153F$$

In Figure 6.11, the analytical solution of the mid-span deflection is compared with the FEA model and measured values from the laboratory tests. The analytical solution is slightly conservative, but has reasonable agreement with the test results and FEA result. Therefore, the analytical method provides a relatively simple solution for predicting the behavior of the reduction in stiffness due to angle bending from the eccentric connections.

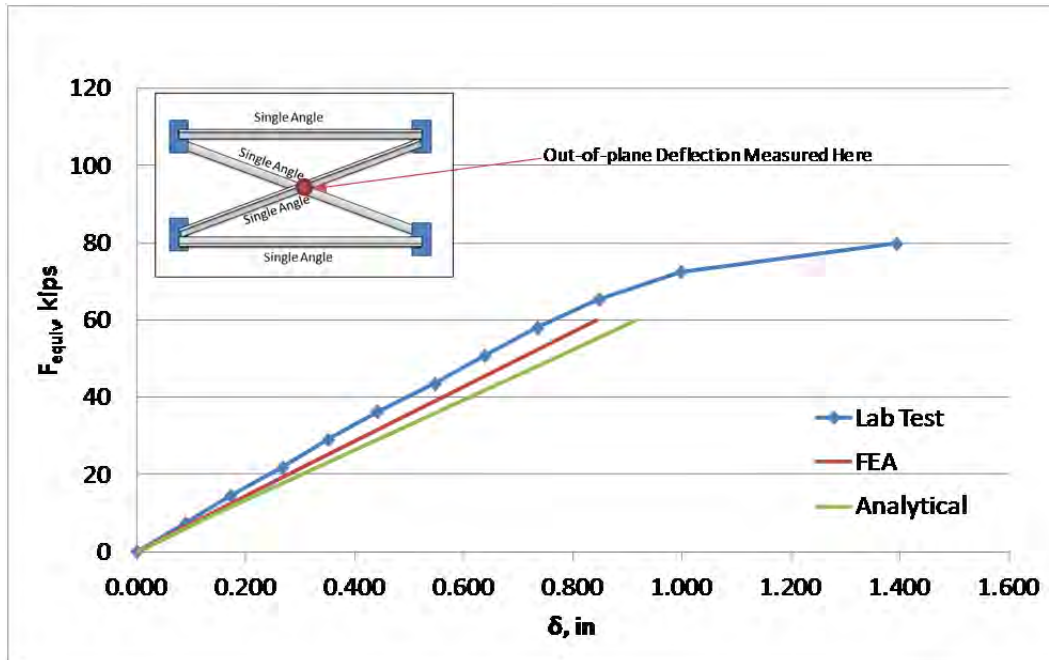


Figure 6.11: Out-of-plane Deflection for X-Frame

Finally, the stiffness reduction value for the diagonal can be directly used to calculate the torsional brace stiffness of the cross frame. Recalling that for the X cross frame, the analytical solution based on the compression-tension model gives a stiffness of 1,579,000 in-k/rad. When this stiffness is corrected to account for the eccentric connections of the angles, the following stiffness results:

$$\begin{aligned}\beta_{b-SX-corrected} &= R\beta_b = 0.62 \times 1,579,000 \\ &= 979,000 \text{ kip-in/rad}\end{aligned}$$

This estimated value is 12% higher than the test result of 872,000 kip-in/rad. The overestimation may be caused by the geometric difference between the truss model and the actual cross frame. The angle (α) between the diagonal and horizontal strut is 22.9° and based on the truss model, the angle is:

$$\alpha = \text{atan}\left(\frac{h_b}{l_c}\right) = \text{atan}\left(\frac{53.74}{114.5}\right) = 25.1^\circ$$

Apparently there is discrepancy between the truss model and the actual cross frame and the actual diagonal is less inclined than it is assumed. This discrepancy originates from the geometric conflicts at a gusset plate where a diagonal and a strut are connected. The test specimen was designed according to the TxDOT standard drawings (Texas Department of Transportation, 2006), where a simplified method was adopted to determine the design parameter of the gusset plate. As shown in Figure 6.12, typical values of “T” and “B” were tabulated in the standard drawing and it causes the line of the diagonal does not pass the working pointing defined by the “S” and “h_b”. And usually a lower angle between these two members would cause a more significant conflict.

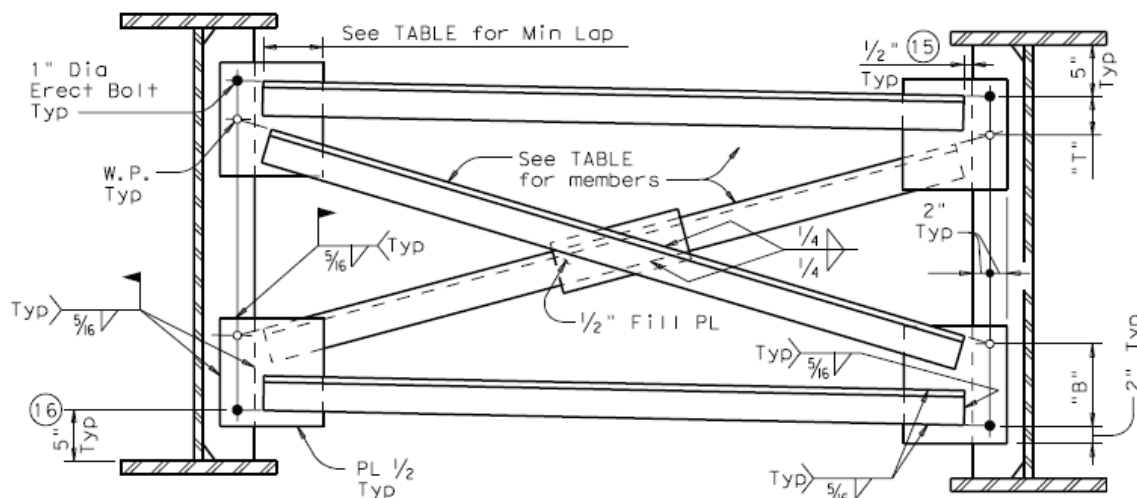


Figure 6.12: Typical TxDOT Cross Frame (Texas Department of Transportation, 2006)

In order to more accurately predict the stiffness of the cross frame, the analytical calculation needs to be revised to account for the possible geometric discrepancy of the cross

frame actually built. According to the revised truss model shown in the Figure 6.13, the effective height of the cross frame is h_b' . Since the top and bottom strut is not contributing in the stiffness of the cross frame, the following equation can be obtained:

$$\beta_{b-sx}' = \frac{A_c E S^2 h_b'^2}{L_c^3} = \frac{A_c E S^2 (S \tan \alpha)^2}{\left(\frac{S}{\cos \alpha}\right)^3} = A_c E S \sin^2 \alpha \cos \alpha \quad (6.27)$$

If Equation (6.27) is used in example of the stiffness of the Single Angle X-Frame specimen, the analytical stiffness is:

$$\beta_{b-sx}' = A_c E S \sin^2 \alpha \cos \alpha \quad \text{From Eq. (6.27)}$$

$$= 2.91 \times 29000 \times 114.5 \times \sin^2 22.9 \times \cos 22.9$$

$$= 1,348,000 \text{ kip-in/rad}$$

$$\beta_{b-sx\text{-corrected}}' = R \beta_b' = 0.62 \times 1,348,000$$

$$= 836,000 \text{ kip-in/rad}$$

The resulting stiffness of the cross frame is 836,000 kip-in/rad which is 4% conservative than the tested value 872,000 kip-in/rad. It can be concluded that the analytical method derived in this section gives a reasonable and accurate prediction.

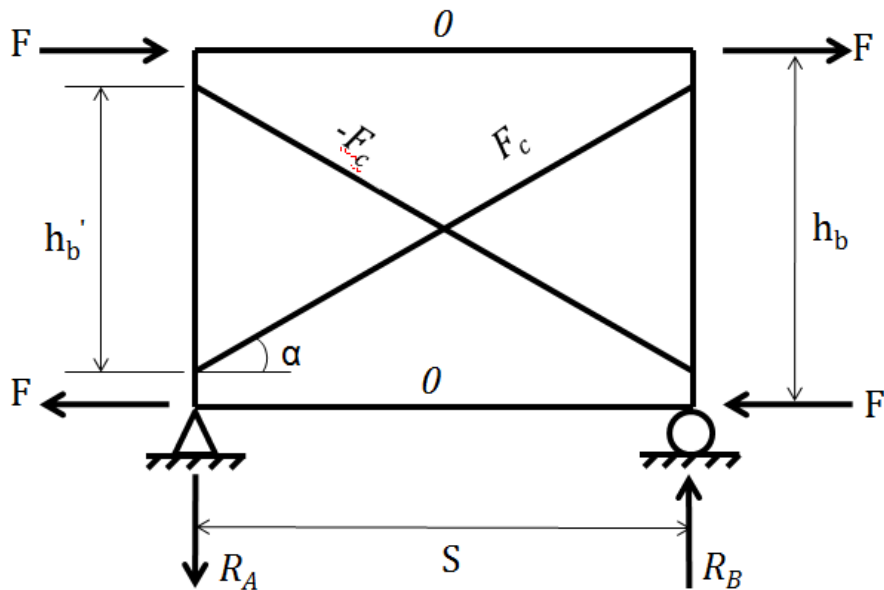


Figure 6.13: Revised Geometry of the Compression-Tension Model

6.3.3 Single Angle K-Frame

The stiffness reduction for a Single Angle K-Frame (R_{ana-SK}) can be also derived from the K-frame model described by Equation (2.12) along with Equation (6.24). The corrected brace stiffness can be calculated as follows:

$$\beta_{b-SK-corrected} = \frac{2ES^2h_b^2}{\frac{8L_c^3}{R_cA_c} + \frac{S^3}{R_hA_h}} \quad (6.28)$$

Where:

R_c = Stiffness reduction factor of the diagonal

R_h = Stiffness reduction factor of half of the bottom struts between the gusset plates. The bottom strut should be regarded as two truss members because the forces in the two branches are in the opposite direction.

The stiffness reduction factor of the K-frame can be evaluated by the following expression:

$$R_{Ana-SK} = \frac{\beta_{b-SK-corrected}}{\beta_b} \quad (6.29)$$

Since the length of the angle members have small impact on the stiffness reduction factor and the diagonal of the K-frame is usually only slightly shorter than the spacing, the stiffness reduction factor for half of the bottom strut can be conservatively used for the whole cross frame:

$$R_{ana-SK} \approx R_h \quad (6.30)$$

The Single Angle K-Frame test specimen is used to demonstrate the effectiveness of using the derived analytical method.

EXAMPLE 6.3

Given:

Angle L4x4x3/8, $I=4.32 \text{ in}^4$, $\bar{y}=1.13 \text{ inch}$

Cross Frame: Single Angle K-Frame: 114.5" (S) x 53.76" (h_b)

$L_c=78.5 \text{ in}$, $S_c/2L_c=0.729$

Solution:

Calculate the stiffness reduction factor for the diagonal:

$$k_L = \frac{EI}{L_c} = \frac{29000 \times 4.32}{78.5} = 1596 \text{ kip} - \text{in/rad} \quad \text{from Eq. (6.8)}$$

$$k_p = 151b = 151 \times 4 = 604 \text{ kip} - \text{in/rad} \quad \text{from Eq. (6.9)}$$

$$\gamma = \frac{1}{\frac{k_p}{2k_L} + 1} = \frac{1}{\frac{604}{2 \times 1596} + 1} = 0.84 \quad \text{from Eq. (6.15)}$$

$$R_c = \frac{1}{1 + 0.8\gamma} = \frac{1}{1 + 0.8 \times 0.84} = 0.60 \quad \text{from Eq. (6.21)}$$

Then calculate the stiffness reduction factor for the branch of the bottom strut:

$$k_L = \frac{EI}{L_c} = \frac{29000 \times 4.32}{57.25} = 2188 \text{ kip} - \text{in/rad} \quad \text{from Eq. (6.8)}$$

$$k_p = 151b = 151 \times 4 = 604 \text{ kip} - \text{in/rad} \quad \text{from Eq. (6.9)}$$

$$\gamma = \frac{1}{\frac{604}{2 \times 2188} + 1} = 0.88 \quad \text{from Eq. (6.15)}$$

$$R_h = \frac{1}{1 + 0.8 \times 0.88} = 0.59 \quad \text{from Eq. (6.21)}$$

The same check can be performed on the accuracy of the γ value. According to Equation 5.8, the resultant moment from eccentric loading is:

$$M_L = \gamma F_c \bar{y} = \gamma F \frac{2L_c}{S_c} \bar{y} = 0.84 \times \frac{1}{0.729} \times F = 1.15F\bar{y} \quad \text{from Eq. (6.13)}$$

The out-of-plane deflection at the mid-span of the compression diagonal:

$$\delta = \frac{M_L L_c^2}{8EI} = \frac{1.15F \times 1.13 \times 78.5^2}{8 \times 29000 \times 4.32} = 0.007F\bar{y} = 0.008F$$

In Figure 6.14, the analytical solution of the mid-span deflection of the compression diagonal is compared with predictions from the FEA model and the measured values. The analytical solution and the FEA result showed very good agreement, while the test results showed lower deflections prior to buckling of the diagonal. Figure 6.14 can prove that the analytical method can provide reasonable predictions of the behavior of the bending due to the eccentricity.

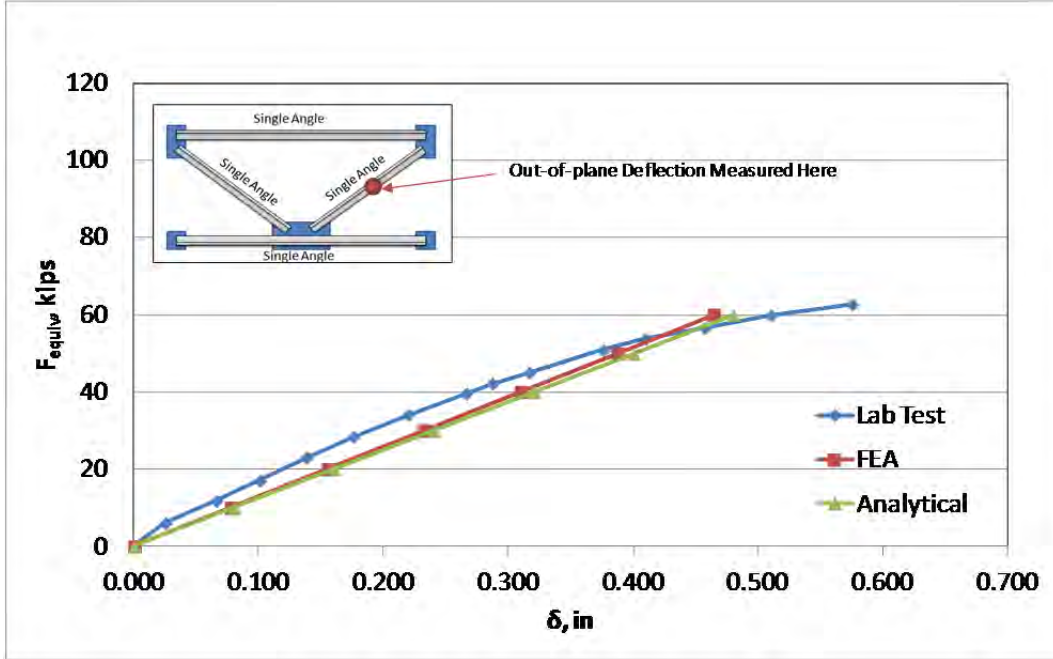


Figure 6.14: Out-of-plane Deflection for K-Frame

From the numerical example, it is seen that the stiffness reduction for the strut and diagonal are practically the same. According to the K frame model, the analytical stiffness of this cross frame is 1,189,000 kip-in/rad. Therefore, the stiffness reduction value for the half bottom strut can be directly used to calculate the stiffness of the cross frame:

$$\begin{aligned}\beta_{b-SK-corrected} &= R_h \beta_b = 0.59 \times 1,189,000 \\ &= 701,500 \text{ kip} - \text{in/rad}\end{aligned}$$

This value has reasonable agreement with the tests stiffness value of 760,000 kip-in/rad and is 8% conservative. It should be noted that the geometric difference observed in the Single Angle X-Frame does not occur in the Single Angle K-Frame case. It is apparently because the K-Frame arrangement usually results in a more inclined diagonal, which has less conflict with the strut. This observation also suggests that the K-Frame has more advantage than an X-Frame in the design of cross frames with a wider spacing.

6.3.4 Single Angle Z-Frame

The stiffness reduction a Single Angle Z-Frame (R_{ana-SZ}) can also be derived from the tension-only model and Equation (6.24). The corrected brace stiffness can be calculated as:

$$\beta_{b-SZ-corrected} = \frac{ES^2 h_b^2}{\frac{2L_c^3}{R_c A_c} + \frac{S^3}{R_h A_h}} \quad (6.31)$$

Then the stiffness reduction factor of the Z-frame can be evaluated by:

$$R_{ana-sz} = \frac{\beta_{b-sz-corrected}}{\beta_b} \quad (6.32)$$

As shown in the K-frame example, the lengths of a member have only a small impact on the R_{member} and the struts of the Z-frame are usually only slightly shorter than the diagonals, the reduction factor for the strut can therefore be conservatively used for the whole cross frame:

$$R_{ana-sz} \approx R_h \quad (6.33)$$

The Single Angle Z-Frame test specimen is used to demonstrate the effectiveness of using the derived analytical method.

EXAMPLE 6.4

Given:

Angle L4x4x3/8, $I=4.32 \text{ in}^4$, $\bar{y}=1.13 \text{ in}$

Cross Frame: Single Angle Z-Frame: 114.5" (S) x 53.76" (h_b)

$L_c= 126.48 \text{ in}$

Solution:

Calculate the stiffness reduction factor for the strut:

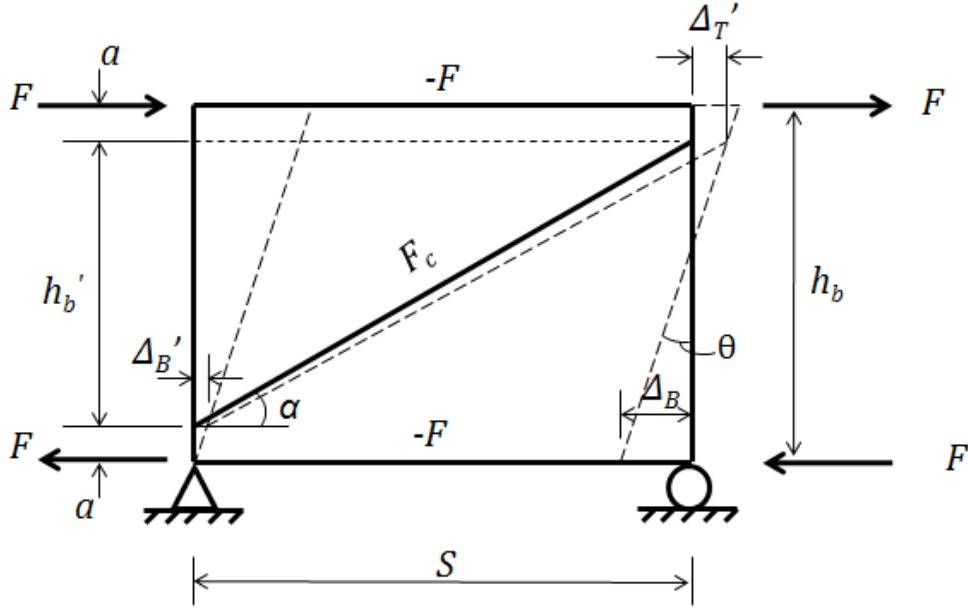
$$k_L = \frac{EI}{S} = \frac{29000 \times 4.32}{114.5} = 1,094 \text{ kip} - \text{in/rad} \quad \text{from Eq.(6.8)}$$

$$k_p = 151b = 151 \times 4 = 604 \text{ kip} - \text{in/rad} \quad \text{from Eq.(6.9)}$$

$$\gamma = \frac{1}{\frac{k_p}{2k_L} + 1} = \frac{1}{\frac{604}{2 \times 1094} + 1} = 0.78 \quad \text{from Eq.(6.15)}$$

$$R_c = \frac{1}{1 + 0.8\gamma} = \frac{1}{1 + 0.8 \times 0.78} = 0.62 \quad \text{from Eq.(6.21)}$$

According to the tension only model results, the analytical stiffness of this cross frame is 575,000 kip-in/rad. However similar to the Single Angle X-Frame, the theoretical brace stiffness for the Z-Frame should be also corrected first to account for the geometric difference between the truss model and the actual cross frame. The revised truss model is shown in Figure 6.15. The deformed shape of the cross frame is shown in dash line. The derivation of the revised torsional brace stiffness is then presented. The designation used in the derivation is defined in Figure 6.15.



L_c' =length of the diagonal

Figure 6.15: Revised Geometry for Tension-only Model

From equilibrium, the force in the diagonal is calculated as:

$$F_c = \frac{2F}{\cos\alpha} \left(\frac{h_b}{h_b'} \right) \quad (6.34)$$

The axial deformation of the diagonal under the F_c is:

$$\Delta_c = (\Delta_T' - \Delta_B') \cos\alpha = \frac{F_c L_c'}{(EA)_c} \quad (6.35)$$

Combine Eq. (6.34) and Eq.(6.35), then it can be obtained:

$$\Delta_T' - \Delta_B' = \frac{2FL_c'}{(EA)_c \cos^2\alpha} \left(\frac{h_b}{h_b'} \right) \quad (6.36)$$

Also the axial deformation of strut under the force F is:

$$\Delta_B = \frac{FS}{(EA)_h} \quad (6.37)$$

In addition, the following relationships can be obtained from the geometry:

$$\Delta_B + \Delta_T' = \theta(h_b' + a) \quad (6.38)$$

$$\Delta_B' = \theta a \quad (6.39)$$

Eq. (6.36) + Eq.(6.37) will give:

$$\Delta_T' - \Delta_B' + \Delta_B = \frac{2FL_c'}{(EA)_c \cos^2 \alpha} \left(\frac{h_b}{h_b'} \right) + \frac{FS}{(EA)_h} \quad (6.40)$$

Eq. (6.38) - Eq.(6.39) will give:

$$\Delta_T' - \Delta_B' + \Delta_B = \theta h_b' \quad (6.41)$$

Equate Eq. (6.40) to Eq. (6.41) and simplify and equation, then the rotation of the cross frame can be calculated as:

$$\theta = \frac{2FL_c'}{(EA)_c \cos^2 \alpha} \left(\frac{h_b}{h_b'^2} \right) + \frac{FS}{(EA)_h h_b'} \quad (6.42)$$

Finally, the modified tension-only stiffness would be:

$$\beta_{b-sk}' = \frac{Fh_b}{\theta} = \frac{Fh_b}{\frac{2FL_c'}{(EA)_c \cos^2 \alpha} \left(\frac{h_b}{h_b'^2} \right) + \frac{FS}{(EA)_h h_b'}} \quad (6.43)$$

Simplifying (6.43) will give:

$$\beta_{b-sk}' = \frac{ES^2 h_b'^2}{\frac{2L_c'^3}{A_c} + \frac{S^3}{A_h} \left(\frac{h_b'}{h_b} \right)} \quad (6.44)$$

By using Equation (6.44), the revised stiffness of the Single Angle Z-frame can be calculated as:

$$\begin{aligned} \beta_{b-sk}' &= \frac{ES^2 h_b'^2}{\frac{2L_c'^3}{A_c} + \frac{S^3}{A_h} \left(\frac{h_b'}{h_b} \right)} = \frac{ES^2 (Stan\alpha)^2}{2 \left(\frac{S}{\cos\alpha} \right)^3 + \frac{S^3}{A_h} \left(\frac{Stan\alpha}{h_b} \right)} \\ &= \frac{ES \sin^2 \alpha \cos \alpha}{\frac{2}{A_c} + \frac{1}{A_h} \left(\frac{S}{h_b} \right) \sin \alpha \cos^2 \alpha} \\ &= \frac{29000 \times 114.5 \times \sin^2 22.9 \times \cos 22.9}{\frac{2}{2.91} + \frac{1}{2.91} \left(\frac{114.5}{53.74} \right) \sin 22.9 \times \cos^2 22.9} \end{aligned}$$

$$= 498,500 \text{ kip} - \text{in/rad}$$

So the stiffness corrected for the reduction can be calculated by:

$$\beta_{b-SK-corrected}' = R_h \beta_b' = 0.62 \times 498,500 = 309,000 \text{ kip} - \text{in/rad}$$

The calculated brace stiffness is 309,000 kip-in/rad, which is about 13% conservative than the measured stiffness of the specimen. Again, the analytical method can provide a reasonable and practical prediction.

6.3.5 Double Angle Z-Frame

The Double Angle Z-Frames that were tested in the laboratory consisted of double angle for the diagonals and single angles for the struts. The double angle diagonal consists of a concentrically loaded member and is not subjected to the stiffness reduction. However the contribution to the stiffness by the single angle struts does need to be reduced to reflect the eccentric connection. The cross frame stiffness can be calculated as:

$$\beta_{b-DZ-corrected} = \frac{ES^2 h_b^2}{\frac{2L_c^3}{A_c} + \frac{S^3}{R_h A_h}} \quad (6.45)$$

Similarly if the geometry discrepancy presented in the Double Angle Z-frame, Equation (6.44) can be used to derive the analytical solution:

$$\beta_{b-DZ-corrected}' = \frac{ES^2 h_b'^2}{\frac{2L_c'^3}{A_c} + \frac{S^3}{R_h A_h} \left(\frac{h_b'}{h_b}\right)} \quad (6.46)$$

Or:

$$\beta_{b-DZ-corrected}' = \frac{ES \sin^2 \alpha \cos \alpha}{\frac{2}{A_c} + \frac{1}{R_h A_h} \left(\frac{S}{h_b}\right) \sin \alpha \cos^2 \alpha} \quad (6.47)$$

The stiffness reduction factor of the Double Angle Z-frame can be evaluated by the following expression:

$$R_{ana-DZ} = \frac{\beta_{b-DZ-corrected}}{\beta_b} \quad (6.48)$$

Similarly, the stiffness of the tested Double Angle Z-Frame can be calculated.

EXAMPLE 6.5

Given:

Angle L4x4x3/8, $I=4.32 \text{ in}^4$, $\bar{y}=1.13 \text{ in}$

Cross Frame: Double Angle Z-Frame: 114.5" (S) x 53.76" (h_b)

$L_c=126.48 \text{ in}$

Solution:

Same as the previous evaluation of Single Angle Z-Frame, the stiffness reduction factor of the struts R_h is 0.62. The stiffness values are given by the following expressions:

$$\begin{aligned}\beta_{b-DZ}' &= \frac{ES\sin^2\alpha\cos\alpha}{\frac{2}{A_c} + \frac{1}{A_h}\left(\frac{S}{h_b}\right)\sin\alpha\cos^2\alpha} && \text{from Eq. (6.46)} \\ &= \frac{29000 \times 114.5 \times \sin^2 22.9 \times \cos 22.9}{\frac{2}{5.82} + \frac{1}{2.91}\left(\frac{114.5}{53.74}\right)\sin 22.9 \times \cos^2 22.9} \\ &= 791,000 \text{ kip} - \text{in/rad}\end{aligned}$$

$$\begin{aligned}\beta_{b-DZ-corrected}' &= \frac{ES\sin^2\alpha\cos\alpha}{\frac{2}{A_c} + \frac{1}{R_h A_h}\left(\frac{S}{h_b}\right)\sin\alpha\cos^2\alpha} && \text{from Eq. (6.47)} \\ &= \frac{29000 \times 114.5 \times \sin^2 22.9 \times \cos 22.9}{\frac{2}{5.82} + \frac{1}{0.62 \times 2.91}\left(\frac{114.5}{53.74}\right)\sin 22.9 \times \cos^2 22.9} \\ &= 631,000 \text{ kip} - \text{in/rad}\end{aligned}$$

If it is needed, the stiffness reduction factor for the cross frame can be calculated with:

$$R_{ana-DZ} = \frac{\beta_{b-DZ-corrected}'}{\beta_b'} = \frac{631,000}{791,000} = 0.80 \quad \text{from Eq. (6.48)}$$

According to the laboratory test, the actual stiffness of this cross frame is 597,000 kip-in/rad. The analytical solution slightly overestimates the stiffness by 5.6%.

6.3.6 Summary of the Analytical Solutions for Stiffness Reduction in Cross Frames

A summary of the results obtained from the analytical solutions is presented in Table 6.1 along with their measured values. The percent error by using this method ranges from -12% to 5.6%, where the negative value represents a conservative prediction. Overall, the derived

analytical method can provide a relatively accurate estimate of the cross frame's stiffness to account for the stiffness reduction due to the eccentricity of the single angle member.

Table 6.1 Summary of Brace Stiffness by Analytical Solution

Cross Frame	R	β_b' (analytical) kip-in/rad	$R\beta_b'$ (analytical) kip-in/rad	β_b (measured) kip-in/rad	Error, %
Single Angle X-frame	0.62	1,348,000	836,000	872,000	-4%
Single Angle K-frame	0.59	1,189,000	701,500	760,000	-8%
Single Angle Z-frame	0.62	498,500	309,000	358,000	-13%
Double Angle Z-frame	0.80	791,000	631,000	597,000	5.6%

For those cross frames composed of single angle member only, the stiffness reduction factors are all near 0.6. And for the cross frame with concentric double angle diagonal, the stiffness reduction is in a much higher value: 0.8. Therefore, this comparison also suggests that using concentric members can effectively help improve the stiffness of cross frames.

6.4 Parametric Studies for the Stiffness Reduction Factor Using Analytical Solutions

The analytical solution derived in Section 6.3 has demonstrated the potential capability in estimating the torsional brace stiffness of cross frames comprised of single angles. In this section, Equations (6.26) and (6.29) are used to perform parametric studies on the Single Angle X-Frame and the Single Angle K-Frame. The study illustrates how the stiffness reduction factor changes with different combinations of variables including: girder spacing (S), brace height (h_b), angle leg size (b) and angle leg thickness (t). The angle members are assumed to be equal leg angles. Values of the parameters used in this study are shown in Table 6.2.

Table 6.2 Summary of Variables in the Parametric Study

h_b , in	S , in	Range of S/h_b	b , in	t , in
48	96, 108, 120, 132, 144	2 – 3	3, 4	1/4, 3/8, 1/2, 5/8
60	96, 108, 120, 132, 144	1.6 – 2.4	3, 4	1/4, 3/8, 1/2, 5/8
72	96, 108, 120, 132, 144	1.3 – 2	4, 5	1/4, 3/8, 1/2, 5/8
84	96, 108, 120, 132, 144	1.4 – 1.7	4, 5	1/4, 3/8, 1/2, 5/8
96	96, 108, 120, 132, 144	1 – 1.5	5, 6	1/4, 3/8, 1/2, 5/8

The resulting stiffness reduction factors by the analytical solution are plotted against the eccentricity of the section \bar{y} . Figure 6.16 and Figure 6.17 show the plots for Single Angle X-Frame and Single Angle K-Frame respectively. As shown in these figures, the analytical solutions cluster in groups. Each group represents one angle section. For example, the group at the upper left corner represents the results from L3x3x1/4, and the group at the right bottom represents L6x6x5/8. In general, with the increase of both b and t , the stiffness reduction factor (R_{ana-SX}) decreases.

In addition, for a particular member (b and t are constant), the variation of the R_{ana-SX} is related to the bending stiffness of the angle or the length of the angle. If the angle member is shorter, or the bending stiffness is higher, R_{ana-SX} is reduced.

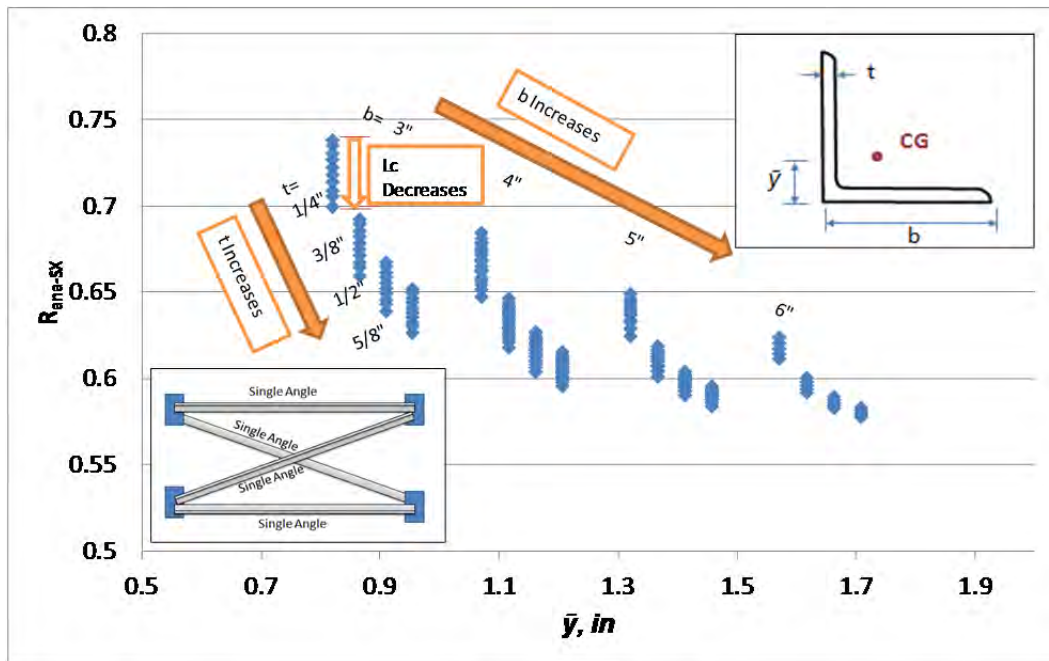


Figure 6.16: Analytical Stiffness Reduction Factor of Single Angle X-Frame

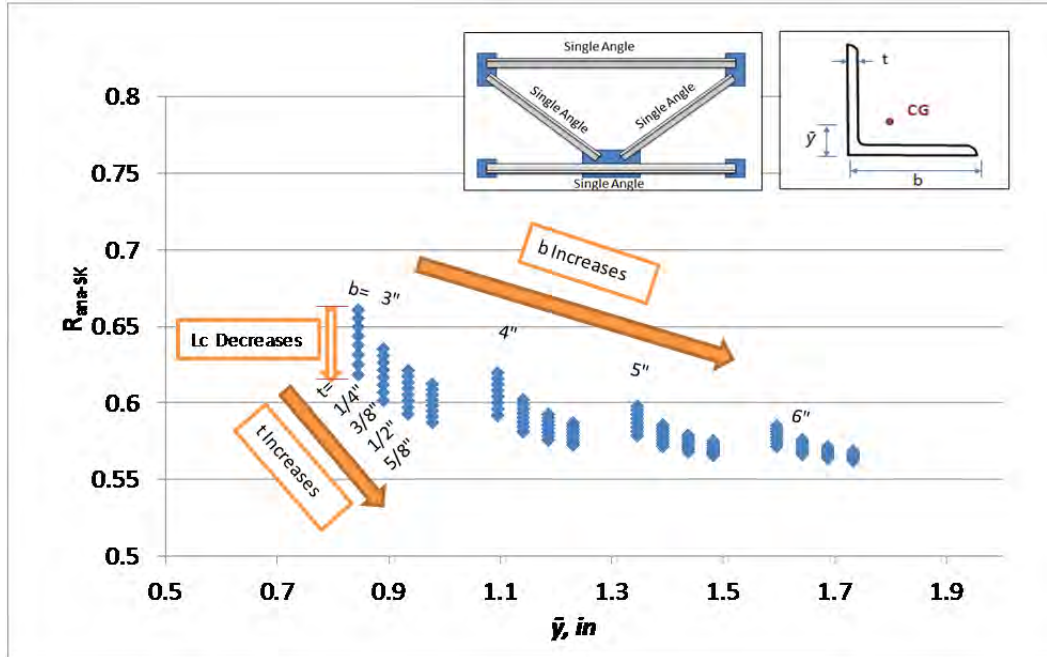


Figure 6.17: Analytical Stiffness Reduction Factor of Single Angle K-Frame

6.5 Conclusions of the Analytical Solution

In this preceding sections, the analytical solution for the stiffness reduction factor of a cross frame composed of single angle members was derived. Equation (6.24) can be used to predict the axial stiffness reduction for an eccentrically loaded single angle member. If it is combined with traditional truss analogy methods, this equation can also be used to predict the stiffness reduction for a cross frame with single angles as well. Analyses based on this equation are done to investigate the behavior of the stiffness reduction for different cross frames. Several conclusions can be drawn from the findings:

- The axial stiffness reduction factor (R_{member}) of an eccentrically connected single angle is significantly related to the bending stiffness of the angle k_L and the bending stiffness of the gusset plate k_p . In general, stiffer angles result in a lower reduction factor (i.e. a more significant reduction in the stiffness). In addition, increasing the stiffness of the gusset plate results in a higher reduction factor (i.e. a less significant reduction in the stiffness). The bending stiffness of the gusset plate can be estimated using Whitmore's method to approximate the geometry.
- The torsional brace stiffness reduction factor of a cross frame can be derived from the member axial stiffness reduction factor. In general, the results obtained from this analytical method provide a reasonable estimate of the stiffness of the cross frame. In addition, the method can also accurately predict the bending behavior of the angles due to the eccentric loading.
- The geometric discrepancy between the truss model and actual built cross frame geometry also plays an important role in finding stiffness of the cross frames. The angle between the diagonal and strut is usually reduced in design to avoid conflict at the gusset plate and the reduction of the angle will cause lower cross frame stiffness. It can be seen

from the examples that the reduction in the stiffness is much more significant for the X-Frame and Z-Frame than the K-frame, because the K-frame arrangement naturally avoids congestion at the gusset plate. This effect was studied in this chapter and the evaluations are also included in validating the analytical solutions.

- Parametric studies using the analytical solution showed that the stiffness reduction of the cross frame is significantly affected by the angle member size (b , t). Increasing the size of the angle members results in a lower magnitude for the reduction factor. In addition, the reduction factor is also related to the global geometry of the cross frame primarily in terms of the diagonal length. Longer diagonals tend to increase the magnitude of R_{frame} . Based upon the range of parameters considered in this study, typical values of R_{frame} range from 0.55 and 0.75.

The derived analytical solutions have been validated with the laboratory results. However, the validity of the analytical method to be used in wider range of geometries is yet unproved. In addition, the analytical method does not include the geometry of the stiffeners and gusset plates, and the differences in these details may cause the stiffness of a cross frame to differ from its theoretical values. Hence, in the following sections, more detailed FEA shell element models will be used in parametric studies to find the stiffness of cross frames for various geometries and results will be compared with the solutions obtained from the herein derived analytical method.

6.6 Parametric Studies for Stiffness of Single Angle X-Frame

6.6.1 Introduction

Discussions in the previous sections have revealed that the analytical truss-type models often used in brace design can lead to significant errors in the stiffness of cross frames comprised of single angle members. Many of the models that are used significantly overestimate the stiffness of the cross frames. To account for the unconservative errors, a stiffness reduction factor was introduced to modify the results calculated from the traditional methods. A derivation of the stiffness reduction factors was provided in Chapter 5 by including the bending deflection in the calculation of the axial stiffness. The results from the stiffness reduction method showed relatively good agreement with the test results.

Due to the significant time and cost required to perform the laboratory experiments, it is not feasible to perform laboratory tests on the wide range of potential cross frame geometries. Instead, the results from the laboratory tests that were conducted were used to verify the finite element models and as well as the analytical solutions.

The FEA shell element models introduced in Chapter 5 were shown to accurately predict the stiffness of different types of cross frames and simulating the behavior of the cross frame under specified load pattern. The verified FEA models can then be used to carry out parametric studies on a wide range of cross frame geometries that can potentially be encountered in practice. Hence, these models can be used to predict the stiffness of the cross frames with various geometries.

In this section, parametric studies on the Single Angle X-Frame are introduced and the parametric studies on the Single Angle K-Frame are presented in the next section. A parametric study was first performed to get the elastic stiffness values of the Single Angle X-Frames with a

wide range of geometries. A statistical analysis on the variation of the resulting stiffness reduction factors was performed to identify the major parameters that should be considered. In addition, the stiffness values estimated from different methods were compared with the parametric results so that advantages and disadvantages of the different methods could be considered.

Following the linear parametrical study, a nonlinear parametric study was also performed. The purpose of this study was to investigate the potential stiffness loss of cross frames due to the second order effects of the compression members. Finally a parametric study on unequal leg angles is discussed and the effect of using these members in cross frames is studied.

6.6.2 Parametric Study with Linear Analysis

According to the derivation earlier in this chapter, the stiffness loss due to the eccentricity is not a function of the load magnitude, so linear (or elastic) analysis can effectively predict this effect. The parameters considered in this study included brace height (h_b), angle leg size (b) and angle leg thickness (t). The angle members in the results presented in this section were assumed to be equal leg angles. Values of the parameters used in this study are shown in the Table 6.3. The values of the parameters were chosen to cover the wide range of bridge geometries and cross frame configurations that might be encountered in practice. The aspect ratio of the cross frame is defined as the ratio of S/h_b , which is in a range of 1 to 3 for the majority of cross frames. The total number of cases that were analyzed was 160. The results from the parametric studies are discussed in the following subsections.

Table 6.3 Summary of Variables in the Parametric Study

h_b , in	S, in	Range of S/h_b	b, in	t, in
48	96, 108, 120, 132, 144	2 – 3	3, 4	1/4, 3/8, 1/2, 5/8
60	96, 108, 120, 132, 144	1.6 – 2.4	3, 4	1/4, 3/8, 1/2, 5/8
72	96, 108, 120, 132, 144	1.3 – 2	4, 5	1/4, 3/8, 1/2, 5/8
84	96, 108, 120, 132, 144	1.1 – 1.7	4, 5	1/4, 3/8, 1/2, 5/8
96	96, 108, 120, 132, 144	1 – 1.5	5, 6	1/4, 3/8, 1/2, 5/8

6.6.3 Parametric Study with Out-of-Plane Bending Constrained

Before the actual parametric analysis was carried out, an analysis with bending in the angles constrained was performed. This analysis does not reflect the actual deformation of the structure, but it can be used to illustrate the difference between cases with eccentricity and cases without. This analysis was carried out in an attempt to identify the source of the reduction in cross frame stiffness compared to the analytical solutions derived for the truss model representation. The actual reduction in the members stiffness may come from sources such as bending in the members or in the shear lag effect since only one leg of the angle is connected. Since the computer models that were used in this section did have the shear lag effect included,

the results presented will demonstrate the impact of the shear lag on the cross frame stiffness. The out-of-plane bending restraint was modeled by restraining the out-of-plane displacement for all angle members. A comparison of the results calculated from the compression and tension model and results from the bending constrained FEA model is shown in Figure 6.18.

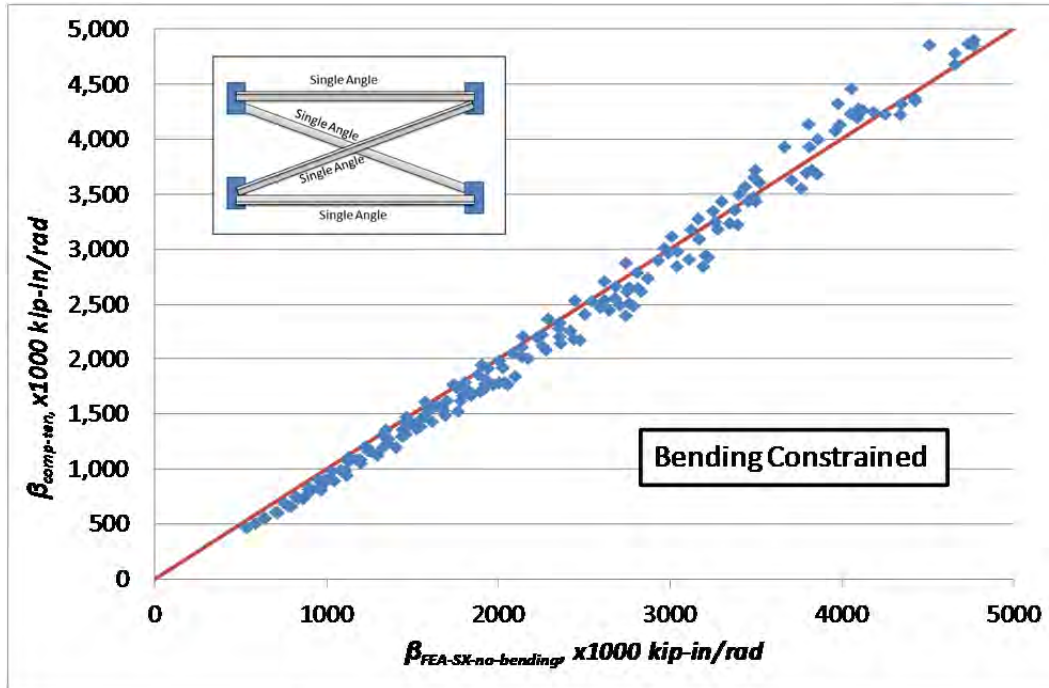


Figure 6.18: $\beta_{comp-ten}$ VS $\beta_{FEA-SX-no-bending}$

It can be seen from the comparison that most data cluster around the line with slope of 1, which indicates that the compression and tension model can effectively predict the stiffness of the cross frames that are simulated by the bending constrained FEA model. The results also demonstrate that the impact of the shear lag in the single angle members on the cross frame stiffness is relatively minimal.

6.6.4 Parametric Study with Out-of-Plane Bending Allowed

The results presented in this section are more indicative of the actual cross frame behavior since the angle members are free to displace in the out of plane direction, similar to the actual boundary conditions from the laboratory tests. After the parametric study on the actual model was performed, the stiffness resulted from the analytical equation using the compression and tension model ($\beta_{comp-ten}$) against the FEA results are plotted in Figure 6.19. The $\beta_{comp-ten}$ value assumes concentric members and does not reflect the impact of out of plane bending. The comparison confirms the previous observation that the compression and tension model significantly overestimates the cross frame stiffness. By comparing Figure 6.18 and Figure 6.19, it can be concluded that the major factor affecting the stiffness reduction is the out-of-plane bending. As shown in Figure 6.20, the overestimation caused by neglecting the out of plane bending can be as high as 95%. The error in this figure is defined as:

$$Error, \% = \frac{\beta_{comp-ten} - \beta_{FEA-SX}}{\beta_{FEA-SX}} \times 100\% \quad (6.49)$$

The focus in this section is not the magnitude of the errors and what parameters lead to the largest errors, but instead in the source of the errors. The results from the parametric studies are used later to develop an expression for the R-factor that can take into account the impact of the wide range of the parameters on the accuracy of the solution.

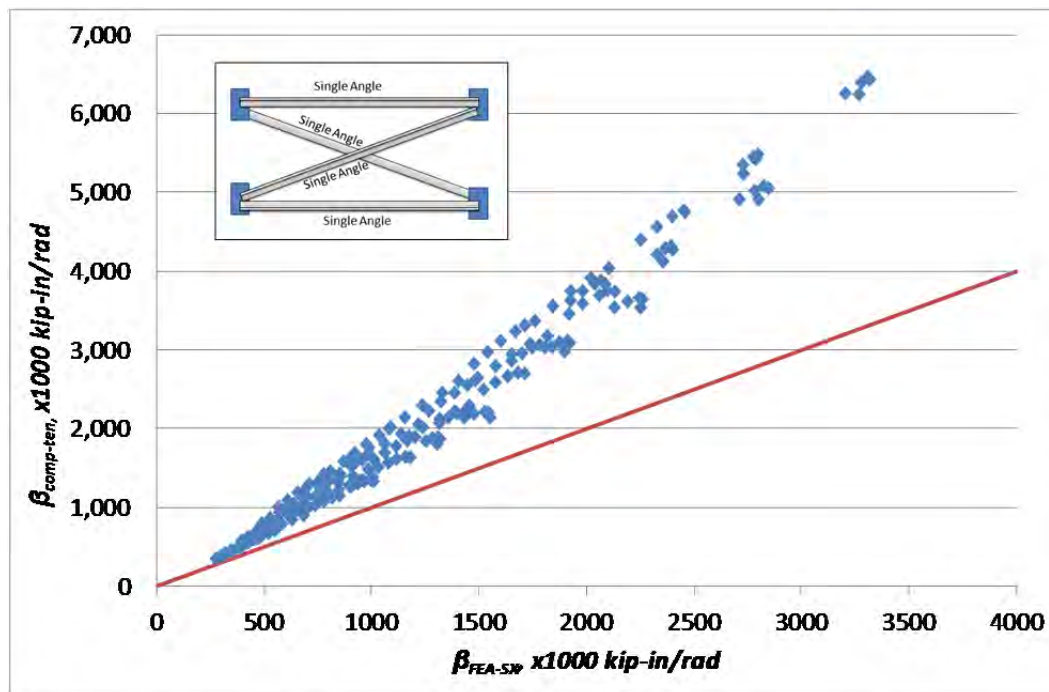


Figure 6.19: $\beta_{comp-ten}$ VS β_{FEA-SX}

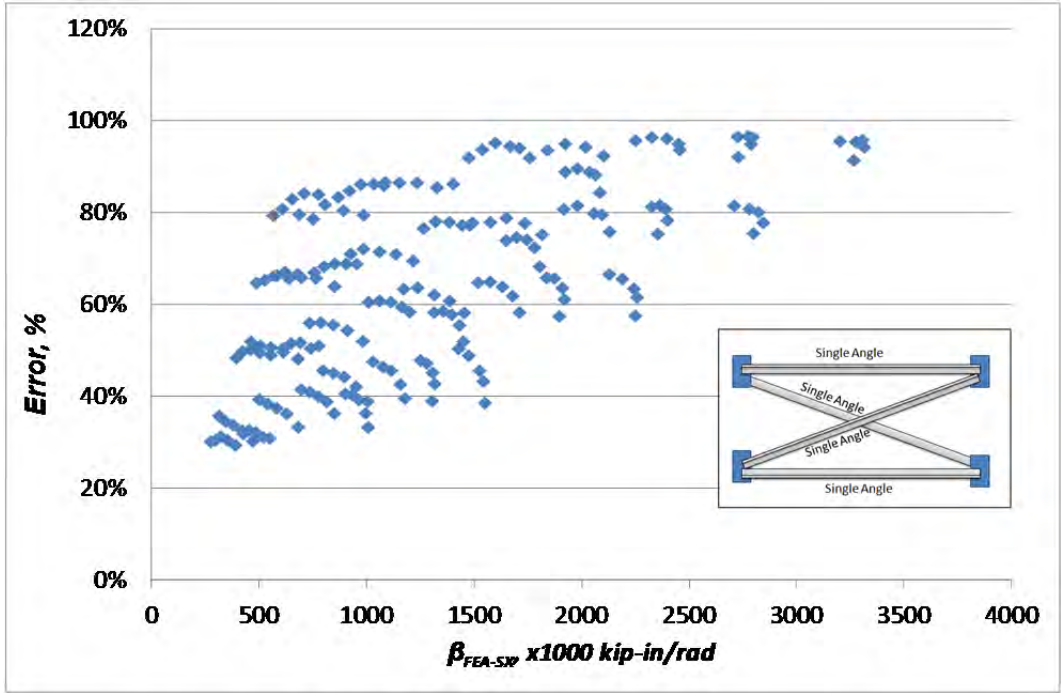


Figure 6.20: Errors of $\beta_{comp-ten}$

6.6.5 Stiffness Estimate Using Analytical Stiffness Reduction Factor

If the analytical stiffness reduction factor derived from Equation 6.26 and the corrected truss model in Equation 6.27 is used, the modified stiffness can be evaluated as:

$$\beta'_{ana-sx} = R_{ana-sx} \beta_{b-sx}' \quad (6.50)$$

The resulting stiffness values from the method are plotted against the FEA results in Figure 6.21. Errors caused by this method are in a range of -20% to 20% as shown in Figure 6.22 (negative values represent conservative estimates).

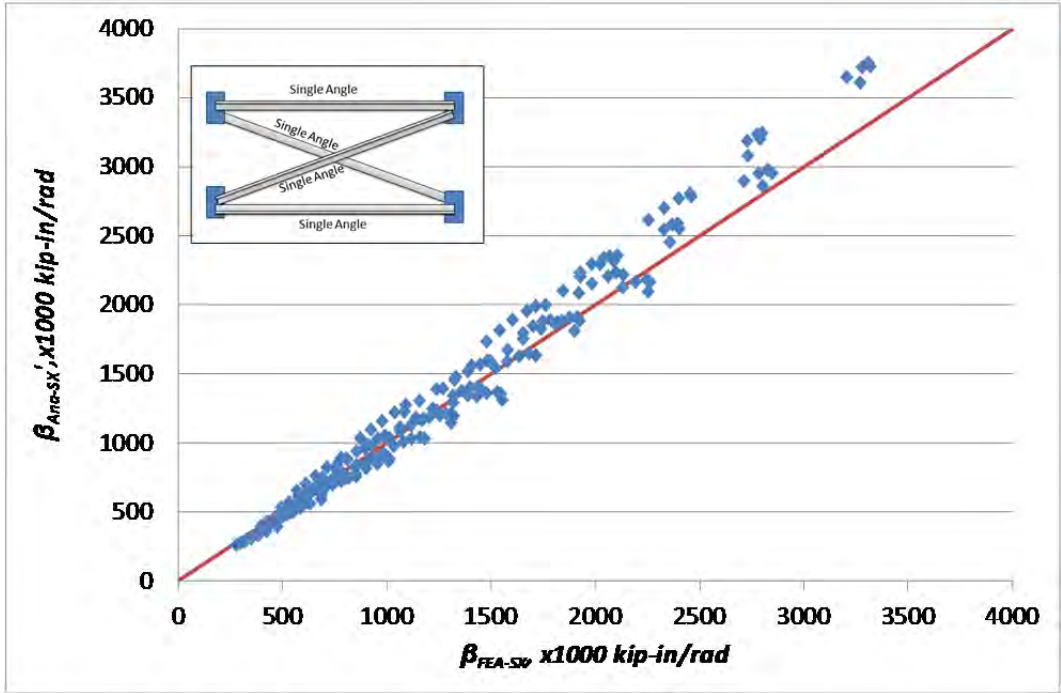


Figure 6.21: β_{ana-SX} VS β_{FEA-SX}

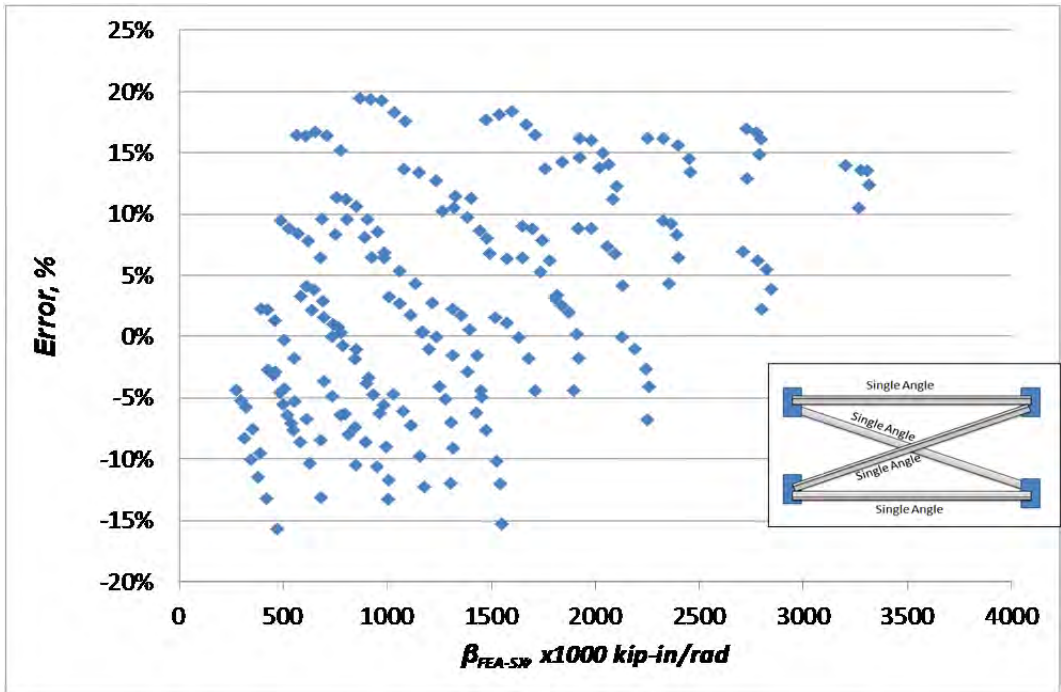


Figure 6.22: Errors of β_{ana-SX}

Based upon a review of the errors of this analytical method, it was apparent that the primary source of the errors in this method was related to the thickness of the angle (t). A plot of the errors against t is shown in Figure 6.22. The figure indicates that for angles with a thickness

of 3/8", the error is in the range of -5% to 8%. For angles with a thickness of 1/4", the range was between -13% and 0% and for an angle with thickness of 5/8", the error range was between 10% and 25%. The variation is likely a result of using a standard connection thickness (0.5"). The analytical method assumes a simplified truss model but the actual cross frame stiffness should include the connection stiffness. For thicker angle members, the connections with 0.5" plate introduce a large flexibility in the cross frame and results in a lower stiffness. Likewise, the connection can result in a higher stiffness for cross frames with thinner angles.

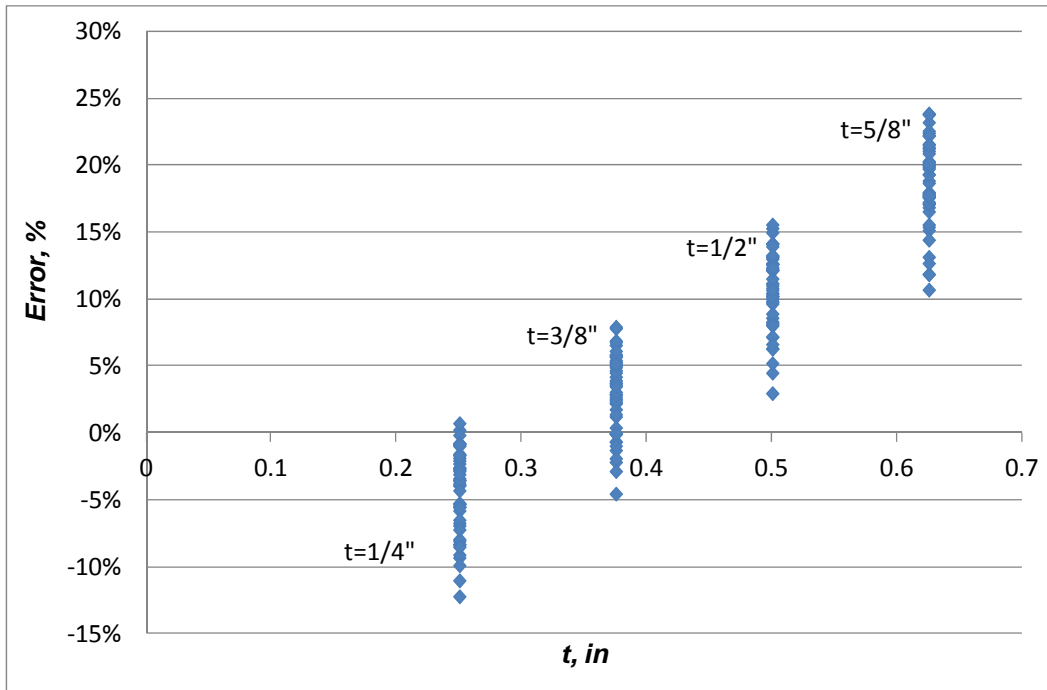


Figure 6.23: Errors of β_{ana-SX} VS. Thickness of Angle (t)

This error might be solved by including the stiffness of the connection in the calculation, however such an approach will lead to increased complexity in the calculations. An easier approach may be to simply find an additional reduction factor account for the unconservative nature of the error. Figure 6.24 shows the comparison between results from the FEA study and the estimated results with an extra reduction factor 0.85.

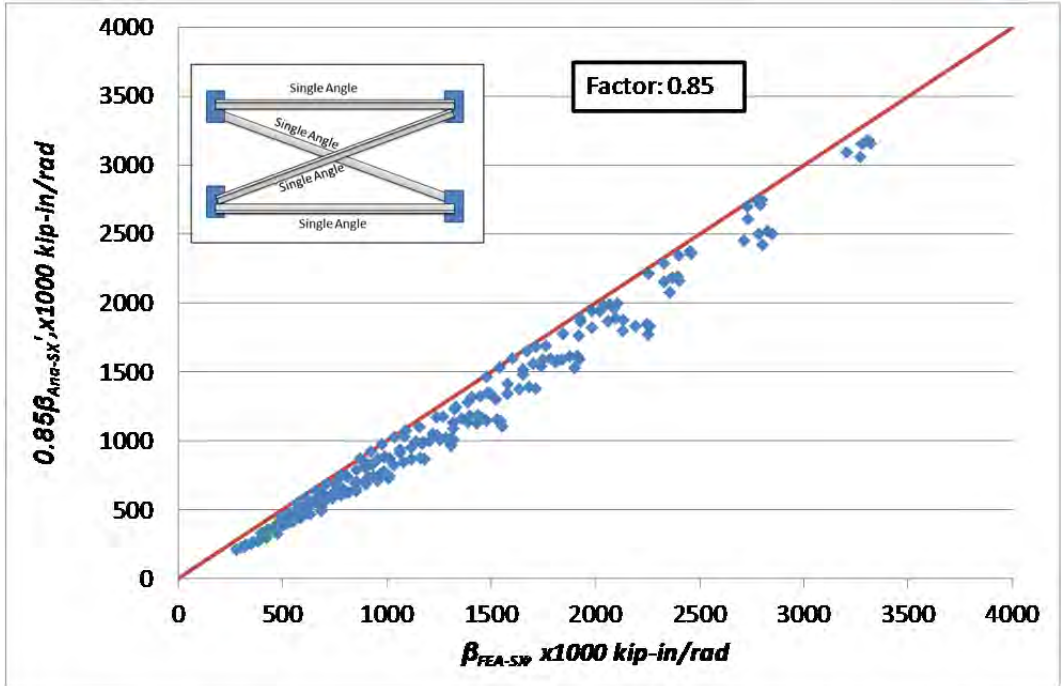


Figure 6.24: $0.85\beta_{ana-SX}$ VS β_{FEA-SX}

The results discussed up to this point have focused on a methodology to include the stiffness reduction due to the eccentricity in the main members of cross frame. However, such a method can be difficult due to the nature of the complex details of a cross frame. For practical reasons, it is therefore worthwhile to find a universal factor of safety to make up the stiffness reduction. According to the discussion in Section 6.3 to Section 6.5, the lower boundary of analytical stiffness reduction factor was 0.55, so a simple uniform stiffness reduction factor of 0.5 provides a simple and conservative solution. Figure 6.25 presents a comparison between the FEA results and the estimates by using the stiffness reduction factor of 0.5. It shows that the modification results in conservative and relatively reasonable estimates of the actual stiffness. The errors in Figure 6.26 showed a range between -35% and 0 (negative values represent conservative estimates).

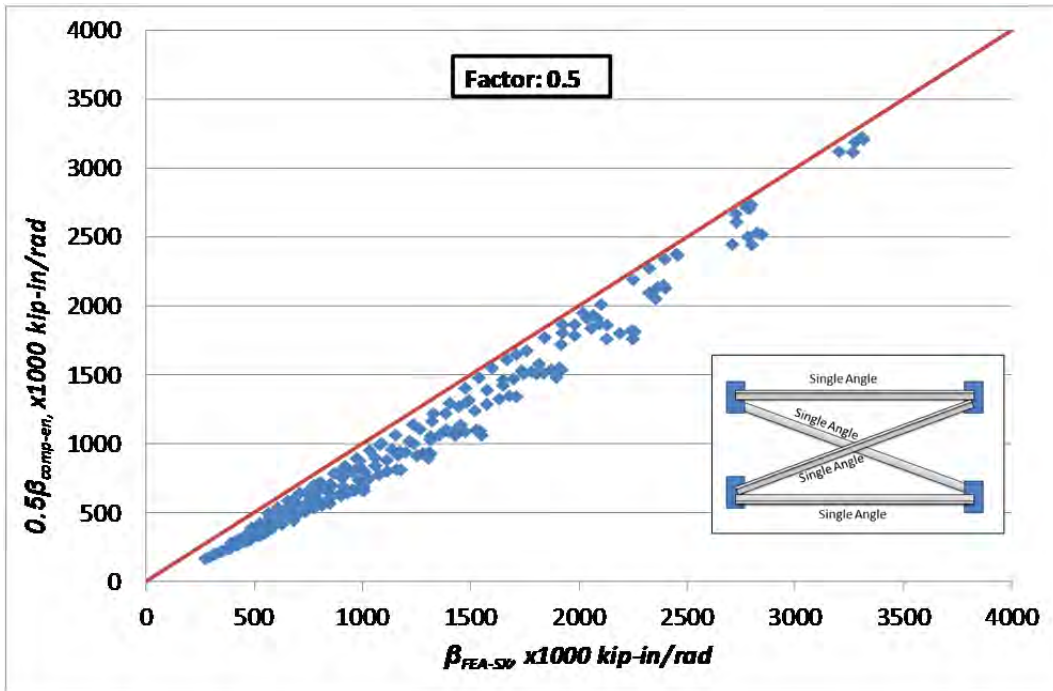


Figure 6.25: $0.5\beta_{comp-ten}$ VS β_{FEA-SX}

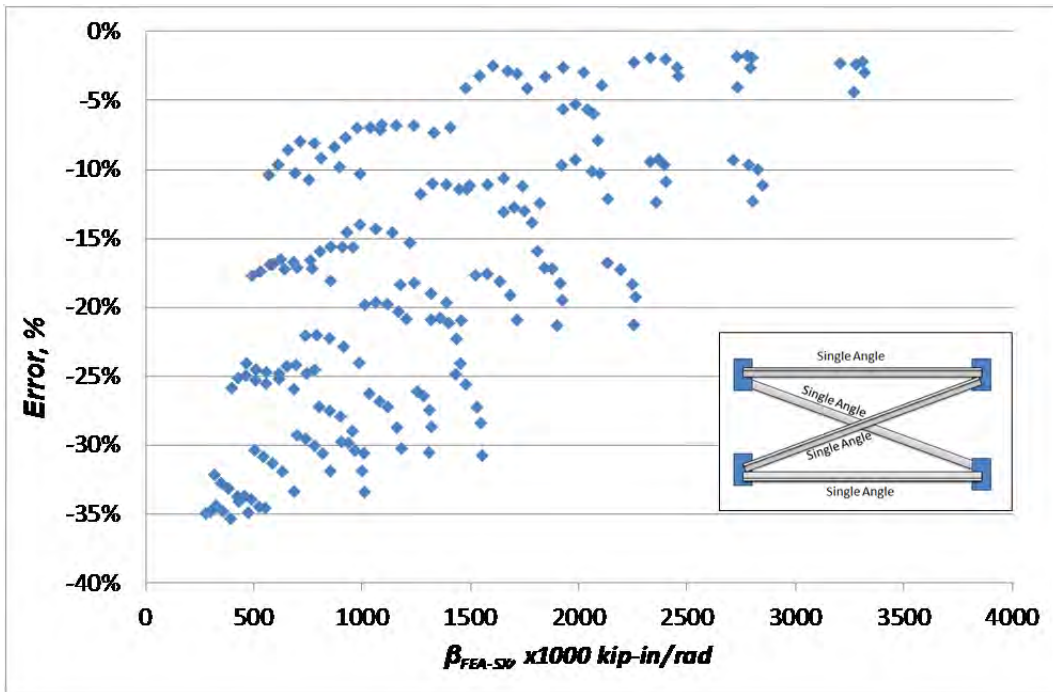


Figure 6.26: Errors of $0.5\beta_{comp-ten}$

The simplified approach provides a practical and quick method for reducing the stiffness of the cross frames as a result of member eccentricity. Such a method also lends itself well to

direct applications to analysis results. During the analysis, the stiffness reduction factor can be incorporated in the model by simply reducing the area of single angles by half.

6.6.6 Stiffness Comparison Using Tension-Only Diagonal Model

The tension-only diagonal assumption for estimating the stiffness of Single Angle X-Frames was traditionally considered conservative because it ignores the contribution of the compression diagonal. On the other hand, the tension-only diagonal model does not consider the stiffness reduction due to the eccentrically loaded single angle member. So the degree of conservatism of the tension-only diagonal assumption is unknown without comparisons of test and computational data. In this section, the FEA parametric results are compared with results from the tension-only diagonal model.

The comparison of results is plotted in Figure 6.27. It can be seen the tension only model always provides conservative estimates (below the 1:1 line) relative to the computational results. The errors of this model are in a range of -50% to -10% (negative values represent conservative estimates). The tension-only diagonal model provides a simple method of evaluating the stiffness of the cross frame system that is conservative relative to the FEA stiffness results.

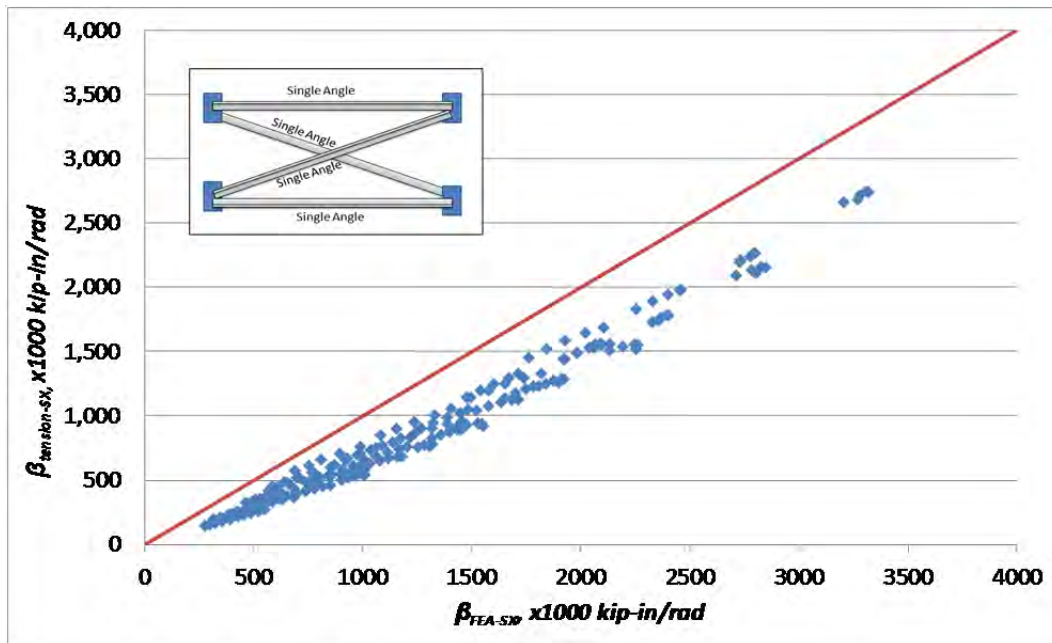


Figure 6.27: $\beta_{tension}$ VS β_{FEA-SX}

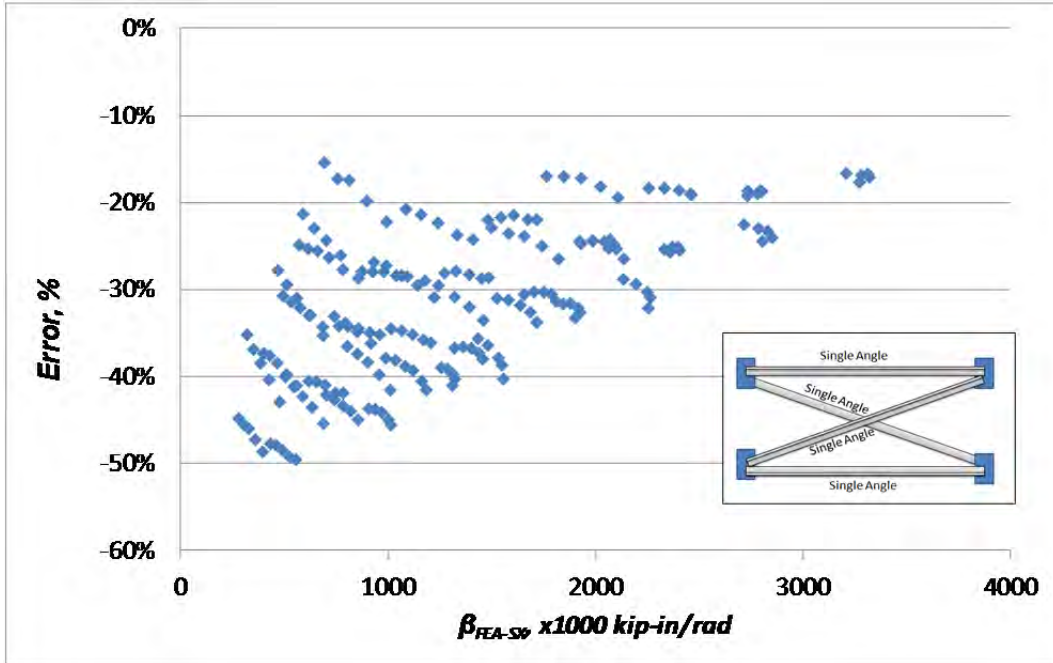


Figure 6.28: Errors of $\beta_{tension}$

6.6.7 Stiffness Reduction from Regression Method

A regression analysis can be used to develop a representative function in estimating stiffness reduction factors that considers the wide range of parameters that were considered. The values of stiffness reduction factors from FEA parametric model is defined as:

$$R_{FEA-SX} = \frac{\beta_{FEA-SX}}{\beta_{comp-ten}} \quad (6.51)$$

Where:

β_{FEA-SX} = Stiffness calculated from FEA model

$\beta_{comp-ten}$ = Stiffness by using compression and tension model in Figure 2.5

The first step in the development of a reduction factor consisted of an investigation of the major geometric factors. A plot between R_{FEA-SX} and \bar{y} was created to study how the angle size affects the stiffness reduction factor. The plot is shown in Figure 6.29 and the data points represent the results from the FEA parametric study. It appears that the trend is similar to the analytical solution shown previously in Figure 6.8. The R_{FEA-SX} is correlated to \bar{y} , b and t . It should be noted that the parameters b , t and \bar{y} are interdependent and any one can be determined from the other two. The data points were separated by groups of b and t . As the sections become larger, the stiffness reduction factor becomes smaller. Within one group, the variation of the data is caused by the overall geometry of the cross frame. The range of the stiffness reduction is between 0.4 and 0.8.

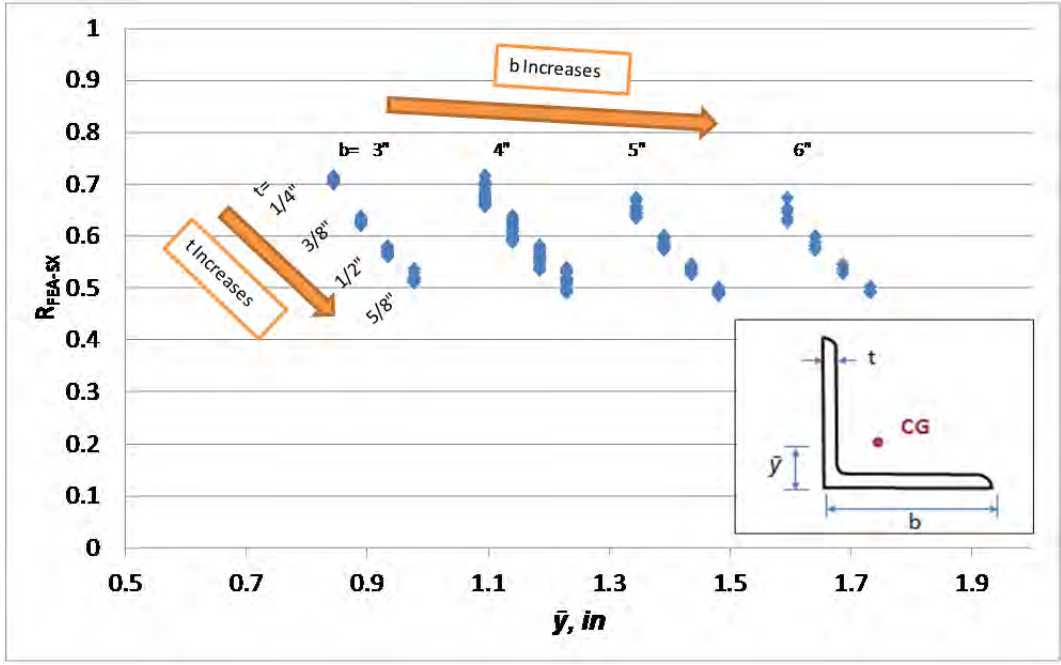


Figure 6.29: R_{FEA-SX} VS \bar{y}

The relationship between the R_{FEA-SX} and the aspect ratio (S/h_b) of the cross frame was investigated and is shown in Figure 6.30. It can be observed that the factor R_{FEA-SX} decreases with the increase of S/h_b ratio. This relationship can be potentially explained by recalling the discussion on angle discrepancy. In that discussion, it was shown that the congestion at the gusset plate could cause the actual angle between the diagonal and struts lower than that presumed by a truss model. This angle discrepancy could cause the actual stiffness values to be lower than the predicted values. In addition, when the aspect ratio (S/h_b) is greater, the congestion at the gusset plate could get more serious, in turn can cause an even larger error.

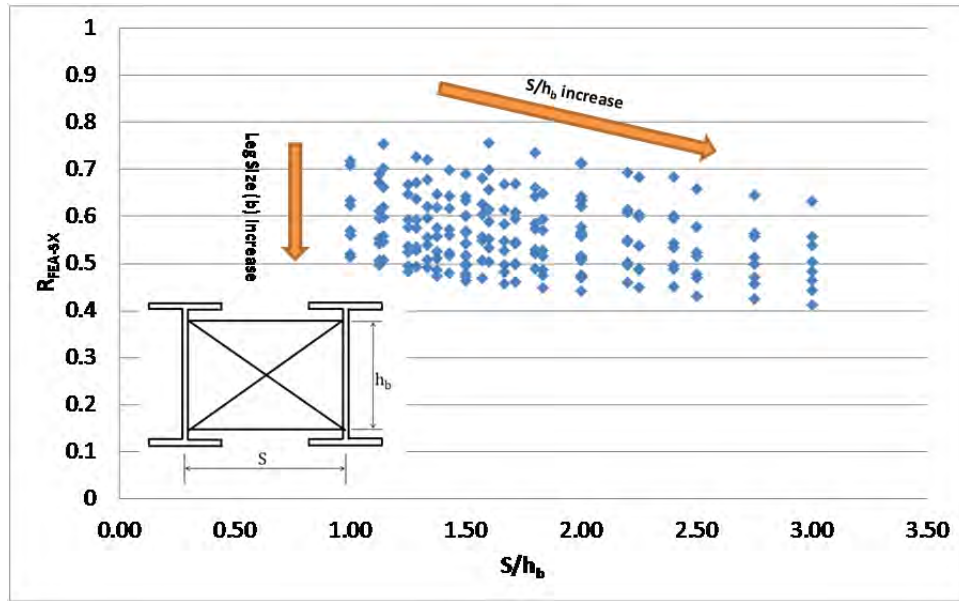


Figure 6.30: R_{FEA-SX} VS S/h_b

This deduction can be proved by using Equation 6.27 to correct the stiffness from analytical model. The following equation can derive the corrected stiffness reduction factor:

$$R_{FEA-SX}' = \frac{\beta_{FEA-SX}}{\beta_{b-SX}'} \quad (6.52)$$

Where:

β_{FEA-SX} = Stiffness calculated from FEA model

β_{b-SX}' = Stiffness corrected for angle discrepancy, defined in Equation (6.27)

The plot of the corrected stiffness reduction factors are presented in Figure 6.31. This figure shows that after the geometrical difference is fixed, the aspect ratio has a very limited impact on the cross frames stiffness.

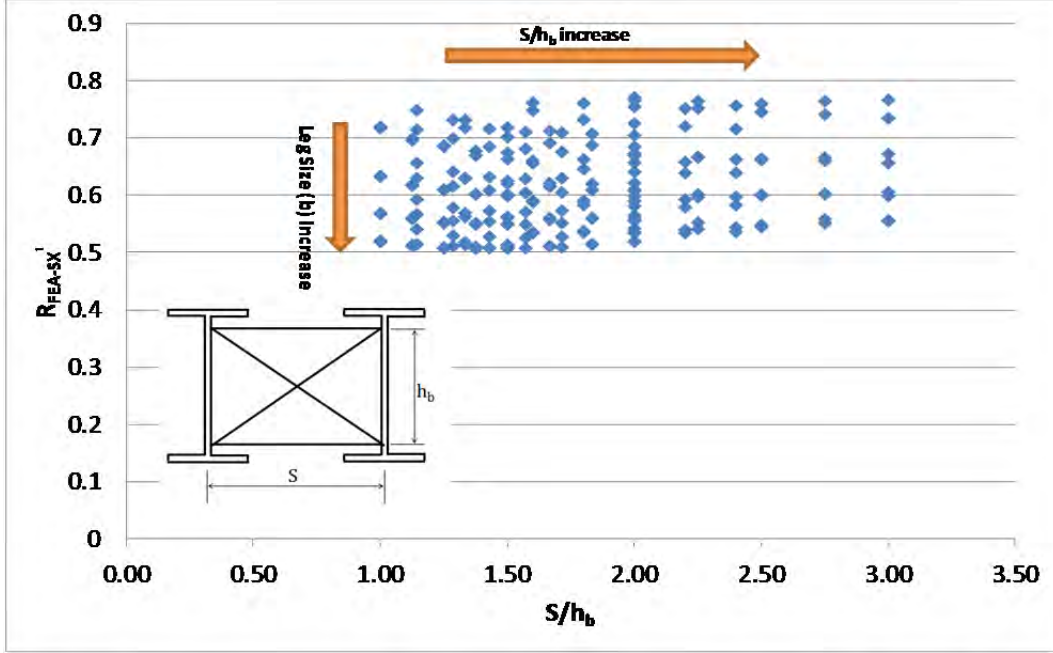


Figure 6.31: R_{FEA-SX}' VS S/h_b

The investigations on the parameters demonstrated that b , t and S/h_b are the primary factors that have impact the values of the stiffness reduction factor, R_{FEA-SX} . Therefore, a more accurate estimation of the stiffness reduction factor can be generated from a regression analysis based on these parameters. The linear regression analysis uses the "least squares" method to fit a line through a set of data. The single dependent variable is referred to as R_{FEA-SX} , with three independent variables: b , t and S/h_b . This regression analysis resulted in a coefficient of determination (R^2) of 0.95, and a standard error σ of 0.0178, which indicates good agreement. The resulting coefficients can be used to form the equation in estimating the dependent variable. This equation is shown in Equation (6.53) .

$$R_{reg-SX} = 1.063 - 0.087 \frac{S}{h_b} - 0.040b - 0.461t \quad (6.53)$$

Using Equations (6.53), the estimated stiffness can be evaluated as:

$$\beta_{reg-SX} = (1.063 - 0.087 \frac{S}{h_b} - 0.040b - 0.461t) \beta_{comp-ten} \quad (6.54)$$

Additionally, since the parameters b , t and \bar{y} are interdependent, \bar{y} instead of b can be included in the regression analysis:

$$R_{est-SX} = 1.063 - 0.087 \frac{S}{h_b} - 0.159\bar{y} - 0.403t \quad (6.55)$$

Figure 6.32 shows the comparison between the resulting stiffness from Equation (6.54) and the results from the FEA parametrical study. The values graphed on the horizontal axis are the FEA results while the values graphed on the vertical axis are the predicted stiffness using Equation 6.1. A reference line with 1:1 slope is also provided in the figure. It can be observed that the estimated values are in very good agreement with the FEA results. The errors between

the estimated results are shown in Figure 6.33. The figure shows that errors are in a range of -10% to 6% (negative values represent conservative estimates).

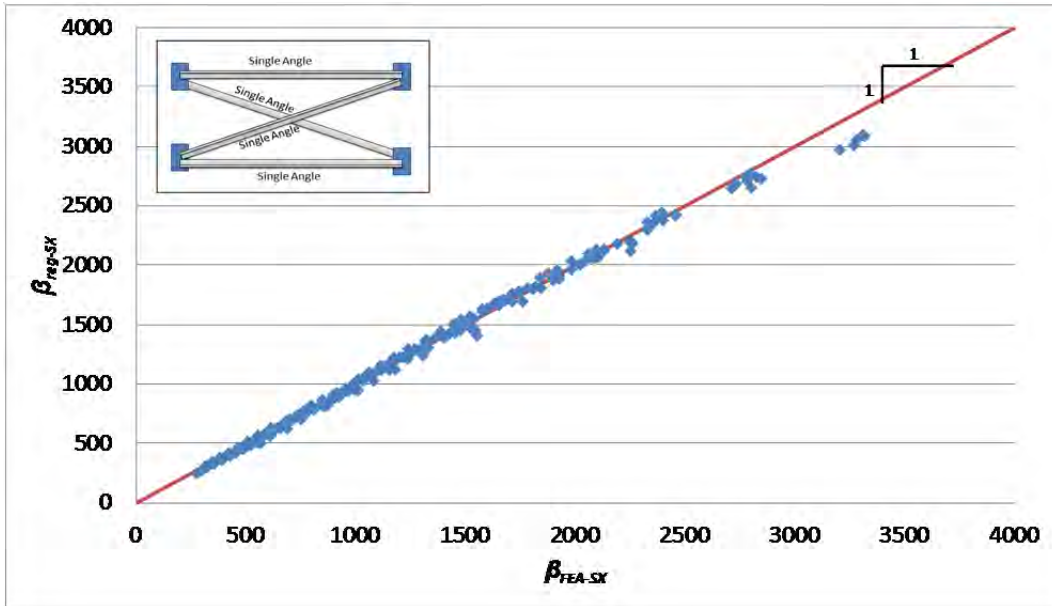


Figure 6.32: β_{reg-SX} VS β_{FEA-SX}

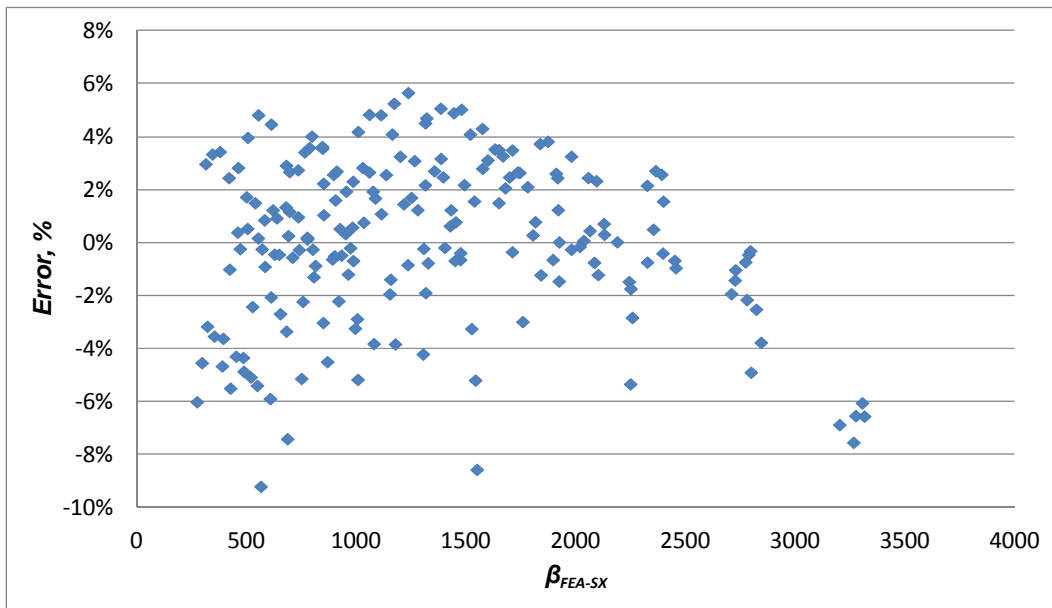


Figure 6.33: Errors of β_{reg-SX}

6.6.8 Parametric Study with Nonlinear Buckling Analysis

The discussion up to this point has focused on the elastic stiffness of cross frames. However, as the load increases, the compression diagonal of a cross frame will go into a plastic range of stress with large deformation. As a result, the stiffness of the cross frame will decrease.

In this section, the finite element parametric study is used to generalize a rule of how the stiffness is affected by the load.

The first step of the generalization is to identify the turning point of the elastic range. The nonlinear buckling analysis outlined in Chapter 4 can be used to generate the buckling curve of the cross frames. One example is shown in Figure 6.34. Visual observation on this curve discovered the starting point of nonlinear range to be around F equals to 60 kips. At this point, the tangential stiffness of the cross frame is 2,143 kip-in/rad, which is 10% reduction from the initial stiffness. Even though the tangential stiffness at this point is subject to 10% reduction, the overall stiffness from $F=0$ to $F=60$ kips is 2,334 kip-in/rad, which is only 1.9% lower than the initial stiffness. Therefore, this range can be still considered as an elastic range. It also can be read from the curve that when force is greater than 60 kips, the stiffness of the cross frame drops dramatically. Since 60 kips is 65% of the ultimate strength 82 kips, it can be concluded that for this cross frame example, when the force is lower than 65% of ultimate strength, the cross frame is still in elastic range.

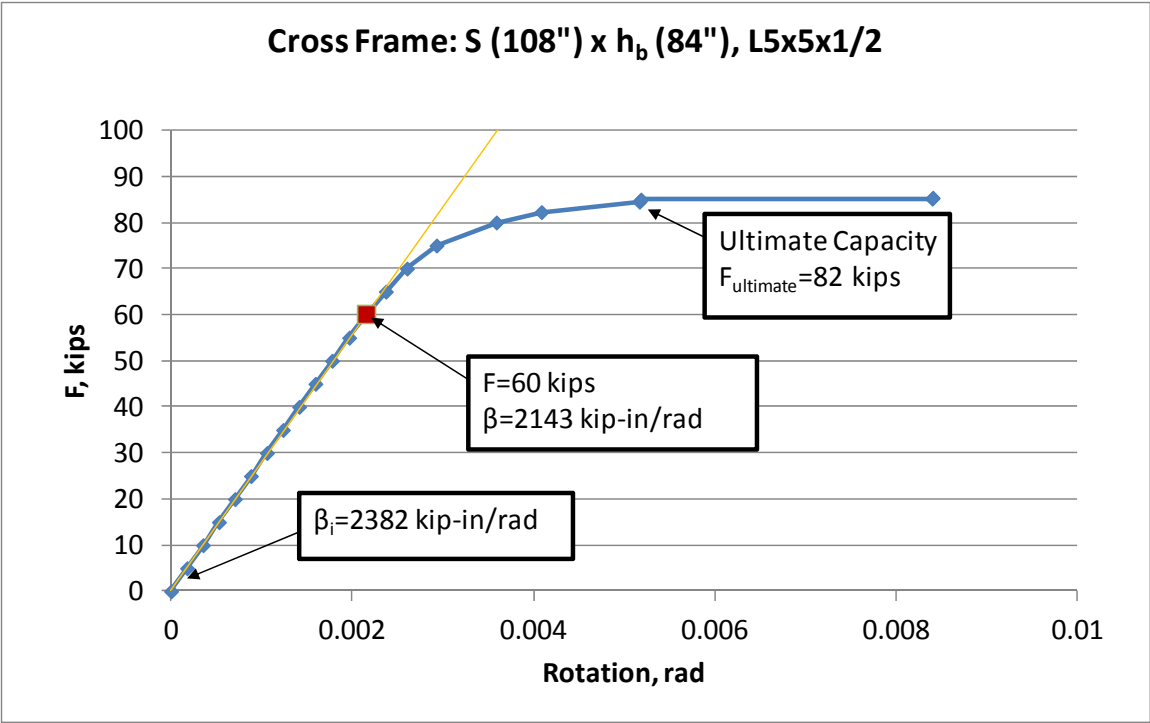


Figure 6.34: Example of Load-Deflection Curve

Since the main characteristic points of a curve have been identified, a parametric study can be performed to generalize the curve. The parametric study performed considered geometric parameters listed in Table 6.4.

Table 6.4. Summary of Variables in the Parametric Study

h_b, in	S, in	Range of S/ h_b	Angle Size
48	96, 108, 120, 132, 144	2 – 3	L3x3x1/4, L4x4x3/8
60	96, 108, 120, 132, 144	1.6 – 2.4	L3x3x1/4, L4x4x3/8
72	96, 108, 120, 132, 144	1.3 – 2	L4x4x3/8, L5x5x1/2
84	96, 108, 120, 132, 144	1.4 – 1.7	L4x4x3/8, L5x5x1/2
96	96, 108, 120, 132, 144	1 – 1.5	L5x5x1/2, L6x6x5/8

As same as the illustrated example problem, 10% of reduction in the tangential stiffness is selected as the starting point of the nonlinearity. A P-value defined by using Equation 6.56 is used to normalize the force:

$$P = \frac{F_{10}}{F_{ult}} \quad (6.56)$$

Where:

F_{10} = the applied force F of the load step when the tangential stiffness is reduced by 10%

F_{ult} = the applied force F when cross frame reaches its ultimate strength

A statistical analysis on the values of P for all of the cases considered in the parametric studies is presented in Figure 6.35. The analysis showed that the value of P ranges from 0.60 to 0.85. Results of this study suggested that as long as the load on the cross frame is limited within 60% of its ultimate strength, the reduction in stiffness caused by softening of the compression diagonal can be ignored and the initial stiffness of the cross frame (elastic stiffness) provides a reasonable estimate of the cross frame stiffness. Such an approach would allow the use of the compression/tension model for the cross frame instead of the tension-only diagonal system.

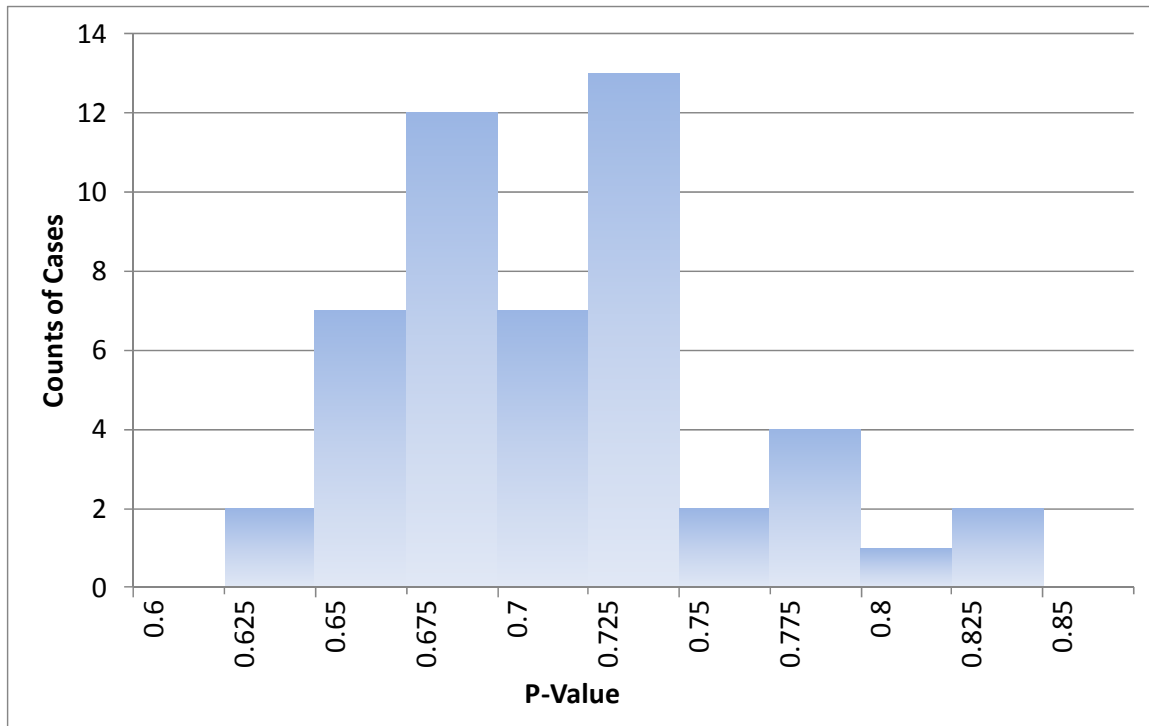


Figure 6.35: Statistics on P

6.6.9 Parametric Study for Cross Frame with Unequal Legs Angles

Surveys on current design practices and standard drawings of state transportation departments suggested that the cross frame systems predominantly utilize equal legs angles. However, compared with equal leg angles, unequal legs angles have the merit of smaller eccentricities if the shorter leg is the outstanding leg. The smaller eccentricity will result in higher cross frame stiffness according to results of the analytical derivation as well as the regression study. In this section, the stiffness of cross frames comprised of unequal leg angles is investigated.

A parametric study was performed by changing the angle leg lengths and thickness. The cross frame size was fixed at a girder spacing of 12 ft. ($S=144$ in) and a cross frame depth of 8 ft ($h_b=96$ in.). The cross section parameters of angle member are shown in Table 6.5. The angle orientation was varied by keeping the leg with the b_1 length in the plane of the connection plates and varying the length of the outstanding leg, b_2 . The angle leg lengths ranged from 3 to 6 inches in 1 inch increments. Four different thickness values were considered for the angles.

Table 6.5 Summary of Cross Section Parameters of Unequal Legs Angle Members

b_1 , in	b_2 , in	t , in
3	3, 4, 5,6	1/4, 3/8, 1/2, 5/8
4	3, 4, 5,6	1/4, 3/8, 1/2, 5/8
5	3, 4, 5,6	1/4, 3/8, 1/2, 5/8
6	3, 4, 5,6	1/4, 3/8, 1/2, 5/8

Note:

1. b_1 is the length of the angle leg in the plane of connection plates.
2. b_2 is the length of the outstanding angle leg.
3. t is the thickness of the angle legs.

The results from the parametric study are summarized in Figure 6.36. The calculated stiffness reduction factors are plotted against the eccentricity for all cross frame sections that were considered. It can be observed that the stiffness reduction factor is affected by \bar{y} and the thickness of the angles t . The trend is similar to that shown in previously for equal leg angles in Figure 6.29.

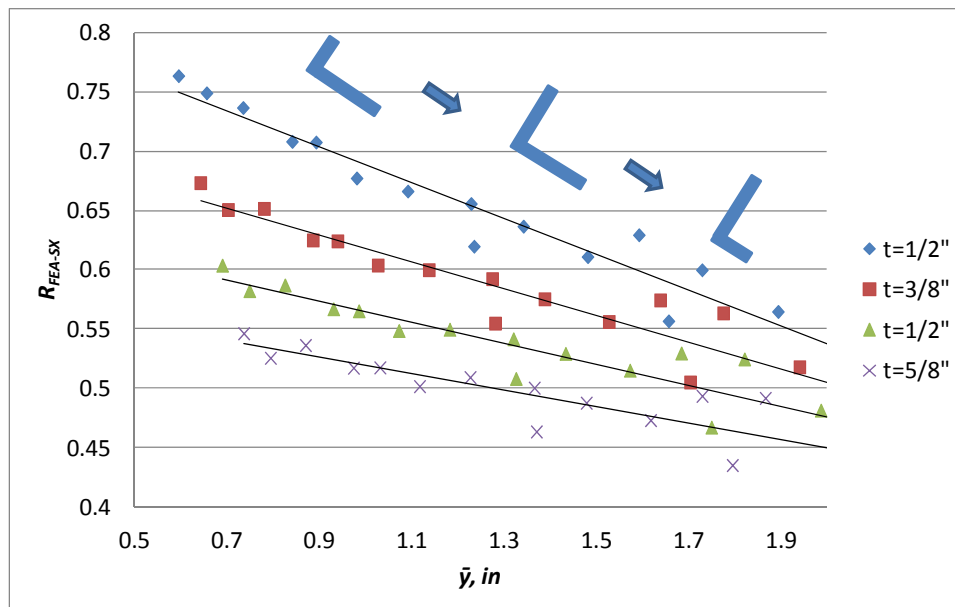


Figure 6.36: R_{FEA-SX} VS \bar{y} for Cross Frame with Unequal Legs Angles

Recall in the parametric study performed on equal leg angle cross frames, Equations (6.53) and (6.55) were generated to predict the stiffness reduction factor. Equation (6.53) shows the stiffness reduction is dependent on variables of t , b and S/h_b , while Equation (6.55) shows the stiffness reduction is dependent on variables \bar{y} , t , and S/h_b . Since Figure 6.36 shows that for unequal leg angle cross frame, \bar{y} and t are also major variables, it is reasonable to expect that

Equation (6.55) could be also used for unequal leg angle cross frames. To examine this supposition, the stiffness resulted from Equation (6.55) is plotted against the FEA results in Figure 6.37. The error of using this method is presented in Figure 6.38. These figures show that, although there is more scatter in the data compared to the equal leg angle case, in general Equation (6.55) can provide a reasonable estimate of the stiffness of cross frames comprised of unequal leg angles.

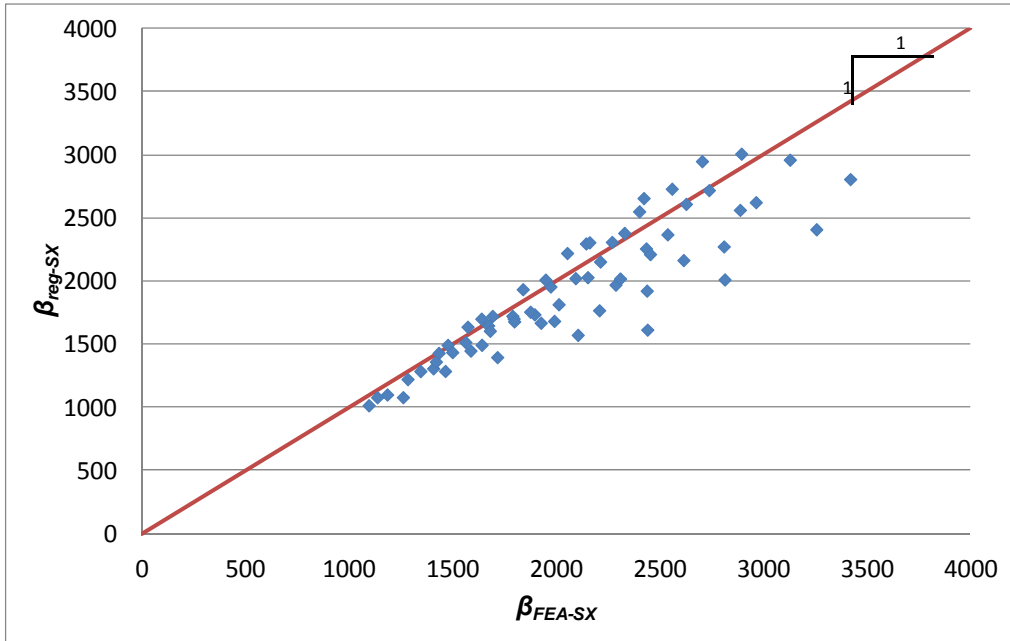


Figure 6.37: β_{reg-SX} VS β_{FEA-SX} for Cross Frame with Unequal Legs Angles

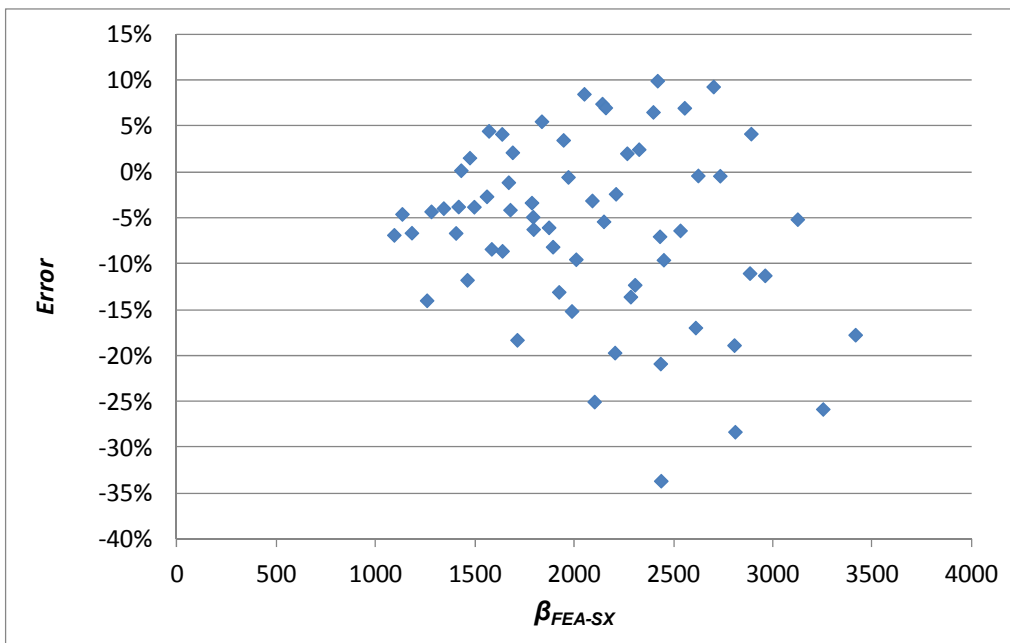


Figure 6.38: $R_{est-SX-adj}$ VS R_{FEA-SX} for Cross Frame with Unequal Legs Angles

6.6.10 Summary of Parametric Studies for Single Angle X-Frame

In this section, parametric studies were performed with the validated FEA Single Angle X-Frame model. The study results were used to compare with several methods in estimating cross frame stiffness. A conclusion of the analysis and comparisons are summarized below:

- The compression and tension model results in unconservative estimates of the cross frame stiffness since it does not include the reduction in stiffness caused by connection eccentricity. The error can be corrected by applying a stiffness reduction factor, R .
- The cross frame stiffness expression based upon the tension-only diagonal system constitutes a viable hand-calculation method in evaluating the stiffness of the Single Angle X-Frame. By ignoring the compression diagonal, this method provides conservative estimates of the stiffness of the cross frame. The conservatism ranged from 10% to 50%.
- An alternative method to the use of the tension-only diagonal system is to utilize the stiffness expression that considers both diagonals and to apply a stiffness reduction factor that reflects the impact of the eccentric connections on the resulting cross frame stiffness. Two methods were used to obtain the stiffness reduction factor. One method was to derive the stiffness reduction factor based upon the analytical method presented. This method resulted in an approximation that tended to be unconservative with increasing angle thickness. Because this method requires a relatively detailed calculation, a simplified method was also investigated which consisted of a simple reduction factor of 0.5. The reduction factor of 0.5 applied to the analytical compression and tension model for the cross frame stiffness was conservative compared to all of the FEA results, but still had reasonable agreement with the computer solutions. The value of 0.5 of the stiffness reduction factor is consistent with the lower boundary (0.55).
- A more accurate estimate of the stiffness reduction factor was also developed based upon a regression analysis of the data from the parametric study results. The resulting expression considers the impact of cross frame angle and geometrical parameters and had good correlation with the FEA results. The stiffness reduction factor is applied to the stiffness of the tension/compression diagonal system stiffness.
- A cross frame stiffness expression that relies on a compression member will also experience a reduction in stiffness as the compression diagonal approaches the buckling capacity. A nonlinear geometrical analysis was carried out considering a wide variety of parameters. The results showed that the reduction in cross frame stiffness was minimal provided the forces in the compression members are kept below 60% of the buckling strength of the corresponding member of the cross frame. For this reason, it is concluded that if design load is less than 60% of the strength of the cross frame, no deduction on cross frame stiffness is necessary.
- A brief parametric study was also provided for cross frames with unequal leg angles. The results of analysis showed that the regression equation (6.55) derived from equal leg angles also provide reasonable estimates of the stiffness of cross frames with unequal leg angles.

6.7 FEA Parametric Studies for Stiffness of Single Angle K-Frame

6.7.1 Introduction

A discussion of the results from a parametric FEA study that was conducted on Single Angle K-Frames is provided in this section. Similar to the studies outlined for Single Angle X-Frame in the previous section the studies begin by focusing on the results from a parametric study using a linear-elastic analysis. The impact of nonlinear geometry associated with the potential buckling of compression members in the cross frame is then considered. Finally, the stiffness of K-frames with unequal leg angles is also investigated.

6.7.2 Parametric Study with Linear Analysis

The basic geometry of the K-frame systems that were modeled in the studies followed typical details employed by TxDOT. The geometries and the force paths in K-frames differ substantially from the single angle X-frames outlined earlier. For the same girder spacing and cross frame depth, K-Frames have much shorter diagonal lengths compared to the X-Frame systems. The shorter compression member length makes the K-Frame more suitable for applications with longer cross frames (longer girder spacing). Such an application with longer cross frames is for end frames of skewed bridge. Because the end cross frame is typically parallel to the skew angle, the resulting cross frame length can become relatively large. Therefore, in this parametric study, higher values of aspect ratio are employed (from 1.3 to 3.75). Table 6.6 summarizes the range of parameters considered in the study.

Table 6.6 Summary of Variables in the Parametric Study

h_b , in	S, in	Range of S/ h_b	b, in	t, in
48	96, 108, 120, 132, 144, 156, 168, 180	2 – 3.75	3, 4	1/4, 3/8, 1/2, 5/8
60	96, 108, 120, 132, 144, 156, 168, 180	1.6 – 3	3, 4	1/4, 3/8, 1/2, 5/8
72	96, 108, 120, 132, 144, 156, 168, 180	1.3 – 2.5	4, 5	1/4, 3/8, 1/2, 5/8
84	108, 120, 132, 144, 156, 168, 180	1.3– 2.1	4, 5	1/4, 3/8, 1/2, 5/8
96	120, 132, 144, 156, 168, 180	1.3 – 1.5	5, 6	1/4, 3/8, 1/2, 5/8

6.7.3 Parametric Study with Out-of-Plane Bending Constrained

Similar to the analysis on Single Angle X-Frames, an analysis with out-of-plane bending constrained is also performed to study the stiffness without considering the bending in single angle members. A plot between results calculated from the K-frame analytical solution and the results from the bending constrained FEA model is shown in Figure 6.39. The analytical stiffness solution is graphed on the vertical axis while the FEA stiffness solution with out-of-plane translation prevented is graphed on the horizontal axis. The red line that is graphed corresponds to a 1:1 slope which would indicate perfect correlation between the two solutions. Results that

graph below the red line indicate that the analytical solution is conservative relative to the FEA solution.

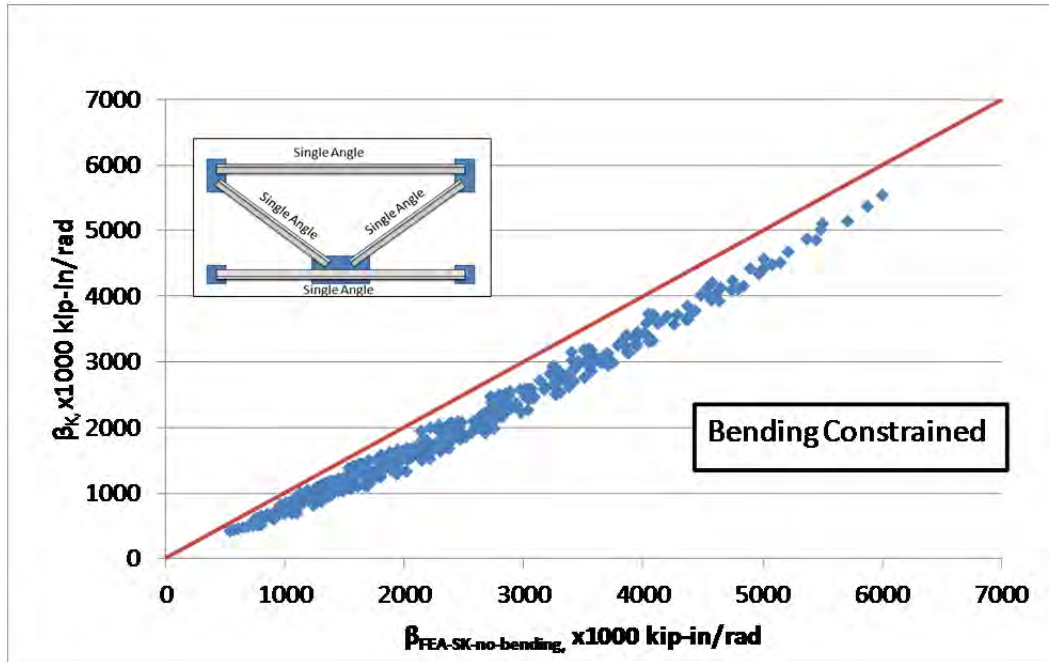


Figure 6.39: β_K VS $\beta_{FEA-SK-no-bending}$

The comparison shows that the analytical stiffness solution for the K-frame model is conservative compared to the FEA model with out-of-plane translations constrained. The conservatism of the truss analogy of K-Frame might be caused by the simplification of a pin connection at the middle of the bottom strut. The actual cross frame is made of a continuous bottom strut and the connection plate for the diagonals at the middle of the bottom strut may also provide some stiffening. The moment restraint and stiffening effect of the connection plate may provide some increase in the stiffness of the K-frame FEA model compared to the analytical solution that was developed based upon a truss model representation of the K-frame. Similar to the X-frame comparison, the effects of shear lag from the eccentric connection appear to have a negligible effect on the stiffness of the cross frame.

6.7.4 Parametric Study with Out-of-Plane Bending Allowed

The previous section showed that the shear lag effects of the eccentric connections had no measurable effect on the stiffness of the cross frame and the analytical solution was actually conservative relative to the FEA solution. The second set of analyses that were conducted consisted of parametric studies with out-of-plane bending allowed. The stiffness estimates by from the analytical K-Frame expression (β_k) is graphed versus the FEA results in Figure 6.40.

Similar to the results observed for the X-frame configuration, the K-Frame truss model greatly overestimates the stiffness of the cross frame. As shown in Figure 6.41, the error ranges from 24% to 97%. As discussed in previous chapters, the source of the error is likely the impact of bending deformations due to eccentric connections in the primary members of the cross frame. The following two subsections focus on developing modifications that can be applied to the

analytical stiffness expression. The modifications consist of a reduction coefficient developed based upon the bending deformations discussed at the beginning of this chapter as well as a reduction coefficient that is based upon a regression analysis from the results of the parametric study.

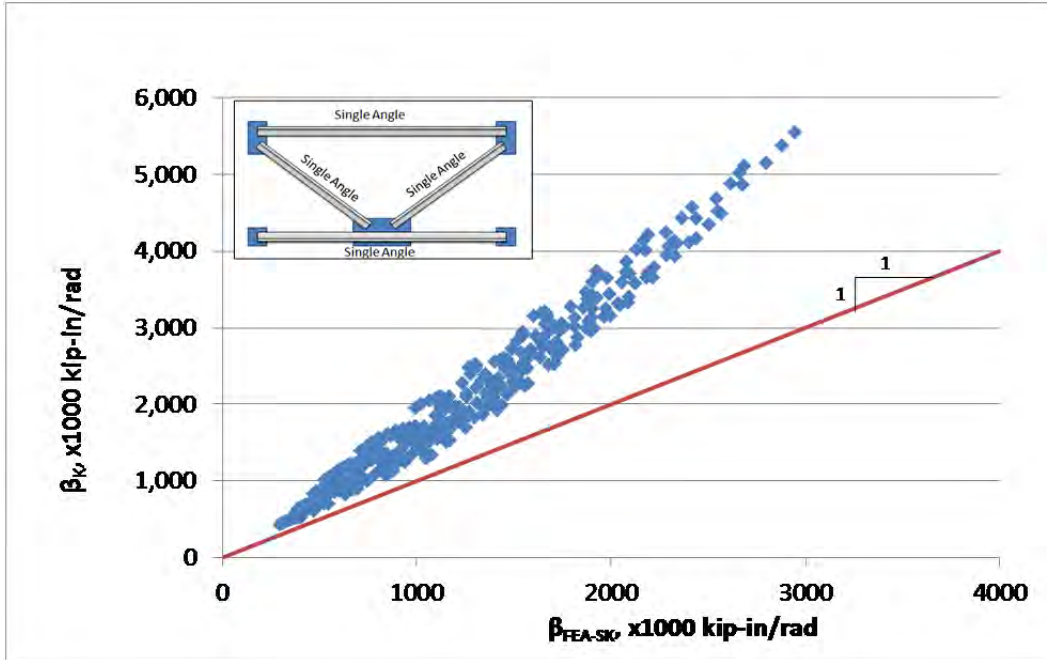


Figure 6.40: β_K VS β_{FEA-SK}

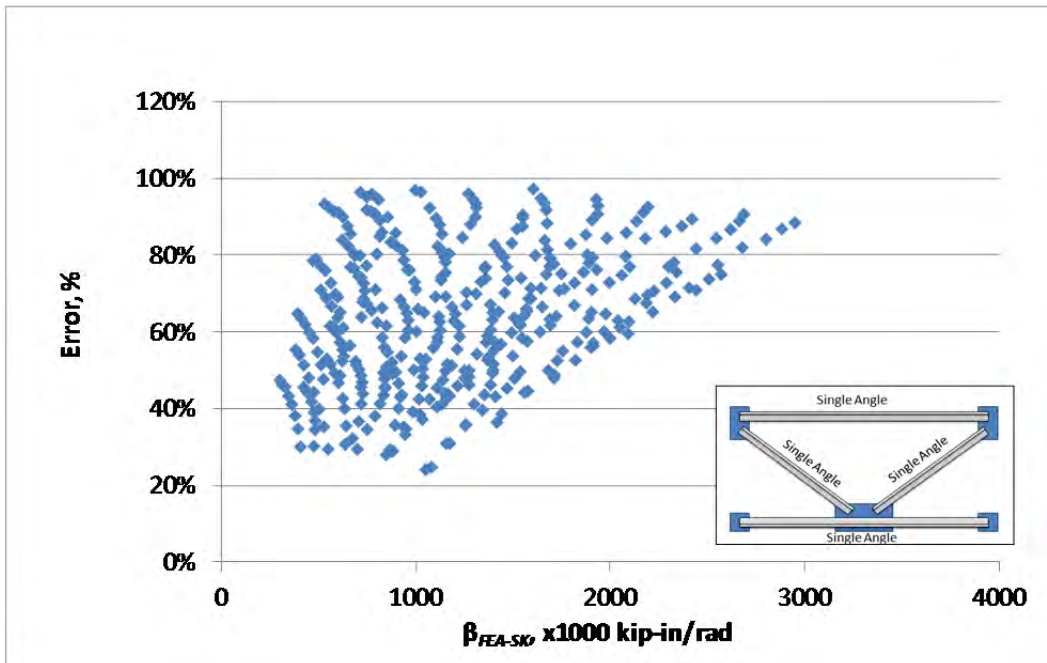


Figure 6.41: Errors of β_K

6.7.5 Estimate Stiffness by Using Analytical Stiffness Reduction Factor

Methods of accounting for the flexural deformations in the members due to moments caused from the eccentric connections were discussed earlier in this chapter. Equation 6.28 can be used to derive the cross frame stiffness with consideration of the analytical stiffness reduction factor. The resulting stiffness values for the wide range of cross frame parameters from this method are plotted against the FEA results in Figure 6.42. Errors caused by this method are in a range of -20% to 20% as shown in Figure 6.43 (negative values represent conservative estimates).

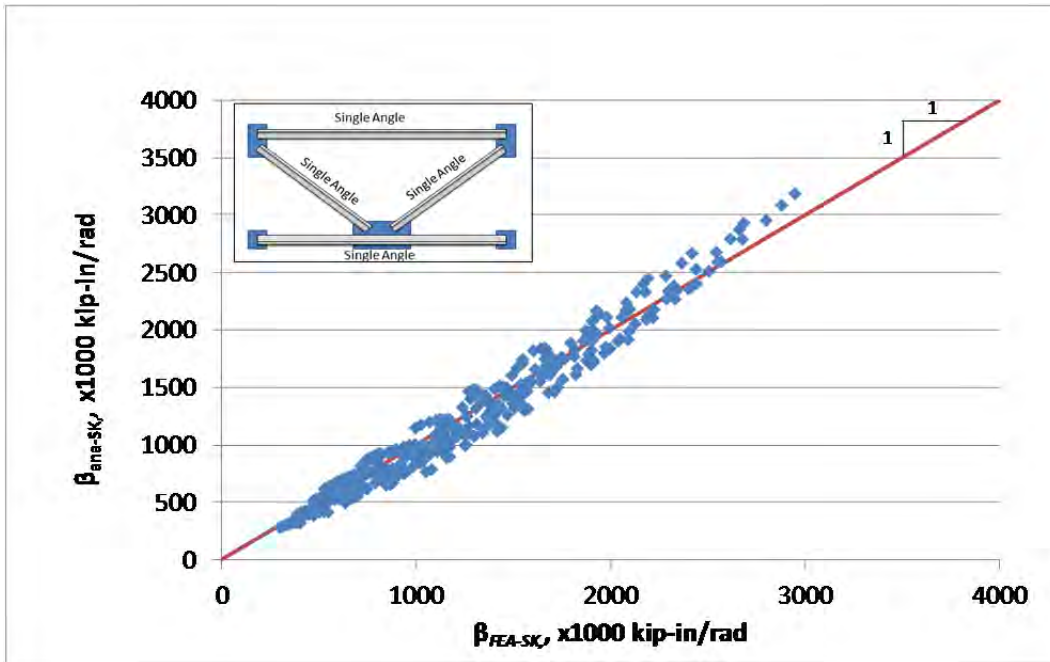


Figure 6.42: β_{ana-SK} VS β_{FEA-SK}

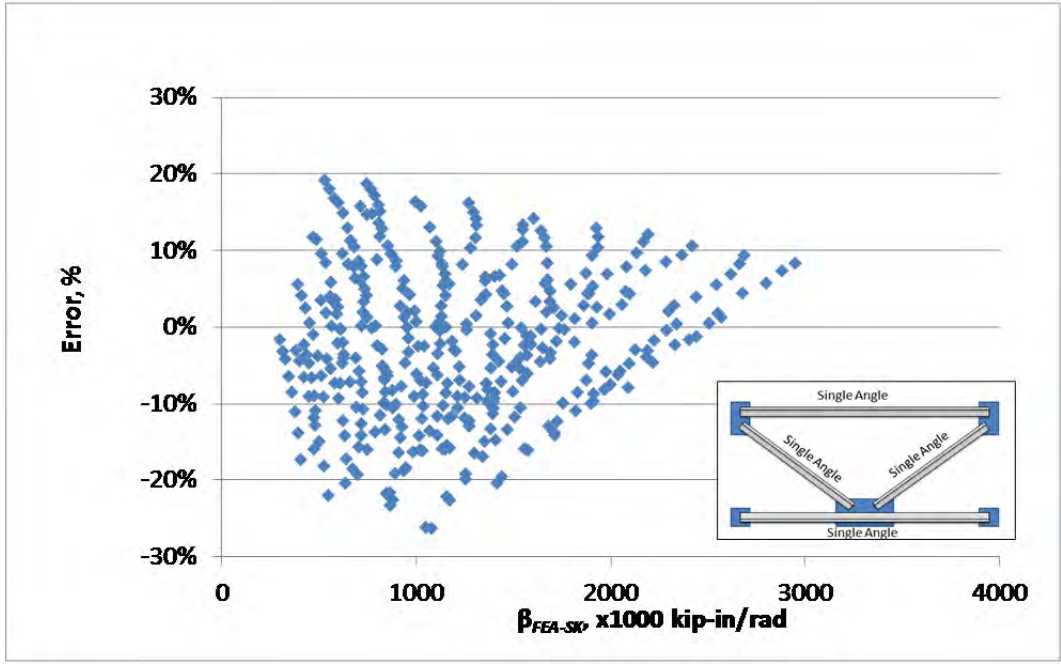


Figure 6.43: Errors of β_{ana-SK}

Similar to the method discussed for the Single Angle X-Frame Section 6.6, a universal stiffness reduction factor of 0.5 can be also employed to simplify the calculation. Figure 6.25 presents a comparison between the FEA results and the estimates by using stiffness reduction factor of 0.5. The errors in Figure 6.45 showed a range between -38% and 0 (negative values represent conservative estimates).

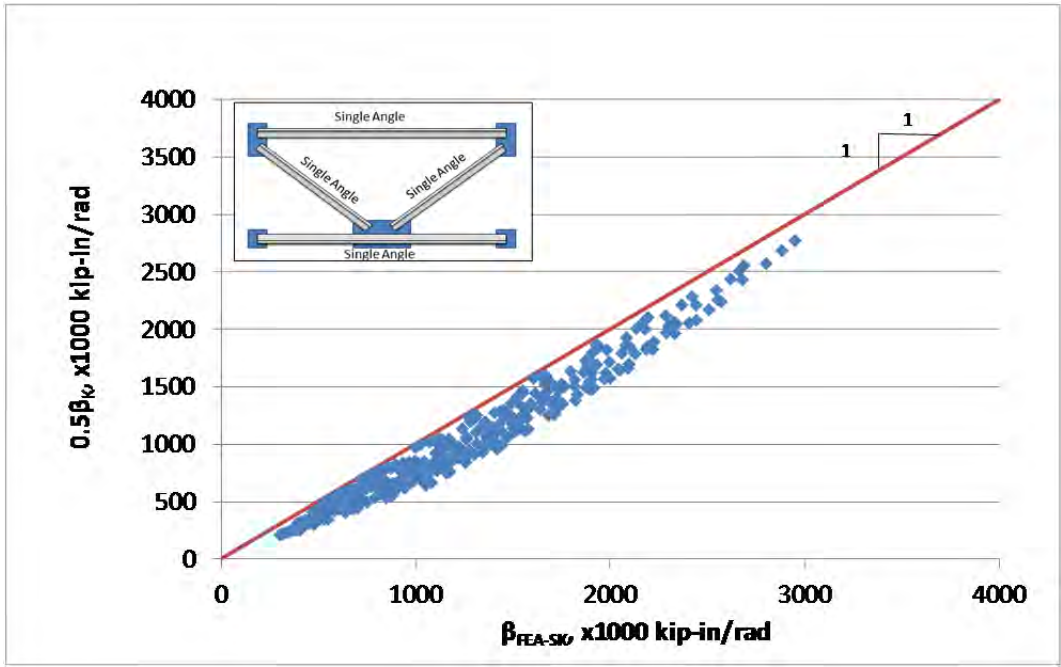


Figure 6.44: $0.5\beta_K$ VS β_{FEA-SK}

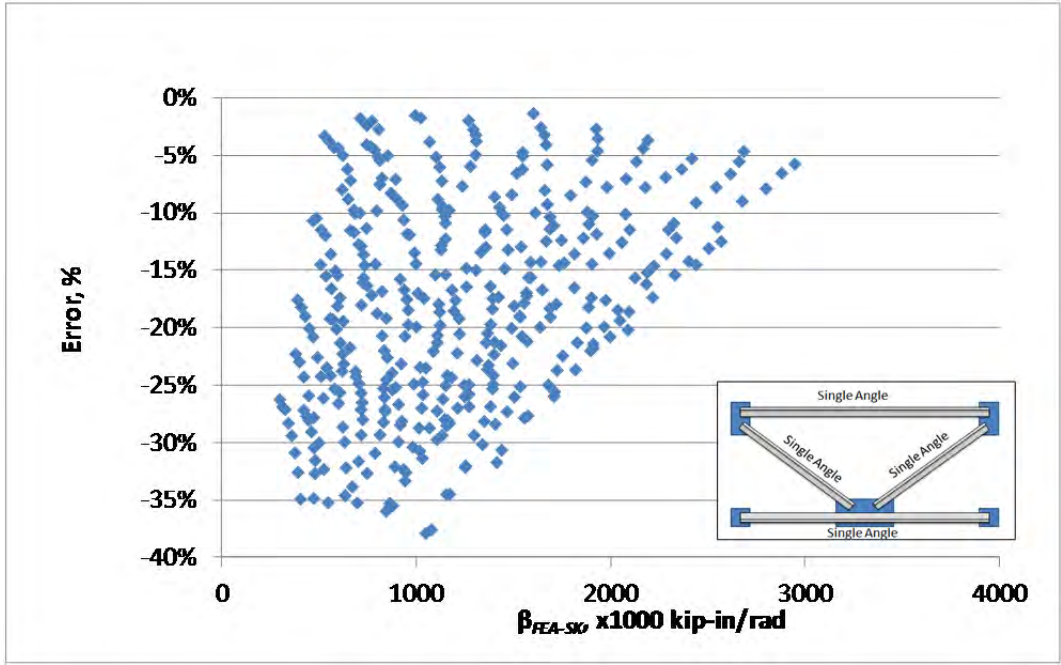


Figure 6.45: Errors of $0.5\beta_K$

6.7.6 Estimate Stiffness with Regression Method

A regression analysis was also carried out on the data from the parametric studies on the K-Frame system to develop a stiffness reduction factor that was representative of the variables that come into play with the wide variety of cross frame geometries that may be used in practice. Similar to the reduction factors outlined for the X frame, the stiffness reduction factor based upon the FEA parametric model is defined as:

$$R_{FEA-SK} = \frac{\beta_{FEA}}{\beta_K} \tag{6.57}$$

Where:

β_{FEA} = Stiffness calculated from FEA model

β_K = Theoretical stiffness by using K-Frame model

The first step in the parametric investigation consisted of determining the major geometric factors that might impact the behavior. A plot between R_{FEA-SK} and \bar{y} was created to study how the angle size could affect the stiffness reduction factor. The plot is shown in Figure 6.46 and the data points represent the results from the FEA models. It can be seen that the data points cluster in groups of b and t . Increases in the thickness of the angles results in a reduction in the stiffness reduction factor gets lower. The stiffness is also related to width of the members; however the impact is not as obvious as that of thickness. Overall, the range of the stiffness reduction is between 0.5 and 0.8.

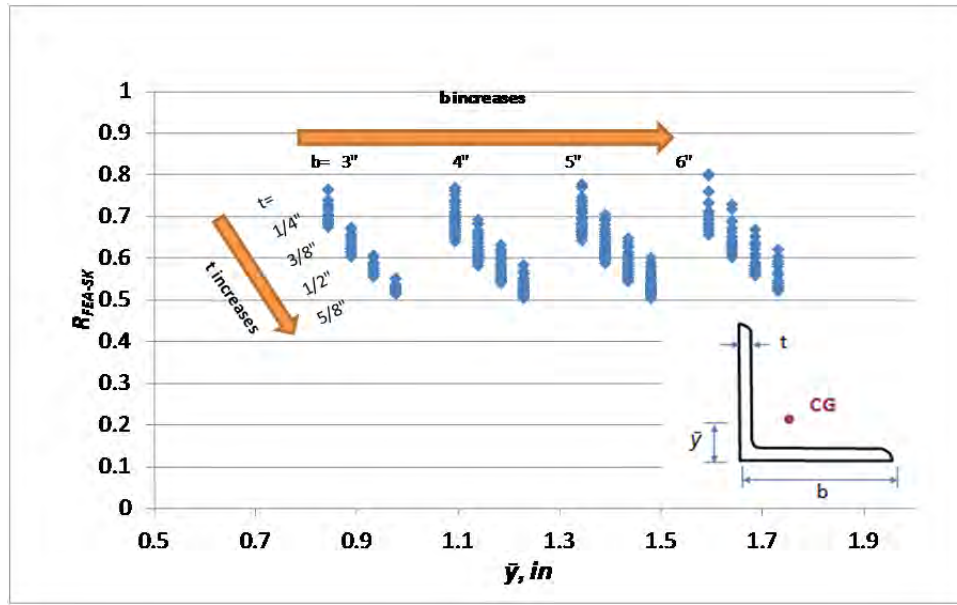


Figure 6.46: R_{FEA-SK} VS \bar{y}

The reduction coefficient, R_{FEA-SK} , is also related to the overall geometry of cross frames. The relation between the R_{FEA-SK} and the aspect ratio of the cross frame is plotted in Figure 6.47. It can be observed that the factor R_{FEA-SK} decreases with the increase of the cross frame's aspect ratio, S/h_b . Therefore for a given girder spacing, reducing the depth of the cross frame results in a larger reduction in the stiffness. This trend is similar to that observed in study of Single Angle X-Frame. However, the trend for the K-Frame is not as significant as was observed for the X-frame systems. For a K-frame, the angle between the diagonal and struts are greater than that of the X-Frame with a same overall geometry. So the congestion at gusset plates is not as serious. This finding also showed that K-frame makes a more effective cross frame when long cross frames is required, for example for end frames of skewed bridges.

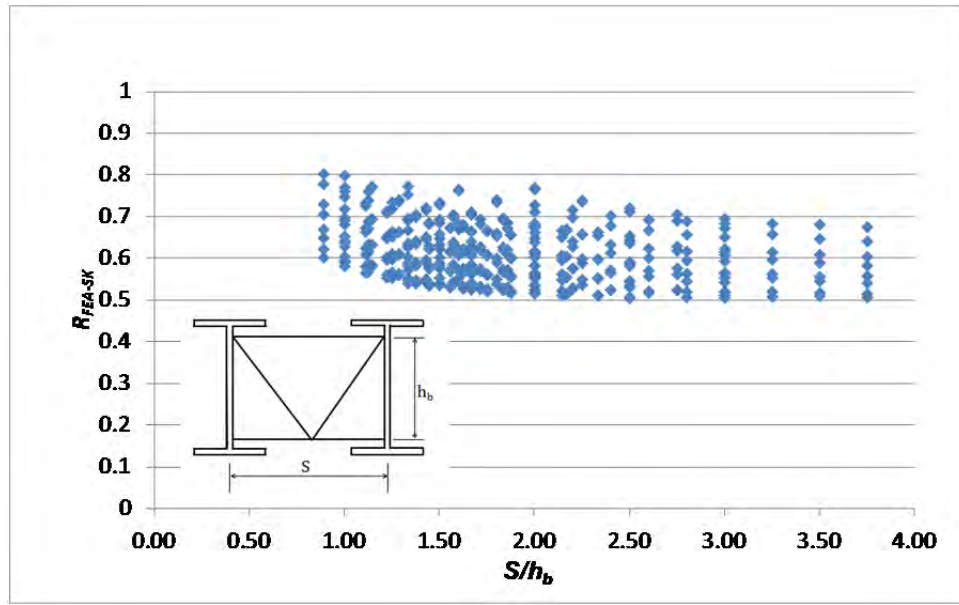


Figure 6.47: R_{FEA-SK} VS S/h_b

After the major parameters identified, the regression analysis described for the X frame could be performed on the parametric results. By performing the regression analysis with the variables b , t and S/h_b , the Equation (6.58) can be composed to estimate the stiffness reduction factor of the Single Angle K-Frame. The R-Squared value of the regression analysis was 0.90 and standard deviation was 0.0223.

$$R_{reg-SK} = 0.943 - 0.042 \frac{S}{h_b} - 0.012b - 0.438t \quad (6.58)$$

Based on Equation (6.58), the estimated stiffness can be evaluated as:

$$\beta_{reg-SK} = (0.943 - 0.042 \frac{S}{h_b} - 0.012b - 0.438t) \beta_K \quad (6.59)$$

Figure 6.48 shows the comparison between the estimated values from the Equation (6.59) and the observations from the FEA analysis. The regression based R value has good correlation with the finite element results as indicated by the red line with the 1:1 slope.

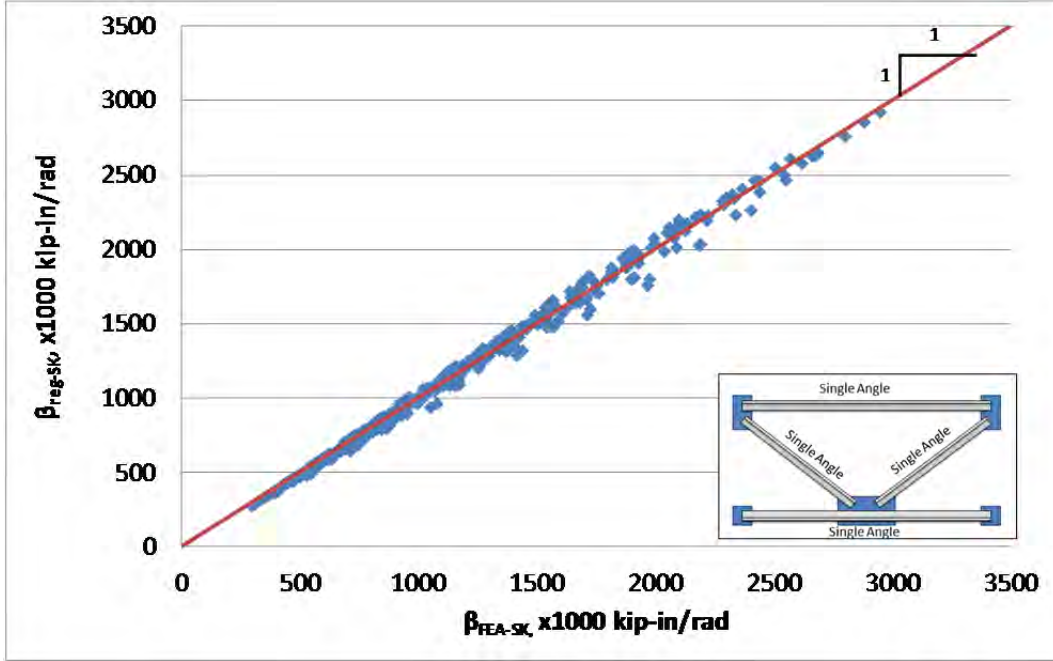


Figure 6.48: β_{reg-SK} VS β_{FEA-SK}

Additionally, if the regression analysis is done on \bar{y} , t and S/h_b , the stiffness reduction factor can be evaluated as:

$$R_{reg-SK} = 0.943 - 0.042 \frac{S}{h_b} - 0.048\bar{y} - 0.420t \quad (6.60)$$

6.7.7 Parametric Study with Nonlinear Buckling Analysis

A parametric study focusing on the nonlinear buckling analysis for Single Angle K-Frame was also carried out to investigate the stiffness reduction based upon the force in the compression members as a function of the buckling resistance. The geometric parameters considered in this study are listed in Table 6.7.

Table 6.7 Summary of Variables in the Parametric Study

h_b , in	S, in	Range of S/ h_b	Angle Size
48	96, 108, 120, 132, 144, 156, 168, 180	2 – 3.75	L3x3x1/4, L4x4x3/8
60	96, 108, 120, 132, 144, 156, 168, 180	1.6 – 3	L3x3x1/4, L4x4x3/8
72	96, 108, 120, 132, 144, 156, 168, 180	1.3 – 2.5	L4x4x3/8, L5x5x1/2
84	108, 120, 132, 144, 156, 168, 180	1.3– 2.1	L4x4x3/8, L5x5x1/2
96	120, 132, 144, 156, 168, 180	1.3 – 1.5	L5x5x1/2, L6x6x5/8

The P value plotted in Figure 6.49 represents the ratio of the load relative to the ultimate load where stiffness of the cross frames drops below 10% of the initial elastic stiffness. The parametric analysis showed that the value of P ranged from 0.59 to 0.81 for the K-frame system. A histogram of values of N is presented in Figure 6.49. The results for the K-frame are similar to the conclusion (approximately) reached for the X-frame system in that if the load on the cross frame is limited 60% of ultimate strength, the reduction in stiffness due to softening of the compression members can be ignored and the initial stiffness of the cross frame (elastic stiffness) can be used.

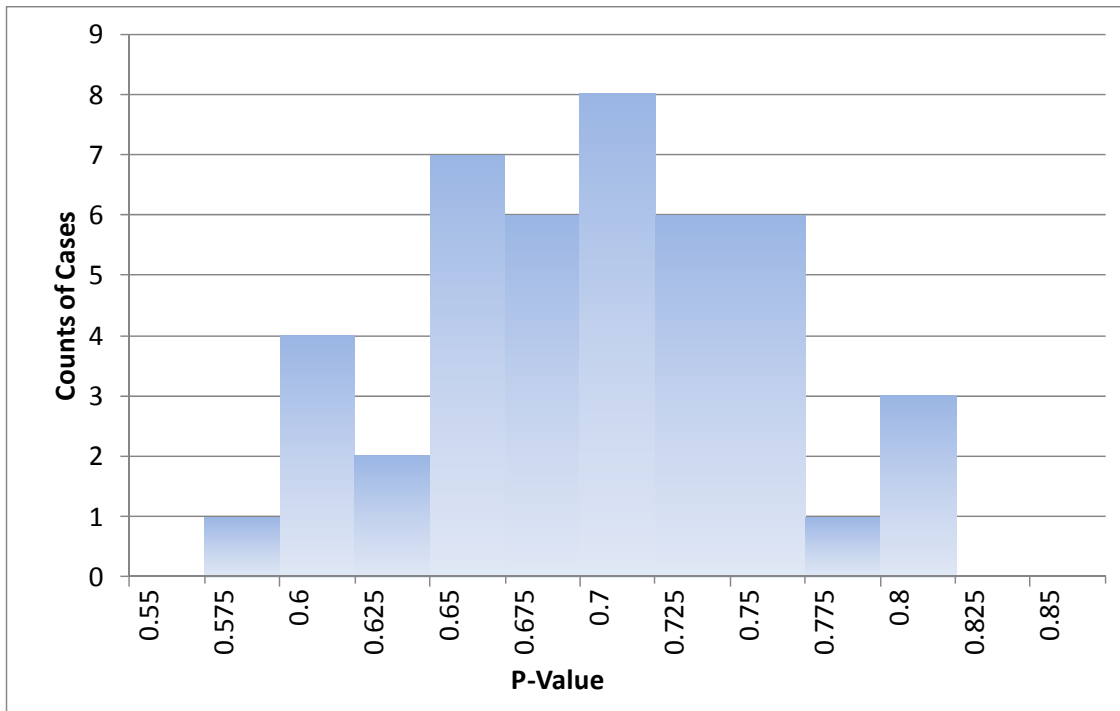


Figure 6.49: Statistics on N

6.7.8 Parametric Study with Unequal Legs

The final parametric study that was undertaken for the K-frame system was to investigate the use of unequal leg angles to reduce the effects of the eccentric connections compared to equal leg angles. The similar study on X-frame systems showed that the equation obtained from the parametric study on the equal leg angle cross frames can be applied to the unequal leg cases. The study for the K-frame system was achieved by changing the lengths and thickness of the angle legs. The cross frame size was fixed at a girder spacing of 12 ft. ($S=144$ in) and a cross frame depth of 8 ft ($h_b=96$ in.). The cross section parameters of the angle members are the same as those used for the X-frames and are shown again in Table 6.8. The angle orientation was varied by keeping the leg with the b_1 length in the plane of the connection plates and varying the length of the outstanding leg, b_2 . The angle leg lengths ranged from 3 to 6 inches in 1 inch increments. Four different thickness values were considered for the angles.

Table 6.8 Summary of Cross Section Parameters of Unequal Legs Angle Members

b_1 , in	b_2 , in	t , in
3	3, 4, 5,6	1/4, 3/8, 1/2, 5/8
4	3, 4, 5,6	1/4, 3/8, 1/2, 5/8
5	3, 4, 5,6	1/4, 3/8, 1/2, 5/8
6	3, 4, 5,6	1/4, 3/8, 1/2, 5/8

Note:

4. b_1 is the length of the angle leg in the plane of connection plates.
5. b_2 is the length of the outstanding angle leg.
6. t is the thickness of the angle legs.

The stiffness reduction factors were calculated for the cross frames considered in the parametric studies using Equation (6.57). The resulting stiffness reduction factors are presented in Figure 6.50 with the corresponding R values on the vertical axis graphed against \bar{y} on the horizontal axis. Similar to the observations from Single Angle X-Frame, the stiffness reduction factor for unequal leg angle K-Frames is related to \bar{y} and t .

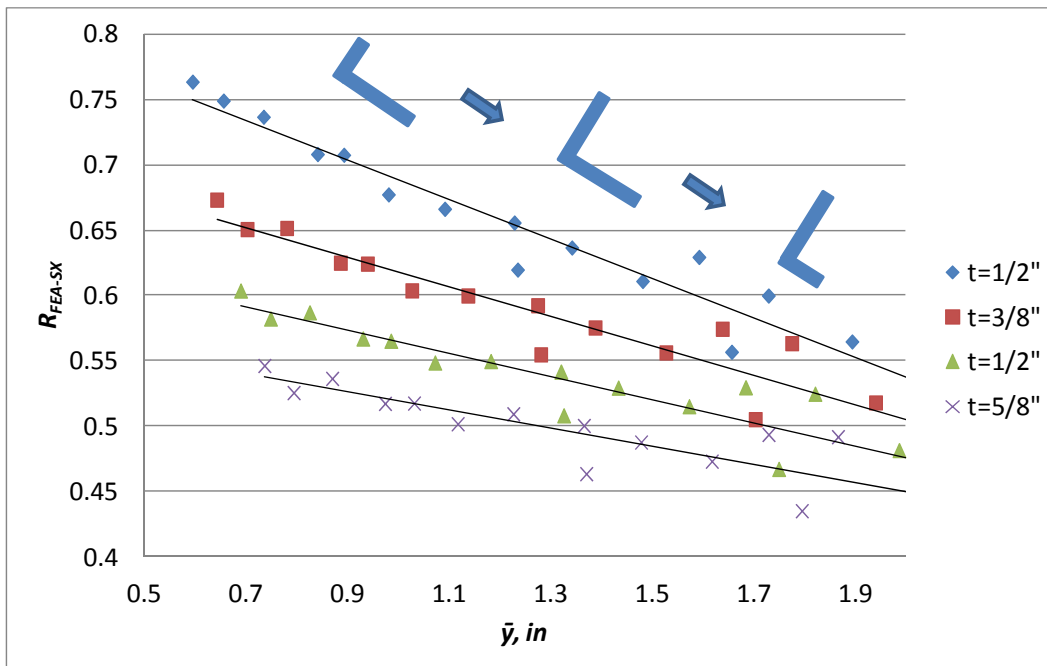


Figure 6.50: R_{FEA-SK} VS \bar{y} for Cross Frame with Unequal Legs Angles

Figure 6.51 shows the plot between the predicted stiffness from Equation (6.60) and that from the parametric study. It can be concluded that the regression equation for the stiffness

reduction coefficient, R , has reasonable agreement with the FEA solutions and can therefore be used in evaluating the stiffness of the unequal leg angle cross frames.

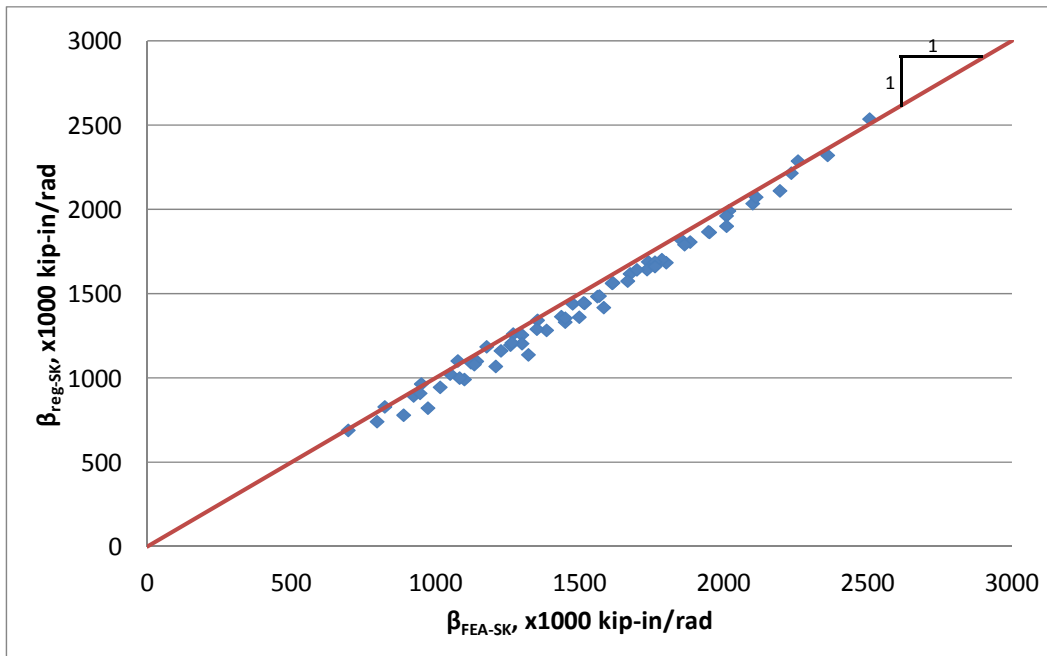


Figure 6.51: β_{reg-SK} VS β_{FEA-SK} for Cross Frame with Unequal Legs Angles

6.7.9 Summary of Parametric Studies for Single Angle K-Frames

In this section, parametric studies were performed with the Single Angle K-Frame systems using the FEA model that had been validated with laboratory test results. Based upon the parametric FEA studies on the K-frame systems, the following conclusions can be drawn:

- The direct use of the analytical K-frame stiffness expression on cross frames composed of single angle members produces unconservative estimates of the cross frame stiffness compared to the stiffness from the FEA studies. The resulting error for the wide range of cross frame systems that were studied ranged from 24% to 97%. The error can be corrected by applying a stiffness reduction factor, R , to the analytical solution that was developed using a truss model.
- Two methods were considered to develop an expression for the stiffness reduction factor. The first method utilized the analytical model developed. This method provided reasonable estimates of the reduction in stiffness of cross frames compared to the analytical truss model. This method does require some significant calculations and therefore a simplified method was also considered in which a universal stiffness reduction factor of 0.5 was considered. The $R=0.5$ provided reasonable estimates of the cross frame stiffness and was conservative compared to the FEA solutions. A more accurate estimate of the stiffness reduction factor was also developed based upon a regression analysis on the results from the parametric FEA study. The

resulting expression (Equation 7.2) considers the impact of cross frame angle and geometrical parameters and had good correlation with the FEA results.

- A cross frame stiffness expression that relies on a compression member will also experience a reduction in stiffness as the compression diagonal approaches the buckling capacity. A nonlinear geometrical analysis was carried out considering a wide variety of parameters. The results showed that the reduction in cross frame stiffness was minimal provided the forces in the compression members are kept below 60% of the buckling strength of the corresponding member of the cross frame. For this reason, it is concluded that if design load is less than 60% of the strength of the cross frame, no deduction on cross frame stiffness is necessary.
- A brief parametric study is also provided for cross frames with unequal leg angles. The results of the analysis showed that the regression Equation (6.60) derived from equal leg angles also provides reasonable estimates of the stiffness of cross frames with unequal leg angles.

Chapter 7. Cross Frame Fatigue Tests

7.1 Introduction

One of the priorities of TxDOT Project 0-6564 was to evaluate the performance of existing cross frame layouts and offer improved details for a more efficient brace. In Chapter 4, proposed connections were tested on a component level to determine stiffness, strength, and fatigue behavior. The MTS Universal Testing Machine used was also able to test the single angle detail in stiffness and strength, but could not perform the fatigue tests. The single angle detail attached to a gusset plate through one leg is an eccentric connection, as seen in Figure 7.1.

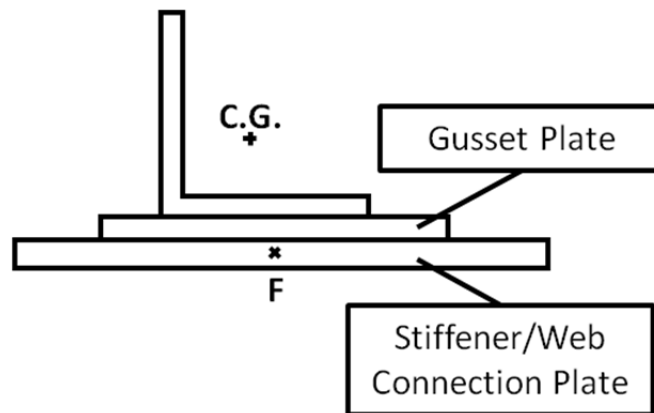


Figure 7.1: Eccentric Single Angle Connection

Due to the eccentricity, a substantial amount of bending is induced in the member, and in turn, a bending moment is applied to the testing machine. Figure 7.2 depicts the magnitude of the bending as seen in the tension test performed to the ultimate strength of the angle.



Figure 7.2: Single Angle Strength Test Bending

With the large amount of observed bending, there is concern that the testing machine could be damaged if cyclic fatigue tests were to be performed. A previous study conducted for the American Institute for Iron and Steel [McDonald and Frank 2009] had similar issues with the angle bending. As an alternative, the researchers opted to test two angle specimens back-to-back, to achieve concentric from the combined members and eliminate the potential damage to the cross head. The resulting orientation was very similar to the double angle member tested as part of the current project, with the exception the angles were not connected to a single gusset plate. The AASHTO fatigue category determined by McDonald and Frank [2009] for the single angles was E', the same as was determined for the double angle connection as outlined in Chapter 4.

While the previous single angle tests provide a baseline understanding of the connection, there is the possibility that the testing boundary conditions are not representative of the real structure. In the cross frame, the gusset plates would be free to bend with the single angle members, potentially further diminishing the fatigue life of the detail. Therefore, full scale cross frame fatigue tests are necessary to determine the appropriate category for these members in the existing brace details. The test setup also allowed the researchers to evaluate the fatigue performance of the other proposed details in a full cross frame system.

In addition, the stiffness of the cross frames utilizing the single angle details obtained in the large scale laboratory tests and accompanying finite element analyses showed a large discrepancy as compared to the appropriate truss analogy for brace stiffness. Perhaps treating the members as axial elements may not be a good representation of the actual behavior, thus necessitating a different test evaluation for the fatigue performance.

In order to verify the fatigue performance of the various cross frame connection details, a test setup was fabricated to allow cyclic loading of the entire cross frame so as to be similar to cross frames in actual bridge applications. This chapter outlines the features of the test setup, discusses the results for five different cross frame types, and makes recommendations for improved cross frame behavior based on the test data and accompanying finite element analyses.

7.2 Cross Frame Fatigue Test Setup

The large scale cross frame fatigue tests were performed at the Ferguson Structural Engineering Laboratory at The University of Texas at Austin. A CAD view of the test setup using SolidWorks 2011 software is shown in Figure 7.3 and the completed laboratory setup is shown in Figure 7.4.

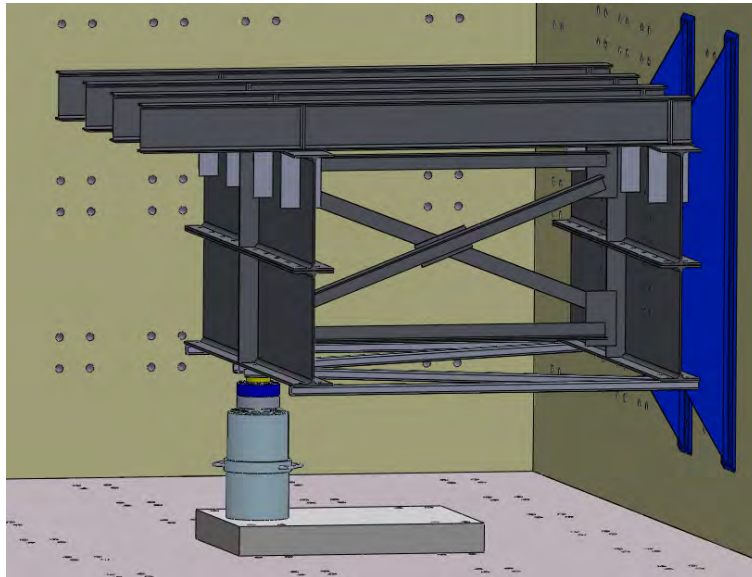


Figure 7.3: CAD Drawing of Cross Frame Fatigue Setup



Figure 7.4: Completed Cross Frame Fatigue Test Setup

Figure 7.5 through Figure 7.8 shows front views and side views of the test setup as well as identifies some key features of the experiment. The following subsections will discuss the various pieces of the test frame and the purpose of each.

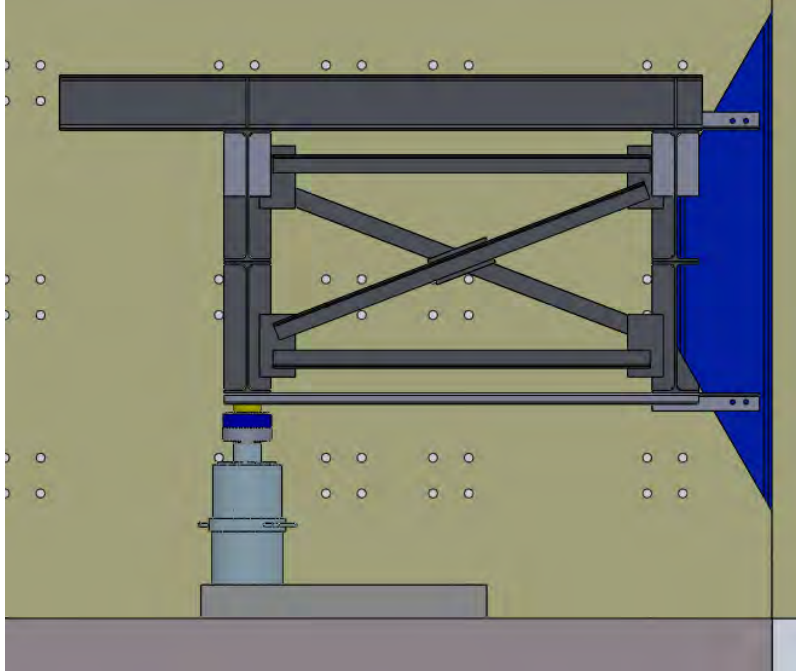


Figure 7.5: Front View of Cross Frame Fatigue Setup

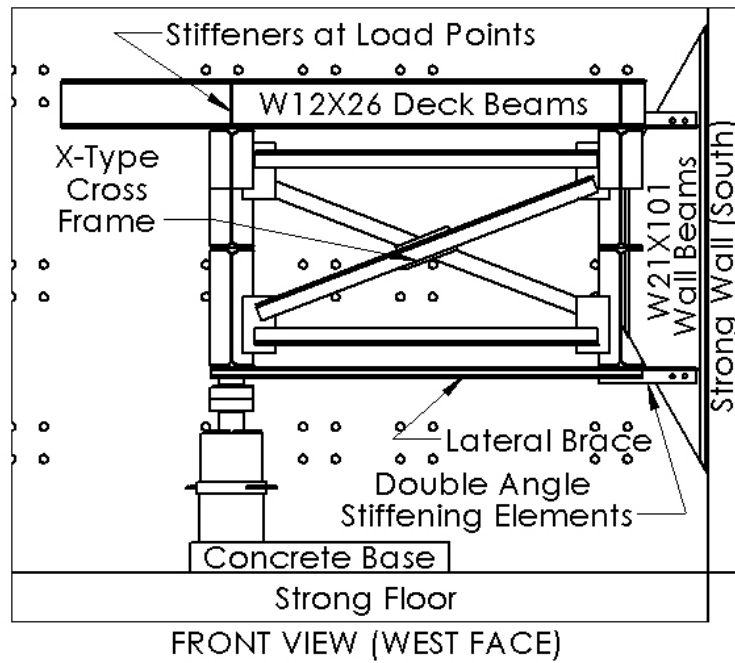


Figure 7.6: Front View of Cross Frame Fatigue Setup (Details)

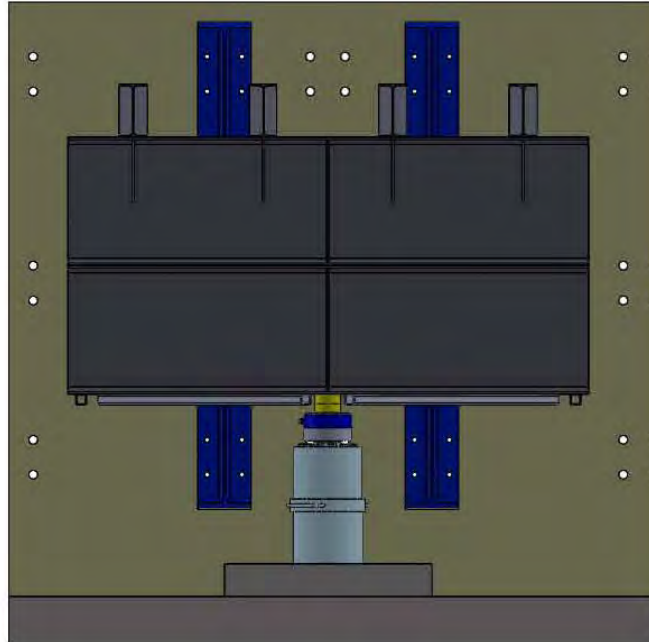


Figure 7.7: Side View of Cross Frame Fatigue Setup

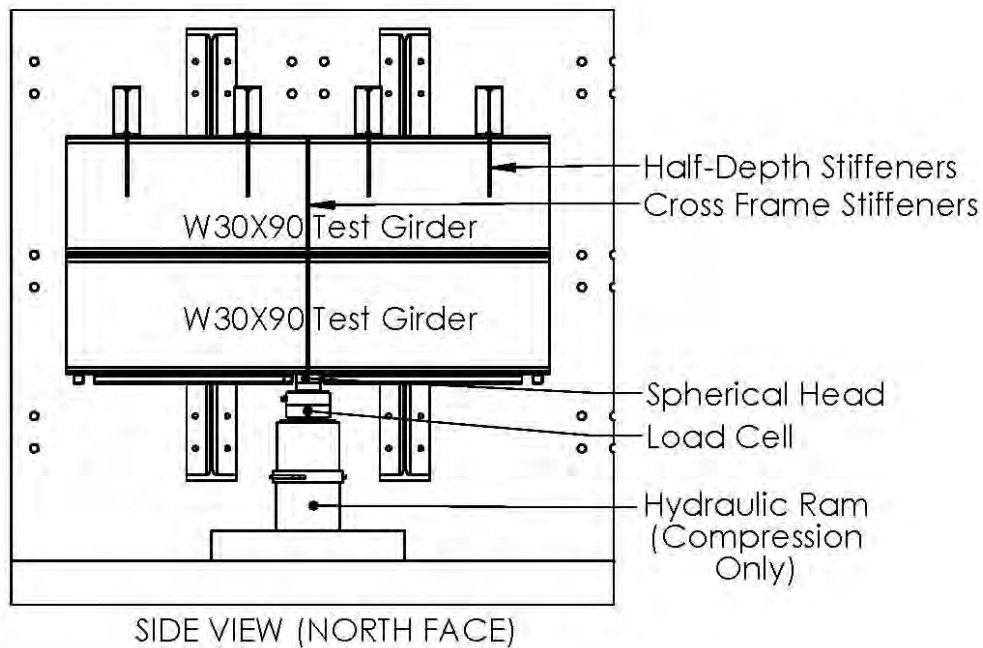


Figure 7.8: Side View of Cross Frame Fatigue Setup (Details)

7.2.1 Built-Up Test Girders

In order to simulate the plate girders typically used in the construction of steel bridges, the researchers used two 10 ft long W30x90 rolled sections, stacked on top of one another, and bolted together along the length of the flange at a 12 in spacing. The bolt spacing was selected

using preliminary FEA ensure that the fully tightened bolts controlled slip between the two wide flange sections and simulated a built up girder. The bolts used were ASTM A490 bolts and were tightened with the assistance of a pneumatic torque wrench. The resulting cross section is approximately 5 ft deep, with a web thickness of 0.47 in. The associated web slenderness ratio (web depth to thickness) is 123, well within the typical range for plate girders frequently used in steel bridges.

7.2.2 Deck Beams

Although a composite concrete deck between the two girders was considered during the design phase of the setup, such a deck would make the removal and installation of cross frames very difficult. Therefore a simulated concrete deck was used by including W12x26 sections spanning between the two test girder sections. Once the concrete deck is cured in a real bridge system, it can provide substantial bracing to the girder sections by acting as a torsional brace attached to the top flanges of the girders. For simplicity in fabrication and repeatability between tests, the W12x26 beams were selected to provide similar rotational restraint to the flanges. Using typical concrete deck depths, reinforcement ratios, and material properties, the EI/L of the concrete deck section was calculated and equated to that of an equivalent steel section, resulting in the placement of four W12x26 beams for the 10 ft girder sections being tested. The deck beams are indicated in Figure 7.6.

7.2.3 Wall Beam Supports

The desired loading condition was to represent the deflection in the cross frame when a truck passes over the brace location. To practically achieve this condition, a vertical load was applied to one test girder, while the deflections of the adjacent test girder were restricted. The differential deflection was achieved in the tests by using a hydraulic actuator to displace one girder while the other girder was anchored to a reaction wall. Two W21x101 girder sections were fabricated and anchored to the wall. One of the test girder webs was then bolted to the W21x101 sections. The wall support is shown in blue in Figure 7.5 and is called out in Figure 7.6.

7.2.4 Double Angle Stiffening Elements

When statically loading the cross frame setup before the first test, a large amount of flange bending occurred at the test girders as a result of the limited attachment length of the wall beam to the girder web. The excessive bending lead to large displacements required to achieve realistic forces in the cross frame members. As a result, a double angle member was bolted to the top and bottom flanges of the test girder adjacent to the wall and bolted to the web of the wall beam. Figure 7.5 and Figure 7.6 show the locations of the double angles.

7.2.5 Lateral Bracing

The 10 ft. simulated girder sections lacked the continuity that would be present in an actual bridge section and there were concerns about the deformational behavior of the bottom flange of the girders. Due to the eccentric loading of the single angle members, deflection out of the plane of the cross frame occurs. This deflection could cause the entire test setup to rotate about the load point. To prevent the rotation and simulate the stiffening effects that would come from girder continuity, bracing was supplied in the form of a lateral truss on the bottom flange.

The lateral truss consisted of HSS2.5x 2.5x1/4. Preliminary FEA results showed that these members did not significantly change the forces in the cross frame and the stresses using the selected member would be minimal so as not to create a fatigue issue. The bottom flange bracing can be seen Figure 7.3, Figure 7.3 and is indicated in Figure 7.6.

7.2.6 Stiffeners

Girder stiffeners were provided to help limit distortion at the cross frame locations as well as the helping to distribute the stiffness of the simulated deck beams. Half-depth stiffeners cut from PL5x1/2 material were selected to help transfer the forces from the test girders into the deck beams. The same plate material comprised the full depth stiffeners situated above the loading ram, which also acted as the cross frame connection plates.

7.2.7 Loading System

To load the cross frame vertically, a 200 kip hydraulic actuator was used to apply compression-only loads, transferred to the girders through a 200 kip load cell and spherical head which allowed rotation of the test girder relative to the loading system. The hydraulic actuator was placed on a concrete pad. Holes were drilled into the concrete pad the actuator rested on. Threaded rods screwed into the base of the actuator extend into the concrete pad to act as a shear key to prevent the actuator from shifting too far out of position during cycling. The actuator, load cell, and spherical head are shown in Figure 7.9. A preload was applied to the system to impose a preload to the cross frame. . Cyclic loads above this preload were then used to produce the desired stress range.



Figure 7.9: (a) Hydraulic Actuator, (b) Load Cell, and (c) Spherical Head

7.2.8 Fabrication Methods

To accommodate the wall beam, the flanges on one side of the test beam were coped to provide continuous support along the depth of the web. The wall support beams had to be long

enough to provide sufficient anchor points to the reaction wall, but also needed fit within the flanges of the test beams. The wall support beams were therefore tapered to form a trapezoid that was long enough to provide sufficient anchoring points to the wall and to fit within the flanges. Since the components of the setup were to be used on a fatigue setup, care was taken in cutting the test setup pieces to the proper length and shape since rough, jagged cuts could present possible fatigue crack initiation points on the test setup. After flame cutting the sections, grinding was performed to improve the surface condition. Figure 7.10 to Figure 7.13 depict the wall support fabrication process.

In addition, all the holes were constructed using a magnetic drill, lubricated by hydraulic oil, to produce holes with minimal defects to minimize potential points of fatigue crack initiation. The smaller lateral truss tubes, double angle stiffening elements, girder stiffeners, and cross frame members and gusset plates were cut using a metal band saw.



Figure 7.10: Drilling Holes for Wall Beams



Figure 7.11: Flame Cutting Web



Figure 7.12: Completed Wall Support



Figure 7.13: Surface Condition (a) After Flame Cut and (b) After Subsequent Grinding

7.3 Cross Frame Specimen Details

The majority of the cross frames were fabricated by the researchers and welded by a welding technician at the Ferguson Structural Engineering Laboratory. The following subsections outline the general procedures performed to create the braces and the measures taken for quality assurance.

7.3.1 Cross Frame Fabrication and Specimen Designation

The cross frame members were cut to appropriate length using a horizontal band saw, which is consistent with the cutting methods used in standard bridge fabrication shops. Different cross sections were used for the members based on the cross frame type and detail summarized in Table 7.1.

Also, the specimen designation adopted for reference in the project is introduced.

Table 7.1: Cross Frame Types and Specimen Designation

Cross Frame Type	Specimen Designation ¹	Cross Frame Member
X Frame, Equal Leg Angles	XF_#	L4x4x3/8
X Frame, Unequal Leg Angles	XF_UL_#	L6x3.5x5/16
K Frame, Equal Leg Angles	KF_#	L4x4x3/8
Z Frame, HSS Tubes	ZF_HSS_#	HSS5x5x3/8 HSS6x3x5/16
Z Frame, Double Equal Leg Angles	ZF_DA_#	2L4x4x3/8

1. The # symbol denotes the specimen number for that type of cross frame.

Once cut, the pieces were laid out on a welding table according to the individual specimen details. In order to assure the proper height of brace, 4x4 wood posts were cut and placed between the top and bottom struts of the cross frame. Using the posts guaranteed the struts were parallel to one another and the proper distance apart. The plates were held in place to the struts using C-clamps, and squared up using the edges of the welding table. The diagonals were then set in place and clamped. Once the cross frame was complete, tack welds were used to maintain the geometry until the prescribed welded details were completed. In general, the tack welds were placed at locations away from potential stress concentrations and were ground smooth before completing the fillet welds. An example of laying out the cross frame is shown in Figure 7.14.



Figure 7.14: Cross Frame Layout during Fabrication

Based upon test results, changes were incorporated into some of the details to improve fatigue behavior and constructability and/or to investigate the effects of different variables. Drawings of each specimen and associated dimensions are given in Appendix A.

7.3.2 Cross Frame Welds

The welding processes performed for each cross frame were conducted in accordance with TxDOT standards regarding weld size and material. The welding machine used was a Miller XMT 450 CC/CV multiprocess inverter with a Miller 70 series wire feeder.

At an early stage in the full scale fatigue tests, the researchers had some of the cross frames fabricated in the Bridge Section of Hirschfeld Industries in San Angelo, Texas. The cross frames were cut and tack welded at FSEL with the final welding completed at Hirschfeld to ensure that the fatigue performance of specimens welded at FSEL were consistent with the quality that would be expected from a bridge fabricator. Members of the research team were present at Hirschfeld to observe the welding process and note the welding electrode and settings.

Two types of wire were used throughout the cross frame fatigue tests. The first was a Lincoln Electric Ultracore® 71A85 flux-cored gas-shielded wire with a 1/16 in diameter. The 71A85 wire is designed for all position welds, meets seismic structural fabrication standards, and should be used with a mixed Argon-CO₂ shielding gas [Lincoln Electric 2013]. The wire was used primarily to weld the cross frame specimens to the girder stiffeners in the test setup due to its ability to better perform vertical and overhead welds. The cross frame specimens fabricated prior to the researchers' visit to Hirschfeld Industries (a Texas steel bridge fabricator) had welds connecting the cross frame members to the gusset plates using this type of welding wire (Specimens XF_1,2,3,4; KF_1,2; ZF_HSS_1; ZF_DA_1).

The second type of wire is the Lincoln Electric Outershield® 70 series for mild steel in the flat and horizontal position and is suited for structural fabrication [Lincoln Electric 2013]. This wire has consistent properties to the one used at Hirschfeld which was a Lincoln Electric Ultracore® 70C wire. The wire had a 5/64 in diameter, greatly increasing the heat input and available weld metal relative to the 1/16 in wire. Since this wire is only suited for flat and horizontal positions, it was used only in the fabrication of the cross frames. The previous Lincoln Electric Ultracore® 71A85 wire was used to attach the specimens to the stiffeners in the test setup.

7.3.3 Testing Procedures

Once the specimens were welded into the setup, researchers would load the cross frames statically to measure the vertical stiffness of the system and to verify the deflections were similar to the FEA model predictions. Figure 7.15 provides a typical view of the test setup and loading direction.



Figure 7.15: Test Setup and Load Application

Since the hydraulic actuators used in the research could only apply compression loads, the stresses in the cross frame members never experienced a reversal. The load was statically applied until the critical member in the brace reached an average tensile stress of 5 ksi based on the readings collected from the member strain gages and accounting for shear lag in the member connection. The 5 ksi stress acted as the baseline tension value in the member and was the minimum stress value in the loading cycle. The desired stress range of the test was then added to this minimum to give the maximum stress value in the loading cycle (i.e. a test with a $S_R = 15$ ksi, would have $S_{\min} = 5$ ksi and $S_{\max} = 20$ ksi including shear lag effects). Once the applied load to achieve the minimum stress value was established, the load was increased to determine the value at the maximum stress and force and displacement measurements were taken.

Due to the complexity of the setup, the force at the minimum stress range was not always uniform for all cross frame specimens of the same type. In addition, once the load range was established, researchers would cycle back and forth 2-5 times until force and displacement measurements had stabilized, making minor adjustments during the process.

Using the load range determined by the described process, the cross frame cycled between the maximum and minimum following a sine curve. The frequency of the test was gradually increased until the setup was no longer stable, meaning the max/min stresses were not being reached, the force feedback error became larger than 10 kips, or the setup or hydraulic ram made uncharacteristic noises. The frequency was then reduced to maintain proper control of the setup and the test was begun.

Each test was run until failure. Researchers monitored the stress ranges in the appropriate elements and recalibrated the applied force range if discrepancies arose. Due to the time-consuming fabrication of the braces, specimens were sometimes temporarily repaired to evaluate fatigue crack growth at secondary locations. These tests are indicated by a, 'A' and a 'B' following the test specimen designation to indicate reuse of the specimen.

7.3.4 Testing Equipment

The test was conducted utilizing a closed-loop force-controlled system. A 30 gallon per minute (gpm) hydraulic pump was used to provide hydraulic oil to the system. The oil flowed into an MTS high-pressure accumulator, which was connected to an MTS Flextest® SE Controller and a 15 gpm servo-valve. The system was monitored by a portable data acquisition system.

The computer software monitors the force response from the load cell attached to the hydraulic ram and controls the flow of the oil into the system via the servo-valve to make sure the desired force range was attained. The following figure graphically depicts the force-controlled system.

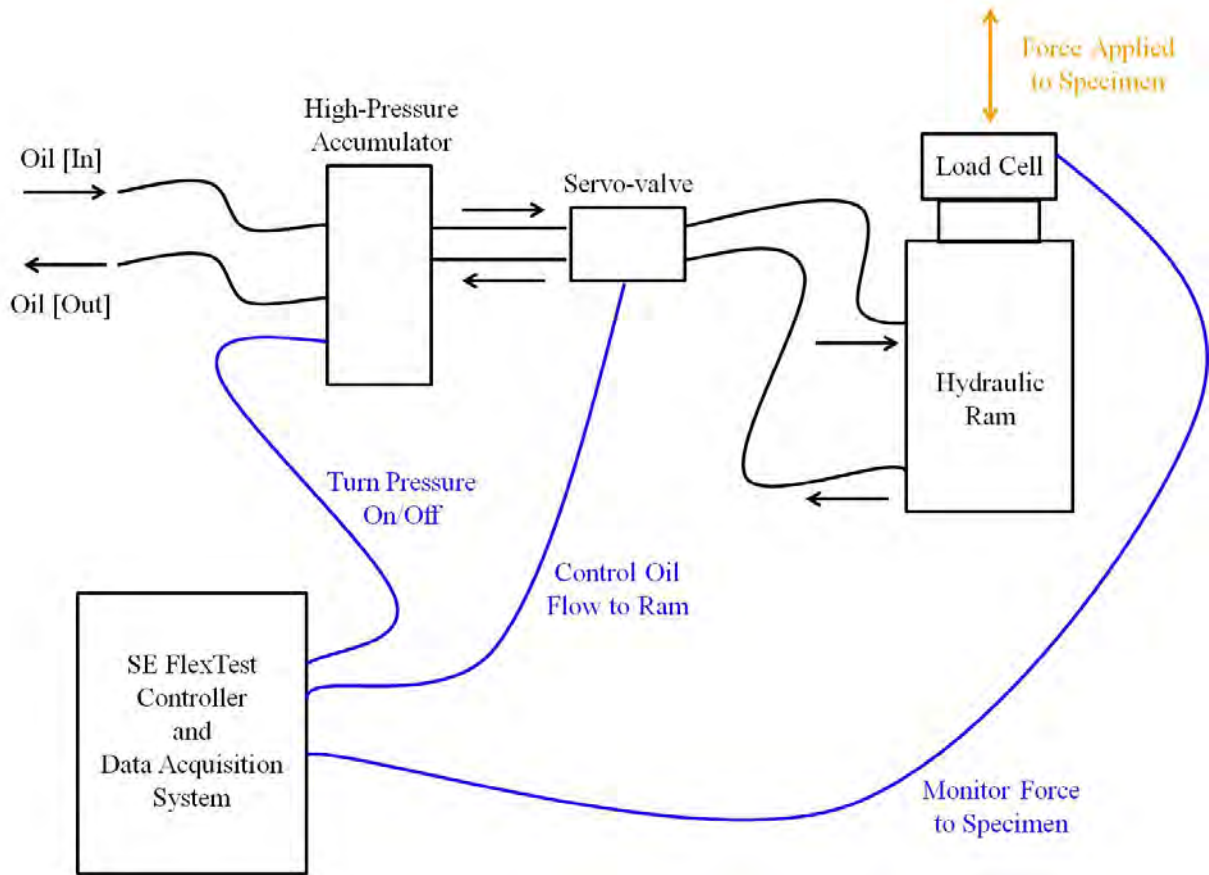
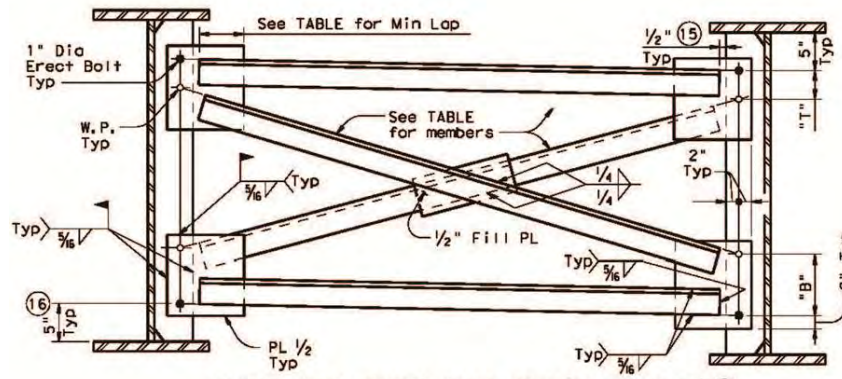


Figure 7.16: Schematic of Force Controlled System

Part I: X Frames—Equal Leg Angles

7.4 X Frame—Equal Leg Angle Design

The initial design of the X frame using equal leg angles followed the TxDOT standard detail for Type E cross frames described in Chapter 2. The angle size was chosen based upon the test frame size, spacing, and girder depth. In addition, the L4x4x3/8 angles were used in the large scale cross frame stiffness tests, providing continuity in the research.



TYPE XF1 THRU XF3 CROSS-FRAMES (17)

For Plate Girders with web depths of 52" to 96". For all locations, including end bearings when Thickened Slab Ends, shown on standard SBTS are used. Minimum stiffener width is 8" for use with these cross-frames.

Figure 7.17: Typical TxDOT X Frame Detail [TxDOT 2010]

A typical view of the X frame specimens in the testing frame is shown in Figure 7.18.



Figure 7.18: Typical X Frame Specimen in Test Setup

When the outside girder is loaded through the hydraulic actuator, the outside edge of the cross frame specimen displaces vertically, inducing tension in one diagonal and compression in the other as depicted in Figure 7.19. The load range in the tests were established to achieve the desired stress range based upon the corresponding output from axial forces calculated based upon the strain gage readings from the cross frame diagonals.

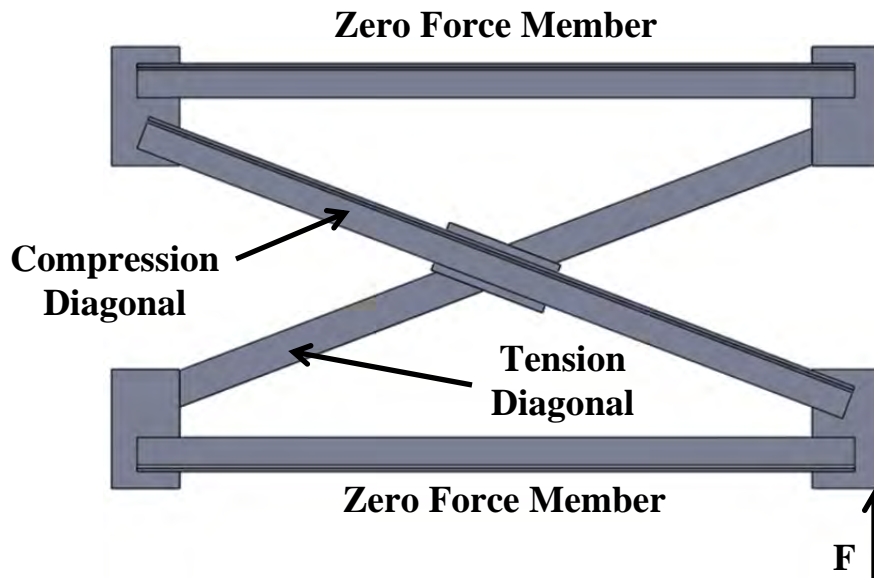


Figure 7.19: Typical X Frame Internal Forces from Load Applied

7.4.1 X Frame Test Variables

A total of 8 X frames with L4x4x3/8 equal leg angles were tested in fatigue with varying geometries. The complete details of each test are summarized in Appendix A.

For discussion purposes, the tests are divided into three primary groups of interest. First, there are the tests that most closely follow the geometry called for in the typical TxDOT detail shown in Figure 7.17. These correspond to test specimens XF_1,3,4.

Secondly, there are the tests that have the same geometry, but the tension diagonal has been oriented on the side of the gusset plate away from the gusset-stiffener connection. The ramification is the critical tension member welds in these specimens do not directly interact with the gusset-stiffener welds. These correspond to test specimens XF 2,5,8. Additionally these tests examined the effect of placing a weld along the back edge of the angle-gusset weld, currently not specified in the typical TxDOT detail.

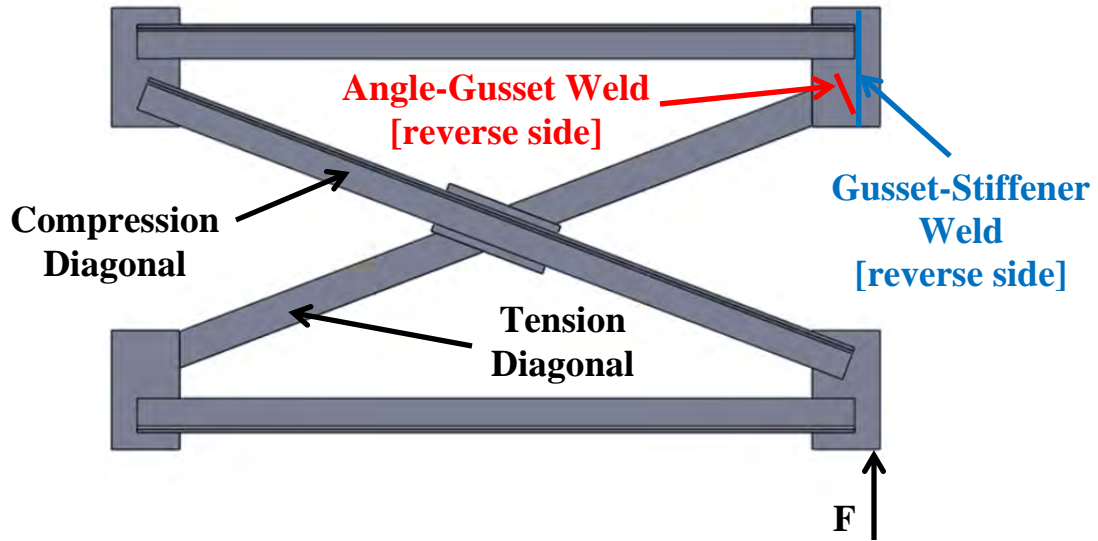


Figure 7.20: X Frame with Tension Diagonal on Stiffener Side of Cross Frame (i.e. XF_1,3,4)

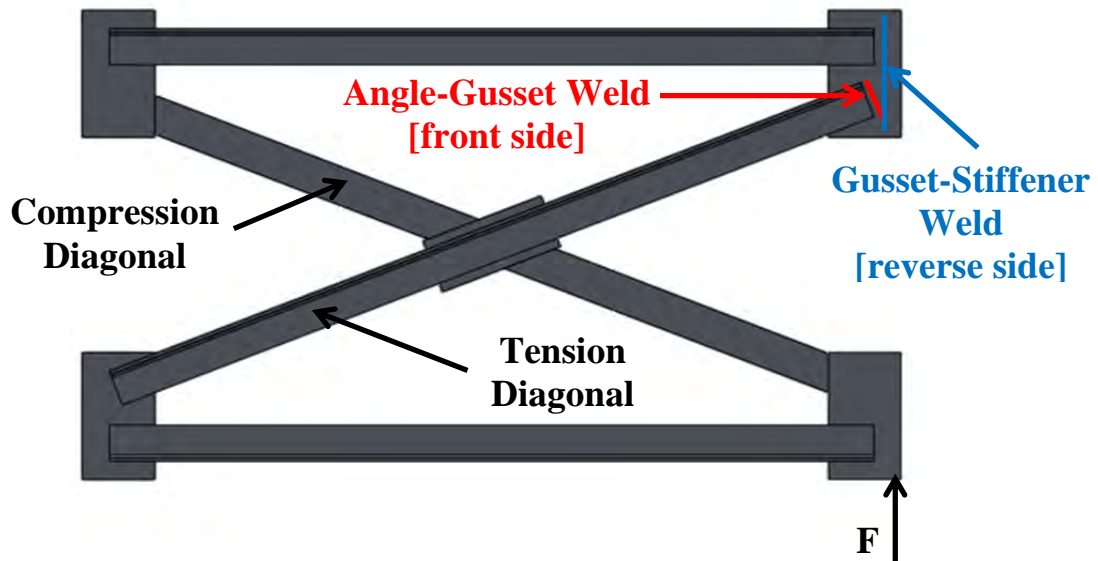


Figure 7.21: X Frame with Tension Diagonal away from Stiffener Side of Cross Frame (i.e. XF_2,5,8)

Lastly, the research team investigated an increased spacing between the end of the angle weld and the gusset-stiffener weld. The tests used a wider gusset plate so that the overlap of the angle diagonals remained constant. These tests correspond to XF_6,7.

7.4.2 X Frame Tests of Current TxDOT Detail (XF_1,3,4)

Specimens XF_1,3,4 were fabricated following details most similar to the current TxDOT detail. The cross frame was welded together and then welded into the test frame. Upon

running the first test, a fatigue crack began propagating from the toe of the angle-gusset weld into the gusset plate at a relatively low fatigue life, much lower than the AASHTO minimum Category E'. Upon subsequent inspection, it was seen the gusset-stiffener weld, typically performed in the field, was intersecting the angle-gusset weld, as seen in Figure 7.22 and Figure 7.23.

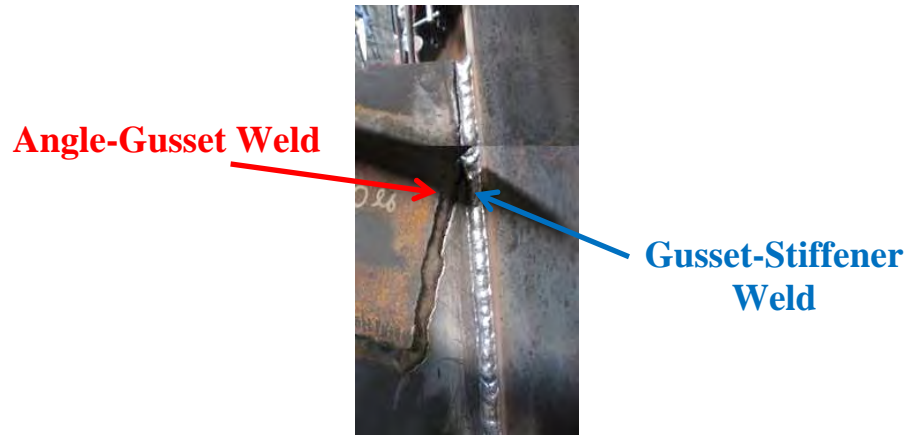


Figure 7.22: Overlap of Angle-Gusset Weld and Gusset-Stiffener Weld (XF_1)

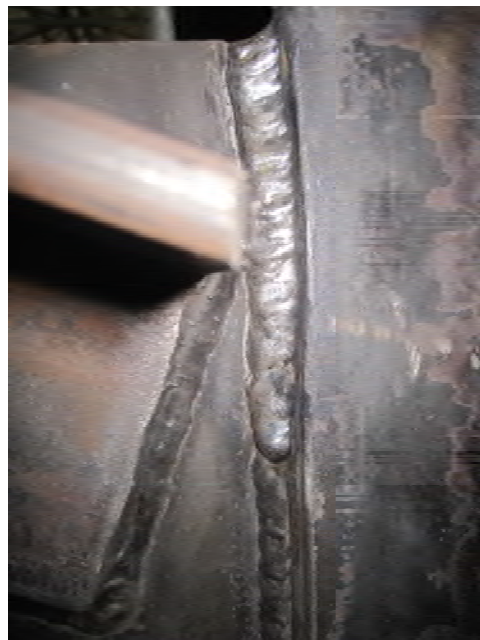


Figure 7.23: Overlap of Angle-Gusset Weld and Gusset-Stiffener Weld (XF_4)

The overlap of any welds in a structure can lead to significant stress concentrations, primarily due to the rapid stress transfer that must occur at the weld boundaries. In addition, residual tension/compression effects from the localized heating of the metal can exacerbate the stresses. In this case, the overlap significantly reduced the fatigue life of the welds.

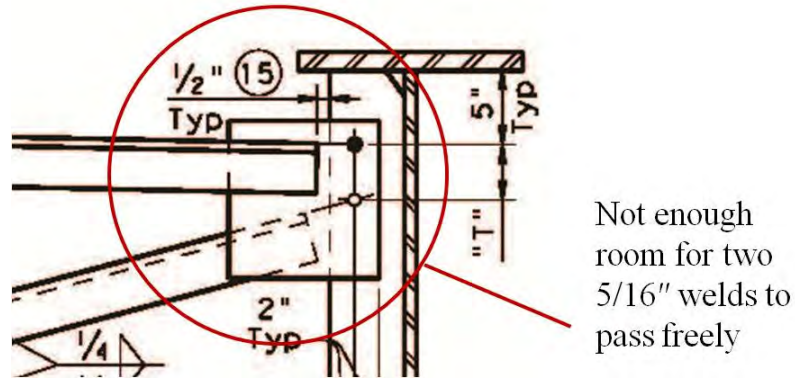


Figure 7.24: Typical TxDOT Spacing between End of Angle and Edge of Stiffener [TxDOT 2010]

The intersecting welds are a direct result of the specified 1/2" spacing between the end of the diagonal and the connection plate edge as shown in Figure 7.24. The fillet dimension of a 5/16" fillet weld used for the angle to gusset plate weld combined with the 5/16" fillet dimension for the gusset to connection plate weld adds up to 5/8" which exceeds the 1/2" spacing and therefore the welds must overlap. It is the recommendation of the researchers to modify this detail immediately to include a larger spacing, as the fatigue behavior is relatively poor, as indicated in Figure 7.25. The details with the overlapping welds had a rating just below E'.

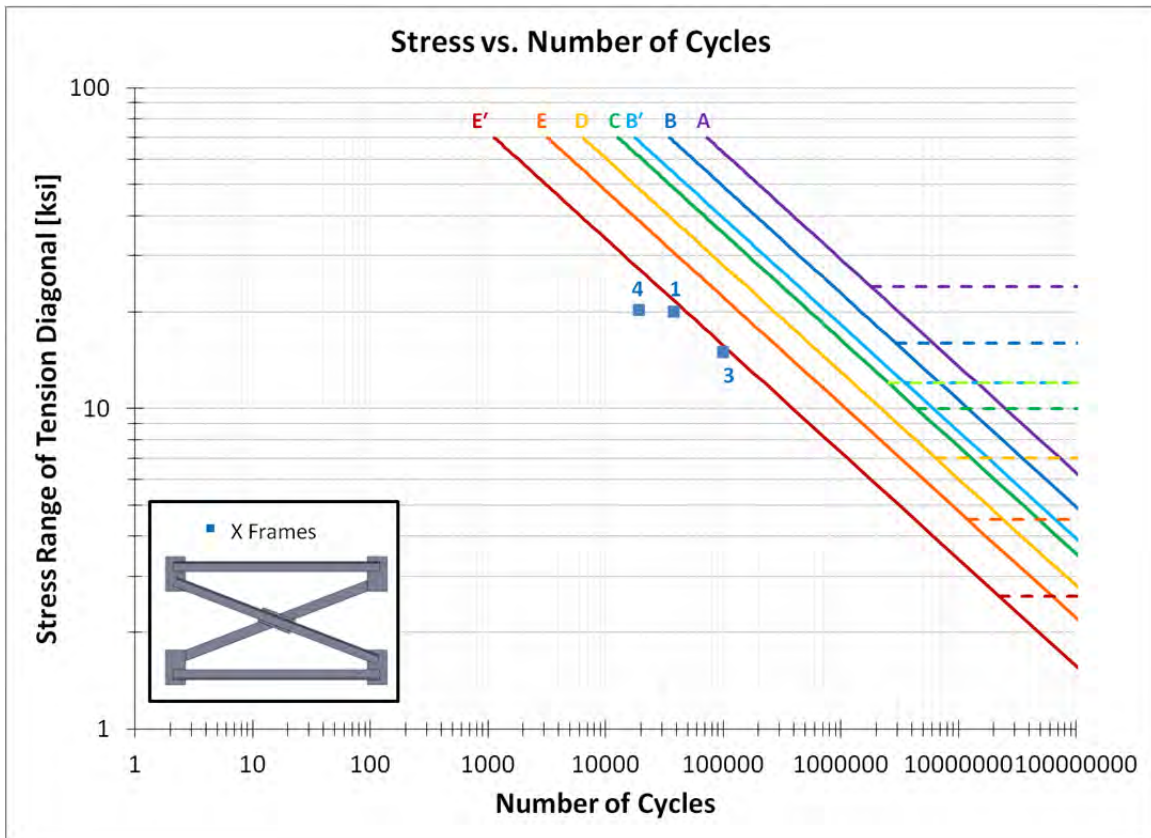


Figure 7.25: Cross Frame Fatigue Results of Specimens XF_1,3,4 with Weld Intersection

7.4.3 X Frame Tests of TxDOT Detail with Tension Diagonal away from Gusset-Stiffener Weld (XF_2,5,8)

Specimens XF_2,5,8 were fabricated with the tension diagonal away from the gusset-stiffener weld to prevent implication of the weld intersection. As the tension/compression diagonal behavior varies depending on location and force placement on the bridge, it was necessary to consider this alternate scenario.

Specimen XF_2 had very good performance, nearly achieving the Category E currently designated in the AASHTO specification [2013]. With the lack of stress concentration at the end weld of the angle-gusset connection as in the other XF tests, these specimens experienced failure at the forward edge of the fillet weld connection propagating into the angle member. This type of failure was consistent with the observations of McDonald and Frank [2009]. An example of a fatigue crack is shown in Figure 7.26.



Figure 7.26: Fatigue Crack at Forward Edge of Fillet Weld into Angle Member (XF_2)

In discussing the X frame detail with fabricators and TxDOT engineers, it was determined an additional transverse fillet weld is sometimes placed along the reverse side of the angle-gusset connection, as indicated in Figure 7.27. This weld is often placed to seal the connection from moisture and prevent/delay corrosion in the connection; however it is not required by the detail specification.

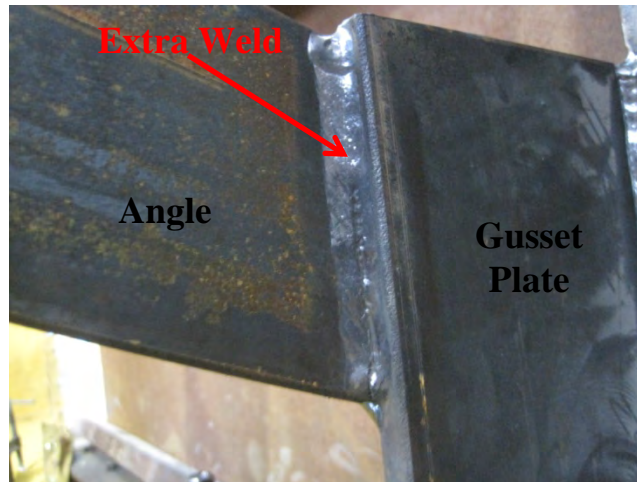


Figure 7.27: Additional Transverse Fillet Weld on Reverse Side of Angle-Gusset Connection (XF_2)

The research team decided to investigate the performance of this connection with and without this detail. Two similar specimens to XF_2 had the same basic geometry, but did not include these welds. Data from the tests indicate the fatigue performance without the weld is worse than when it is included. Both XF_5 and XF_8 failed to achieve category E' at failure due to lack of the weld. As mentioned before, XF_5 was repaired with plates welded to reinforce the cracked portion, so that additional test data could be obtained. The test marked XF_5B corresponds to a second failure in the tension diagonal at the other end of the diagonal from failure XF_5A.

A summary of the test data for this set of specimens is given in Figure 7.28.

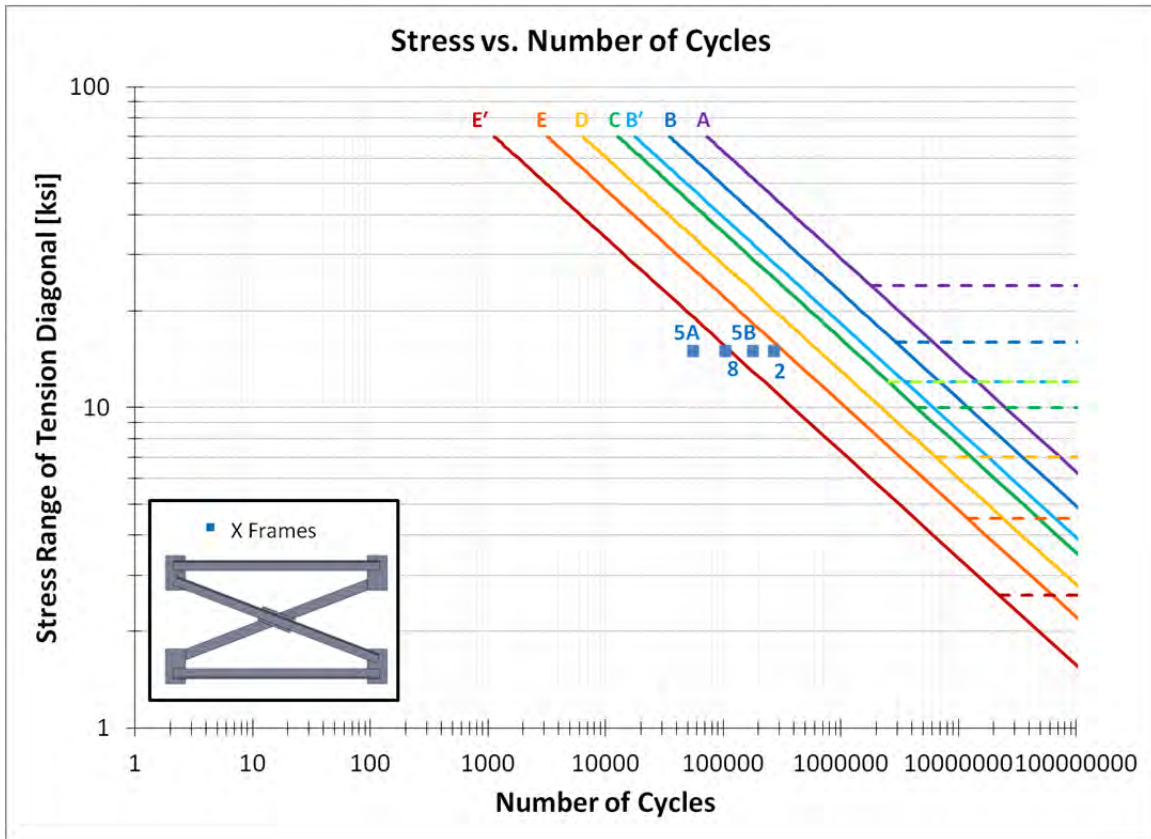


Figure 7.28: Cross Frame Fatigue Results of Specimens XF_2,5,8 with Tension Diagonal away from Gusset-Stiffener Weld; XF_5,8 has No Additional Transverse Weld

7.4.4 X Frame Tests of TxDOT Detail with Increased Spacing between Angle-gusset Weld and Gusset-Stiffener Weld (XF_6,7)

The final series of tests on the X frames with equal leg angles examined the effect of an increased gusset width, which in turn allowed a larger space between the end weld of the angle-gusset connection and the gusset-stiffener weld. Recall the overlap of these welds in XF_1,3,4 led to a significant reductions in the fatigue life.

To determine the spacing, finite element modeling was used to vary the gap until an optimal distance was found. When the angle is placed in tension, a hot spot stress develops in the gusset plate approximately 0.75"-1" away from the gusset toe of the angle-gusset weld as shown in Figure 7.29.

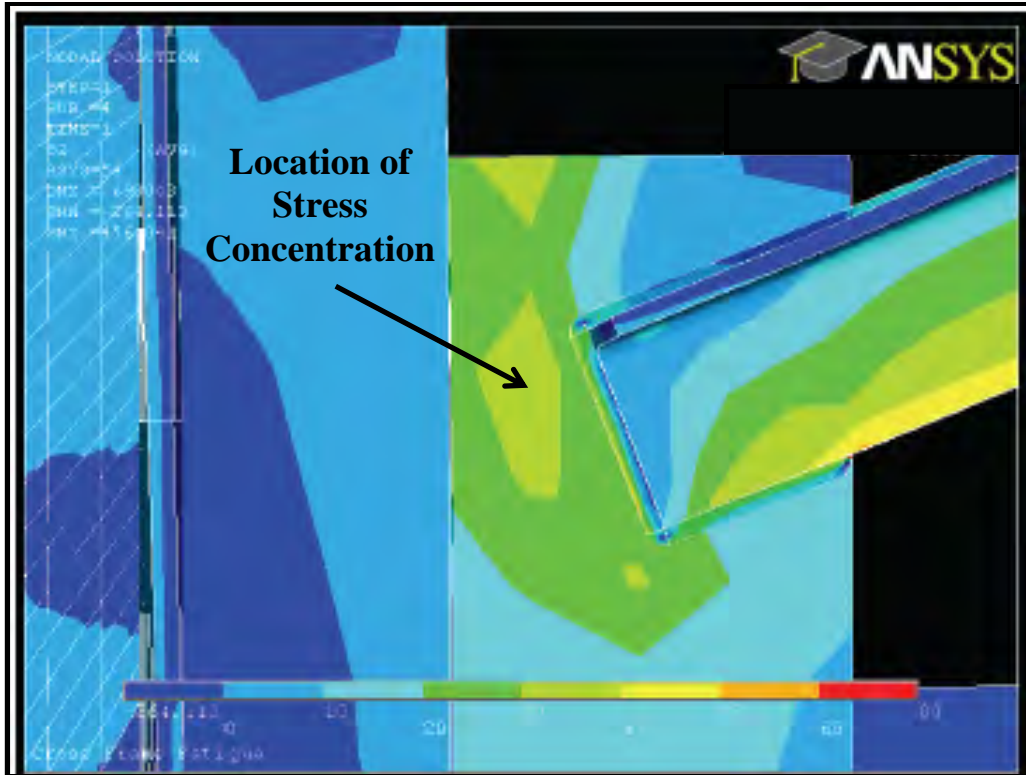


Figure 7.29: Hot Spot Stress in Gusset Plate due to Angle-Gusset Connection

Due to the location of the stress concentration, the distance between the stiffener edge and tension angle was increased from 0.5" to 2.5". The extra spacing allows the highest portion of the stress concentration to be in the gusset plate, instead of at the toe of the gusset-stiffener weld. To keep the details comparable, the gusset plate width was also increased by 2" so the angle overlap remained similar.

The extra spacing substantially increases the fatigue performance, as shown in Figure 7.30 with tests XF_6,7 reaching Category E.

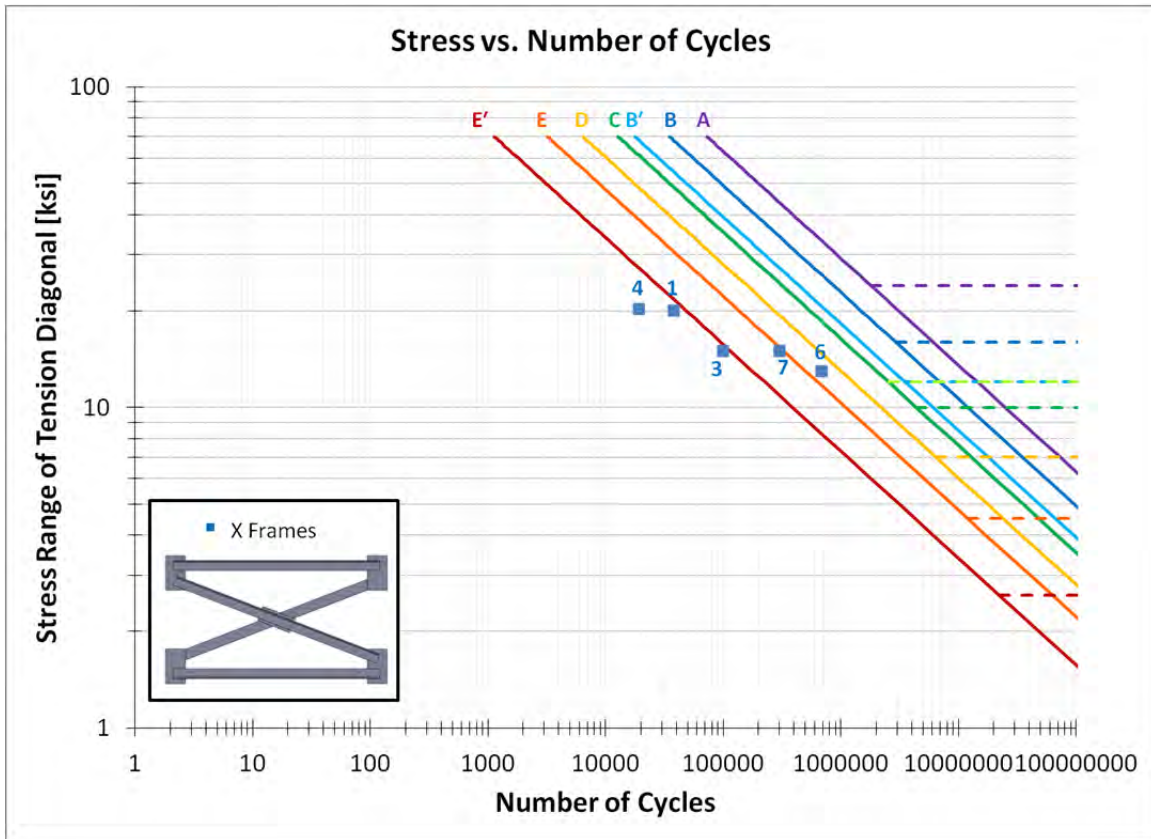


Figure 7.30: Cross Frame Fatigue Results of Specimens XF_6,7 with Increased Weld Spacing (Relative to Typical TxDOT Details in XF_1,3,4)

Although the stress concentration was reduced, failure emanated from the toe of the angle-gusset weld and propagated into the gusset plate. However, the overall performance of these cross frames was superior to the other specimens. A typical failure crack is shown in Figure 7.31.

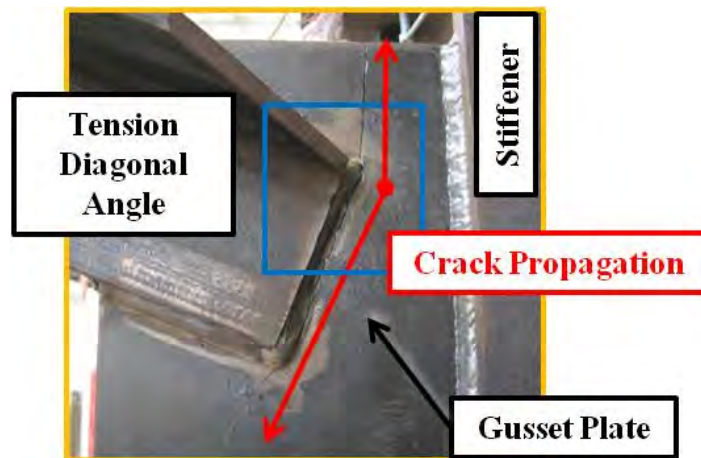


Figure 7.31: Typical Failure Crack in X Frame with Increased Weld Spacing (XF_6)

7.4.5 X Frame Conclusions

The following figure summarizes the cross frame fatigue test data on the series of X frames with equal leg angles.

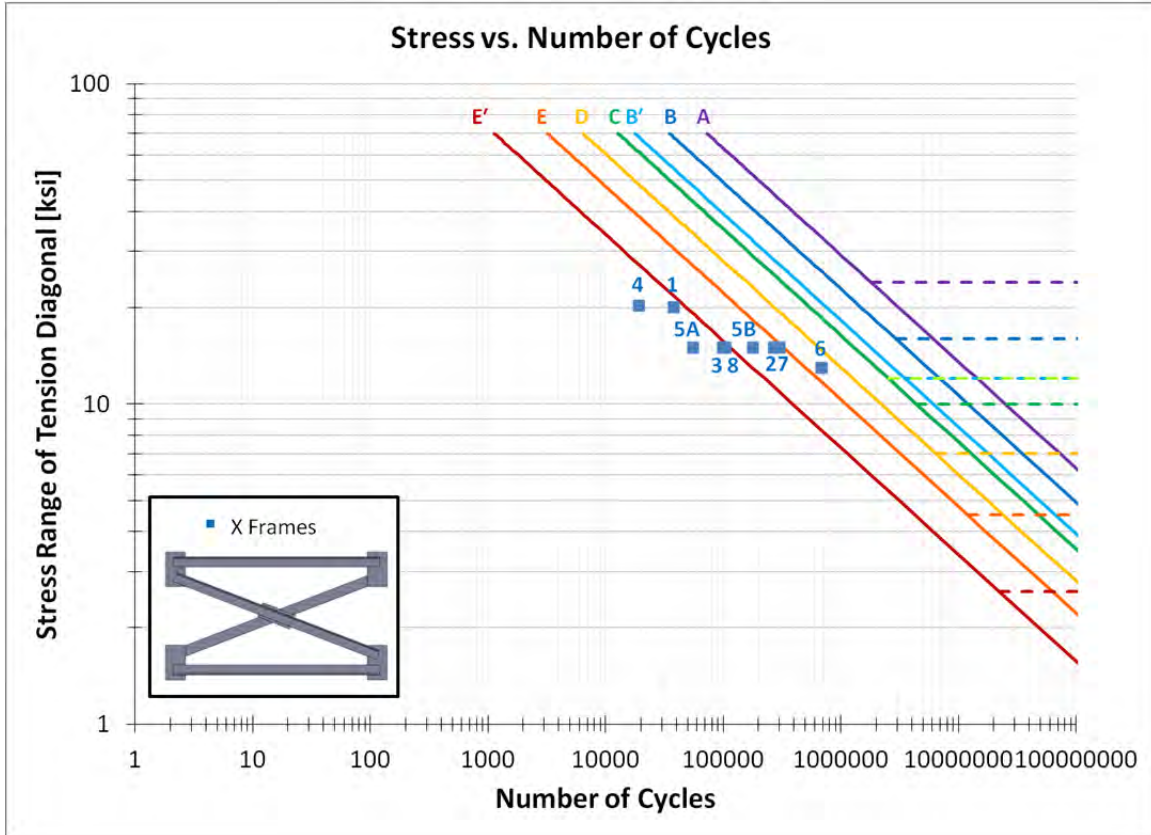


Figure 7.32: Cross Frame Fatigue Results of X Frames with Equal Leg Angles

The testing showed a variety of failure mechanisms. First and foremost, the TxDOT recommendation of 0.5 in between the end of the diagonal member and the stiffener shown in Figure 7.17 leads to poor fatigue behavior. Increasing this spacing to 2.5 in resulted in significant improvement of life. In addition, in cases where the direction of tension in the diagonals is known, such as curved or severely skewed bridges, the angle in tension should be detailed so it attaches to the gusset plates on the same side as the top and bottom struts. Finally, increased fatigue life is obtained by including the additional transverse weld on the reverse side of the angle along the gusset plate edge. Due to the fabrication techniques for X frames, this additional weld will not substantially increase cost.

Part II: X Frames—Unequal Leg Angles

7.5 X Frame—Unequal Leg Angle Design

In addition to the equal leg specimens, 3 specimens with unequal legs were examined using L6x3.5x3/16 members. The primary purpose of investigation was to examine the performance of the unequal leg angle cross frame relative to the equal leg X frames. As

discussed in Chapter 5, the unequal leg X frame provides moderately more stiffness than the equal leg counterpart for the same area of steel. The result is mainly due to the reduced eccentricity of the angle member. With a reduced eccentricity of the unequal leg angle, it is perceived the fatigue performance should be the same as the equal leg angle X frame, if not better.

The typical TxDOT details for X frames were followed for the unequal leg specimens, however, the gusset plate depths were increased to accommodate the wider angle sections. Details on the test specimens are given in Appendix A. The unequal leg angle specimen is shown in Figure 7.33 and a typical test is shown in Figure 7.34.

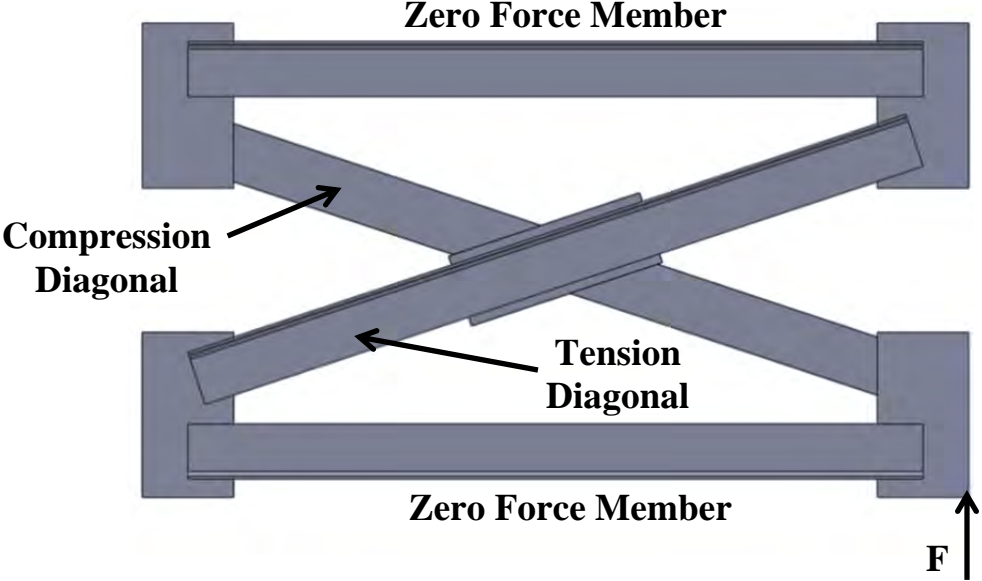


Figure 7.33: Typical Unequal Leg X Frame Specimen with Internal Forces due to Load



Figure 7.34: Typical Unequal Leg X Frame in Test Setup

Similar to the X Frame Equal Leg series, specimens with the tension diagonal on both sides of the gusset plate were considered. The specimens with designation XF_UL_1,2 had the tension diagonal on the side away from the gusset-stiffener weld, while XF_UL_3 had the tension diagonal on the same side as the gusset-stiffener weld. XF_UL_3 also included the increased gusset plate spacing which helped to reduce the stress concentration discussed in XF_6,7.

Typical unequal leg X frame fatigue cracks are shown in the following figures.



Figure 7.35: Typical Unequal Leg X Frame Fatigue Crack (XF_UL_1,2)



Figure 7.36: Typical Unequal Leg X Frame Fatigue Crack (XF_UL_3)

Results from the fatigue tests seem to indicate the reduced eccentricity may lead to formation of the fatigue crack at the forward edge of the fillet weld propagating into the angle member. All three specimens failed in this manner.

Additionally, specimen XF_UL_3 did not have additional transverse welds along the reverse side of the angle at the gusset edge.

The following is a summary of the X frame unequal leg angle fatigue test results.

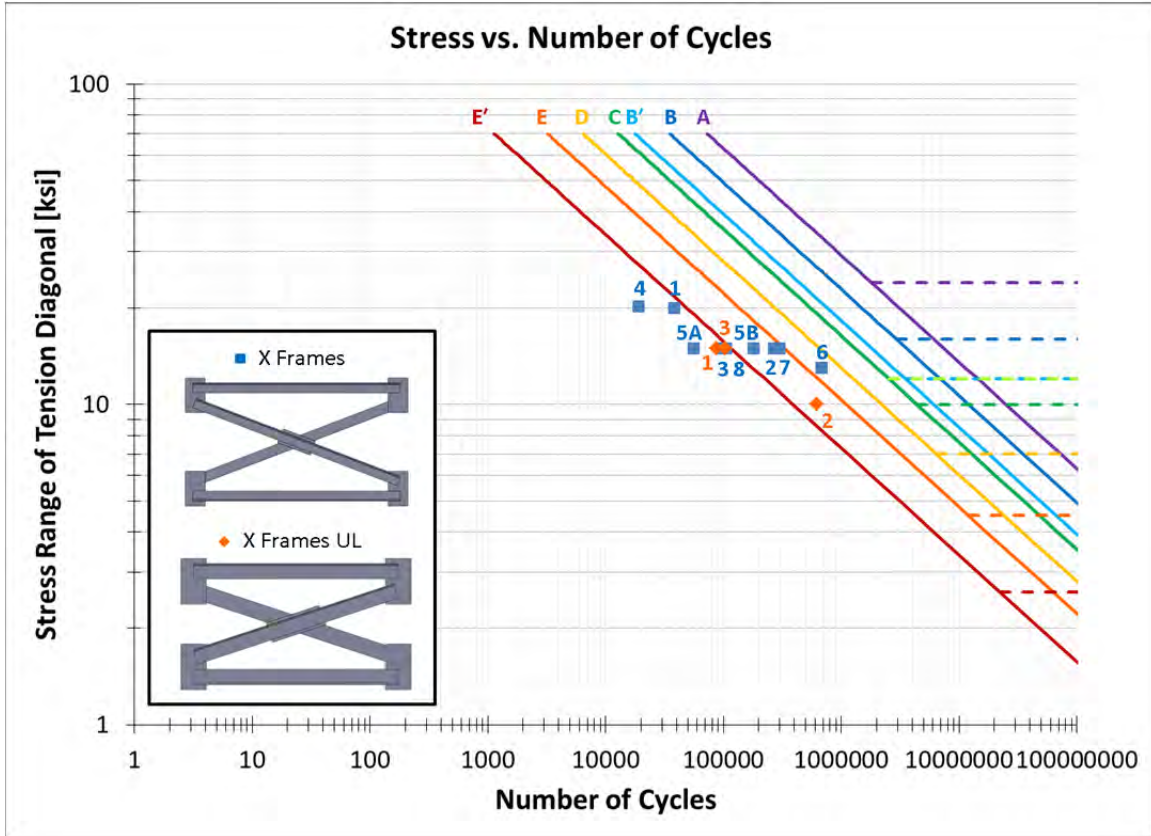


Figure 7.37: Cross Frame Fatigue Results of Unequal Leg Angles

Results from the tests seem to indicate the unequal leg angles provide about the same performance as their equal leg counterparts when similar testing conditions are examined. It is concluded the unequal leg angles may offer a viable alternative to equal leg angles, as their fatigue performance is similar but they have slightly higher cross frame stiffness results.

Part III: K Frames—Equal Leg Angles

7.6 K Frame—Equal Leg Angle Design

K frames were also tested as part of the research program. The K-frames utilized L4x4x3/8 angles and were constructed in accordance with the typical TxDOT standard details [2010]. The following figure indicates the requirements for the K frame geometry.

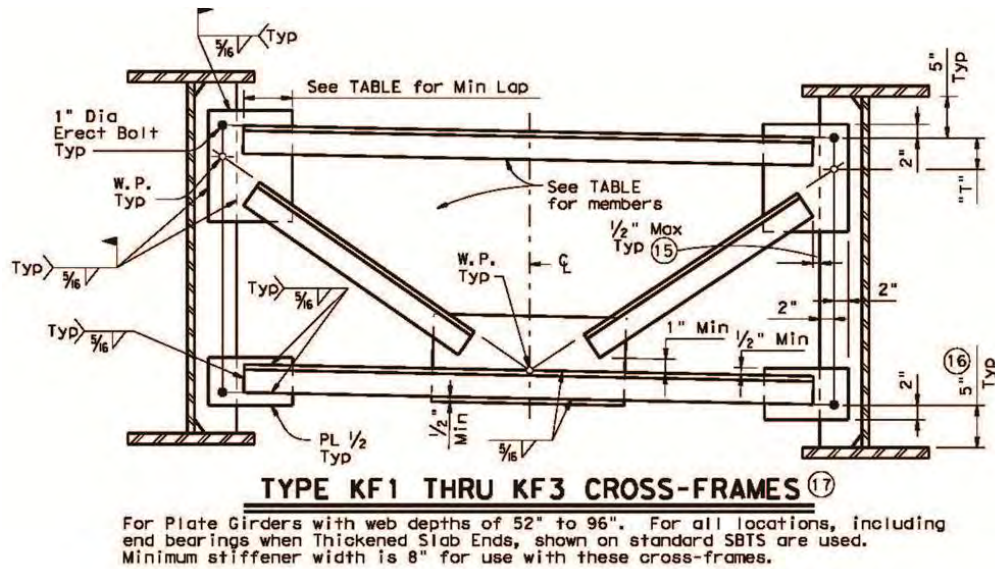


Figure 7.38: TxDOT Standard K Frame Detail [2010]

A typical view of the K frame specimen in the testing frame is shown in Figure 7.39.



Figure 7.39: Typical K Frame Specimen in Test Setup

As with the other tests, the hydraulic actuator raises the outside girder causing a differential vertical displacement between the ends of the cross frame. The cyclic load induces tension in one diagonal and compression in the other (see Figure 7.40). The axial forces in the diagonals and struts were monitored using strain gages and the load range set to achieve the desired stress range.

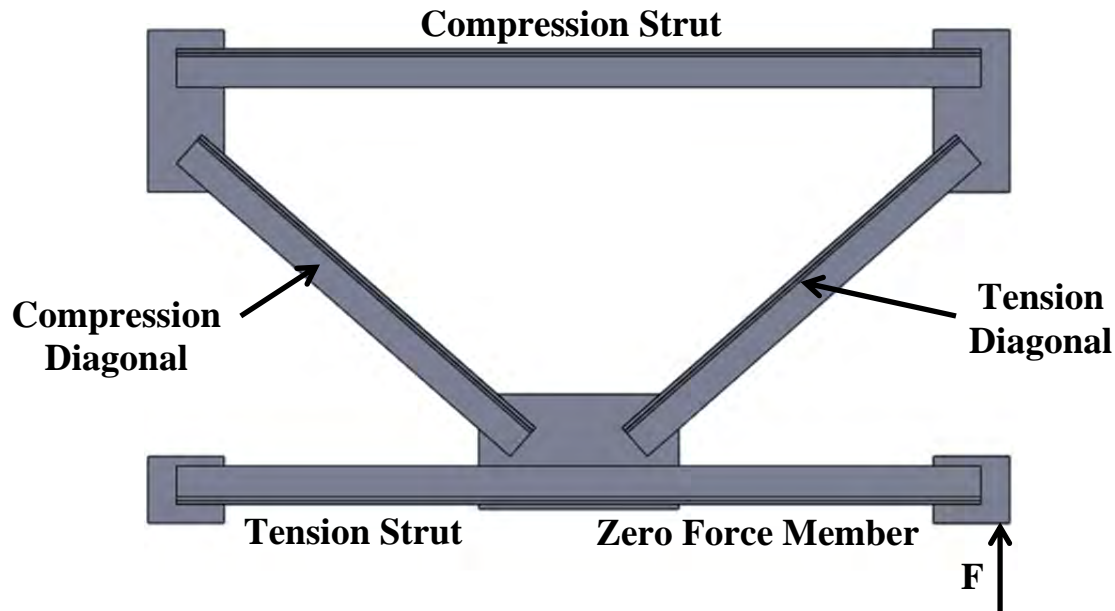


Figure 7.40: Typical K Frame Internal Forces from Load Applied

7.6.1 K Frame Test Variables

A total of 5 K frames with L4x4x3/8 equal leg angles were tested in fatigue with varying geometries. Two additional tests were performed on the K frame which included an L4x4x3/4 angle for a strut and an increased thickness of plate for the center gusset plate connection. The complete details of each test are summarized in Appendix A.

The 7 tests performed on K frames are divided into three groups of test parameters. First, the tests most similar to the TxDOT detail are assessed. These correspond to specimens KF_2,3,4 and used equal leg L4x4x3/8 members.

Secondly, tests were run on K frames whose orientation was rotated 180 degrees (flipped vertically to change the orientation of the diagonals) from the TxDOT standard, corresponding to specimens KF_1,5. These tests incorporated the same basic geometry as KF_2,3,4 with the L4x4x3/8 members.

Lastly, tests were performed on K frames whose members were increased to L4x4x3/4 members and the center gusset plate thickness was increased from 0.5" to 0.75". The reasoning behind these changes is examined, as well as the difference in fatigue performance.

Similar to the X frames, tests were performed with and without a transverse weld on the reverse side of the angle connecting the angle to the gusset plate edge. The necessity of the backside weld is very important from a fabrication standpoint. If the weld can be omitted, the ease of fabrication is dramatically improved since the K-frame can be fabricated without the necessity of flipping the cross frame.

7.6.2 K Frame Tests of Current TxDOT Detail (KF_2,3,4)

Specimens KF_2,3,4 were fabricated following details most similar to the current TxDOT detail. The cross frame members were welded to the gusset plates, and the cross frame system was then welded into the test frame.

The primary cause of fatigue in cross frames is from the differential deflection of adjacent girders due to truck traffic passing over the girders. The loading that was used was the same as in the previously discussed tests with the outside girder deflected upwards. In order for the tests to be comparable to the TxDOT detail shown in Figure 7.38, the orientation of the cross frames had to be rotated to match the loading, as shown in Figure 7.41.

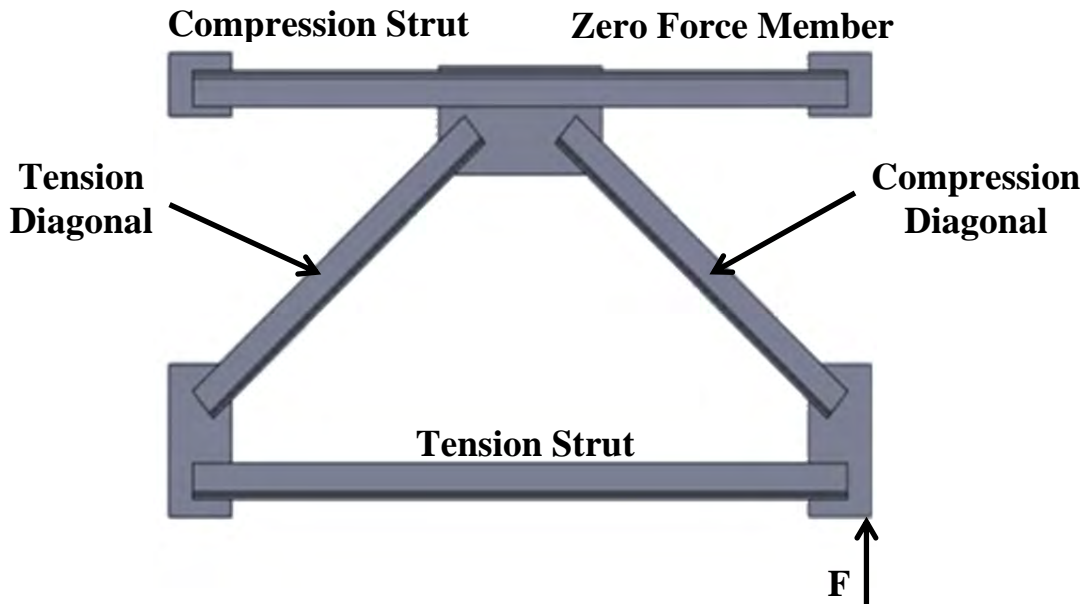


Figure 7.41: K Frame Orientation in Test Setup as given by TxDOT Detail (KF_2,3,4)

One potential concern in flipping the cross frame was the positioning of the steel deck girders (which simulate the concrete deck), relative to the struts. Using the finite element model of the test specimen, axial forces were measured for the struts with the load applied upward (as in the lab tests) and downward (as in typical bridge loading). The change in axial force was deemed minimal, and there was virtually no difference in the subsequent magnitude of deflection.

Finally, it is important to note the axial forces labeled in Figure 7.41 are those based on a simplistic truss analysis of the cross frame. Measured forces, along with finite element models, indicated the “zero force member” in fact had substantial stress at the connections and in specimens KF_2,3,4 was the first location to fail. An example of a fatigue crack at this location is shown in Figure 7.42.

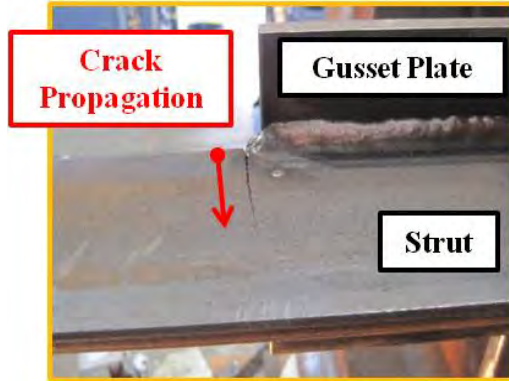


Figure 7.42: K Frame with Fatigue Crack in Strut (KF_2)

In order to consider why the K frames failed at this location, it is necessary to examine the main mode in which forces are induced in the cross frame. As previously stated, differential deflection of the cross frame leads to fatigue of the brace. If the cross frame shown in Figure 7.41 undergoes a displacement, rather than an applied force, the struts must rotate to accommodate the movement. In a true truss analysis, the “zero force member” labeled in the figure would simply undergo rigid body rotation and would not pick up force. However, since the angle-gusset welds are not perfect hinges and develop some moment in the connection, the strut undergoes double curvature bending, similar to a beam. This bending of the member caused stress/strain, which is what the strain gages measured. The stress due to the bending led to a stress concentration that eventually resulted in a fatigue crack.

In order to gain further information on the fatigue behavior of the axially loaded angle members (the diagonals), the aforementioned fatigue crack was often repaired to permit additional testing. An example of the repair is shown in Figure 7.43.

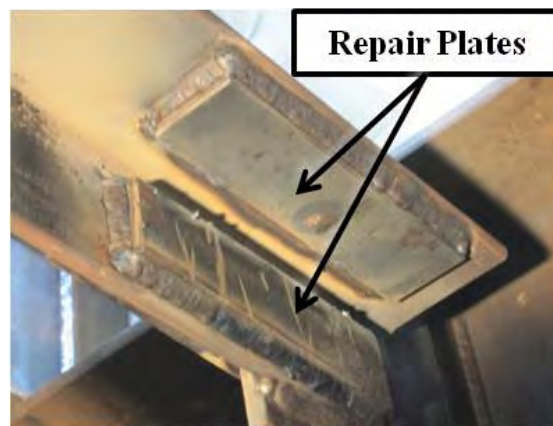


Figure 7.43: K Frame Fatigue Crack Repair in Strut (KF_2)

Once repaired, the cross frames continued to cycle until failure occurred in the tension diagonal, as seen in Figure 7.44.



Figure 7.44: K Frame Fatigue Crack in Tension Diagonal (KF_2)

The results from the fatigue tests indicate the current TxDOT K frame detail to be between the AASHTO Category E' and E details (see Figure 7.45). Due to the relatively low stress range in the struts, the failure due to the bending stresses significantly decreased the life (Failure A). Once repaired, the failure in the angle members (Failure B) behaved similar to the predicted behavior of McDonald and Frank [2009] as well as the behavior seen in X frame specimens XF_2,5,8. In fact, the K frame angles provide better performance than the X frames if there was a mechanism to ensure failure in the diagonals.

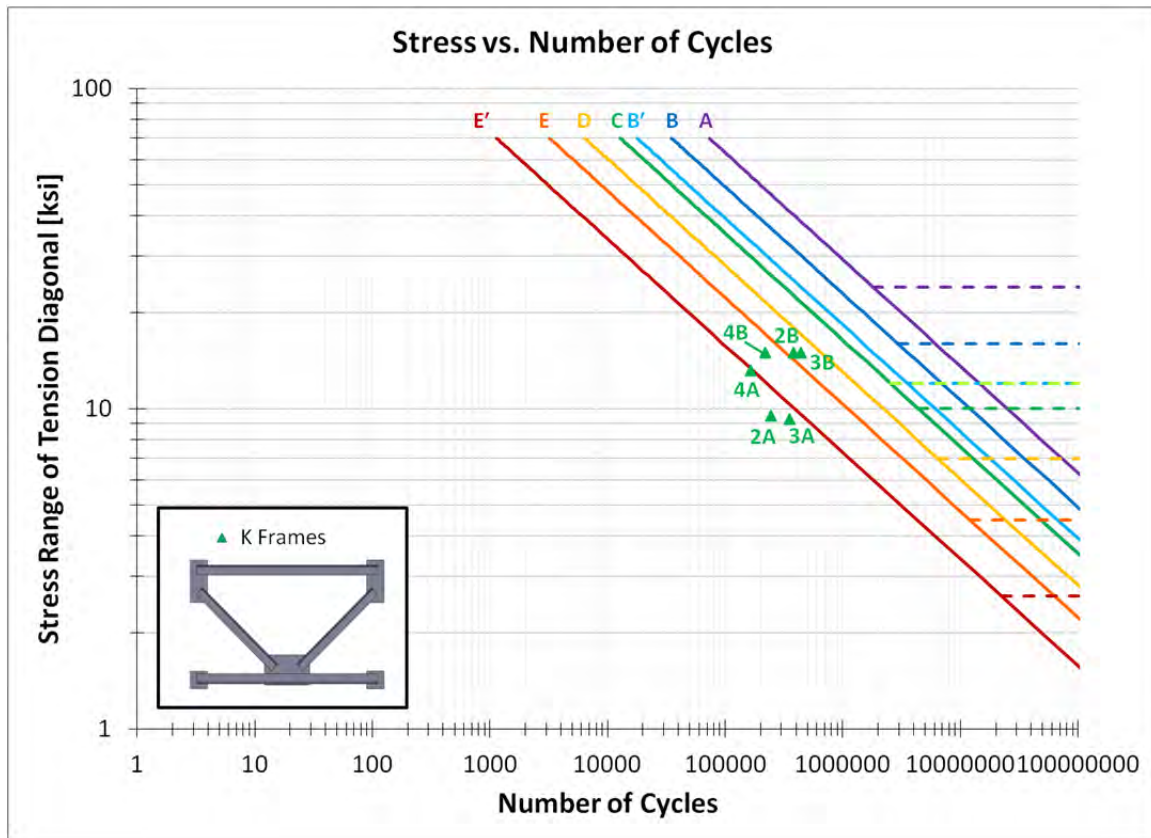


Figure 7.45: Cross Frame Fatigue Results of Specimens KF_2,3,4

Finally, it is noted that specimens KF_3,4 did not include the an additional transverse weld on the reverse side of the angle member along the gusset edge (see Figure 7.46). Based on the results from these fatigue tests (and on specimens KF_5,6,7), it is believed there is no correlation between fatigue life and the presence of the backside weld in K frames. It is recommended for design these welds be optional, especially due to the advantage for fabrication. Unlike the X frame, all the members of the K frame are on one side of the gusset plate. This allows for more rapid fit-up of the cross frame, as well as welding, since the cross frame does not need to be flipped during fabrication. The reduced handling requirements can lead to improved economy in the fabrication process.

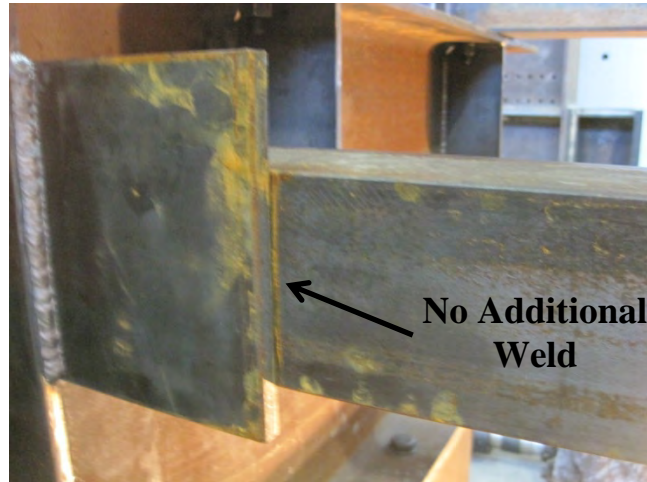


Figure 7.46: Absence of Additional Transverse Weld on Reverse Side of Angle

Finally, one additional observation was taken from this series of tests. The current typical detail shown in Figure 7.38 has the outstanding leg of both struts on the same side (see figure below). The orientation for the bottom strut as shown was used in KF_4, while KF_2,3 had the outstanding legs symmetrical as shown in Figure 7.40.

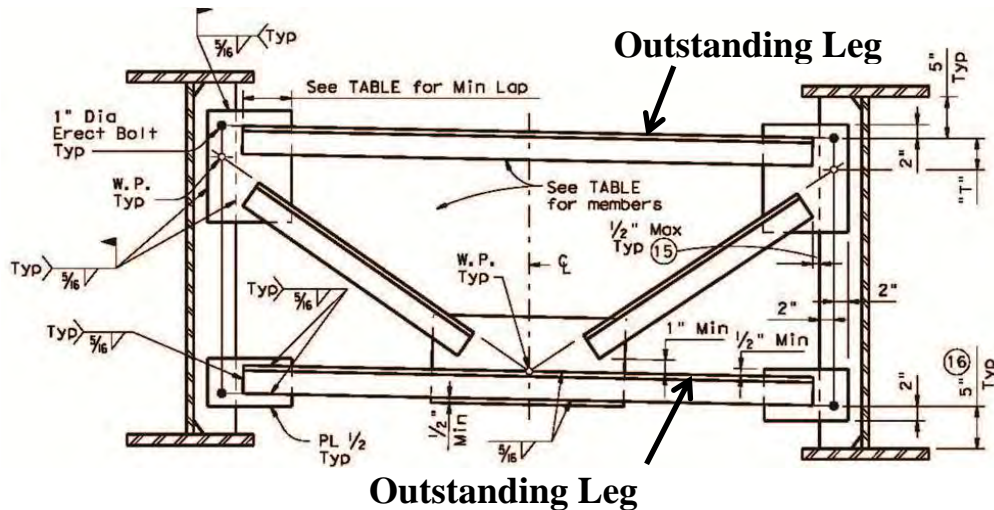


Figure 7.47: TxDOT Standard K Frame Detail with Strut Orientation Indicated [2010]

As seen in the test data of Figure 7.45 and confirmed by subsequent FEA, the TxDOT typical orientation increases the amount of bending stress at the connection of the strut, and leading to a reduced amount of cycles to failure. Therefore, it is recommended to flip the bottom strut to have the outstanding leg on the bottom of the K-frame.

7.6.3 K Frame Tests of TxDOT Detail Rotated 180 Degrees (KF_1,5)

Specimens KF_1,5 were fabricated with the same geometry as KF_2,3,4 but were positioned in the test frame upside down relative to the location of the applied load as seen in Figure 7.48. Often in construction, the K frames are installed in both orientations. In terms of cross frame stiffness, both orientations provide the same torsional restraint. Therefore, the researchers wanted to determine the most advantageous arrangement of the brace.

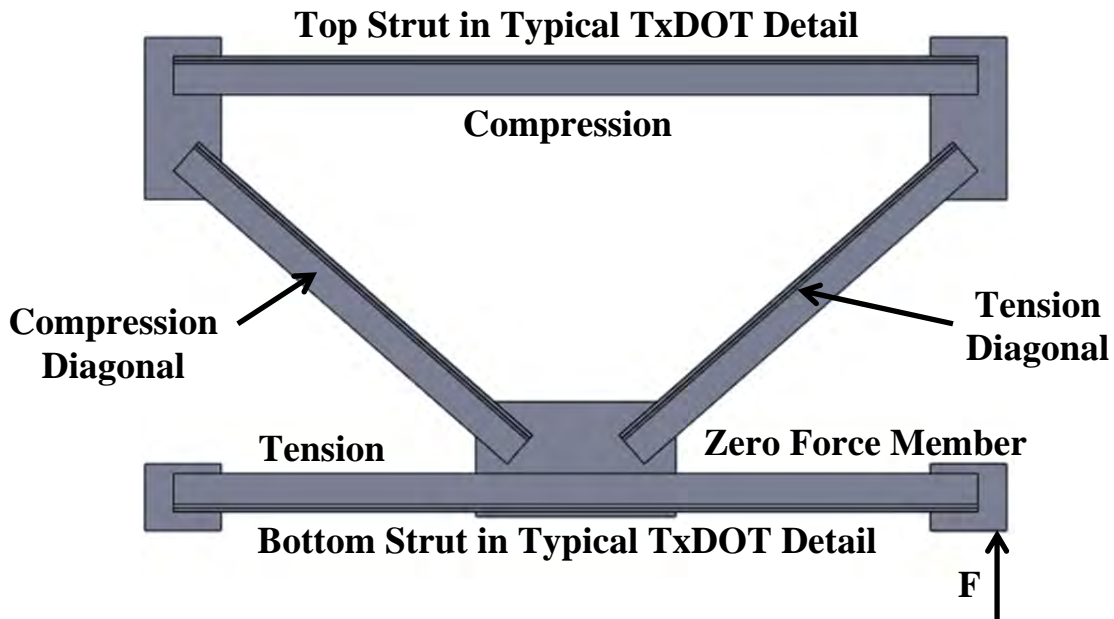


Figure 7.48: Cross Frame Orientation of KF_1,5

Following the aforementioned truss analogy, the expected failure location would be expected in either the tension diagonal or the tension portion of the bottom strut. Monitoring the stress in the cross frame members showed the tension strut to have nearly the same axial force as the diagonal, partially due to the vertical bending deformation at the connection. The results of two tests are shown in Figure 7.49 and an example of the crack forming in the tension strut is shown in Figure 7.50.

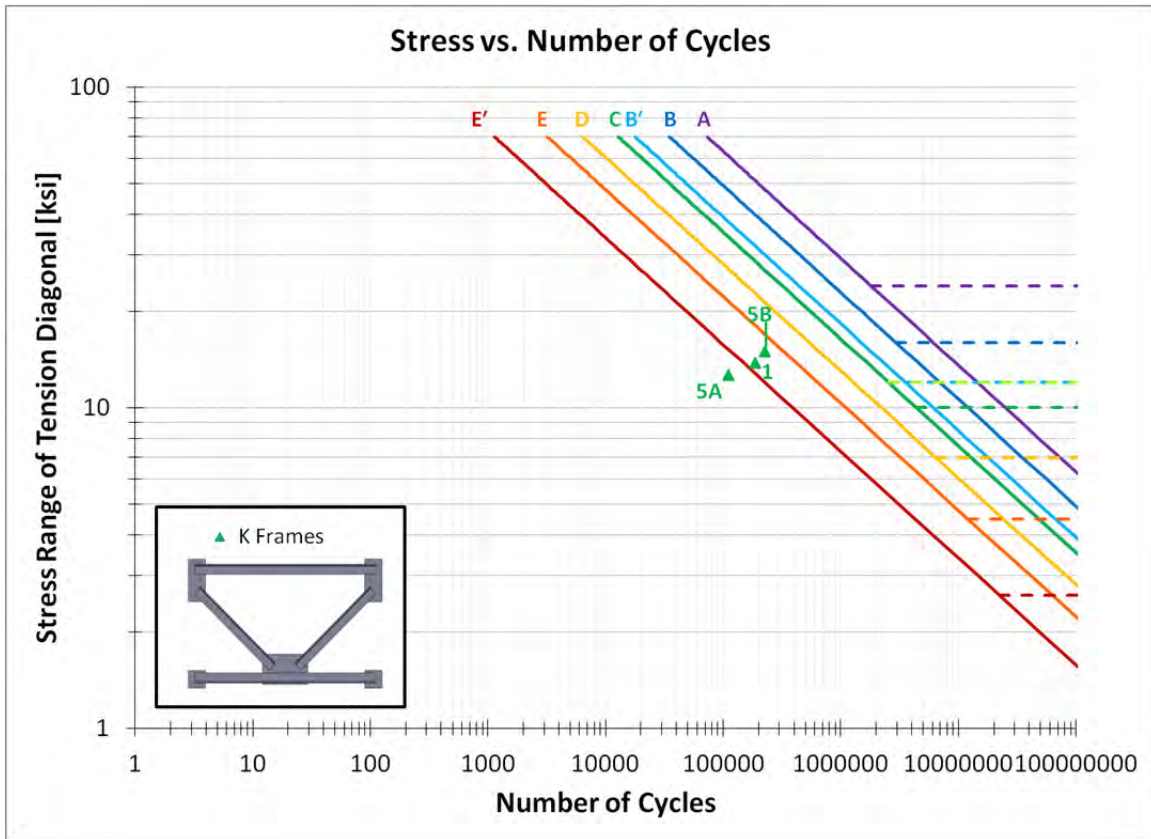


Figure 7.49: Cross Frame Fatigue Results of Specimens KF_1,5



Figure 7.50: Crack in Tension Strut (KF_1)

When compared to the normal orientation of the K Frame in the previous section, the fatigue performance of the rotated specimens is inferior to the former. Therefore, the orientation shown in the typical TxDOT Standard Details provides longer fatigue life for this type of brace.

7.6.4 K Frame Tests with L4x4x3/4 Strut (KF_6,7)

As noted earlier, the failure of many of the cross frames consisted of cracking in the top strut (in the flipped orientation) of the strut due to excessive bending of the angle members. In many instances the crack was repaired so that the test could be extended to look at the behavior of other components of the cross frame. These tests are labeled with the “A” and the “B” to denote a cross frame in which the initial crack was repaired. The research team wanted to try to avoid the cracking problem in the struts and therefore the final series of tests on the K frames involved using a larger, stiffer strut to decrease the bending stress in the member and a thicker center gusset plate. The purpose of these modifications was to extend the life of the cross frame by eliminating failure in the gusset plates and struts, so the K frame would fail by fatigue in the diagonal members. The preferred mode of failure is a fatigue crack at the forward edge of the fillet weld, propagating into the angle as discussed in the X frame test series. This failure mode correlates with the results published by McDonald and Frank [2009] and subsequently referenced in the AASHTO Specification [2013].

The primary geometry remained the same as KF_2,3,4, but with the modifications indicated by the following figure.

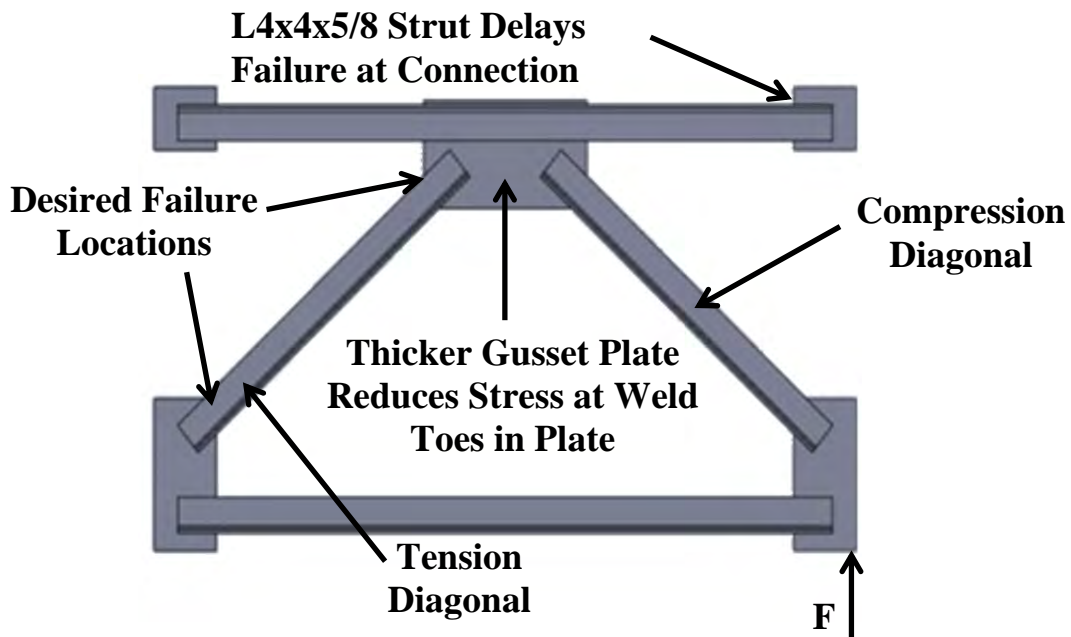


Figure 7.51: K Frame Specimen Details (KF_6,7)

The tests showed these modifications to improve the fatigue behavior of the K frame, with the result of cracking in the tension diagonal member. Results for KF_6,7 are plotted with the other data for comparison in Figure 7.52 and an example of the fatigue crack at failure is shown in Figure 7.53.

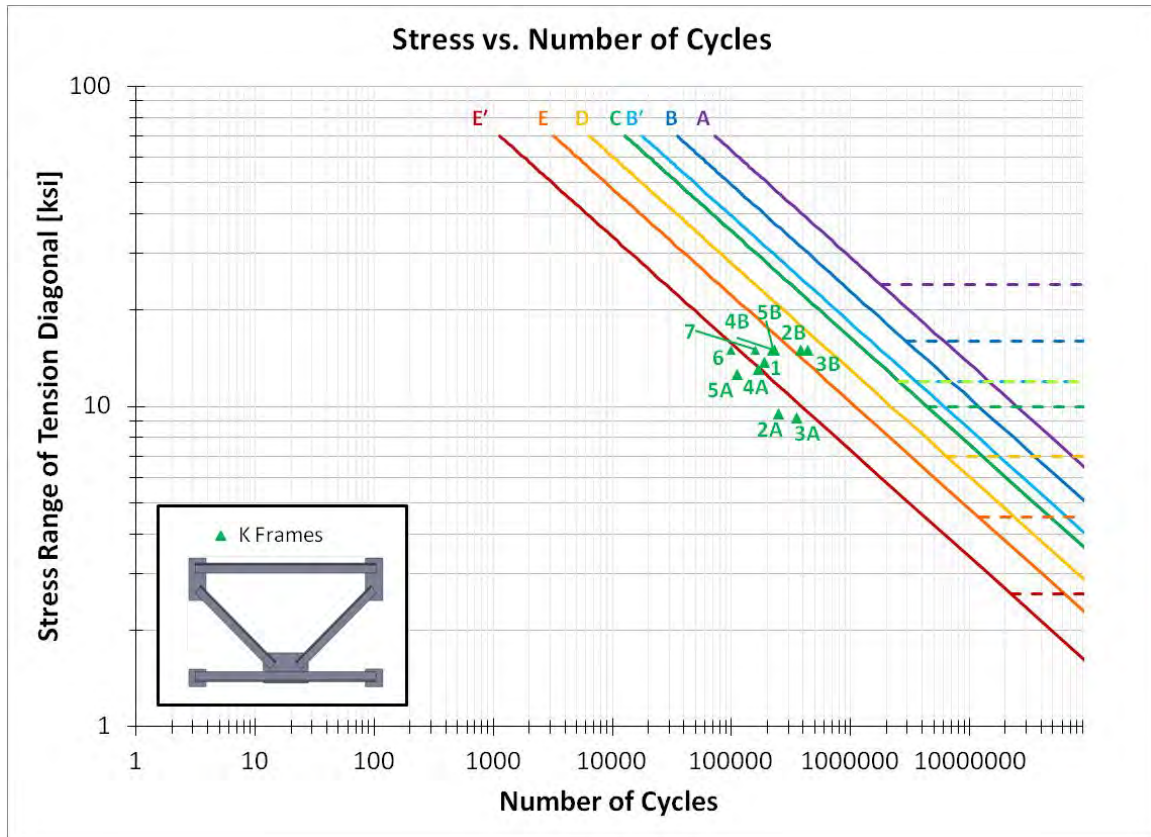


Figure 7.52: Cross Frame Fatigue Results of K Frame Specimens



Figure 7.53: Fatigue Crack in Tension Diagonal (KF_7)

7.6.5 K Frame Conclusions

Figure 7.52 summarizes the results for the K frame tests. The testing showed two primary failure mechanisms: bending of the struts leading to relatively low fatigue life and failure in the tension diagonal, either at the forward edge of the fillet weld connection propagating into the

angle member, or at the back weld of the connection propagating into the plate as seen in the X Frame series of tests.

It is concluded the current orientation of the TxDOT Standard Detail offers the highest fatigue performance, and the following modifications can be made to increase fatigue life:

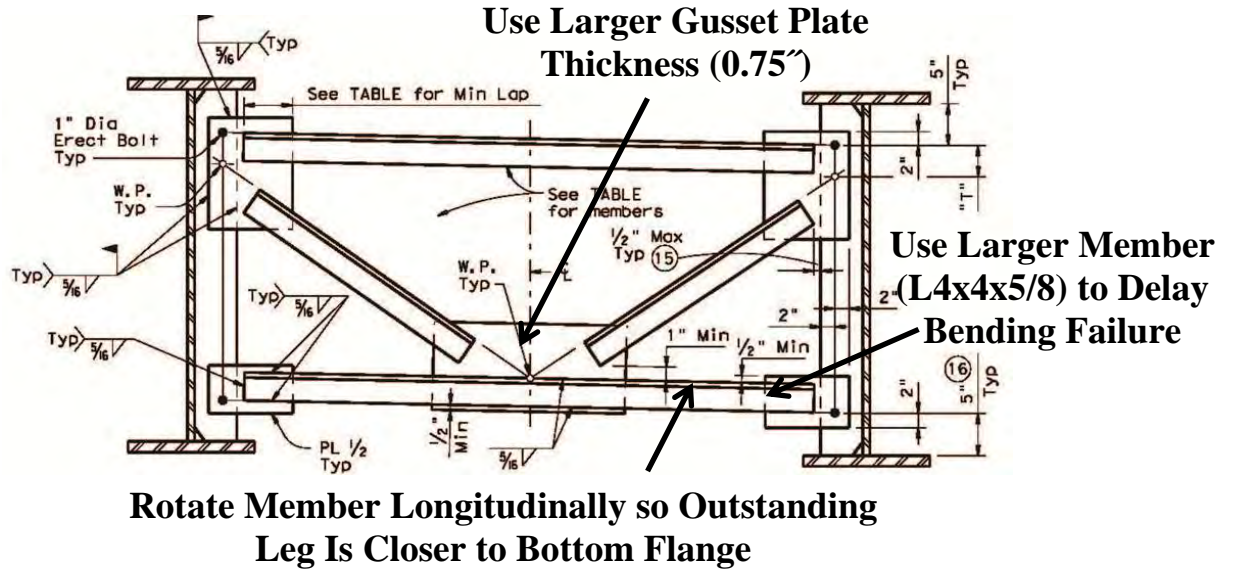


Figure 7.54: Suggested Improvements to TxDOT Standard K Frame Detail

Additionally, it is noted the extra transverse weld on the reverse side of the angles does not have a correlation to fatigue life based on the tests conducted herein; therefore, for ease of fabrication, these welds should not be required.

In terms of stiffness, K frames generally offer lower stiffness than X frames for typical girder spacings and girder depths (except for shallow, wide cross frames). However, if the stiffness calculated is still adequate for a given bridge design, then K frames would be preferred due to the more simple fabrication that does not require flipping of the cross frame. The following graph compares the stiffness ratio of X frames to K frames for various inclinations (degrees) for the diagonal (based on the X frame). Results are shown for several different angle sizes.

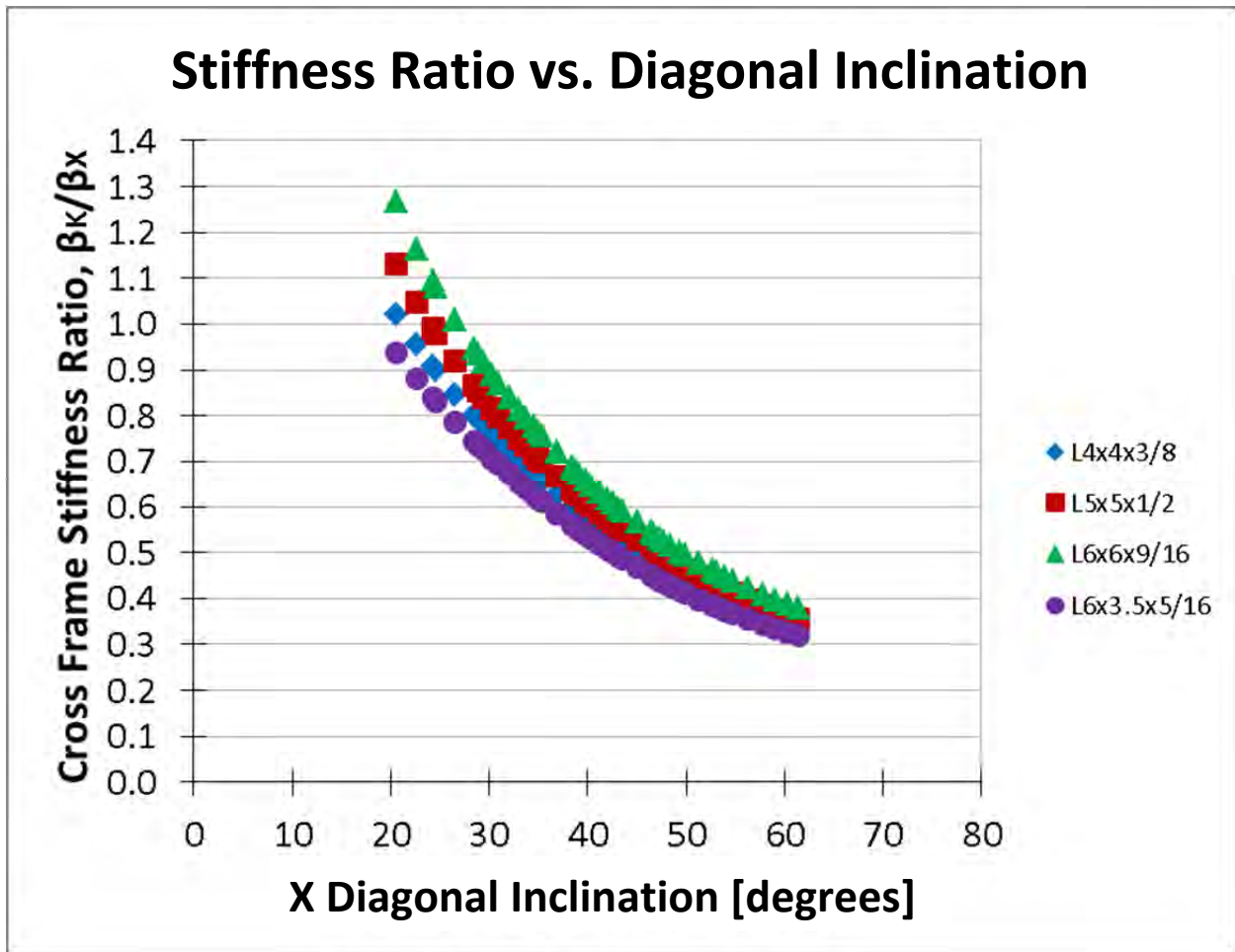


Figure 7.55: X Frame to K Frame Comparison for Different Geometries and Cross Sections

Part IV: Z Frames—HSS Tubes

7.7 Z Frame—HSS Tube Design

Based on the results from the small scale experiments, Z frames were also further investigated to examine their fatigue behavior. The first series of Z-frames utilized HSS 5x5x3/8 square tubes with knife plate connections. A second size diagonal was used in the final test with the HSS section to investigate the impact of the member proportions on the fatigue behavior. The following figures show the specimen in the setup and internal forces generated by the applied loading.



Figure 7.56: Z Frame HSS Specimen in Fatigue Test Setup

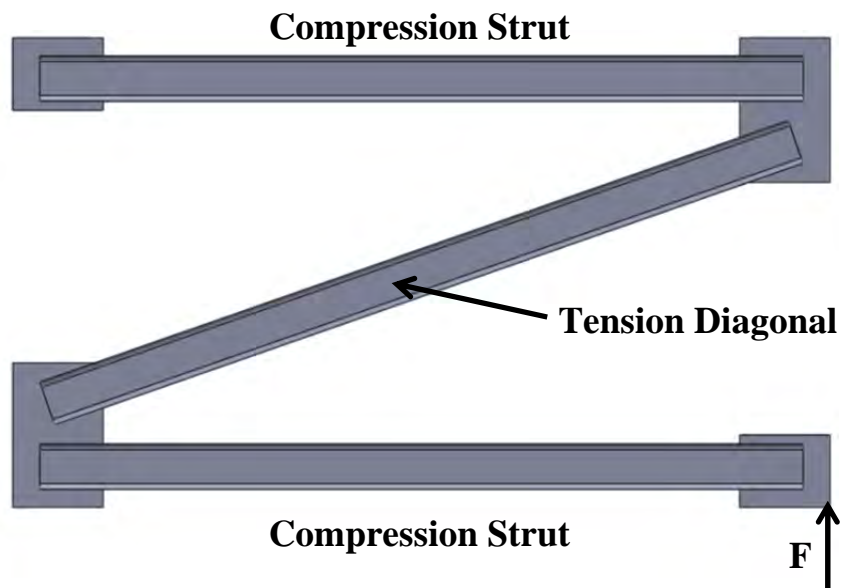


Figure 7.57: Z Frame HSS Internal Forces due to Fatigue Test Loading

7.7.1 Z Frame HSS Test Variables

A total of 4 Z frames with HSS members were tested in fatigue. The geometry of the specimens was adapted from the TxDOT Standard Details for X frames, using the width of the HSS tubes to size the gusset plate widths and depths.

The first three tests utilized HSS5x5x3/8 members connected to the gusset plates using the knife plate detail. The same size tube was studied in the small scale laboratory experiments and showed a promising Category E or better detail in axial fatigue. These specimens are noted as ZF_HSS_1,2,3.

A fourth test was conducted near the termination of the project using a rectangular HSS6x3x5/16 to better compare to the stiffness of the angle cross frames, and to examine the effect of the height of the tube.

7.7.2 Z Frame Tests using HSS5x5x3/8 Members (ZF_HSS_1,2,3)

As discussed in Chapters 2 and 4, the HSS5x5x3/8 member was chosen as an equivalent size tube to provide a similar capacity in compression as an L4x4x3/8 angle in tension.

To help alleviate stress concentrations at the forward toe of the fillet weld, a stress relief hole was included on specimens ZF_HSS_1,2. While this technique showed promise in improving the fatigue life of the axial specimens, it was readily apparent to the researchers that construction of this detail in cross frames would be difficult. During fabrication, it was difficult to precisely locate the drilled hole to provide the stress shadowing effect and to fit it up with the gusset plates accordingly.

The third specimen did not contain the stress relief hole, and provided similar performance to the other specimens. In addition, this specimen was fabricated using a plasma torch rather than a band saw to cut the slots. From the test results, no difference in fatigue behavior is noted.

The following figures show typical cracks in the HSS square members.



Figure 7.58: Typical Z Frame HSS Fatigue Crack (ZF_HSS_2)



Figure 7.59: Typical Z Frame HSS Fatigue Crack (ZF_HSS_3)

The typical mode of failure was the introduction to cracks at the tube toe of the forward edge of the fillet weld propagating into the tube. Additionally, cracks may have initiated at the critical stress point on the circular stress relief hole, or at material notches in the plasma cut slot. These failures were consistent with the small scale fatigue tests. Once fatigue cracking had initiated, some specimens developed cracks through the throat of the fillet weld, typically only after the primary cracks had become quite large.

The results from the fatigue tests are given in Figure 7.60.

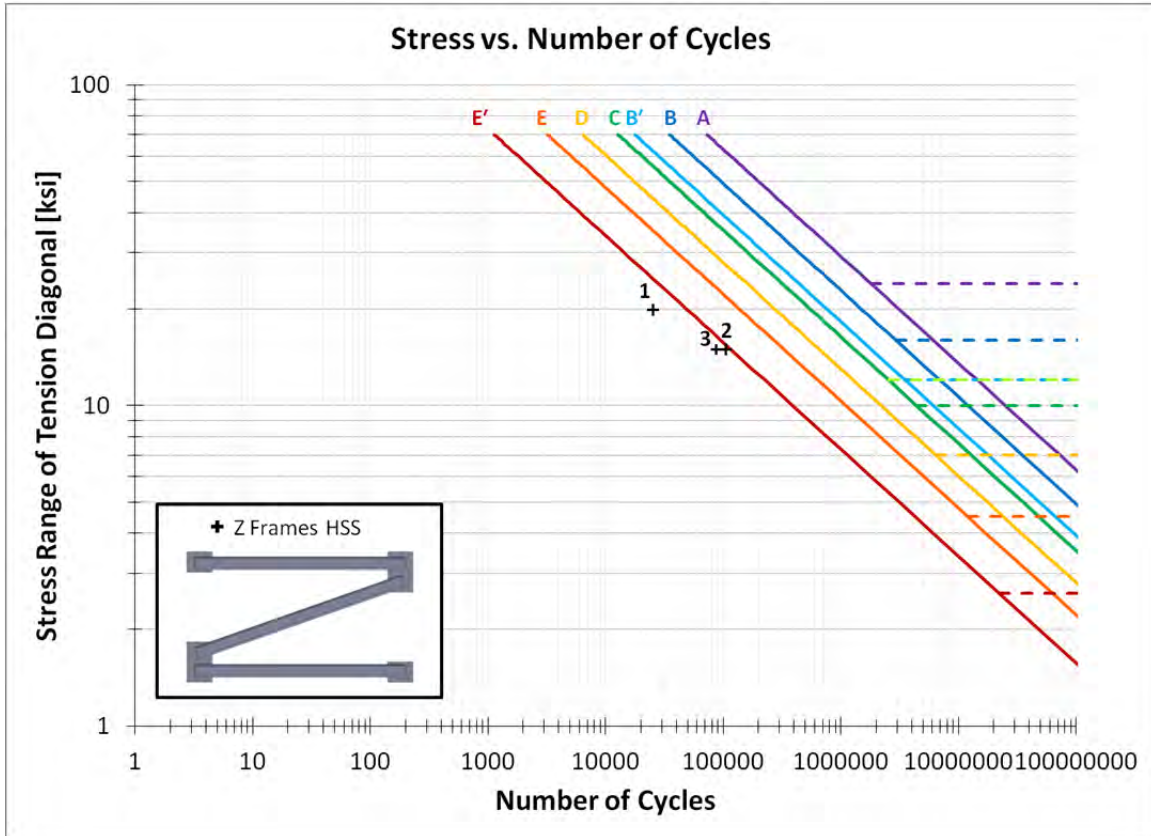


Figure 7.60: Cross Frame Fatigue Results of Specimens ZF_HSS_1,2,3

From the test data, it is seen the HSS tube specimens failed at a stress state corresponding to less than a Category E' detail using the AASHTO Specification. This result was surprising considering the superior performance determined by the small scale laboratory tests and underscored the importance of full scale testing. Based upon the small scale component tests, the Z-frame with the HSS sections would have been the top recommendation based upon fatigue performance. However, the full scale tests demonstrated shortcomings in some HSS sections for application in cross frames bracing.

Upon further investigation, it was determined, that like the K frames, the singular diagonal in tension is subjected to a substantial amount of bending due to the fixity of the connections and the applied vertical load. To determine the magnitude, specimen ZF_HSS_2 was instrumented with strain gages at the quarter points of the tube (rather than mid-length as done in ZF_HSS_1). The stress on the top face of the tube was nearly 2.0 times the average stress of the member. This correlates to a significant increase in stress concentration at the connection (see Figure 7.61).

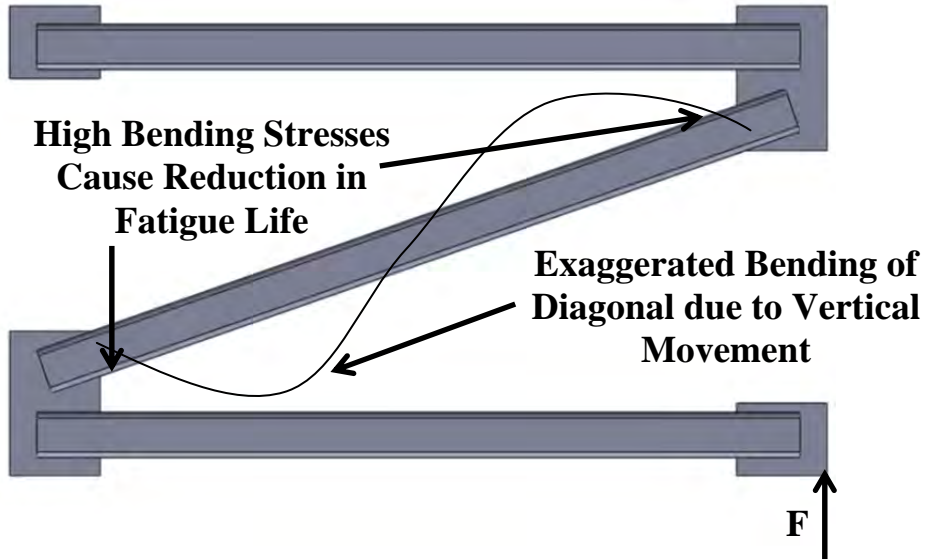


Figure 7.61: Large Bending Stress Causes Loss of Fatigue Life in Z Frames

7.7.3 Z Frame Tests using HSS6x3x5/16 Members (ZF_HSS_4)

Since the bending stress is proportional to the distance from the centroid, it was theorized that a rectangular tube, with the short width in the vertical direction, would help to lower the bending stress and improve fatigue performance. The following figures show the specimen in the test setup along with examples of fatigue cracks.



Figure 7.62: Rectangular HSS Z Frame in Test Setup



Figure 7.63: Example of Fatigue Crack (ZF_HSS_4)

The result from this test showed the rectangular HSS tube significantly improved the fatigue life to Category E. The stress increase due to bending of the tube was reduced from 2.0 times to 1.6 times. Figure 7.64 shows the fatigue test results for all the Z frame HSS specimens.

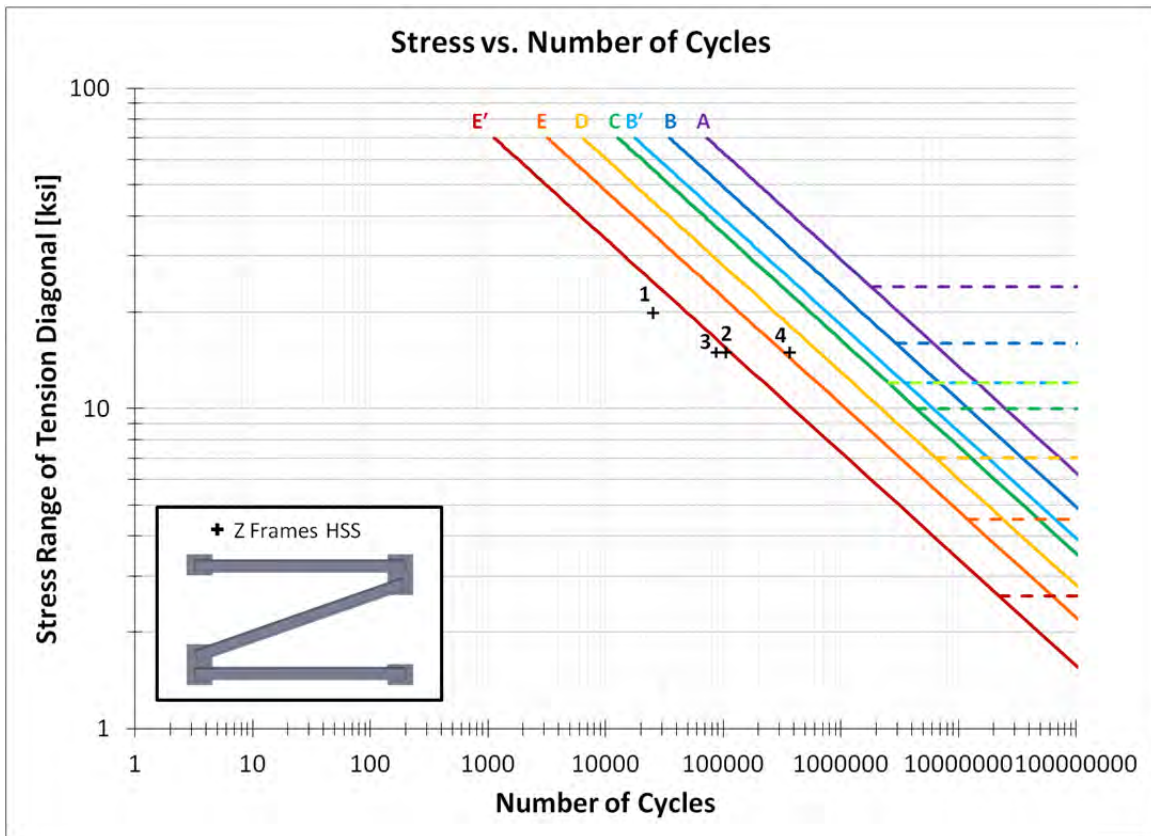


Figure 7.64: Cross Frame Fatigue Results of Z Frame HSS Specimens

7.7.4 Z Frame HSS Conclusions

Due to the relatively large cross frame stiffness of the Z Frame HSS, differential girder deflection tended to introduce a substantial amount of bending into the cross frame members and particularly the diagonal. When the tension bending stress is added to the axial tension induced from differential deflection, the fatigue performance was significantly reduced. However, despite cracking early, the tubes exhibit a large amount of resiliency since cracks propagated to nearly 3/4 the perimeter of the member before sudden fracture.

The final specimen tested utilized a rectangular HSS tube with the gusset plate inserted into slots made in the longer portion of the tube. The rectangular tube resulted in significant decreases in the bending induced stresses (since it is proportional to the distance from the neutral axis) and resulted in a specimen that achieved adequate fatigue life for design and may offer improved life relative to the single angle X and K frames.

Part V: Z Frames—Equal Leg Double Angles

7.8 Z Frame—Equal Leg Double Angle Design

Z frames with L4x4x3/8 double angles were tested in the full scale cross frame fatigue setup as well. Although the fatigue performance of the single angles couldn't be tested with the small scale tests, these tests indicated that the built-up double angles offer improved structural performance versus the single angle detail due to the concentric nature of the geometry. The following figures highlight the test details.



Figure 7.65: Z Frame Double Angle Specimen in Fatigue Test Setup

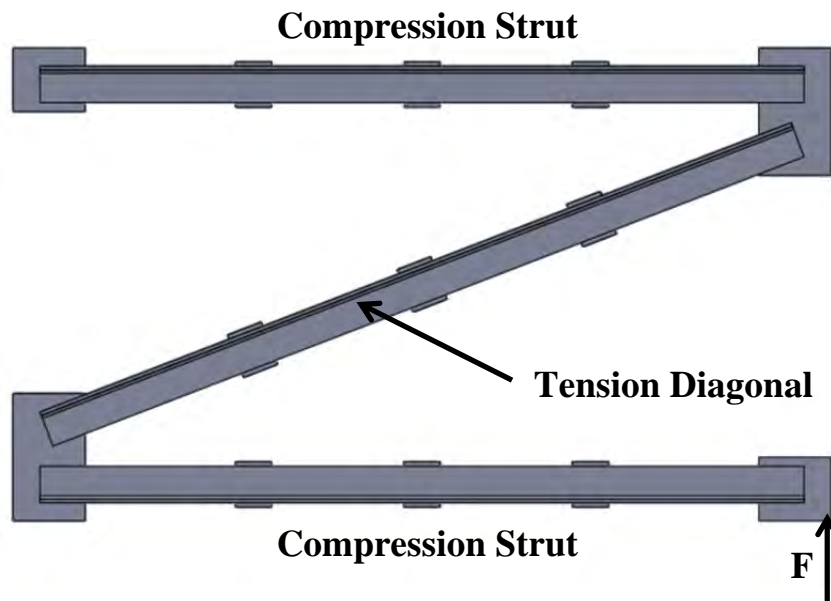


Figure 7.66: Z Frame Double Angle Internal Forces due to Fatigue Test Loading

7.8.1 Z Frame Double Angle Test Variables

A total of three Z frames with 2L4x4x3/8 members were tested in fatigue. The geometry of the specimens were adapted from the TxDOT Standard Details for X frames, but eliminating one diagonal and using double angle members. The gusset plates were modified where only a single member framed into the connection. The specimen designation for these tests is ZF_DA_1,2,3.

7.8.2 Z Frame Tests using 2L4x4x3/8 Members (ZF_DA_1,2,3)

As discussed in Chapters 2 and 4, from a stiffness and strength perspective, the double angle members offer the same if not better performance than the single angle counterparts due to the concentric nature of the connection. To verify their use in full scale cross frames, fatigue tests on the entire assembly were performed. Results from the tests are shown in Figure 7.67 and example of fatigue cracks are given in Figure 7.68 to Figure 7.70.

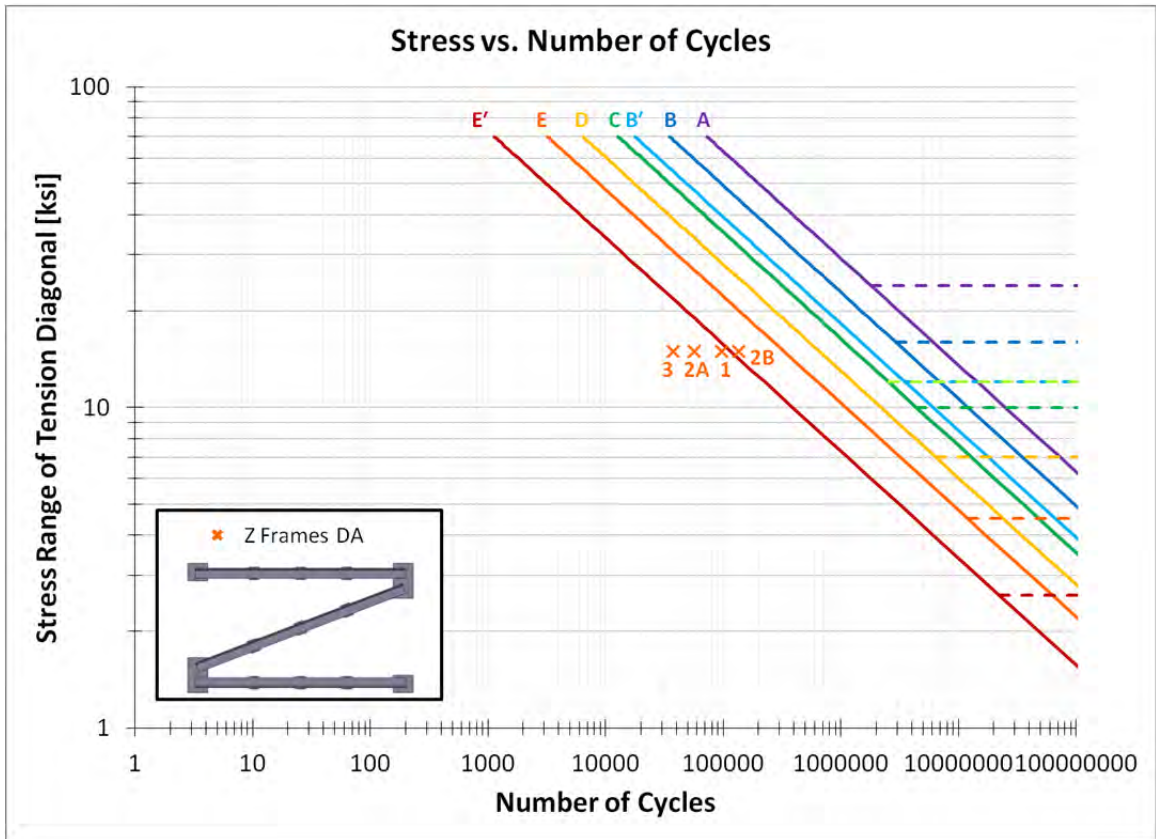


Figure 7.67: Cross Frame Fatigue Results of Z Frame DA Specimens



Figure 7.68: Typical Z Frame Double Angle Fatigue Crack (ZF_DA_1)



Figure 7.69: Typical Z Frame Double Angle Fatigue Crack (ZF_DA_2)

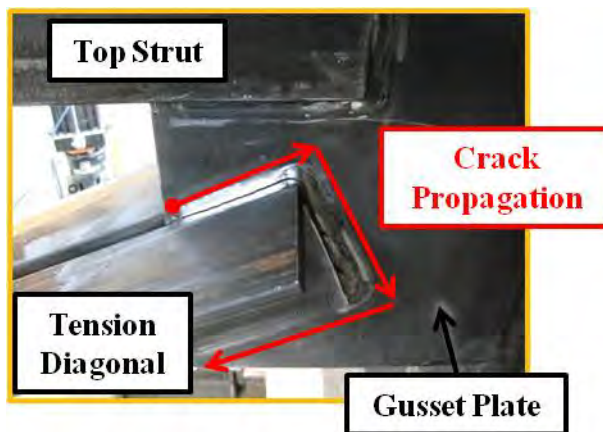


Figure 7.70: Typical Z Frame Double Angle Fatigue Failure Mode (ZF_DA_3)

Similar to the Z Frame HSS specimens, the diagonal of the ZF_DA specimens undergoes a substantial amount of bending due to the displacement of the system (see Figure 7.61). The bending significantly reduces the fatigue life, and in the case of the double angles, reduces it to less than Category E' in the AASHTO Specification.

Like the X frame series of tests, some cracks formed at the forward edge of the fillet weld, but into the heel of the double angle members. Other failure cracks were observed due to interaction between the angle-gusset welds and gusset-stiffener field weld. The most interesting failure mechanism, observed in two of the three specimens at the end of the fatigue life, was the failure depicted in Figure 7.70. The failure began at the heel of the angle, but rather than propagating into the angle or into the plate, the crack ran along the weld throat of the connection. Once through the longitudinal weld, it continued through the transverse weld, and then worked its way forward on the other longitudinal weld. Once the member disconnected, the test was complete.

While the behavior was interesting, the failure occurred at relatively low values and most likely does not represent a viable alternative to cross frame design.

7.8.3 Z Frame Double Angle Conclusions

Due to the high cross frame stiffness of the Z Frame Double Angle, a substantial amount of bending was introduced to the diagonal, similar to the HSS specimens. The bending stresses cause the angles to crack early and have a low fatigue life. Although the concentric nature of the angles improves the stiffness, it seems to have a detriment on fatigue life and the researchers believe that this layout may not achieve adequate fatigue life for design. The Z frame double angle layout is currently not recommended for design, based upon the full scale cross frame fatigue tests.

7.9 Summary of Conclusions

Fatigue tests on 25 full scale cross frames were conducted as part of the research. The major conclusions from the test program are as follows:

- K frames may be a desirable choice for cross frame applications since the layout of the members can save fabrication time since the welding can be conducted from one side, thereby eliminating the need to flip the cross frame. However, the designer must check the K frame can provide adequate stiffness for bridge stability.
- K frames and X frames have very similar fatigue performance.
- Improvements to the TxDOT Standard Detail for K frames are:
 - Thicker center gusset plate extends fatigue life.
 - Use of larger angle on the bottom chord improves the fatigue performance.
 - Flipping the bottom chord vertically so that the outstanding leg is closer to the bottom flange improves fatigue performance.
 - The transverse weld between the gusset plate and the angle of the K-frame on reverse side of the angle does not change performance and should therefore not be required in the detail.
- Improvement to the TxDOT Standard Detail for X frames are:
 - The minimum spacing between the end of angles and edge of stiffener should be increased from 0.5" to 2.5" to minimize interaction/stress concentration between the angle-gusset end weld and gusset-stiffener edge field weld. The current detail does not allow enough room for the two welds to pass freely, resulting in overlap of welds and a reduction in the fatigue life.
 - The inclusion of an additional transverse weld on the reverse side of the angle improves fatigue performance and should be included. Since the cross frame already needs to be flipped to facilitate other welds, this additional well has a relatively minimal cost.
- X frames with unequal leg angle members have similar performance as the X frames with equal leg angles. The reduced eccentricity of unequal leg angles moderately increases the stiffness but does not seem to change the fatigue performance.
- Z frames with square HSS tubes can have substantial bending in the diagonal. The performance is similar to the use of angles, so the additional cost is therefore not justified.

- Z frames with rectangular HSS tubes seem to offer a viable alternative to X frames and K frames.
- Z frames with double angle members should not be used due to relatively poor fatigue performance relative to the other systems that were tested.

Chapter 8. Finite Element Studies of Cross Frame Forces

8.1 Introduction

In order to evaluate the force demands on the cross frame members, a finite element study was undertaken to determine the range of forces experienced by cross frame members for different bridge geometries. The cross frame forces were considered for the case of construction loading on the bridge where the girders are not composite, as well as for the case of live load acting on the completed composite bridge. This chapter describes this study.

8.2 Comparison to Commercial Software

As discussed earlier, the use of the typical eccentric single angle connection detail leads to a reduction in cross frame stiffness. The effect of the cross frame stiffness has a different impact on stability induced forces versus forces induced due to passing truck traffic. From the perspective of stability bracing, a lower cross frame stiffness can lead to an unsafe system since the bracing must possess adequate stiffness to provide effective bracing. Even if the brace is adequate from a stiffness perspective, a reduction in the stiffness will result in a larger force induced due to stability effects on the system. The effect of the cross frame stiffness on forces induced in the cross frame due to truck traffic actually result in the opposite effect compared to stability induced forces. In analyzing bridge behavior, a reduction in stiffness usually results in a reduction in force on the cross frame members. In general, stiffer elements attract higher forces; therefore modeling decisions related to the bracing that might be made by designers or within the computer software programs can have a significant impact on the resulting forces in the bracing and the impact on the girder itself. Overestimating the stiffness of the cross frame in the finished bridge may result in perceived fatigue problems that are not actually realistic.

It is therefore of interest to further investigate the implications of the methods used by commercial bridge design software in modeling the stiffness of the cross frames. Discussions with TxDOT designers have revealed cases where the fatigue stresses in the cross frames have controlled the design of the braces on some projects. It is a difficult design predicament, as increasing the area of the cross frame members in hopes of reducing the fatigue stress range in turn, increases the axial stiffness of the member which increases the forces attracted by the brace. By using the reduction factor discussed in Chapter 6, the stiffness properties of the cross frame can be more accurately modeled, potentially reducing the forces in the members and lowering the fatigue stresses. The following sections highlight a case study in which the fatigue stresses of the cross frame members governed the design, ultimately requiring engineers to add an extra girder line to the project.

8.2.1 Case Study Details

The plans and details of the bridge modeled for comparison in this study were provided by TxDOT and consist of two phases that will be referred to as the “initial design” and the “final design”. The initial design contains plans for a single span curved I-girder bridge using 8 girders and the TxDOT XF2 cross frame detail. During design, fatigue issues were indicated by the bridge software package, which consisted of a grillage model. After adjusting the girder cross sectional properties, cross frame spacing, and cross frame member type, the fatigue stress range

in the cross frames were still larger than acceptable. The solution resulted in the final design, which includes an additional girder line, adds two extra lines of cross frames, and increases the area of the cross frame members to the TxDOT XF3 detail. The following subsections describe the bridge in full detail.

Initial Design

The initial design of the bridge consisted of 8 single span curved girders spaced at 8.571 ft. The outermost girder on the curve had a length of 164.991 ft and a radius of curvature of 1943.86 ft. The girder cross section details are highlighted in Table 8.1 and the full bridge plans are given in Appendix B.

Table 8.1: Initial Design Bridge Details

Initial Design	
Girder Properties	
Number of Girders	8
Girder Spacing	8.571 ft
Deck Overhang	3 ft
Radius of Curvature	1883.86-1943.86 ft
Number of Spans	1
Span Length	159.713-164.991 ft
Web Depth	68 in
Web Thickness	0.625 in
Girder Spacing	8.57 ft
Flange Width	24 in
Top Flange Thickness	1-1.25 in
Bottom Flange Thickness	1-2.25 in
Dapped End Length	85 in (both ends)
Dapped End Depth	42 in (both ends)
Bracing Information	
Cross Frame Arrangement	Radial, Equal Spaces
Total Number of Cross Frames	12
Cross Frame Spacing	14.52-15.00 ft
Cross Frame Type	TxDOT XF2
Angle Type	L5x5x1/2
Angle Area	4.75 in ²
Brace Height	58 in
Intermediate Stiffeners	
Stiffener Width	8 in
Stiffener Thickness	0.50 in
Bearing Stiffeners	
Stiffener Width	11 in
Stiffener Thickness	1.25 in

The bridge geometry and cross sections were modeled using a commercial grillage type analysis program that helps designers check the various strength, service, and fatigue limit states required by the AASHTO LRFD Bridge Design Specification. Output from the software provided by TxDOT indicated the stresses in the cross frame members in the initial design exceeded the Fatigue I limit state. Therefore, designers needed to modify the geometry to satisfy the requirements.

The easiest way to try to satisfy the requirements is to increase the area of the cross frame members, thereby lowering the stress in the members, assuming the force remains the same. However, when the area of the cross frame members is increased, the associated stiffness of the brace is also increased. The increase in system stiffness leads to the attraction of larger forces, potentially not reducing the stress range in the members.

Final Design

TxDOT engineers attempted to satisfy the Fatigue I limit state by modifying the initial design cross frame member areas, girder spacing, and number of cross frame lines. Finally the designers were forced to add an additional girder line which reduced the girder spacing, and add additional cross frame lines and larger cross frame member areas to satisfy the design requirements. The final design details are given in Table 8.2.

Table 8.2: Final Design Bridge Details

Final Design	
Girder Properties	
Number of Girders	9
Girder Spacing	7.5 ft
Deck Overhang	3 ft
Radius of Curvature	1883.86-1943.86 ft
Number of Spans	1
Span Length	159.713-164.991 ft
Web Depth	68 in
Web Thickness	0.625 in
Flange Width	24 in
Top Flange Thickness	1.25 in
Bottom Flange Thickness	1-2 in
Dapped End Length	85 in (both ends)
Dapped End Depth	42 in (both ends)
Bracing Information	
Cross Frame Arrangement	Radial, Equal Spaces
Total Number of Cross Frames	14
Cross Frame Spacing	12.28-12.69 ft
Cross Frame Type	TxDOT XF3
Angle Type	L6x6x9/16
Angle Area	6.45 in ²
Brace Height	58 in
Intermediate Stiffeners	
Stiffener Width	8 in
Stiffener Thickness	0.50 in
Bearing Stiffeners	
Stiffener Width	11 in
Stiffener Thickness	1 in

Output from the grillage software provided by TxDOT indicated the stresses in the cross frame members in the final design satisfied all fatigue limit states.

8.2.2 Software for Steel Bridge Analysis

The advantage of using a three dimensional finite element software package is the ability to extensively model the bridge girders, stiffeners, cross frames, deck, and other components in a more complete fashion. However, it is unrealistic that bridge designers would be able to model every project in such detail, and use of sophisticated modeling techniques requires specialized expertise and time. As an appropriate alternative, there are a variety of commercial software packages that allow the designers to input the bridge geometry, apply loads, and perform appropriate analyses to make sure the bridge meets the design specifications.

Many of these software packages perform a grillage or grid analysis on the completed bridge structure. In a grid analysis, the structure is simplified into a two-dimensional plane with all the applied loads acting perpendicular to the plane [Topkaya and Williamson 2003]. The members are usually modeled as line elements which are assumed to be axially rigid and have three degrees of freedom at each node, namely transverse displacement, rotation about the member's strong axis, and rotation about the member's longitudinal axis. Bending about the weak axis is typically ignored [Topkaya and Williamson 2003].

Grid analyses are computationally efficient, but can sometimes lead to oversimplification of the structure. Of particular concern is the modeling of the cross frames. In order to create the grid, the cross frames are simplified into an equivalent beam element. The equivalent beam is given a moment of inertia and torsional constant based on different structural analogies of the cross frame system. Some programs may use the equations outlined in Chapter 2 for torsional brace stiffness to size the equivalent beam. Other programs use a truss model analogy, performing a secondary analysis on the cross frame to determine the stiffness properties.

Determination of Equivalent Beam for Grid Analysis

Many bridge engineers make use of analysis software that carries out a grillage analysis on bridge projects involving complex geometry as well as curved girders. Cross frames in the grillage models are modeled using a single line element (beam element) that must have a specific moment of inertia to capture the appropriate stiffness of the cross frame. In order to determine the properties of the bracing beam elements, the cross frame is modeled as a truss, including both the cross frame members and the connection plates as part of the truss model. In many situations the software may internally use assumptions about the characteristics of the cross frame. A review of the documentation for the software will provide an indication of how the moment of inertia is determined. One modeling technique that is used consists of releasing one side of the brace and providing a roller type boundary condition while the other side of the brace is pinned. The top and bottom nodes of the brace are supported on both sides. A moment is applied to the released end by placing a unit force couple at the top and bottom nodes. Figure 8.1 denotes the boundary and loading conditions for this analysis. Figure 8.2 shows the associated deflected shape of the brace.

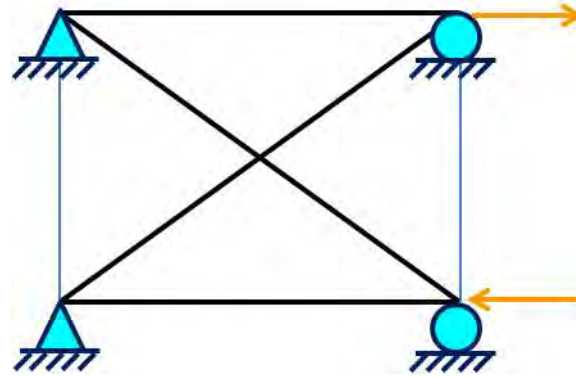


Figure 8.1: Boundary and Loading Conditions for Cross Frame Rotation Calculation in Typical Grillage Model

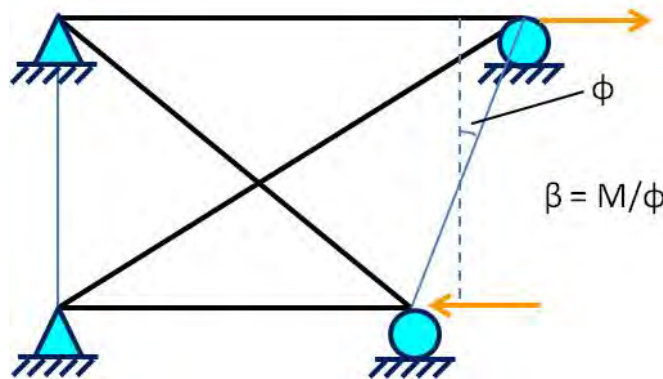


Figure 8.2: Displaced Shape Cross Frame Stiffness Calculation in Typical Grillage Model.

The horizontal displacements of the top and bottom nodes on the released side are calculated using a truss analysis; in the case of the X-type bracing, the analysis will be indeterminate in degree. The resulting displacements are used to calculate the rotation of the brace (ϕ) by taking the total displacement measured and dividing by the brace height (similar to the procedure outlined in Chapter 2). Ultimately, this provides the cross frame stiffness by dividing the applied moment by the rotation of the brace.

The rotational stiffness of a fixed-pinned beam subjected to a moment at the free end is given by the following and graphically exhibited in:

$$M = 4 \frac{EI}{L} \times \theta \quad (8.1)$$

where,

M = Applied Moment

E = Young's Modulus

I = Moment of Inertia

L = Length of the Beam

θ = Rotation at the Free End

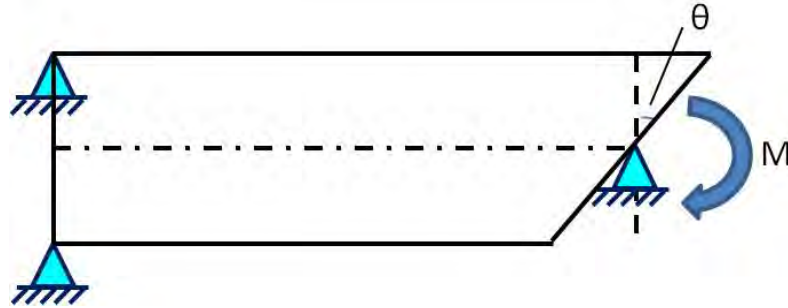


Figure 8.3: Displaced Shape of Equivalent Beam in Grillage Model

Equating the rotation of the cross frame from the analysis to the rotation of the beam element at the free end (using the same applied moment), an equivalent moment of inertia can be calculated for use in the grid analysis. The torsional constant for the beam element is calculated by summing the torsional constants of the individual members of the cross frame.

A comparison of the truss model cross frame stiffness and the beam element equivalent moment of inertia was conducted for the two phases of this case study. The truss model analysis was conducted using MASTAN2. A summary of the grillage model input and calculation results is presented in Table 8.3.

Table 8.3: Calculation of Beam Equivalent Moment of Inertia

	Original Design	Final Design
Girder Web Depth	68 in	68 in
Height of Brace	58 in	58 in
Girder Spacing	8.57 ft	7.5 ft
Distance from Cross Frame Connection to Center of Girder	6 in	0 in
Angle Member	L5x5x1/2	L6x6x9/16
Angle Area	4.75 in ²	6.45 in ²
Length of Strut	90.85 in	90 in
Length of Diagonal	107.8 in	107.1 in
MASTAN 2 Results		
UX of Top Node	0.0004125 in	0.0003019 in
UX of Bottom Node	-0.0004125 in	-0.0003019 in
Rotation (MASTAN2)	1.422 x 10 ⁻⁵ rad	1.041 x 10 ⁻⁵ rad
Equivalent Beam Calculations		
I _{equivalent} (Calculated)	3194 in ⁴	4323 in ⁴
I _{equivalent} (Grillage Input)	3111 in ⁴	4133 in ⁴
Percent Difference	+2.7%	+4.6%

Determination of Cross Frame Forces from Equivalent Beam

Once the grid analysis is complete, the grillage software often applies the resulting moments and shear forces on the equivalent beam to the truss model of the cross frame. Shear is distributed equally to both top and bottom nodes (provided the node location is able to resist vertical loads), and the moment is reapplied as a force couple. The forces in the cross frame members are determined using a structural analysis.

8.2.3 ANSYS Model*Geometry and Properties*

In order to evaluate the cross frame forces predicted by the grillage model software, comparison to a three-dimensional finite element software was conducted. The model constructed followed typical techniques used in previous research to obtain brace forces in plate girder systems [Quadrato 2010, Stith 2010]. The girders were constructed using 8-noded shell elements. The girders were modeled along a horizontal curve as given by the plan dimensions and contained the dapped end detail specified. Stiffeners were placed at each cross frame

location, also made from the 8-noded shell elements. The stiffeners were placed at the exact location and connected to the web elements using constraint equations.

The cross frames were modeled using line elements that framed into the web-flange interface, connecting at the nodes of the stiffeners. A concrete deck was also provided using shell elements that framed in along the top flange of the girders. Elastic section properties of the concrete were employed, consistent with the deck thickness and compressive strength of concrete provided in the output from the TxDOT supplied grillage model analysis.

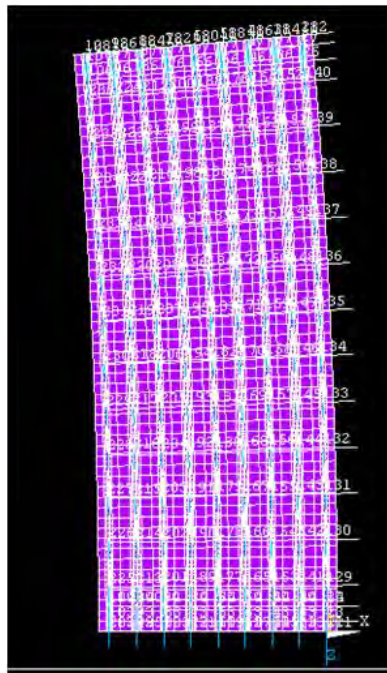


Figure 8.4: Top View of ANSYS Model

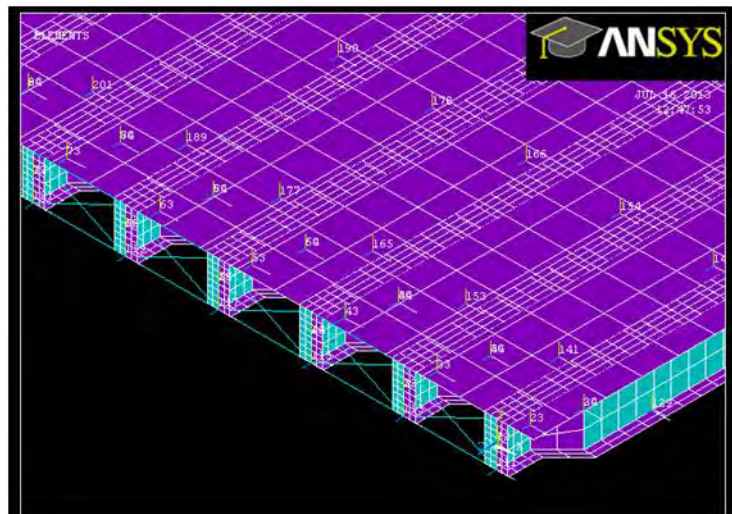


Figure 8.5: Isometric View of ANSYS Model

Application of Loads

With commercial bridge modeling software, determining the specific technique for placement of loads and their associated magnitudes may not be clear. Therefore, loads were applied in ANSYS consistent with the current AASHTO LRFD Specification [2013] for Fatigue I and Fatigue II limit states.

The specification calls for a design lane load of 0.64 klf (kips/linear ft) to be applied over a 10 ft width per lane. The lane load did not include the 1.15 impact factor [AASHTO 2013]. Using the grillage software output, the bridge was assumed to contain 4 design lanes of traffic. The lane live load was divided equally amongst the deck nodes on which it acted, as shown in Figure 8.6.

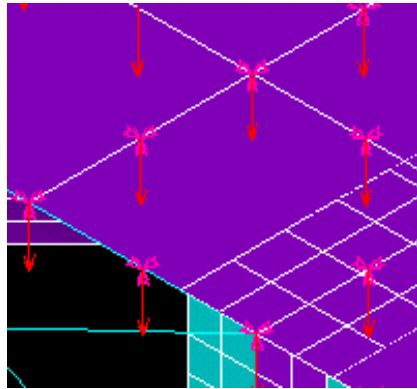


Figure 8.6: Application of Design Lane Live Load in ANSYS

Superimposed on the design lane load is either the design truck or tandem, applied as moving point loads within the design lane. The design truck has a fixed 30 ft spacing between the rear axles as specified for fatigue analyses. The moving point loads are multiplied by the 1.15 impact factor.

A schematic is shown in Figure 8.7 on how the point loads were applied. Corner nodes of the deck shell elements were set on a 3 ft grid. The point loads were then applied at the nearest node for analysis. The truck (or tandem) was run along the outside girder first, and repeated across the width of the bridge.

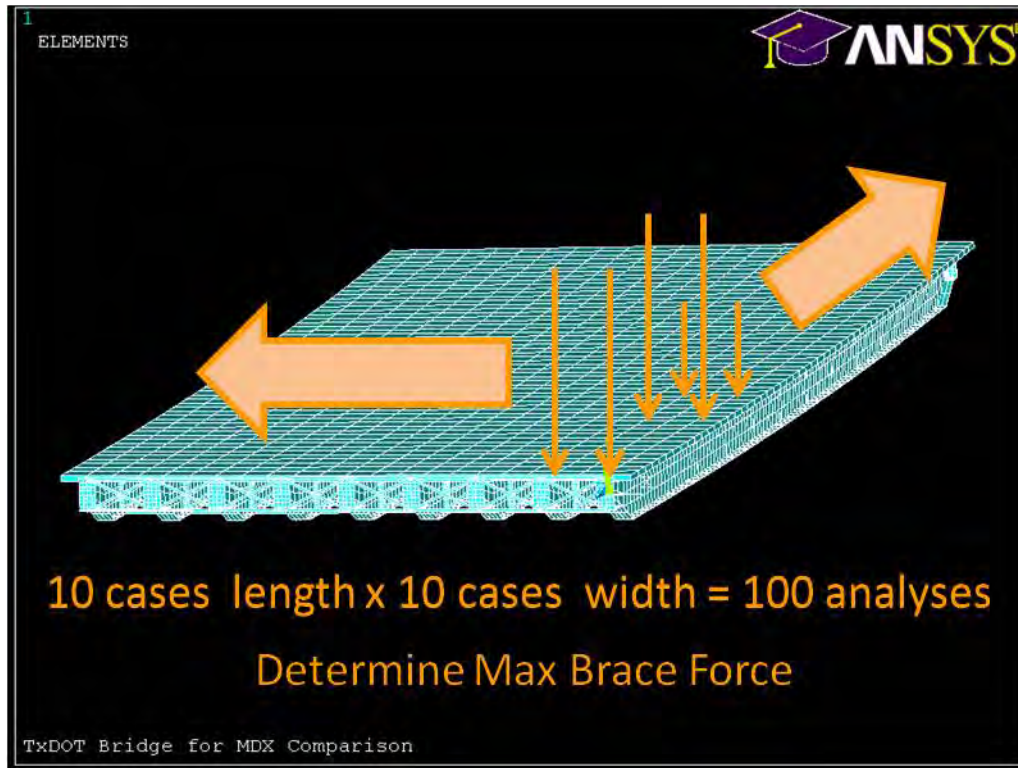


Figure 8.7: Application of Design Truck Loads in ANSYS

Determination of Cross Frame Line Element Area

In order to compare with the results given to the research team by TxDOT, the area of the line elements were selected to first model the equivalent stiffness calculated by the grillage model. Since the grillage model accounted for the actual height of brace, and the cross frames in the ANSYS model framed into the web-flange interface, slight modifications to the area of the line elements were made.

8.2.4 Initial Design Comparison

Analysis was performed on the initial design geometry to the best extent available from the provided plans. The fatigue truck and tandem were each run at the 100 different locations outlined in Figure 8.7, and the maximum force in each cross frame member was identified.

As previously discussed, the initial design was controlled by the Fatigue I limit state. Analysis in ANSYS showed the truck to induce much larger force in the cross frames than the tandem for the given geometry. The location of the maximum forces due to the suite of analysis cases was in the center bay, in the braces near the center. See Figure 8.8 for more detail.

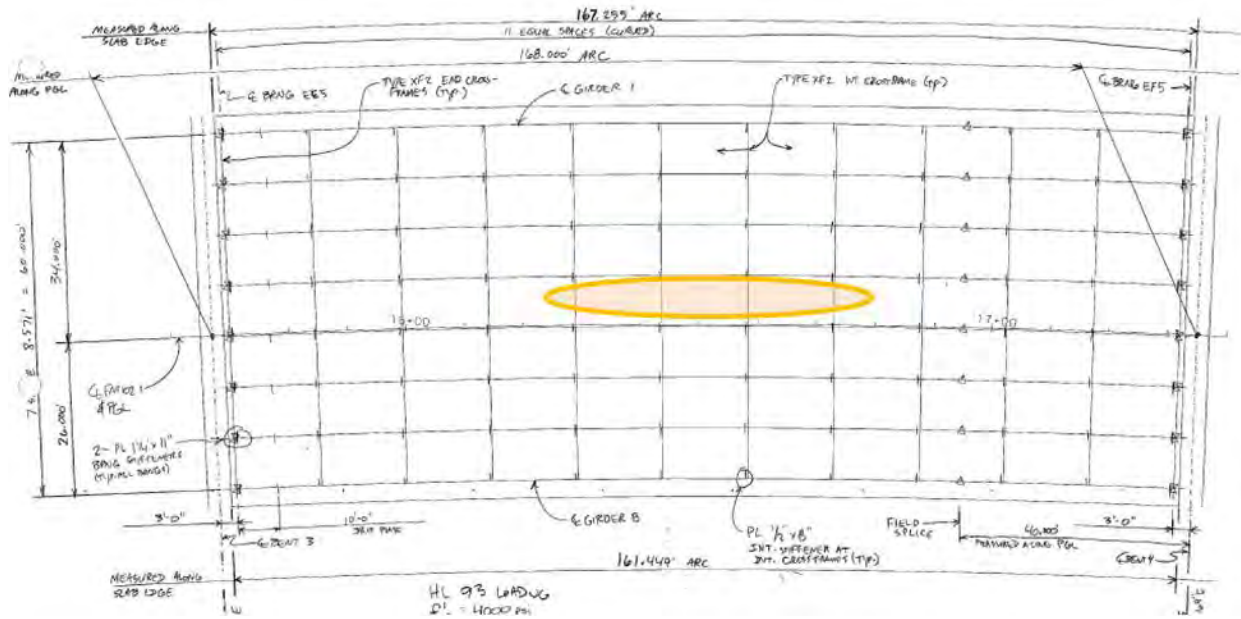


Figure 8.8: Location of Maximum/Minimum Forces in ANSYS and Grillage Model (Initial Design)

When considering fatigue, it is important to consider the range of force a given cross frame member may experience. The range of force is the value provided by the grillage model output and is what the ANSYS forces will be compared against. From the information obtained by the authors, it seems the grillage model software takes the maximum force in each cross frame member due to the series of loads and subtracts the minimum force in each member found for the same series of loads. This approach is very conservative as it assumes that every “cycle” must now consist of the placement of a truck in the precise locations to provide both the maximum and minimum possible forces.

Results from the initial design analysis showed fair agreement between the ANSYS and grillage model output. The results for the center bay are given in Table 8.4.

Table 8.4: Results for Cross Frame Member Forces in Center Bay of Initial Design

Initial Design Comparison- Bay 4

Loading Condition: Fatigue I, Design Truck

Maximum Brace Forces (ANSYS)				
Brace	Top Chord [k]	Bottom Chord [k]	Diagonal 1 [k]	Diagonal 2 [k]
1	1.90	0.00	3.10	3.30
2	1.27	9.67	8.63	6.33
3	1.75	16.49	12.01	9.44
4	2.06	20.05	13.33	10.45
5	2.37	21.29	14.12	10.60
6	2.49	21.91	14.58	10.43
7	2.50	22.22	14.84	10.63
8	2.41	22.27	14.79	11.22
9	2.11	21.97	14.40	11.56
10	1.77	18.55	13.12	10.67
11	1.30	10.84	9.21	7.00
12	1.92	0.96	2.67	3.54

Minimum Brace Forces (ANSYS)				
Brace	Top Chord [k]	Bottom Chord [k]	Diagonal 1 [k]	Diagonal 2 [k]
1	-0.13	0.00	-5.01	-4.44
2	0.00	-5.43	-3.44	-5.72
3	0.00	-8.40	-3.92	-6.17
4	0.00	-8.93	-3.45	-6.15
5	0.00	-9.72	-2.91	-6.63
6	0.00	-10.20	-2.78	-7.06
7	0.00	-10.60	-2.77	-7.24
8	0.00	-10.62	-2.91	-6.98
9	0.00	-10.48	-3.65	-6.83
10	0.00	-10.03	-4.06	-6.74
11	0.00	-6.91	-3.89	-5.96
12	0.00	-1.31	-4.41	-5.83

Force Range (ANSYS)				
Brace	Top Chord [k]	Bottom Chord [k]	Diagonal 1 [k]	Diagonal 2 [k]
1	2.04	0.00	8.11	7.75
2	1.27	15.10	12.07	12.05
3	1.75	24.88	15.93	15.61
4	2.06	28.98	16.78	16.60
5	2.37	31.01	17.03	17.23
6	2.49	32.11	17.36	17.49
7	2.50	32.81	17.61	17.86
8	2.41	32.89	17.70	18.20
9	2.11	32.44	18.05	18.38
10	1.77	28.59	17.18	17.40
11	1.30	17.75	13.10	12.96
12	1.92	2.27	7.07	9.37

Force Range (Grillage Model)				
Brace	Top Chord [k]	Bottom Chord [k]	Diagonal 1 [k]	Diagonal 2 [k]
1	0.25	0.25	3.00	3.00
2	13.47	13.47	4.45	4.45
3	24.27	24.27	6.09	6.09
4	31.50	31.50	5.85	5.85
5	35.92	35.92	6.17	6.17
6	38.69	38.69	6.53	6.53
7	38.69	38.69	6.53	6.53
8	35.92	35.92	6.17	6.17
9	31.50	31.50	5.85	5.85
10	24.27	24.27	6.09	6.09
11	13.47	13.47	4.45	4.45
12	0.25	0.25	3.02	3.02

One important observation from the obtained data is the discrepancy between the force range in the top chords of these braces. Since the ANSYS software includes modeling of the concrete deck as well as the three dimensional location of the cross frames relative to the deck, the force range in the top strut is very low. The grillage model cannot identify this extra restraint, making the force range in the top chord quite high. Additionally, due to the way the cross frames are modeled as equivalent beams in the grillage model, the top and bottom chords undergo the same force range as well as the diagonals. This differs from the ANSYS model predictions.

In addition, there is a sizable discrepancy between the force ranges in the diagonals. Due to the roller and pin restraints inherent to the cross frame in the grillage model (see Figure 8.2), the diagonals are not experiencing larger forces since the roller/pin supports will take some of the applied load. This is contradictory to the findings given in Chapter 5 and 6 where the diagonals of the X frame are the primary load carrying members of the system.

Despite these differences, the maximum force range still occurs in the bottom strut in both models, the magnitude of which was similar for most locations.

8.2.5 Final Design Comparison

The next stage in the case study was to compare the force ranges from the ANSYS model to the grillage model for the final geometry. The comparison was done for the Fatigue II limit

state, which was indicated by the output of the grillage model software to be the controlling scenario. The location of the maximum force range was again identified at the braces towards the very center of the bridge, as indicated in Figure 8.9.

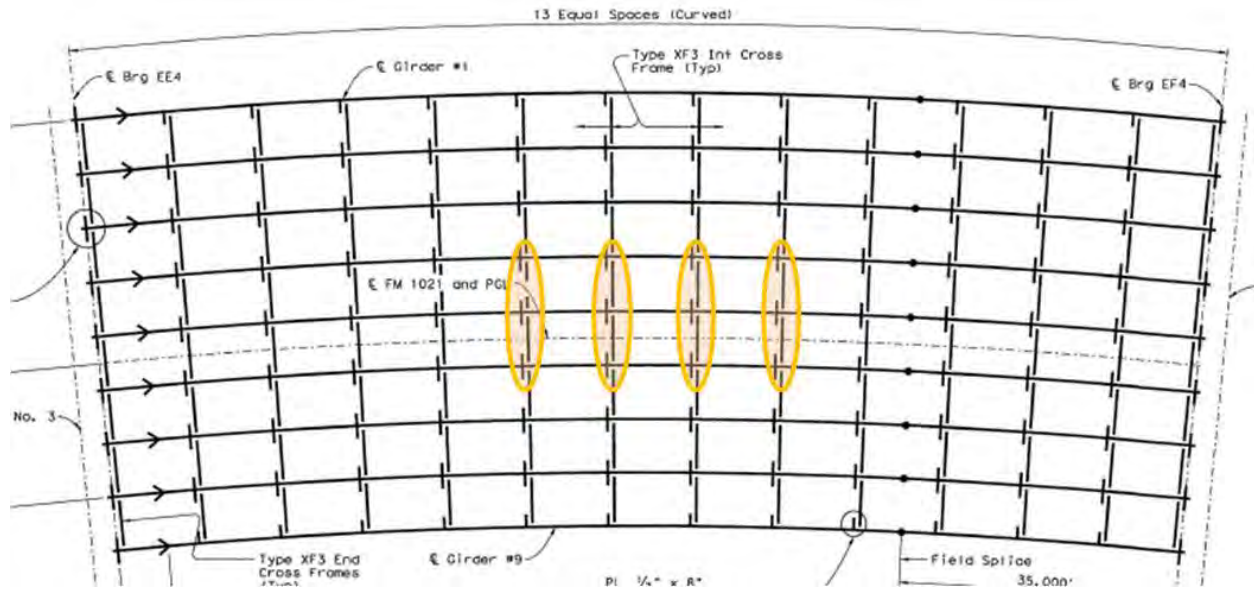


Figure 8.9: Location of Maximum/Minimum Forces in ANSYS and Grillage Model (Final Design)

As discussed for the initial design, the force ranges in the braces were compared and found to be in relative agreement for the maximum values. For this loading condition ANSYS indicated the force range to be slightly higher. A sample of the data is shown in Table 8.5.

Table 8.5: Results for Cross Frame Member Forces in Center Bays of Final Design

Final Design Comparison- Bay 5

Loading Condition: Fatigue II, Design Truck

Maximum Brace Forces (ANSYS)				
Brace	Top Chord [k]	Bottom Chord [k]	Diagonal 1 [k]	Diagonal 2 [k]
1	0.86	0.00	1.33	1.29
2	0.72	4.86	3.88	3.22
3	1.00	7.22	4.91	4.12
4	1.27	8.27	5.25	4.44
5	1.50	9.32	5.47	4.80
6	1.68	9.82	5.59	4.84
7	1.78	10.00	5.62	4.78
8	1.79	10.02	5.73	4.86
9	1.71	9.92	5.79	4.95
10	1.56	9.60	5.77	5.00
11	1.34	9.13	5.73	5.02
12	1.06	8.19	5.41	4.72
13	0.70	5.34	4.15	3.57
14	0.93	0.71	0.49	1.94

Minimum Brace Forces (ANSYS)				
Brace	Top Chord [k]	Bottom Chord [k]	Diagonal 1 [k]	Diagonal 2 [k]
1	-0.19	0.00	-3.02	-2.99
2	0.00	-2.71	-2.06	-2.48
3	0.00	-4.57	-1.89	-2.94
4	0.00	-5.30	-1.45	-3.25
5	0.00	-5.41	-1.42	-3.28
6	0.00	-5.42	-1.34	-3.36
7	0.00	-5.39	-1.24	-3.39
8	0.00	-5.58	-1.23	-3.46
9	0.00	-5.74	-1.32	-3.49
10	0.00	-5.92	-1.43	-3.51
11	0.00	-5.81	-1.58	-3.53
12	0.00	-5.34	-2.03	-3.35
13	0.00	-3.19	-2.14	-2.55
14	-0.02	-0.74	-3.04	-2.96

Force Range (ANSYS)				
Brace	Top Chord [k]	Bottom Chord [k]	Diagonal 1 [k]	Diagonal 2 [k]
1	1.05	0.00	4.35	4.28
2	0.72	7.57	5.94	5.70
3	1.00	11.79	6.80	7.06
4	1.27	13.57	6.70	7.69
5	1.50	14.73	6.89	8.07
6	1.68	15.24	6.92	8.20
7	1.78	15.39	6.86	8.17
8	1.79	15.60	6.96	8.32
9	1.71	15.66	7.11	8.44
10	1.56	15.52	7.20	8.51
11	1.34	14.94	7.31	8.55
12	1.06	13.52	7.44	8.07
13	0.70	8.53	6.29	6.13
14	0.95	1.44	3.54	4.90

Force Range (Grillage Model)				
Brace	Top Chord [k]	Bottom Chord [k]	Diagonal 1 [k]	Diagonal 2 [k]
1	0.01	0.01	0.08	0.08
2	6.39	6.39	0.59	0.59
3	9.28	9.28	1.15	1.15
4	11.56	11.56	1.00	1.00
5	13.25	13.25	1.44	1.44
6	13.73	13.73	0.67	0.67
7	13.99	13.99	0.63	0.63
8	13.99	13.99	0.63	0.63
9	13.73	13.73	0.67	0.67
10	13.22	13.22	1.44	1.44
11	11.48	11.48	0.99	0.99
12	5.95	5.95	2.98	2.98
13	3.98	3.98	2.26	2.26
14	0.00	0.00	0.06	0.06

The previous discrepancies in the force ranges in the top chords and diagonals are again observed in the data. The maximum force range was identified in the bottom strut of the braces and showed fair agreement between the two models, especially considering the number of unknown characteristics about the internal calculations of the grillage software.

8.2.6 Use of R Factor for Calculation of Force Range

The final stage of the case study was to examine the effect of properly modeling the cross frame stiffness of the system. As discussed in Chapter 6, the use of single angle members leads to significant reductions in cross frame stiffness due to the eccentricity of the member. The research has proposed the use of a reduction factor, R, in which the eccentricity can be accounted for and an accurate prediction of cross frame stiffness can be made utilizing the truss model equations.

Since stiffer members will tend to attract more force, it is theorized the predicted force ranges in the cross frame members using line element models are in fact, higher than the actual forces experienced. To quantify this effect, more analysis was performed on the initial TxDOT

design to see if including the R factor reduced the cross frame forces. The results of the series of analyses are given in Table 8.6.

Table 8.6: Results for Cross Frame Member Forces in Center Bay of Initial Design Including the R Factor

Initial Design Comparison- Bay 4
Loading Condition: Fatigue I, Design Truck

Force Range (ANSYS)					Force Range with R Factor (ANSYS)				
Brace	Top Chord [k]	Bottom Chord [k]	Diagonal 1 [k]	Diagonal 2 [k]	Brace	Top Chord [k]	Bottom Chord [k]	Diagonal 1 [k]	Diagonal 2 [k]
1	2.04	0.00	8.11	7.75	1	1.32	0.00	7.01	6.85
2	1.27	15.10	12.07	12.05	2	0.41	8.70	7.54	7.47
3	1.75	24.88	15.93	15.61	3	0.65	15.80	10.94	10.78
4	2.06	28.98	16.78	16.60	4	0.82	20.12	12.55	12.37
5	2.37	31.01	17.03	17.23	5	0.93	22.39	13.27	13.23
6	2.49	32.11	17.36	17.49	6	0.97	23.89	13.76	13.77
7	2.50	32.81	17.61	17.86	7	0.97	24.56	13.97	14.07
8	2.41	32.89	17.70	18.20	8	0.93	24.13	13.93	14.16
9	2.11	32.44	18.05	18.38	9	0.81	22.49	13.68	13.80
10	1.77	28.59	17.18	17.40	10	0.66	18.29	12.21	12.11
11	1.30	17.75	13.10	12.96	11	0.43	10.80	8.29	8.11
12	1.92	2.27	7.07	9.37	12	0.96	0.82	6.43	7.24

Referencing the above results, one can see the force range is reduced significantly when the R factor is accounted for in the analysis. For reference purposes, the R factor for the given cross frame geometry was nearly 0.50.

For the cross frame members with the largest force ranges, inclusion of the reduction factor results in a 25% decrease in the cross frame force range. In terms of design, this reduced force can help alleviate fatigue design problems. The following table examines the ratio between the force range with the R factor included to the original ANSYS predicted force range.

Table 8.7: Ratio of Cross Frame Member Forces in Center Bay of Initial Design Including the R Factor to the Original Calculation

Ratio of Force Range With/Without R Factor (ANSYS)				
Brace	Top Chord [k]	Bottom Chord [k]	Diagonal 1 [k]	Diagonal 2 [k]
1	0.65	-	0.86	0.88
2	0.32	0.58	0.62	0.62
3	0.37	0.63	0.69	0.69
4	0.40	0.69	0.75	0.74
5	0.39	0.72	0.78	0.77
6	0.39	0.74	0.79	0.79
7	0.39	0.75	0.79	0.79
8	0.39	0.73	0.79	0.78
9	0.38	0.69	0.76	0.75
10	0.37	0.64	0.71	0.70
11	0.33	0.61	0.63	0.63
12	0.50	0.36	0.91	0.77

Referencing Table 8.7 it is clear the proper modeling of the stiffness of the cross frame not only effects stability calculations, but also serves an important role in the determination of cross frame fatigue force ranges. Reductions of 20-30% were typical in the most heavily loaded braces, while other braces can see upwards of 60-70% reductions.

8.2.7 Application of R to General Computer Software

In the analysis considered, the R factor was applied to the member cross sectional area and the resulting forces were obtained from the ANSYS finite element software. Although this is one viable solution, an alternative would be to apply the reduction factor to the modulus of elasticity, that way stress calculations performed by the program would remain accurate. In addition, the change in elasticity may be an easier way to apply the reduction factor to all the cross frames. Since the stiffness of the members is proportional to AE/L , both methods are acceptable.

8.2.8 Case Study Conclusions

The following conclusions summarize the information obtained in performing this case study:

- The method in which grillage analysis software determine cross frame “beams” with an equivalent moment of inertia may not result in accurate stiffness and fatigue behavior of the cross frame.
- Increasing the stiffness of a cross frame in a bridge model will increase the amount of force the members of the brace experience.
- To more accurately predict the forces in the cross frames, the reduction factor R can be applied to the cross sectional area or modulus of elasticity of the line element cross frame members.
- Including the reduction factor can lead to 20-30% decreases in the fatigue force range for the most heavily loaded members.

The importance of using the R factor to better estimate the cross frame force ranges is highlighted by the initial and final design considered in this case study. Due to fatigue forces calculated by the analysis program, designers were forced to use 35% larger cross frame members, two additional intermediate cross frame lines, and one extra girder line. These additions significantly increased the cost of the project and may not have been necessary due to the overestimation of cross frame force ranges.

Chapter 9. Conclusions and Recommendations

9.1 Introduction

TxDOT Project 0-6564 was initiated to improve cross frame behavior. The project sought to examine the current details used in practice and to propose alternative designs which could offer increased performance in strength, stiffness, and fatigue.

To accomplish these broad goals, the research team performed numerous experimental tests and computational analyses on the cross frame members, the member connections, the cross frame system, and the cross frame as part of the overall bridge geometry. The results of these tests and analyses are presented in this chapter.

9.2 Applicability of Cast Steel Connections

In developing an efficient cross frame, the research team investigated the use of tubular members for inclusion in the cross frame design. By using tubular members, effective braces with only one diagonal are possible, as shown in the Z frame layout in Figure 9.1.

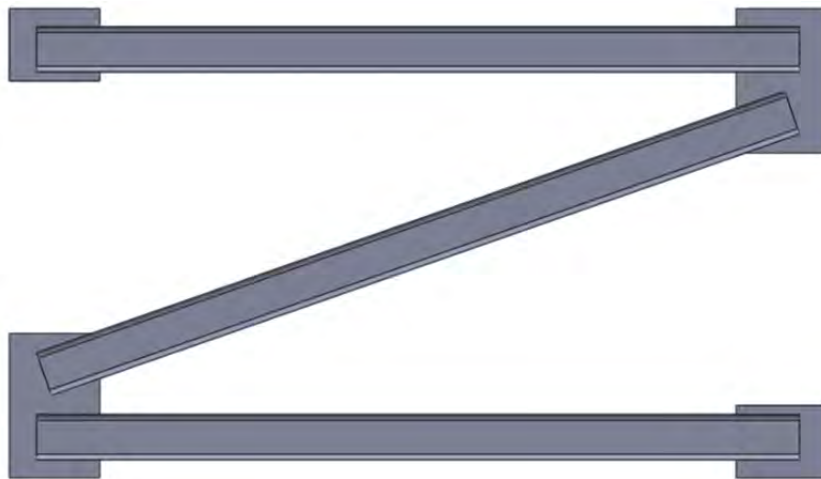


Figure 9.1: Z Frame Cross Frame Layout

Using tubular members to connect to the gusset plates can lead to difficult fabrication techniques, so one proposed solution was to develop a steel casting that was engineered to seal the end of the tube, connect easily to the tube via a fillet welded connection, and taper to a flat plate which could be welded to the gusset plate or cross frame connection plate. The casting developed is shown in Figure 9.2.



Figure 9.2: Cast Steel Connection

Ultimately, the fillet weld between the cast steel connection and tube did not meet the fatigue design limits set forth in the AASHTO LRFD Bridge Design Specification [2013]. However, the research regarding the cast steel connection resulted in the following conclusions:

- Cast steel components can be engineered for use in steel bridge design.
- During the design and fabrication process, it is important to have a good working relationship with the foundry, which will assist the engineer in developing the molds used for creating the connection.
- Since the components are created from molten steel, the engineer is able to have control over the material properties of the final product.
- Steel castings can be made in a weathering steel grade similar to ASTM A709, Grade 50W.
- The steel castings produced for the research had very good strength properties, including a yield strength of 68.2 ksi, a tensile strength of 85.1 ksi, and an elongation at fracture of 0.29.
- The steel castings developed had very good toughness, recording Charpy V-notch test values of 110.7 ft-lb at 40°F and 84.0 ft-lb at -40°F.
- A variety of quality control techniques are available to ensure the castings are free from internal and surface defects.

9.3 Cross Frame Member Strength, Stiffness, and Fatigue Tests

The next stage of the research considered the individual cross frame member behavior with a variety of connections identified for potential use with the tubular members, as well as conventional connections with single and double angle members. Figure 9.3 shows each of the members tested for ultimate strength, stiffness, and fatigue performance.

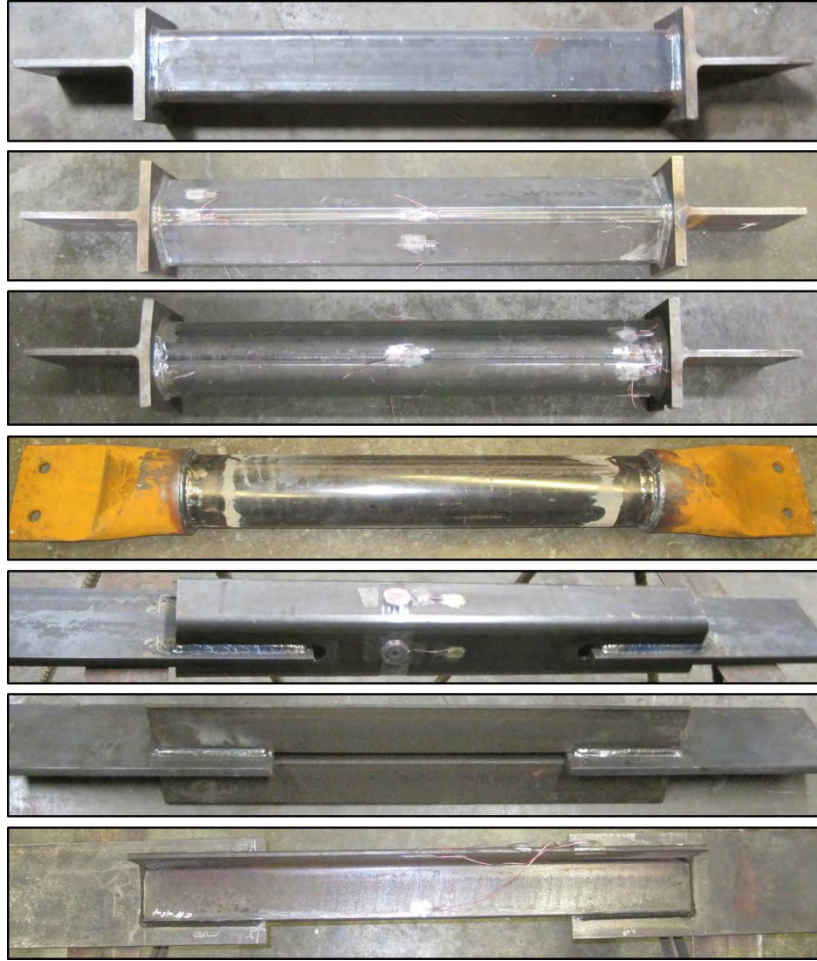


Figure 9.3: Test Specimens- (a) T-Stem and Square HSS, (b) T-Stem and Diamond HSS, (c) T-Stem and Round HSS, (d) Cast Connection, (e) Knife-Plate Connection, (f) Double Angle Connection, and (g) Single Angle Connection

Based upon the individual member tests, the following conclusions were drawn:

Strength and Stiffness Tests

- Simplified formulas for design typically neglect the effect of the connections on the stiffness of the member (and subsequently of the overall cross frame system).
- The Square, Round, and Diamond T-stem connections performed poorly in stiffness and strength due to a large stress concentration that forms in the tubular member in line with the stem of the T. The T-stem members failed in strength at a lower value than predicted by conventional tension member and connection formulas.
- The cast connection provides a concentric connection with an even stress distribution to the tube. The strength properties exceeded the predicted strength of typical tension member and connection formulas.
- The knife-plate connection was more difficult to fabricate, but offered good strength and stiffness properties.

- The double angle connection offered good strength and stiffness properties. It is important to properly size the connection plate for this arrangement.
- The single angle connection has adequate strength properties, but relatively poor stiffness behavior. The eccentricity of the angle member relative to the applied load results in a moment on the member. The moment further decreases the stiffness of the member. A basic schematic is shown in Figure 9.4.

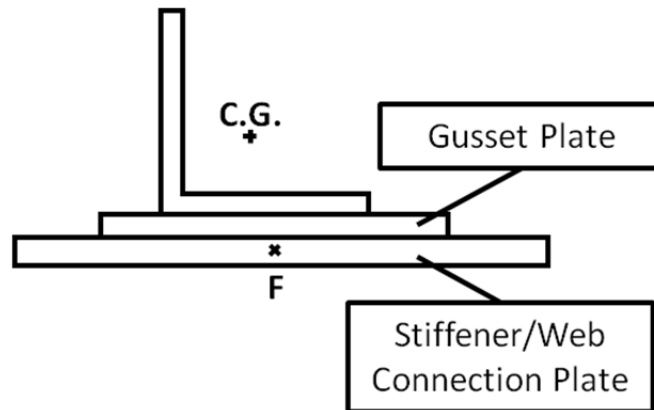


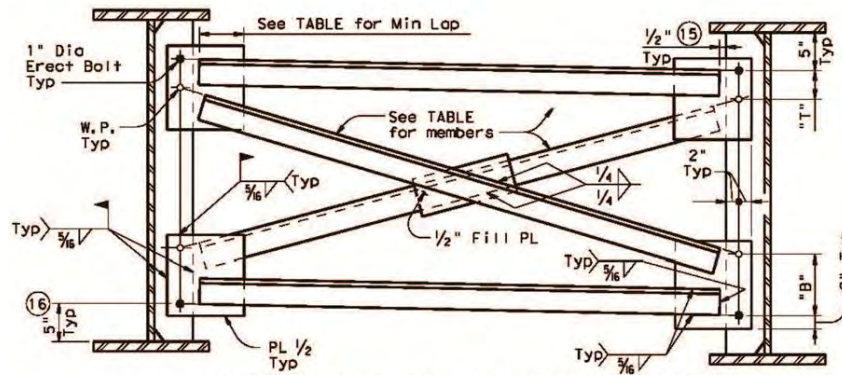
Figure 9.4: Eccentricity of Load Relative to Angle Center of Gravity

Fatigue Tests

- The Square, Round, and Diamond T-stem connections performed poorly in fatigue, most likely due to the transversely loaded fillet weld that has a slight load eccentricity when examined on the local level.
- The cast steel connection performed poorly in fatigue, similar to the T-stem connections.
- The knife-plate connections offered adequate performance, with 5 of 6 specimens achieving AASHTO Category E. The stress relief hole further increases the fatigue life, while using the saw or torch to cut the slots seems to have no effect.
- The double angle members meet the requirements of AASHTO Category E'. The cracks should form in the angles as long as the stress range in the gusset plate is not larger than in the member.
- The single angle member could not be tested due to the amount of bending that occurs due to the eccentric load pattern. An alternative test setup described in Chapter 7 determined the fatigue behavior of these members.

9.4 Full Scale Cross Frame Stiffness and Ultimate Strength Tests

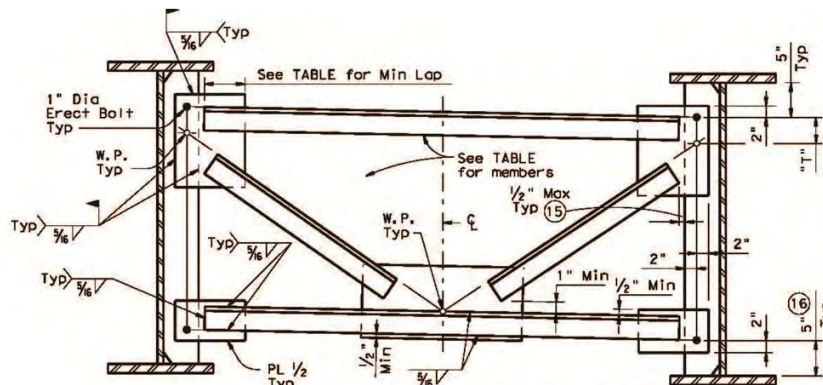
Based on the success of the knife-plate and double angle member tests, full scale cross frame stiffness and ultimate strength tests were carried out for these members in the Z frame layout. In addition, the current TxDOT single angle X frame and K frame details were considered to evaluate the performance. These standard details are given in Figure 9.5 and Figure 9.6.



TYPE XF1 THRU XF3 CROSS-FRAMES (17)

For Plate Girders with web depths of 52" to 96". For all locations, including end bearings when Thickened Slab Ends, shown on standard SBTS are used. Minimum stiffener width is 8" for use with these cross-frames.

Figure 9.5: TxDOT Standard X Frame Detail [2010]



TYPE KF1 THRU KF3 CROSS-FRAMES (17)

For Plate Girders with web depths of 52" to 96". For all locations, including end bearings when Thickened Slab Ends, shown on standard SBTS are used. Minimum stiffener width is 8" for use with these cross-frames.

Figure 9.6: TxDOT Standard K Frame Detail [2010]

In total, seven cross frame arrangements were tested to measure the stiffness and strength properties. The following summarizes the major conclusions.

- Stiffness tests showed that the stiffnesses of cross frames are typically the same for loadings in opposite directions. One exception is the Single Angle Z-Frame, which has shown significant stiffness reduction when the diagonal is in compression.
- Failure of the cross frame usually occurs when critical compressive components lost its stability, which could be buckling of cross frame member, or buckling of gusset plates.
- For the Single Angle X-Frame, the mid-span spacer plate can be considered as a bracing point for the compression diagonal.
- In all cases using single angle members, the reduction in member stiffness due to the eccentricity of the load severely lowers the overall cross frame stiffness by as much as 50%.

- Use of the tension-only model for X-type cross frames is erroneous. The tests indicate that the compression and tension diagonals develop equal but opposite loads, and thus should be treated as a tension-compression system.
- The tension-only models could accurately predict the stiffness of the Z frames when concentric members (HSS with knife-plate connections, double angles) were used.
- The reduction in stiffness of the unequal leg X-frame was less than the equal leg X-frame with the same member area. Therefore, unequal leg X-frames may provide improved performance.
- In terms of ultimate strength, the braces had no reserve capacity once the critical compression member buckled.

9.5 Cross Frame Stiffness and Ultimate Strength Parametric Studies

The results from the large scale tests were used to validate finite element models used to determine the adequacy of current formulas for brace stiffness. General results from the computer analyses indicate the following:

- When there are single angle members in a cross frame, the analytical models usually overestimate the stiffness capacity of the cross frame because of the eccentric loads that are transferred by the angles.
- Line element truss models used to represent the cross frames consider the full stiffness of the member and will therefore not account for stiffness reductions due to eccentric loading.
- The tension-only analytical and computer models for the Square Tube Z-frame and Double Angle Z Frame 2 accurately predict the stiffness of the brace.
- In all cases, the shell element computer models developed in ANSYS can accurately predict the brace stiffness, however it is not practical for everyday design.

A series of parametric studies was performed to develop a reduction factor to account for the stiffness reduction due to the eccentricity of the single angle cross frame members.

$$R_{frame} = \frac{\beta_a}{\beta_b} \quad (9.1)$$

Where:

β_a = Actual stiffness of the cross frame

β_b = Theoretical stiffness of a cross frame as defined in Chapter 2

Based upon the results, the following equations were developed.

For X-type cross frames:

$$R_{est-SX} = 1.063 - 0.087 \frac{S}{h_b} - 0.159\bar{y} - 0.403t \quad (9.2)$$

Where:

S = Girder spacing

h_b = Height of the brace

\bar{y} = Distance from connection plate to angle center of gravity

t = Thickness of the angle

For K-type cross frames:

$$R_{reg-SK} = 0.943 - 0.042 \frac{S}{h_b} - 0.048\bar{y} - 0.420t \quad (9.3)$$

Additionally the following conclusions are noted:

- The compression and tension model for the X-type cross frames and the K-type cross frame model results in erroneous estimates of the cross frame stiffness since it does not include the reduction in stiffness caused by connection eccentricity. The error can be corrected by applying a stiffness reduction factor, R .
- The cross frame stiffness expression based upon the tension-only diagonal system constitutes a possible hand-calculation method in evaluating the stiffness of the single angle X-Frame. By ignoring the compression diagonal, this method provides estimates of the stiffness of the cross frame that are from 10 to 50-percent less than the actual stiffness. Note that underestimating cross frame stiffness will generally be conservative when evaluating girder stability. However, underestimating cross frame stiffness may be unconservative when checking cross frames for fatigue.
- A simplified method was also investigated which consisted of a simple reduction factor of 0.5. The reduction factor of 0.5 applied to the analytical compression and tension model or K frame model for the cross frame stiffness was conservative compared to all of the FEA results, but still had reasonable agreement with the computer solutions. The value of 0.5 of the stiffness reduction factor is consistent with the lower boundary (0.55).
- A more accurate estimate of the stiffness reduction factor was also developed based upon a regression analysis of the data from the parametric study results. The resulting expression considers the impact of cross frame angle and geometrical parameters and had good correlation with the FEA results. The stiffness reduction factor is applied to the stiffness of the tension/compression diagonal system stiffness.
- A cross frame stiffness expression that relies on a compression member will also experience a reduction in stiffness as the compression diagonal approaches the buckling capacity. A nonlinear geometrical analysis was carried out considering a

wide variety of parameters. The results showed that the reduction in cross frame stiffness was minimal provided the forces in the compression members are kept below 60% of the buckling strength of the corresponding member of the cross frame. For this reason, it is concluded that if design load is less than 60% of the strength of the cross frame, no deduction on cross frame stiffness is necessary.

- A brief parametric study was also provided for cross frames with unequal leg angles. The results of analysis showed that regression equations derived from equal leg angles also provides reasonable estimates of the stiffness of cross frames with unequal leg angles.

9.6 Full Scale Cross Frame Fatigue Tests

Fatigue tests on 25 separate specimens were conducted as part of the research. The major conclusions from the test program are as follows:

- The current AASHTO classification of the single angle detail as Category E may be unconservative. The eccentricity of the member when tested in the actual arrangement seems to indicate a lower bound to the data of Category E'.
- K frames are desirable for design as the layout and fabrication reduces labor time and costs, provided no additional transverse welds are used on the reverse side of the angles. However, the designer must check the K frame can provide adequate stiffness for bridge stability.
- K frames and X frames have very similar fatigue performance.
- Possible improvements to the TxDOT Standard Detail for K frames are:
 - Thicker center gusset plate extends fatigue life.
 - Use of larger angle on the bottom chord improves fatigue performance.
 - Rotating the bottom chord longitudinally so the outstanding leg is closer to the bottom flange improves fatigue performance.
 - Use of additional transverse weld on reverse side of angle does not change performance and should therefore not be included in order to simplify fabrication.
- Possible improvements to the TxDOT Standard Detail for X frames are:
 - The minimum spacing between the end of angles and edge of stiffener should be increased from 0.5" to 2.5" to minimize interaction/stress concentration between the angle-gusset end weld and gusset-stiffener edge field weld. The current detail does not allow enough room for the two welds to pass freely, resulting in overlap of welds and a severe reduction in fatigue life.
 - The inclusion of an additional transverse weld on the reverse side of the angle improves fatigue performance and should be included.
- X frames with unequal leg angle members have similar performance as the X frames with equal leg angles. The reduced eccentricity of unequal leg angles moderately increases the stiffness and does not seem to change the fatigue performance.

- Z frames with square HSS tubes can have substantial bending in the diagonal. The performance is similar to the use of angles, so the additional cost may not be justified.
- Z frames with rectangular HSS tubes may offer a viable alternative to X frames and K frames.
- Z frames with double angle members should be avoided.

9.7 Comparison of Cross Frame Fatigue Forces to Commercial Software

A comparison using FEA software to commercial software was performed, which showed the reduction in stiffness inherent to the single angle members leads to a reduction in fatigue-induced forces. By including the reduction factor R, the forces experienced in fatigue were reduced by 20-30% in the case study, which could lead to significant savings in the number of cross frames necessary, the angle cross-section selected, and potentially less girder lines.

9.8 Recommendations to Improve Current TxDOT Cross Frame Details

Based upon the observations in the full scale cross frame fatigue tests, the following modifications to the existing TxDOT detail are recommended.

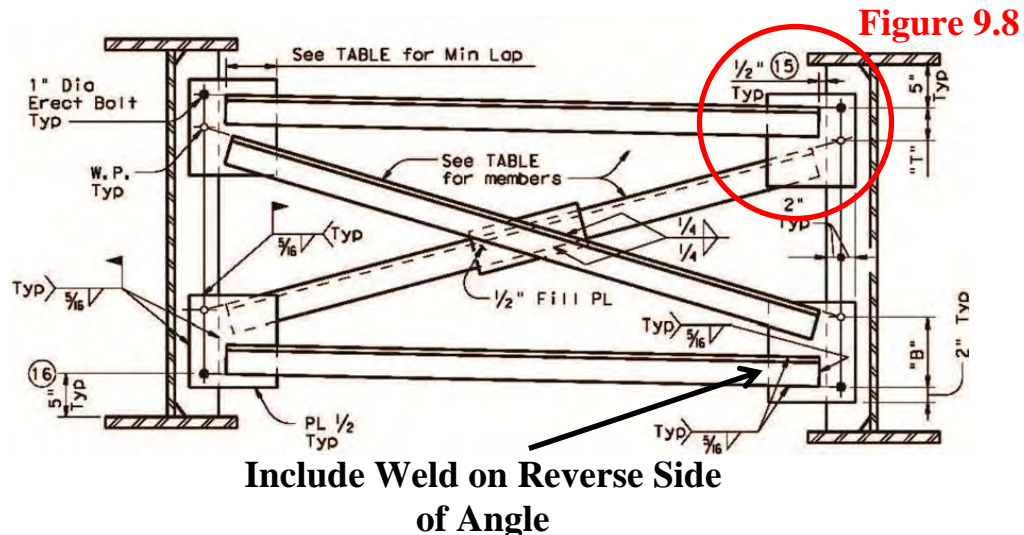


Figure 9.7: Suggested Improvements to TxDOT Standard X Frame Detail

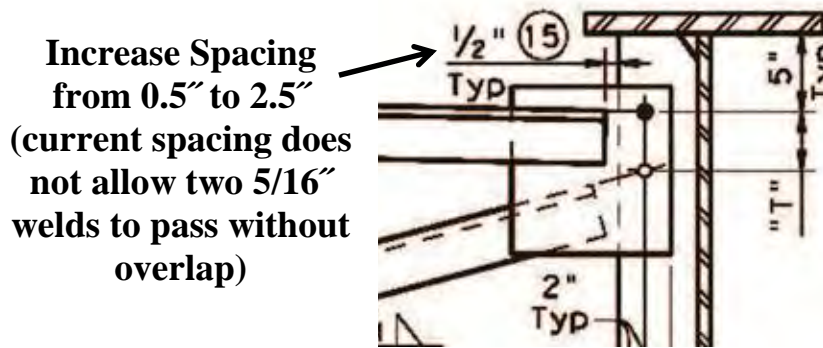


Figure 9.8: Increased Spacing between End of Angle and Edge of Stiffener

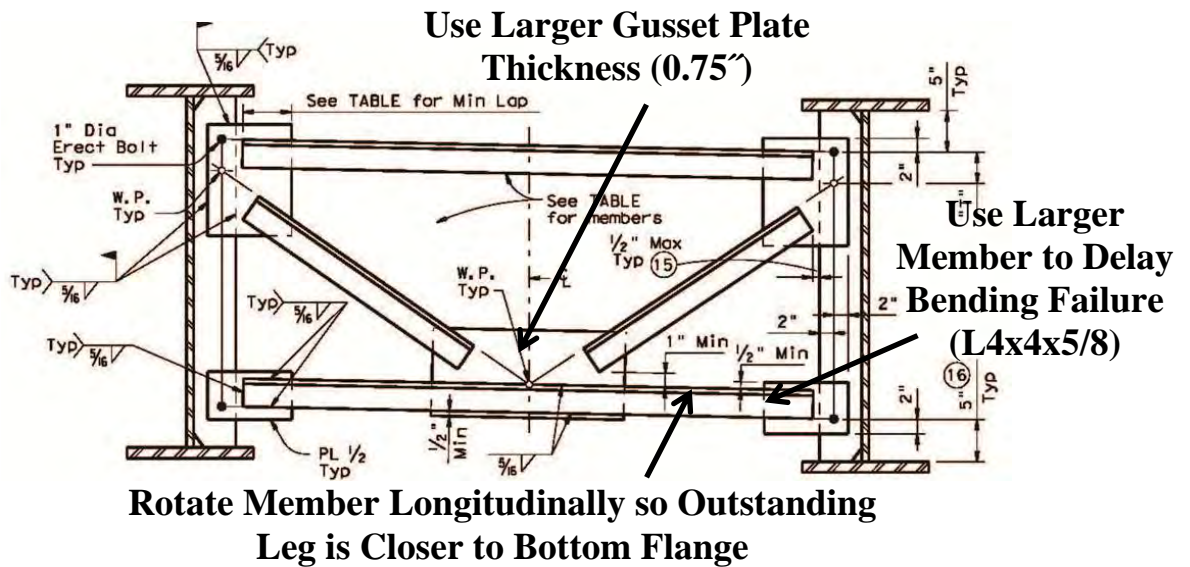


Figure 9.9: Suggested Improvements to TxDOT Standard K Frame Detail

References

- AASHTO/NSBA Steel Bridge Collaboration. (2003). *Guidelines for Design for Constructibility*. AASHTO.
- AASHTO/NSBA Steel Bridge Collaboration. (2011). G13.1 Guidelines for Steel Girder Bridge Analysis.
- Adan, S., and Gibb, W. (2008). "Inelastic Cyclic Testing of the Kaiser Bolted Bracket Moment Connection." *ASCE Structures Congress Conference Proceedings*.
- American Institute of Steel Construction (AISC). (2005). *Steel Construction Manual, 13th Edition*.
- American Institute of Steel Construction (AISC). (2010). *Steel Construction Manual, 14th Edition*.
- American Association of State Highway and Transportation Officials, *AASHTO LRFD Bridge Design Specifications, 4th Edition*, 2007.
- American Association of State Highway and Transportation Officials, *AASHTO LRFD Bridge Design Specifications, 5th Edition*, 2010.
- American Association of State Highway and Transportation Officials, *AASHTO LRFD Bridge Design Specifications, 6th Edition*, 2012.
- American Welding Society. (2010). *AWS D1.1/D1.1M: 2010 Structural Welding Code-Steel*, XXth edition. American Welding Society, Miami, FL.
- ANSYS Inc. (2011). "Elements Reference." *Release 11.0 Documentation for ANSYS*.
- ASCE. (1997). ASCE10-97-Design of Latticed Steel Transmission Structures.
- Barth, A. S., & Bowman, M. D. (2001). Fatigue Behavior of Welded Diaphragm-to-Beam Connections. *Journal of Structural Engineering* , 127 (10), pp.1145-1152.
- Battistini, Anthony. "Skewed Cross Frame Connection Stiffness." *Master's Thesis presented to The University of Texas*. Austin, TX, December 2009.
- Brannon, S., McElrath, M., Reddy, R., and Counselor, S. (2001, October). "Navigating the Ripples of Flow Coating." *Modern Casting*, 29-31.
- Chang, C. S. (2005). Computer Simulation for Steel Bridge Construction. *Proc., World Steel Bridge Symposium*.
- Connor, L., editor. (1987). *Welding Handbook, 8th Edition*. Volume 1, American Welding Society. Miami, FL.
- de Oliveira, Juan-Carlos. "Cast Steel Connector for Tubular Braces in Seismic Building Applications." *Master's Thesis presented to The University of Toronto*. Toronto, Ontario, Canada, 2006.

- de Oliveira, J.C., Packer, J., and Christopoulos, C. (2008, March) “Cast Steel Connectors for Circular Hollow Section Braces under Inelastic Cyclic Loading.” *Journal of Structural Engineering*, 134 (3), 374-383.
- de Oliveira, C., and Stine, T. (2008, July). “Convenient Connections.” *Modern Steel Construction*.
- Dowswell, B. and Barber, S. (2005). “Shear Lag in Rectangular Hollow Structural Sections Tension Members: Comparison of Design Equations to Test Data.” *Practice Periodical on Structural Design and Construction* 10 (3), 195-199.
- FHWA. (2009). Load Rating Guidance and Examples For Bolted and Riveted Gusset Plates In Truss Bridges.
- Federal Highway Administration. (2001, March) “Steel Bridge Fabrication Technologies in Europe and Japan.” Report No. FHWA-PL-01-018.
- Frank, K.H. (2008). “CE 383D: Steel Bridge Design” Class Notes. The University of Texas at Austin.
- Frank, K.H and Fisher, J.W. (1979). “Fatigue Strength of Fillet Welded Cruciform Joints.” *Journal of the Structural Division*, 105 (ST9), 1727-1740.
- Fraser, R. E. (2000). Behaviour of Distortion-Induced Fatigue Cracks in Bridge Girders. *Structural Engineering Report* , No. 235.
- Heins, C. P., & Potocko, R. A. (1979, August). Torsional Stiffening of I-Girder Webs. *ASCE Journal of the Structural Division* , 1689-1698.
- Helwig, T. A. (1994, August). Lateral Bracing of Bridge Girders by Metal Deck Forms. *PhD. Dissertation Submitted to University of Texas* . Austin, TX.
- Helwig, T., & Fan, Z. (2000). Field and Computational Studies of Steel Trapezoidal Box Girder Bridges, TxDOT Research Report 1395-3. The University of Houston.
- Herman, R. S., Helwig, T. A., & Chong, Z. (2007). Use of Lean-On Cross-Frame Bracing in Steel Girder Bridges. *Structures Congress: New Horizons and Better Practices* (p. 79). Long Beach: ASCE.
- Haldimann-Sturm, S.C., and Nussbaumer, A. (2008). “Fatigue Design of Cast Steel Nodes in Tubular Bridge Structures.” *International Journal of Fatigue*, 30, 528-537.
- Liu, Y., Dawe, J.L., and Li, L. (2006). “Experimental Study of Gusset Plate Connections for Tubular Bracing.” *Journal of Constructional Steel Research*, 62, 132-143.
- Maddox, S.J. (2008). “Status Review on Fatigue Performance of Fillet Welds.” *Journal of Offshore Mechanics and Arctic Engineering*, 130, 031006-1 – 031006-10.
- Martinez-Saucedo, G., and Packer, J.A. (2009). “Static Design Recommendations for Slotted End HSS Connections in Tension.” *Journal of Structural Engineering*, 135 (7), 797-805.

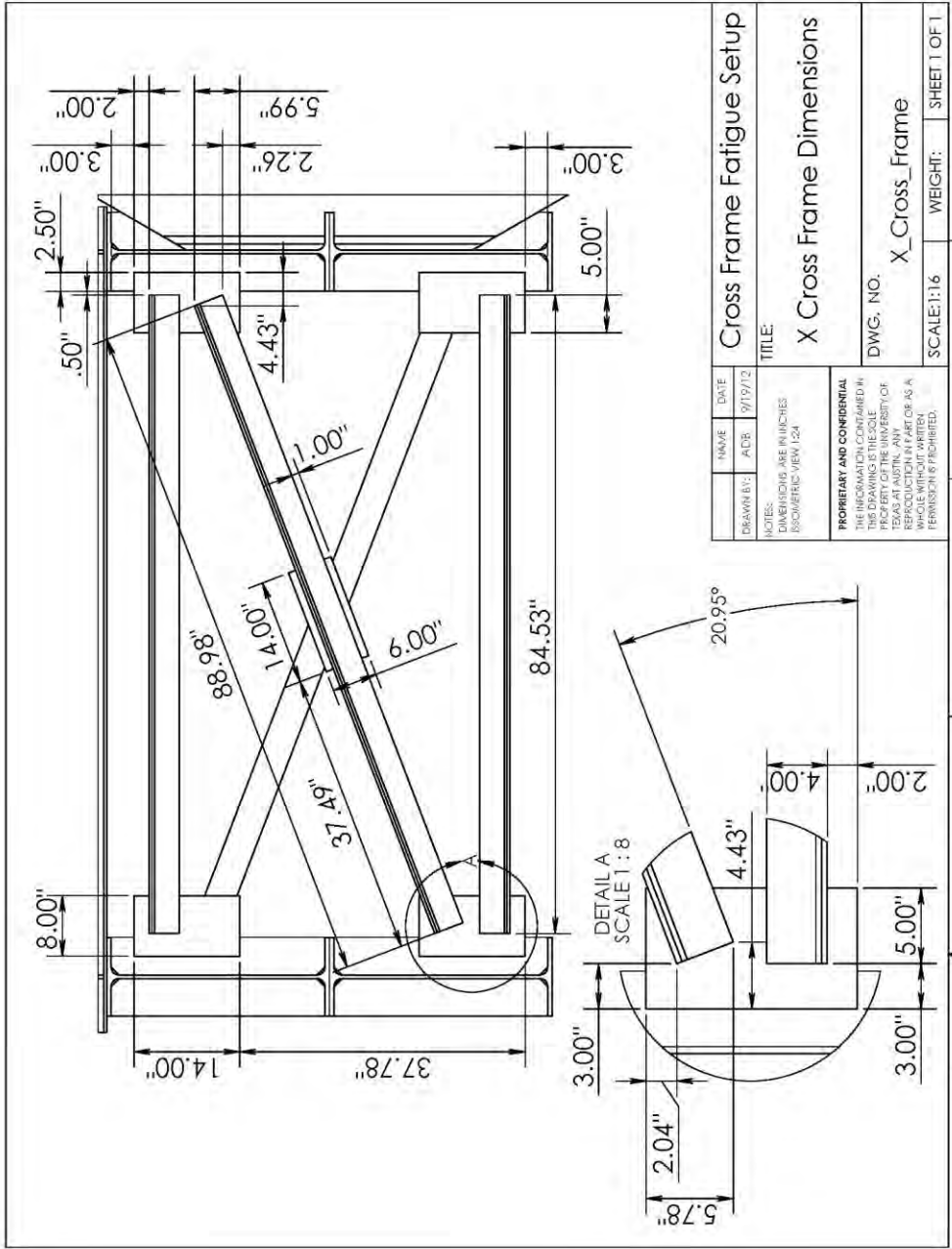
- MASTAN2, v3.3.1. Ziemian, R.D., and McGuire, W. (2013). Downloaded from Internet: <http://www.mastan2.com/>
- McDonald, G. and Frank, K. (2009, December). "The Fatigue Performance of Angle Cross-Frame Members in Bridges." Report FSEL No: 09-1 at the University of Texas at Austin.
- Mori, T.; Kainuma, S.; and Ichimiya, M. (2000). "A Study of Fatigue Crack Initiation Points in Load-Carrying Type Fillet Welded Joints." *IIW Document No. XIII-1832-2000*.
- Munse, W.H. (1964). *Fatigue of Welded Structures*. New York: Welding Research Council.
- Ningbo Yinzhou KST Machinery Co. Ltd (2010). "Investment Casting." Retrieved August 29, 2010: <http://www.casting-investment.com/investment-casting-process.htm>
- Ojalvo, M., & Chambers, R. (1977). Effects of Warping Restraints on I-Beam Buckling. *ASCE Journal of the Structural Division* , 103 (ST12), 2351-2360.
- Ozgur, C. a. (2007). Behavior and Analysis of a Curved and Skewed I-Girder Bridge. *Proc., World Steel Bridge Symposium*.
- Quadrato, Craig. "Stability of Skewed I-shaped Girder Bridges Using Bent Plate Connections." *Dissertation presented to The University of Texas*. Austin, TX, May 2010.
- Soderberg, E. (2010, March). "Colossal Cranes." *2010 STEER Conference*, Ferguson Structural Engineering Laboratory at the University of Texas at Austin, Presentation
- Steel Founders' Society of America. (2009). "SFSA: Overview of the Casting Process." Retrieved December 17, 2009: <http://www.sfsa.org/sfsa/cstintcp.php#prcint2.4>
- Stith, Jason. (2010) "Predicting the Behavior of Horizontally Curved I-Girders During Construction." *Dissertation presented to The University of Texas*. Austin, TX, August 2010.
- SSRC. (2010). *Stability Design Criteria for Metal Structures* (Six ed.). (R. Ziemian, Ed.) New York: Wiley & Sons.
- SSRC. (1998). *Structural Stability Research Council*. (T. V. Galambos, Ed.) New York: Wiley & Sons.
- Taylor, A., & Ojalvo, M. (1966, April). Torsional Restraint of Lateral Buckling. *Journal of the Structural Division* , 115-129.
- Texas Department of Transportation. (2006, April). Miscellaneous Details Steel Girders and Beams. Retrieved December 14, 2009, from Texas Department of Transportation: <ftp://ftp.dot.state.tx.us/pub/txdot-info/cmd/cserve/standard/bridge/spgdste1.pdf>

- Texas Steel Quality Council. (2007, April 1). *Preferred Practices for Steel Bridge Design, Fabrication, and Erections*. Retrieved May 9, 2008, from Texas Department of Transportation: http://www.dot.state.tx.us/publications/bridge/steel_bridge.pdf
- Timoshenko, S., & Gere, J. M. (1961). *Theory of Elastic Stability*. New York: McGraw-Hill.
- Topkaya, C., and Williamson, E.B. (2003). "Development of computational software for analysis of curved girders under construction loads." *Computers and Structures*, 81, 2087-2098.
- Totten, G.E., Funatani, K., and Xie, L. (2004). *Handbook of Metallurgical Process Design*. New York: Marcel Dekker, Inc., 353-356.
- Turco, G. (2009, November). "Wichita Falls Ramp 'T': Torsional Bracing Retrofit To 3-Span Steel Plate Girder Units." *2009 World Steel Bridge Symposium*, National Steel Bridge Alliance, Presentation.
- Wahr, Andrew. "The Fatigue Performance of Cross Frame Connections." *Master's Thesis Presented to The University of Texas*. Austin, TX, August 2010.
- Wang, L. (2002, August). Cross-Frame and Diaphragm Behaviour for Steel Bridges with Skewed Supports. *Ph.D. Dissertation Submitted to the University of Houston* . Houston, TX.
- Wang, L., & Helwig, T. A. (2008). Stability Bracing Requirements for Steel Bridge Girders with Skewed Supports. *Journal of Bridge Engineering* , 13 (2), 149-157.
- Whisenhunt, T. W. (2004). Measurement and Finite Element Modeling of the Non-Composite Deflections of Steel Plate Girder Bridges. *M.S. Thesis Submitted to North Carolina State University* . Raleigh, NC.
- Whitmore, R. (1952). Experimental Investigation of Stresses in Gusset Plates, Bulletin No. 16, Engineering Experiment Station,. University of Tennessee.
- Willibald, S., Packer, J.A., and Martinez-Saucedo, G. (2006). "Behaviour of Gusset Plate Connections to Ends of Round and Elliptical Hollow Structural Section Members." *Canadian Journal of Civil Engineering*, 33, 373-383.
- Winter, G. (1958). Lateral Bracing of Columns and Beams. *Journal of the Structural Division Proceedings of the American Society of Civil Engineers* , 84 (ST2), 1561-1 - 1561-22.
- Winterling, J. (2007). Monitoring Dead Load and Construction Stresses of a Heavily Skewed HPS Bridge. *M.S. Thesis Submitted to the University of Delaware* . Newark, DE.
- Yura, J. B. (1992). *Bracing of Steel Beams in Bridges*. Austin, TX: TxDOT.
- Yura, J. (2001). "Fundamentals of Beam Bracing." *Engineering Journal*, First Quarter, 11-26.

Yura, J., Helwig, T., Reagan, H., & Zhou, C. (2008). Global Lateral Buckling of I-Shaped Girder Systems. *Journal of Structural Engineering* , 134 (9), 1-8.

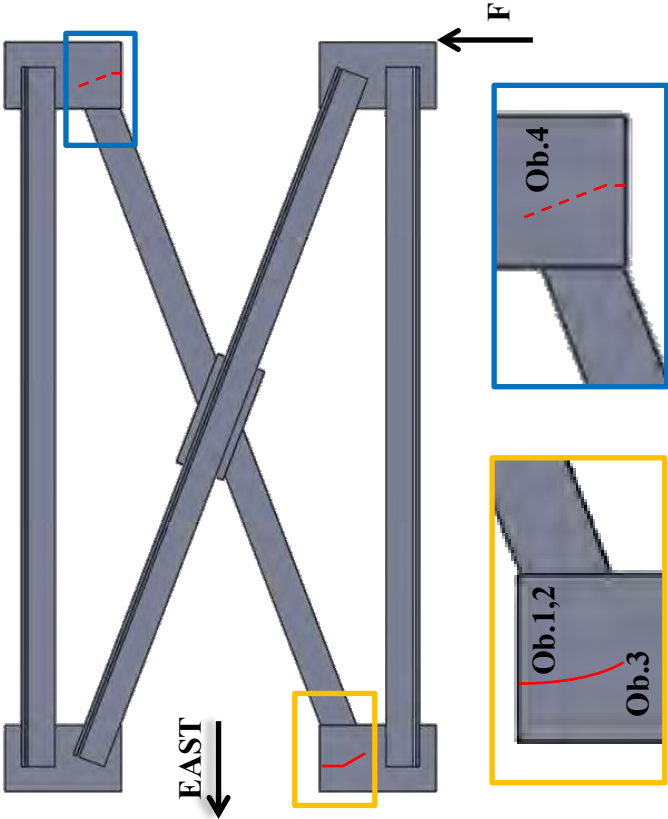
Zhou, C. (2006, December). Utilizing Lean-On Cross-Frame Bracing for Steel Bridges. *Ph.D. Dissertation Submitted to the University of Houston* . Houston, TX.

APPENDIX A
Cross Frame Fatigue Test Details



DRAWN BY:	NAME	DATE	Cross Frame Fatigue Setup X Cross Frame Dimensions
ADG	ADG	9/19/72	
NOTES: DIMENSIONS ARE IN INCHES ISOMETRIC VIEW 1:24			DWG. NO. X_Cross_Frame
PROPRIETARY AND CONFIDENTIAL THE INFORMATION CONTAINED IN THIS DRAWING IS THE SOLE PROPERTY OF THE UNIVERSITY OF TEXAS AT AUSTIN. ANY REPRODUCTION IN PART OR AS A WHOLE WITHOUT WRITTEN PERMISSION IS PROHIBITED.			
SCALE: 1:16		WEIGHT:	SHEET 1 OF 1

1 2 3 4 5

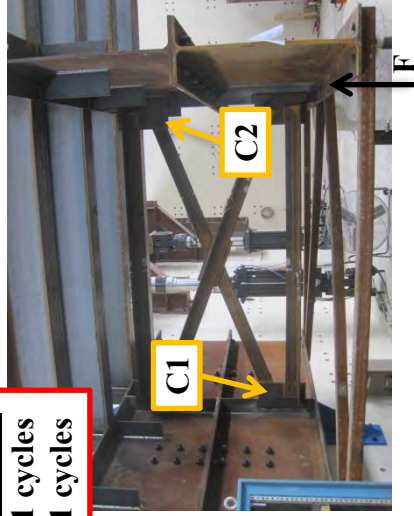
<p>Test Specimen: XF1</p>	<p>Crack Locations:</p> 
<p>Test Dates: 11/2/2012 – 11/4/2012</p>	
<p>Primary Failure Location: Gusset Plate</p> <p>$S_R = 20.03$ ksi (tension diagonal)</p> <p>$N = 38,201$ cycles</p> <p>AASHTO Fatigue Category: < E'</p>	
<p>Average Weld Size: Leg: 0.33" Throat: 0.32"</p>	
<p>Stiffness: Initial: 84.61 k/in Final: 79.34 k/in</p> <p>6.23% loss of stiffness</p>	<p>Details:</p> <ul style="list-style-type: none"> • TxDOT Standard X-Type Cross Frame Detail • First test completed in testing program • MTS 407 controller used • Tension diagonal of cross frame positioned on the back side of the cross frame • Tension diagonal angle-gusset plate weld intersected gusset-stiffener field weld
<p>Observations:</p> <ol style="list-style-type: none"> 1. Cracking occurred along the gusset toe of the gusset-stiffener weld above the weld intersection, and along the gusset toe of the angle-gusset weld below the intersection 2. The intersection of welds leads to a large tensile stress transfer, making it the likely point of crack initiation. The crack was already large when first observed, but Test Specimen XF4 confirmed this theory. 3. The curved nature of crack on back of gusset suggests downward propagation of crack by bending effects. 4. A smaller, hairline crack, similar in pattern, was seen at the opposite side of the tension diagonal. 	

Test Specimen: XF1

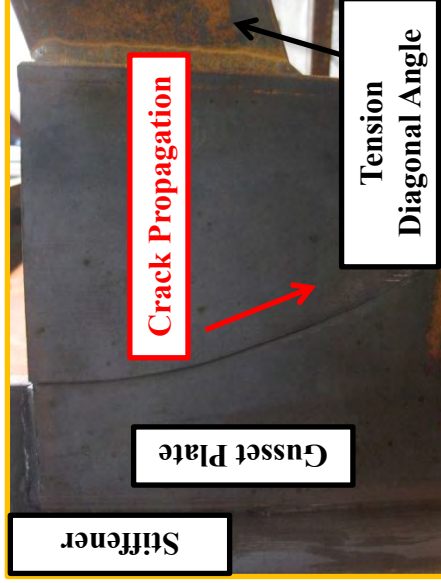
First Observed Crack

C1: N = 38,201 cycles

C2: N = 38,201 cycles

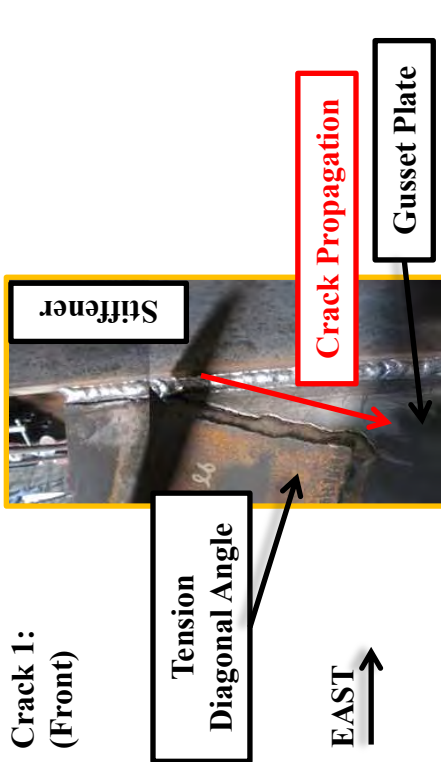


Crack 1:
(Back)

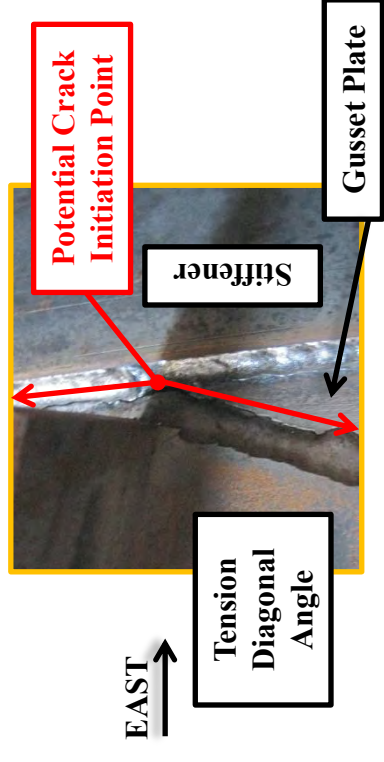


The curved nature of the crack suggests downward propagation due to bending.

Crack 1:
(Front)

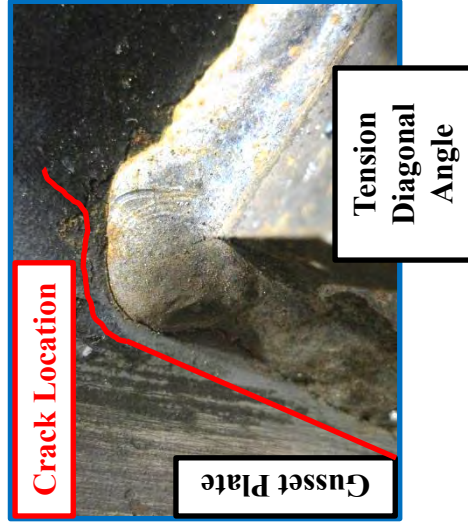
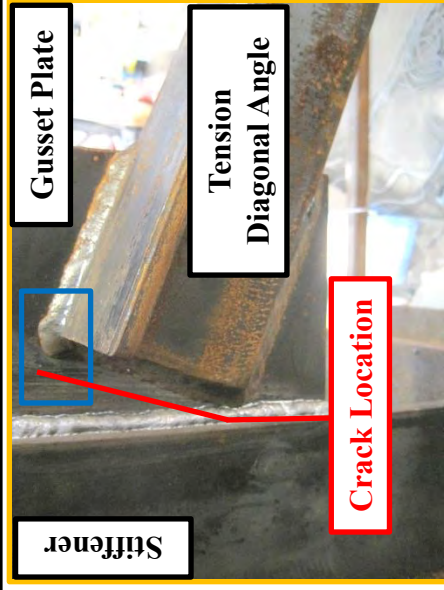


The crack was large when first observed. The crack is along the gusset toe of the gusset-stiffener weld and the gusset toe of the angle-gusset weld. It is believed to have initiated at the weld intersection, which would occur by strictly following the TxDOT Standard Detail.

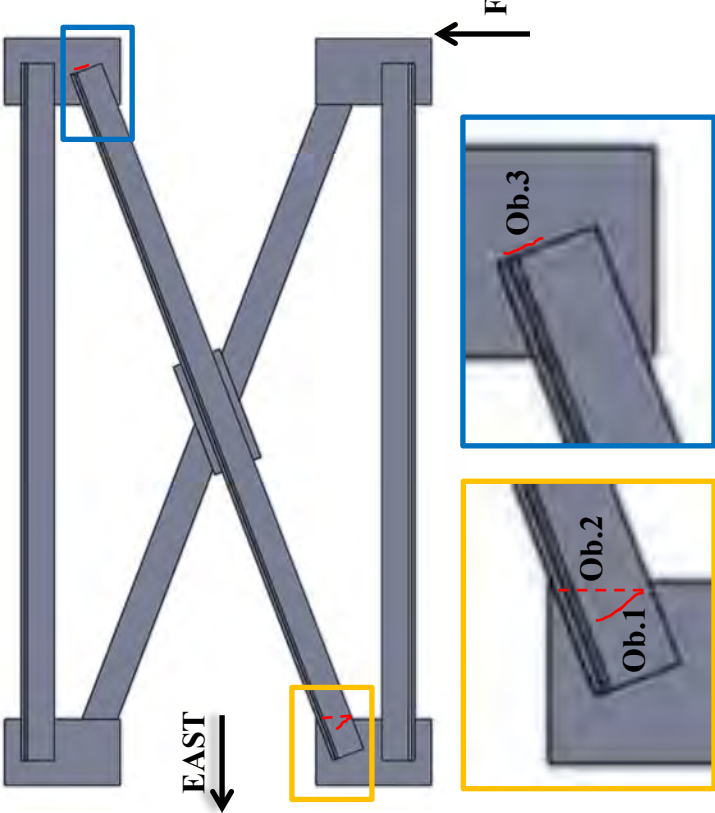


Test Specimen: XF1

Crack 2:



A similar crack to the primary failure occurred at the other end of the tension diagonal. The crack followed the gusset toe of the angle-gusset connection above the point of weld intersection and the gusset toe of the gusset-stiffener connection below the intersection.

<p>Test Specimen: XF2</p>	<p>Crack Locations:</p> 
<p>Test Dates: 11/12/2012 – 11/19/2012</p>	
<p>Primary Failure Location: Tension Diagonal</p> <p>$S_R = 15.00$ ksi (Effective Stress Range)</p> <p>$A_g = 2.85$ in²</p> <p>$U = 0.749$</p> <p>$N = 271,111$ cycles</p> <p>AASHTO Fatigue Category: E'</p>	
<p>Average Weld Size: Leg: 0.31" Throat: 0.33"</p>	<p>Stiffness: Initial: 88.25 k/in Final: 82.37 k/in</p> <p>6.67% loss of stiffness</p>
<p>Details:</p> <ul style="list-style-type: none"> • TxDOT Standard X-Type Cross Frame Detail • Tension diagonal of cross frame positioned on the front side of the cross frame • Compression diagonal angle-gusset plate weld intersected gusset-stiffener field weld 	<p>Observations:</p> <ol style="list-style-type: none"> 1. First crack initiated at the forward edge of angle-gusset weld at angle toe and propagated into the angle 2. Crack eventually began propagating through throat of the back side angle-gusset weld 3. Crack also seen at failure at gusset toe of angle-gusset weld of the tension diagonal on the opposite end from failure

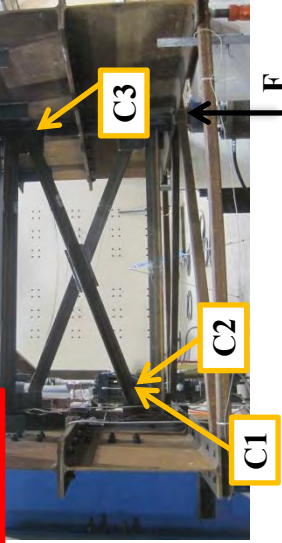
Test Specimen: XF2

First Observed Crack

C1: N = 271,111 cycles

C2: N = 271,111 cycles

C3: N = 271,111 cycles



EAST
→

Crack 2:



EAST
→

The crack also propagated through the weld throat on the angle back side fillet weld.

Crack 1:

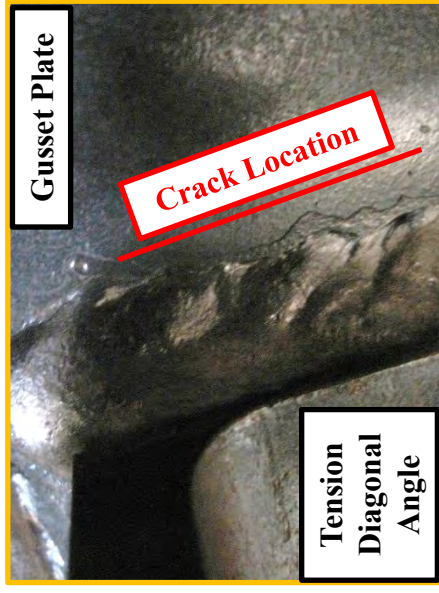
EAST
→



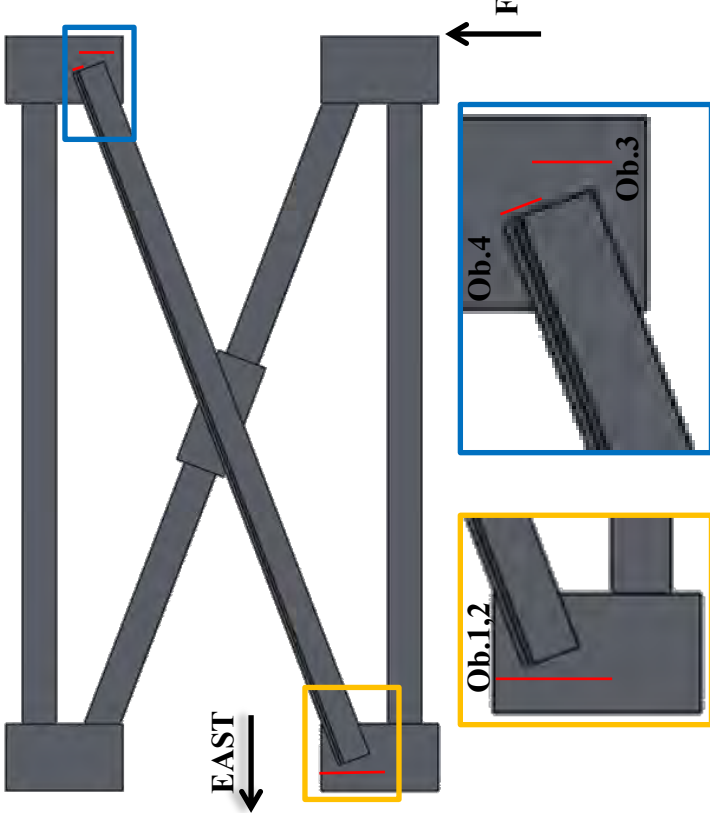
The first crack initiated at the forward edge of the fillet weld at the angle weld toe and propagated into angle.

Crack 3:

EAST
→



A small crack was also seen at failure at the gusset toe of the angle-gusset weld near the gusset stress concentration.

<p>Test Specimen: XF3</p>	<p>Crack Locations:</p> 
<p>Test Dates: 11/29/2012 – 12/3/2012</p>	
<p>Primary Failure Location: Gusset Plate $S_R = 15$ ksi (Tension Diagonal) $N = 99,120$ cycles AASHTO Fatigue Category: < E'</p>	
<p>Average Weld Size: Leg: 0.31" Throat: 0.29"</p>	
<p>Stiffness: Initial: 87.65 k/in Final: 84.59 k/in 3.49% loss of stiffness</p>	
<p>Details:</p> <ul style="list-style-type: none"> • TxDOT Standard X-Type Cross Frame Detail but tension diagonal length 1/2" shorter to prevent weld intersection • Tension diagonal of cross frame positioned on the back side of the cross frame • Tension diagonal angle-gusset weld did not intersect gusset-stiffener weld but was separated by 3/16" to 1/4" at closest point 	
<p>Observations:</p> <ol style="list-style-type: none"> 1. Crack initiated along gusset toe of gusset-stiffener weld at bottom end of tension diagonal. 2. Although the welds did not intersect, the crack still initiated in the gusset plate. 3. A similar crack was seen at the top end of the tension diagonal. The crack was along the gusset toe of the gusset-stiffener weld. The crack did not extend to the top/bottom of gusset plate suggesting the initiation occurred where the welds are near intersection, then the crack propagates in both directions. 4. Another crack was observed in the gusset toe in the angle-gusset weld near the angle end stress concentration. 	

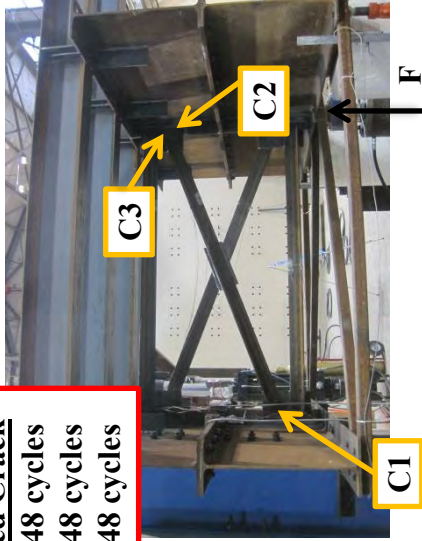
Test Specimen: XF3

First Observed Crack

C1: N = 77,648 cycles

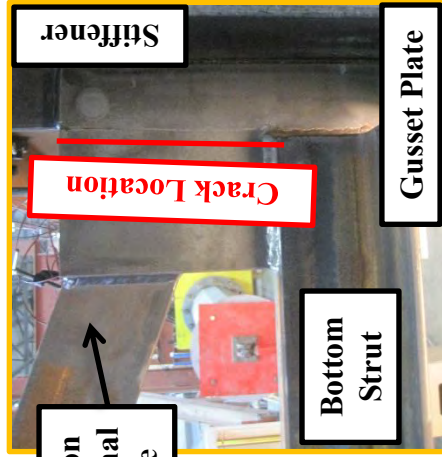
C2: N = 77,648 cycles

C3: N = 77,648 cycles



EAST
←

Crack 1:
(Back)

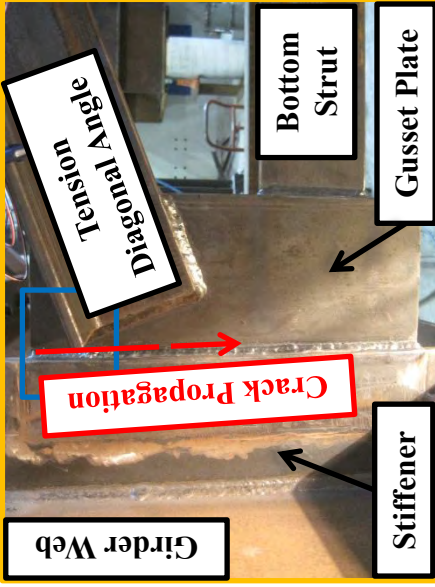


Tension
Diagonal
Angle

EAST
→

View of
the crack
on the
back side
of the
gusset
plate.

Crack 1:
(Front)



EAST
←

The first crack began near the weld intersection but had reached a length of 4" from the top of the gusset plate along the gusset toe of the gusset to stiffener weld when first seen. It continued propagating downward.



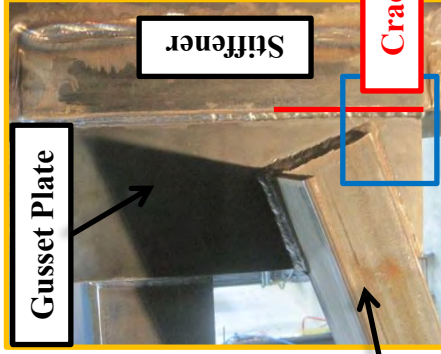
EAST
←

A close-up of
the crack.

Tension
Diagonal
Angle

Test Specimen: XF3

Crack 2:



EAST

Tension Diagonal Angle

Crack Location



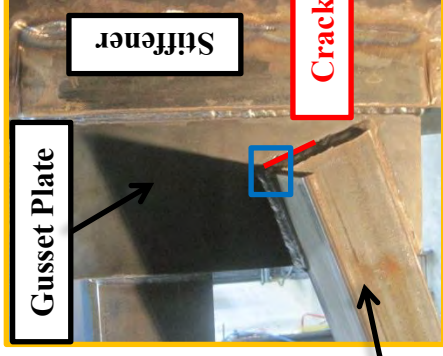
EAST

Gusset Plate

Crack Location

A similar crack formed at the other end of the tension diagonal along the gusset toe of the gusset-stiffener weld.

Crack 3:



EAST

Tension Diagonal Angle

Crack Location

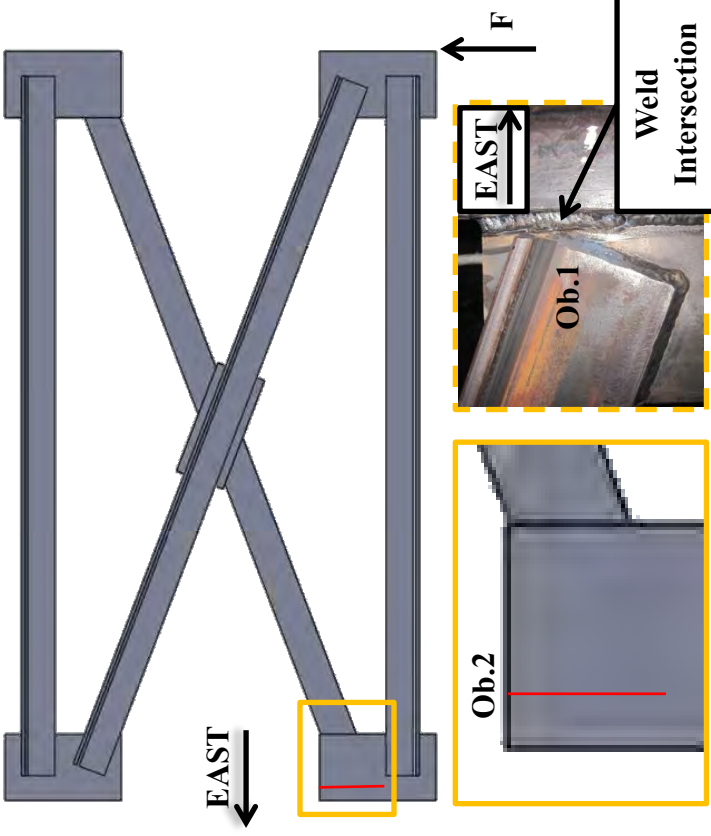


EAST

Tension Diagonal Angle

Crack Location

Another crack was observed on the gusset toe of the angle-gusset weld near the stress concentration associated with the angle end.

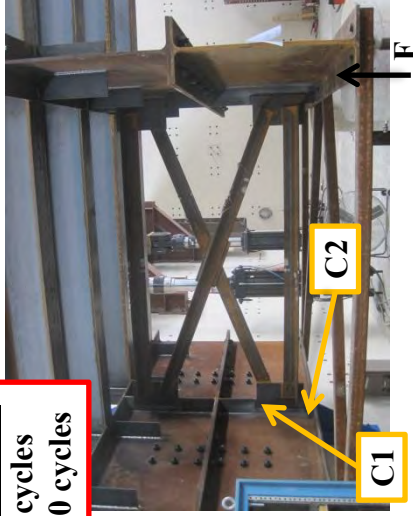
<p>Test Specimen: XF4</p>	<p>Crack Locations:</p> 
<p>Test Dates: 12/14/2012 – 12/18/2012</p>	
<p>Primary Failure Location: Gusset Plate</p> <p>$S_R = 20.27$ ksi</p> <p>$N = 19,078$ cycles</p> <p>AASHTO Fatigue Category: < E'</p>	
<p>Average Weld Size: Leg: 0.32" Throat: 0.31"</p>	
<p>Stiffness: Initial: 88.75 k/in Final: 79.21 k/in</p> <p>10.7% loss of stiffness</p>	
<p>Details:</p> <ul style="list-style-type: none"> • TxDOT Standard X-Type Cross Frame Detail • Tension diagonal of cross frame positioned on the back side of the cross frame • Tension diagonal angle-gusset weld purposefully intersected with gusset-stiffener weld to be similar to XF1 	
<p>Observations:</p> <ol style="list-style-type: none"> 1. Initial weld was undersized and did not intersect as welder attempted to avoid intersection. The weld was ground out from the top of the gusset to 2" below the intersection point, and then welded again to intersect. 2. Crack initiated along gusset toe of gusset-stiffener weld at the location of weld intersection and then propagated upward to the edge of the gusset plate and downward along the gusset toe ($N=2774$ at first crack). 3. Cracks were discovered in the stiffener after the first sign of cracking in the gusset plate was observed. Ultimately it was a combination of the two cracks which led to the stopping of the test. 	

Test Specimen: XF4

First Observed Crack

C1: N = 2774 cycles

C2: N = 11,620 cycles



EAST
→

Crack 1:
(Back)



EAST
→

View of the crack on the back side of the gusset plate.

Crack 1:
(Front)



EAST
→

Tension
Diagonal
Angle

Gusset Plate

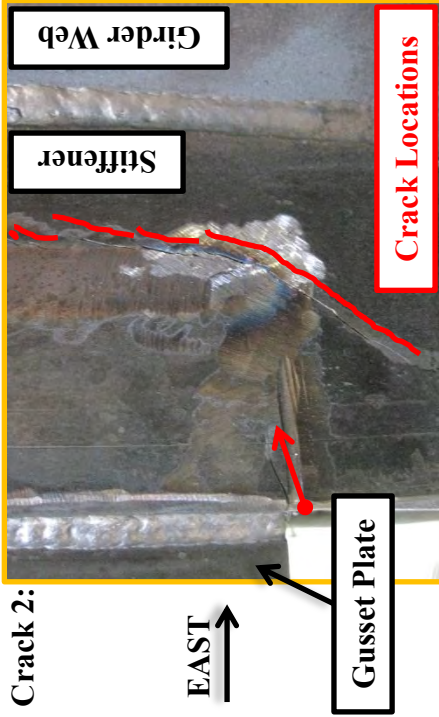
The first crack began at the weld intersection and extended upward to edge of gusset plate and downward along gusset toe.



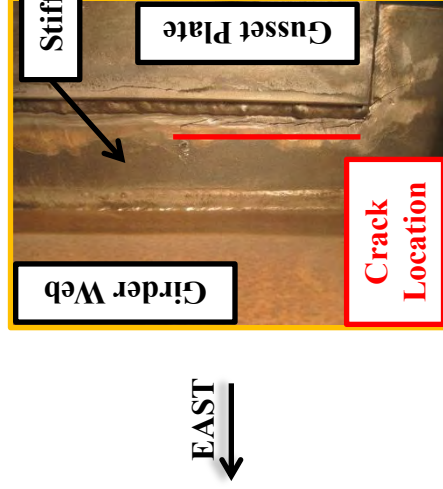
EAST
→

Crack Location

Test Specimen: XF4



Stiffness of cross frame was 83.30 k/in at the time stiffener cracks were noticed. (6.13% loss)



Cracks were observed in the stiffener due to the repeated grinding out and welding of multiple specimens.

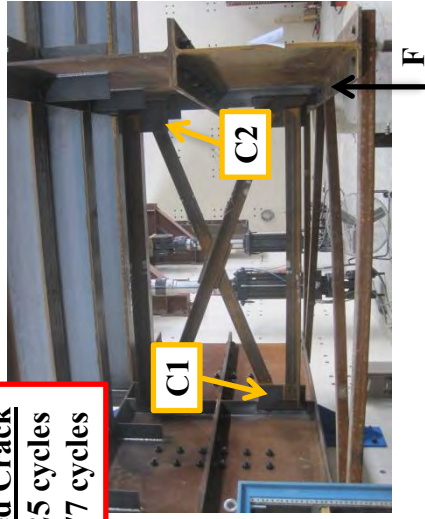
Test Specimen: XF5		Crack Locations:
Test Dates: 3/8/2013 – 3/14/2013	Secondary Failure: Tension Diagonal $S_R = 15.00$ ksi (Effective Stress Range) $A_g = 2.95$ in ² $U = 0.734$ $N = 179,907$ cycles AASHTO Fatigue Category: E'	
Primary Failure: Tension Diagonal $S_R = 15.00$ ksi (Effective Stress Range) $A_g = 2.95$ in ² $U = 0.734$ $N = 55,774$ cycles AASHTO Fatigue Category: < E'	Stiffness: Initial: 89.12 k/in Final: 82.73 k/in 7.17% loss of stiffness Average Weld Size: Leg: 0.32" Throat: 0.31"	Details: <ul style="list-style-type: none"> • TxDOT Standard X-Type Cross Frame Detail with members 1" short prevent weld intersection • The back of the angle was not welded to gusset • Tension diagonal of cross frame positioned on the front side of the cross frame • After tension diagonal cracked on one end, it was repaired to allow cracking at the other end
Observations: <ol style="list-style-type: none"> 1. First crack initiated at the forward edge of angle-gusset weld at angle toe and propagated into the angle 2. Second crack initiated at the forward edge of angle-gusset weld at angle heel and propagated into the angle 3. Repair of first crack resulted in system with similar stiffness as the original 		

Test Specimen: XF5

First Observed Crack

C1: N = 55,625 cycles

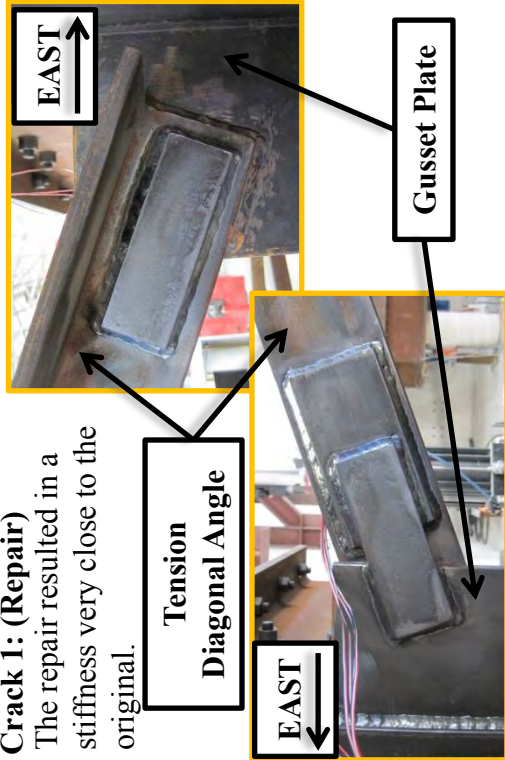
C2: N = 66,777 cycles



EAST ←

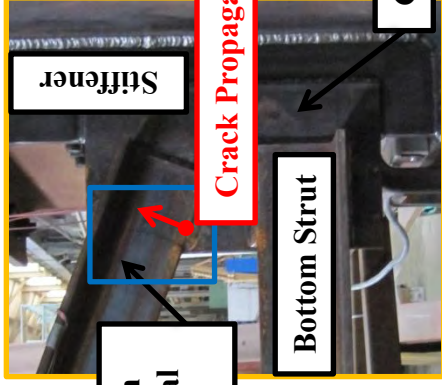
Crack 1: (Repair)

The repair resulted in a stiffness very close to the original.



EAST ←

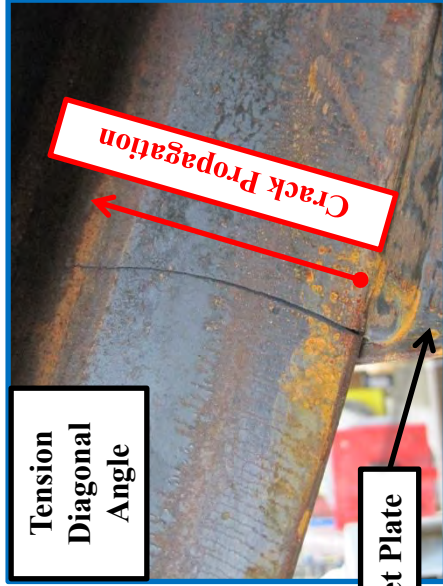
Crack 1: (Front)



Tension Diagonal Angle

EAST →

The first crack occurred at the forward edge of the angle-gusset connection initiating at the angle toe and propagating into the angle. A close up is shown below.



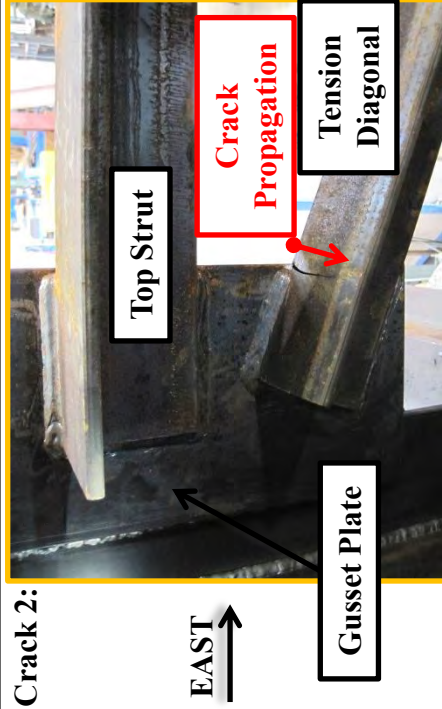
Tension Diagonal Angle

EAST →

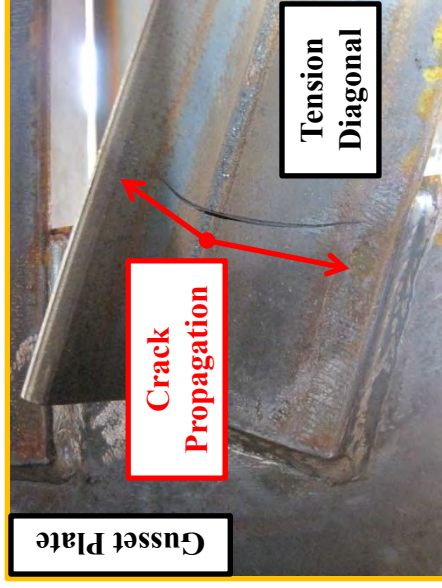
Gusset Plate

Test Specimen: XF5

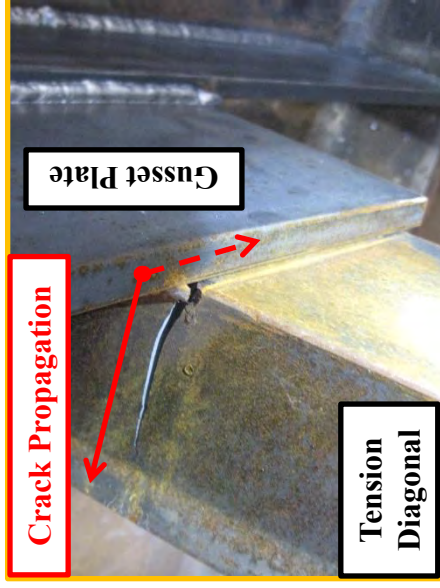
Crack 2:



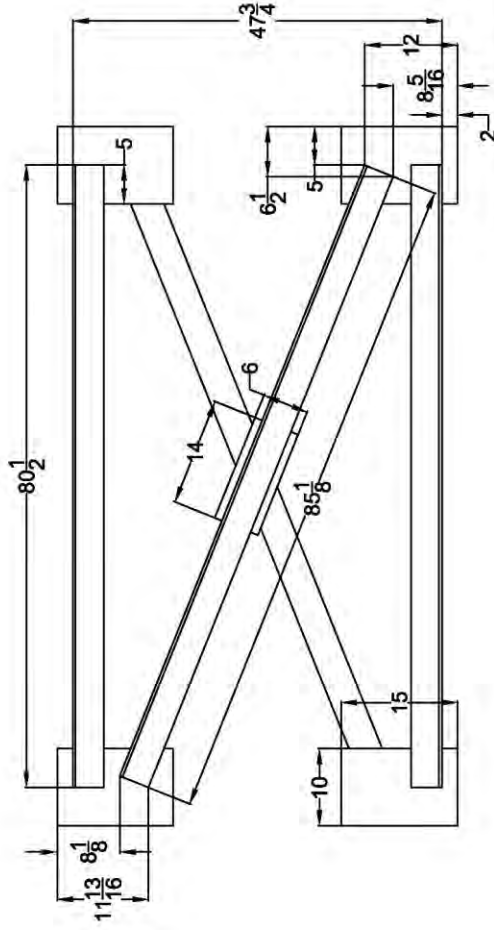
After the repair (N = 55,774 cycles), testing of the specimen continued. There was no sign of a crack at this location at the time of repair. At N = 66,777 cycles, a small crack was seen to initiate at the angle toe at the forward edge of angle-gusset connection and propagating into the heel of the angle (seen using magnifying glass). The crack propagated through the angle thickness and along both angle legs until failure.



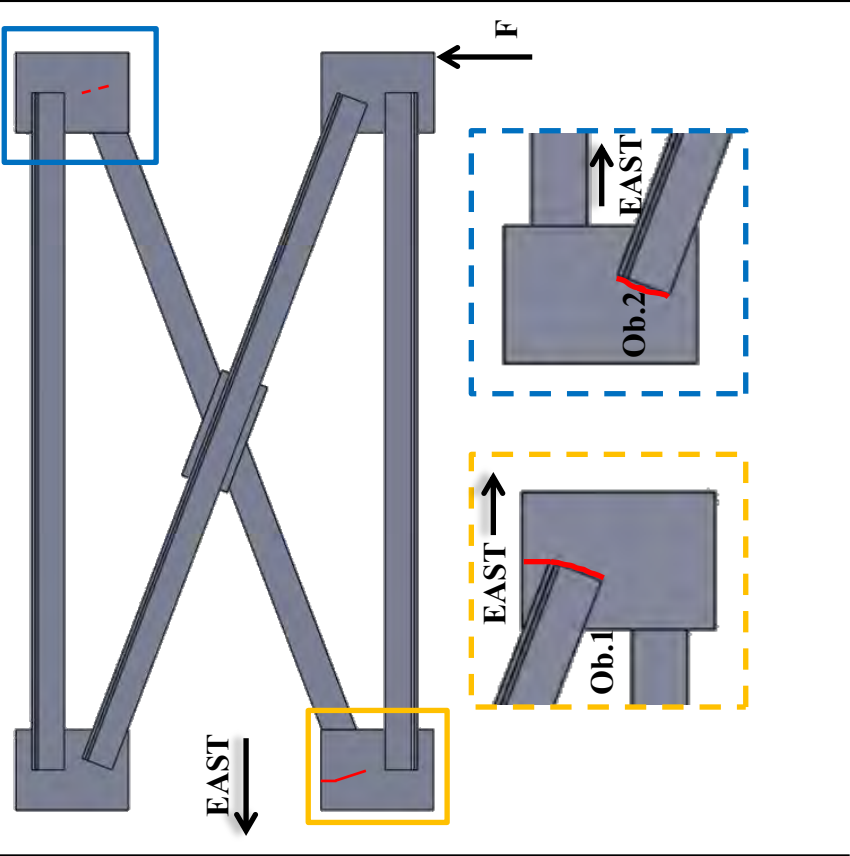
View of crack on the inside face of the angle.



Top view of crack initiating at angle heel..



Cross Frame Fatigue Test	
X Frame 10" Gusset	
Scale: 1:16	Sheet 1 of 1

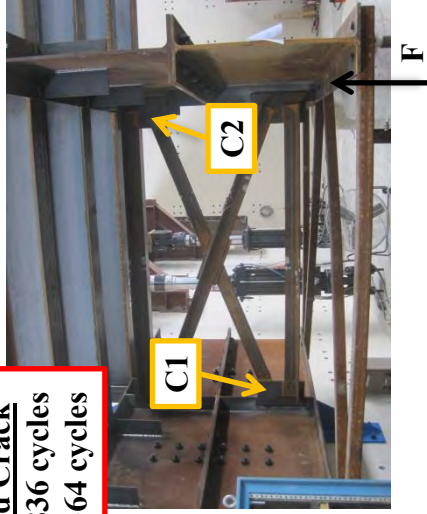
<p>Test Specimen: XF6</p>	<p>Crack Locations:</p> 	
<p>Test Dates: 4/9/2013 – 4/19/2013</p>		
<p>Primary Failure Location: Gusset Plate</p> <p>$S_R = 13.00$ ksi (Tension Diagonal)</p> <p>$N = 683,364$ cycles</p> <p>AASHTO Fatigue Category: E</p>		
<p>Stiffness: Initial: 97.97 k/in Final: 86.22 k/in</p> <p>12.0% loss of stiffness</p>		
<p>Average Weld Size: Leg: 0.31" Throat: 0.34"</p>		
<p>Details:</p> <ul style="list-style-type: none"> • TxDOT Standard X-Type Cross Frame Detail with members 4" short prevent weld intersection • The gusset plates were 2" wider to maintain the same overlap as XF1-5 and the angle of the diagonals remained consistent • Tension diagonal of cross frame positioned on the back side of the cross frame to see if increased space between angle-gusset weld and gusset-stiffener weld improves plate fatigue 		
<p>Observations:</p> <ol style="list-style-type: none"> 1. First crack initiated at the back edge of angle-gusset weld at gusset toe and propagated into the gusset plate to the free edge 2. Second, similar crack found at opposite end of tension diagonal during final stiffness test 		

Test Specimen: XF6

First Observed Crack

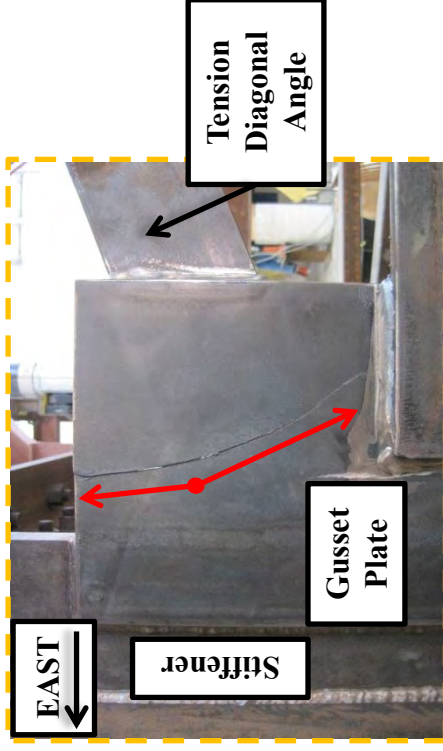
C1: N = 369,836 cycles

C2: N = 683,364 cycles



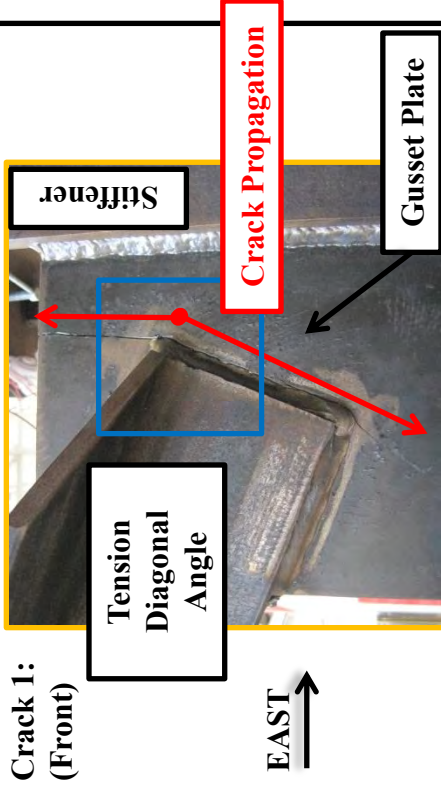
EAST ←

Crack 1: (Back)



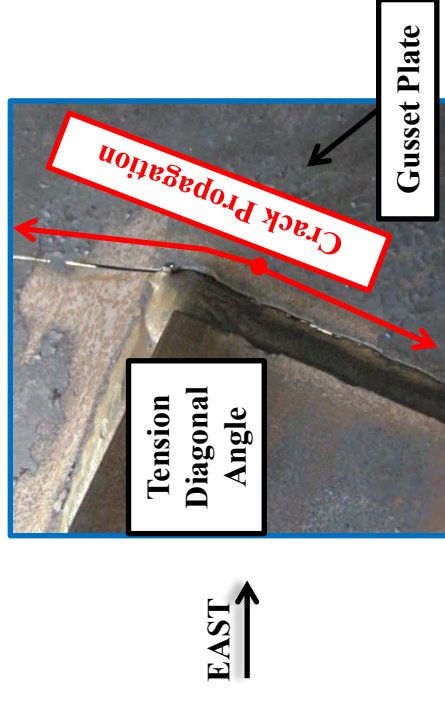
EAST ←

Crack 1:
(Front)



EAST →

The first crack occurred at the back edge of the angle-gusset connection initiating at the gusset toe and propagating into the plate. A close up is shown below.

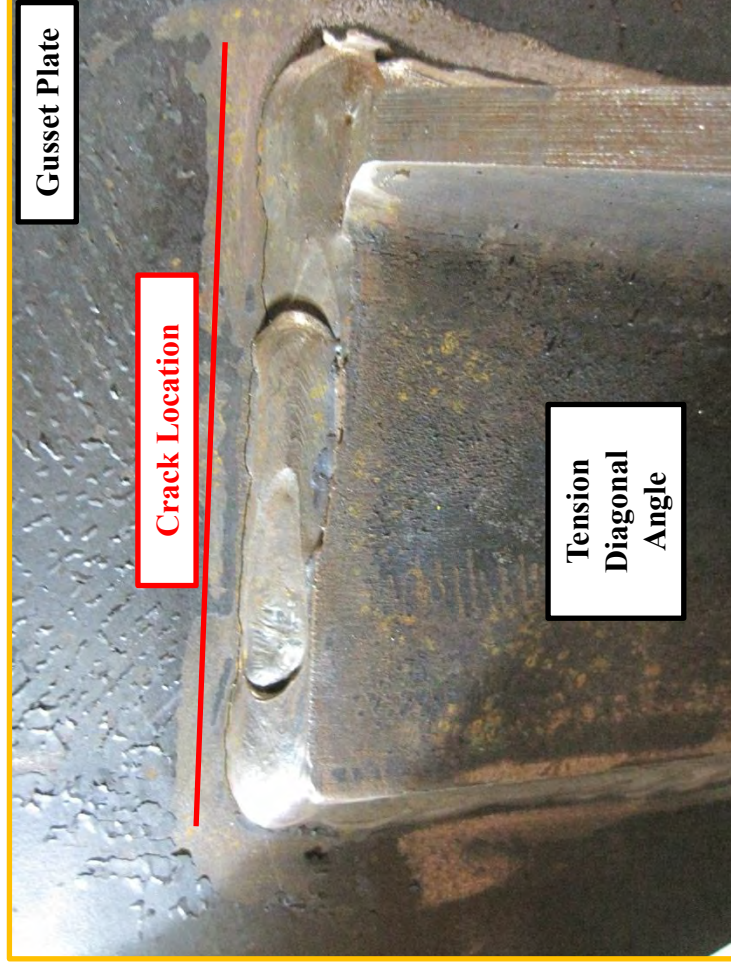


EAST →

Gusset Plate

Test Specimen: XF6

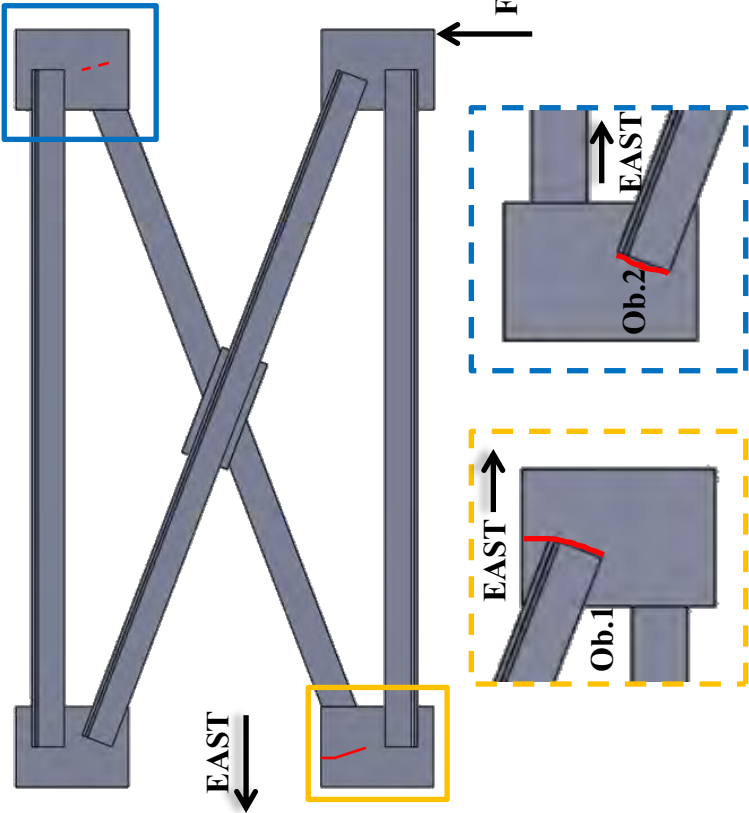
**Crack 2:
(Front)**



EAST →

The second crack occurred at the opposite side of the tension diagonal along the back edge of the angle-gusset connection initiating at the gusset toe and propagating into the plate. The crack was first observed at failure.

There is also damage to the mill scale seen in this photo. It is possible some local yielding occurred by placing the angle further from the gusset-stiffener connection.

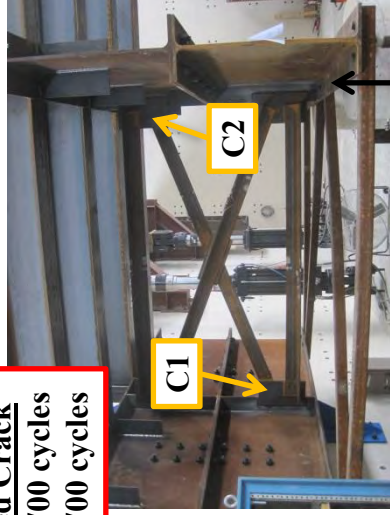
<p>Test Specimen: XF7</p>	<p>Crack Locations:</p> 
<p>Test Dates: 5/30/2013 – 6/4/2013</p>	
<p>Primary Failure Location: Gusset Plate</p> <p>$S_R = 15.00$ ksi (Tension Diagonal)</p> <p>$N = 300,001$ cycles</p> <p>AASHTO Fatigue Category: almost E</p>	
<p>Stiffness: Initial: 98.12 k/in Final: 82.19 k/in</p> <p>16.2% loss of stiffness</p>	
<p>Average Weld Size: Leg: 0.31" Throat: 0.32"</p>	
<p>Details:</p> <ul style="list-style-type: none"> • TxDOT Standard X-Type Cross Frame Detail with members 4" short prevent weld intersection • The gusset plates were 2" wider to maintain the same overlap as XF1-6 and the angle of the diagonals remained consistent • Tension diagonal of cross frame positioned on the back side of the cross frame to validate results of XF_6 that increased space between angle-gusset weld and gusset-stiffener weld improves plate fatigue 	
<p>Observations:</p> <ol style="list-style-type: none"> 1. First crack initiated at the back edge of angle-gusset weld at gusset toe and propagated into the gusset plate to the free edge 2. Second, similar crack found at opposite end of tension diagonal at the same time first crack was observed. 	

Test Specimen: XF7

First Observed Crack

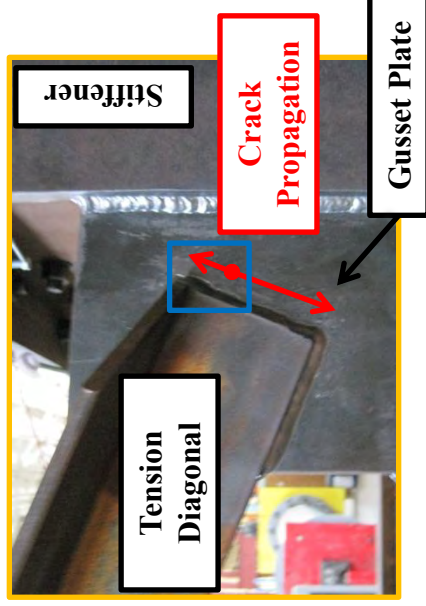
C1: N = 175,700 cycles

C2: N = 175,700 cycles



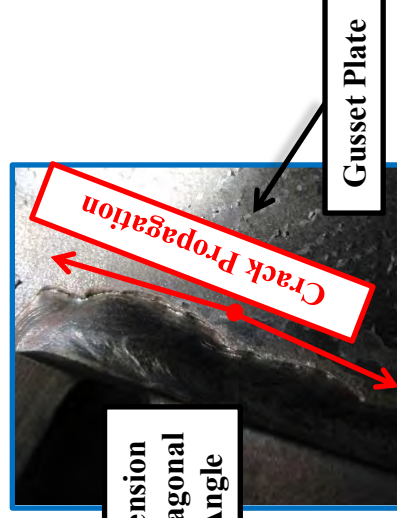
EAST ←

Crack 1:
(Front)



EAST →

The first crack occurred at the back edge of the angle-gusset connection initiating at the weld toe and propagating into the plate. Close ups are shown below. Note how the crack follows the weld toe. There is also minor undercut at this connection but it is within acceptable tolerances.



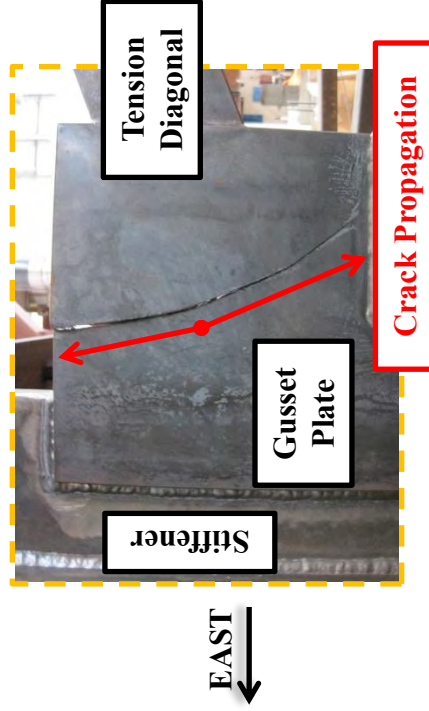
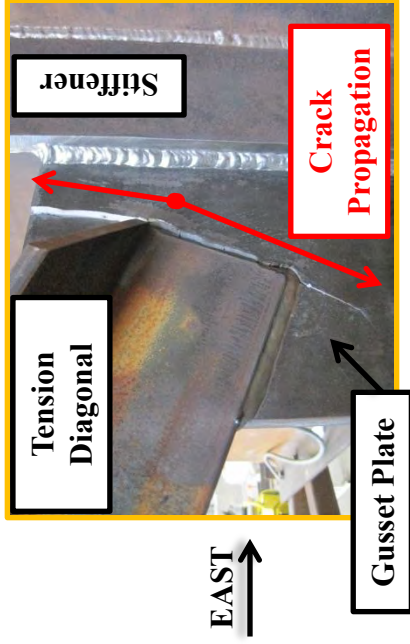
EAST →



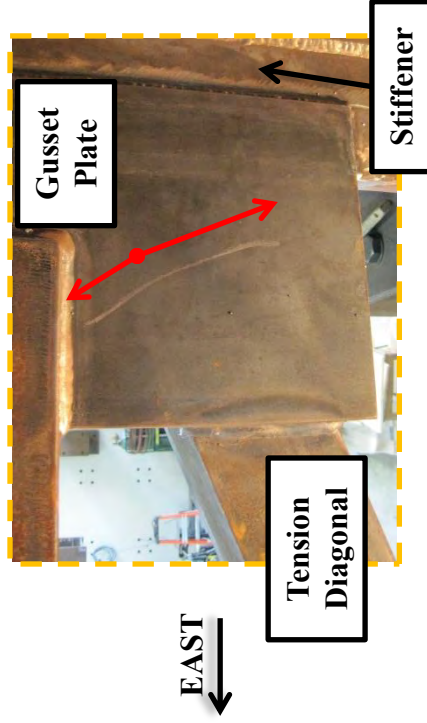
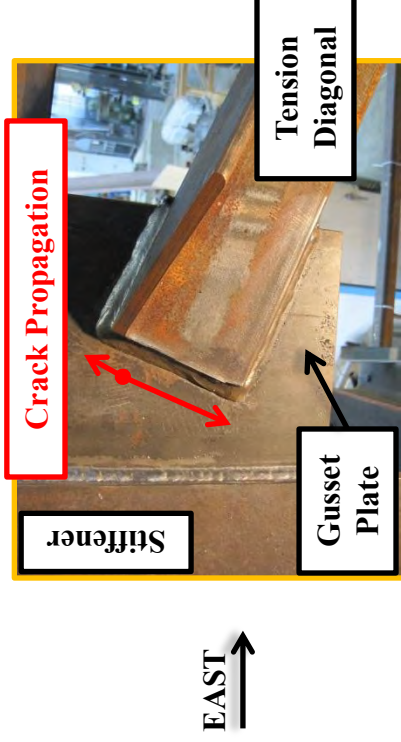
EAST →

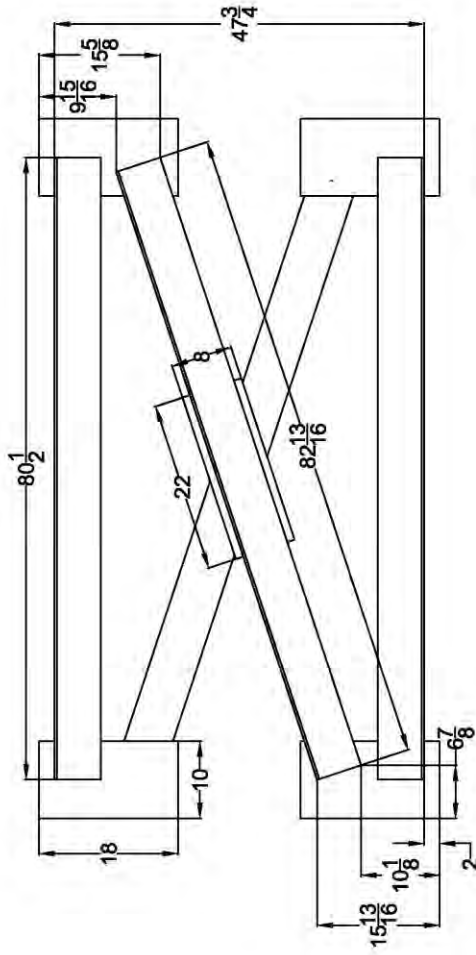
Test Specimen: XF7

Crack 1: (Failure- N=300,001)



Crack 2: (Failure- N=300,001)



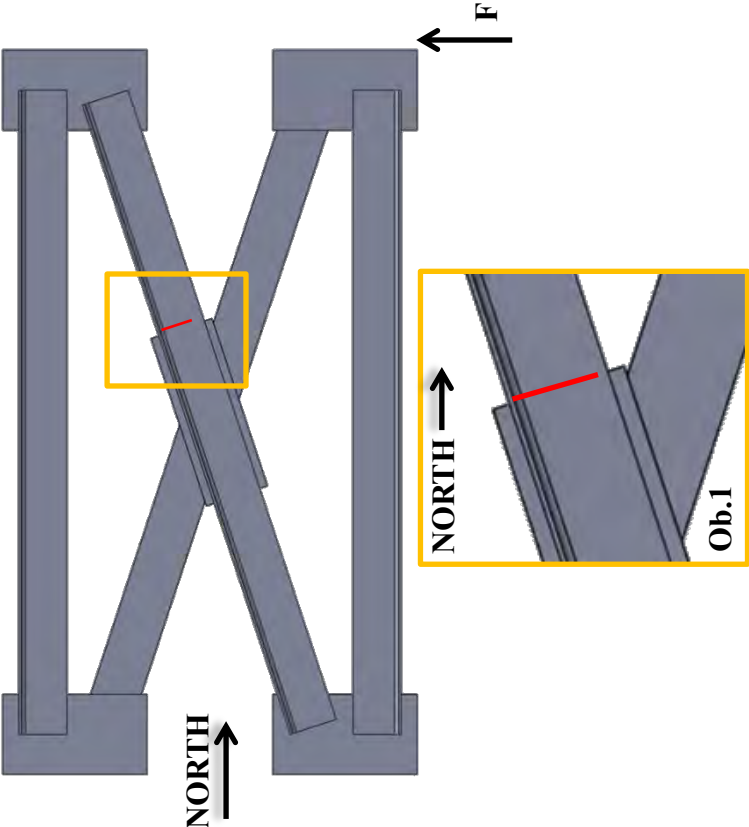


Cross Frame Fatigue Test

Unequal Leg Angle
X Frame 10" Gusset

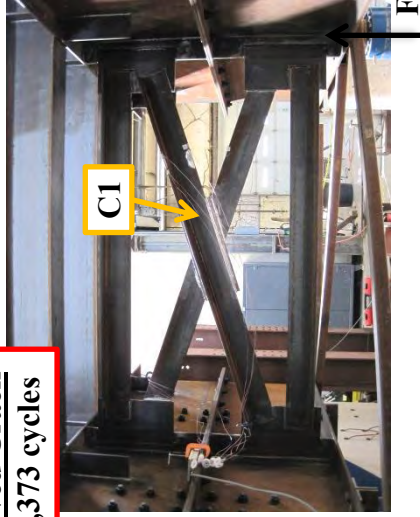
Unequal_X_Frame_10_Gusset

Scale: 1:16 Sheet 1 of 1

<p>Test Specimen: XF_UL_1</p>	<p>Crack Locations:</p> 
<p>Test Dates: 4/10/2013 – 4/12/2013</p>	
<p>Primary Failure Location: Angle</p> <p>$S_R = 15.00$ ksi</p> <p>$N = 86,970$ cycles</p> <p>AASHTO Fatigue Category: < E'</p>	
<p>Stiffness: Initial: 94.32 k/in Final: 66.12 k/in</p> <p>29.9% loss of stiffness</p>	
<p>Average Weld Size: Leg: 0.31" Throat: 0.31"</p>	
<p>Details:</p> <ul style="list-style-type: none"> • Unequal leg L6 x 3.5 x 5/16 members • TxDOT Standard X-Type Cross Frame Details for L4 x 4 x 3/8 followed for overlap • TxDOT Standard X-Type Cross Frame Details for L6 x 6 x 9/16 followed for plate geometry • Angles 1" shorter to prevent weld intersection • Tension diagonal of cross frame positioned on the front side of the cross frame to prevent interaction of angle-gusset weld and gusset-stiffener weld 	
<p>Observations:</p> <ol style="list-style-type: none"> 1. First crack initiated at the angle toe of the angle-center plate weld at the heel of the angle and propagated along both legs of the angle 	

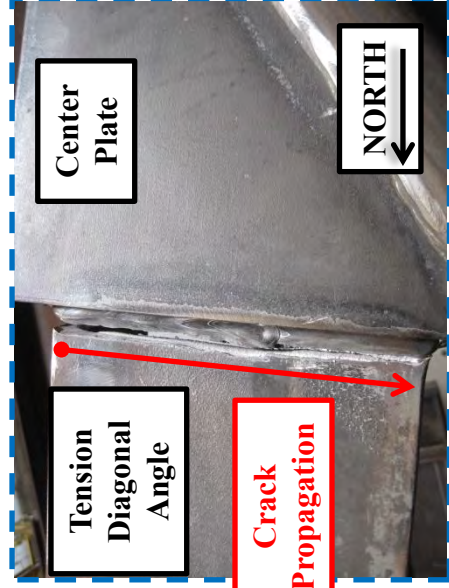
Test Specimen: XF_UL_1

First Observed Crack
C1: N = 83,373 cycles



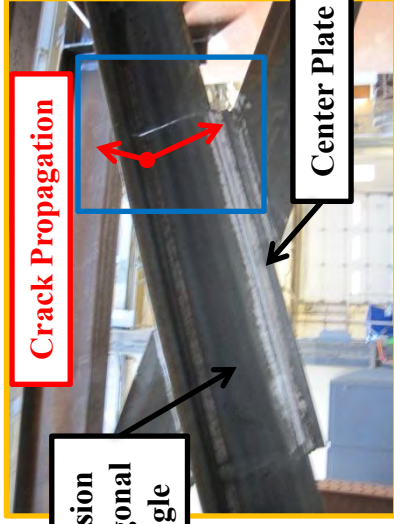
NORTH
→

Crack 1: (Back- Horizontal Long Leg)



NORTH
←

Crack 1:
(Front)



Tension
Diagonal
Angle

NORTH
→

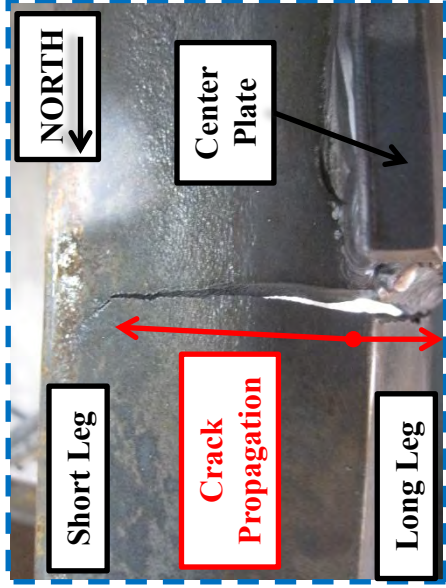
The crack occurred at the heel of the angle along the angle toe of the angle-center plate weld and propagating into the angle legs. The crack was not observed sooner as previous experiments did not lead researchers to monitor this location.

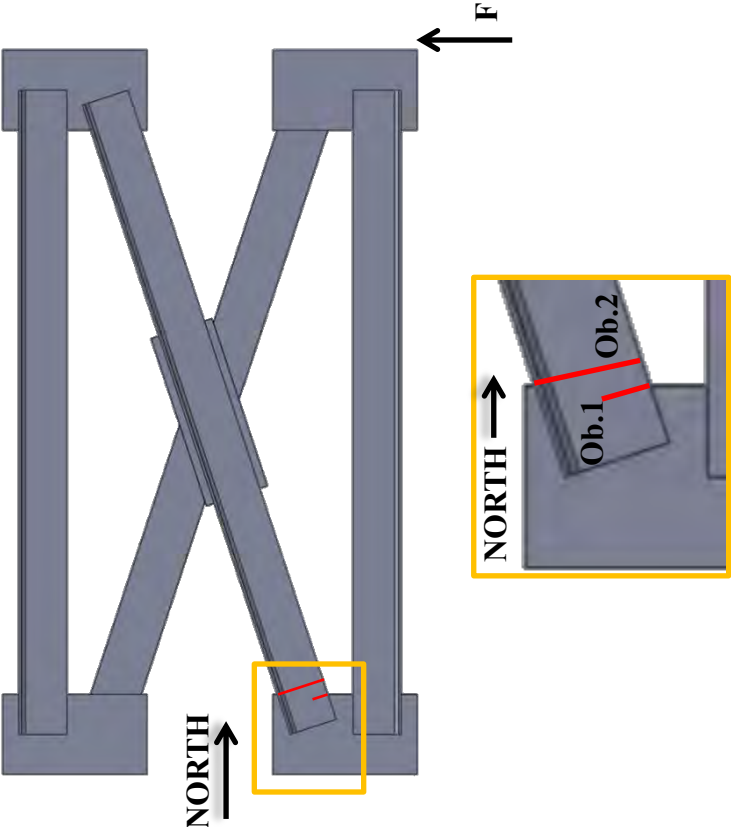


NORTH
→

Test Specimen: XF_UL_1

Crack 1: (Top-Outstanding Short Leg)



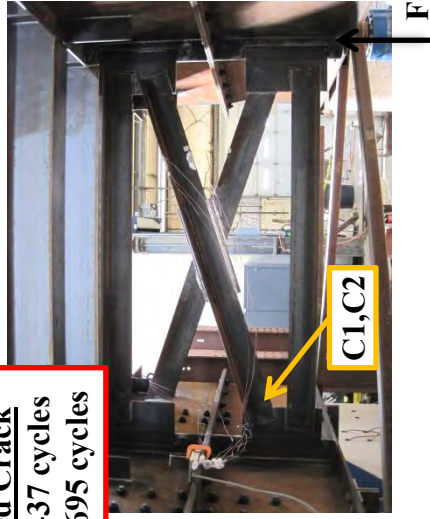
<p>Test Specimen: XF_UL_2</p>	<p>Crack Locations:</p> 
<p>Test Dates: 5/8/2013 – 5/20/2013</p>	
<p>Primary Failure Location: Angle</p> <p>$S_R = 15.00$ ksi</p> <p>$N = 620,464$ cycles</p> <p>AASHTO Fatigue Category: E'</p>	
<p>Stiffness: Initial: 94.32 k/in Final: 74.5 k/in</p> <p>21.0% loss of stiffness</p>	
<p>Average Weld Size: Leg: 0.30" Throat: 0.31"</p>	
<p>Details:</p> <ul style="list-style-type: none"> • Unequal leg L6 x 3.5 x 5/16 members • TxDOT Standard X-Type Cross Frame Details for L4 x 4 x 3/8 followed for overlap • TxDOT Standard X-Type Cross Frame Details for L6 x 6 x 9/16 followed for plate geometry • Angles 1" shorter to prevent weld intersection • Tension diagonal of cross frame positioned on the front side of the cross frame to prevent interaction of angle-gusset weld and gusset-stiffener weld 	
<p>Observations:</p> <ol style="list-style-type: none"> 1. First crack initiated at the forward toe of the angle-gusset plate weld at the toe of the angle and propagated into the angle. 2. A second crack formed in the member nearby, eventually propagating across the section. 	

Test Specimen: XF_UL_2

First Observed Crack

C1: N = 295,437 cycles

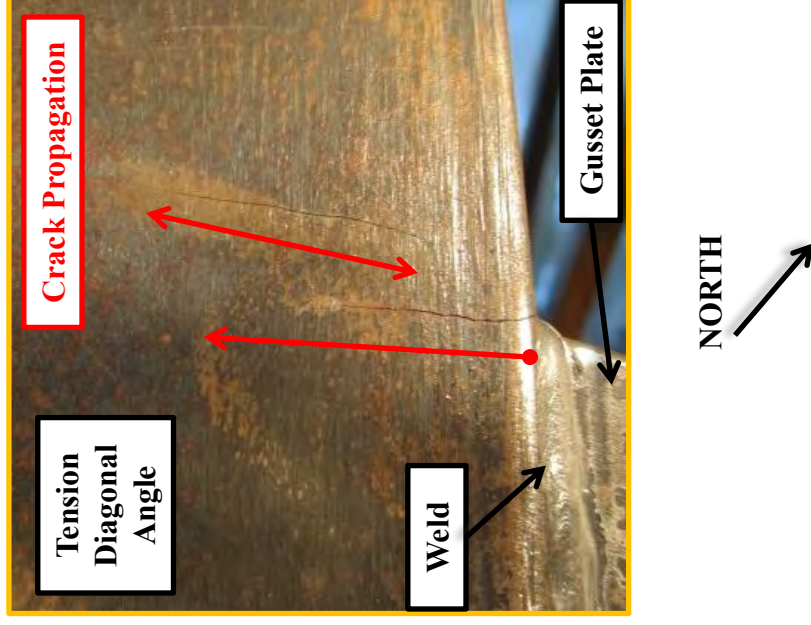
C2: N = 607,695 cycles



NORTH
→

The first crack observed formed at the forward edge of the angle-gusset fillet weld, propagating into the angle toe and across the leg. The second crack was observed in the member, most likely originating at the toe of the backside weld and propagating through the thickness.

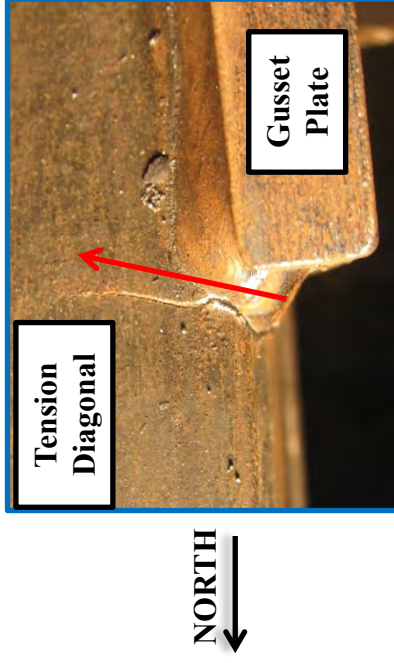
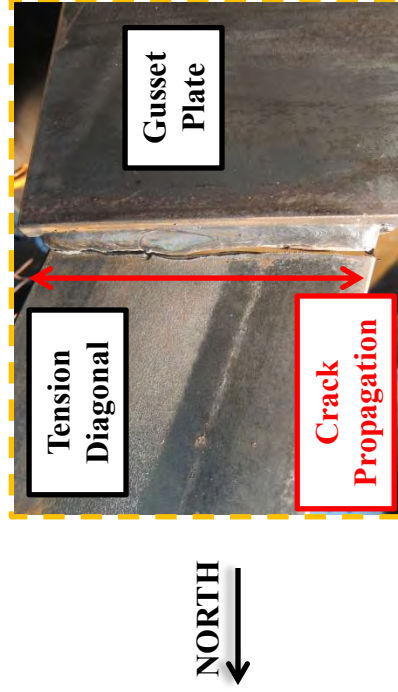
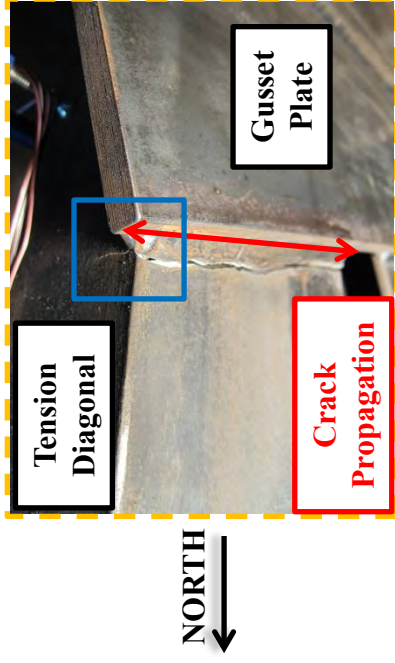
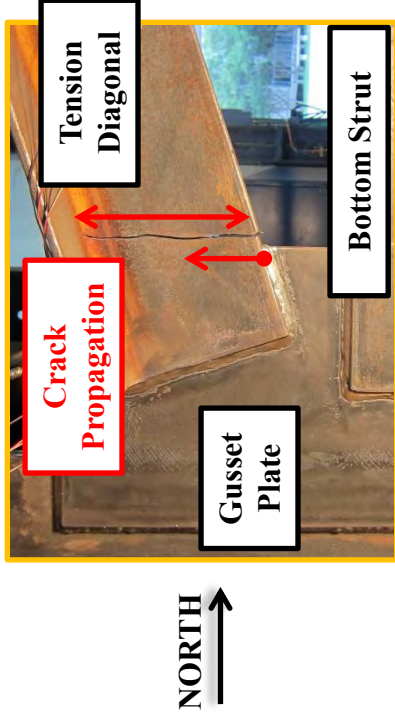
Crack 1,2:(N=607,695)

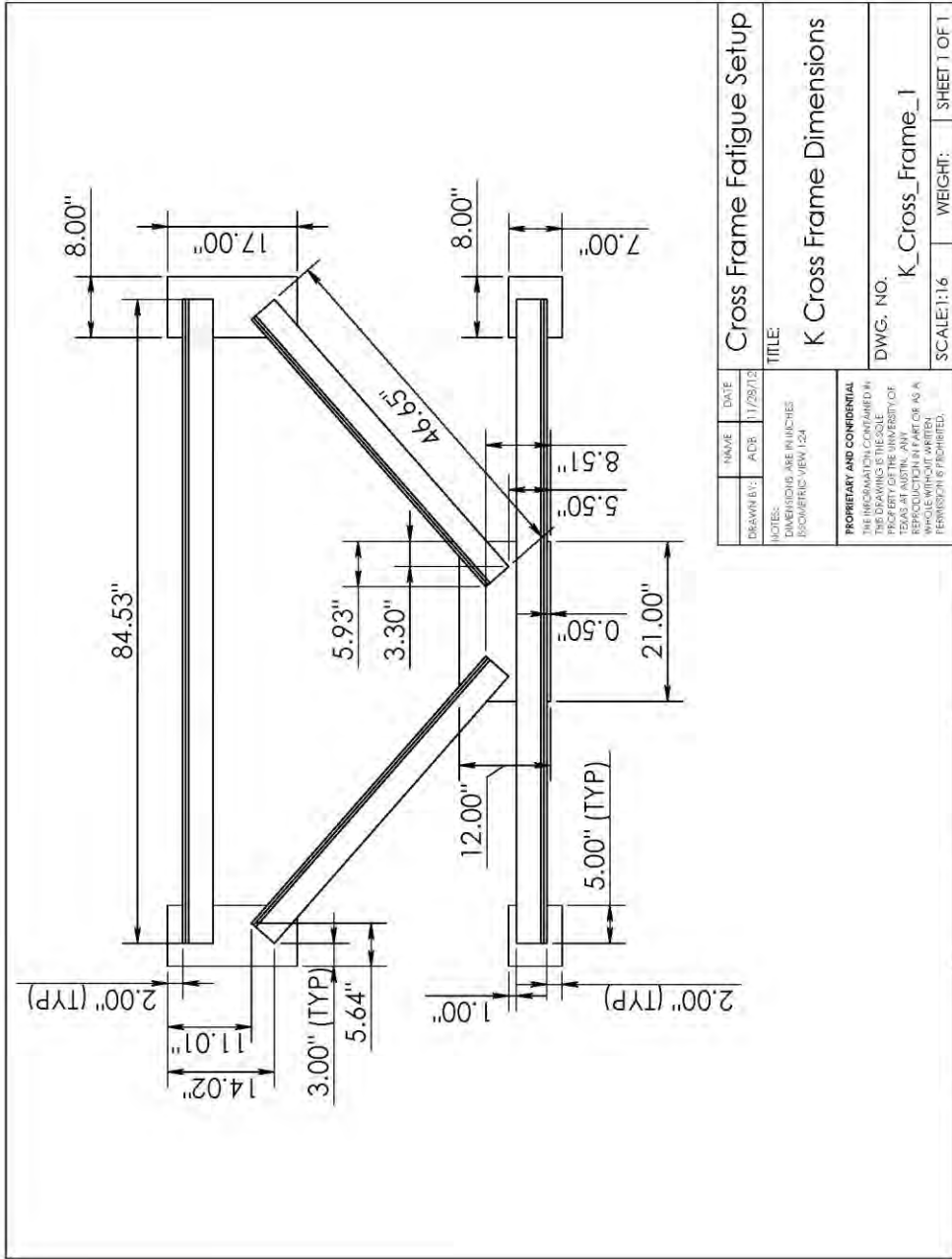


NORTH
↗

Test Specimen: XF_UL_2

Crack 2: (Failure- N=620,464)





DRAWN BY:	NAME	DATE
ADP	ADP	1/29/12

Cross Frame Fatigue Setup

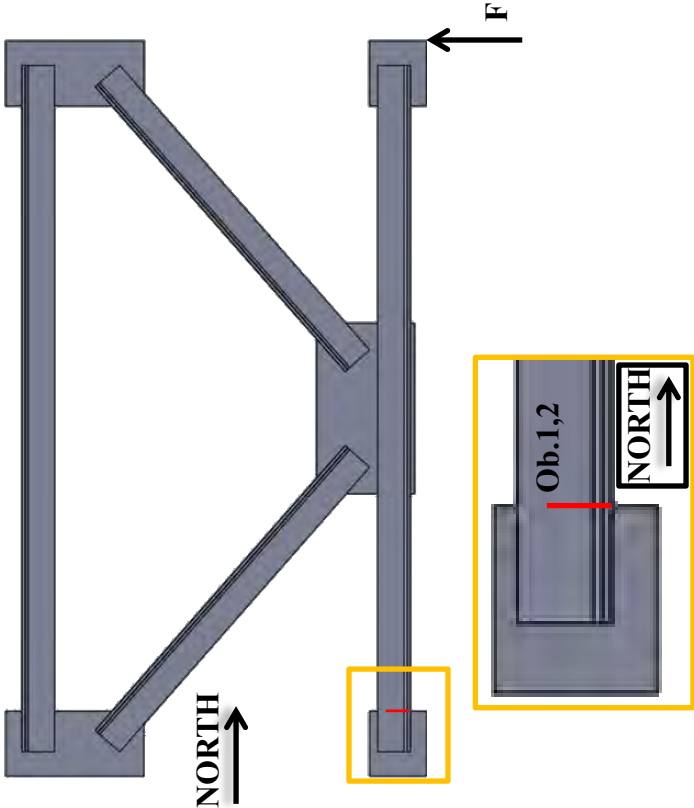
TITLE
K Cross Frame Dimensions

DWG. NO.
K_Cross_Frame_1

SCALE: 1:16 WEIGHT: SHEET 1 OF 1

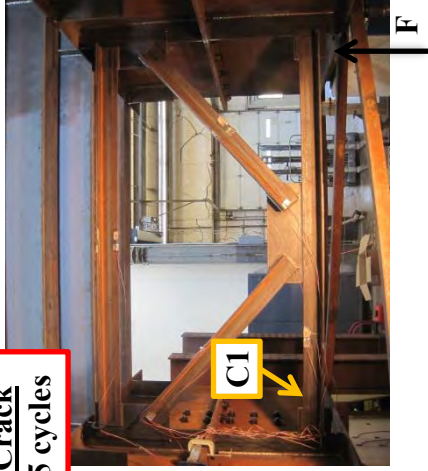
PROPRIETARY AND CONFIDENTIAL
THE INFORMATION CONTAINED HEREIN IS UNCLASSIFIED AND IS THE PROPERTY OF THE UNIVERSITY OF TEXAS AT AUSTIN. ANY REPRODUCTION IN PART OR AS A WHOLE WITHOUT WRITTEN PERMISSION IS PROHIBITED.

NOTES:
DIMENSIONS ARE IN INCHES
ISOMETRIC VIEW 124

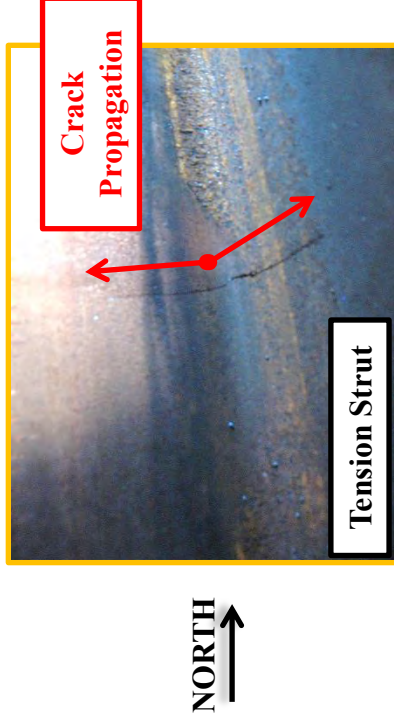
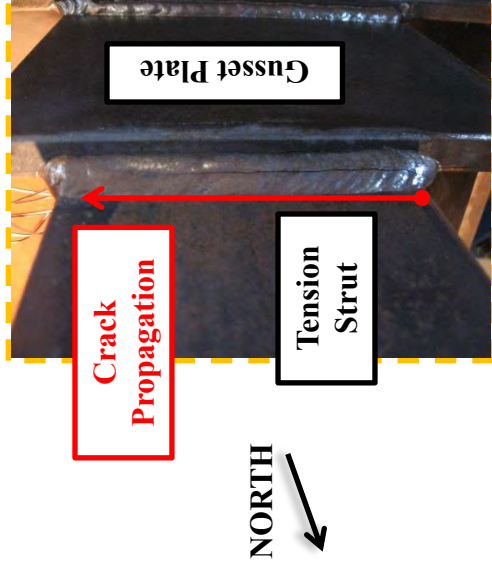
<p>Test Specimen: KF_1</p>	<p>Crack Locations:</p> 
<p>Test Dates: 1/22/2013 – 1/28/2013</p>	
<p>Primary Failure Location: Tension Strut $S_R = 13.76$ ksi $N = 186,732$ cycles AASHTO Fatigue Category: E'</p>	
<p>Stiffness: Initial: 90.04 k/in Final: 67.30 k/in 25.3% loss of stiffness</p>	
<p>Average Weld Size: Leg: 0.31" Throat: 0.30"</p>	
<p>Details:</p> <ul style="list-style-type: none"> • TxDOT Standard K-Type Cross Frame Details for L4 x 4 x 3/8 • Orientation of struts and diagonals were inverse of typical TxDOT layout (typical detail has center gusset plate attached to strut opposite loaded flange) 	
<p>Observations:</p> <ol style="list-style-type: none"> 1. First crack seen in the loaded strut, starting at the back side weld and propagating through the angle member. 2. The measured force was higher than that predicted by a truss analogy, and was close to the stress range of 15 ksi targeted in the tension diagonal. 	

Test Specimen: KF_1

First Observed Crack
C1: N = 182,825 cycles



Crack 1: (N=182,825)



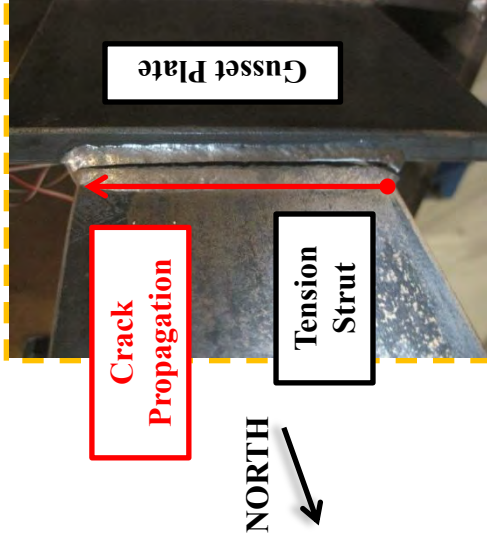
The crack began at the forward edge of the fillet weld near the transverse weld and propagated into the angle heel and through the weld throat.

Test Specimen: KF_1

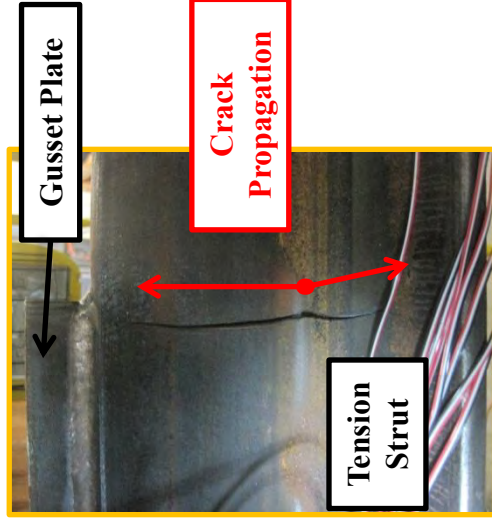


NORTH
↑

Crack 1: (Failure- N=186,732)



NORTH
↓



NORTH
↑

The crack continued to grow through both angle legs until the stress range could not be maintained.

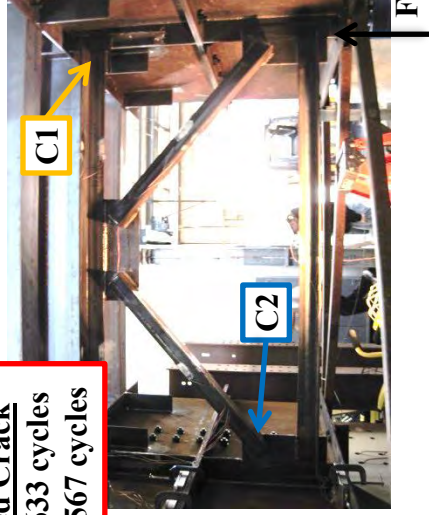
<p>Test Specimen: KF_2</p>		<p>Crack Locations:</p>
<p>Test Dates: 2/14/2013 – 3/1/2013</p>	<p>Secondary Failure: Tension Diagonal $S_R = 15.00$ ksi (Effective Stress Range)</p> <p>$N = 437,412$ cycles AASHTO Fatigue Category: E</p> <p>Stiffness: Initial: 91.57 k/in Final: 45.54 k/in 50.3% loss of stiffness</p>	
<p>Primary Failure: Strut $S_R = 9.51$ ksi (Effective Stress Range)</p> <p>$N = 244,633$ cycles AASHTO Fatigue Category: < E'</p> <p>Stiffness: Initial: 89.56 k/in Final: 75.08 k/in 16.2% loss of stiffness</p> <p>Average Weld Size: Leg: 0.32" Throat: 0.31"</p>	<p>Details:</p> <ul style="list-style-type: none"> • TxDOT Standard K-Type Cross Frame Details for L4 x 4 x 3/8 • Orientation of struts and diagonals follow TxDOT detail- strut near unloaded flange has outstanding leg on opposite side 	
<p>Observations:</p> <ol style="list-style-type: none"> 1. First crack seen in the strut, starting at the toe of the back side weld and propagating through the angle member, most likely due to bending of the member (truss model indicates it is a zero force member). 2. The strut was repaired to continue testing the tension diagonal. 3. The tension diagonal cracked, originating at the angle toe of the backside angle-gusset weld. 		

Test Specimen: KF_2

First Observed Crack

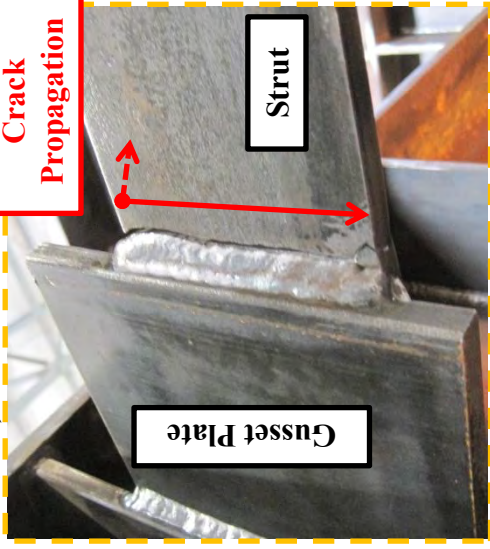
C1: N = 244,633 cycles

C2: N = 410,567 cycles



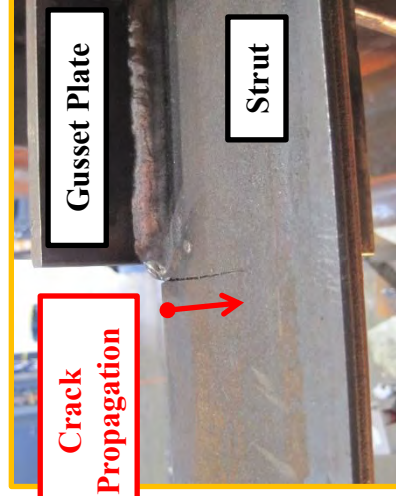
NORTH →

Crack 1: (N=244,633)

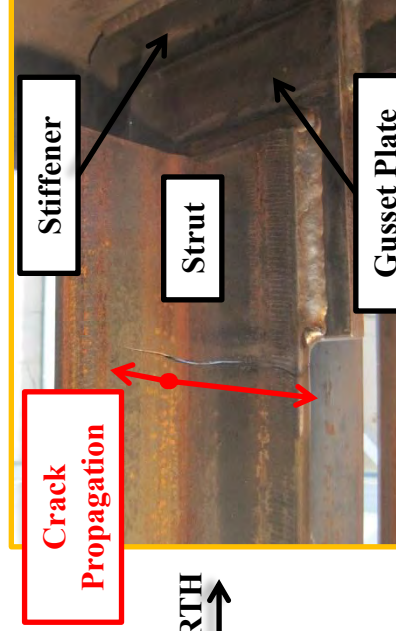


NORTH →

The crack began at the forward edge of the back side fillet weld and propagated into the angle heel along each leg.



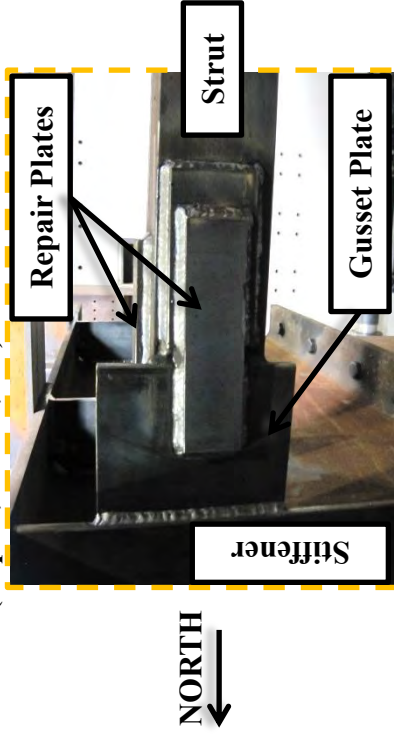
NORTH →



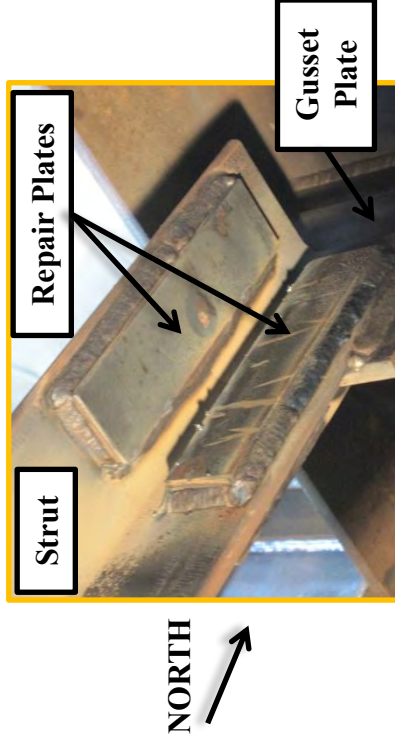
NORTH →

Test Specimen: KF_2

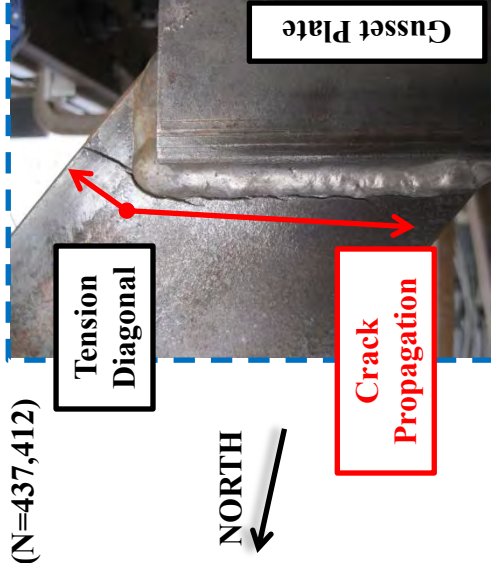
Crack 1: (Repair, N=244,633)



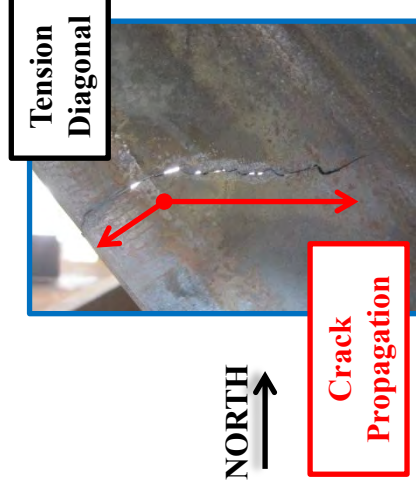
The first crack was repaired to further investigate the performance of the diagonal angle in tension. The stiffness post-repair (91.57 kip/in) was similar to the original stiffness of the specimen (89.56 kip/in).



Crack 2: (N=437,412)



The second crack formed in the tension diagonal at the corner of the backside angle weld. The crack propagated along the weld toe into the angle.



Test Specimen: KF_3		<p>Crack Locations:</p>
<p>Test Dates: 3/12/2013 – 3/21/2013</p> <p>Primary Failure: Strut $S_R = 9.27$ ksi (Effective Stress Range) $N = 379,672$ cycles AASHTO Fatigue Category: < E'</p>	<p>Secondary Failure: Tension Diagonal $S_R = 15.00$ ksi (Effective Stress Range) $N = 379,672$ cycles AASHTO Fatigue Category: E</p>	
<p>Stiffness: Initial: 87.06 k/in Final: 59.17 k/in 32.0% loss of stiffness</p>		
<p>Average Weld Size: Leg: 0.32" Throat: 0.31"</p>		
<p>Details:</p> <ul style="list-style-type: none"> TxDOT Standard K-Type Cross Frame Details for L4 x 4 x 3/8 Orientation of struts and diagonals follow TxDOT detail- strut near unloaded flange has outstanding leg on opposite side No backside welds were used 		
<p>Observations:</p> <ol style="list-style-type: none"> First crack seen in the strut, starting at the toe of the forward edge of the angle-gusset fillet weld and propagating into the angle heel, most likely due to bending of the member. A second crack developed shortly after in the tension diagonal member at the forward edge of the angle-gusset fillet weld and propagating into the angle heel. The cracks grew somewhat simultaneously, and therefore a repair was not necessary. 		

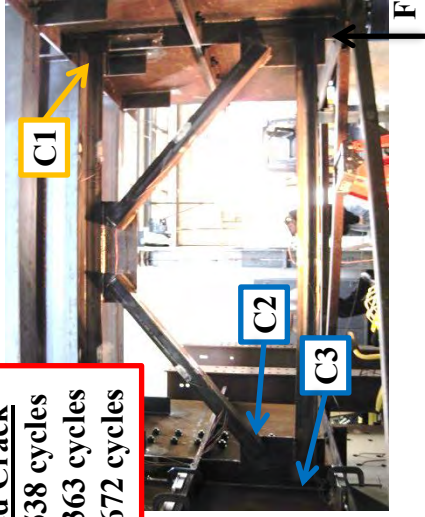
Test Specimen: KF_3

First Observed Crack

C1: N = 220,538 cycles

C2: N = 270,363 cycles

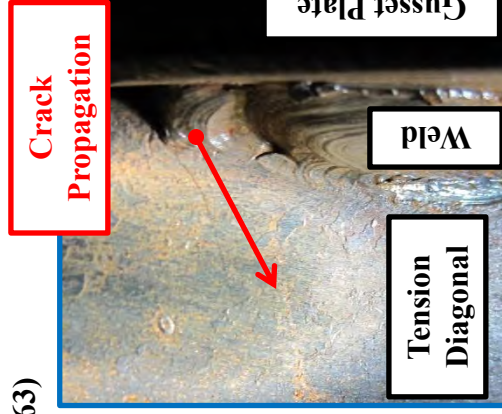
C3: N = 379,672 cycles



NORTH
↑

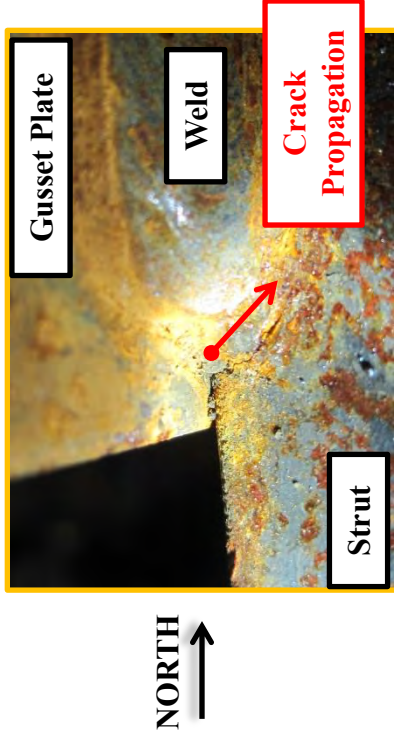
Crack 2: (N=270,363)

A second crack was observed in the tension diagonal at the forward edge of the fillet weld and propagated into the angle heel along each leg.



EAST
↓

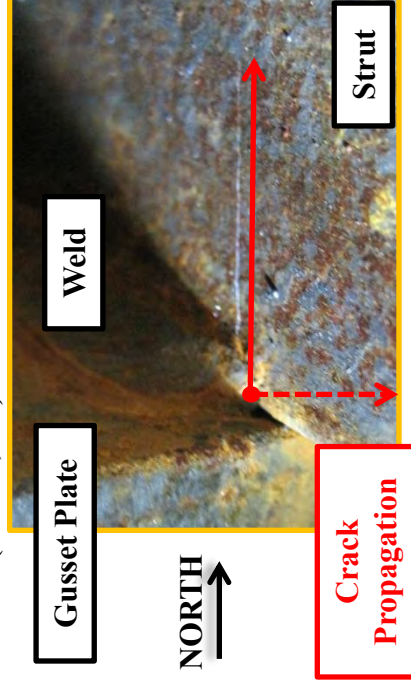
Crack 1: (N=220,538)



NORTH
↑

The strut crack at first observation.

Crack 1: (N=270,363)

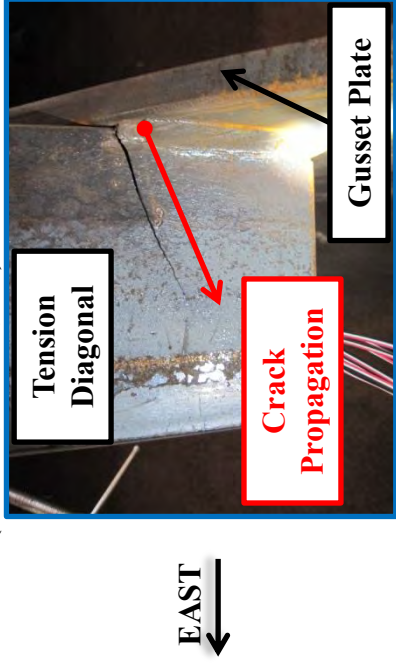


NORTH
↑

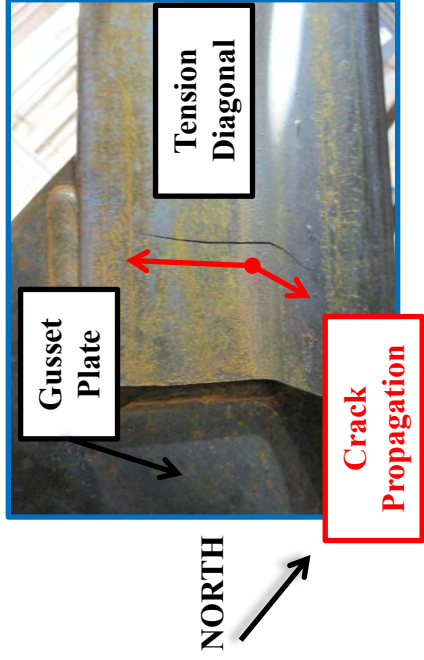
The crack began at the forward edge of the fillet weld and propagated into the angle heel along each leg.

Test Specimen: KF_3

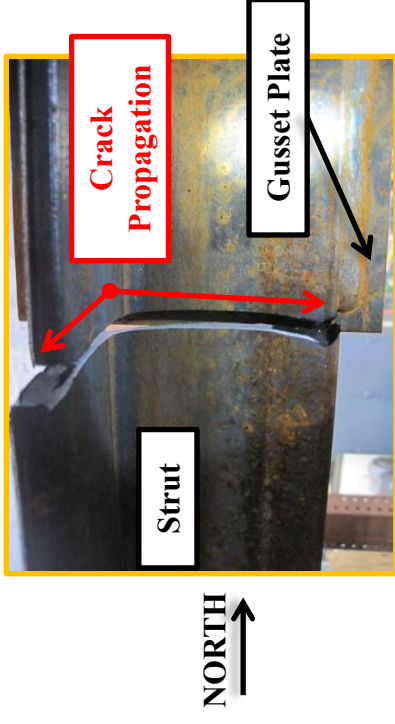
Crack 2: (Failure, N=379,672)



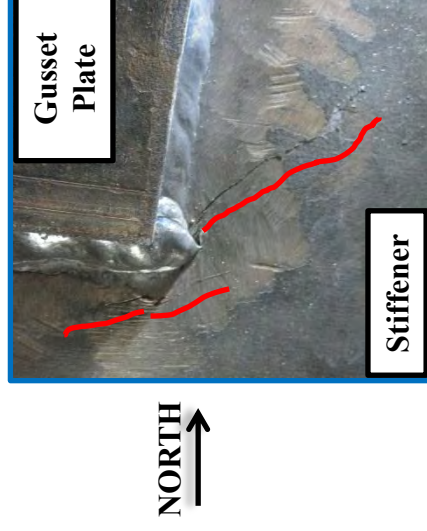
The second crack was quite large at complete fracture of crack 1.



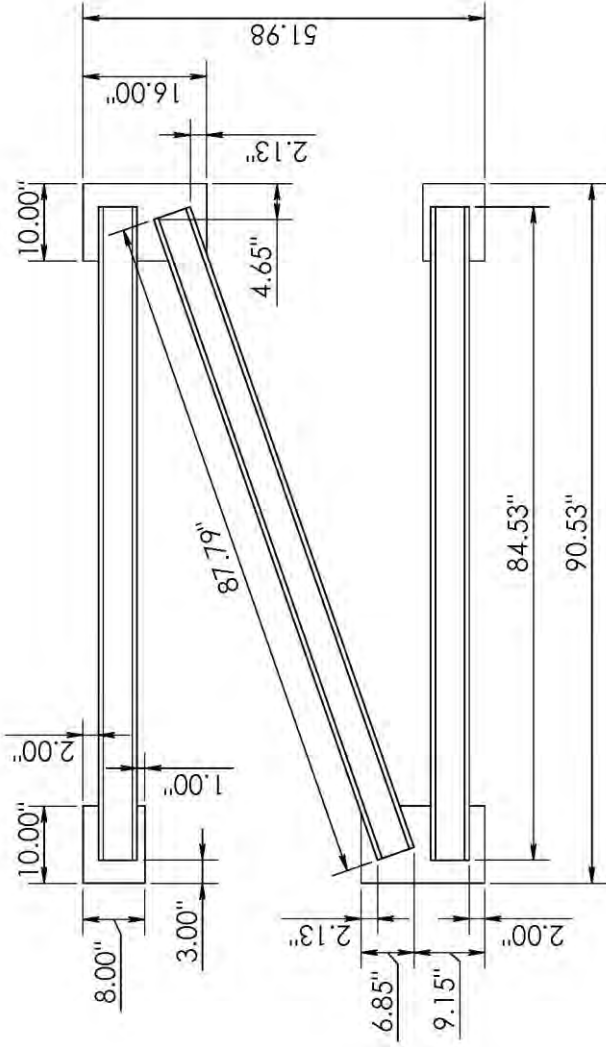
Crack 1: (Failure, N=379,672)



Crack 3: (Failure, N=379,672)

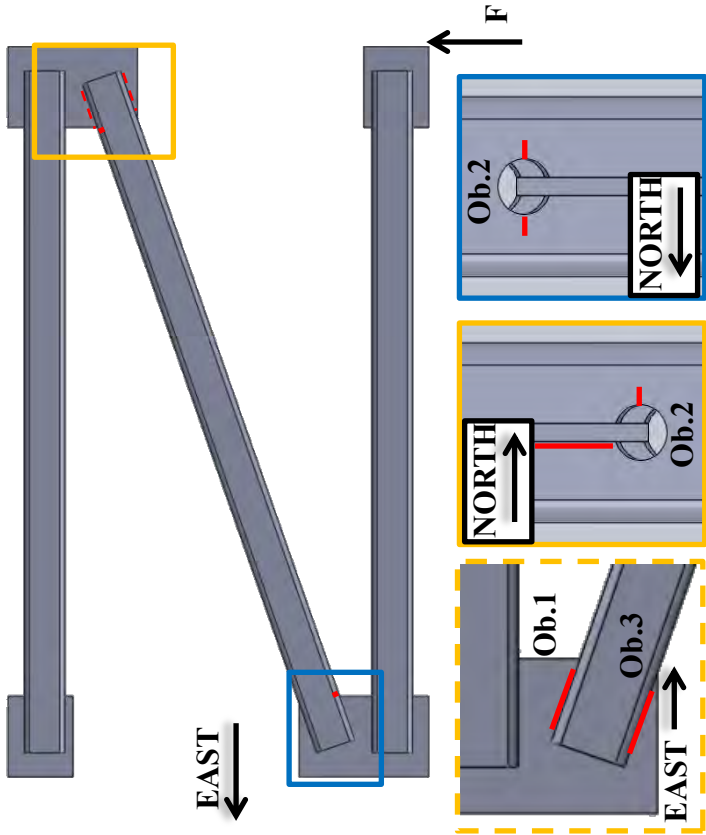


Small stiffener cracks were seen at the conclusion of the test. It was deemed not to be significant enough to affect the results.



NAME	DATE	Cross Frame Fatigue Setup	
DRAWN BY: ADR	1/8/13	TITLE:	
NOTES: DIMENSIONS ARE IN INCHES ISOMETRIC VIEW 1:24			
PROPRIETARY AND CONFIDENTIAL THIS INFORMATION CONTAINED HEREIN IS THE SOLE PROPERTY OF THE UNIVERSITY OF TEXAS AT AUSTIN. ANY REPRODUCTION OR DISSEMINATION OF THIS INFORMATION AS A WHOLE OR IN PART IS PROHIBITED WITHOUT PERMISSION OF THE UNIVERSITY OF TEXAS AT AUSTIN			
DWG. NO. Z_Cross_Frame_HSS		SCALE: 1:16	
WEIGHT:		SHEET 1 OF 1	

1 2 3 4 5

<p>Test Specimen: ZF_HSS_1</p>	<p>Crack Locations:</p> 
<p>Test Dates: 1/22/2013 – 1/23/2013</p>	
<p>Primary Failure Location: Weld</p> <p>$S_R = 20.00$ ksi (Diagonal)</p> <p>$N = 25,179$ cycles</p> <p>AASHTO Fatigue Category: < E'</p>	
<p>Stiffness: Initial: 96.65 k/in Final: 82.35 k/in</p> <p>14.8% loss of stiffness</p>	
<p>Average Weld Size: Leg: 0.31" Throat: 0.29"</p>	
<p>Details:</p> <ul style="list-style-type: none"> • TxDOT Standard X-Type Cross Frame Details for L5 x 5 x 1/2 followed for Z frame layout with HSS 5 x 5 x 3/8 • Stress relief hole of 1-5/8" used at connection 	
<p>Observations:</p> <ol style="list-style-type: none"> 1. First crack observation showed a full fracture through the throat of the tension diagonal fillet weld located at the top gusset plate on the top of the HSS on the SW side. 2. At the same time, cracks were also visible at the stress relief holes. 3. As the testing continued, the welds at the top gusset plate continued to crack. The top weld on the NW side cracked, originating at the back of the connection and moving forward through the weld throat. Shortly after the bottom weld on the SW side cracked ending the test. 	

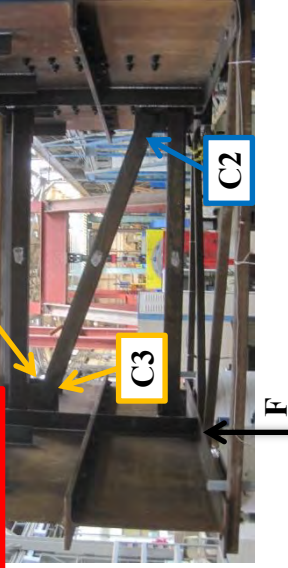
Test Specimen: ZF_HSS_I

First Observed Crack

C1: N = 23,672 cycles

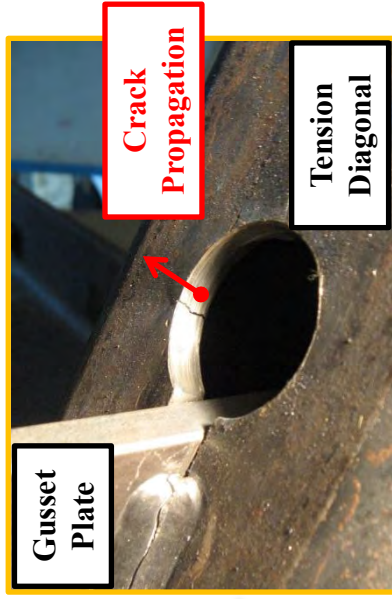
C2: N = 23,672 cycles

C3: N = 25,179 cycles



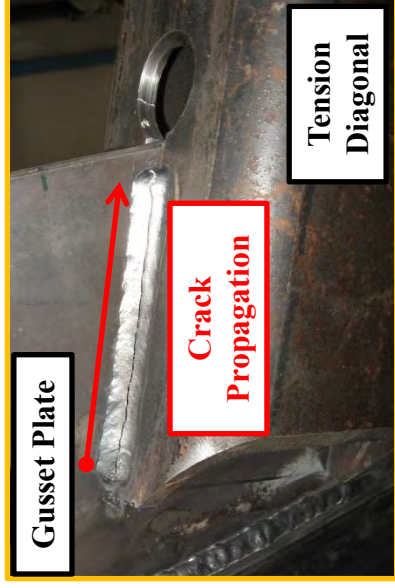
EAST ←

Crack 2: (Top West- Stress Relief Hole- N=23,672)



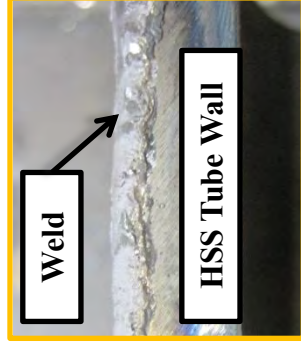
EAST →

Crack 1:



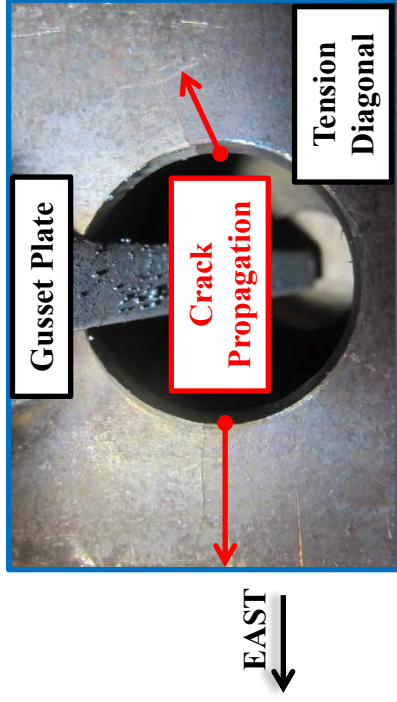
EAST →

The crack began at the end of the connection and propagated towards the stress relief hole. The weld was later examined. The fillet weld was undersized at 3/16" (supposed to be 5/16") and the weld had significant voids and defects as shown below.

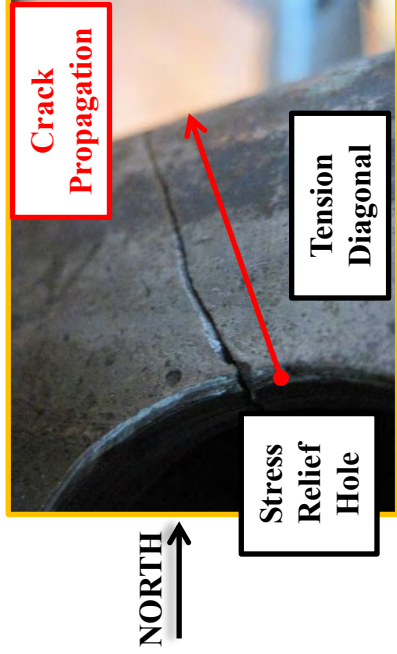


Test Specimen: ZF_HSS_1

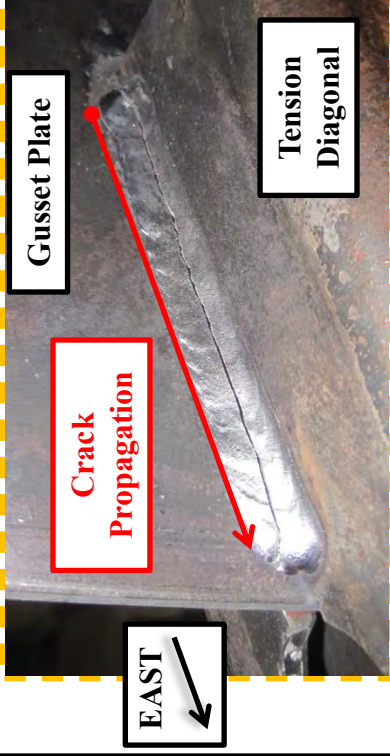
Crack 2: (Bottom East- Stress Relief Hole)



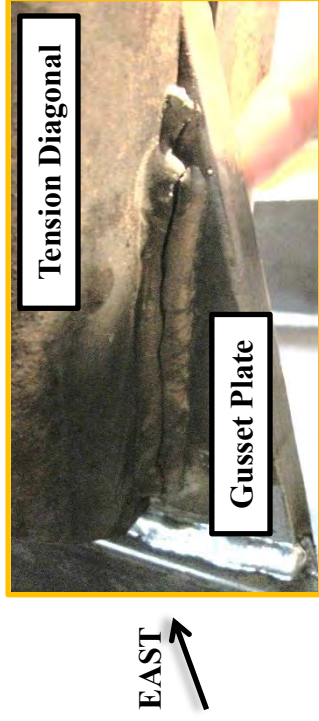
Crack 3: (Top West- Stress Relief Hole- N=25,179)

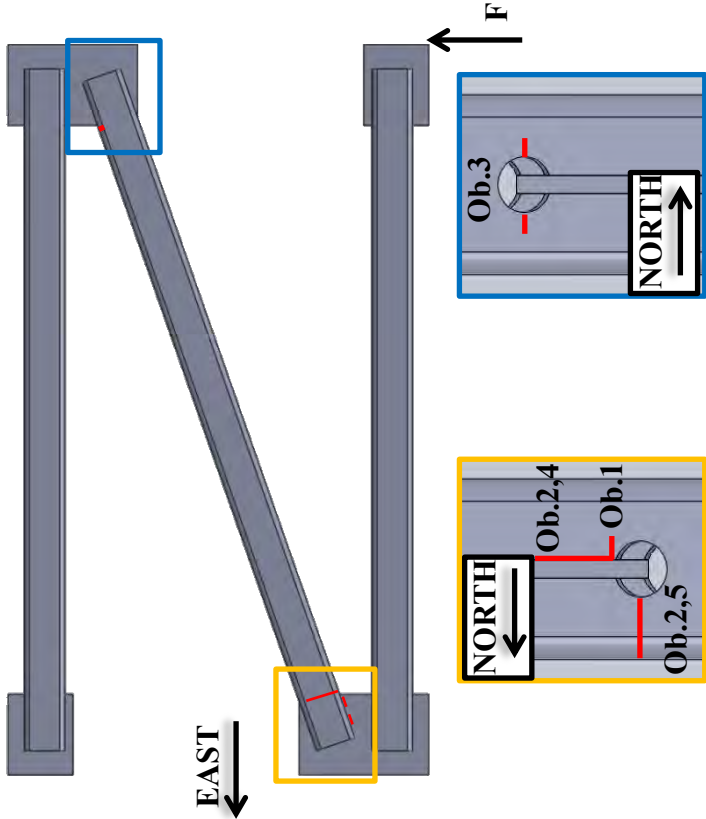


Crack 3: (NW Top Weld)



After crack 1 had completely fractured the weld, another crack began at the end of the top NW connection and propagated towards the stress relief hole (above). Once this fractured, the bottom SW connection fractured (below).



<p>Test Specimen: ZF_HSS_2</p>	<p>Crack Locations:</p> 
<p>Test Dates: 3/19/2013 – 3/22/2013</p>	
<p>Primary Failure Location: Member</p> <p>$S_R = 15$ ksi</p> <p>$A_{eff} = 4.03$ in² $U = 0.659$</p> <p>$N = 104,747$ cycles</p> <p>AASHTO Fatigue Category: almost E'</p>	
<p>Stiffness: Initial: 100.3 k/in Final: 77.81 k/in</p> <p>22.4% loss of stiffness</p>	
<p>Average Weld Size: Leg: 0.31" Throat: 0.32"</p>	
<p>Details:</p> <ul style="list-style-type: none"> • TxDOT Standard X-Type Cross Frame Details for L5 x 5 x 1/2 followed for Z frame layout with HSS 5 x 5 x 3/8 • Stress relief hole of 1-5/16" used at connection 	
<p>Observations:</p> <ol style="list-style-type: none"> 1. First crack seen at the forward edge of the fillet weld on the south face of the bottom of the east connection. 2. A second crack was observed at the bottom stress relief hole at the east connection. A small crack was seen in the throat of the south facing weld on the bottom of the east connection. 3. Cracks were observed at the west connection on both sides of the top stress relief hole. 4. The throat weld fully propagated through the connection. 5. The crack from the stress relief hole continued to grow until the member fractured. 	

Test Specimen: ZF_HSS_2

First Observed Crack

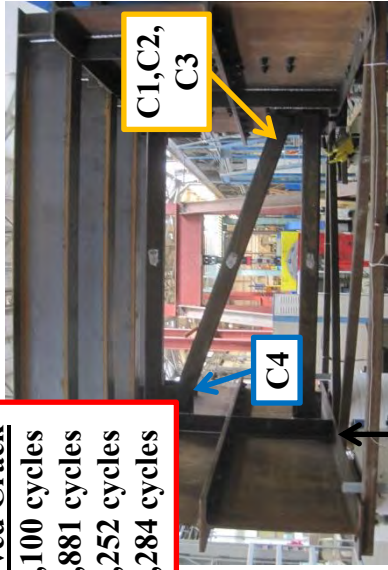
C1: N = 32,100 cycles

C2: N = 50,881 cycles

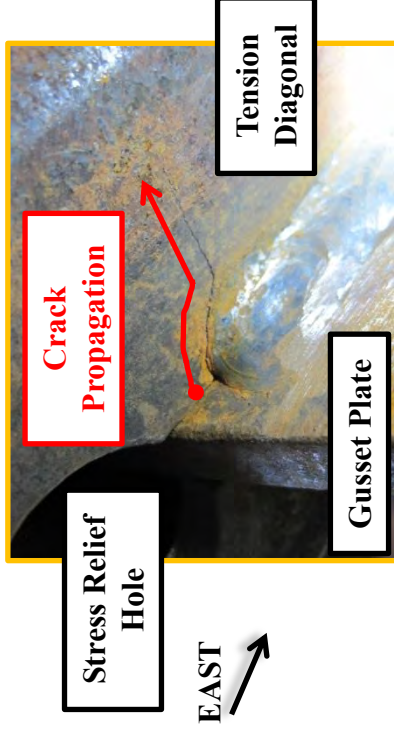
C3: N = 58,252 cycles

C4: N = 63,284 cycles

EAST ←

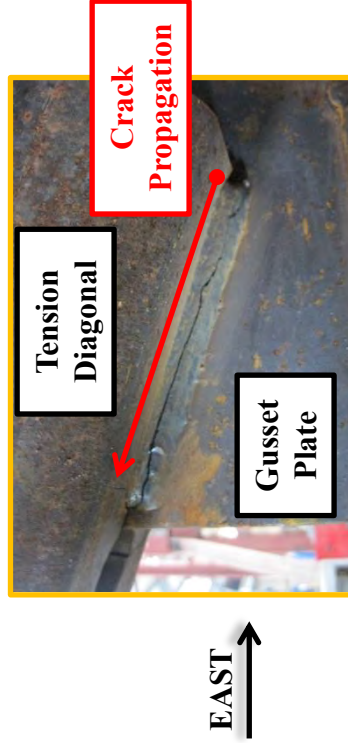


Crack 1: (Bottom East- N=32,100)



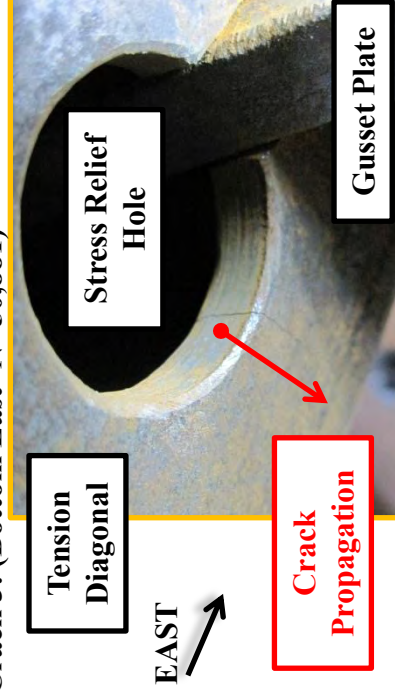
The crack began at the forward edge of the fillet weld and propagated into the HSS member.

Crack 2: (Bottom East- N=50,881)



The second crack was observed in the throat of the weld at 50,881 cycles. It continued to grow until it completely fractured at 86,712 cycles.

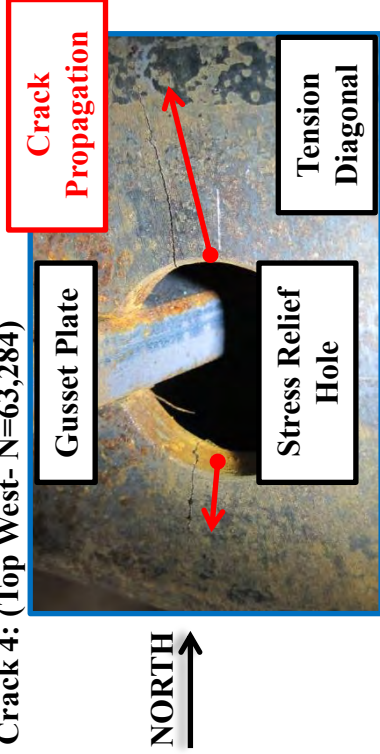
Crack 3: (Bottom East- N=50,881)



A crack was also observed at the stress relief hole, which would eventually grow into the failure crack.

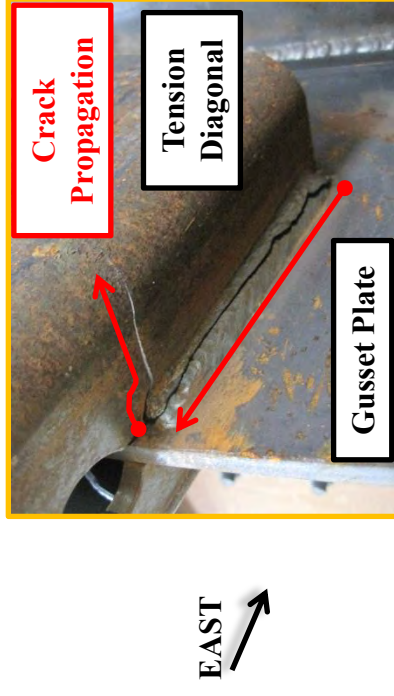
Test Specimen: ZF_HSS_2

Crack 4: (Top West- N=63,284)

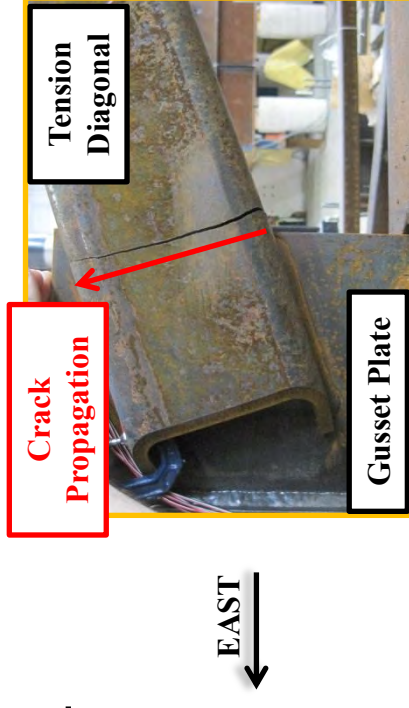
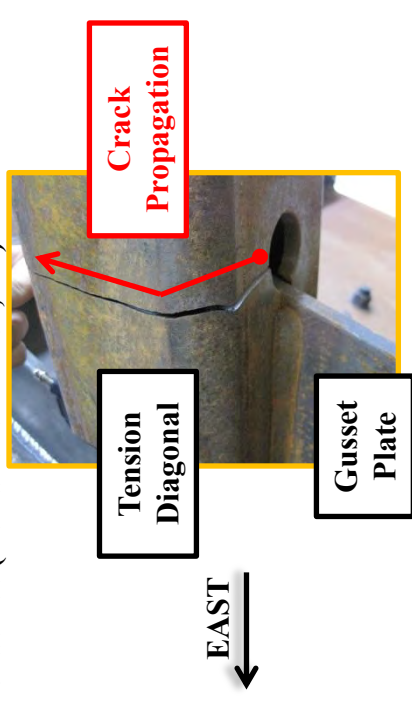


The fourth cracks were seen at the top stress relief hole at the west connection.

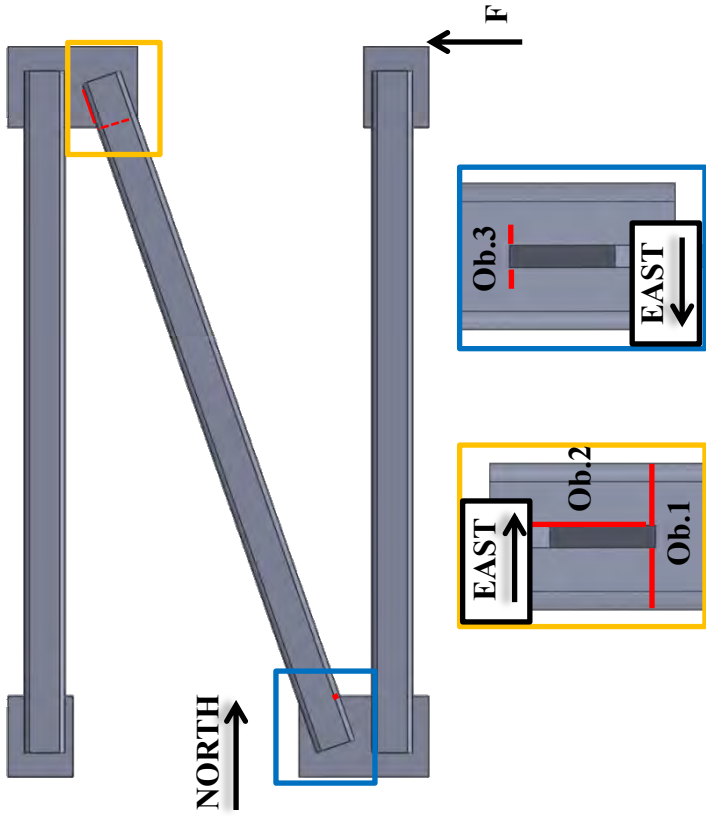
Crack 1, 2: (At Failure, N=104,747)



Crack 3: (At Failure- N=104,747)



The crack observed earlier at the stress relief hole eventually propagated through North half of the tube resulting in fracture of the member.

<p>Test Specimen: ZF_HSS_3</p>	<p>Crack Locations:</p> 	
<p>Test Dates: 5/30/2013 – 6/3/2013</p>		
<p>Primary Failure Location: Member $S_R = 15$ ksi (Diagonal) $N = 86,014$ cycles AASHTO Fatigue Category: < E'</p>		
<p>Stiffness: Initial: 104.4 k/in Final: 65.55 k/in 37.2% loss of stiffness</p>		
<p>Average Weld Size: Leg: 0.31" Throat: 0.32"</p>		
<p>Details:</p> <ul style="list-style-type: none"> • TxDOT Standard X-Type Cross Frame Details for L5 x 5 x 1/2 followed for Z frame layout with HSS 5 x 5 x 3/8 • Slots were cut using plasma torch; no stress relief hole 		
<p>Observations:</p> <ol style="list-style-type: none"> 1. First cracks seen at the forward edge of the fillet welds on the top face of the north connection propagating into the tube. 2. A second crack formed at the top northeast connection at the back of the fillet weld and propagated through the weld throat towards the forward edge of the connection. 3. Cracks were later observed at the forward edge of the fillet welds on the bottom face of the south connection propagating into the tube. 		

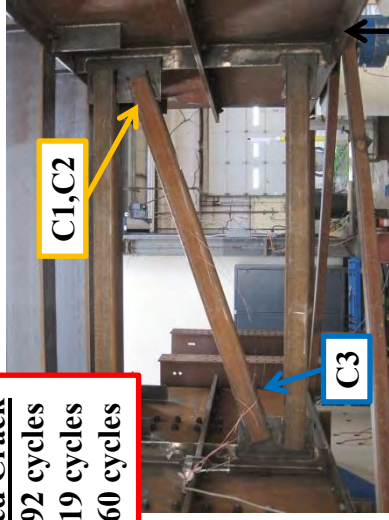
Test Specimen: ZF_HSS_3

First Observed Crack

C1: N = 19,892 cycles

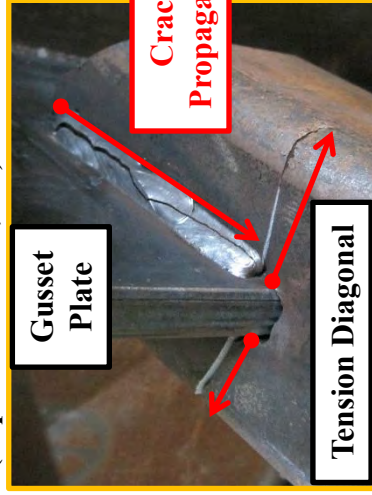
C2: N = 41,419 cycles

C3: N = 45,960 cycles



NORTH
→

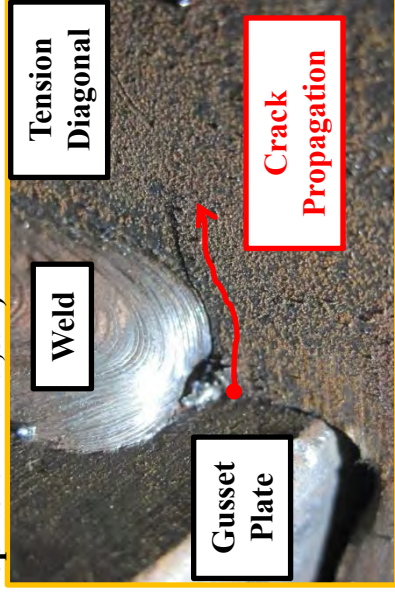
Crack 1,2: (Top North- N=86,014)



EAST
→

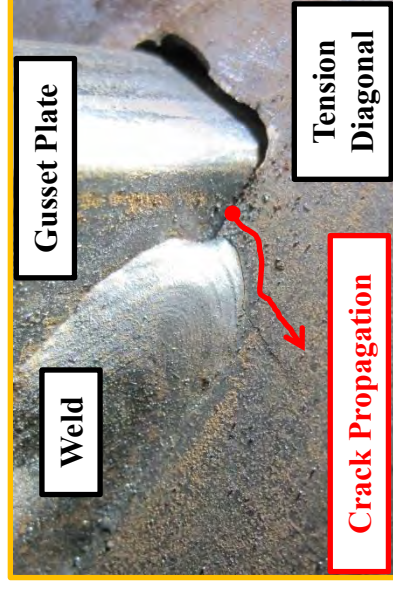
The second crack was observed in the throat of the weld at the back end of the connection at 41,419 cycles. It continued to grow until the tube fractured at 86,014 cycles.

Crack 1: (Top North- N=19,892)



EAST
→

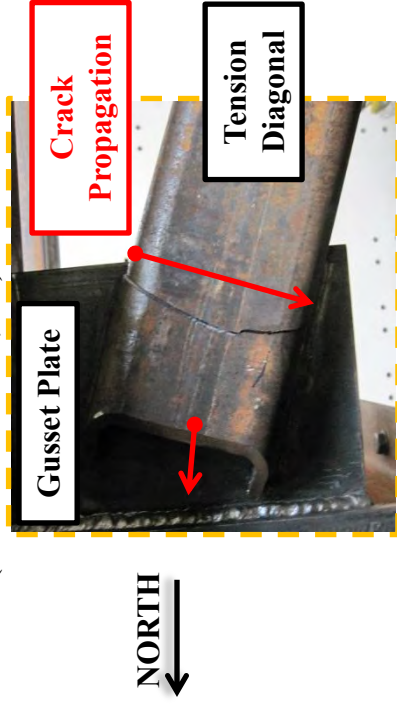
The crack began at the forward edge of the fillet welds and propagated into the HSS member.



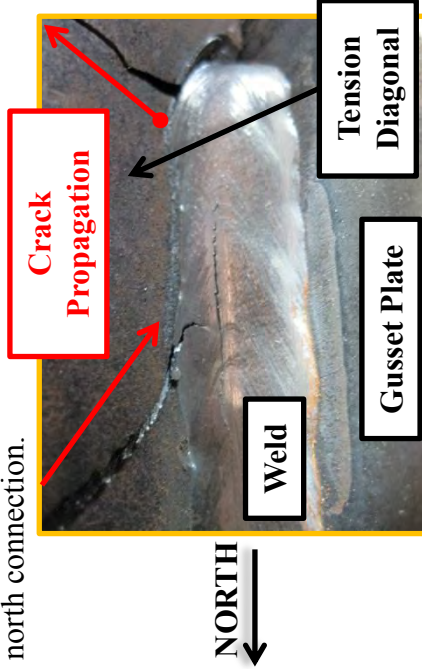
EAST
→

Test Specimen: ZF_HSS_3

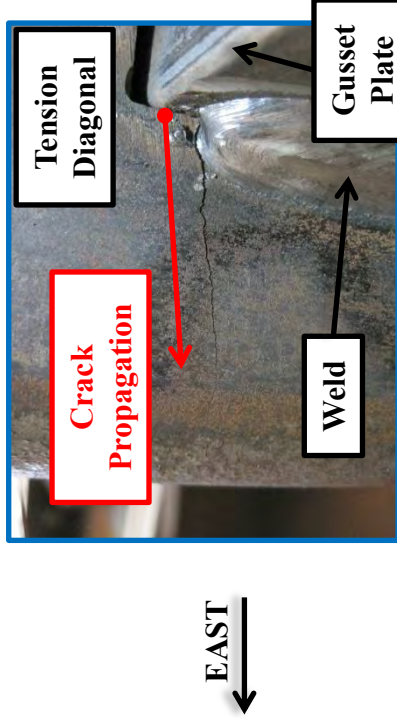
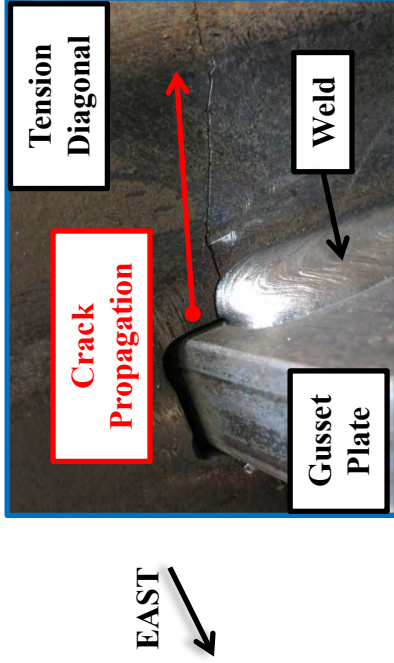
Crack 1: (West Face- N=86,014)



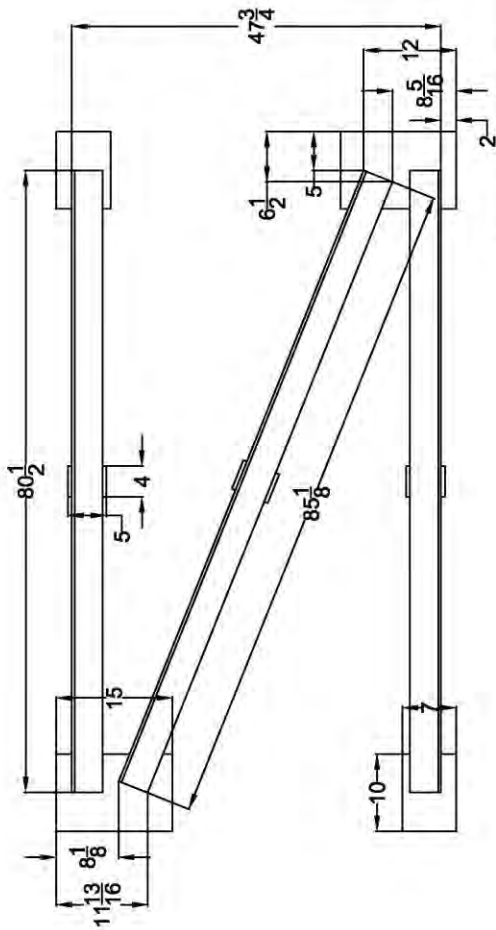
The first crack eventually propagated completely through the HSS tube. Near failure additional cracks formed at the forward toe of the fillet weld on the bottom face of the north connection.



Crack 3: (Bottom South, N=86,014)



Cracks were also observed at the south connection on the bottom face originating at the forward edge of the fillet welds and propagating into the tube.



Cross Frame Fatigue Test	
Double Angle Z Frame 10" Gusset	
Double Angle_10_Gusset	
Scale: 1:16	Sheet 1 of 1

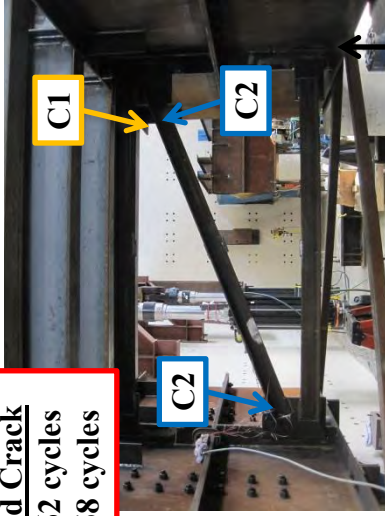
<p>Test Specimen: ZF_DA_1</p>	<p>Crack Locations:</p>
<p>Test Dates: 2/14/2013 – 2/18/2013</p>	
<p>Primary Failure Location: Weld $S_R = 15.00$ ksi (Diagonal) $N = 97,060$ cycles</p> <p style="text-align: center;">AASHTO Fatigue Category: < E'</p>	
<p>Stiffness: Initial: 195.0 k/in Final: 123.9 k/in 36.4% loss of stiffness</p>	
<p>Average Weld Size: Leg: 0.32" Throat: 0.32"</p>	
<p>Details:</p> <ul style="list-style-type: none"> • TxDOT Standard X-Type Cross Frame Details for L4 x 4 x 3/8 followed for Z frame layout • Angles on back side of cross frame cut 1/2" shorter to prevent weld intersection 	
<p>Observations:</p> <ol style="list-style-type: none"> 1. First crack appeared to initiate at a tack weld at the heel of the SW angle and propagated along the weld through the throat 2. Secondary cracks formed in the NW angle heel and the SE and NE angle toes consistent with double curvature of member 	

Test Specimen: ZF_DA_1

First Observed Crack

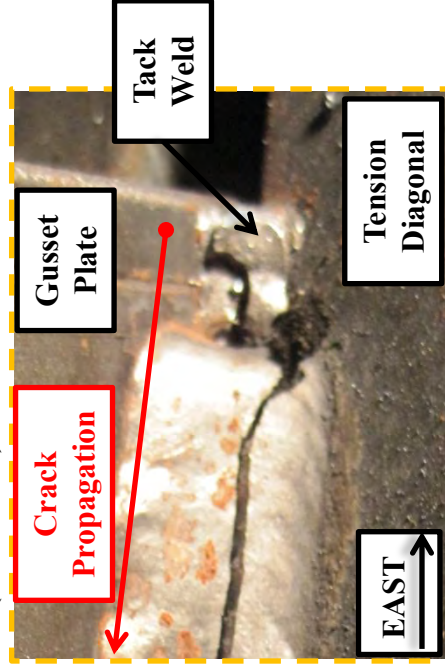
C1: N = 90,862 cycles

C2: N = 94,058 cycles

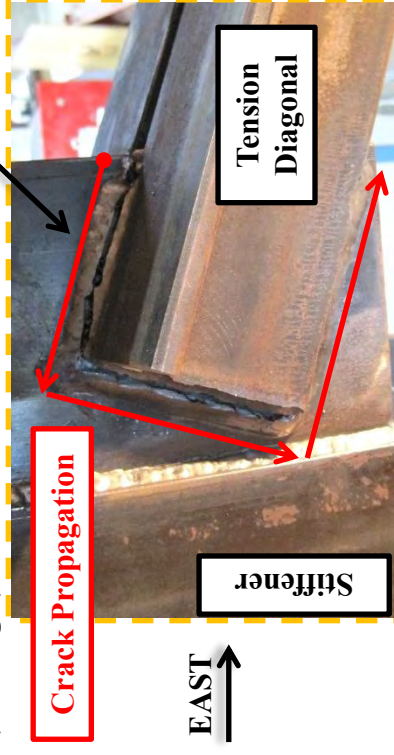


EAST ←

Crack 1: (Tack Weld)

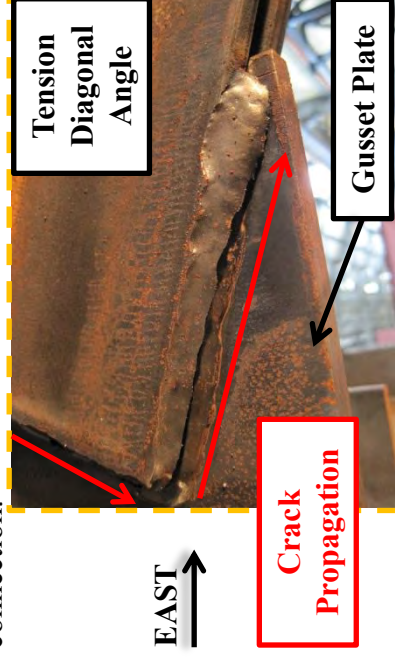


Crack 1:
(SW Angle)



EAST →

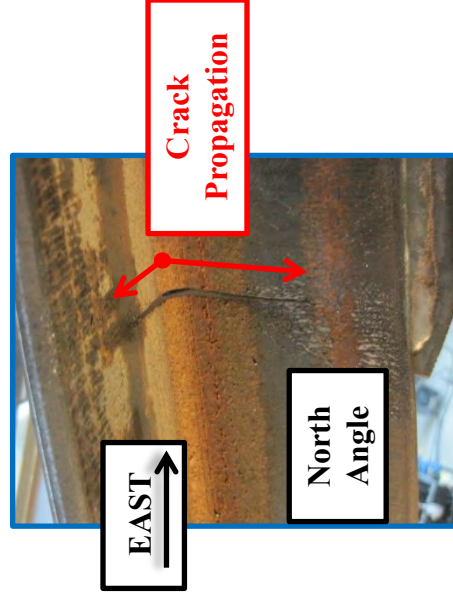
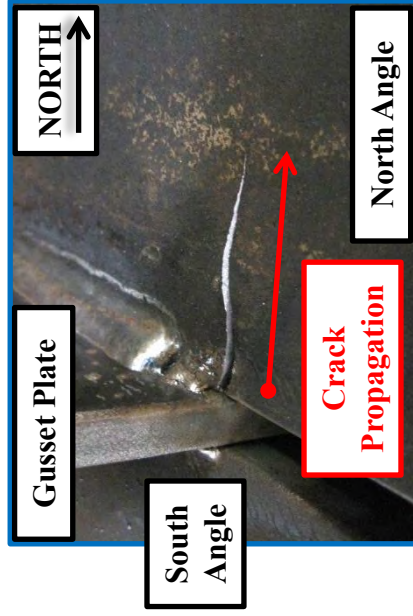
The crack began at a tack weld at the heel of the south angle of the diagonal at the west connection. The crack propagated through the throat of the weld around the connection.



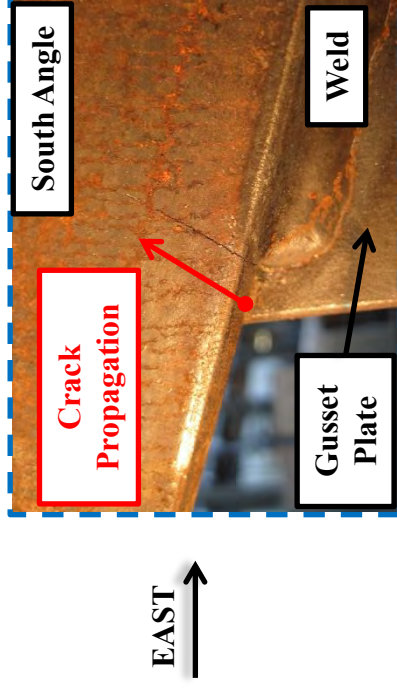
EAST →

Test Specimen: ZF_DA_1

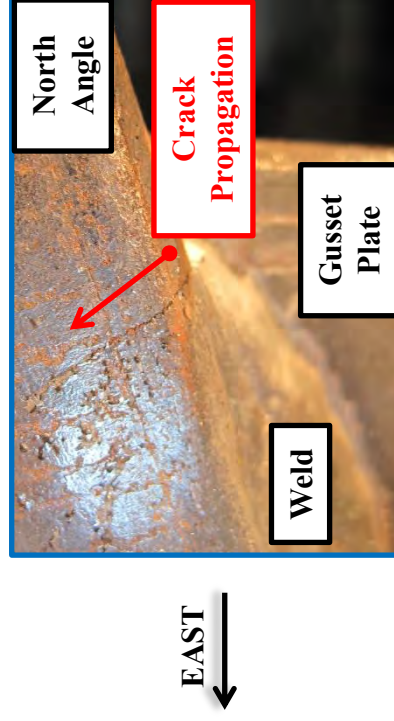
Crack 2: (NW Angle- Top)



Crack 2: (SE Angle)



Crack 2: (NE Angle)



<p>Test Specimen: ZF_DA_2</p>		<p>Crack Locations:</p>
<p>Test Dates: 2/22/2013 – 3/2/2013</p>	<p>Primary Failure: Gusset-Stiffener Weld $S_R = 15.00$ ksi (Diagonal) (Effective Stress Range)</p> <p>$N = 56,793$ cycles AASHTO Fatigue Category: <math>E'</math></p>	
<p>Secondary Failure: Angle-Gusset Weld $S_R = 15.00$ ksi (Effective Stress Range)</p> <p>$N = 134,638$ cycles AASHTO Fatigue Category: E'</p>	<p>Stiffness: Initial: 193.4 k/in Final: 166.5 k/in 13.9% loss of stiffness</p> <p>Average Weld Size: Leg: 0.32" Throat: 0.32"</p>	<p>Details:</p> <ul style="list-style-type: none"> • TxDOT Standard X-Type Cross Frame Details for L4 x 4 x 3/8 followed for Z frame layout • Angles on back side of cross frame cut 1/2" shorter to prevent weld intersection • Welded at Hirschfeld Industries
<p>Observations:</p> <ol style="list-style-type: none"> 1. First crack initiated at gusset toe of gusset-stiffener weld and propagated along the weld toe through the plate 2. A secondary crack formed at the SW angle heel at the forward weld toe propagating through the weld throat and around the connection consistent with a stress concentration caused by double curvature of the diagonal 3. An additional crack was seen at the NW angle heel originating at the angle toe and propagating into the angle 		

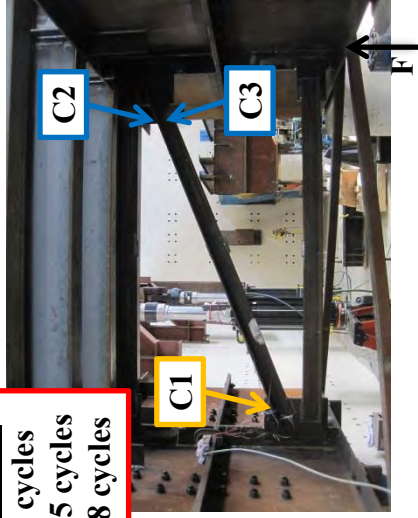
Test Specimen: ZF_DA_2

First Observed Crack

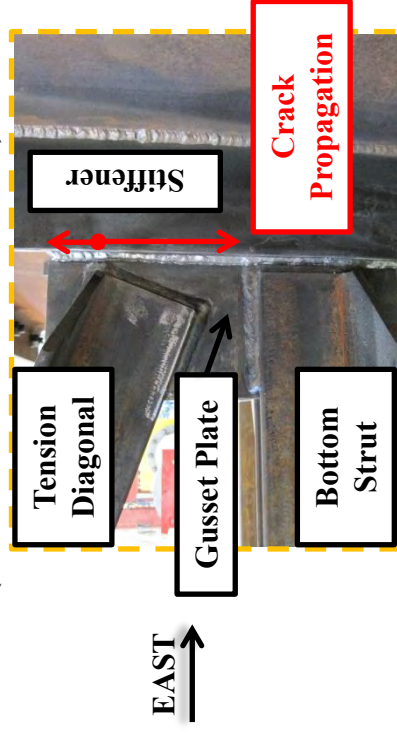
C1: N = 44,354 cycles

C2: N = 122,175 cycles

C3: N = 134,638 cycles

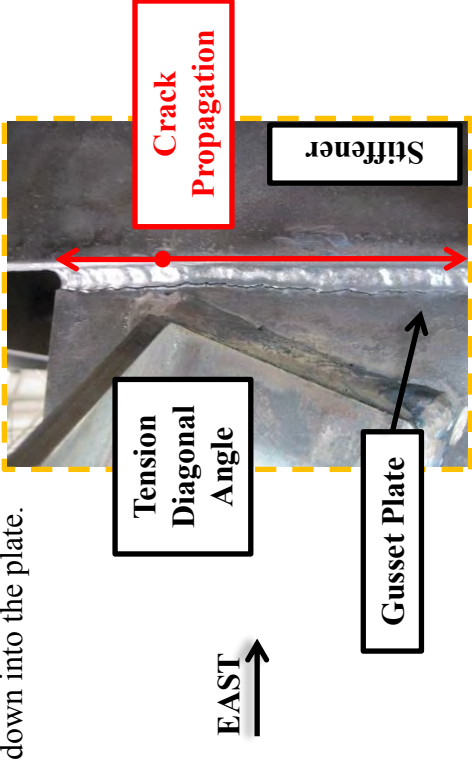
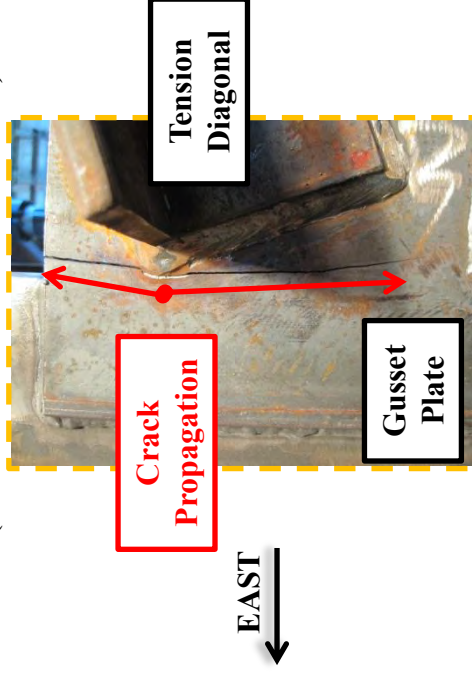


Crack 1: (Bottom East Gusset- South Face)



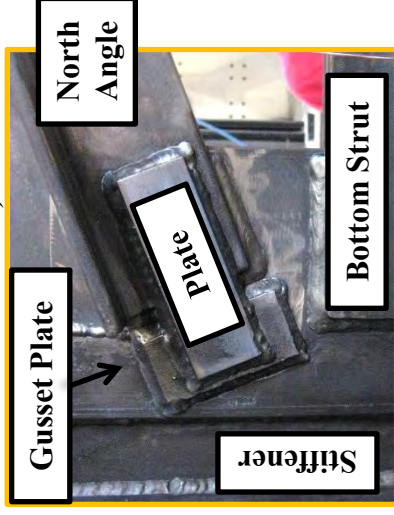
The crack began near the intersection of the angle-gusset weld and the gusset-stiffener weld. It began at the gusset toe of the gusset-stiffener weld and propagated up and down into the plate.

Crack 1: (Bottom East Gusset- North Face)



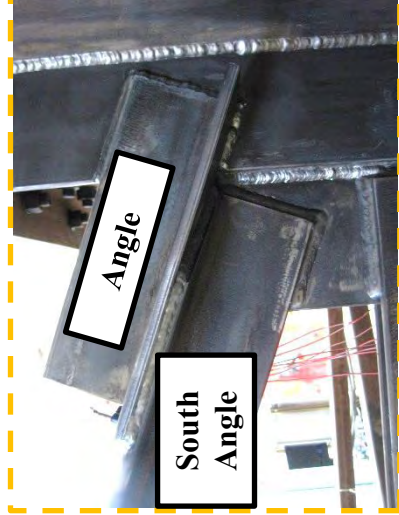
Test Specimen: ZF_DA_2

Repair: (Bottom East Gusset Plate)



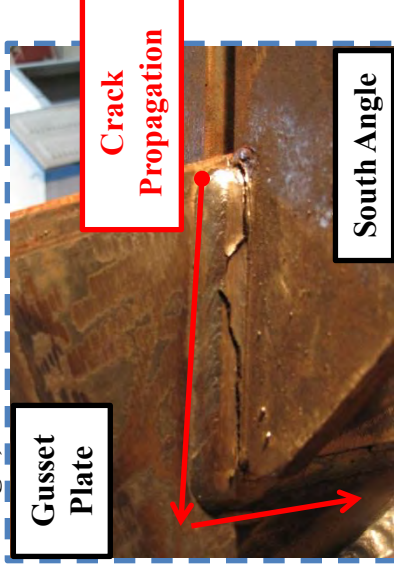
EAST ←

The crack was repaired by grinding out the crack and inserting a double groove weld. An additional plate and angle were used to bridge the crack. The repaired stiffness was very similar to the original stiffness.



EAST →

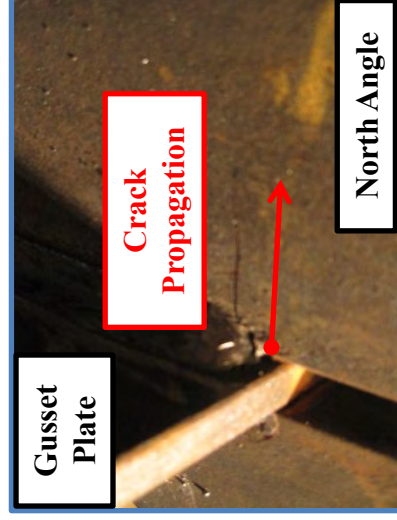
Crack 2: (SW Angle)



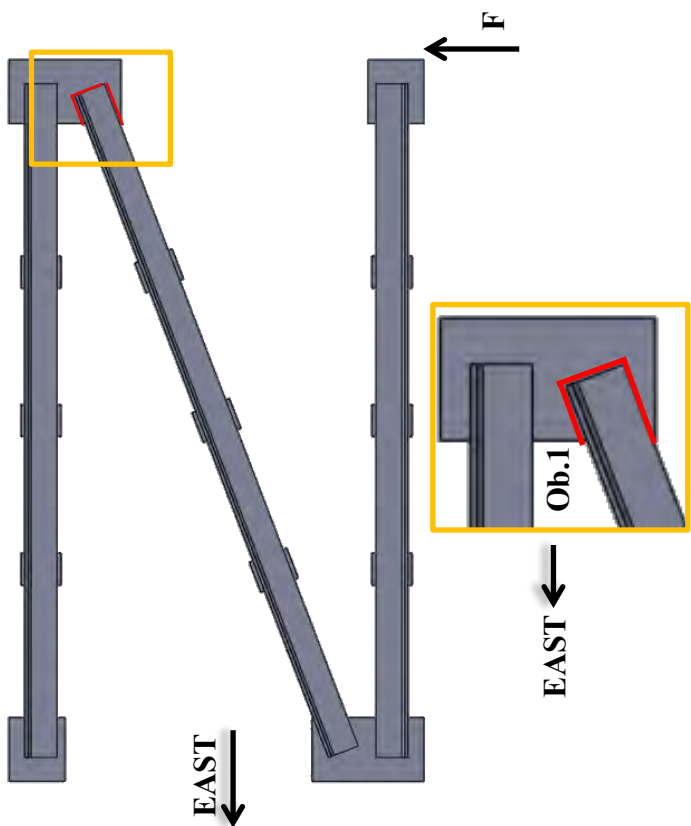
EAST →

Very similar to ZF_DA_1, the crack began at the forward edge of the connection and worked its way around the weld through the throat.

Crack 3: (NW Angle)



EAST ←

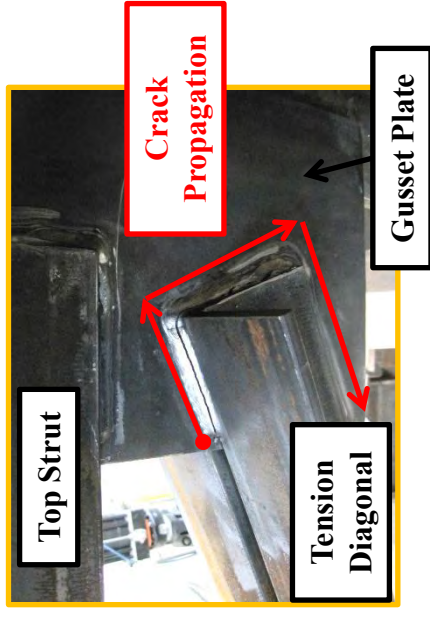
<p>Test Specimen: ZF_DA_3</p>	<p>Crack Locations:</p> 
<p>Test Dates: 5/7/2013 – 5/8/2013</p>	
<p>Primary Failure Location: Weld $S_R = 15.00$ ksi $N = 37,442$ cycles AASHTO Fatigue Category: < E'</p>	
<p>Stiffness: Initial: 212.7 k/in Final: 164.2 k/in 22.8% loss of stiffness</p>	
<p>Average Weld Size: Leg: 0.30" Throat: 0.33"</p>	
<p>Details:</p> <ul style="list-style-type: none"> • TxDOT Standard X-Type Cross Frame Detail with members 4" short prevent weld intersection • The gusset plates were 2" wider to maintain the same overlap as XF1-6 and the angle of the diagonals remained consistent 	
<p>Observations:</p> <ol style="list-style-type: none"> 1. First crack initiated at the NW angle heel at the forward weld toe propagating through the weld throat and around the connection consistent with a stress concentration caused by double curvature of the diagonal. 	

Test Specimen: ZF_DA_3

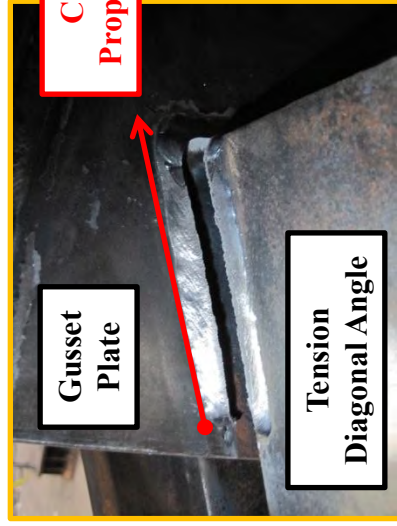
First Observed Crack
C1: N = 36,797 cycles



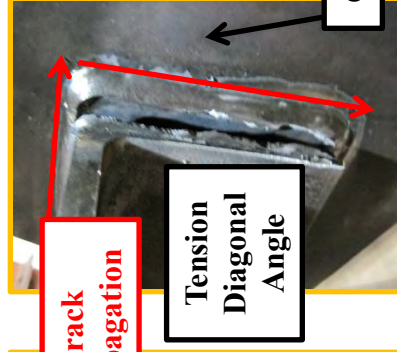
Crack 1: (Top West Gusset- North Face- At Failure)



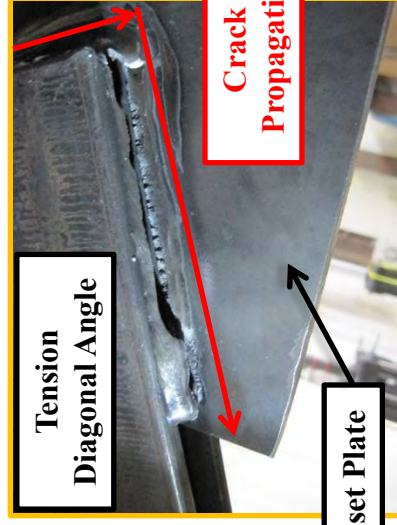
← EAST



← EAST

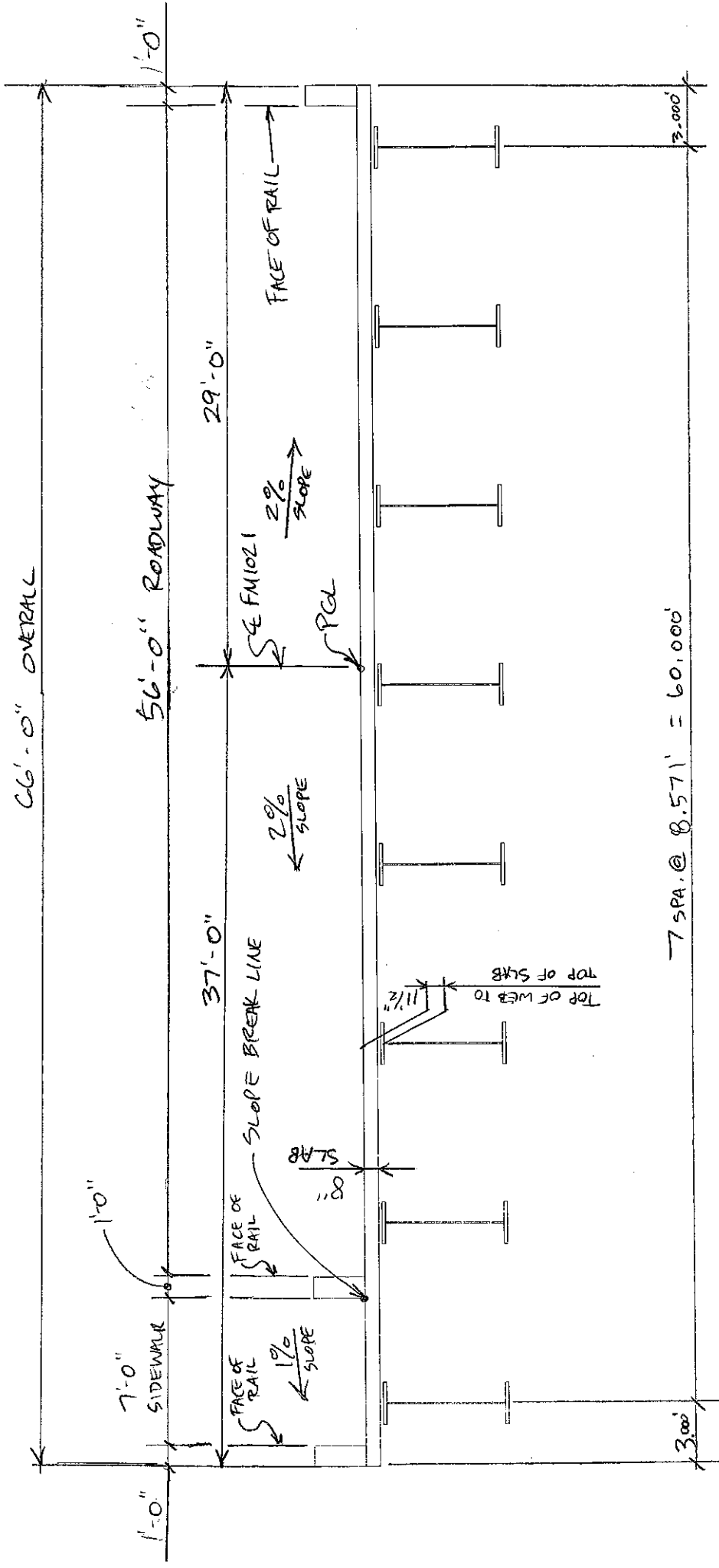


← EAST



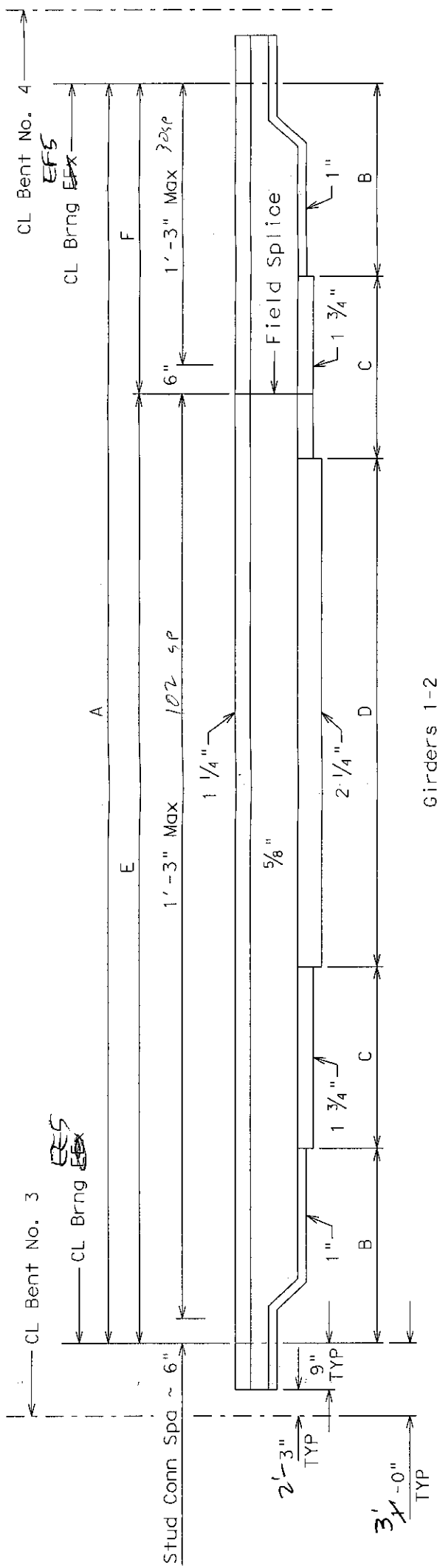
The crack began at the forward edge of the fillet weld at the heel of the angle and continued around connection.

APPENDIX B
TxDOT Bridge Details for FEA Comparison



STANDARD SLAB REINFORCING.

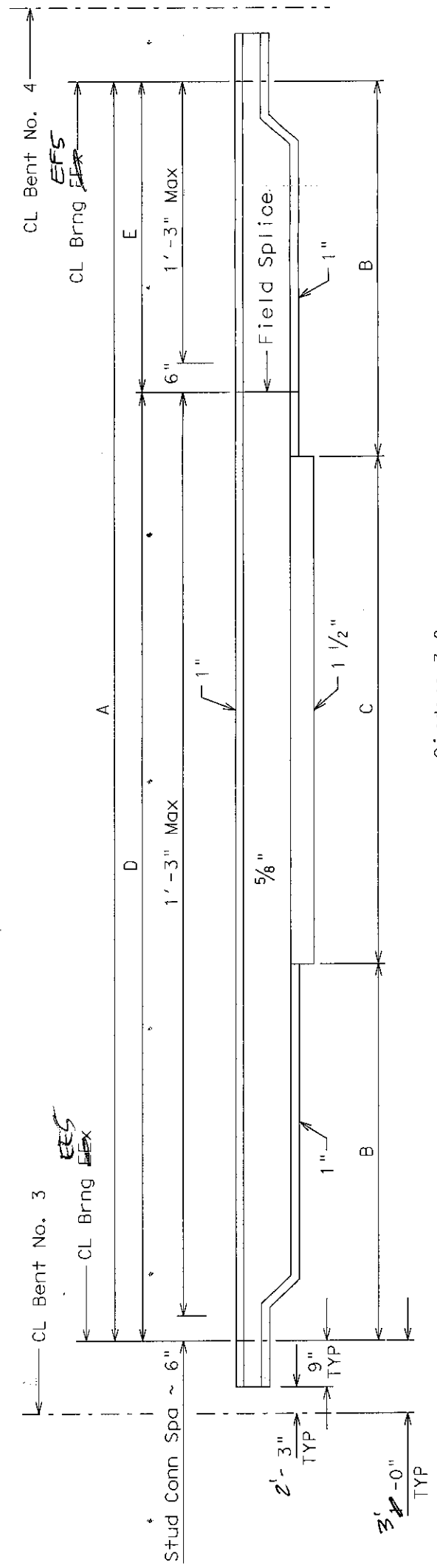
24" FLANGE WIDTH
 60" WEB DEPTH
 ALL STEEL SHALL
 CONFORM TO
 A709 GR 50W
 ALL STEEL IS
 TO REMAIN
 UNPAINTED



Girders 1-2

Girder	A	B	C	D	E	F
1	164.991	27.495	20.000	70.000	127.225	37.765
2	164.237	27.118	20.000	70.000	127.096	37.141

133
 133

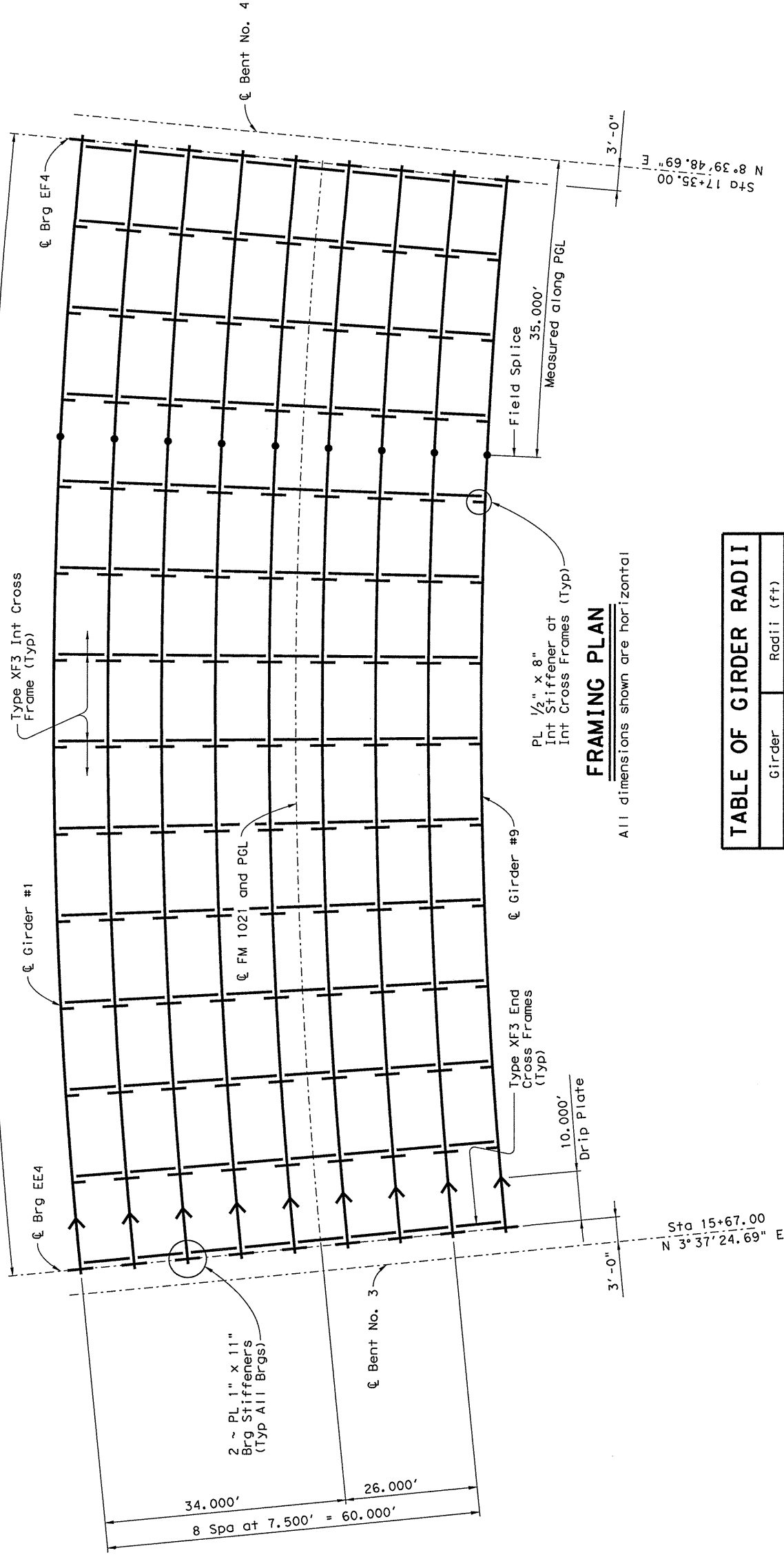


Girders 3-8

Girder	A	B	C	D	E
3	163.483	46.741	70.000	126.103	37.380
4	162.729	46.364	70.000	125.542	37.187
5	161.975	45.987	70.000	124.981	36.994
6	161.221	45.610	70.000	124.420	36.801
7	160.467	45.233	70.000	123.859	36.608
8	159.713	44.856	70.000	123.298	36.415

131
 131
 130
 130
 129
 128

13 Equal Spaces (Curved)



FRAMING PLAN

All dimensions shown are horizontal

TABLE OF GIRDER RADII

Girder	Radii (ft)
1	1943.86
2	1936.36
3	1928.86
4	1921.36
5	1913.86
PGL	1909.86
6	1906.36
7	1898.86
8	1891.36
9	1883.86

BENT REPORT

SPAN	GIRDER	BENT NO. 3 (S 3 37 24.69 W)		BENT NO. 4 (S 8 39 48.69 W)		GIRDER SLOPE
		D	S	D	S	
3	GIRDER 1	90	0	90	0	0.0348
	GIRDER 2	90	0	90	0	0.0350
	GIRDER 3	90	0	90	0	0.0351
	GIRDER 4	90	0	90	0	0.0352
	GIRDER 5	90	0	90	0	0.0354
	GIRDER 6	90	0	90	0	0.0355
	GIRDER 7	90	0	90	0	0.0357
	GIRDER 8	90	0	90	0	0.0358
	GIRDER 9	90	0	90	0	0.0359
TOTAL		67.500		67.500		

HL93 LOADING Sheet 2 of 5



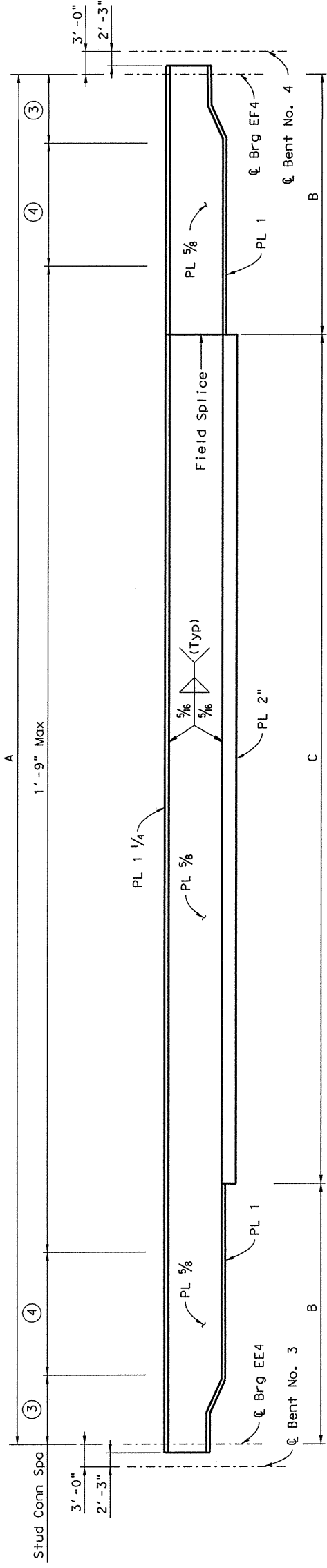
168.00' PLATE GIRDER SPAN
(SPAN 3)

UPRR OVERPASS



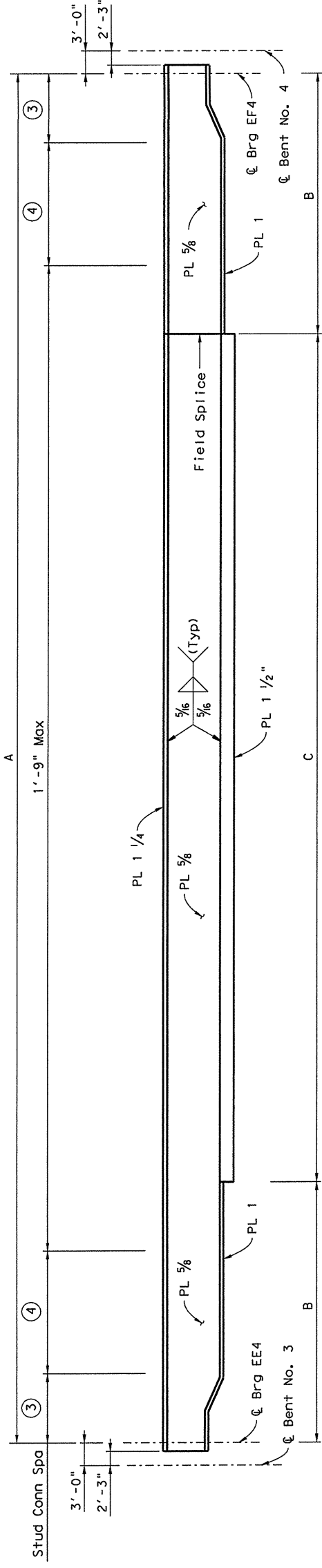
Jeff Tomkins
11/24/12

FILE: 7329sp01.dgn	DW: JPT	CK: TCG	CR: JPT
© TPOOT	DISTRICT: LRD	FEDERAL AID PROJECT:	SHEET: 15
JULY, 2011	COUNTY: MAYERLICK	CONTROL SECT: 1229 01	JOB HIGHWAY: FM1021
REVISIONS:			



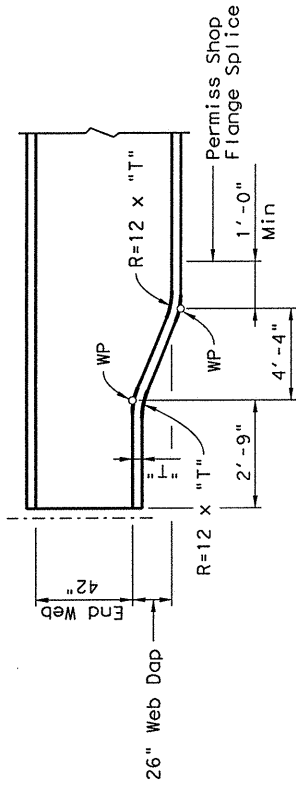
GIRDER NOS. 1-2 ELEVATION

- ③ 4 Spa at 6" = 2'-0"
- ④ 15 Spa at 1'-0" = 15'-0"



GIRDER NOS. 3-9 ELEVATION

Girder	A	B	C
1	164.991	32.623	99.745
2	164.331	32.486	99.360
3	163.671	32.348	98.975
4	163.012	32.211	98.590
5	162.352	32.073	98.205
6	161.692	31.936	97.820
7	161.032	31.798	97.436
8	160.373	31.661	97.051
9	159.713	31.524	96.666



DAPPED END DETAIL

All Web Plates are 68" deep except at ends. See Dapped End detail
 All Flange Plates are 24" wide
 All steel shall conform to A709 Gr 50

PLATE GIRDER FABRICATION NOTE:
 All structural steel including stiffeners and diaphragms shall conform to ASTM A709 Gr 50, unless noted otherwise, and shall be paid for at the unit price bid for Structural Steel (Plate Girder)
 All steel surfaces shall be cleaned and painted with System II in accordance with Item 446. Use an appearance coat as directed by the Engineer.
 Girder tension flanges and webs are classified as tension components and shall conform to Item 442.3(1)
 All dimensions shown in Girder Elevations are horizontal arc dimensions
 Except at changes in section, shop or field flange and web splices in plate girders may be located as desirable to optimize plate lengths and erection procedures, except that splices will not be allowed where a 40' or less unspliced length would suffice; neither will tension flange splices be allowed within .05S either side of interior bearings, within .10S either side of interior span centerline, nor within the range between .30S and .50S from the end bearings (S=length c.c. Bearing of Span in which the splice is made)
 Flange and Web Splices shall be made by full penetration groove welds in accordance with the Item "Steel Structures". Field Splices shall be made by full penetration groove welds or, at the Contractor's option, may be bolted. See sheet 5 of 5 for Optional Bolted Field Splice Details

HL93 LOADING Sheet 3 of 5

Texas Department of Transportation
 Bridge Division

168.00' PLATE GIRDER SPAN (SPAN 3)

UPRR OVERPASS

FILE: T329sp01.dgn DN: JPT CK: TGG DR: TGG CK: JPT SHEET
 © TxDOT JULY, 2011 DISTRICT LRD FEDERAL AID PROJECT
 REVISIONS COUNTY MAVERICK CONTROL SECT JOB HIGHWAY
 1229 01 042 FM1021

216

